frontiers | Research Topics

Nitrate from field to stream: characterization and mitigation

Edited by
Yefang Jiang, Jana Levison and Keith Schilling

Published in
Frontiers in Environmental Science



FRONTIERS EBOOK COPYRIGHT STATEMENT

The copyright in the text of individual articles in this ebook is the property of their respective authors or their respective institutions or funders. The copyright in graphics and images within each article may be subject to copyright of other parties. In both cases this is subject to a license granted to Frontiers.

The compilation of articles constituting this ebook is the property of Frontiers.

Each article within this ebook, and the ebook itself, are published under the most recent version of the Creative Commons CC-BY licence. The version current at the date of publication of this ebook is CC-BY 4.0. If the CC-BY licence is updated, the licence granted by Frontiers is automatically updated to the new version.

When exercising any right under the CC-BY licence, Frontiers must be attributed as the original publisher of the article or ebook, as applicable.

Authors have the responsibility of ensuring that any graphics or other materials which are the property of others may be included in the CC-BY licence, but this should be checked before relying on the CC-BY licence to reproduce those materials. Any copyright notices relating to those materials must be complied with.

Copyright and source acknowledgement notices may not be removed and must be displayed in any copy, derivative work or partial copy which includes the elements in question.

All copyright, and all rights therein, are protected by national and international copyright laws. The above represents a summary only. For further information please read Frontiers' Conditions for Website Use and Copyright Statement, and the applicable CC-BY licence.

ISSN 1664-8714
ISBN 978-2-8325-7169-9
DOI 10.3389/978-2-8325-7169-9

Generative AI statement
Any alternative text (Alt text) provided alongside figures in the articles in this ebook has been generated by Frontiers with the support of artificial intelligence and reasonable efforts have been made to ensure accuracy, including review by the authors wherever possible. If you identify any issues, please contact us.

About Frontiers

Frontiers is more than just an open access publisher of scholarly articles: it is a pioneering approach to the world of academia, radically improving the way scholarly research is managed. The grand vision of Frontiers is a world where all people have an equal opportunity to seek, share and generate knowledge. Frontiers provides immediate and permanent online open access to all its publications, but this alone is not enough to realize our grand goals.

Frontiers journal series

The Frontiers journal series is a multi-tier and interdisciplinary set of open-access, online journals, promising a paradigm shift from the current review, selection and dissemination processes in academic publishing. All Frontiers journals are driven by researchers for researchers; therefore, they constitute a service to the scholarly community. At the same time, the *Frontiers journal series* operates on a revolutionary invention, the tiered publishing system, initially addressing specific communities of scholars, and gradually climbing up to broader public understanding, thus serving the interests of the lay society, too.

Dedication to quality

Each Frontiers article is a landmark of the highest quality, thanks to genuinely collaborative interactions between authors and review editors, who include some of the world's best academicians. Research must be certified by peers before entering a stream of knowledge that may eventually reach the public - and shape society; therefore, Frontiers only applies the most rigorous and unbiased reviews. Frontiers revolutionizes research publishing by freely delivering the most outstanding research, evaluated with no bias from both the academic and social point of view. By applying the most advanced information technologies, Frontiers is catapulting scholarly publishing into a new generation.

What are Frontiers Research Topics?

Frontiers Research Topics are very popular trademarks of the *Frontiers journals series*: they are collections of at least ten articles, all centered on a particular subject. With their unique mix of varied contributions from Original Research to Review Articles, Frontiers Research Topics unify the most influential researchers, the latest key findings and historical advances in a hot research area.

Find out more on how to host your own Frontiers Research Topic or contribute to one as an author by contacting the Frontiers editorial office: frontiersin.org/about/contact

Nitrate from field to stream: characterization and mitigation

Topic editors

Yefang Jiang — Charlottetown Research and Development Centre, Agriculture and Agri-Food Canada (AAFC), Canada

Jana Levison — University of Guelph, Canada

Keith Schilling — The University of Iowa, United States

Citation

Jiang, Y., Levison, J., Schilling, K., eds. (2025). *Nitrate from field to stream: characterization and mitigation*. Lausanne: Frontiers Media SA.

doi: 10.3389/978-2-8325-7169-9

Table of contents

05 Editorial: Nitrate from field to stream: Characterization and mitigation
Yefang Jiang, Jana Levison and Keith Schilling

In-field studies

08 A diverse rotation of corn-soybean-winter wheat/double crop soybean with cereal rye after corn reduces tile nitrate loss
Lowell E. Gentry, Corey A. Mitchell, John M. Green, Carlos Guacho, Eric Miller, Dan Schaefer, Annette K. Vasquez and Zhongjie Yu

21 Assessing the potential of diverse pastures for reducing nitrogen leaching
Scott L. Graham, Jack Pronger, Johannes Laubach, John E. Hunt, Graeme N. D. Rogers, Sam Carrick, David Whitehead, Malcolm McLeod, Grace Mitchell and Paul Mudge

33 Risk for nitrogen leaching after application of solid manure in autumn differs between manure types
Sofia Delin, Kristina Mårtensson and Holger Johnsson

46 Dissolved nitrous oxide emissions associated with agricultural drainage water as influenced by manure application
D. L. Burton, H. D. M. Wilts and J. A. MacLeod

Downstream nitrate mitigation

59 Agricultural nitrate attenuation in a small groundwater-influenced wetland system
Leah M. Crossley, Kerry T. B. MacQuarrie and Serban Danielescu

73 Quantifying the impact of a constructed wetland on downstream nitrate concentrations and loads in the U.S. Midwest
Elliot Anderson, Keith E. Schilling, Craig L. Just and Bong Chul Seo

87 Ditch management using low-grade weirs: an opportunity for mitigating water quality and quantity impacts
J. S. Strock and A. Z. Ranaivoson

Improved quantification of nitrate

100 Quantifying rain-driven NO_3-N dynamics in headwater: value of applying SISO system identification to multiple variables monitored at the same high frequency
Nick A. Chappell

109 Insights on nitrate transport in a shallow, sandy aquifer at various temporal and spatial scales
Christina Zeuner, Jana Levison and Marie Larocque

131 Regression-based machine learning models for nitrate and chloride prediction in surface water in a small agricultural sand plain sub-watershed in southwestern Ontario, Canada
Ahmed Elsayed, Jana Levison, Andrew Binns, Marie Larocque and Pradeep Goel

153 Large variability of nitrate load estimated from sparse measurements by typical methods in Atlantic Canada
Kang Liang, Yefang Jiang, Keith Fuller, Marcos Cordeiro, Xuesong Zhang, Junyu Qi, Xiaoyuan Geng, Tao Liu, Qian Zhang, Mohammad Amir Azimi and Fan-Rui Meng

166 Nutrient dynamics in restored and unrestored urban streams in the Piedmont ecoregion of South Carolina
Emily N. Jordan, Debabrata Sahoo, Calvin B. Sawyer, Jeremy W. Pike, Dara M. Park, Sarah A. White and Brian E. Haggard

Evaluating nitrate at the watershed scale

183 Impacts of climate change and best management practices on nitrate loading to a eutrophic coastal lagoon
Alexandra C. Oliver, Barret L. Kurylyk, Lindsay H. Johnston, Nicole K. LeRoux, Lauren D. Somers and Rob. C. Jamieson

199 The contribution of red clover to nitrate loading in an agricultural watershed
Yefang Jiang, Mohammad Amir Azimi, Fan-Rui Meng and Kang Liang

212 Comparative modeling of nitrogen losses in a tile-drained watershed using SWAT model: uncertainty and calibration considerations
Junyu Qi, Robert Malone, Kang Liang, Kevin Cole, Bryan Emmett, Daniel Moriasi, Muhammad Rizwan Shahid and Michael Castellano

231 Simulation and attribution analysis of agricultural nitrogen non-point source pollution in Huang-Huai-Hai Plain based on the InVEST model
Ying Yu, Weiqiang Chen, Guangxing Ji, Yulong Guo, Yinan Chen, Siyu Sheng, Yaru Deng and Qianwen Weng

frontiers | Frontiers in Environmental Science

TYPE Editorial
PUBLISHED 07 November 2025
DOI 10.3389/fenvs.2025.1730350

Check for updates

OPEN ACCESS

EDITED AND REVIEWED BY
Yuncong Li,
University of Florida, United States

*CORRESPONDENCE
Yefang Jiang,
yefang.jiang@agr.gc.ca
Jana Levison,
jlevison@uoguelph.ca
Keith Schilling,
keith-schilling@uiowa.edu

RECEIVED 22 October 2025
REVISED 27 October 2025
ACCEPTED 28 October 2025
PUBLISHED 07 November 2025
CORRECTED 11 November 2025

CITATION
Jiang Y, Levison J and Schilling K (2025) Editorial: Nitrate from field to stream: Characterization and mitigation.
Front. Environ. Sci. 13:1730350.
doi: 10.3389/fenvs.2025.1730350

COPYRIGHT
© 2025 Jiang, Levison and Schilling. This is an open-access article distributed under the terms of the Creative Commons Attribution License (CC BY). The use, distribution or reproduction in other forums is permitted, provided the original author(s) and the copyright owner(s) are credited and that the original publication in this journal is cited, in accordance with accepted academic practice. No use, distribution or reproduction is permitted which does not comply with these terms.

Editorial: Nitrate from field to stream: Characterization and mitigation

Yefang Jiang[1]*, Jana Levison[2]* and Keith Schilling[3]*

[1]Charlottetown Research and Development Centre, Agriculture and Agri-Food Canada (AAFC), Charlottetown, PE, Canada, [2]College of Engineering, University of Guelph, Guelph, ON, Canada, [3]Iowa Geological Survey, University of Iowa, Iowa City, IA, United States

KEYWORDS

agriculture, nutrients, water quality, beneficial management practice, nitrate leaching

Editorial on the Research Topic
Nitrate from field to stream: characterization and mitigation

Introduction

Agricultural production plays a vital role in ensuring global food security. Nitrogen (N), an essential nutrient for crop growth, is often applied to agricultural systems as inorganic fertilizer, manure, or added to the soil via legume fixation to increase crop yields. However, excess N, in the form of nitrate, readily leaches from agricultural systems, harming water quality in groundwater, rivers, streams, lakes, and estuaries. Despite efforts to improve practices for agricultural N management, groundwater nitrate levels still often exceed drinking water guidelines for human health in many regions (Bijay-Singh and Craswell, 2021). High nitrate levels are a leading reason for violations at regulated U.S. drinking water utilities (Pennino et al., 2017). In the EU, a recent report showed that 14% of drinking water wells surpass the nitrate concentration limit (European Environment Agency, 2024a). Excessive nitrate leaching in the U.S. Corn Belt has been linked to the formation of large hypoxic zones in the Gulf of America and about one-third of coastal waters and rivers (Metaxoglou and Smith, 2025). Additionally, lakes in the EU are considered eutrophic partly due to high nitrate runoff from agricultural areas (European Environment Agency, 2024b). In Canada, nitrate contamination from agriculture affects many aquifers, including those in Abbotsford- Sumas, Assiniboine Delta, Annapolis Valley, and Prince Edward Island. When nitrate enters stream networks, some of it is converted to N_2O through denitrification, contributing roughly 10% of global N_2O emissions and thus to global warming (Beaulieu et al., 2011).

This Research Topic brings together articles advancing the science of identifying and reducing N losses from agricultural fields to streams. The Research Topic covers various aspects of N loss characterization and mitigation, including in-field N management, downstream mitigation, innovative monitoring strategies, and assessment at watershed scales. It provides a comprehensive overview of current research, highlighting new monitoring and mitigation strategies, as well as the sources, dynamics, and controls of N loss.

In-field studies

Four of the 16 studies examined the effects of beneficial management practices (BMPs) on N losses at the field scale. These included a diverse crop rotation in the Midwest US (Gentry et al.), multi-species pasture mixes for livestock production in New Zealand (Graham et al.), manure application timing and carbon-to-nitrogen (C/N) ratios in Germany (Delin et al.), and different fertility sources for potatoes in Prince Edward Island (PEI), Canada (Burton et al.). The diverse crop rotation was found to reduce nitrate leaching by up to 50% compared to conventional corn-soybean rotations. The inclusion of new rotational crops sometimes delayed planting under unfavorable weather, potentially compromising yields. While these rotations show promise for improving the resilience of row crop production, further research is needed to identify varieties and seeding rates that maximize yield and profitability under variable conditions (Gentry et al.). A multi-species pasture mix, hypothesized to reduce nitrate leaching from livestock operations, did not outperform the conventional two-species mix, underscoring the need for rigorous BMP evaluation before adoption (Graham et al.). Research on manure management showed that early fall application with a C/N ratio of 10 significantly increased nitrate leaching, whereas a higher ratio (up to 18) did not, highlighting the importance of both timing and composition in managing nitrate losses (Delin et al.).

Implementing BMPs to reduce nitrate leaching may inadvertently increase nitrous oxide (N_2O) emissions, a potent greenhouse gas. However, measuring both nitrate leaching and N_2O emissions together is uncommon in BMP studies, making it difficult to assess the trade-offs of N losses between the two pathways. One article reported on both tile drainage nitrate, dissolved N_2O, and soil surface N_2O emissions from a conventional potato-barley-red clover rotation in PEI (Burton et al.). The study found that nitrate losses via tile drainage from the potato phase were an order of magnitude greater than N_2O emissions from both tile drainage and the soil surface. Since tile drainage represents only a portion of total soil drainage (Jiang et al., 2011), total nitrate leaching is likely even higher. This large disparity suggests that the priority of mitigating N loss from the rotation should be placed on nitrate leaching. The results also emphasize the importance of measuring both nitrate and N_2O losses when evaluating BMPs to prioritize mitigation efforts effectively.

Downstream nitrate mitigation

Two studies evaluated constructed wetlands for nitrate removal in contrasting climates: Atlantic Canada (Crossley et al.) and Iowa, US (Anderson et al.). Another investigated the capacity of a low-grade weir to remove nitrate from a tile-drained ditch in Minnesota, US (Strock and Ranaivoson). Despite their different settings, the constructed wetlands removed 39% and 74% of incoming nitrate flux, respectively, whereas the weir increased nitrate removal by 58%. These articles highlight that temporarily retaining high-nitrate water in wetlands or behind weirs in flowing streams can be an effective strategy for reducing nitrate in agricultural watersheds.

Although the results are promising, Anderson et al. (2025) further noted that nitrate removal by the wetland on the experimental tributary accounted for only a small fraction of the total watershed nitrate load. Scaling up to remove 74% of the nitrate load across the entire Mud Creek watershed would require more than 1,800 wetlands of similar size, highlighting the impracticality of relying solely on wetlands for watershed-scale mitigation. This stresses the importance of placing BMP assessments under a broad watershed context.

Improved quantification of nitrate

Although nitrate is frequently monitored at many sites, concentrations can be highly variable in response to rainfall runoff. They can be difficult to estimate at local and regional scales, given the limited availability of calibration data. Some articles focused on improving N monitoring using a variety of approaches. Chappell (2025) used high-resolution monitoring of nitrate and hydrological dynamics to develop a model to quantify the rain-driven nitrate dynamics in a small headwater basin in the United Kingdom. In a sandy sub-catchment of an agriculturally intense region in Canada, Zeuner et al. (2025) evaluated data Research Topic methods at varying spatial scales and frequency (e.g., monthly sampling, 2-h auto-sampling, and *in situ* multiparameter instruments) to better understand groundwater N transport. High-frequency sampling using autosamplers was useful to capture storm-related transport of nitrate, but some issues were identified with data collection (e.g., impacts of sediment transport; power failure). When data are sparse, Elsayed et al. (2025) showed that machine learning (ML) regression models can be developed to quantify nitrate and other surface water concentrations using a variety of easily measured input variables, including hydrological, meteorological, and field conditions. In a different approach to sparse nitrate data, Liang et al. (2025) first demonstrated that the lack of adequate monitoring data can lead to substantial biases in nitrate load estimation and then showed how the use of a process-based watershed model can be used to improve load estimation when there are systematic data gaps in the monitoring record.

The transformation and loss of nitrate and other nutrients within the stream network can be very difficult to quantify. Jordan et al. (2025) report on the efficacy of using nutrient injection experiments as a monitoring tool to assess nutrient retention efficiency in stream reaches of South Carolina. They found that the presence of engineered pools in restored stream channels can help to trap and reduce nutrients. The effectiveness of temporarily trapping and treating nitrate within channels is consistent with results shared by Strock and Ranaivoson (2025) for their low-grade weir site in Minnesota.

Evaluating nitrate at the watershed scale

The impacts of nitrate loss and transport at smaller field or reach scales are often manifested at the outlets of larger watersheds (Danalatos et al., 2022). Developing watershed-scale mitigation strategies and quantifying their impacts often necessitates the use of models. Two independent studies assessed the impacts of land use on nitrate loads in two agricultural watersheds in PEI using the SWAT model (Oliver et al.; Jiang et al.). Both found that replacing forage red clover in the conventional potato-cereal-forage rotation in PEI with soybean effectively reduced nitrate loads. Also using SWAT, Qi et al. (2025) conducted comparative modeling (using the original and new

tile drainage and N modules) to assess model performance for simulation of N-loss in a typical Midwestern tile-drained watershed, noting that when observations are scarce, the processes in the new N module can magnify uncertainty in N-gas-flux estimates. In a distinctly different modeling approach, the Source List Model and the InVEST Model were used to assess total nitrogen emissions, including nitrate losses into rivers, as well as their sources, in the Huang-Huai-Hai Plain (5,423 km^2) of China (Yu et al.). Despite considerable uncertainties in the models, they yielded similar proportions of emissions from various sources and provided meaningful insights for developing management strategies in the region.

Concluding thoughts on special issue

The series of articles published in this Research Topic of Frontiers in Environmental Science highlights the challenges of evaluating and mitigating nitrate loss from fields to streams, while also serving to underline the interconnectedness of the research. Reducing nitrate loss at the field scale may be the first line of defense against excessive off-site transport, but this research Research Topic also shows that there are downstream remedial measures that can be taken to reduce nitrate once it has left the field. Once strategies are in place, improving quantification of nitrate loads and evaluating watershed-scale effectiveness using analytical and numerical models will be needed to document long-term performance. Overall, while the special Research Topic can include only a small sampling of the type of research being conducted by the scientific community on nitrate loss, mitigation, and transport, the Research Topic captures the many facets of this work that will be useful to a wide range of stakeholders.

We would like to express our sincere gratitude to all the authors for their contributions to this Research Topic and to the reviewers for their detailed evaluations and insightful comments that strengthened the manuscripts.

Author contributions

YJ: Writing – original draft, Writing – review and editing. JL: Writing – original draft, Writing – review and editing. KS: Writing – original draft, Writing – review and editing.

Funding

The author(s) declare that no financial support was received for the research and/or publication of this article.

Conflict of interest

The authors declare that the research was conducted in the absence of any commercial or financial relationships that could be construed as a potential conflict of interest.

The author(s) declared that they were an editorial board member of Frontiers, at the time of submission. This had no impact on the peer review process and the final decision.

Correction note

This article has been corrected with minor changes. These changes do not impact the scientific content of the article.

Generative AI statement

The author(s) declare that no Generative AI was used in the creation of this manuscript.

Any alternative text (alt text) provided alongside figures in this article has been generated by Frontiers with the support of artificial intelligence and reasonable efforts have been made to ensure accuracy, including review by the authors wherever possible. If you identify any issues, please contact us.

Publisher's note

All claims expressed in this article are solely those of the authors and do not necessarily represent those of their affiliated organizations, or those of the publisher, the editors and the reviewers. Any product that may be evaluated in this article, or claim that may be made by its manufacturer, is not guaranteed or endorsed by the publisher.

References

Beaulieu, J. J., Tank, J. L., Hamilton, S. K., Wollheim, W. M., Hall, R. O., Jr., Mulholland, P. J., et al. (2011). Nitrous oxide emission from denitrification in stream and river networks. *Proc. Natl. Acad. Sci.* 108 (1), 214–219. doi:10.1073/pnas.1011464108

Bijay-Singh, and Craswell, E. (2021). Fertilizers and nitrate pollution of surface and ground water: an increasingly pervasive global problem. *SN Appl. Sci.* 3, 518. doi:10.1007/s42452-021-04521-8

Danalatos, G. J. N., Wolter, C., Archontoulis, S. V., and Castellano, M. J. (2022). Nitrate losses across 29 Iowa watersheds: measuring long-term trends in the context of interannual variability. *J. Environ. Qual.* 51 (4), 708–718. doi:10.1002/jeq2.20349

European Environment Agency (2024a). Nitrate in groundwater in Europe. Available online at: https://www.eea.europa.eu/en/analysis/indicators/nitrate-in-groundwater-8th-eap.

European Environment Agency (2024b). Nutrients in freshwater in Europe. Available online at: https://www.eea.europa.eu/en/analysis/indicators/nutrients-in-freshwater-in-europe#:~:text=Rivers%20that%20drain%20land%20with,time%20series%20show%20different%20patterns.

Jiang, Y., Zebarth, B. J., and Love, J. (2011). Long-term simulations of nitrate leaching from potato production systems in Prince Edward Island, Canada. *Can. Nutr. Cycl. Agroecosyst.* 91 (3), 307–325. doi:10.1007/s10705-011-9463-z

Metaxoglou, K., and Smith, A. (2025). Agriculture's nitrogen legacy. *J. Environ. Econ. Manag.* 130, 103132. doi:10.1016/j.jeem.2025.103132

Pennino, M. J., Compton, J. E., and Leibowitz, S. G. (2017). Trends in drinking water nitrate violations across the United States. *Environ. Sci. Technol.* 51, 13450–13460. doi:10.1021/acs.est.7b04269

frontiers | Frontiers in Environmental Science

TYPE Original Research
PUBLISHED 11 February 2025
DOI 10.3389/fenvs.2025.1506113

Check for updates

OPEN ACCESS

EDITED BY
Keith Schilling,
The University of Iowa, United States

REVIEWED BY
Yansheng Li,
Chinese Academy of Sciences (CAS), China
Calvin Wolter,
The University of Iowa, United States

*CORRESPONDENCE
Lowell E. Gentry,
lgentry@illinois.edu

RECEIVED 04 October 2024
ACCEPTED 06 January 2025
PUBLISHED 11 February 2025

CITATION
Gentry LE, Mitchell CA, Green JM, Guacho C, Miller E, Schaefer D, Vasquez AK and Yu Z (2025) A diverse rotation of corn-soybean-winter wheat/double crop soybean with cereal rye after corn reduces tile nitrate loss.
Front. Environ. Sci. 13:1506113.
doi: 10.3389/fenvs.2025.1506113

COPYRIGHT
© 2025 Gentry, Mitchell, Green, Guacho, Miller, Schaefer, Vasquez and Yu. This is an open-access article distributed under the terms of the Creative Commons Attribution License (CC BY). The use, distribution or reproduction in other forums is permitted, provided the original author(s) and the copyright owner(s) are credited and that the original publication in this journal is cited, in accordance with accepted academic practice. No use, distribution or reproduction is permitted which does not comply with these terms.

A diverse rotation of corn-soybean-winter wheat/double crop soybean with cereal rye after corn reduces tile nitrate loss

Lowell E. Gentry[1]*, Corey A. Mitchell[1], John M. Green[1], Carlos Guacho [1], Eric Miller[2], Dan Schaefer[3], Annette K. Vasquez[1] and Zhongjie Yu[1]

[1]Department of Natural Resources and Environmental Sciences, University of Illinois, Urbana, IL, United States, [2]Producer and Landowner in Piatt County, Monticello, IL, United States, [3]Illinois Fertilizer and Chemical Association, Bloomington, IL, United States

Artificial drainage via subterranean drainage pipes called tiles transport nitrate from fields to streams, impairing downstream surface waters. Increased crop rotational diversity may conserve nitrogen, support greater system resiliency, and reduce tile nitrate loss. This 9-year study compares tile nitrate loss under a 3-year rotation of corn-soybean-winter wheat/double crop soybean plus cereal rye after corn versus a conventionally managed 2-year corn-soybean rotation. Tile flow and tile nitrate concentration were measured from 2015 through 2023 to determine annual flow weighted mean concentrations and loads of tile nitrate. Cereal rye following corn greatly reduced annual tile nitrate; however, more than 6 Mg ha^{-1} of above ground biomass may have decreased soybean yield. Winter wheat was efficient at using split-applied fertilizer nitrogen (N) as annual tile nitrate concentrations were reduced similar to cereal rye. Double crop soybean after winter wheat may be the most productive phase of the rotation; however, an early killing freeze greatly reduced soybean yield and increased tile nitrate loss. Interestingly, the subsequent corn crop may have benefitted from this unexpected N source. Overall, tile nitrate loss was approximately 50% less in the diverse 3-year rotational system, suggesting that a more diverse rotational system is efficient at retaining N, conserving nitrogen in the field, and reducing N loss to surface water. This study demonstrated proof of concept that a more diverse crop rotation can reduce tile nitrate loss from fields to streams, while maintaining crop productivity.

KEYWORDS

tile drainage, nitrate, diverse crop rotation, cover crop, corn, soybean, winter wheat, doublecrop soybean

1 Introduction

Nitrate loss from agricultural fields via subterranean drainage pipes called tiles is a major source of riverine nitrate load in central Illinois (David et al., 1997; David et al., 2010; Gentry et al., 1998; Gentry et al., 2009; Tilman et al., 2011; Mitchell et al., 2000; Pittelkow et al., 2017). A recent report by the Census of Agriculture estimated that approximately

3.6 million hectares in Illinois (36% of the total farmland) contain tile drainage (USDA National Agricultural Statistics Service, 2017). The predominant cropping system in Illinois is a 2-year rotation of corn (*Zea Mays* L.) and soybean (*Glycine max* L.) with nearly a 50: 50 mix of corn and soybean produced annually in central Illinois. Current Illinois fertilizer N recommendations for corn in central Illinois is approximately 200 kg ha^{-1} based on the Maximum Return to Nitrogen calculator [Home:: Nitrogen Rate Calculator (cornnratecalc.org)]; whereas soybean does not require fertilizer N (Vonk et al., 2024). Typical losses of riverine nitrate in central Illinois headwater streams average approximately 30 kg ha^{-1} yr^{-1} (Gentry et al., 2014) with nitrate concentrations in the spring frequently greater than the US EPA drinking water standard of 10 mg L^{-1} NO_3^-N (Royer et al., 2006). A contributing factor to large riverine nitrate loads in these extensively tile-drained watershed is the common practice of applying fertilizer N for next year's corn production in the late fall following soybean harvest (Welch et al., 1971; Randall and Vetsch, 2005; Gentry et al., 2014). Moving fall N application to the spring has been shown to reduce tile nitrate (David et al., 2015; Pittelkow et al., 2017; Gentry et al., 2024). Various split applications of fertilizer N applied in the spring, at planting, and early side-dress can reduce tile nitrate loss (Clark et al., 2020; Gentry et al., 2024); however, legacy N from previous fertilizer N applications contributes to tile nitrate loss for several years, masking immediate gains in water quality from improved fertilizer N use efficiency (David et al., 2016a; Yu et al., 2024).

Another important source of tile and riverine N load is nitrate liberated from soil N mineralization, especially following soybean (Gentry et al., 2001; Gentry et al., 2024). Although the soybean crop depletes soil N (Ciampitti and Salvagiotti, 2018), there is more soil inorganic N available to corn following soybean than when corn follows corn, reducing the fertilizer N requirement of rotated corn (Sawyer et al., 2006; Gentry et al., 2013). This rotation effect formerly known as the soybean N credit is largely due to greater net soil N mineralization following soybean than corn (Green and Blackmer, 1995; Gentry et al., 2001). Although both crops have residue with a wide carbon (C): N ratio, corn has approximately 3 times more crop residue than soybean. Therefore, corn residue has a greater N immobilization potential which can result in reduced plant available N as well as reduced tile nitrate loss during the non-growing season. In contrast, the soybean phase may be the weak link in soil C replenishment during the corn-soybean rotation, resulting in the loss of long-term soil organic C following soybean (Coulter et al., 2009).

Longer and more diverse crop rotations have been shown to benefit corn (Kazula and Lauer, 2018), and soybean (Janovicek et al., 2021), reduce nutrient loss (Hanrahan et al., 2024), suppress disease (Peralta et al., 2018), improve soil health (Baldwin-Kordick et al., 2022) and increase system resiliency (Bowles et al., 2020). A more diverse rotation with winter wheat (*Triticum Aestivum* L.) may indirectly benefit corn and soybean production by breaking pest cycles (Rocha et al., 2021). However, adding winter wheat after soybean may directly benefit wheat by providing the opportunity to scavenge mineralized N in the fall, generally before the tile drainage season begins. Although winter wheat receives fertilizer N, it is often split applied in the spring when the crop is actively growing and may be inherently more efficient than fertilizer N application to corn. Another benefit of adding winter wheat is the possibility of producing double crop soybean in the same year. A 3-year rotation of corn, soybean and winter wheat plus double crop soybean is a common cropping system in southern Illinois and the winter wheat/double crop soybean phase of the rotation can be the most profitable (Schnitkey et al., 2022; Shrestha et al., 2021).

Overwintering grass cover crops such as cereal rye (*Secale cereale L.*) can act as a N catch crop, accumulating soil inorganic N and reducing tile nitrate loss (Kaspar et al., 2012). Gentry et al. (2024) used cereal rye after corn in a 2-year corn and soybean rotation to reduce tile nitrate by more than 40%. Historically, cereal rye cover crops have been used to reduced soil erosion (Basche et al., 2016), weed pressure (Nichols et al., 2020b), and weed seedbank (Nichols et al., 2020a). Producing sufficient cereal rye biomass to reduce tile nitrate also contributes extra C to the system, which may enhance N immobilization (Basche et al., 2016). Several studies indicate a yield penalty with cereal rye before corn (Crandall et al., 2005; Qin et al., 2021), but not before soybean (Ruffo et al., 2004; Behnke et al., 2020; Silva et al., 2024) likely due to its N fixing capability. Additionally, using cereal rye before soybean reduces the risk of enhancing nitrous oxide production from the interaction of cover crop decomposition and added fertilizer N (Preza-Fontes et al., 2021).

Using a systems approach, the objective of this study was to evaluate crop yield and tile nitrate loss in a more diverse 3-year crop rotation of corn-soybean-winter wheat/double crop soybean plus cereal rye following corn (experimental treatment) versus a conventionally managed 2-year crop rotation of corn and soybean with full width tillage and fall fertilizer N application (control treatment). We hypothesized that the diverse rotation with a longer duration of living roots and greater C input compared to the conventional system could reduce tile nitrate loss. In addition, we hypothesize that the diverse rotation may support greater corn and soybean grain yields. The control treatment was produced by summing tile flow and tile loads from two adjacent fields on the opposite phase of the 2-year rotation, which represented the integrated loss of nitrate from field tiles to streams across central Illinois. The experiment was replicated in time with a 9-year period of record (2015–2023) for the 3-year rotation versus an 8-year period of record (2016–2023) for the 2-year rotation. Additionally, this systems comparison study assessed N retention in the predominant cropping system of southern Illinois, investigating the outcome of moving this cropping system north into the intensively tile drained region of central Illinois.

2 Materials and methods

2.1 Site description and experimental design

This field study was conducted on a private farm in southern Piatt County, IL and is in Upper Kaskaskia River watershed. The predominant soil types on this farm are Drummer and Flanagan (fine-silty, mixed, superactive, mesic Typic Endoaquolls) containing approximately 4% organic matter and are characterized as poorly drained with 0%–2% slopes (Soil Survey Staff, Natural Resources Conservation Services and USDA, 2024). Based on data collected near Tuscola IL, the 30-year mean annual precipitation is 1041 mm and the mean annual temperature is 11.2°C. Precipitation was

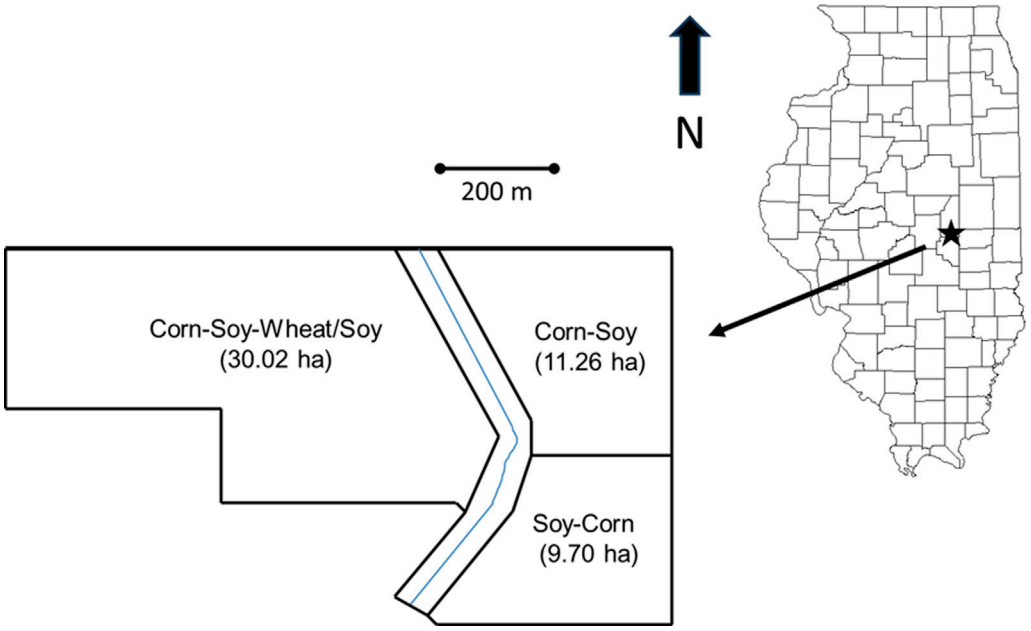


FIGURE 1
Study site field layout and location within Piatt County, Illinois.

measured on site using a Davis Instruments Vantage Pro2 Plus weather station and expressed on a water year basis (October 1-September 30).

Prior to the initiation of this study, the entire farm was either planted to corn or soybean in a corn-soybean rotation with winter wheat planted only the year of tile installation. In the summer of 2014, a pattern tile system was installed, creating a field plot with a drainage area of 30.02 ha (Figure 1). Tiles (10.2 cm in diameter) were installed to an average depth of approximately 1.2 m and lateral tiles were spaced 30.1 m apart throughout the field. The tile outlet discharged to a dredged ditch that divided the farm. This field plot was under the 3-year rotation beginning with corn in 2015. That same year, on the other side of the ditch, three adjacent pattern tile systems were installed with drainage areas of 8.10, 3.16, and 9.70 ha. Tile size, depth, and spacing were the same as the other field and tile outlets discharged into the dredged ditch. By isolating the two smaller tile systems into one field, two distinct field plots were created with drainage areas of 11.26 and 9.70 ha (Figure 1). These field plots were under the conventionally managed 2-year rotation and maintained on the opposite phase of the rotation. Combining the tile data across both phases of the 2-year rotation created a larger drainage area of 20.96 ha for the control treatment, closer in size to the experimental treatment. During the study period, three cycles through the 3-year rotation and four cycles through the 2-year rotation were completed.

2.2 Crop management

Field operations are listed chronologically in Supplementary Tables S1, S2 including dates for crop planting and harvest, cereal rye planting and termination, tillage, and fertilizer applications. The aim was to plant corn and soybean in late April through mid-May, plant winter wheat in early October, and harvest wheat and plant double crop soybean before July 4th. In the 2-year rotation corn was planted in April in 2017 and 2018; however, wet months of May in 2019 and 2020 delayed corn planting until early June. Similar to corn, soybean planting in the 2-year rotation was delayed until June in 2019; however, in 2020 soybean was planted in April before the wet period. In the diverse 3-year rotation, corn was planted in April in 2015 and 2018, and May in 2021. Soybean in the diverse rotation was planted in May in 2016 and 2022; however, planting was delayed until June in 2019. Wheat was planted in early to mid-October. An early wheat harvest on 27 June 2017, allowed for an early double crop soybean planting. Wheat harvest was July 6th and seventh in 2020 and 2023, delaying double crop soybean planting. The 3-year rotation requires greater planning, more equipment initially, and timeliness of field operations.

2.3 Cover crop management

Cereal rye was planted in October following corn in the 3-year rotation (Supplementary Table S2). Cereal rye was drill-planted at 67 kg ha^{-1} and terminated in the spring prior to soybean planting in 2016 and 2022; however, in 2019, soybean was planted directly into live cereal rye Cereal rye termination dates were in April of 2016, June of 2019, and May of 2022. Above ground cereal rye biomass was randomly collected from a 0.25 m^2 area from nine locations across the field. Samples were dried at 65°C for 48 h and weighed. Cover crop biomass was ground and analyzed for N concentration by combustion analysis (A&L Great Lakes Laboratories, Inc., Ft. Wayne, IN).

2.4 Fertilizers

Conventionally managed corn in the 2-year rotation received fertilizer N at a rate of 202 kg ha^{-1} (Supplementary Table S1). Depending on precipitation following crop harvest, fertilizer N was applied in the fall as anhydrous ammonia with a nitrification inhibitor after soil temperatures were less than 10°C at the 10 cm depth. In 2016 and 2017, N application occurred at planting as a starter fertilizer (UAN at 32%) and the remainder at early side-dress (UAN at 32%). In 2018 and 2019, fertilizer N was applied at a 2/3rds rate in the fall with the remainder nearly equally split between the starter fertilizer at planting and at early side-dress. In 2020–2023, fertilizer N was applied at a 2/3rds rate in the fall with the remainder applied at planting. Soybean received no fertilizer N. Overall, both field plots under the 2-year rotation received 808 kg ha^{-1} over the 8-year period (101 kg ha^{-1} yr^{-1}).

In the 3-year rotation, fertilizer N was applied to corn at a rate of 202 kg ha^{-1} and winter wheat at a rate of 134 kg ha^{-1}, whereas soybean received no N (Supplementary Table S2). For corn, starter fertilizer N (22–45 kg ha^{-1}) was applied at planting (UAN at 32%) with the remainder at early side-dress (UAN at 32%). Starter fertilizer N rate was increased over time in the 3-year rotation, decreasing the N rate at side-dress. For wheat, 18–26 kg ha^{-1} of N was applied with fertilizer phosphorus (P) in the fall while the remainder was split applied (50:50 or 40:60) in March and April. Overall, the field under the 3-year rotation received 1008 kg ha^{-1} over the 9-year period (112 kg ha^{-1} yr^{-1}).

For all three study fields, P and potassium (K) fertilizers were co-applied in the fall each year at recommended rates based on the Illinois Agronomy Handbook (University of Illinois, 2021), except for an accidentally omission of fertilizer application in 2019 following corn harvest in the field plots under the 2-year rotation. Fertilizer P was applied as triple super phosphate to corn and soybean; whereas mono-ammonium phosphate was applied to wheat to provide N to the wheat seedling. Fertilizer K was applied as muriate of potash (Supplementary Tables S1, S2).

2.5 Tillage

Conventional tillage in the 2-year rotation consisted of full width tillage either in the spring or fall; however, wet weather limited fall tillage operations in some years (Supplementary Table S1). Conventional tillage implements were either a field cultivator, chisel-plow or disk-chisel. In the 3-year rotation, strip-till occurred before corn either in the fall or early spring; whereas soybean, winter wheat, and double crop soybean were no-till planted (Supplementary Table S2).

2.6 Crop grain harvest

As with tillage operations, planting and harvest dates were controlled by the weather, and planting delays occurred during the wet springs of 2018 and 2019, which led to late harvests (Supplementary Tables S1, S2). Crop grain yields were determined using a yield monitor and represent whole field averages. Yield monitor was calibrated using a weigh wagon and moisture meter in the field and measuring grain weight over a predetermined area. Yield maps and field yield averages were determined by PAC Interactive (Monticello, IL). Crop grain yields are presented at 15.5, 13.0, and 14.5% moisture for corn, soybean and winter wheat, respectively.

2.7 Herbicides

The herbicide programs for both cropping systems were designed to include multiple modes of action to control the onslaught of herbicide-tolerant weeds (Supplementary Table S3). There were eight different herbicide compounds applied to cover pre-emergence and post-emergence applications to corn and soybean in both the 2-year and 3-year rotations. In addition, the 3-year rotation received glyphosate as a preplant application to terminate the cereal rye cover crop and again as a post-emergence double crop soybean. Winter wheat received only one herbicide compound as a post-emergence application.

2.8 Tile monitoring

Drain tile flow was monitored with a 45° V-notch weir stoplog fitted at the bottom of an in-line water control structures (Agri Drain, Inc., Adair, IA). Water height within the structure was determined using a combination pressure transducer and datalogger (Solinst, Inc., Georgetown, Ontario, Canada). Tile flow rate was calculated using the v-notch weir equation described by Chun and Cooke (2008). Flow was logged on 15-minute intervals and daily average flow was calculated using the 96 logged data points per day. During extreme precipitation events, rising ditch water submerged tile outlets, impeding tile flow. When this occurred, tile flow was manually set to zero until water height in the control structures began to recede. At that point, we assumed a linear increase in tile flow until maximum flow resumed (Li et al., 2020).

Tile nutrient concentrations were determined from 500 mL water samples collected using automated water samplers (ISCO 3700, Teledyne, Lincoln, NE) or from grab samples during periods when air temperatures decreased below 0°C. Samplers were set to sequential time mode on an 8-h basis to capture nutrient concentration changes during tile flow events. If no flow events occurred, tile water samples were collected weekly. Tile water samples were collected from automated samplers within 24 h. Samples were vacuum filtered through a 0.45 um membrane and analyzed for nitrate. Nitrate-N concentrations were measured using ion chromatography (ICS-1600, Dionex, Sunnyvale, CA) with a minimum detection limit of 0.1 mg N L^{-1}. We used linear interpolation to estimate nitrate concentration for each day between tile sampling dates. Annual tile nitrate loads were calculated by multiplying daily average flow by daily nitrate concentration, expressed on a water year basis. Annual flow-weighted mean concentration (FWMC) of nitrate-N was calculated by dividing annual tile load by annual tile flow. Overall FWMC of tile nitrate-N was calculated by summing annual tile loads and dividing by the sum of annual tile flows over the period of record for each cropping systems.

TABLE 1 Crop grain yields in both phases of the conventionally managed 2-year rotation and in the 3-year rotation from 2015 through 2023.

Year	2-Year rotation				3-Year rotation	
	Corn-Soy		Soy-Corn		Corn-Soy-Wheat	
	Crop	Yield (Mg ha^{-1})	Crop	Yield (Mg ha^{-1})	Crop	Yield (Mg ha^{-1})
2015	NC	—	NC	—	Corn	15.9
2016	Corn	13.7	Soy	5.8	Soy	5.0
2017	Soy	5.3	Corn	15.2	Wheat/Soy	6.6/3.7
2018	Corn	17.0	Soy	5.8	Corn	16.6
2019	Soy	5.6	Corn	13.9	Soy	5.0
2020	Corn	13.6	Soy	5.4	Wheat/Soy	6.2/1.3
2021	Soy	5.4	Corn	14.3	Corn	15.1
2022	Corn	14.9	Soy	5.5	Soy	5.7
2023	Soy	5.6	Corn	14.6	Wheat/Soy	7.1/2.4

Note: NC = No crop.
Wheat/Soy yields are reported separately when both crops are grown in the same year.

2.9 Data analysis

A balanced T-test analysis was conducted to evaluate differences in the average annual tile flow, tile nitrate load, FWMC of nitrate, and crop grain yield between the two conventionally managed field plots under either a corn-soybean or soybean-corn rotation (n = 4) over the 8-year period of record. Without significant differences between the two conventionally managed fields, an annual integrated tile flow, tile nitrate load, and FWMC of tile nitrate was calculated across corn and soybean phases to create the control treatment. The 3-year rotation represented the experimental treatment. T-test analysis was conducted to evaluate differences in tile flow, tile FWMC of nitrate, and nitrate load between the experimental treatment, (n = 9) and the control treatment (n = 8). T-test analysis was conducted on corn and soybean grain yields to evaluate differences between the experimental treatment (n = 3) and the control treatment (n = 8). All analyses were performed using R Statistical Software (v4.2.2; R Core Team, 2022).

3 Results

3.1 Crop grain yield

Precipitation during the growing season on this farm was sufficient to produce crop yields that equaled or surpassed the county yield estimate each year of this study. In the two conventionally managed field plots, corn grain yields ranged from 13.6 Mg ha^{-1} in 2020 to 17.0 Mg ha^{-1} in 2018, averaging 14.7 over the 8 growing seasons (Table 1). Conventionally managed soybean grain yields varied minimally during this same period, ranging from 5.3 Mg ha^{-1} in 2017 to 5.8 Mg ha^{-1} in 2016, equaled again in 2018, with an average of 5.5 Mg ha^{-1}.

There was no comparison between the two rotational cropping systems for corn yield in 2015 as the control treatment was initiated in 2016. Corn grain yields were 2% less in 2018 and 6% greater in 2021 in the 3-year versus the 2-year rotation. Soybean grain yields were 11% and 13% less, and 4% greater, in 2016, 2019, and 2022, respectively, in the 3-year versus the 2-year rotation. Average crop grain yields in the 3-year rotation were 15.9 Mg ha^{-1} for corn, 5.3 Mg ha^{-1} for soybean, 6.6 Mg ha^{-1} for winter wheat, and 2.5 Mg ha^{-1} for double crop soybean. There were no significant differences between average corn ($p > 0.05$) and soybean ($p > 0.05$) yields between the experimental treatment and the control. Double-crop soybean grain yield varied widely and ranged from a low of 1.3 Mg ha^{-1} due to an early frost versus 3.7 Mg ha^{-1} when allowed to reach maturity.

3.2 Cereal rye cover crop

Depending on termination date, cereal rye biomass production varied more than four-fold during the study. The late termination on 2 June 2019, produced the greatest amount of above ground cereal rye biomass (5.94 Mg ha^{-1}), with early termination on 16 April 2016, producing the least biomass (1.37 Mg ha^{-1}), and termination on 10 May 2022, producing an intermediate amount (2.38 Mg ha^{-1}) (Table 2). Cereal rye biomass N accumulation ranged from 24 to 46 kg ha^{-1} representing less than a two-fold increase as biomass N concentration decreased with increasing biomass production, widening the C:N ratio (Table 2). With approximately 43% C, cereal rye biomass added from 0.6 to 2.5 Mg ha^{-1} of C to the 3-year rotation.

3.3 Precipitation and tile flow

Annual precipitation at this research site ranged from 818 to 1192 mm from 2015–2023, averaging 1012 mm, which was only 3% less than the 30-year average of 1041 mm (Table 3). Compared to the 30-year average, annual precipitation was 15% greater in 2016 and 21% less in 2017. Annual precipitation was characterized as average

TABLE 2 Cereal rye biomass and biomass nitrogen in above ground biomass before soybean in the 3-year rotation from 2015 through 2023.

Year	Cereal rye biomass and Biomass N		
	Biomass (Mg ha^{-1})	Biomass N (%)	Biomass N (kg ha^{-1})
2015–2016	1.37	1.70	23.5
2018–2019	5.94	0.77	45.7
2021–2022	2.38	1.19	28.4

TABLE 3 Annual precipitation and annual tile flows in both phases of the conventionally managed 2-year rotation and in the 3-year rotation from 2015 through 2023.

Year	Precipitation	2-Year rotation				3-Year rotation	
		Corn-Soy		Soy-Corn		Corn-Soy-Wheat	
	(mm)	Crop	Tile flow (mm)	Crop	Tile flow (mm)	Crop	Tile flow (mm)
2015	1,153	NC	—	NC	—	Corn	119
2016	1,192	Corn	179	Soy	185	Soy	117
2017	818	Soy	132	Corn	101	Wheat/Soy	114
2018	961	Corn	98	Soy	64	Corn	50
2019	1,097	Soy	276	Corn	217	Soy	177
2020	1,045	Corn	273	Soy	243	Wheat/Soy	272
2021	957	Soy	102	Corn	100	Corn	95
2022	987	Corn	230	Soy	153	Soy	115
2023	894	Soy	83	Corn	58	Wheat/Soy	71

Note: NC = No crop.

in 2020, above average in in 2015, 2016, and 2019, and below average in 2017, 2018, 2021, 2022, and 2023.

At this site, tile flow most frequently occurred from January through June, averaging 125 days of flow per year; however, with consecutive wet years in 2015 and 2016, tile flow occurred every month in 2016. Generally, years with greater annual precipitation produced greater annual tile flow. An exception was in 2020 when most of the precipitation occurred during the first 6 months, greatly elevating annual tile flow for all three field plots. Combined tile flow from all three field plots accounted for approximately 15% of the annual precipitation during the study period. There were no significant differences for annual tile flow between the two conventionally managed field plots ($p > 0.05$) (Table 3). Although annual tile flow was less under the diverse 3-year rotation, there was no significant difference between the experimental treatment and the control treatment ($p > 0.05$) (Table 3).

3.4 Pattern of tile nitrate concentrations

The pattern of tile nitrate concentration in tiles under the two conventionally managed field plots demonstrated elevated tile nitrate concentrations under corn compared to soybean (Figures 2A, B). Tile nitrate concentrations increased during the spring under corn, whereas under soybean concentrations remained relatively unchanged in 2018, 2020, and 2023. Tile nitrate concentrations were greater than 10 mg L^{-1} in 35% of the samples and less than 5 mg L^{-1} in 15% of the samples collected in the 2-year rotation.

In contrast, the pattern of tile nitrate concentrations in the 3-year rotation was dissimilar to the pattern observed in tiles under the 2-year rotation (Figure 2C). Tile nitrate was greater than 10 mg L^{-1} in only 1% of the samples and less than 5 mg L^{-1} in 70% of the samples in the 3-year rotation. Tile nitrate concentrations decreased under cereal rye each year and under winter wheat in 2023. Following the severe freeze and premature death of the double crop soybean in October of 2020, tile nitrate concentrations were elevated in 2021 (Figure 2C). When tile flow began in March of 2021, the initial tile nitrate concentrations were greater than all other years, gradually increasing to 9 mg L^{-1} prior to starter fertilizer N application at corn planting. Following side-dress fertilizer N application that year, tile nitrate reached 14 mg L^{-1} during high tile flow in June causing substantial nitrate loss.

3.5 Annual tile flow weighted mean nitrate concentrations

The annual FWMC of tile nitrate in the two field plots in the 2-year rotation ranged from 6.9 to 12.7 mg L^{-1} under corn and from

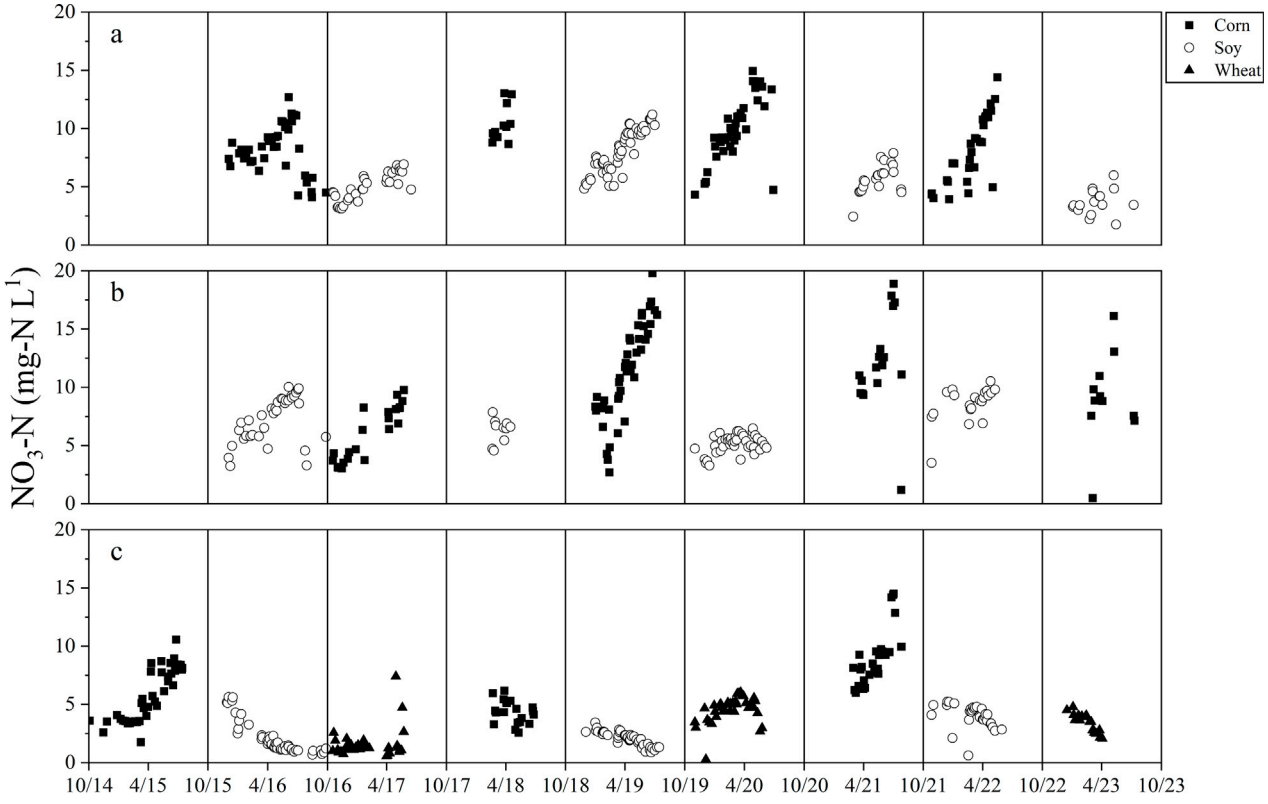


FIGURE 2
(A–C) Pattern of tile nitrate concentrations in both phases of the conventionally managed 2-year rotation and in the 3-year rotation from 2015 through 2023. Water years are separated by vertical lines and crop phases are represented by squares for corn, circles for soybean, and triangles for winter wheat/double-crop soybean.

TABLE 4 Annual tile flow weighted mean nitrate concentrations and annual tile nitrate loads in both phases of the conventionally managed 2-year rotation and in the diverse 3-year rotation from 2015 through 2023.

Year	2-Year rotation						3-Year rotation		
	Corn-Soy			Soy-corn			Corn-Soy-wheat		
	Crop	NO_3–N (mg L^{-1})	NO_3–N (kg ha^{-1})	Crop	NO_3–N (mg L^{-1})	NO_3–N (kg ha^{-1})	Crop	NO_3–N (mg L^{-1})	NO_3-N (kg ha^{-1})
2015	NC	—	—	NC	—	—	Corn	6.5	7.7
2016	Corn	7.4	13.3	Soy	6.2	11.4	Soy	2.0	2.3
2017	Soy	5.3	7.0	Corn	6.9	6.9	Wheat/ Soy	1.9	2.2
2018	Corn	9.8	9.6	Soy	6.2	3.9	Corn	4.5	2.2
2019	Soy	8.2	22.5	Corn	12.7	27.6	Soy	1.9	3.4
2020	Corn	9.6	26.2	Soy	5.2	12.6	Wheat/ Soy	4.7	12.7
2021	Soy	5.7	5.8	Corn	12.1	12.1	Corn	10.4	9.8
2022	Corn	8.5	19.4	Soy	8.7	13.2	Soy	4.1	4.7
2023	Soy	3.7	3.1	Corn	9.6	5.6	Wheat/ Soy	3.2	2.3

Note: NO_3–N (mg/L) = FWMC; NO_3–N (kg/ha) = Load; NC = No crop.

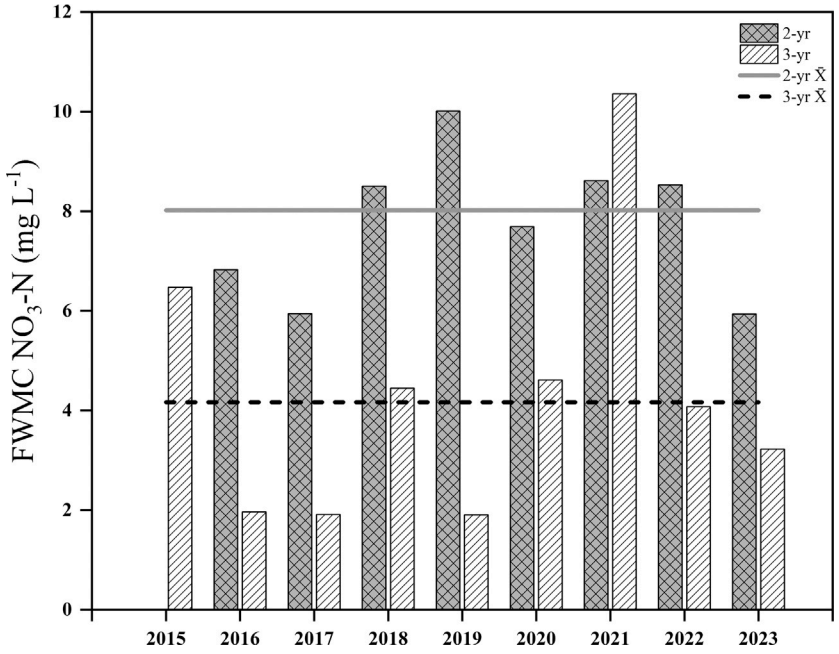


FIGURE 3
Annual tile flow weighted mean nitrate concentrations across both phases of the conventionally managed 2-year rotation compared to the 3-year rotation from 2015 through 2023. Horizontal lines represent overall tile flow weighted mean nitrate concentration over three cycles of the diverse rotation and four cycles of the conventional rotation.

3.7 to 8.7 mg L^{-1} under soybean (Table 4). The overall FWMC of tile nitrate in each field plot over the 8-year period of record was not significantly different (7.7 and 8.3 mg L^{-1}) ($p > 0.05$). The annual integrated FWMC of tile nitrate across both phases of the 2-year rotation ranged from 5.9 mg L^{-1}–9.9 mg L^{-1} (Figure 3). The overall integrated FWMC of tile nitrate across both crop phases of the 2-year rotation over the 8-year period of record was 8.0 mg L^{-1} and represented nitrate loss from the control treatment (Figure 3).

In the 3-year rotation annual FWMC of tile nitrate under corn ranged from 4.5 to 10.4 mg L^{-1} (Table 4). Annual FWMC of nitrate under soybean ranged from 1.9 to 4.1 mg L^{-1} (Table 4) Annual FWMC of tile nitrate under winter wheat/double crop soybean ranged from 1.9 to 4.7 mg L^{-1} (Table 4). The overall FWMC of tile nitrate in the 3-year rotation over the 9-year period of record was 4.2 mg L^{-1}, which was significantly less than the control treatment ($p < 0.05$) (Figure 3).

3.6 Tile nitrate load

Annual tile nitrate loads ranged from 5.6 kg ha^{-1} in 2023 to 27.6 kg ha^{-1} in 2019 under corn in the 2-year rotation, while tile nitrate loads under soybean ranged from 3.1 kg ha^{-1}–22.5 kg ha^{-1} in those same years (Table 4). Average annual tile nitrate loads in the 2-year rotation under conventional corn and conventional soybean were 15.1 kg ha^{-1} and 9.9 kg ha^{-1} during the 8-year period of record. Average annual tile nitrate loads from the two conventionally managed field plots were not significantly different at 11.7 and 13.4 kg ha^{-1}. The overall average tile nitrate load in the 2-year rotation over the 8-year period of record was 12.5 kg ha^{-1}.

In the 3-year rotation, the greatest tile nitrate load occurred during the wet spring of 2020 under the wheat/double crop soybean phase (Table 4). The second greatest annual load occurred in 2021 following the early freeze of the double crop soybean crop. Annual tile nitrate loads in the 3-year rotation ranged from 2.2 to 12.7 kg ha^{-1}, averaging 4.9 kg ha^{-1} over the 9-year period of record (Table 4), which was significantly less than the control ($p < 0.05$) (Figure 3). Note: With the inherent challenges in measuring tile flow; tile nitrate concentration data may better differentiate treatment response.

4 Discussion

4.1 Crop yields

Growing conditions were favorable to produce above average corn and soybean yields on this farm compared with Piatt County estimates. The average grain yields of conventionally managed corn and soybean were 14.7 Mg ha^{-1} and 5.5 Mg ha^{-1} at this site which were 7% and 15% greater than the county yield estimates over the 8-year period of record (Table 1). Piatt County's corn and soybean yields consistently rank amongst the highest producing counties in Illinois with record corn and soybean yields of 15.2 Mg ha^{-1} and 5.1 Mg ha^{-1} in 2018 (USDA National Agricultural Statistics Service, 2022). This county produced the largest soybean yields in Illinois for 3 years in a row during the study period (2020, 2021, and 2022), producing the largest soybean yield for any county in the entire U.S. in 2022 (USDA National Agricultural Statistics Service, 2022). These data clearly indicate that our study site was located in one of the most productive areas in the U.S Corn Belt.

With the predominant cropping system under a corn and soybean rotation in central Illinois, there are few fields under winter wheat production and no county yield estimate. Winter wheat is generally not grown on the productive tile drained soils of central Illinois due to lower economic return compared to corn and soybean (G. Schnitkey, personal communication). However, on sloping lands in southern Illinois, winter wheat is more commonly grown and is often followed by double-crop soybean. With more time to grow wheat and soybean in the same year, this phase of the corn-soybean-wheat rotation can be the most profitable in southern Illinois. At the latitude of this study site, however, producers are aware of the risk of early frost, which can negatively impact double crop soybean yield and profitability. It is interesting to note that the USDA has updated frost-free dates twice in the past 12 years due to recent data trends, moving frost-free zone boundaries approximately 100 km north. With lengthening growing seasons, the 3-year rotation of corn-soybean-wheat/double crop soybean may become more common in the intensively tile drained watershed of central Illinois (USDA National Agricultural Statistics Service, 2022).

Numerous studies (Davis et al., 2012; Gaudin et al., 2015; Bowles et al., 2020) suggest longer more diverse crop rotations may enhance both corn and soybean yields, however, our results were mixed. In general, earlier crop planting dates at this site produced greater grain yields for both corn and soybean. In 2018, the weather supported an extended grain filling period and produced large corn grain yields for both cropping systems that were approximately 10% greater than the record-breaking county estimate. In 2021, corn grain yield was 0.8 Mg ha^{-1} greater in the 3-year rotation which may have been related to the unexpected N source from the frozen double crop soybean.

Soybean yields in the 3-year rotation were decreased in 2016 and 2019 due to issues related to the cereal rye cover crop. In 2016, soybean planting was delayed 17 days by wet soil conditions in the 3-year rotation following cover crop termination, decreasing yield potential and overall soybean grain yield. In 2019, a large cover crop biomass was produced due to wet conditions preventing timely termination. Without a roller crimper, the soybean crop emerged in standing cereal rye, reducing early plant vigor likely due to the combination of less light interception by the developing crop and greater N immobilization following cover crop senescence (Nevins et al., 2020). In 2022, however, soybean grain yield was greater in the 3-year rotation, which is approximately the amount of yield increase needed to offset the price of establishing and terminating cereal rye before soybean.

Winter wheat grain yields at this site were 32% greater than average winter wheat yields in the southern Illinois region (USDA National Agricultural Statistics Service, 2022). Double-crop soybean grain yield was 67% of the full season soybean yield when allowed to reach maturity while only 25% of the full season soybean yield after the killing freeze. Double-crop soybean planting date is critical, therefore, searching for high yielding wheat varieties that mature several days earlier is an important goal of current wheat breeding programs (J. Rutkowski, personal communications). To maximize yield and profitability of this cropping system, nested microplot studies are being initiated at this site to evaluate wheat varieties and seeding rates for double crop soybean.

4.2 Fertilizer N application

The timing of conventional fertilizer N application to corn varies due to convenience and risk for a given farmer (David et al., 2015). In central Illinois, approximately half of the fields under corn receive fertilizer N in the fall (Gentry et al., 2014). Following university guidelines, the application of fall N with a nitrification inhibitor occurred only after soil temperatures were consistently less than 4°C (University of Illinois Agronomy Handbook). Numerous studies report increased tile nitrate loss under fall fertilizer N application (Welch et al., 1971; David et al., 2015; Pittelkow et al., 2017; Gentry et al., 2024). Split-application of fertilizer N has been proposed to reduce tile nitrate loss, improving synchronization of fertilizer application with crop growth (Dinnes et al., 2002). Testing this hypothesis in central Illinois, Gentry et al. (2024) evenly split-applied fertilizer N in the fall and spring and found approximately a 10% reduction in tile nitrate compared to 100% applied in the fall. With more producers split-applying fertilizer N, we chose to split-apply a 2/3rds fertilizer N rate in the fall with the remainder in the spring to represent conventional fertilizer application. Although we used the same total fertilizer N rate for corn in both rotational cropping systems, fall fertilizer N application occurred 6 out of the 8 years in the 2-year rotation, increasing tile nitrate loss. In the 3-year rotation, fertilizer N was split-applied in season for both corn and wheat for improved synchrony between application and uptake. Overall, the 3-year rotation received approximately 10% more fertilizer N than the 2-year rotation (112 vs. 101 kg ha^{-1} yr^{-1}).

4.3 Herbicides

The advent of herbicides has made modern agriculture more efficient and more profitable by reducing reliance on mechanical weed control. Regardless of tillage differences between the cropping systems, herbicide use was similar and can be considered conventional for both rotational cropping systems as corn and soybean as well as the double crop soybean in the diverse rotation required an additional herbicide application of glyphosate. Wheat production required less herbicide application compared to corn and soybean production. Weeds were effectively eliminated from both cropping systems and played no role in experimental outcomes.

4.4 Tillage

With effective herbicidal control of weeds in conventional cropping systems, tillage is a method of managing crop residue, especially for corn; however, soil conditioning is also a consideration as a warm seedbed speeds germination and enhances early crop growth (Licht and Al-kaisi, 2005). Soil disturbance from tillage aerates the soil, energizing soil microorganisms, and stimulating soil N mineralization, which may decrease soil organic C (Randall et al., 1997; Balesdent et al., 2000). Therefore, we hypothesize that tillage has the potential to increase nitrate leaching and tile nitrate loss compared to no-till and reduced tillage systems. In contrast,

however, no-till improves soil aggregate stability and soil structure, which increases water infiltration rates and possibly tile nitrate loss.

An interesting phenomenon that has occurred in the 3-year rotation is the return and establishment of earthworms (*Lumbricus teresteres* L.). Tillage is clearly detrimental to earthworm survivability and no-till systems have been shown to have increased abundance (Kladivko et al., 1997). With precision farming techniques, moving the center of the tilled strip 25 cm each corn year in a 76 cm row width completely tills the entire field every 9 years under the 3-year rotation. Although conventional herbicide practices occurred in both rotational cropping systems, visual inspection indicated worm middens in the 3-year rotation and none in the two conventionally managed fields under corn and soybean, suggesting that full width tillage limited the prevalence of worms rather than herbicide toxicity. Anecdotally, this past spring we observed short-term ponding following an intense precipitation event only in the conventionally managed field plots, suggesting that infiltrations rates are different between the two cropping systems. This study is on-going and water infiltration rate studies are planned to evaluate the influence of earthworms on tile flow and nitrate loss over time.

4.5 Cereal rye

The conservation technique of adding a cereal rye cover crop after corn in a corn-soybean rotation has been shown to greatly reduce tile nitrate concentrations and loads (Kaspar et al., 2012; Ruffatti et al., 2019; Waring et al., 2020; Gentry et al., 2024). Cereal rye following corn can capture unused fertilizer N and mineralized N during the non-crop growing season that may leach to tiles. Cereal rye biomass and biomass N accumulation was sufficient to decrease tile nitrate each time through the rotation with the greatest reduction in tile nitrate occurring when cereal rye was terminated in early June in 2019. Unlike end-of-pipe nitrate remediation techniques such as wetlands (Kovacic et al., 2000; Tilman et al., 2011), woodchip bioreactors (Christianson et al., 2011; David et al., 2016b), and saturated riparian buffers (Singh et al., 2024) that only treat the symptom of a declining soil C stock (i.e., tile nitrate loss from soil N mineralization), cereal rye adds carbon to the system, directly treating the cause of tile nitrate loss. Management practices that conserve N in the field have a strategic advantage over remediation techniques that return N to the atmosphere via denitrification.

In Illinois cover crops are being adopted on sloping lands and are more easily integrated into animal livestock operations (Plastina et al., 2023), whereas in the flat rich soils of central Illinois there are few livestock animals and less than 5% of the area in cover crops (USDA National Agricultural Statistics Service, 2022). The greatest impetus behind cover crop adoption is preventing soil erosion, while the greatest impediment is cost of cover crop establishment and termination (David et al., 2015; Roth et al., 2018). Cereal rye covers the soil quickly in the spring and is the most widely used cover crop in Illinois due to winter hardiness. Cereal rye is also known to suppress weed germination and growth (Kaspar et al., 2012), potentially offsetting some of the cover crop production cost by reducing herbicide use. Using a roller crimper at the appropriate cereal rye growth stage is an effective termination strategy, creating a thick mat of residue that reduces weed pressure, retains soil moisture, and reduces soil temperature (Mirsky et al., 2011). The additional C input from cereal rye can tie up soil nitrate via microbial N immobilization (McSwiney et al., 2010; Nevins et al., 2020). Simple stoichiometry indicates that to build soil organic matter, soil N will need to increase concomitantly with soil C, therefore, net N immobilization may be the key to soil C sequestration (Cao et al., 2021).

4.6 Tile nitrate concentration

Yu et al. (2024) measured the natural abundance of heavy isotopes in tile water and identified sources as fertilizer N, soil organic matter decomposition, and legacy nitrate with a release lag time of several years. Legacy N may explain the muted tile nitrate response to a reduced fertilizer N rate (75%) treatment in a replicated tile drainage experiment in central Illinois that surprisingly decreased corn yield more than tile nitrate loss (Gentry et al., 2024). Similar to that study, tile nitrate concentrations in the conventionally managed plots were greater under corn than soybean. Tile nitrate concentrations tended to increase through the spring with numerous samples during the corn phase containing greater than the US EPA drinking water standard of 10 mg L^{-1} nitrate-N, especially during the wet springs of 2019 and 2020. Even though fertilizer N application in the fall was limited to 2/3rds of the full rate, fall N appeared to increase tile nitrate loss (2017 through 2023) compared to years without fall N application (2015 and 2016). Although no fall fertilizer N was applied in the first 2 years of the study, tile nitrate concentrations increased in the spring, suggesting the source was in part from soil N mineralization.

The downward trend in tile nitrate in the spring under cereal rye demonstrated the efficacy of an overwintering grass cover crops to act as a catch crop, absorbing mineralized N as well as legacy N during the non-crop growing season. Winter wheat appeared effective at utilizing fertilizer N, especially in the spring of 2023, when the pattern of tile nitrate concentrations was similar to years under cereal rye. Compared to conventional corn, fertilizer N was spoon-fed to winter wheat with approximately 20% of the fertilizer N applied with the phosphorus fertilizer in the fall and the remainder split applied in the spring. Wheat was actively growing when fertilizer N was applied in the spring, which reduced tile nitrate loss despite the input of fertilizer N and concurrent soil N mineralization following soybean production.

The early freeze in 2020 that reduced double crop soybean yield occurred during mid grain fill (R5 growth stage) when soybean leaves, stems, and nodules contain high N concentrations (Bender et al., 2015). We speculate that organic N from soybean roots and shoots leaked into the soil, nitrified, and leached to tiles during the subsequent spring. Even with the annual FWMC of tile nitrate greater than 10 mg L^{-1} in 2021, the overall FWMC was only 4.2 mg L^{-1} in the 3-year rotation, compared to the overall FWMC of tile nitrate of 8.0 mg L^{-1} in the 2-year rotation, indicating a 50% reduction in FWMC of tile nitrate with the diverse cropping system. This unique long-term drainage study provided proof of concept that a longer more diverse cropping system can reduce tile nitrate loss, while maintaining system productivity.

4.7 Tile nitrate loads

Average annual tile nitrate loads from the conventionally managed field plots on this farm were less than reported for other tile nitrate studies in central Illinois (David et al., 1997; Royer et al., 2006; Rufatti et al., 2019; Gentry et al., 2024). Annual tile flow in this study may be a conservative estimate due to the assumption that tile flow stopped during high ditch water flow. Similar to Gentry et al. (2024), 60% of the tile nitrate load occurred under corn and 40% under soybean. Annual tile nitrate loads in the 2-year rotation clearly demonstrated that years with below normal precipitation transport the least amount of tile nitrate and tile flow generally ranked in order with annual precipitation. In the 3-year rotation, crop phase had a greater influence on annual tile nitrate load as cereal rye and winter wheat greatly reduced tile nitrate concentrations and loads. Additionally, tile flow tended to cease earlier under winter wheat compared to under corn or soybean, helping to reduce tile nitrate load.

The two wettest years (2019 and 2020) produced the greatest tile nitrate loads under conventionally managed corn as the combination of fall fertilizer N application and wet spring conditions delaying corn planting, exacerbated tile nitrate loads those years (27.6 and 26.2 kg ha^{-1}). The largest annual difference in tile nitrate loads between the two cropping systems occurred in 2019 when cereal rye accumulated 6 Mg ha^{-1} of above-ground biomass and annual tile nitrate load was only 3.4 kg ha^{-1}, representing a 90% reduction in tile nitrate load. This comparison demonstrates the magnitude of tile nitrate reduction possible in a row crop production system without having to convert to a perennial crop (McIsaac et al., 2010; Heaton et al., 2008).

4.8 Systems comparison

Using an overwintering grass cover crop to reduce tile nitrate loss is not a new idea as Armsby (1884) suggested using rye to keep growing roots in the soil as extensively as possible to curtail N loss from manured plots. With cereal rye after corn and winter wheat after soybean, the 3-year rotation had living roots 30 out of 36 months versus 10 out of 24 months in the conventionally managed 2-year rotation. Available C is a critical factor in N retention in soils and extra C added into the diverse 3-year cropping systems may tighten the N cycle (McSwiney et al., 2010), sequestering C and reducing tile nitrate loss. Overall, by maintaining crop yields and reducing tile nitrate loss, this study may be the first of its kind to demonstrate sustainable intensification in a high-yielding, dry land production system in the US Corn Belt (Cassman and Grassini, 2020; Heaton et al., 2013; Tilman et al., 2011).

The most challenging aspects of managing the diverse rotation was readiness and timeliness of field operations due to the limited number of days to conduct field work in the spring. The first-time cereal rye was grown following corn the decision not to plant soybean in the 3-year rotation on May 5th (conventional soybean planting date) may have been a costly misstep as it led to reduced yield. The combination of the 17-day planting delay and the use of a shorter season maturity soybean variety may explain the grain yield reduction. Three years later, when wet weather delayed cover crop termination in 2019, soybean was "planted green" and the large amount of cereal rye biomass interfered with both the physical planting operation and early soybean growth (Reed et al., 2019).

Consideration for balancing cover crop biomass production with timely row crop management must be weighed against nutrient loss reduction goals. Using a replicated tile drainage study, Gentry et al. (2024) found that cereal rye biomass accumulation of approximately 1 Mg ha^{-1} was sufficient to significantly reduce tile FWMC of nitrate, whereas this study indicated that 6 Mg ha^{-1} may be more than required. Therefore, we recommend producers aim for at least 1 Mg ha^{-1} of above ground biomass (stem length 15–20 cm) to 6 Mg ha^{-1} (beginning flowering) to maximize tile nitrate reduction and weed control without decreasing soybean yield.

This study demonstrated winter wheat was efficient at using split-applied fertilizer N and helped reduce the loss of mineralized N following soybean. Winter wheat occupies the space of an overwintering grass cover crop and demonstrated the potential to reduce tile nitrate during its phase of the 3-year rotation. Planting double crop soybean after winter wheat can be highly productive at this latitude, however, early frost greatly reduced soybean yield and increased tile nitrate loss. Interestingly, the subsequent corn crop appeared to be benefitted from this unexpected N source.

Future studies at this research site will focus on refining management practices within the diverse cropping system and documenting economic viability and competitiveness with the conventional 2-year rotation. This study suggests the common rotation of corn-soybean-wheat/double crop soybean in southern Illinois is efficient at retaining N and reducing N loss. Overall, this study demonstrated proof of concept that a more diverse crop rotation can greatly reduce tile nitrate loss from fields to streams, while maintaining crop productivity.

Data availability statement

The raw data supporting the conclusions of this article will be made available by the authors, without undue reservation.

Author contributions

LG: Conceptualization, Funding acquisition, Investigation, Writing–original draft. CM: Data curation, Investigation, Writing–review and editing. JG: Investigation, Methodology, Writing–review and editing. CG: Formal Analysis, Investigation, Writing–review and editing. EM: Conceptualization, Investigation, Methodology, Writing–review and editing. DS: Conceptualization, Investigation, Methodology, Writing–review and editing. AV: Investigation, Writing–review and editing. ZY: Funding acquisition, Project administration, Writing–review and editing.

Funding

The author(s) declare that financial support was received for the research, authorship, and/or publication of this article. We thank the Illinois Nutrient Research and Education Council (Grant number:

2015-5-360350-374) for their generous continuous support of this long-term research project.

Conflict of interest

The authors declare that the research was conducted in the absence of any commercial or financial relationships that could be construed as a potential conflict of interest.

Generative AI statement

The author(s) declare that no Generative AI was used in the creation of this manuscript.

Publisher's note

All claims expressed in this article are solely those of the authors and do not necessarily represent those of their affiliated organizations, or those of the publisher, the editors and the reviewers. Any product that may be evaluated in this article, or claim that may be made by its manufacturer, is not guaranteed or endorsed by the publisher.

Supplementary material

The Supplementary Material for this article can be found online at: https://www.frontiersin.org/articles/10.3389/fenvs.2025.1506113/full#supplementary-material

References

Armsby, H. P. (1884). Loss of nitrogen from arable soils. *Science* 3, 17–19. doi:10.1126/science.ns-3.48.17

Baldwin-Kordick, R., De, M., Lopez, M. D., Liebman, M., Lauter, N., Marino, J., et al. (2022). Comprehensive impacts of diversified cropping on soil health and sustainability. *Agroecol. Sustain. Food Syst.* 46 (3), 331–363. doi:10.1080/21683565.2021.2019167

Balesdent, J., Chenu, C., and Balabane, M. (2000). Relationship of soil organic matter dynamics to physical protection and tillage. *Soil Tillage Res.* 53, 215–230. doi:10.1016/S0167-1987(99)00107-5

Basche, A. D., Archontoulis, S. V., Kaspar, T. C., Jaynes, D. B., Parkin, T. B., and Miguez, F. E. (2016). Simulating long-term impacts of cover crops and climate change on crop production and environmental outcomes in the Midwestern United States. *Agric. Ecosyst. Environ.* 218, 95–106. doi:10.1016/j.agee.2015.11.011

Behnke, G. D., Kim, N., and Villamil, M. B. (2020). Agronomic assessment of cover cropping and tillage practices across environments. *Agron. J.* 112 (5), 3913–3928. doi:10.1002/agj2.20337

Bender, R. R., Haegele, J. W., and Below, F. (2015). Nutrient uptake, partitioning, and remobilization in modern soybean varieties. *Agron. J.* 107, 563–573. doi:10.2134/agronj14.0435

Bowles, T. M., Mooshammer, M., Socolar, Y., Calderón, F., Cavigelli, M. A., Culman, S. W., et al. (2020). Long-term evidence shows that crop-rotation diversification increases agricultural resilience to adverse growing conditions in North America. *One Earth* 2 (3), 284–293. doi:10.1016/j.oneear.2020.02.007

Cao, Y., He, Z., Zhu, T., and Zhao, F. (2021). Organic-C quality as a key driver of microbial nitrogen immobilization in soil: a meta-analysis. *Geoderma* 383, 114784. doi:10.1016/j.geoderma.2020.114784

Cassman, K. G., and Grassini, P. (2020). A global perspective on sustainable intensification research. *Nat. Sustain.* 3, 262–268. doi:10.1038/s41893-020-0507-8

Chun, J. A., and Cooke, R. A. (2008). Technical note: Calibrating Agridrain water level control structures using generalized weir and orifice equations. *Appli. Enginee. Agricu.* 24 (5), 595–602. doi:10.13031/2013.25274

Christianson, L. E., Bhandari, A., and Helmers, M. J. (2011). Pilot-scale evaluation of denitrification drainage bioreactors: reactor geometry and performance. *J. Environ. Eng.* 137, 213–220. doi:10.1061/(ASCE)EE.1943-7870.0000316

Ciampitti, I. A., and Salvagiotti, F. (2018). New insights into soybean biological nitrogen fixation. *Agron. J.* 110, 1185–1196. doi:10.2134/agronj2017.06.0348

Clark, J. D., Fernandez, F. G., Camberato, J. J., Carter, P. R., Fergusun, R. B., Franzen, D. W., et al. (2020). Weather and soil in the US Midwest influence the effectiveness of single- and split-nitrogen applications in corn production. *Agron. J.* 112 (6), 5288–5299. doi:10.1002/agj2.20446

Coulter, J. A., Nafziger, E. D., and Wander, M. M. (2009). Soil organic matter response to cropping system and nitrogen fertilization. *Agron. J.* 101, 592–599. doi:10.2134/agronj2008.0152x

Crandall, S. M., Ruffo, M. L., and Bollero, G. A. (2005). Cropping system and nitrogen dynamics under a cereal winter cover crop preceding corn. *Plant Soil* 268 (1), 209–219. doi:10.1007/s11104-004-0272-x

David, M. B., Drinkwater, L. E., and McIsaac, G. F. (2010). Sources of nitrate yields in the Mississippi River basin. *J. Environ. Qual.* 39, 1657–1667. doi:10.2134/jeq2010.0115

David, M. B., Flint, C. G., Gentry, L. E., Dolan, M. K., Czapar, G. F., Cooke, R. A., et al. (2015). Navigating the socio-bio-geo-chemistry and engineering of nitrogen management in two Illinois tile-drained watersheds. *J. Environ. Qual.* 44, 368–381. doi:10.2134/jeq2014.01.0036

David, M. B., Gentry, L. E., Cooke, R. A., and Herbstritt, S. M. (2016a). Temperature and substrate control woodchip bioreactor performance in reducing tile nitrate loads in east-central Illinois. *J. Environ. Qual.* 45, 822–829. doi:10.2134/jeq2015.06.0296

David, M. B., Gentry, L. E., Kovacic, D. A., and Smith, K. M. (1997). Nitrogen balance in and export from an agricultural watershed. *J. Environ. Qual.* 26, 1038–1048. doi:10.2134/jeq1997.00472425002600040015x

David, M. B., Mitchell, C. A., Gentry, L. E., and Salemme, R. K. (2016b). Chloride sources and losses in two tile-drained agricultural watersheds. *J. Environ. Qual.* 45, 341–348. doi:10.2134/jeq2015.06.0302

Davis, A. S., Hill, J. D., Chase, C. A., Johanns, A. M., and Liebman, M. (2012). Increasing cropping system diversity balances productivity, profitability and environmental health. *PLoS One* 7, e47149. doi:10.1371/journal.pone.0047149

Dinnes, D. L., Karlen, D. L., Jaynes, D. B., Kaspar, T. C., Hatfield, J. L., Colvin, T. S., et al. (2002). Nitrogen management strategies to reduce NO_3 leaching in tile-drained midwestern soils. *Agron. J.* 94, 153–171. doi:10.2134/agronj2002.0153

Gaudin, A. C. M., Tolhurst, T. N., Ker, A. P., Janovicek, K., Tortora, C., Martin, R. C., et al. (2015). Increasing crop diversity mitigates weather variations and improves yield stability. *PLoS One* 10, e0113261. doi:10.1371/journal.pone.0113261

Gentry, L. E., Below, F. E., David, M. B., and Bergerou, J. A. (2001). Source of the soybean N credit in maize production. *Plant Soil* 236, 175–184. doi:10.1023/A:1012707617126

Gentry, L. E., David, M. B., Below, F. E., Royer, T. V., and McIsaac, G. F. (2009). Nitrogen mass balance of a tile-drained agricultural watershed in east-central Illinois. *J. Environ. Qual.* 38, 1841–1847. doi:10.2134/jeq2008.0406

Gentry, L. E., David, M. B., and McIsaac, G. F. (2014). Variation in riverine nitrate flux and fall nitrogen fertilizer application in East-Central Illinois. *J. Environ. Qual.* 43, 1467–1474. doi:10.2134/jeq2013.12.0499

Gentry, L. E., David, M. B., Smith, K. M., and Kovacic, D. A. (1998). Nitrogen cycling and tile drainage nitrate loss in a corn/soybean watershed. *Agric. Ecosyst. Environ.* 68, 85–97. doi:10.1016/S0167-8809(97)00139-4

Gentry, L. E., Green, J. M., Mitchell, C. A., Andino, L. F., Rolf, M. K., Schaefer, D., et al. (2024). Split fertilizer nitrogen application with a cereal rye cover crop reduces tile nitrate loads in a corn-soybean rotation. *J. Environ. Qual.* 53 (1), 90–100. doi:10.1002/jeq2.20530

Gentry, L. F., Ruffo, M. L., and Below, F. E. (2013). Identifying factors controlling the continuous corn yield penalty. *Agron. J.* 105, 295–303. doi:10.2134/agronj2012.0246

Green, C. J., and Blackmer, A. M. (1995). Residue decomposition effects on nitrogen availability to corn following corn or soybean. *Soil Sci. Soc. Am. J.* 59, 1065–1070. doi:10.2136/sssaj1995.03615995005900040016x

Hanrahan, B. R., King, K. W., and Stinner, J. H. (2024). Nitrogen balances and losses in conservation cropping systems across a tile-drained landscape in Ohio, United States. *J. Soil Wat. Conserv.* 79 (3), 145–154. doi:10.2489/jswc.2024.00055

Heaton, E. A., Dohleman, F. G., and Long, S. P. (2008). Meeting US biofuel goals with less land: the potential of Miscanthus. *Glob. Chang. Biol.* 14, 2000–2014. doi:10.1111/j.1365-2486.2008.01662.x

Heaton, E. A., Schulte, L. A., Berti, M., Langeveld, H., Zegada-Lizarazu, W., Parrish, D., et al. (2013). Managing a second-generation crop portfolio through sustainable

intensification: examples from the USA and the EU. *Biofuels, Bioprod. Biorefining* 7 (6), 702–714. doi:10.1002/bbb.1429

Janovicek, K., Hooker, D., Weersink, A., Vyn, R., and Deen, B. (2021). Corn and soybean yields and returns are greater in rotations with wheat. *Agron. J.* 113, 1691–1711. doi:10.1002/agj2.20605

Kaspar, T. C., Jaynes, D. B., Parkin, T. B., Moorman, T. B., and Singer, J. W. (2012). Effectiveness of oat and rye cover crops in reducing nitrate losses in drainage water. *Agric. Water Manage.* 110, 25–33. doi:10.1016/j.agwat.2012.03.010

Kazula, M. J., and Lauer, J. G. (2018). The influence of crop rotation on corn total biomass production. *J. Soil Water Conserv.* 73 (5), 541–548. doi:10.2489/jswc.73.5.541

Kladivko, E. J., Akhouri, N. M., and Weesies, G. (1997). Earthworm populations and species distributions under no-till and conventional tillage in Indiana and Illinois. *Soil Biol. Biochem.* 29, 613–615. doi:10.1016/s0038-0717(96)00187-3

Kovacic, D. A., David, M. B., Gentry, L. E., Starks, K. M., and Cooke, R. A. (2000). Effectiveness of constructed wetlands in reducing nitrogen and phosphorus export from agricultural tile drainage. *J. Environ. Qual.* 29, 1262–1274. doi:10.2134/jeq2000.0047242500290004033x

Li, Z., Chu, M. L., Gentry, L., Li, Y., Mitchell, C., and Arai, Y. (2020). Passive detection of phosphorus in agricultural tile waters using reactive hybrid anion exchange resins. *Water* 12, 2808. doi:10.3390/w12102808

Licht, M. A., and Al-Kaisi, M. (2005). Strip-tillage effect on seedbed soil temperature and other soil physical properties. *Soil Tillage Res.* 80, 233–249. doi:10.1016/j.still.2004.03.017

McIsaac, G. F., David, M. B., and Mitchell, C. A. (2010). Miscanthus and switchgrass production in central Illinois: impacts on hydrology and inorganic nitrogen leaching. *J. Environ. Qual.* 39, 1790–1799. doi:10.2134/jeq2009.0497

McSwiney, C. P., Snapp, S. S., and Gentry, L. E. (2010). Use of N immobilization to tighten the N cycle in conventional agroecosystems. *Ecol. Appl.* 20, 648–662. doi:10.1890/09-0077.1

Mirsky, S. B., Curran, W. S., Mortensen, D. A., Ryan, M. R., and Shumway, D. L. (2011). Timing of cover crop management effects on weed suppression in no-till planted soybean using a roller crimper. *Weed Sci.* 59, 380–389. doi:10.1614/WS-D-10-00101.1

Mitchell, J. K., McIsaac, G. F., Walker, S. E., and Hirschi, M. C. (2000). Nitrate in river and subsurface drainage flows from an east central Illinois watershed. *Trans. ASAE* 43, 337–342. doi:10.13031/2013.2709

Nevins, C. J., Lacey, C., and Armstrong, S. (2020). The synchrony of cover crop decomposition, enzyme activity, and nitrogen availability in a corn agroecosystem in the Midwest United States. *Soil Tillage Res.* 197, 104518. doi:10.1016/j.still.2019.104518

Nichols, V., English, L., Carlson, S., Gailans, S., and Liebman, M. (2020a). Effects of long-term cover cropping on weed seedbanks. *Front. Agron.* 2, 591091. doi:10.3389/fagro.2020.591091

Nichols, V., Martinez-Feria, R., Weisberger, D., Carlson, S., Basso, B., and Basche, A. (2020b). Cover crops and weed suppression in the US Midwest: a meta-analysis and modeling study. *Agric. Environ. Lett.* 5 (1), e20022. doi:10.1002/ael2.20022

Peralta, A. L., Sun, Y., McDaniel, M. D., and Lennon, J. T. (2018). Crop rotational diversity increases disease suppressive capacity of soil microbiomes. *Ecosphere* 9, e02235. doi:10.1002/ecs2.2235

Pittelkow, C. M., Clover, M. W., Hoeft, R. G., Nafziger, E. D., Warren, J. J., Gonzini, L. C., et al. (2017). Tile drainage nitrate losses and corn yield response to fall and spring nitrogen management. *J. Environ. Qual.* 46, 1057–1064. doi:10.2134/jeq2017.03.0109

Plastina, A., Acharya, J., Marcos, F. M., Parvej, M. R., Licht, M. A., and Robertson, A. E. (2023). Does grazing winter cereal rye in Iowa, USA, make it profitable? *Renew. Agric. Food Syst.* 38, e45. doi:10.1017/S1742170523000388

Preza-Fontes, G., Pittelkow, C. M., Greer, K. D., Bhattarai, R., and Christianson, L. E. (2021). Split nitrogen application with cover cropping reduces subsurface nitrate losses while maintaining corn yields. *J. Environ. Qual.* 50 (6), 1408–1418. doi:10.1002/jeq2.20283

Qin, Z., Guan, K., Zhou, W., Peng, B., Villamil, M. B., Jin, Z., et al. (2021). Assessing the impacts of cover crops on maize and soybean yield in the U.S. Midwestern agroecosystems. *Field Crops Res.* 273, 108264. doi:10.1016/j.fcr.2021.108264

Randall, G. W., Huggins, D. R., Russelle, M. P., Fuchs, D. J., Nelson, W. W., and Anderson, J. L. (1997). Nitrate losses through subsurface tile drainage in conservation reserve program, alfalfa, and row crop systems. *J. Environ. Qual.* 26, 1240–1247. doi:10.2134/jeq1997.00472425002600050007x

Randall, G. W., and Vetsch, J. A. (2005). Nitrate losses in subsurface drainage from a corn–soybean rotation as affected by fall and spring application of nitrogen and nitrapyrin. *J. Environ. Qual.* 34, 590–597. doi:10.2134/jeq2005.0590

R Core Team (2022). *R: a language and environment for statistical computing*. Vienna: R Foundation for Statistical Computing. Available at: https://www.R-project.org/.

Reed, H. K., Karsten, H. D., Curran, W. S., Tooker, J. F., and Duiker, S. W. (2019). Planting green effects on corn and soybean production. *Agron. J.* 111, 2314–2325. doi:10.2134/agronj2018.11.0711

Rocha, L. F., Pimentel, M. F., Bailey, J., Wyciskalla, T., Davidson, D., Fakhoury, A. M., et al. (2021). Impact of wheat on soybean cyst nematode population density in double-cropping soybean production. *Front. Plant Sci.* 12, 640714. doi:10.3389/fpls.2021.640714

Roth, R. T., Ruffatti, M. D., O'Rourke, P. D., and Armstrong, S. D. (2018). A cost analysis approach to valuing cover crop environmental and nitrogen cycling benefits: a Central Illinois on farm case study. *Agric. Syst.* 159, 69–77. doi:10.1016/j.agsy.2017.10.007

Royer, T. V., David, M. B., and Gentry, L. E. (2006). Timing of riverine export of nitrate and phosphorus from agricultural watersheds in Illinois: implications for reducing nutrient loading to the Mississippi River. *Environ. Sci. Technol.* 40, 4126–4131. doi:10.1021/es052573n

Ruffatti, M. D., Roth, R. T., Lacey, C. G., and Armstrong, S. D. (2019). Impacts of nitrogen application timing and cover crop inclusion on subsurface drainage water quality. *Agric. Water Manage.* 211, 81–88. doi:10.1016/j.agwat.2018.09.016

Ruffo, M. L., Bullock, D. G., and Bollero, G. A. (2004). Soybean yield as affected by biomass and nitrogen uptake of cereal rye in winter cover crop rotations. *Agron. J.* 96, 800–805. doi:10.2134/agronj2004.0800

Sawyer, J., Nafziger, E., Randall, G., Bundy, L., Rehm, G., and Joern, B. (2006). *Concepts and rationale for regional nitrogen rate guidelines for corn. Publ. PM 2015*. Ames: Iowa State Univ.

Schnitkey, G., Zulauf, C., Swanson, K., Paulson, N., Baltz, J., and Coppess, J. (2022). *Projected wheat double-crop soybean profitability in 2023*. Champaign: Department of Agricultural and Consumer Economics, University of Illinois at Urbana-Champaign, 126. farmdoc daily (12).

Shrestha, R. K., Richer, E., Clevenger, W. B., Davis, M., and Lindsey, L. E. (2021). Effect of mono-relay-and double-crop systems on yield and profitability. *Agron. J.* 113, 1747–1757. doi:10.1002/agj2.20598

Silva, T. S., Mourtzinis, S., McMechan, A. J., Carmona, G. I., Potter, B. D., Tilmon, K. J., et al. (2024). Cereal rye cover crop termination at or before soybean planting has minimal effect on soybean yield across the midwestern US. *Field Crops Res.* 312, 109393. doi:10.1016/j.fcr.2024.109393

Singh, G., Davis, M., Nelson, K. A., and Kaur, G. (2024). Drainage water management, woodchip bioreactor, and saturated riparian buffer as stacked conservation practices for improving crop yields and water quality. *Environ. Technol. Innovation* 36, 103779. doi:10.1016/j.eti.2024.103779

Soil Survey Staff, Natural Resources Conservation Services, and USDA (2024). Web soil survey Available at: https://websoilsurvey.sc.egov.usda.gov.

Tilman, D., Balzer, C., Hill, J., and Befort, B. L. (2011). Global food demand and the sustainable intensification of agriculture. *Proc. Natl. Acad. Sci. U. S. A.* 108 (50), 20,260–20,264. doi:10.1073/pnas.1116437108

University of Illinois (2021). *Illinois Agronomy Handbook*. Dep. Crop Sci. Univ. Ill. A. T. Urbana–Champaign. Available at: http://extension.cropsci.illinois.edu/handbook/ (Accessed September 13, 2024).

USDA National Agricultural Statistics Service (2017). *NASS - quick stats*. USDA national agricultural Statistics Service. Available at: https://data.nal.usda.gov/dataset/nass-quick-stats.

USDA National Agricultural Statistics Service (2022). *NASS – Census of agriculture*. USDA national agricultural Statistics Service. Available at: https://www.nass.usda.gov/Publications/AgCensus/2022/#full_report.

Vonk, J., Nafziger, E. D., and Preza-Fontes, G. (2024). Soybean response to nitrogen fertilizer in different soils. *Crop Forage Turfgrass Mgmt* 10, e20304. doi:10.1002/cft2.20304

Waring, E. M., Lagzdins, A., Pederson, C., and Helmers, M. J. (2020). Influence of no-till and a winter rye cover crop on nitrate losses from tile-drained row-crop agriculture in Iowa. *J. Environ. Qual.* 49, 292–303. doi:10.1002/jeq2.20056

Welch, L. F., Mulvaney, D. L., Oldham, M. G., Boone, L. V., and Pendleton, J. W. (1971). Corn yields with fall, spring, and side-dress nitrogen. *Agron. J.* 63 (1), 119–123. doi:10.2134/agronj1971.00021962006300010037x

Yu, Z., Hu, Y., Gentry, L. E., Yang, W. H., Margenot, A. J., Guan, K., et al. (2024). Deciphering the isotopic imprint of nitrate to reveal nitrogen source and transport mechanisms in a tile-drained agroecosystem. *Water Resour. Res.* 129 (8), e2024JG008027. doi:10.1029/2024JG008027

frontiers | Frontiers in Environmental Science

TYPE Original Research
PUBLISHED 24 September 2024
DOI 10.3389/fenvs.2024.1445212

Check for updates

OPEN ACCESS

EDITED BY
Yefang Jiang,
Agriculture and Agri-Food Canada (AAFC), Canada

REVIEWED BY
Vicki Burgggraaf,
AgResearch Ltd., New Zealand
Serban Danielescu,
Environment and Climate Change Canada (ECCC), Canada

*CORRESPONDENCE
Scott L. Graham,
grahams@landcareresearch.co.nz

RECEIVED 06 June 2024
ACCEPTED 04 September 2024
PUBLISHED 24 September 2024

CITATION
Graham SL, Pronger J, Laubach J, Hunt JE, Rogers GND, Carrick S, Whitehead D, McLeod M, Mitchell G and Mudge P (2024) Assessing the potential of diverse pastures for reducing nitrogen leaching.
Front. Environ. Sci. 12:1445212.
doi: 10.3389/fenvs.2024.1445212

COPYRIGHT
© 2024 Graham, Pronger, Laubach, Hunt, Rogers, Carrick, Whitehead, McLeod, Mitchell and Mudge. This is an open-access article distributed under the terms of the Creative Commons Attribution License (CC BY). The use, distribution or reproduction in other forums is permitted, provided the original author(s) and the copyright owner(s) are credited and that the original publication in this journal is cited, in accordance with accepted academic practice. No use, distribution or reproduction is permitted which does not comply with these terms.

Assessing the potential of diverse pastures for reducing nitrogen leaching

Scott L. Graham[1]*, Jack Pronger[2], Johannes Laubach[1], John E. Hunt[1], Graeme N. D. Rogers[1], Sam Carrick[1], David Whitehead[1], Malcolm McLeod[2,3], Grace Mitchell[2] and Paul Mudge[2]

[1]Manaaki Whenua—Landcare Research, Lincoln, New Zealand, [2]Manaaki Whenua—Landcare Research, Hamilton, New Zealand, [3]Waikato Regional Council, Hamilton, New Zealand

Mitigation practices for nitrogen leaching losses from livestock agriculture are needed to protect freshwater quality and increase the efficiency of agricultural production. Within New Zealand, the most common pasture type is a two-species mix of perennial ryegrass (*Lolium perenne*) and white clover (*Trifolium repens*). Ecological theory suggests that increasing species and functional diversity improves ecosystem function, including nitrogen (N) retention. Use of more diverse pasture types, including a mix of pasture grasses, legumes and other forbs, particularly plantain (*Plantago lanceolata*), with functional traits, including winter activity, deep-rooting, N fixation, and biological inhibition of nitrification in the soil, is a potential mitigation practice that requires further verification with long-term field measurements. Here we utilize a network of large lysimeters to make field-based measurements of N leaching from 5–8 species diverse pasture, including plantain, under a range of soil, climate and management conditions, for comparison with losses from traditional ryegrass-clover pasture. Over 3 years of measurements, leaching from fully established diverse pasture was 2–80 kg N ha^{-1} y^{-1}. No differences were observed in dry matter production or N leaching of diverse pasture compared to ryegrass-clover lysimeters. Large losses, up to 120 kg N ha^{-1}, were observed during periods when pasture was not fully established, including cultivation and sowing of new pasture, depending on season. Timing of management activities could be optimized to minimize these losses. These data provide critical assessment of diverse pasture as a mitigation approach for reducing N losses. Further work on diverse pastures should include higher diversity mixes as well as consideration of animal mediated effects of diverse pasture diets on N inputs.

KEYWORDS

nitrogen leaching, soil hydrology, mitigation, grassland, grazing, plant diversity, *Plantago lanceolata*

1 Introduction

Leaching of nitrogen (N) from livestock agriculture negatively affects surface and groundwater quality, contributing to both ecological and human health consequences. Management practices to mitigate leaching losses are needed to minimize the environmental impact of livestock grazing, as well as increase the efficiency of

agricultural practices, as nutrients lost to leaching could otherwise support production. Increasing species diversity of pastures is a management practice with the potential to reduce N losses. However, there is an insufficient number of long-term field studies of leaching losses from more diverse pastures to verify a mitigation effect.

There is a positive relationship between plant species diversity, productivity, and N retention of grassland ecosystems established in the ecological literature (Tilman et al., 1996; Hector et al., 1999; Hooper et al., 2005). Such effects arise from complementarity amongst functional traits affecting resource acquisition. Multispecies mixes, compared to monocultures, lose less N to leaching, although there can be complex changes in the processes contributing to N loss (Dijkstra et al., 2007). In addition to reducing N leaching, other benefits of increasing diversity include enhanced soil carbon stocks (Lange et al., 2015), increased soil water infiltration (Fischer et al., 2015), and increased resistance to drought (Isbell et al., 2015). The diversity-ecosystem function concepts from the ecological literature can be applied to grazing landscapes, where increasing diversity of pastures has the potential to increase productivity and environmental sustainability of grazing land (Sanderson et al., 2004; Vibart et al., 2016).

Pastures in New Zealand are most often a two species mix of perennial ryegrass (*Lolium perenne*) and white clover (*Trifolium repens*), henceforth "ryegrass-clover." However, there is increasing adoption of more diverse pastures with four or more species, including a mixture of grasses, legumes, and forbs, henceforth "diverse pasture." The species mixtures of diverse pasture are generally selected to possess beneficial functional traits, such as greater cool-season activity to increase N uptake during winter drainage seasons (Malcolm et al., 2014), deep-rooting species that contribute to higher belowground biomass (McNally et al., 2015) and greater legume content to enhance N fixation, decreasing reliance on chemical fertilizers (Peoples et al., 2009). Species such as plantain (*Plantago lanceolata*) are known to affect N transformations in the soil, so-called biological nitrification inhibitors, reducing both N leaching and nitrous oxide (N_2O) emissions (Di et al., 2016; Gardiner et al., 2018; Podolyan et al., 2020). Animal mediated effects have been documented, including changes in amounts and concentrations of N in excreta of livestock fed on diverse pasture and plantain diets (Vibart et al., 2016; Pinxterhuis et al., 2024). Such changes to amounts and concentrations of N inputs have implications for N leaching losses.

Malcolm et al. (2014) made direct measurements of N leaching from lysimeters with mixes of up to four species. Following application of a simulated urine patch, leaching from 4-species diverse pasture was not different from perennial ryegrass-clover lysimeters. However, lysimeters containing winter-active Italian ryegrass (*Lolium multiflorum*) leached 24%–54% less than perennial ryegrass-clover due to higher dry matter production and N uptake, demonstrating the importance of seasonal activity for reducing N losses. While this single study did not find a mitigation effect of diverse pasture, further field measurements across different soil types and management intensities are needed to identify the mitigation potential of diverse pastures for reducing N losses.

The objective of this study was to provide field-scale measurements of N leaching losses from diverse pasture on contrasting soil types and for a range of management intensities, from low-input, non-irrigated sites to high-intensity effluent irrigated sites, for comparison with N losses from ryegrass-clover pasture. We employed a network of large lysimeters to make direct measurements of leaching losses from diverse and ryegrass-clover pastures. These measurements provide critical assessment of diverse pastures as a mitigation approach, reducing N losses from livestock agriculture. Our dataset will likewise contribute to process-based modelling of N leaching in these systems and inform decision support tools for farmers, regulators, and land managers.

2 Methods

2.1 Lysimeter sites

2.1.1 Ashley Dene Research and Development Station

The Lincoln University Ashley Dene Research and Development Station (ADRDS) is a 190-ha commercial dairy farm in Canterbury, South Island, New Zealand (43°38′56.2″S, 172°21′04.1″E, 32 m a.s.l., Supplementary Figure S1). The mean annual air temperature is 12°C, with maximum and minimum temperatures of 34° and −4°C respectively. The site receives c. 780 mm y^{-1} of precipitation. Much of the farm receives 200–400 mm y^{-1} irrigation during the growing season (October – April). Dairy effluent (henceforth "effluent"), collected from the milking shed into storage ponds, is applied by irrigator to a portion of the pasture area. The ADRDS is on flat land and the soil is derived from glacial alluvium. Stony silt loam topsoil overlies sandy subsoil, with stone contents of up to 70%. The soil classification is Typic Orthic Brown Soil (Hewitt, 2010).

Lysimeters were installed at three sites across ADRDS: one receiving irrigation and effluent from a central pivot irrigator (EI), one receiving irrigation with water only from a linear irrigator (OI) and one non-irrigated site (NI). All measurement sites are within 500–700 m of each other. Six large lysimeters, 2 m diameter and 1.5 m depth, were constructed *in situ* from an undisturbed column of soil at the EI and NI site in 2016. Following 4 years of measurements of drainage and leaching from lucerne (*Medicago sativa*), these lysimeters were sprayed off with glyphosate, the soil inside the lysimeters was cultivated to 250 mm depth, and re-sown with 5–8 species diverse pasture, including plantain (Table 1). A subset at EI were converted in a similar fashion to ryegrass-clover pasture for comparison. Three other lysimeters, 2 m diameter and 1.2 m depth, had been constructed at OI in 2014. Following a crop cycle in maize, these lysimeters were likewise sprayed off and converted to diverse pasture. The pasture species mixes and sowing rates were selected based on commonly used mixes and advice from commercial seed suppliers. EI was converted in autumn (April) 2020, while OI and NI were converted in spring (October) 2020. Further details of the ADRDS lysimeter sites and construction can be found in Carrick et al. (2017), Graham et al. (2019) and Graham et al. (2022).

TABLE 1 Species mixes planted in diverse and ryegrass-clover pasture lysimeters at the Ashley Dene Research and Development Station effluent irrigated (EI) site, irrigated only (OI) site, non-irrigated site, and the Tihoi non-irrigated (TN) site.

Site	Pasture type	No. of lysimeters	Species mix	Sowing rate (kg ha^{-1})
EI	Diverse	3	Perennial ryegrass (*Lolium perenne*)	12
OI	Diverse	3	Italian ryegrass (*Lolium multiflorum*)	6
			Plantain (*Plantago lanceolata*)	4
			Red clover (*Trifolium pratense*)	3
			White clover (*Trifolium repens*)	2
NI	Diverse	6	Tall fescue (*Festuca arundinacea*)	15
			Perennial ryegrass (*Lolium perenne*)	4
			Lucerne (*Medicago sativa*)	4
			Plantain (*Plantago lanceolata*)	4
			Cocksfoot (*Dactylis glomerata*)	3
			Subterranean clover (*Trifolium subterraneum*)	2
			White clover (*Trifolium repens*)	2
			Phalaris (*Phalaris aquatica*)	1
TN	Diverse	12	Perennial ryegrass (*Lolium perenne*)	16
			Italian ryegrass (*Lolium multiflorum*)	2
			Cocksfoot (*Dactylis glomerata*)	2
			Plantain (*Plantago lanceolata*)	4
			Red clover (*Trifolium pratense*)	4
			White clover (*Trifolium repens*)	2
EI	Ryegrass-clover	3	Perennial ryegrass (*Lolium perenne*)	21
TN	Ryegrass-clover	8	White clover (*Trifolium repens*)	4

2.1.2 Tihoi

The Tihoi lysimeter site (TN) is on a commercially operated sheep and beef farm in the hill country of Waikato, North Island, New Zealand (38°39′51.1″S, 175°44′43.8″E, 564 m a.s.l., Supplementary Figure S1). The mean annual air temperature is 11°C, with maximum and minimum temperatures of 30° and −5°C. The site receives c. 1,400 mm y^{-1} of precipitation distributed through the year, although summer droughts do occur. The soil is a deep, relatively stone-free volcanic pumice classified as Typic Orthic Pumice Soil (Hewitt, 2010).

In 2016, twenty non-irrigated lysimeters, 0.9 m diameter and 1.5 m depth, were constructed from undisturbed soil and arranged around a central drainage collection caisson. Following 5 years of measurement of drainage and leaching from lucerne and ryegrass-clover, in spring (October) 2020, the lysimeters were sprayed off with glyphosate, cultivated to 150 mm and re-sown with 6 species diverse pasture (12 lysimeters) and ryegrass-clover pasture (8 lysimeters) (Table 1), evenly distributed across the previous lucerne and ryegrass-clover histories. Further details of lysimeter construction can be found in McLeod (2020).

2.2 Drainage volume and leachate collection

At EI, OI and NI, drainage volume from the lysimeters was measured by tipping bucket gauges (0.03 mm drainage resolution), logged continuously by a datalogger. A subsample of leachate was accumulated continuously and was periodically collected for analysis of total N, NO_3^- (including NO_2^-) and ammoniacal N (NH_3 and NH_4^+) concentrations by an accredited commercial laboratory following each large drainage event. At TN, lysimeter drainage was into 80 L reservoirs and the drainage volumes since the previous sampling event were manually recorded and a subsample was collected for analysis. Sampling occurred approximately every 20–60 mm of drainage.

2.3 Dry matter harvest

Dry matter production on the lysimeters was measured 5–7 times per year, simulating a grazing cycle appropriate to pasture growth for each site. At EI, OI, and NI, biomass was clipped to a simulated grazing height of 50 mm within a 0.25 m^2 quadrat. Subsequently biomass was cut and removed on the remainder of the lysimeter. At TN, biomass was sampled from the entire lysimeter area. The samples were dried at 60°C for 48 h and weighed for dry mass. Seasonally, the clipped biomass was sorted into grasses, legumes, plantain, and other forbs. A subset of the samples was ground and analyzed for analysis of N content of dry matter.

2.4 N inputs

Additions of excreta from grazing animals were simulated in a manner appropriate to each management system at EI, OI and NI.

Approximately every second dry matter harvest event, once establishment of pasture was complete, fresh dung (1.1–2.5 kg) was added to the lysimeter in a 300 mm diameter circular patch and synthetic urine (1.1–2.5 L) with a N content of 6 g N L^{-1} (Clough et al., 1998) was applied to a separate location in a 300 mm diameter circular patch. Amounts and timing were varied to reflect dry matter production and assumed supplemental feed according to the intensity of each management system (Graham et al., 2022). No assumptions were made on the effect of a diet of the different pasture types on N inputs and ryegrass-clover and diverse pasture lysimeters at a given site received the same inputs of dung and urine.

Due to the smaller area of the TN lysimeters, inputs from excreta were simulated though a single application of 2.1 L synthetic urine (McLeod, 2020) each year. Dung was not applied to the TN lysimeters, as it is long-lasting on the soil surface and repeated application would negatively affect dry matter production. Applications of urine occurred in late-summer or autumn each year.

2.5 N uptake and surplus calculations

N uptake by plants (N_U) as a component of the lysimeter N balance was calculated from Equation 1:

$$N_U = p_G M_H c_G + p_L M_H c_L + p_P M_H c_P + p_O M_H c_O \quad (1)$$

where M_H is the harvested dry matter from each lysimeter, p_G, p_L, p_P, and p_O are the proportions of harvested dry matter represented by grass, legumes, plantain and other forbs, respectively, and c_G, c_L, c_P, and c_O are the N concentration of grass, legumes, plantain and other forbs. Since a portion of N in legumes comes from fixation of atmospheric N (N_F), and not uptake from the soil, this amount was estimated from Equation 2:

$$N_F = p_L M_H c_L f_F \quad (2)$$

where f_F is the fraction of N coming from fixation. For the effluent irrigated site, f_F was estimated as 0.55, based on previous measurements of lucerne under this management (Graham et al., 2022). For the lower intensity sites, f_F was estimated as 0.80, based on measurements from low-input, non-irrigated lucerne.

As a metric of the balance of N inputs and uptake and removal by harvest, surplus N (N_S) was calculated by Equation 3:

$$N_S = N_I + N_F - N_U \quad (3)$$

where N_I is the total input of N from fertilizer, effluent and animal excreta.

2.6 Statistical analysis

The statistical significance of differences in the annual total of soil drainage, N leaching and dry matter production between ryegrass-clover and diverse pasture was tested at the EI and TN sites with a Welch's t-test. This was applied separately for each full year of measurement: Year 1 (October 2020-September 2021), Year 2 (October 2021-September 2022) and Year 3 (October 2022-September 2023). The test was also applied to the cumulative totals for 3 years of measurement.

To determine the drivers of annual N leaching, a linear regression approach was used. A maximal model of annual N leaching loss was constructed, including total annual water input (precipitation and irrigation), drainage volume, grass fraction, plantain fraction, clover fraction, nitrogen surplus and pasture type were included as explanatory factors. Interactions between drainage and N surplus and water input and N surplus were also investigated. This model was then minimized by dropping factors in a stepwise fashion to minimize Akaike's Information Criterion. Analyses were conducted in R v4.2.1 (R Core Team, 2022). Since there was potential for non-linearity in the responses of N leaching to the explanatory variables, as well as correlations amongst the explanatory variables, an alternative Random Forest modelling approach was conducted using the "randomForest" package in R (Liaw and Wiener, 2002). Additional, and likely correlated, explanatory variables (including dry matter harvest, N input, N uptake) were included in this approach. The importance of each explanatory variable in the Random Forest analysis was estimated based on the percentage change in mean square error associated with each variable. Both modelling approaches were assessed based on a test subset made up of 30% of the original dataset, held out during model fitting.

3 Results

3.1 Drainage and N leaching

The EI lysimeters were the first to be converted from lucerne to diverse or ryegrass–clover pasture in autumn 2020. N losses in the first 6 months following conversion exceeded 120 kg N/ha, higher than the annual loss recorded for any of the sites and measurement years (Figure 1). This high loss could be attributable to low N uptake by the pasture early in establishment, coinciding with high drainage volumes with the onset of winter rain. Sources of N driving this loss are likely to involve mineralization of soil organic matter and dead lucerne biomass, in combination with residual N from animal excreta inputs preceding conversion, and the continued input of 25 kg N ha^{-1} as effluent while the soil was actively draining.

By the start of Year 1 (October 2020), the pasture was well established at EI. Leaching losses for ryegrass–clover and diverse pasture lysimeters were similar at 27 and 28 kg N ha^{-1} y^{-1}, respectively (Figure 1; Table 2). In Year 2, a wet winter led to cumulative N leaching from ryegrass-clover of 80 kg N ha^{-1} y^{-1}, 2.8 times greater than diverse pasture ($p < 0.05$). However, lysimeter measurements were interrupted between late-July to November 2022 due to unusually high groundwater levels and inundation of lysimeter instrumentation, introducing some uncertainty into the annual total. The losses during this period were likely low, as few drainage events were recorded at the OI site, which remained operational. In Year 3, N losses from diverse pasture were not statistically different from ryegrass-clover. Once again, the measurements were interrupted by high groundwater levels

10.3389/fenvs.2024.1445212

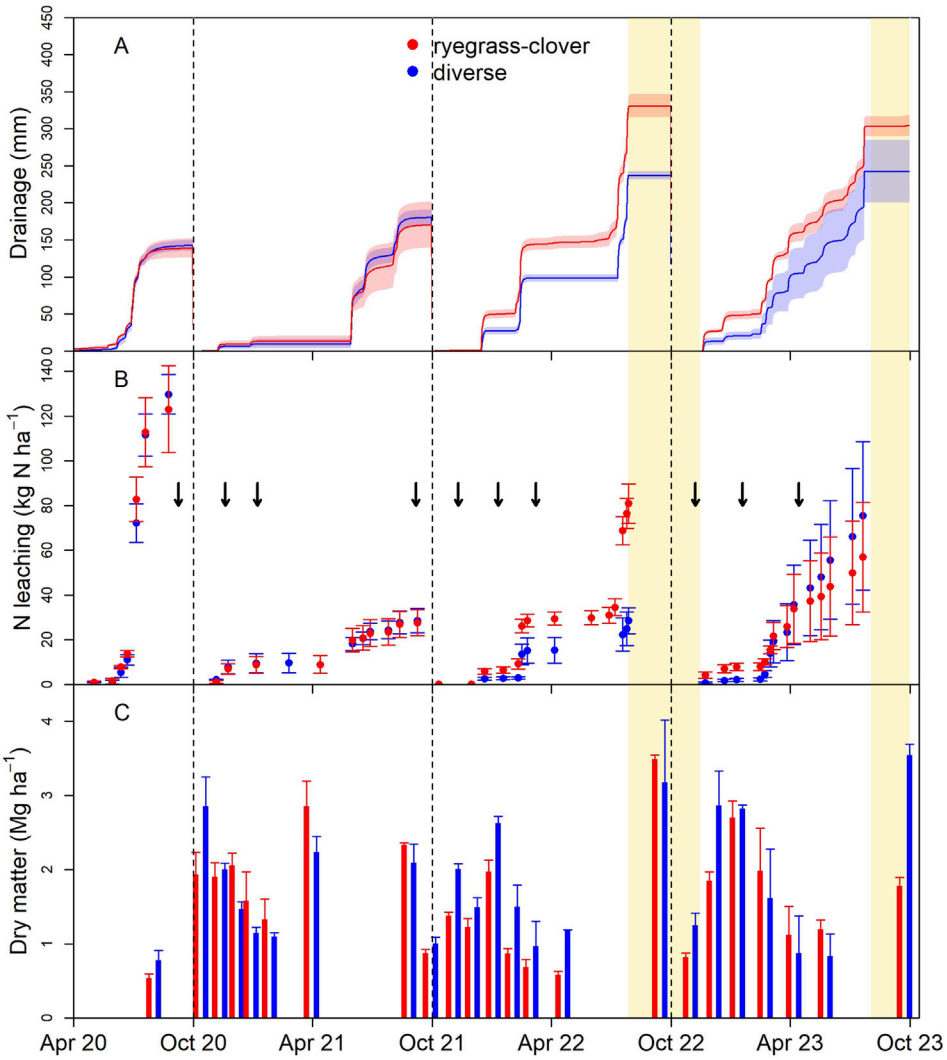


FIGURE 1
Lysimeter drainage volume (±SEM) **(A)**, cumulative leached nitrogen **(B)**, and dry matter harvest mass **(C)** following conversion to diverse (blue) or ryegrass–clover (red) pasture in April 2020 and for three subsequent leaching years (October to September) at a site on the Ashley Dene Research and Development Station irrigated with water and effluent (EI); arrows indicate the timing of additions of dung and urine to the lysimeters and the gold-shaded regions indicate periods of lysimeter inoperability due to high groundwater levels.

between August and September 2023 introducing uncertainty into the annual sum.

At OI, the lysimeters leached 26 kg N ha^{-1} y^{-1} in Year 1. The largest losses were in the period immediately following conversion in October 2020 (Figure 2; Table 2). Excess irrigation during this period contributed to drainage during the period when pasture establishment was incomplete and N uptake was low. In Year 2 and Year 3, when pasture was fully established, the losses were lower than Year 1 and the EI site, at 3 and 11 kg N ha^{-1} y^{-1}, respectively. This reflects the lower N input relative to EI.

At NI, N leaching was 71 kg N ha^{-1} y^{-1} in Year 1, larger than those of any of the other sites in Year 1, despite lower N inputs (Figure 3; Table 2). This was likely due to low pasture production and N uptake resulting from poor germination and establishment. In Year 2, the site was re-sown, but losses were 40 kg N ha^{-1} y^{-1}, corresponding with continued low dry matter production. By Year 3, when pasture establishment was complete, the losses were low, 5 kg N ha^{-1} y^{-1}. Drainage volumes at NI were similar to EI and OI, reflecting the predominant winter drainage season. However, both EI and OI had growing season drainage events that were not observed at NI (Figures 1–3). These drainage events were the direct effect of irrigation and could have been prevented through improved irrigation management.

At TN, N leaching losses in Year 1 from diverse pasture lysimeters were not significantly different from ryegrass-clover lysimeters and were small relative to the ADRDS sites (Figure 4; Table 2). There was a trend for enhanced losses from ryegrass-clover pasture throughout the summer of Year 2, despite similar drainage volumes. However, following a second addition of synthetic urine patch in May 2022, and a wet winter, which lead to high drainage volumes, cumulative N losses from ryegrass-clover and diverse pasture were similar by the end of Year 2, 92 and 98 kg N ha^{-1} y^{-1}, respectively. Throughout Year 3, drainage volumes and N losses continued to be similar for both ryegrass-

TABLE 2 Annual totals (±SE) for site variables, nitrogen inputs, and nitrogen losses for diverse and ryegrass–clover pasture lysimeters at effluent irrigated (IE), irrigated only (OI) and non-irrigated sites (NI) at the Ashley Dene Research and Development Station and the Tihoi non-irrigated (TN) site for Year 1 (October 2020 – September 2021), Year 2 (October 2021 – September 2022) and Year 3 (October 2022 – September 2023) since conversion to pasture; values affected by periods of lysimeter inoperability are indicated with an asterisk.

Variable		IE		OI	NI	TN	
		Ryegrass-clover	Diverse	Diverse	Diverse	Ryegrass-clover	Diverse
Year 1	Precipitation (mm)	603	603	603	603	1,285	1,285
	Irrigation (mm)	326	326	107	-	-	-
	Drainage (mm)	170 ± 30	180 ± 10	345 ± 21	182 ± 8	595 ± 50	608 ± 16
	Dry matter harvest (Mg ha^{-1})	13.7 ± 0.2	12.6 ± 0.7	3.5 ± 0.2	0.9 ± 0.1	7.6 ± 0.4	8.9 ± 0.4
	Nitrogen inputs (kg N ha^{-1})						
	Effluent	110	110	-	-	-	-
	Fertilizer	110	110	23	23	22	22
	Dung	41	41	9.5	-	-	-
	Urine	89	89	21	-	207	207
	N leaching (kg N ha^{-1})	**27.5 ± 5.8**	**28.6 ± 5.4**	**26.3 ± 4.9**	**71.1 ± 6.0**	**8.1 ± 2.8**	**2.3 ± 0.4**
Year 2	Precipitation (mm)	843	843	843	843	1,572	1,572
	Irrigation (mm)	220	220	71	-	-	-
	Drainage (mm)	331 ± 15*	237 ± 5*	330 ± 36	312 ± 9*	1,014 ± 79	1,062 ± 20
	Dry matter harvest (Mg ha^{-1})	10.7 ± 0.2	13.6 ± 0.8	9.5 ± 0.6	2.5 ± 0.2	7.9 ± 0.4	9.0 ± 0.4
	Nitrogen inputs (kg N ha^{-1})						
	Effluent	151*	151*	-	-	-	-
	Fertilizer	140	140	25	25	-	-
	Dung	45	45	29	-	-	-
	Urine	97	97	63	-	207	207
	N leaching (kg N ha^{-1})	**80.8 ± 8.9***	**28.4 ± 5.7***	**3.1 ± 0.4**	**40.7 ± 3.0***	**92.9 ± 12.1**	**98.1 ± 10.5**
Year 3	Precipitation (mm)	805	805	805	805	1,630	1,630
	Irrigation (mm)	448	448	148	-	-	-
	Drainage (mm)	304 ± 14*	242 ± 42*	224 ± 24	202 ± 6*	1,139 ± 59	1,166 ± 41
	Dry matter harvest (Mg ha^{-1})	11.1 ± 1.2	13.5 ± 1.7	11.6 ± 0.9	5.9 ± 0.6	14.3 ± 0.7	15.1 ± 0.5
	Nitrogen inputs (kg N ha^{-1})						
	Effluent	84*	84*	-	-	-	-
	Fertilizer	209	209	25	25	-	-
	Dung	67	67	59	34	-	-
	Urine	144	144	125	71	207	207
	N leaching (kg N ha^{-1})	**56.9 ± 24.4***	**75.3 ± 33.1***	**10.5 ± 5.5**	**4.9 ± 0.7***	**32.3 ± 5.4**	**9.6 ± 13.8**

clover and diverse pasture. The third urine patch was added to the lysimeters in March 2023. Year 3 leaching losses from diverse pasture were 51 kg N ha^{-1} y^{-1} compared to 32 kg N ha^{-1} y^{-1} from ryegrass-cover. However, again this difference was not significant.

Due to the treatment of the entire lysimeter as a urine patch at TN, the losses from the lysimeters are not representative of the whole field. A single grazing event leads to 1%–3% of the area receiving urine patches (Haynes and Williams, 1993; Moir et al., 2011). On an annual basis, the assumption is that 25% of the area receives urine patches (Cameron et al., 2013). Lysimeter measurements can be scaled up to the entire field using this assumption, and the finding that losses from pasture not receiving urine are generally low, ~2 kg N ha^{-1} y^{-1} (McLeod, 2020). Thus, the field-scale losses at TN were 2–26 kg N ha^{-1} y^{-1} across the measurement years.

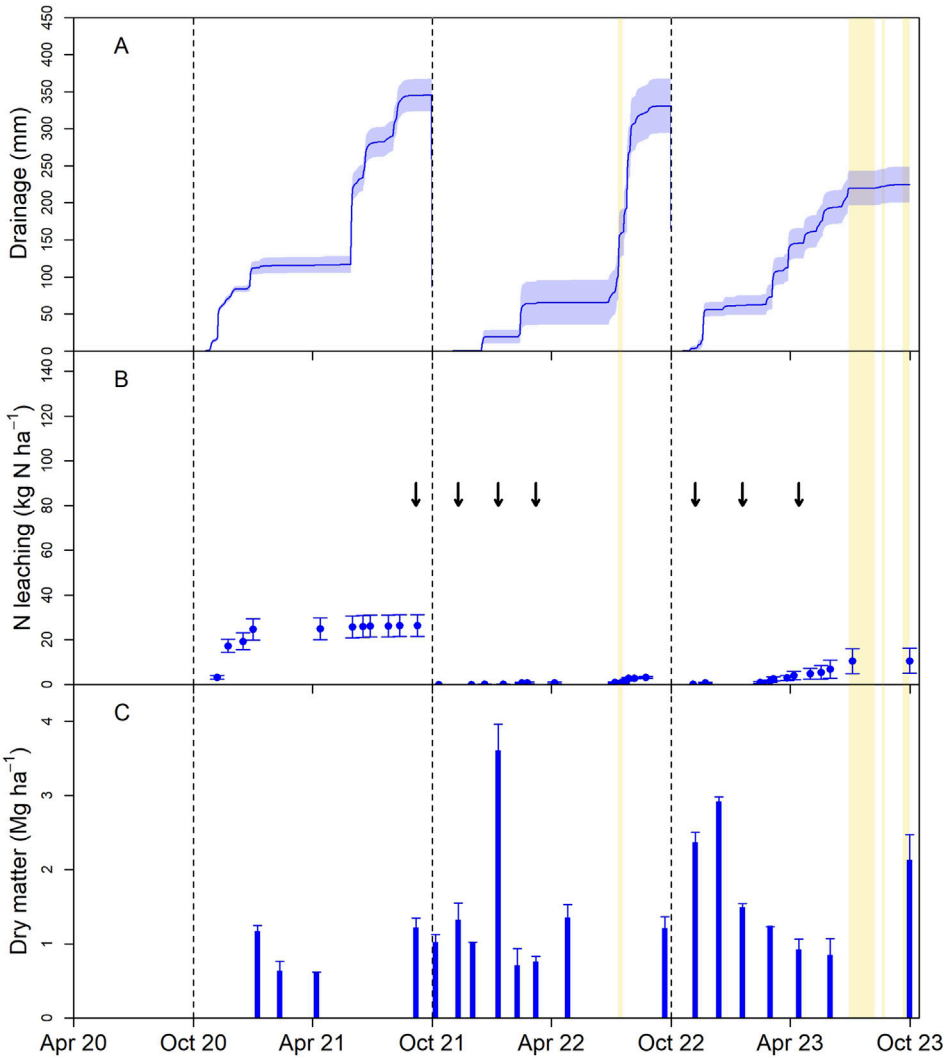


FIGURE 2
Cumulative drainage volume (±SEM) **(A)**, cumulative leached nitrogen **(B)**, and dry matter harvest mass **(C)** for diverse pasture in an area of the Ashley Dene Research and Development Station irrigated with water-only (OI) for 3 years following conversion to diverse pasture in October 2020; arrows indicate the timing of additions of dung and urine to the lysimeters, and gold-shaded regions indicate periods of lysimeter inoperability due to high groundwater levels.

3.2 Dry matter production and N uptake

At EI, pasture dry matter production during Year 1 was similar for ryegrass–clover and diverse pasture types under effluent irrigation, at 13.7 and 12.6 Mg dry matter ha^{-1} y^{-1} (Figure 1; Table 2). In Year 2, production by diverse pasture was 27% greater than that of ryegrass-clover. In Year 3, biomass production by diverse pasture lysimeters was again statistically similar to ryegrass-clover, at 13.5 and 11.1 Mg ha^{-1} y^{-1}, respectively. Cumulative production for the entire 3-year measurement period was also similar for the two pasture types. As with dry matter production, N uptake only differed by pasture type in Year 2, when N uptake by diverse pasture was 15% greater than ryegrass-clover. The additional 41 kg N ha^{-1} y^{-1} uptake explains the lower leaching losses in Year 2 at EI.

The increase in biomass production by diverse pasture relative to ryegrass–clover in Year 2 at EI also corresponded with a change in the functional group representation. In Year 1 the biomass of diverse pasture was 79% grass (Figure 5). In Year 2, the plantain and clover proportions increased to 32% and 21%, respectively, with the grass proportion decreasing to 44%. However, in Year 3, the plantain content was reduced to 5% while clover content increased to 27%.

Despite lower N inputs, dry matter production at OI was 70%–85% of that at EI in Year 2 and Year 3, at 9.5 and 11.6 Mg ha^{-1} y^{-1} (Figure 2; Table 2). The OI lysimeters also had the highest plantain content amongst the ADRDS sites, with 43% plantain, 38% clover and 17% grass in Year 2 (Figure 5).

Dry matter production at NI was low in Year 1 due to the failed pasture establishment (Figure 3; Table 2). In Year 2 the site was re-sown, but production remained only 18%–27% of that at other sites. Production increased in Year 3 and harvested dry matter was 5.9 Mg ha^{-1} y^{-1}, 44% of that by diverse pasture at EI.

Dry matter production of the diverse pasture lysimeters at TN was not statistically different from the ryegrass-clover lysimeters

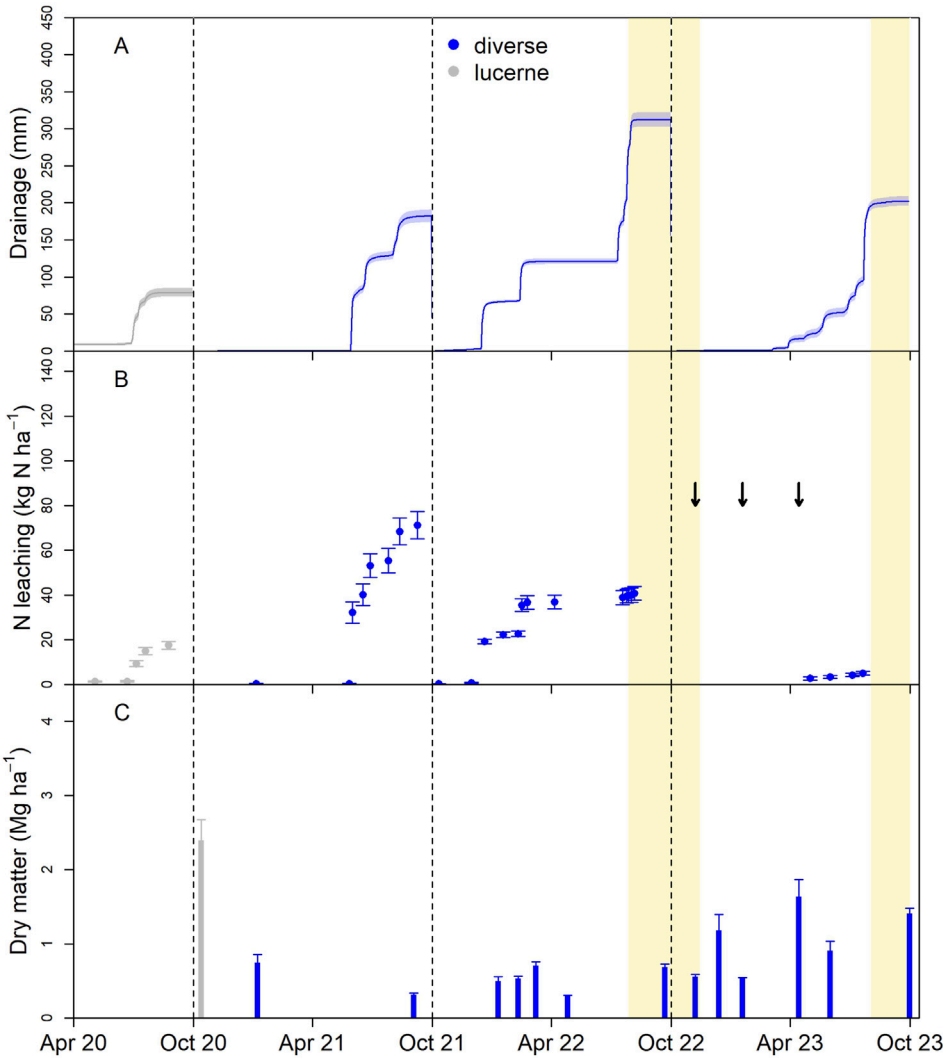


FIGURE 3
Lysimeter drainage volume (±SEM) **(A)**, cumulative leached nitrogen **(B)**, and dry matter harvest mass **(C)** following conversion to diverse pasture in a non-irrigated (NI) area of the Ashley Dene Research and Development Station; arrows indicate the timing of additions of dung and urine to the lysimeters, and the gold-shaded regions indicate periods of lysimeter inoperability due to high groundwater levels.

(Figure 4; Table 2). Likewise, there were no significant differences in N uptake. Annual dry matter production at TN was responsive to seasonal water availability, as biomass production was 67%–80% greater in Year 3 compared to Year 2, due to high summer rainfall which contributed to year-round soil drainage, in contrast to the relatively dry summer in Year 2. Uptake of N associated with the high dry matter production also explains the lower leaching losses in Year 3 relative to Year 2, despite similar drainage volumes and N input. Plantain was the primary contributor to harvest biomass in Year 1, representing 55% of dry matter (Figure 5). This dropped to 8% in Year 3, with a commensurate increase in grass fraction.

Nitrogen content of the different functional groups varied, particularly for legumes. However, there was no difference in the N content of bulk, unsorted dry matter harvested from different pasture types at either EI or TN. The N contents of dry matter were 25.5 g N kg^{-1} for grass, 39.8 g N kg^{-1} for clovers, 22.5 g N kg^{-1} for plantain and 29.9 g N kg^{-1} for other forbs.

3.3 Drivers of annual N leaching

The minimized linear model of annual N leaching included pasture type, water input, drainage volume, grass fraction, plantain fraction, N surplus and an interaction between N surplus and water input. This model explained 51% of variability in lysimeter N leaching in the test dataset across the sites, years of measurement, and pasture types. Although pasture type was included in the minimal model, an analysis of variance associated with the different factors revealed that only site, N surplus, drainage volume, plantain fraction and the interaction between drainage and N surplus were significant ($p < 0.05$) (Supplementary Figure S2; Table 1).

The Random Forest approach explained 71% of the variability in the test dataset. Analysis of the importance of each explanatory variable, as estimated from percentage increase in mean square error, confirmed the importance of drainage volume and water input, followed by N input and surplus. Plantain fraction and other

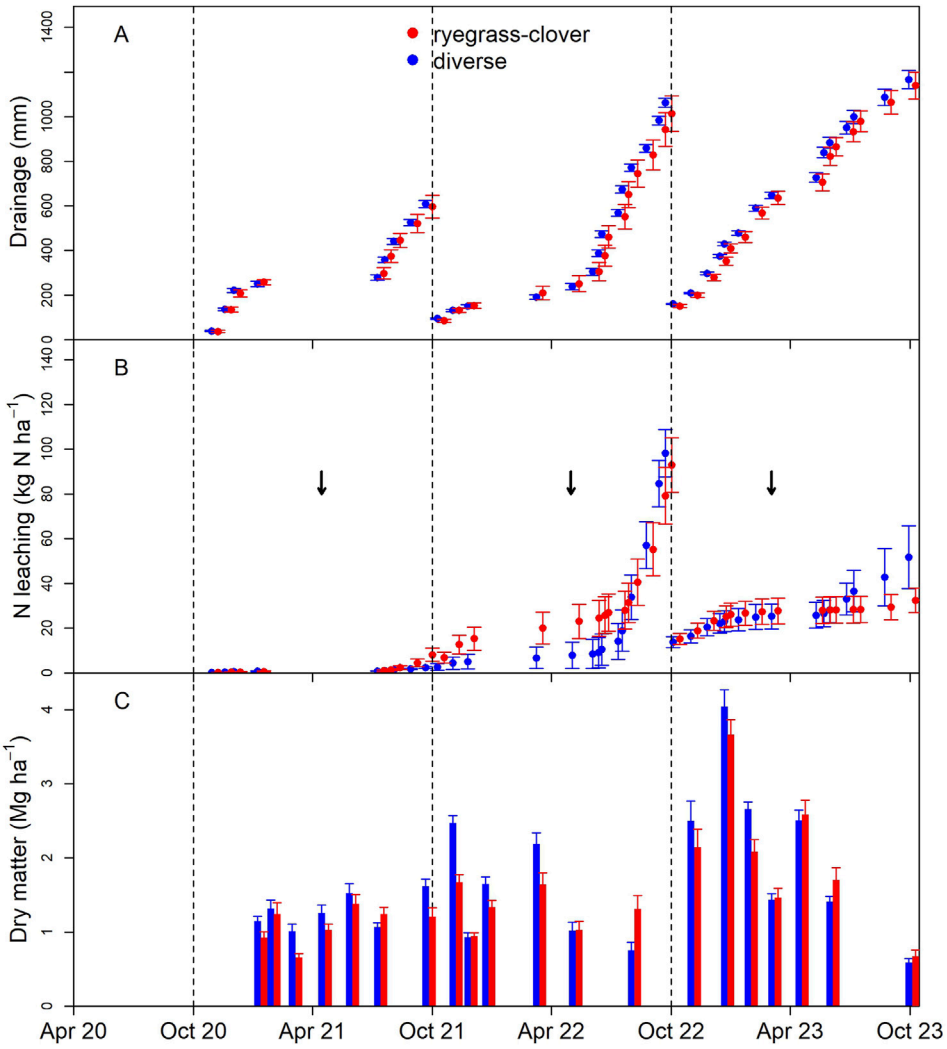


FIGURE 4
Cumulative drainage volume (±SEM) **(A)**, cumulative leached nitrogen **(B)**, and dry matter harvest mass **(C)** from lysimeters planted with diverse and ryegrass–clover pasture during Year 1 (October 2020 – September 2021), Year 2 (October 2021 – September 2022) and Year 3 (October 2022 – September 2023) since conversion from lucerne at the Tihoi non-irrigated site (TN); arrows indicate the timing of additions of synthetic urine to the lysimeters.

vegetation-related variables followed with pasture type occupying the lowest level of importance (Supplementary Figures S3, S4).

4 Discussion

Across the measurement sites, which represented contrasting soils, climatic conditions and a range of management intensities, field-scale N leaching losses from established diverse pasture were 2–80 kg N ha^{-1} y^{-1}, well within the range of values previously measured for grazed pastures (Cameron et al., 2013). Although there were isolated instances in which significant effects of pasture type were observed (e.g., Year 2 at EI), these effects were inconsistent, and none contributed to a change in cumulative leaching loss over the three measurement years. This is similar to a previous study in New Zealand that found no difference between ryegrass-clover and diverse pasture lysimeter leaching (Malcolm et al., 2014). Neither drainage volume nor pasture production differed consistently for diverse and ryegrass-clover lysimeters, contributing to the absence of an effect of pasture type on N leaching.

The result that leaching losses from diverse pasture were not different from ryegrass-clover would appear to be at odds with the ecological literature, which suggests that production and nutrient retention are increased with increasing diversity in grasslands (Tilman et al., 1996; Dijkstra et al., 2007). However, some studies suggest that it is the presence of specific functional groups, and not diversity, that effects productivity and N losses (Hooper and Vitousek, 1998). In the current study, we investigated minimally diverse mixes of 5–8 species, where in some cases only one species filled a functional role. The proportional representation of different functional groups (grass, clover, plantain, other forbs) was also variable through time and, by the end of the study tended to be similar for the different pasture types. Thus, our results may not represent the full potential of increased pasture diversity.

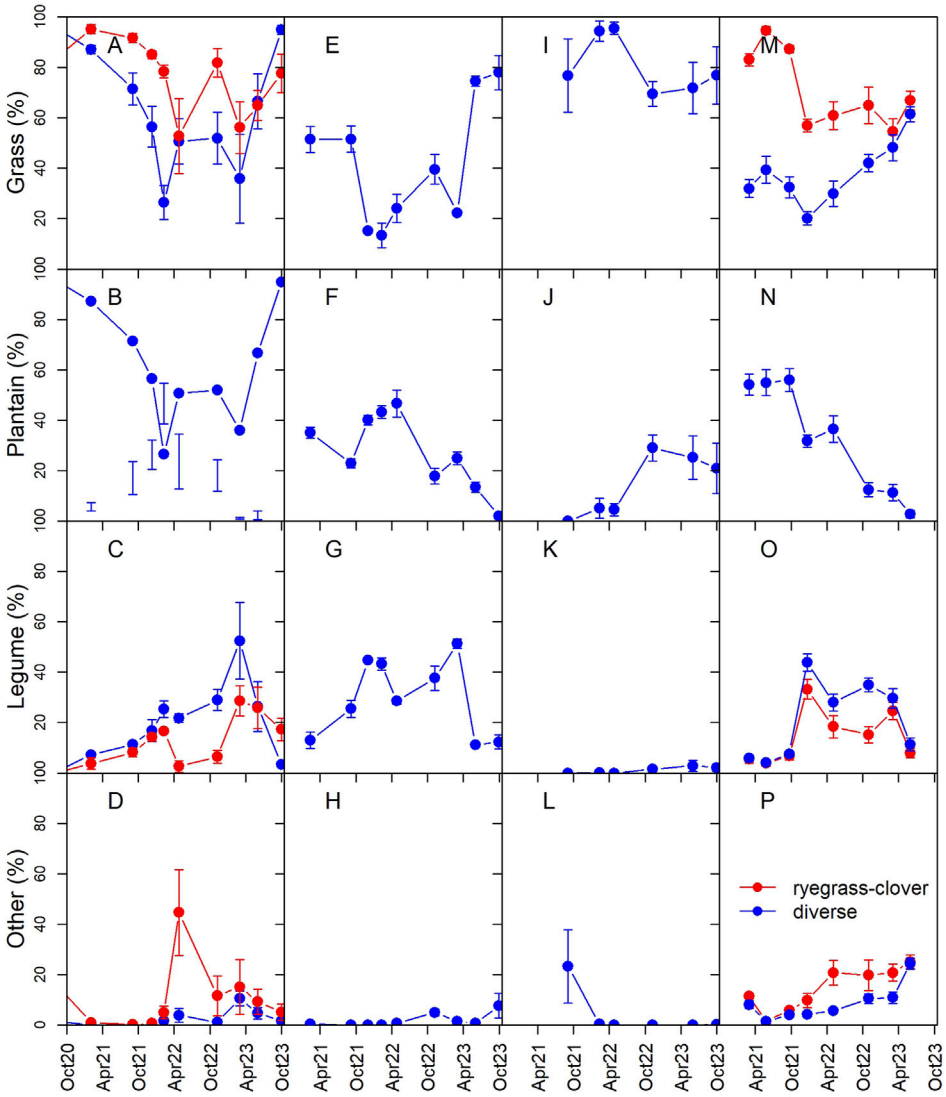


FIGURE 5
Seasonal and interannual variation in the percentage of dry matter harvested from diverse and ryegrass-clover pasture lysimeters represented by each functional group, including grass, plantain, legumes and other forbs for the Ashley Dene Research and Development Station effluent irrigated (EI) site **(A–D)**, irrigated only (OI) site **(E–H)**, non-irrigated (NI) site **(I–L)** and the Tihoi (TN) site **(M–P)**.

Empirical modelling confirmed the importance of water input, drainage volume and N input and surplus as drivers of N loss, as has been shown previously (Cameron et al., 2013). However, plantain fraction was also identified as a significant driver of N leaching by both the linear regression and Random Forest modelling approaches. This may be an artefact arising from the distribution of plantain across measurement sites and measurement years. N leaching from diverse pasture lysimeters was similar to ryegrass-clover lysimeters in most cases at the comparison sites. However, across the entire dataset, the highest plantain fraction was observed at TN in Year 1, when N losses from both pasture types were low. The plantain fraction subsequently decreased during years 2 and 3 when drainage amounts were higher and subsequent urine patches had been applied. At Ashley Dene, the highest plantain contents were observed at the irrigated only site, which had low N losses due to a low N input compared to the effluent irrigated site. However, the lower losses from diverse pasture in Year 2 at the effluent irrigated site also coincided with the highest plantain content. Hence, it is difficult to draw a definitive conclusion on the effect of plantain on N leaching losses from our data alone.

The inclusion of plantain fraction as an important driver of N leaching is supported by the literature from grazed grasslands, which has shown that including plantain in pastures at moderate rates (30%–40%) can decrease N leaching losses by 20%–60% (Pinxterhuis et al., 2024). However, in contrast to the current study, this result included animal mediated effects of diet on N excretion by animals. Plantain content was variable across sites and through time, despite identical sowing rates. Use of plantain as a mitigation approach will depend on its persistence in the pasture. Regular over-sowing of plantain has been investigated as a management intervention which would reduce N losses without affecting farm profitability (Robertson et al., 2023).

Another potential pathway to realizing the benefits of diversity for mitigating N losses may be through sowing highly diverse pastures. In contrast to the minimally diverse mixes investigated here, highly diverse mixes may have better outcomes due to the inclusion of functional redundancy in the initial species mix and a wider variation in functional traits (Orwin et al., 2022). Such mixes may have a lower risk of degradation over time, and their impact on ecosystem function is likely to improve over time as complementarity amongst species increases (Cardinale et al., 2007; Zheng et al., 2024).

The strongest effect on N loss observed in this study was that of management. The highest level of N input (363–505 kg N/ha/y) at the EI site resulted in the highest field-scale losses, 27–80 kg N ha^{-1} y^{-1}. At the remaining sites, where N input was generally less than 200 kg N ha^{-1} y^{-1}, the losses were 2–26 kg N ha^{-1} y^{-1} (excluding years with conversion-related N losses). In addition to N input, irrigation contributed to the effects of management intensity on N leaching. At Ashley Dene, drainage events were observed at the EI and OI lysimeters which were not present in the NI lysimeters. The drainage and associated N losses in these events were a direct result of irrigation management, and thus could be avoided through improved irrigation practices. However, these intensive management practices also lead to 15%–205% more dry matter production by the EI site, relative to NI and OI sites.

Pasture conversion was another important source of management-driven N losses. Losses of over 120 kg N ha^{-1} followed an autumn cultivation and re-sowing at the EI site. This large loss was likely driven by the combination of winter drainage, high residual N in the soil from the previous lucerne crop, and low N uptake by the recently sown pasture. Drainage triggered by irrigation at the OI lysimeters before pasture establishment was complete contributed substantially to the 26 kg N ha^{-1} y^{-1} loss in Year 1. Conversely, no large loss was observed for the TN site following successful spring establishment of diverse and ryegrass-clover pasture. These results suggest that conversion activities should be carried out in a manner that prioritizes complete ground coverage and establishment before the winter drainage season.

Empirical modelling of lysimeter drainage could only explain 51%–71% of the variability in lysimeter N leaching, highlighting the need for process-based modelling to disentangle the effects of seasonal dynamics of drainage, N uptake by plants and amounts and timing of N inputs on N leaching losses. Process-based modelling will allow for optimization of the production benefits of intensive practices, such as irrigation, effluent application, and high stocking rates, versus environmental impacts, such as N leaching. Additional co-benefits and trade-offs with other environmental impacts of mitigation practices, such as use of more diverse pasture, need to be considered. For instance, measurements of net greenhouse gas emissions from more diverse pasture demonstrated that a mitigation effect can be shown for N_2O emissions, which were 39% lower for diverse pasture relative to ryegrass-clover (Laubach et al., 2023). However, the net emissions, considering all greenhouse gasses, were higher from diverse pasture due to the less favorable CO_2 balance. This demonstrates the need for considering a wide range of environmental impacts through process-based modelling. Process-based modelling will likewise facilitate investigation of a wide range of climate and management scenarios, making the results more generalizable for use by decision makers and in the development of decision support tools.

5 Conclusion

Nitrogen leaching losses measured for fully established diverse pasture were 2–80 kg N ha^{-1} y^{-1}, varying with plant production, volume and timing of drainage, and quantity and timing of N inputs. Harvested dry matter, drainage volume and leaching losses from 5–8 species diverse pasture were not consistently different from ryegrass-clover pasture. Although no mitigation effect of diverse pasture was observed in this case, these results should not be extrapolated to high diversity pasture mixes, which should be verified separately. As well, further work is needed to account for animal mediated effects of diverse pasture diets on N inputs to the system. In this study, the most important driver of N leaching losses was management intensity, with higher losses being associated with higher N inputs. Timing of management activities should also be optimized to ensure full pasture cover leading into the drainage season, as high losses of 120 kg N ha^{-1} y^{-1} were observed during the winter drainage season following autumn cultivation and sowing of new pasture in this study. This dataset will be used, along with process-based modelling, to inform decision support tools support farmers and regulators to reduce leaching losses from pasture-based livestock grazing systems.

Data availability statement

The datasets presented in this study can be found in online repositories. The names of the repository/repositories and accession number(s) can be found below: Manaaki Whenua - Landcare Research DataStore (https://doi.org/10.7931/AFSM-BC10).

Author contributions

SG: Writing–review and editing, Writing–original draft, Investigation, Funding acquisition, Formal Analysis, Conceptualization. JP: Writing–review and editing, Investigation, Conceptualization. JL: Writing–review and editing, Data curation, Conceptualization. JH: Writing–review and editing, Methodology, Investigation. GR: Writing–review and editing, Methodology, Investigation. SC: Writing–review and editing, Funding acquisition, Conceptualization. DW: Writing–review and editing, Funding acquisition, Conceptualization. MM: Writing–review and editing, Methodology, Investigation. GM: Writing–review and editing, Investigation. PM: Writing–review and editing, Funding acquisition, Conceptualization.

Funding

The author(s) declare that financial support was received for the research, authorship, and/or publication of this article. This work was funded by the Ministry for Primary Industries Sustainable Land Management and Climate Change Freshwater Mitigation Fund (project 406345).

Acknowledgments

We are grateful to the Lincoln University Ashley Dene Research and Development Station and Tihoi landowners for use of their farms for this study. We thank Brendon Malcolm for helpful comments on an early draft of the manuscript.

Conflict of interest

The authors declare that the research was conducted in the absence of any commercial or financial relationships that could be construed as a potential conflict of interest.

Publisher's note

All claims expressed in this article are solely those of the authors and do not necessarily represent those of their affiliated organizations, or those of the publisher, the editors and the reviewers. Any product that may be evaluated in this article, or claim that may be made by its manufacturer, is not guaranteed or endorsed by the publisher.

Supplementary material

The Supplementary Material for this article can be found online at: https://www.frontiersin.org/articles/10.3389/fenvs.2024.1445212/full#supplementary-material

References

Cameron, K. C., Di, H. J., and Moir, J. L. (2013). Nitrogen losses from the soil/plant system: a review. *Ann. Appl. Biol.* 162, 145–173. doi:10.1111/aab.12014

Cardinale, B. J., Wright, J. P., Cadotte, M. W., Carroll, I. T., Hector, A., Srivastava, D. S., et al. (2007). Impacts of plant diversity on biomass production increase through time because of species complementarity. *Proc. Natl. Acad. Sci.* 104, 18123–18128. doi:10.1073/pnas.0709069104

Carrick, S., Rogers, G., Cameron, K., Malcolm, B., and Payne, J. (2017). Testing large area lysimeter designs to measure leaching under multiple urine patches. *N. Z. J. Agric. Res.* 60, 205–215. doi:10.1080/00288233.2017.1291527

Clough, T. J., Ledgard, S. F., Sprosen, M. S., and Kear, M. J. (1998). Fate of 15N labelled urine on four soil types. *Plant Soil* 199, 195–203. doi:10.1023/a:1004361009708

Di, H. J., Cameron, K. C., Podolyan, A., Edwards, G. R., De Klein, C. A., Dynes, R., et al. (2016). The potential of using alternative pastures, forage crops and gibberellic acid to mitigate nitrous oxide emissions. *J. Soils Sediments* 16, 2252–2262. doi:10.1007/s11368-016-1442-1

Dijkstra, F. A., West, J. B., Hobbie, S. E., Reich, P. B., and Trost, J. (2007). Plant diversity, CO_2, and N influence inorganic and organic N leaching in grasslands. *Ecology* 88, 490–500. doi:10.1890/06-0733

Fischer, C., Tischer, J., Roscher, C., Eisenhauer, N., Ravenek, J., Gleixner, G., et al. (2015). Plant species diversity affects infiltration capacity in an experimental grassland through changes in soil properties. *Plant Soil* 397, 1–16. doi:10.1007/s11104-014-2373-5

Gardiner, C. A., Clough, T. J., Cameron, K. C., Di, H. J., Edwards, G. R., and De Klein, C. a.M. (2018). Potential inhibition of urine patch nitrous oxide emissions by Plantago lanceolata and its metabolite aucubin. *N. Z. J. Agric. Res.* 61, 495–503. doi:10.1080/00288233.2017.1411953

Graham, S. L., Laubach, J., Hunt, J. E., Eger, A., Carrick, S., and Whitehead, D. (2019). Predicting soil water balance for irrigated and non-irrigated lucerne on stony, alluvial soils. *Agric. Water Manag.* 226, 105790. doi:10.1016/j.agwat.2019.105790

Graham, S. L., Laubach, J., Hunt, J. E., Mudge, P. L., Nuñez, J., Rogers, G. N. D., et al. (2022). Irrigation and grazing management affect leaching losses and soil nitrogen balance of lucerne. *Agric. Water Manag.* 259, 107233. doi:10.1016/j.agwat.2021.107233

Haynes, R. J., and Williams, P. H. (1993). "Nutrient cycling and soil fertility in the grazed pasture ecosystem," in *Advances in agronomy*. Editor D. L. Sparks (Academic Press), 119–199.

Hector, A., Schmid, B., Beierkuhnlein, C., Caldeira, M. C., Diemer, M., Dimitrakopoulos, P. G., et al. (1999). Plant diversity and productivity experiments in European grasslands. *Science* 286, 1123–1127. doi:10.1126/science.286.5442.1123

Hewitt, A. E. (2010). *New Zealand soil classification*. Lincoln, New Zealand: Manaaki Whenua Press.

Hooper, D. U., Chapin Iii, F. S., Ewel, J. J., Hector, A., Inchausti, P., Lavorel, S., et al. (2005). Effects of biodiversity on ecosystem functioning: a consensus of current knowledge. *Ecol. Monogr.* 75, 3–35. doi:10.1890/04-0922

Hooper, D. U., and Vitousek, P. M. (1998). Effects of plant composition and diversity on nutrient cycling. *Ecol. Monogr.* 68, 121–149. doi:10.1890/0012-9615(1998)068[0121:eopcad]2.0.co;2

Isbell, F., Craven, D., Connolly, J., Loreau, M., Schmid, B., Beierkuhnlein, C., et al. (2015). Biodiversity increases the resistance of ecosystem productivity to climate extremes. *Nature* 526, 574–577. doi:10.1038/nature15374

Lange, M., Eisenhauer, N., Sierra, C. A., Bessler, H., Engels, C., Griffiths, R. I., et al. (2015). Plant diversity increases soil microbial activity and soil carbon storage. *Nat. Commun.* 6, 6707–6708. doi:10.1038/ncomms7707

Laubach, J., Hunt, J. E., Graham, S. L., Buxton, R. P., Rogers, G. N. D., Mudge, P. L., et al. (2023). Mitigation potential and trade-offs for nitrous oxide emissions and carbon balances of irrigated mixed-species and ryegrass-clover pastures. *Agric. For. Meteorology* 330, 109310. doi:10.1016/j.agrformet.2023.109310

Liaw, A., and Wiener, M. (2002). Classification and regression by randomForest. *R. News* 2, 18–22. Available at: https://CRAN.R-project.org/doc/Rnews/.

Malcolm, B., Cameron, K., Di, H., Edwards, G., and Moir, J. (2014). The effect of four different pasture species compositions on nitrate leaching losses under high N loading. *Soil Use Manag.* 30, 58–68. doi:10.1111/sum.12101

Mcleod, M. (2020). *Nitrogen leaching under grazed lucerne*. Lincoln, New Zealand: Manaaki Whenua - Landcare Research. Contract Report LC3701.

Mcnally, S. R., Laughlin, D. C., Rutledge, S., Dodd, M. B., Six, J., and Schipper, L. A. (2015). Root carbon inputs under moderately diverse sward and conventional ryegrass-clover pasture: implications for soil carbon sequestration. *Plant Soil* 392, 289–299. doi:10.1007/s11104-015-2463-z

Moir, J. L., Cameron, K. C., Di, H. J., and Fertsak, U. (2011). The spatial coverage of dairy cattle urine patches in an intensively grazed pasture system. *J. Agric. Sci.* 149, 473–485. doi:10.1017/s0021859610001012

Orwin, K. H., Mason, N. W. H., Berthet, E. T., Grelet, G., Mudge, P., and Lavorel, S. (2022). Integrating design and ecological theory to achieve adaptive diverse pastures. *Trends Ecol. and Evol.* 37, 861–871. doi:10.1016/j.tree.2022.06.006

Peoples, M. B., Brockwell, J., Herridge, D. F., Rochester, I. J., Alves, B. J. R., Urquiaga, S., et al. (2009). The contributions of nitrogen-fixing crop legumes to the productivity of agricultural systems. *Symbiosis* 48, 1–17. doi:10.1007/bf03179980

Pinxterhuis, J. B., Judson, H. G., Peterson, M. E., Navarrete, S., Minnée, E., Dodd, M. B., et al. (2024). Implementing plantain (Plantago lanceolata) to mitigate the impact of grazing ruminants on nitrogen losses to the environment: a review. *Grass and Forage Sci.* 79, 144–157. doi:10.1111/gfs.12649

Podolyan, A., Di, H. J., and Cameron, K. C. (2020). Effect of plantain on nitrous oxide emissions and soil nitrification rate in pasture soil under a simulated urine patch in Canterbury, New Zealand. *J. Soils Sediments* 20, 1468–1479. doi:10.1007/s11368-019-02505-1

R Core Team (2022). *R: a language and environment for statistical computing*. 4.2.1 ed. Vienna, Austria: R Foundation for Statistical Computing.

Robertson, C., Schipper, L., Pinxterhuis, I., Edwards, J. P., Doole, G., and Romera, Á. (2023). New Zealand dairy farm system solutions that balance reductions in nitrogen leaching with profitability – a case study. *N. Z. J. Agric. Res.*, 1–21. doi:10.1080/00288233.2023.2269136

Sanderson, M. A., Skinner, R. H., Barker, D. J., Edwards, G. R., Tracy, B. F., and Wedin, D. A. (2004). Plant species diversity and management of temperate forage and grazing land ecosystems. *Crop Sci.* 44, 1132–1144. doi:10.2135/cropsci2004.1132

Tilman, D., Wedin, D., and Knops, J. (1996). Productivity and sustainability influenced by biodiversity in grassland ecosystems. *Nature* 379, 718–720. doi:10.1038/379718a0

Vibart, R. E., Vogeler, I., Dodd, M., and Koolaard, J. (2016). Simple versus diverse temperate pastures: aspects of soil–plant–animal interrelationships central to nitrogen leaching losses. *Agron. J.* 108, 2174–2188. doi:10.2134/agronj2016.04.0193

Zheng, L., Barry, K. E., Guerrero-Ramírez, N. R., Craven, D., Reich, P. B., Verheyen, K., et al. (2024). Effects of plant diversity on productivity strengthen over time due to trait-dependent shifts in species overyielding. *Nat. Commun.* 15, 2078. doi:10.1038/s41467-024-46355-z

frontiers | Frontiers in Environmental Science

TYPE Original Research
PUBLISHED 13 November 2024
DOI 10.3389/fenvs.2024.1488638

Check for updates

OPEN ACCESS

EDITED BY
Yefang Jiang,
Agriculture and Agri-Food Canada (AAFC), Canada

REVIEWED BY
Holger Rupp,
Helmholtz Association of German Research Centres (HZ), Germany
Yvonne Uwituze,
Government of Prince Edward Island, Canada

*CORRESPONDENCE
Sofia Delin,
sofia.delin@slu.se

RECEIVED 02 September 2024
ACCEPTED 31 October 2024
PUBLISHED 13 November 2024

CITATION
Delin S, Mårtensson K and Johnsson H (2024) Risk for nitrogen leaching after application of solid manure in autumn differs between manure types.
Front. Environ. Sci. 12:1488638.
doi: 10.3389/fenvs.2024.1488638

COPYRIGHT
© 2024 Delin, Mårtensson and Johnsson. This is an open-access article distributed under the terms of the Creative Commons Attribution License (CC BY). The use, distribution or reproduction in other forums is permitted, provided the original author(s) and the copyright owner(s) are credited and that the original publication in this journal is cited, in accordance with accepted academic practice. No use, distribution or reproduction is permitted which does not comply with these terms.

Risk for nitrogen leaching after application of solid manure in autumn differs between manure types

Sofia Delin[1]*, Kristina Mårtensson[2] and Holger Johnsson[2]

[1]Department of Soil and Environment, Swedish University of Agricultural Sciences, Skara, Sweden, [2]Department of Soil and Environment, Swedish University of Agricultural Sciences, Uppsala, Sweden

Manure application performed in autumn requires regulation due to the risk of nitrogen (N) leaching during winter. On the other hand, application of manure in spring can pose some practical problems depending on the risk for N immobilization and the difficulty in ploughing heavy clay soils during this time of year. The risk for leaching is likely to differ between different soil texture and manure characteristics. In this study, we sought to estimate the risk for nitrogen leaching depending on the carbon/nitrogen ratio (C/N) of the manure, time for manure application, and soil type. We combined 3-year lysimeter experiments with 2-year field plot experiments and laboratory soil incubations and compared results with those from an empirical model. We compared effects of manure application on two soils (silty clay and loamy sand) and solid manures with different representing C/N ratios. In incubations, only manure with a C/N-ratio below 14 contributed with significant amounts of leachable N during the first months after application. In the lysimeter study, N leaching was unaffected by the timing of the application of the manure with C/N-ratio 18. However, regarding manure with C/N-ratio 10, N leaching was elevated with 10–15 kg N per ha after manure application in October compared to November and March on both soil types. The mineral N analyses from soil profiles in the field experiments showed a similar pattern, however, the increase was higher on the loamy sand compared to the silty clay. The ammonia emissions did not differ between manure types, but were on average 24% of applied NH_4-N after application in October when air temperature was on average 12°C compared to only 3% of applied NH_4-N in November and March when air temperature was on average 5°C. Similar to lysimeter results, the modelled N leaching was higher the earlier the manure application occurred in autumn. However, the model also predicted increased leaching for the manure with a high C/N-ratio, and a smaller effect on leaching on clay soil. Considering this, the model calculations overestimated the leaching effects from manure with a high C/N-ratio and underestimated the leaching effects on clay soil.

KEYWORDS

nitrogen leaching, soil type, lysimeter, solid manure, C/N ratio, spring sowing, manure application, NLeCCS system

1 Introduction

Manure application that is carried out in autumn poses a risk for nitrogen leaching during the following winter period, which has a low crop uptake and large drainage runoff (Aronsson et al., 2014), particularly before spring sowing when there is no crop. This risk is therefore dependent on when the manure is applied during the year (Thomsen, 2005). Different manure application times may also mean different time for soil incorporation by ploughing, which can also affect nitrogen leaching (Stenberg et al., 1999; Norberg and Aronsson, 2024). The composition of nitrogen compounds in the manure can also influence whether or not leaching is affected, in which solid manure with less mineral nitrogen can be expected to have an insignificant effect on leaching (Shepherd and Newell-Price, 2016; Pedersen B. N. et al., 2021).

There are currently no reported Swedish leaching experiments regarding solid manure in autumn before a spring crop, but there are results available from Denmark (Hansen et al., 2004; Thomsen, 2005) and the United Kingdom (Smith et al., 2002). Indeed, Thomsen (2005) showed in a lysimeter experiment on loamy sand that nitrate leaching, after application of manure in December and in March, was the same size for unmanured lysimeters, whereas leaching was higher after manure application in September. Moreover, in two parallel plot experiments on a sandy loam with nearly twice as much precipitation as in the lysimeter experiments, Hansen et al. (2004) reported that N utilization was lower after application in both September and December compared to application in spring. This suggests both autumn applications suffered from increased leaching losses. In four experiments on sandy soils in the United Kingdom, application of 200 kg total N with solid farmyard manure in October resulted in an average 4 kg N ha^{-1} increase in nitrate leaching compared to the unmanured control (Smith et al., 2002). Solid fractions with a C/N-ratio ranging from 7 to 10 from separated slurry also caused a significant increase in N leaching after autumn application to winter wheat in Danish experiments (Sørensen and Rubæk, 2012). Solid manures (>20% DM) may, however, have a larger C/N-ratio and a smaller fraction of mineral nitrogen.

Approximately 40% of the animal farms with cattle and pigs in Sweden have management systems with solid manure and deep litter (SCB, 2020). In 2018/19, 1,800,000 tons of solid manure from cattle, 800,000 tons of deep litter from cattle, and 60,000 tons of solid manure from pigs were distributed on Swedish agricultural land (SCB, 2020). Depending on, for instance, both the type and amount of bedding material as well as the storage time, these types of manure may vary considerably in their chemical composition (Ayadi et al., 2015; Keskinen et al., 2017). A manure from a housing with generous amounts of bedding material, that has also not yet been decomposed during storage, will have a much higher proportion of carbon compared to a manure with less bedding material or a manure that already been degraded during storage. The C/N-ratio for solid beef manure normally varies between 11 and 16 but can also be above 20 from systems with a large amount of straw bedding (Qian and Schoenau, 2002; Loro, 2005). With a higher ratio of carbon compared to nitrogen in the manure, more nitrogen will be immobilized by soil biota and there is consequently less in mineral form (Delin et al., 2012) that is available for crop uptake and leaching. This type of manure can be both more practical and beneficial for crop production to apply and incorporate in autumn, particularly on clay soils whose soil structure benefit from ploughing in autumn compared to spring (Njøs and Børresen, 1991). However, manure application with a lower C/N-ratio in autumn may lead to nutrient leaching during winter (Aronsson et al., 2014) and on lighter soils, where spring ploughing is suitable, manure application in spring has resulted in greater yields of spring-sown cereals compared to application in autumn (Hansen et al., 2004).

In Sweden, the main part of the agricultural land is designated as nitrate vulnerable zones that are regulated by the European Union Nitrates Directive. According to current regulations for manure application within these zones, solid manures may be applied in October but not in November-February prior to spring sowing. The intention of this regulation is to limit nitrogen leaching. However, results from Denmark (Thomsen, 2005) and modelling calculations from Sweden (Johnsson and Hoffman, 1995) both suggest that early autumn application enhances leaching more so than if manure is applied in late autumn. In addition, solid manures may vastly differ in chemical composition and if they pose a risk for leaching or not. The risk may also differ between soils with different texture (Hina, 2024).

Swedish data on how nitrogen leaching is affected by time for application of solid manure depending on manure and soil characteristics would enable a better basis for both regulations and recommendations for farmers that would lead to limited nitrogen leaching. This is important to assure safe water quality and to limit environmental impacts such as eutrophication of our waters. The objective of this study was to describe the nitrogen (N) dynamics following the application of different kinds of solid manures to bare soil in Sweden to estimate the risk for nitrogen leaching during the first year after application depending on the carbon/nitrogen ratio (C/N) of the manure, the time for manure application, and the soil type.

2 Materials and methods

2.1 Combination of experiments in the field, lab and in outdoor lysimeters

In order to study the effects of solid manure application on several variables, we combined lysimeter experiments with field plot experiments and laboratory soil incubations. The lysimeter experiments were included to study nutrient leaching and the field experiments to study ammonia emissions, grain yield, and soil mineral nitrogen profiles. In the soil incubations we studied the course of net N mineralisation for a greater number of manures. In all experiments, the same two soils representing clay soil and sandy soil (Table 1) and the two manure types representing a high and low C/N-ratio (Table 2) were included. Manure A, which represented a solid farmyard manure with a relatively low C/N-ratio of 10, originated from a sow stable with moderate amounts of straw bedding compared to a deep litter. Manure B represented a solid manure with a relatively high C/N-ratio of 18 and was acquired from a deep litter for dairy heifers. The lysimeter facility and one of the field experiments were located at Lanna Research Station (58°20 N, 13°7 E) and another field experiment was located at Fotegården

10.3389/fenvs.2024.1488638

TABLE 1 Soil characteristics for the two soils used in lysimeters, field experiments, and incubations (where only the 0–30 cm is relevant for the incubations).

Depth (cm)	Lanna			Fotegården		
	0–30	30–60	60–90	0–30	30–60	60–90
Ca-AL (mg 100g^{-1})	93	16.4	41.1	257	266	230
P-AL (mg 100g^{-1})	14.8	2.2	4.3	3	11.8	19.1
Al-AL	88.4	22.1	4.1	22.5	33.8	33.3
Fe-AL	19.8	11.6	9.5	41.4	12.3	17.2
K-AL	4	1.3	2.9	10.7	13.9	18.7
pH	6.7	7.3	7.5	6.3	6.4	6.7
CEC (cmol kg^{-1})	19	21	19	7.3	1.4	2.3
Base saturation (%)	88	93	94	61	48	80
Clay (%)	45	55		5.6	4.5	2.7
Silt (%)	42	51		7.3	3.4	4.8
Sand (%)	10	4		81	89	91
SOM (%)	2.9	0.4		5.4	2.6	0.9

TABLE 2 Characteristics of the two types of manure used in lysimeters, field experiments, and incubations.

Manure	A	B
From animal	Sow	Heifer
Dry matter, %	20	22
Total N, kg ton^{-1}	8.0	4.8
NH_4-N, kg ton^{-1}	1.9	0.7
C/N-ratio	10	18
Total *p*, kg ton^{-1}	2.4	1.2
Total K, kg ton^{-1}	7.0	9.4
Total Mg, kg ton^{-1}	1.5	1.3
Total Ca, kg ton^{-1}	5.0	4.2

(58°28 N, 13°14 E), 17 km north from Lanna (Figure 1). Weather data was only recorded at Lanna (Figure 2), but data from a weather station in close to Fotegården confirms that temperatures are very similar and that precipitation may be a bit higher at Fotegården. The hydrological year (July-June) 2014/2015 had unusually high precipitation in August and a milder winter than usual (Figure 2).

2.2 Field experiments

2.2.1 Experimental design

Two 2-year field experiments were conducted on fields with different soil conditions (Table 1). One field had loamy sand at the farm Fotegården. For that experiment, three different times of application of two different solid manures (Table 2) were compared with two unmanured controls with different levels of mineral nitrogen fertilizer (Table 3). The lower level of mineral fertilizer was the same as in manured treatments and the higher similar as the expected N fertilization effect of manure N. These treatments were included for comparison, to evaluate the effects of manure N. The other experiment was located at Lanna Research Station in a field with silty clay soil (Table 1). For this experiment, the times for manure application were limited to the two times in autumn and with only one of the manures (Table 3). The reason for the limitation of application times at this site was that this type of soil would not be feasible to plough in spring. To limit costs, only the manure type that was expected to have larger impact on yield and soil mineral N levels was included. The experiments had a randomized block design with three replicates at Fotegården and four replicates at Lanna. Each individual plot was 4 m wide and 15 m long. The experiments were established in autumn 2013 starting with manure application according to plan (Table 3) and was finished after harvest in 2015.

2.2.2 Manure application and ammonia emission

Manure amounts corresponding to approximately 150 kg total N ha^{-1}, i.e. 20 tons ha^{-1} of manure A and 30 tons ha^{-1} of manure B were distributed within the plots using pitchforks. Ammonia emissions were measured from the time of application until ploughing, which was approximately 24 h. For this, an equilibrium concentration method dynamic technique, with chambers and passive diffusion samplers, was used (Svensson, 1994). In each plot with manure application, one or two 0.3 m × 0.4 m large metal frames were inserted into the soil on which ventilated chambers were then placed. We put one diffusive sampler both inside and outside each chamber to estimate the equilibrium concentration using Equation 1. To determine suitable exposure periods, the NH_3 concentration in the ventilated chambers was measured with detection tubes. This usually resulted in one sampler during the first 3–5 h and a new one for the remaining 19–21 h. To ensure the correct manure amount where ammonia emissions were carried out, the amount of manure applied within the frames was weighed separately on a finer scale.

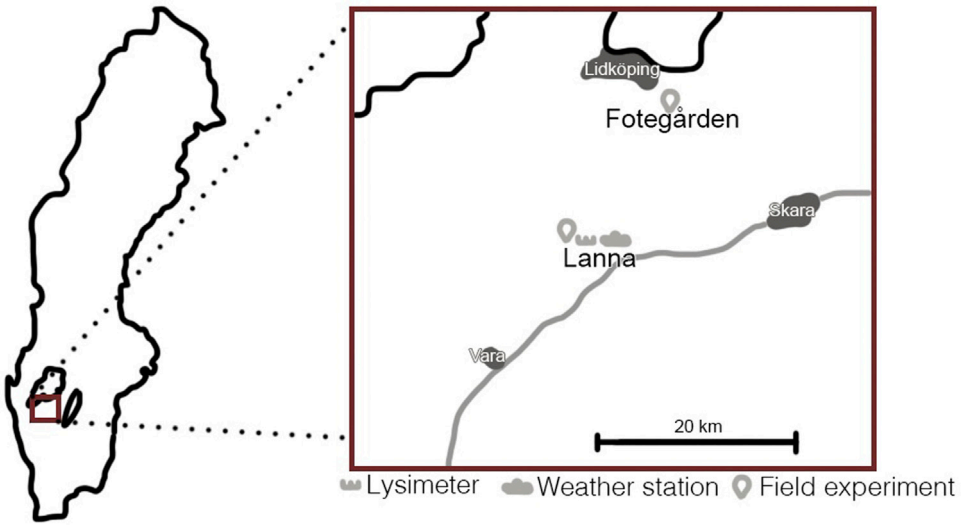


FIGURE 1
Location of field experiments, lysimeter facility and weather station.

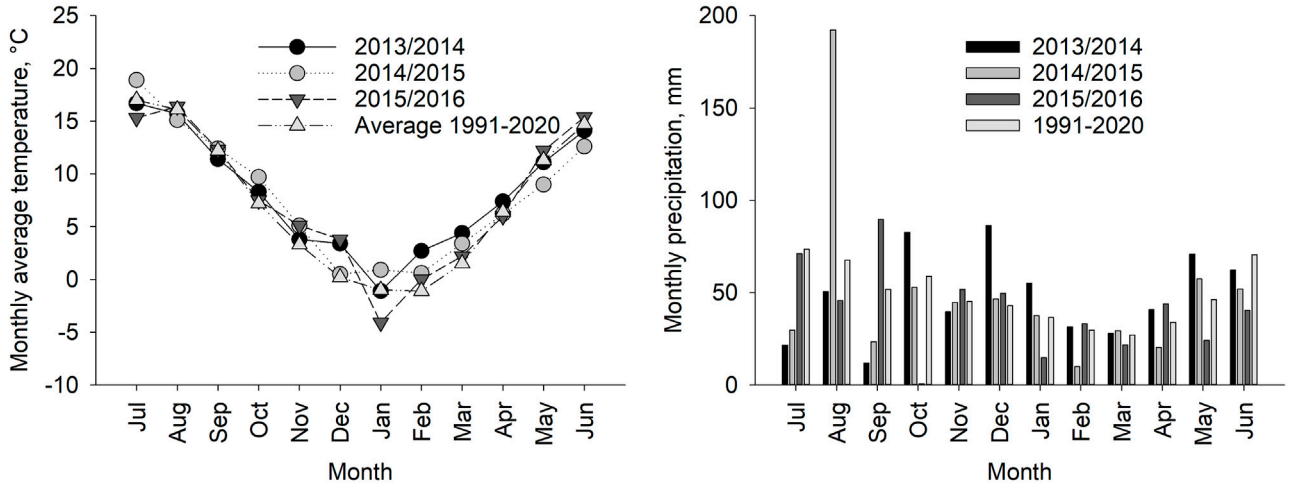


FIGURE 2
Monthly averages of air temperature and monthly accumulated precipitation at Lanna research station during the experimental period.

$$E = (C_{eq} - C_a)K_Z \quad (1)$$

Where E is the ammonia emission, C_{eq} denotes the equilibrium concentration of NH_3 measured inside the chambers, C_a the ambient NH_3 concentration measured outside the chambers and K_Z the mass transfer coefficient which was set to 10 mm s^{-1} (Svensson and Ferm, 1993).

2.2.3 Crop management and yield measurements

The ploughing, harrowing, and sowing was all performed with conventional equipment. Mineral fertilizer corresponding to 40 kg N ha^{-1} was applied in all plots with a boom fertilizer spreader in connection to sowing. Another 40 kg N ha^{-1} was applied in the 80 kg N ha^{-1} treatment with a plot spreader. The grain yield was measured with a plot combine in 20 m^2 large areas within each plot and grain samples were taken plot-wise for an analysis of nitrogen content using near infrared transmission (NIT) spectroscopy.

2.2.4 Soil mineral nitrogen

Soil samples were taken in March 2014, February/March 2015, and September 2015 for determination of mineral nitrogen (NH_4-N and NO_3-N) in the soil profile. For this, 18 cores from the 0–30 cm soil layer, 9 cores from the 30–60 cm, and 60–90 cm depths were mixed to composite samples for each plot and depth. The samples were stored at a frozen temperature until analysis. The samples were milled and homogenized in a frozen state. Subsamples of 40 g were extracted with 100 mL 2 M KCl (Mulvaney, 1996). The ammonium (NH4+) and nitrate (NO3-) analyses were then carried out using

TABLE 3 Treatments in the field experiments where × indicates which treatments are included at the sites Lanna (L) and Fotegården (F).

	L	F	Manure type	Time for application	Mineral fertilizer
1	×	×	No manure		40 kg N ha^{-1}
2	×	×	No manure		80 kg N ha^{-1}
3	×	×	Low C/N-ratio	Early autumn (1 October[a])	40 kg N ha^{-1}
4		×	Deep litter	Early autumn (1 October[a])	40 kg N ha^{-1}
5	×	×	Low C/N-ratio	Late autumn (25 November[a])	40 kg N ha^{-1}
6		×	Deep litter	Late autumn (25 November[a])	40 kg N ha^{-1}
7		×	Low C/N-ratio	spring (25 March[a])	40 kg N ha^{-1}
8		×	Deep litter	spring (25 March[a])	40 kg N ha^{-1}

[a]Exact dates for manure application is presented in supplementary material (Supplementary Table S1).

TABLE 4 Treatments in the lysimeter experiment and corresponding treatment 1-8 in field experiments (Table 3) at Lanna (L) and Fotegården (F).

	Manure type	Time for application	Soil type	Corresponding field treatment
A	No manure		Loamy sand	F1
B	Low C/N-ratio	Early autumn (1 October)	Loamy sand	F3
C	Deep litter	Early autumn (1 October)	Loamy sand	F4
D	Low C/N-ratio	Late autumn (25 November)	Loamy sand	F5
E	Deep litter	Late autumn (25 November)	Loamy sand	F6
F	Low C/N-ratio	spring (25 March)	Loamy sand	F7
G	Deep litter	spring (25 March)	Loamy sand	F8
H	No manure		Silty clay	L1
I	Low C/N-ratio	Early autumn (1 October)	Silty clay	L3
J	Low C/N-ratio	Late autumn (25 November)	Silty clay	L5

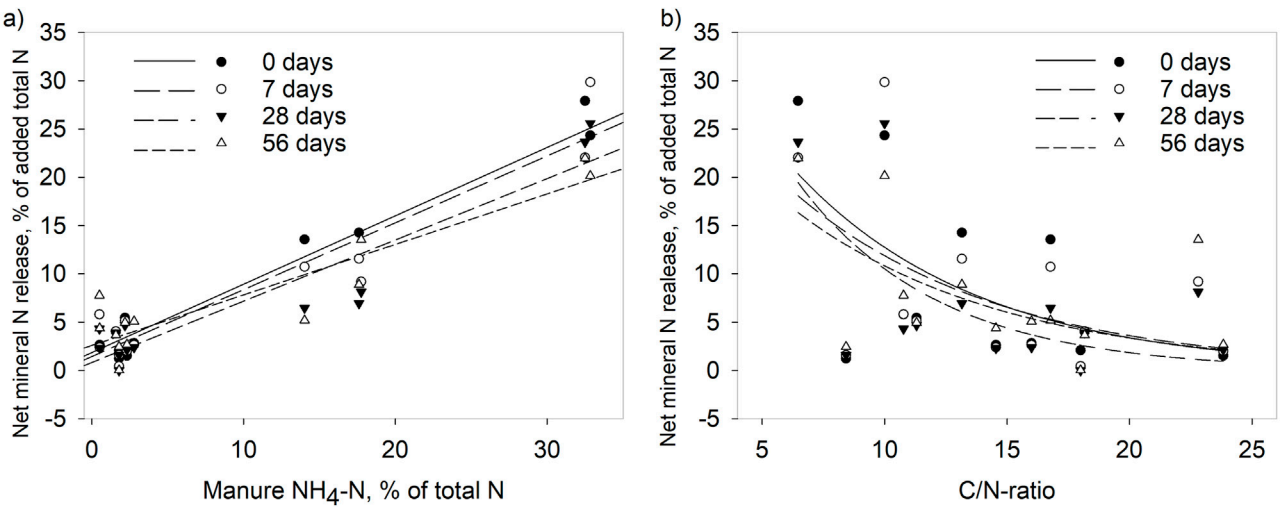


FIGURE 3
Results of incubations showing net mineral N release from manure addition expressed as percentage of total N added with manure and plotted against **(A)** manure content of NH_4-N and **(B)** manure C/N-ratio.

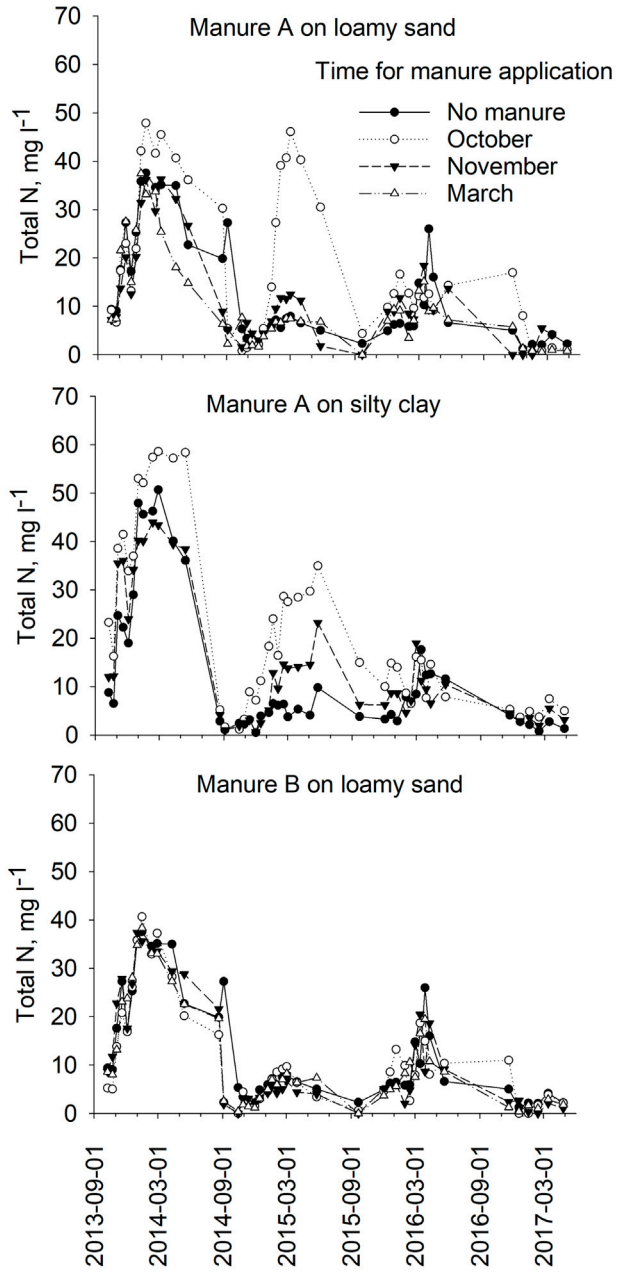


FIGURE 4
Nitrogen concentration at different sampling dates for the different treatments.

colorimetric methods on a Seal AA3 auto-analyzer (SEAL Analytical Inc., Mequon, Wisconsin, United States).

2.2.5 Statistics

Differences in yield and mineral N in subsoil was analyzed statistically with one-way ANOVA for each location and occasion separately. Tukey's test (confidence interval of 95%) was used to investigate differences between the treatments. To verify assumptions for ANOVA, normal probability tests were performed in Mintab.

2.3 Lysimeter experiments

2.3.1 Lysimeters

Differences in N leaching between treatments with three different times of application of the two different solid manures (Table 2) was compared with an unmanured control in a lysimeter experiment (Table 4) involving the two soil types (Table 1). The treatments were the same as in the field experiments, except there was only one unmanured control. For the collection of undisturbed soil monoliths for the experiment, we used a drilling technique described by Persson and Bergström (1991). To carry out this method, we used a corer consisting of a steel cylinder with cutting teeth at the bottom, into which plastic pipes were inserted to encase the soil columns. The steel cylinder rotates and carves out soil cores that were gently pushed into the pipes. The lysimeter containers had an inner diameter of 0.295 m, a length of 1.18 m, and were made of polyvinyl chloride (PVC). This depth correspond to the standard drainage depth of around 1 m on Swedish agricultural soils, which means that water collected at this depth represents drainage water. Twenty-one soil columns with loamy sand, that were 0.8 m in length, were collected from the same field that was used in the field experiment at Fotegården. This slightly more shallow depth was chosen for practical reasons, as deeper soil cores required much more force from the drill leading to compacted and unrepresentative soil columns. A further nine soil columns with silty clay soil were used from a field nearby the field experiment at Lanna. The monoliths were collected in June 2013 and then stored in a cool barn for 6 weeks before they were entered into the ground in the lysimeter facility, which was placed at Lanna, around 500 m from the field experiment on clay soil. Grass was sown between the lysimeters, in order to reduce the weather exposure of the crop. The construction was very similar to the one decribed by Bergström and Johansson, (1991) with water sampled underground individually for each lysimeter.

2.3.2 Manure

The manure was homogenized and divided into 205 g and 137 g large portions of heifer and sow manure respectively, to correspond to 20- and 30- tons ha^{-1} or roughly 150 kg ha^{-1} total N when applied to the lysimeters. For the homogenization we first used scissors to cut the straw in the manure into 2–3 cm long pieces, before mixing it all with a spoon. The portions were stored in the freezer until manure application during the following 3-year period. Manure was applied in either October, November or March depending on treatment (Table 3) during three consecutive years starting in autumn 2013. Prior to manure application, the upper 15 cm of soil was removed and placed in a bucket. The manure was then applied, and the removed soil was returned on top. This procedure simulated manure application with immediate incorporation by ploughing. We only carried out this procedure once per year in each lysimeter, meaning that they had different ploughing times depending on time for manure application. For the unmanured treatment, ploughing was simulated in this way in October in 2013 and 2015 and in November in 2014. To avoid any difference in plant cover for different treatments (which could affect leaching) weeds were removed in all lysimeters at all times of manure application.

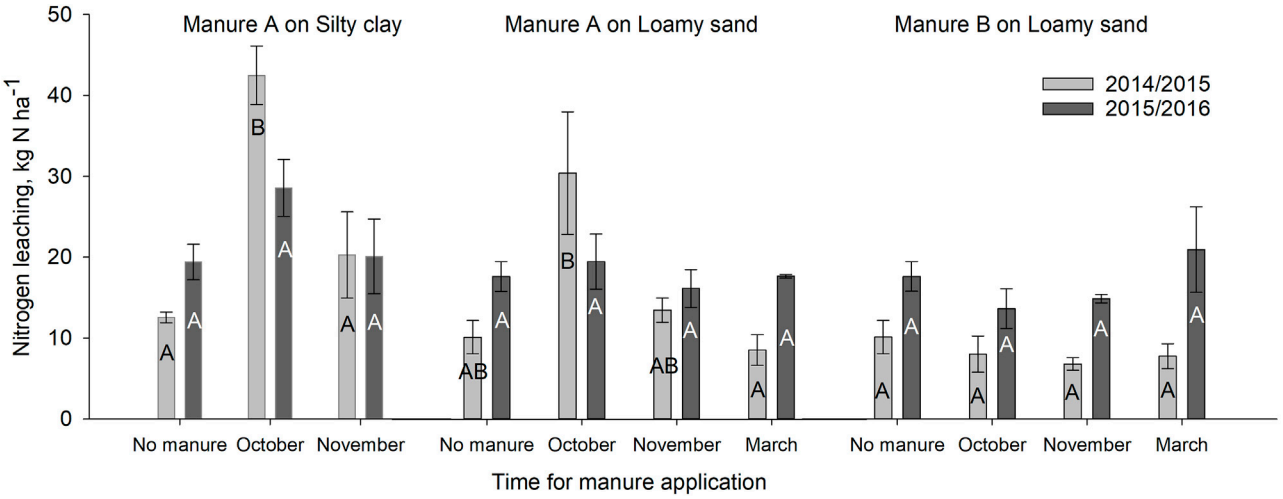


FIGURE 5
Yearly nitrogen leaching throughout the years (October-September) following the manure applications 2014/2015 and 2015/2016 which compare treatments with manure application applied at different times of the year for each manure type and soil type separately. Error bars show standard error, and the same letter indicates that the treatments are not significantly different from other treatments with the same soil and manure type within the same year.

TABLE 5 Grain yield in the field experiments at the two sites during the two different years. The same letter indicates treatments do not differ significantly ($p < 0.05$) within that experiment.

Manure	Application time	Mineral fertilizer kg N ha^{-1}	Silty clay								Loamy sand			
			2014			2015					2014		2015	
No		40	3,282		B	3,098			C		4,034	A	6,290	A
No		80	4,384	A		4,624	A				5,206	A	6,458	A
C/N 10	October	40	4,441	A		3,951		B			4,669	A	7,156	A
C/N 18	October	40									5,290	A	7,703	A
C/N 10	November	40	3,619		B	3,360			C		4,948	A	7,561	A
C/N 18	November	40									4,734	A	6,934	A
C/N 10	spring	40									4,644	A	7,068	A
C/N 18	spring	40									4,717	A	6,326	A

2.3.3 Crop management

In the years following manure application (2014–2016) and the next year with continued leaching measurements (2017), spring cereals were grown with spring oats in 2014 and 2016, spring barley in 2015, and spring wheat in 2017. The sowing was done by hand in three rows with a 10 cm distance. In addition to the applied manure, all lysimeters received mineral N fertilizer as 50 kg N ha^{-1} broadcasted ammonium nitrate (YaraBela AXAN) immediately after sowing. Weeds were removed by hand shortly after emergence. The crop was harvested at ripening by cutting the straw 10–15 cm above ground. Due to birds and moles eating parts of the harvest in 2014 and 2015, the yield measurements from the lysimeters are unreliable and thus not presented.

2.3.4 Water sampling

The drainage water from each lysimeter was assembled in containers placed underground in basement and transported in connecting pipes through free drainage. This water was sampled every second week during periods with enough drainage water (>40 mL per lysimeter) after which the containers were emptied. Throughout the periods with very large amounts of drainage water, sampling was done with only a 1-week interval, to avoid overflow in the water collection containers. During the first few months (until March 2014), the accumulated drainage runoff for the sampling period was measured in connection with sampling. After this, scales with continuous logging were installed and values for drainage runoff were logged for each 15 min period.

TABLE 6 Nitrogen leaching, including 95% confidence interval (95%conf), according to calculations made with the NLeCCs system (Johnsson et al., 2016) with different manure application times, soils, and C/N ratio.

Soil	Manure		N Leaching	
	Time	C/N	year 1	95% conf
			kg Nha^{-}	kg Nha^{-1}
sandy loam	30-sep	20	50.0	4.5
sandy loam	14-okt	20	45.6	4.5
sandy loam	15-nov	20	39.6	4.4
sandy loam	30-dec	20	37.9	4.3
sandy loam	14-mar	20	36.6	4.3
sandy loam	30-sep	13	56.7	5.0
sandy loam	14-okt	13	50.6	4.8
sandy loam	15-nov	13	41.6	4.5
sandy loam	30-dec	13	38.5	4.4
sandy loam	14-mar	13	36.8	4.3
clay	30-sep	13	14.6	1.8
clay	14-okt	13	12.7	1.6
clay	15-nov	13	10.2	1.5
clay	30-dec	13	9.5	1.4
clay	14-mar	13	9.1	1.4

2.3.5 Water analysis

The total N concentrations in drainage water were determined by using the combustion method, according to the European standard (SS-EN 12260:2004). The instrument used was TOC-VCPH, including TNM-1 and ASI-V (Shimadzu). The sum of N in NO3- and NO2- was determined by the photometric method according to the standard SS-EN ISO 15293–1:2013, and the instrument used was a Gallery Discrete Analyzer (Thermo Fisher Scientific).

2.3.6 Leaching calculations and statistical analysis

Nitrogen leaching was calculated for each lysimeter by multiplying the measured drainage volumes by its nitrogen concentration for each sampling period. The calculated leaching was then summarized for each year ranging from 1st October until 30th September. Differences in yearly leakage between treatments on the sandy soil were analyzed using a three-way factorial ANOVA with manure type, soil type, and application time as the independent variables. Tukey's test (confidence interval of 95%) was used to investigate differences among treatments. To verify assumptions for ANOVA, normal probability tests were performed on the residuals. Only for the very last dates of nitogen concenteration, assumptions were not met. For this data, the Box-cox transformation options "No transformation" and "Optimal λ" were tested to see if transformation was required. Since data transformation did not have any significant effects on the results, the results of comparing non-transformed data are presented.

2.4 Soil incubations

Two incubation experiments were performed for this study. In the first, the relations between mineral N content in soil after manure addition and the C/N-ratio of the manure was studied using thirteen different manures from various animals (cattle, pigs, sheep, horses and minks) and the loamy sand soil from

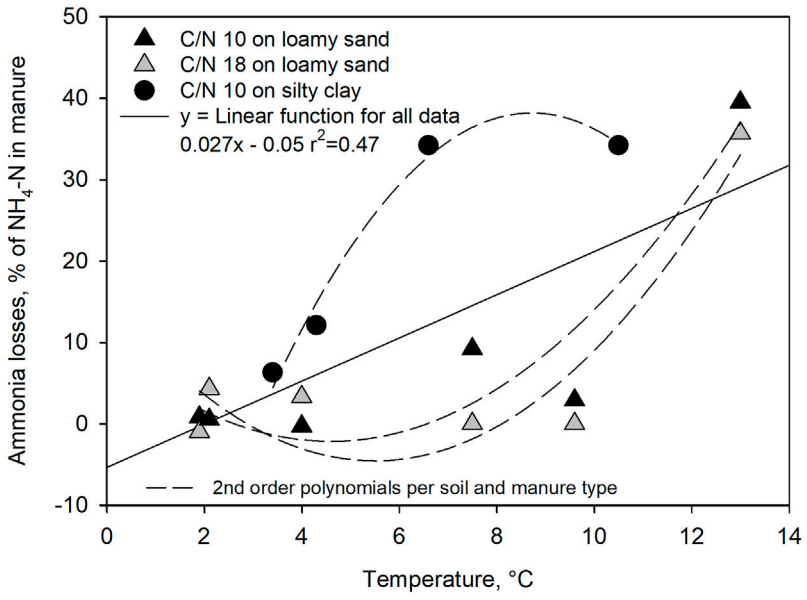


FIGURE 6
ammonia emission from manure application until ploughing (20 h) depending on temperature after application with the two manure types on the two soil types.

10.3389/fenvs.2024.1488638

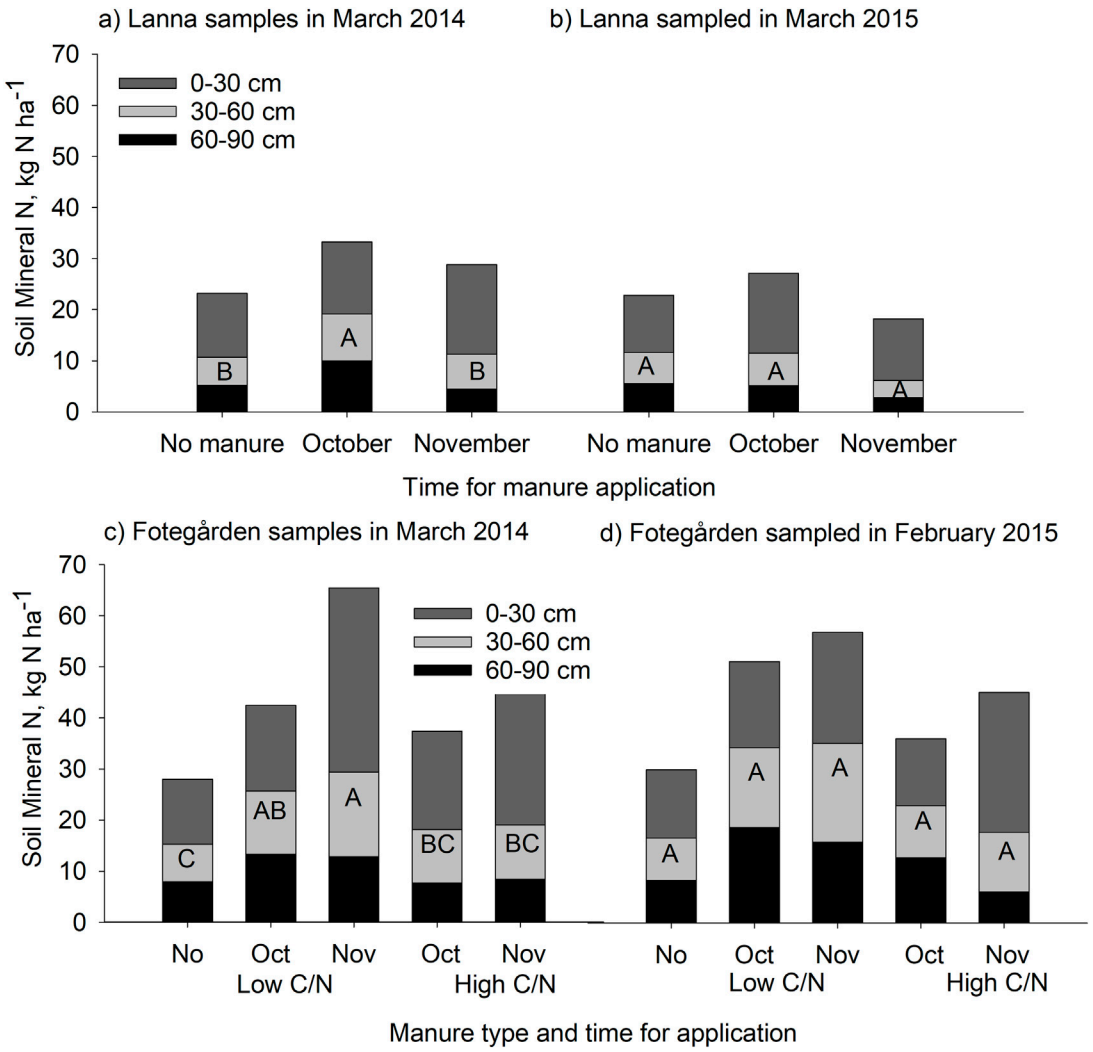


FIGURE 7
Soil Mineral N in soil profiles in the experiment at Lanna in **(A)** March 2014 and **(B)** March 2015 and in the experiment at Fotegården in **(C)** March 2014 and **(D)** February 2015. Bars that don't share the same letter differ significantly ($p < 0.05$) in soil mineral N content in the subsoil (30–90 cm depth).

Fotegården (Table 1). In the second incubation, the effects of soil type on mineral N content in soil was studied by repeating the incubation with two manures (Table 2) on the silty clay soil from Lanna (Table 1). The incubations were performed in metal cylinders that were 5 cm high and 7 cm wide. Manure corresponding to 6-ton dry matter ha^{-1} was sandwiched between two layers of soil that was watered to 50 or 60% of water holding capacity on the silty clay and loamy sand, respectively. The cylinders with loamy sand were prepared by adding 125 g soil, then the manure and finally another 125 g of soil. Due to the soil structure of the silty clay, it could not be prepared in the same way. Instead, those cylinders were taken out from the field. When arriving in the lab the soil was gently pushed so that half the column entered a second cylinder, and it was then divided into two parts with a knife. After adding the manure to one of the half-filled cylinders, the other half could be returned. To obtain equal amounts of soil in all the cylinders, some soil was removed from each one until the soil weight reached 300 g. The reason for adding the manure as a layer in the middle, rather than mixing it with the soil, was to imitate when manure is incorporated by ploughing and to retain a field like structure of the silty clay.

The cylinders were placed in 10°C and sampled after 0, 7, 28 and 56 days. To prevent the soil from drying out and to also maintain an aerobic environment, the cylinders were placed on grids in closed boxes that were aerated at least twice a week. A sufficient amount of cylinders were prepared to sample three replicates at each sampling date. At sampling, the whole cylinders were poured into plastic bags and put in the freezer. The samples were milled in a frozen state and subsamples of 40 g were extracted with 100 mL 2 M KCl (Mulvaney, 1996). The ammonium (NH_{4+}) and nitrate (NO_{3-}) analyses were then carried out using colorimetric methods on a Seal AA3 auto-analyzer (SEAL Analytical Inc., Mequon, Wisconsin, United States).

From the results the amount of mineral N supplied from manure addition to soil was calculated by subtracting the min N content from the unmanured control. This is hereafter referred to as *Net*

mineral N release, expressed as % of added total N. It provides a measure of potentially plant-available N from manure, and was calculated according to Equation 2:

$$\text{Net mineral N release} = \frac{\text{Mineral N in soil with slurry} - \text{Mineral N in control soil}}{\text{Total N added with slurry}} \quad (2)$$

2.5 Modelling

To ensure the results from these experiments were in line with models that describe nitrogen leaching after manure application, nitrogen leakage was calculated using the NLeCCS system (Johnsson et al., 2022), which includes the SOILNDB simulation tools (Johnsson et al., 2002). This system is used for calculations of leakage to report to different commissions for water protection (HELCOM, OSPAR and EEA). The model setup from the PLC6-calculations was used (Johnsson et al., 2016). The NLeCCS method calculates nitrogen leaching from arable land, using a 30-year climate data series assumed to represent normal climate. Climate conditions and agricultural management represent leaching regions. The climate series was run a total of 500 times with a crop sequence that included the crops grown in the leaching region in the proportion reported by Statistics Sweden (SCB, 2014). Also, the fertilizer regimes (*Only mineral fertilization* and *Manure fertilization with supplementary mineral fertilization*) were distributed in the crop sequence according to Statistics Sweden (SCB, 2014). The calculated leaching region was lr 5a (Johnsson et al., 2016).

Calculations of nitrogen leaching after application of manure at five different points between 30 September and 14 March, before sowing of spring barley, was made for a crop sequence where manure application occurred a sufficient number of times. Ploughing was carried out the day after manure application. Calculations were made for similar soil types (clay and sandy loam) and for manure types with similar C/N-ratios and ammonium contents as in our experiments, as well as the leaching region where the experiments were performed.

3 Results

3.1 Soil incubations

The measured increase in mineral N content in soil directly after manure addition correlated well (r^2_{adj} = 0.92***) but was only about 80% of what was added with manure (Figure 3A). Also, after 7, 28, and 56 days there was a strong correlation (r^2_{adj} = 0.84–0.89***), but with somewhat flatter regression lines (Figure 3A). The later measurements indicated a net immobilisation of around 25% of the added ammonium N until day 56 in the treatments with the highest amounts of ammonium added, while for the manures with initial low contents of ammonium N added there was a slight net mineralisation of up to 4% of total N added. There was not any significant correlation (r^2_{adj} = 0.18–0.30) between the C/N-ratio of the manure and net mineral N release to soil from manure addition, although there was a tendency (p = 0.06) for exponential decay (Figure 3B). However, none of the manures with C/N-ratios above 11 resulted in mineral N contents above 15% mineral N of added total N at any time throughout the measuring period.

3.2 Nitrogen leaching in lysimeters

The nitrogen concentration in drainage water was higher during certain periods in treatments B and I, which are the treatments where manure A (with a low C/N-ratio) is applied in early autumn on loamy sand and silty clay respectively (Figure 4). In treatment B (on sandy soil), the nitrogen concentration was significantly higher compared to other treatments on that soil in sampling dates from 19 January 2015 until 31 March 2015. This means a time lag of 3.5 months between surface application in beginning of October until significant effect appeared in leachate. In treatment I (on silty clay) the nitrogen concentration was significantly higher than in the treatment without manure on that soil, and occasionally also higher than in the treatment with later manure application, during the period 13 November 2014 until 7 January 2017, which is a time lag of only 1.5 months between surface application and effect on leachate.

During the first year of measurement (1 October 2013–30 September 2014), the nitrogen concentration was unusually high in all treatments, likely due to mineralisation of dead plant material during the period after drilling up the soil monoliths. Therefore, the focus is hereafter mainly given to the two following years (1 October 2014–30 September 2016), as they could be considered to better mirror a field situation. Due to the high nitrogen concentrations in drainage water during the first year of measurements, leaching during this year was also high and ranged from 58 to 119 kg N ha^{-1}. The highest leaching that was measured within each soil type was in the treatments with early autumn application of manure A, but there were no significant differences within the soil types. For the two following years (Figure 5), early autumn application of manure A was significantly higher in both years on the silty clay and in the year 2014/2015 on the loamy sand. The evaluation was on average for both years 10 kg N per ha on loamy sand (p = 0.07) and 15 kg ha^{-1} on silty clay (p = 0.02) compared to application in November (Figure 5).

3.3 Results from field experiments

3.3.1 Grain yield

The grain yield was similar between application times of manure, with no significant yield differences on the loamy sand (Table 5). However, on the clay soil the yield was significantly lower after application in November compared to October (Table 5).

3.3.2 Ammonia emissions

The measured ammonia emissions varied between 0% and 40% of applied NH_4-N (Table 6). The emission was positively correlated with temperature (Figure 6). The average temperature after manure application in October was 10°C, which resulted in an average ammonia emission of 24% of NH_4-N. In November and March, the temperatures were on average only 3°C and 5°C and the average ammonia emissions were limited to 4% and 2% of NH_4-N respectively. The differences in ammonia emissions between

occasions with high temperatures could not be explained by differences in wind speed. There were no significant differences in emissions depending on manure or soil type, although the emissions on clay soil appeared as though they were larger (Figure 6).

3.3.3 Soil mineral N profiles

On clay soil, soil mineral nitrogen in the subsoil (30–90 cm) was elevated with 8 kg N ha^{-1} in March 2014 after application of manure A in October compared to application in November or no manure application (Figure 7A). In the following year, there was no significant differences found in soil mineral nitrogen in the subsoil (30–90 cm) between any of the manured treatments and the unmanured control (Figure 7B). On the sandy soil, application of manure A at both times in autumn and in both years elevated the soil mineral N content in subsoil in February-March with 10–18 kg N ha^{-1}, although in the second year this was not statistically significant (p = 0.09) (Figures 7C, D). Application of manure B did not lead to any significant elevation of soil mineral nitrogen in subsoil (Figures 7C, D).

3.4 Nitrogen leaching according to model

The nitrogen leaching during the first year after manure application, as calculated according to the NLeCCS system (Table 6), was higher the earlier the manure application was carried out before sowing. Leaching was higher after manure application in the autumn and when the ammonium content of the manure was higher and the C/N-ratio lower, but any differences depending on these manure characteristics were rather small (Table 6). Differences in leaching between soil types were high with small differences concerning the effect on leaching between earliest and latest application date on the clay soil compared to on the sandy loam (Table 6).

4 Discussion

4.1 Conformity between lysimeter and field experiments

The lysimeter study showed a similar trend of leaching from the silty clay as from the loamy sand (Figure 5). Likewise, the mineral N content in the soil profiles that were taken in late winter or early spring in the field experiments (Figure 7) reveal that nitrogen from manure applied in early autumn has moved down to the subsoil on both soil types in 2014. However, in the lysimeters, the leaching effects tended to be higher on the silty clay, whereas in the field experiments the increased mineral N content in subsoil was half as much on the silty clay as on the loamy sand. The higher transport of mineral N in the lysimeter could be due to edge effects in the lysimeter. As the soil dries, large cracks are formed in this type of soil, both in the field and in the lysimeters. However, cracking along the edges in the lysimeter may have increased this effect, which is also indicated by the quite short time lag of only 1.5 months between manure application and effect on leachate on this soil compared to 3.5 months on the lighter soil. The lighter soil was lacking macropores, and therefor had a slower response on drainage from heavy rainfall than the structured silty clay soil. Another observed difference is that on the loamy sand, there was no difference in subsoil mineral N between the two different application times in autumn, whereas on the silty clay subsoil it was only elevated after late autumn application, similar to the lysimeter experiments. The somewhat lower effect on the clay soil shown in the field experiments exhibits a closer similarity with previous observations at Lanna (Aronsson and Stenberg, 2010) and from fine textured soils in general (Hina, 2024). Since low leaching from clay soils are, at times, explained by assumed higher denitrification losses (Aronsson and Stenberg, 2010) which occur on water saturated soil (Bouwman, 1996), one could speculate that the denitrification losses may have been smaller in the lysimeters. Indeed, because they often appeared to be dry, they may never have become as saturated with water, which can be the case under field conditions when ground water level occasionally rises above the drainage depth, since that should not be possible in the freely drained lysimeters. However, Wallman and Delin (2022) found from measurements of drainage water from lysimeters in the same facility and within the same soil from the same field, that leaching levels were similar to those measured from a tile drained field facility in that very same field where the lysimeters were collected. Hence, the large effects on leaching that also occurred on the silty clay cannot be ignored.

4.2 Measured and modelled leaching

The modelled higher leaching with earlier manure application (Table 6) was in accordance with the results with Manure A in the lysimeter study. However, as opposed to the lysimeter study where the effects of Manure B on leaching were insignificant, the effect of manure application according to the model was very similar regardless of the ammonium content or the C/N-ratio. Negligible leaching after application of manure with a high C/N-ratio, as found in the lysimeter study, is supported by previous literature (Shepherd and Newell-Price, 2016; Pedersen B. N. et al., 2021). This implies that the effect of the C/N-ratio is underestimated by the model. Another disparity between the modelled and experimental results were the differences between the soil types. According to the model, leaching effects on the clay soil were rather small compared to lighter soil which is in line with other publications (Hina, 2024), as discussed above. Considering both the literature (Hina, 2024) and the results from the field experiments (Figure 7) the modelled effects of soil type may be more representative than what was observed in the lysimeter study.

4.3 Conformity with other studies

The leaching results after application of the low C/N-ratio manure were in line with those found by Thomsen (2005), who also concluded that manure applied in early autumn increased leaching losses compared to later applications that were carried out in winter or spring. However, Thomsen (2005) and Hansen

et al (2004) also found that early application improved crop N utilization, which was not applicable to the results in our field experiments, in which the yield was unaffected on the loamy sand and affected in the opposite direction on the clay soil. Reduced crop yield after late compared to early autumn ploughing was, on the other hand, in accordance with results from Stenberg et al. (1999), who suggested this to be an effect of increased growth of weeds in the late ploughed treatment. That there is a temperature dependence of ammonia emissions from manure is known from previous research and the increase from less than 5% to 20%–40% with higher emissions at fine textured soils is in line with what Pedersen J. et al. (2021) presented for animal slurries with high DM content.

4.4 Implementation

The results indicate that the risk for leaching after autumn application differ depending on the composition of the manure. Therefore, restrictions may only be relevant for manure with C/N-ratios below 14 or based on the amount of ammonium nitrogen content. Applying the manure late rather than early was unbeneficial for yield as opposed for leaching and current restrictions that only allow application before a certain date does not serve any purpose when it comes to the limitation of leaching. If farmers find it better to apply the manure later, it could also benefit from lower leaching.

5 Conclusion

The results confirm that the risk for leaching is dependent on the nitrogen and carbon composition of the manure. According to the results in this study, the risk for leaching is predominantly for manure with a C/N-ratio below 14 and the amount of leachable nitrogen is very similar to the amount of mineral nitrogen that was applied from the start. Nitrogen leaching was higher after application of manure with a low C/N-ratio in October compared to both November and April. It was affected similarly on clay soil as on sandy soil, however, indications from soil profiles suggest that leaching from clay soil may be smaller under field condition, as indicated by model calculations. The lower ammonia emissions at cooler temperatures later in the autumn also support that manure application would cause lower nitrogen losses in total after application late rather than early in the autumn. Only on clay soils, when soil conditions in late autumn may be too wet to succeed with ploughing without soil structural damage and therefore lower crop yield, earlier application can be motivated.

Data availability statement

The raw data supporting the conclusions of this article will be made available by the authors, without undue reservation.

Author contributions

SD: Conceptualization, Funding acquisition, Investigation, Project administration, Visualization, Writing–original draft, Writing–review and editing. KM: Formal Analysis, Writing–review and editing. HJ: Formal Analysis, Writing–review and editing.

Funding

The authors declare that financial support was received for the research, authorship, and/or publication of this article. This study was funded by the Swedish Research Council FORMAS (grant number 2012-00676).

Acknowledgments

Thanks to Ingrid Thomsen at Aarhus University for valuable guidance during the planning of this project, especially concerning the incubation experiments. Thanks to Lars Bergström for advice, Rolf Tunared for construction and Göran Johansson, Maria Stenberg and Tobias Carlsson for practical assistance with the lysimeter facility. Thanks to the staff at Lanna Research station for assistance with experiments in the field and in lysimeters. Thanks to all the farmers that contributed with manure and to the farmers at Fotegården that gave access to their land and their soil. Thanks also to Martin Ferm for supervision regarding ammonia emission measurements.

Conflict of interest

The authors declare that the research was conducted in the absence of any commercial or financial relationships that could be construed as a potential conflict of interest.

Publisher's note

All claims expressed in this article are solely those of the authors and do not necessarily represent those of their affiliated organizations, or those of the publisher, the editors and the reviewers. Any product that may be evaluated in this article, or claim that may be made by its manufacturer, is not guaranteed or endorsed by the publisher.

Supplementary material

The Supplementary Material for this article can be found online at: https://www.frontiersin.org/articles/10.3389/fenvs.2024.1488638/full#supplementary-material

References

Aronsson, H., Liu, J., Ekre, E., Torstensson, G., and Salomon, E. (2014). Effects of pig and dairy slurry application on N and P leaching from crop rotations with spring cereals and forage leys. *Nutrient Cycl. Agroecosyst.* 98, 281–293. doi:10.1007/s10705-014-9611-3

Aronsson, H., and Stenberg, M. (2010). Leaching of nitrogen from a 3-yr grain crop rotation on a clay soil. *Soil Use Manag.* 26, 274–285. doi:10.1111/j.1475-2743.2010.00277.x

Ayadi, F. Y., Spiehs, M. J., Cortus, E. L., Miller, D. N., and Djira, G. D. (2015). Physical, chemical, and biological properties of simulated beef cattle bedded manure packs. *Trans. ASABE* 58, 797–811. doi:10.13031/trans.58.10962

Bergström, L., and Johansson, R. (1991). Leaching of nitrate from monolith lysimeters of different types of agricultural soils. *J. Environ. Qual.* 20, 801–807. doi:10.2134/jeq1991.00472425002000040015x

Bouwman, A. F. (1996). Direct emission of nitrous oxide from agricultural soils. *Nutrient Cycl. Agroecosyst.* 46, 53–70. doi:10.1007/bf00210224

Delin, S., Stenberg, B., Nyberg, A., and och Brohede, L. (2012). Potential methods for estimating nitrogen fertilizer value of organic residues. *Soil Use Manage.* 28, 283–291. doi:10.1111/j.1475-2743.2012.00417.x

Hansen, E. M., Thomsen, I. K., and Hansen, M. N. (2004). Optimizing farmyard manure utilization by varying the application time and tillage strategy. *Soil Use* 20, 173–177. doi:10.1111/j.1475-2743.2004.tb00353.x

Hina, N. S. (2024). Global meta-analysis of nitrate leaching vulnerability in synthetic and organic fertilizers over the past four decades. *Water* 16, 457. doi:10.3390/w16030457

Johnsson, H., and Hoffmann, M. (1995). Beräkning av kväveutlakning vid olika spridningstidpunkter för stallgödsel. Avdelningen för vattenvårdslära, Sveriges lantbruksuniversitet. Teknisk rapport 11.(In Swedish)

Johnsson, H., Larsson, M., Mårtensson, K., and Hoffmann, M. (2002). SOILNDB: a decision support tool for assessing nitrogen leaching losses from arable land. *Environ. Model. and Softw.* 17, 505–517. doi:10.1016/S1364-8152(02)00013-0

Johnsson, H., Mårtensson, K., Lindsjö, A., Persson, K., Andrist Rangel, Y., and Blombäck, K. (2016). "Läckage av näringsämnen från svensk åkermark," in *Beräkningar av normalläckage av kväve och fosfor för 2013. SMED Rapport Nr 189 2016.* (In Swedish).

Johnsson, H., Mårtensson, K., Lindsjö, A., Persson, K., and och Blombäck, K. (2022). NLeCCS – a system for calculating nutrient leakage from arable land. *Ekohydrologi* 177. Uppsala: Sveriges lantbruksuniversitet.

Keskinen, R., Saastamoinen, M., Nikama, J., Särkijärvi, S., Myllymäki, M., Salo, T., et al. (2017). Recycling nutrients from horse manure: effects of bedding type and its compostability. *Agric. Food Sci.* 26, 68–79. doi:10.23986/afsci.60443

Mulvaney, R. L. (1996). "Nitrogen—inorganic forms," in *Methods of Soil Analysis, Part 3-Chemical Methods*. Editor D. L. Sparks, A. L. Page, R. H. Helmke, P. N. Leoppert, M. A. Soltanpour, C. T. Tabatabai, et al. Soil Science Society of America Book Series. (Madison, Wisconsin, United States: American Society of Agronomy and Soil Science Society of America), 1123–1184. Available at: https://doi.org/10.2136/sssabookser5.3.c38.

Loro, P. (2005). "Characterization of solid beef manure," in *A study funded by the manitoba cattle producers association* (Final Report).

Njøs, A., and Børresen, T. (1991). Long-term experiment with straw management, stubble cultivation, autumn and spring ploughing on a clay soil in S.E. Norway. *Soil Tillage Res.* 21, 53–66. doi:10.1016/0167-1987(91)90005-i

Norberg, L., and Aronsson, H. (2024). Effects of spring and autumn tillage, catch crops, and pig manure application on long-term nutrient leaching from a loamy sand. *Eur. J. Agron.* 156, 127156. doi:10.1016/j.eja.2024.127156

Pedersen B. N., B. N., Eriksen, J., Christensen, B. T., and Sørensen, P. (2021). Fertilizer replacement value and leaching of nitrogen applied to spring barley in cattle deep litter: a 3-year lysimeter study. *Soil Tillage Res.* 209, 104954. doi:10.1016/j.still.2021.104954

Pedersen, J., Nyord, T., Feilberg, A., and Labouriau, R. (2021). Analysis of the effect of air temperature on ammonia emission from band application of slurry. *Environ. Pollut.* 282, 117055. doi:10.1016/j.envpol.2021.117055

Persson, L., and Bergström, L. (1991). Drilling method for collection of undisturbed soil monoliths. *Soil. Sci. Soc. Am. J.* 55, 285–287.

Qian, P., and Schoenau, J. (2002). Availability of nitrogen in solid manure amendments with different C:N ratios. *Can. J. Soil Sci.* 82, 219–225. doi:10.4141/S01-018

SCB (2014). Gödselmedel i jordbruket 2012/2013. Mineral-och stallgödseltill olika grödor samt hantering och lagring av stallgödsel. (Use of fertilisers and animal manure in agriculture in 2012/13). *Stat. Meddel. MI 30 SM*, 1403. Available at: https://www.scb.se/contentassets/211cde08daf74ac9acf844721b15ab46/mi1001_2012b13_sm_mi30sm1402.pdf.

SCB (2020). Gödselmedel i jordbruket 2018/19 Mineral-och stallgödsel till olika grödor samt hantering och lagring av stallgödsel. (Use of fertilisers and animal manure in agriculture in 2018/19). *Statiska Meddel. MI 30 SM* 1402, 156. ISSN 1403-8978.

Shepherd, M. A., and Newell-Price, J. P. (2016). The effects of pig manure type and application timing and frequency on nitrate leaching from a seven-course arable rotation on a retentive alluvial soil. *Soil Use Manag.* 32, 117–126. doi:10.1111/sum.12223

Smith, K. A., Beckwith, C. P., Chalmers, A. G., and Jackson, D. R. (2002). Nitrate leaching following autumn and winter application of animal manures to grassland. *Soil Use Manag.* 18, 428–434. doi:10.1111/j.1475-2743.2002.tb00262.x

Sørensen, P., and Rubæk, G. H. (2012). Leaching of nitrate and phosphorus after autumn and spring application of separated solid animal manures to winter wheat. *Soil Use Manag.* 28, 1–11. doi:10.1111/j.1475-2743.2011.00382.x

Stenberg, M., Aronsson, H., Linden, B., Rydberg, T., and Gustafson, A. (1999). Soil mineral nitrogen and nitrate leaching losses in soil tillage systems combined with a catch crop. *Soil Tillage Res.* 50, 115–125. doi:10.1016/s0167-1987(98)00197-4

Svensson, L. (1994). A new dynamic chamber technique for measuring ammonia emissions from land-spread manure and fertilizers. *Acta Agric. Scand. Sect. B–Soil and Plant Sci.* 44, 35–46. doi:10.1080/09064719409411255

Svensson, L., and Ferm, M. (1993). Mass transfer coefficient and equilibrium concentration as key factors in a new approach to estimate ammonia emission from livestock manure. *J. Agric. Eng. Res.* 56, 1–11. doi:10.1006/jaer.1993.1056

Thomsen, I. K. (2005). Crop N utilization and leaching losses as affected by time and method of application of farmyard manure. *Eur. J. Agron.* 22, 1–9. doi:10.1016/j.eja.2003.10.008

Wallman, M., and Delin, S. (2022). Nitrogen leaching from tile-drained fields and lysimeters receiving contrasting rates and sources of nitrogen. *Soil Use Manage.* 38, 596–610. doi:10.1111/sum.12724

frontiers | Frontiers in Environmental Science

TYPE Original Research
PUBLISHED 06 December 2024
DOI 10.3389/fenvs.2024.1479754

Check for updates

OPEN ACCESS

EDITED BY
Jana Levison,
University of Guelph, Canada

REVIEWED BY
Ziyi Li,
University of Illinois at Urbana-Champaign, United States
Hao Wang,
University of Minnesota Twin Cities, United States

*CORRESPONDENCE
D. L. Burton,
dburton@dal.ca

RECEIVED 12 August 2024
ACCEPTED 11 November 2024
PUBLISHED 06 December 2024

CITATION
Burton DL, Wilts HDM and MacLeod JA (2024) Dissolved nitrous oxide emissions associated with agricultural drainage water as influenced by manure application.
Front. Environ. Sci. 12:1479754.
doi: 10.3389/fenvs.2024.1479754

COPYRIGHT
© 2024 Burton, Wilts and MacLeod. This is an open-access article distributed under the terms of the Creative Commons Attribution License (CC BY). The use, distribution or reproduction in other forums is permitted, provided the original author(s) and the copyright owner(s) are credited and that the original publication in this journal is cited, in accordance with accepted academic practice. No use, distribution or reproduction is permitted which does not comply with these terms.

Dissolved nitrous oxide emissions associated with agricultural drainage water as influenced by manure application

D. L. Burton[1]*, H. D. M. Wilts[2] and J. A. MacLeod[3]

[1]Department of Plant, Food, and Environmental Sciences, Dalhousie University, Truro, NS, Canada, [2]Department of Biology, University of Prince Edward Island Faculty of Science, Charlottetown, PE, Canada, [3]Retired, Charlottetown, PE, Canada

Nitrous oxide (N_2O) is highly water soluble and can be readily transported in waters draining from agricultural fields. Relatively few studies have quantified N_2O losses through agricultural tile drainage systems and none have compared the effect of different sources of applied nitrogen or their timing of application. While IPCC guidelines provide estimates of emissions from agricultural drainage water, the uncertainty in these estimates is relatively high. This research quantifies N_2O loss in tile drainage water, as influenced by nitrogen source and timing. The study site was located at Agriculture Canada research station, Harrington, PE, Canada and consisted of 12 plots with subsurface drainage systems installed at approximately 80 cm, separated by buffer drains. Three swine manure treatments were considered with inorganic fertilizer (ammonium nitrate) as a control, each replicated three times. Manure treatments included fall and spring application of solid swine manure and spring application of liquid swine manure, all applied to supply 120 kg N ha^{-1}. The magnitude of N_2O loss, as measured from samples collected at the tile outlets, demonstrated significant episodic emissions. Annual cumulative dissolved N_2O emissions ranged from 0.1 to 5.69 kg N ha^{-1} (mean 0.83 kg N ha^{-1}), while emissions from the soil surface were 0.09–1.16 kg N ha^{-1} (mean 0.33 kg N ha^{-1}). N_2O emissions in tile water were not significantly affected by the form of N applied, however tile drain length significantly impacted tile water N_2O concentration. IPCC coefficients for N_2O emissions from agricultural drainage water would underestimate actual N_2O emissions at this site.

KEYWORDS

nitrous oxide-N_2O, drainage water, nitrogen loss by drainage, nitrate, greenhouse gas emmissions, nitrogen source, nitrogen timing

Introduction

Nitrous oxide (N_2O) is a long-lived and potent GHG with a global warming potential 298 times that of carbon dioxide and is also the leading anthropogenic cause of stratospheric ozone depletion (IPCC, 2021; WMO, 2014). Agriculture is the largest anthropogenic source of N_2O (Janzen et al., 1999; Flessa et al., 2002; IPCC, 2023; Syakila and Kroeze, 2011) producing over 60% of N_2O emissions globally from inorganic (fertilizer) and organic (manure) sources (IPCC, 2022), with annual contributions of 2.8 Gt CO_2-eq yr^{-1} (IPCC, 2023). In Prince Edward Island (PEI), Canada, agricultural activities are responsible for

approximately 90% of human induced N_2O emissions, with direct emissions from denitrification on agricultural soils, and indirect emissions that occur after nitrogen has been transported off agricultural fields, accounting for 80% of N_2O released (Environment and Climate Change Canada, 2022). In humid and sub-humid climates such as PEI microbial denitrification is the dominant process responsible for N_2O production in agricultural soils due to anoxic conditions that frequently develop as a result of high precipitation rates (Aulakh et al., 1984; Gauder et al., 2012; Granli and Bøckman, 1994; Kavdir et al., 2008).

Our understanding of global N_2O dynamics remains incomplete due to the existence of unknown or poorly quantified sources and sinks of N_2O and the complexity and interaction of mechanisms controlling the known N_2O sources (Baggs, 2011; Chapuis-Lardy et al., 2007). N_2O is produced in soils as a result of ammonia oxidation, nitrification and denitrification, and it's production is affected by climatic factors such as soil temperature, moisture, and freeze-thaw cycles (Shakoor et al., 2021; Choudhary et al., 2002; Maag and Vinther, 1996; Granli and Bøckman, 1994; Gillam et al., 2007), as well as management practices such as nitrogen addition, tillage, and cropping system (Venterea et al., 2011). There is a need to measure N_2O emissions from a greater range of agricultural sources and from a greater diversity of areas, both regionally and within the landscape, to allow improved quantification of national N_2O emissions inventories (Rochette and McGinn, 2008). Understanding the spatial and temporal nature of emission processes is also important in refining and accurately estimating emissions. The IPCC recognizes indirect N_2O emissions from agriculture, including those resulting from nitrogen leaching and runoff (N_2O_L). There is a greater degree of uncertainty in indirect N_2O emissions, as fewer studies have quantified these sources (Nevison, 2000; Quesnel et al., 2019; ECCC, 2022). Furthermore, indirect sources can be difficult to measure, since emissions are removed from their point of origin (Reay et al., 2003; Roper et al., 2013) and, in the case of dissolved N_2O emissions, may be confounded by subsurface soil interactions (Quesnel et al., 2019). The steps outlined by the IPCC in calculating indirect N_2O emissions involve several assumptions, relying on general nitrogen cycling principles and a limited amount of field data (ECCC, 2022). There is a need for further quantification and study of the factors influencing indirect N_2O emissions.

Leaching and run off are estimated to account for more than 75% of indirect N_2O emissions from agriculture, with leaching being the largest contributor, and represents one of largest sources of uncertainty in estimates of agricultural N_2O emissions (Nevison, 2000; Tian et al., 2019). In Canada's National Inventory Report to the IPCC the fraction of nitrogen that is lost through leaching and runoff ($FRAC_{LEACH}$) is estimated as a function of the ratio of precipitation to evapotranspiration and ranges from 5% in the more arid regions of the country to 30% in the more humid regions of the country (ECCC, 2022). The percentage of this nitrogen lost as N_2O (N_2O_L) from N leached from agricultural soils is estimated using leaching/runoff emission factor (EF_5) of 0.0075 kg N_2O-N kg^{-1} N leached (IPCC, 2019). Nevison (2000) indicated several uncertainties in the proposed IPCC methodology for calculating the N_2O emissions through leaching and run off. Since emissions from this source are likely to be significantly influenced by climate there is a need for data from a broader range of agroecosystems. The factor further assumes a relationship between N_2O and NO_3^- concentration in agricultural drainage water. This relationship has not been well documented with some studies (Sawamoto et al., 2003) showing little or no relationship between N_2O and NO_3^- in drainage waters, with high dissolved N_2O concentrations in the fall corresponding with low NO_3^- levels. This disconnect was explained by spatial differences in where these processes were occurring; increased dissolved N_2O concentrations were attributed to subsoil denitrification which occurred during or after NO_3^- leaching had occurred (Sawamoto et al., 2003). As a result, there is a need to develop appropriately documented regional emission coefficients.

Subsurface tile drainage is a management practice used in imperfectly and poorly drained agricultural fields to prevent water logging, lower a perched water table, and drain excess water from fields (Valayamkunnath et al., 2022). Subsurface tile drainage also decreases soil structural damage, erosion, and increases the length of the effective growing season by allowing earlier access to fields (Valayamkunnath et al., 2022). In Atlantic Canada, tile drainage water flows intermittently during year and drainage events can occur during the winter period, when temperatures in the soil profile rise above freezing. Peak drainage events typically occur during spring thaw, which may coincide with peak surface N_2O emissions. In northern climates, up to 70% of N_2O emissions from agricultural soils are thought to occur during spring thaw, as a result of enhanced microbial activity and the release of N_2O trapped under a frozen ice layer (Risk et al., 2013; 2014; Wagner-Riddle et al., 2017). Tile drains intercept the flow of the water draining from the root zone and its composition is often considered to be representative of the nutrients draining from an agricultural field (Valayamkunnath et al., 2022). Several studies have documented that loss of nitrogen through subsurface tile drainage is substantial (Nangia et al., 2010; Quesnel et al., 2019; Milburn et al., 1997; Drury et al., 1993; Randall et al., 1997). In more humid agroecosystems such as PEI, it has been concluded that 15%–50% of the applied nitrogen reaches surface water via subsurface drainage (Jiang et al., 2012). Most studies of nitrogen loss in tile drainage have focused on the losses of NO_3 and NH_4^+ (Drury et al., 1993; Klavidko et al., 1991; Randall et al., 1997), however fewer studies have examined dissolved N_2O (Bruun et al., 2017; Hack and Kaupenjohann, 2002; Hama-Aziz et al., 2017; Reay et al., 2004; Reay et al., 2009; Quesnel et al., 2019).

Nitrous oxide produced below the soil surface results in the accumulation of N_2O in the soil profile due to impeded gas transport by water-filled pores and/or formation of frozen layer during winter and spring thaw (Burton and Beauchamp, 1994; Heincke and Kaupenjohann, 1999). Nitrous oxide is highly soluble in water and its solubility increases as the water temperature decreases (DelVecchia et al., 2023). During winter and spring, cold water moves through the soil profile when N_2O concentrations are elevated (Burton and Beauchamp, 1985). These conditions result in a high potential for N_2O transport and loss in tile drainage water (Valayamkunnath et al., 2022). Moreover, agricultural fields with tile drainage expedite the movement of water from the field and therefore decrease the likelihood of further N_2O reduction in the subsurface (Hack and Kaupenjohann, 2002; Valayamkunnath et al., 2022). Dowdell et al. (1979) noted significant amounts of dissolved N_2O (8.1–277.3 μg N_2O-N L^{-1}) in water draining from agricultural

fields. Similarly, other studies have variously reported dissolved N_2O concentrations in tile drainage water from agricultural systems ranging from 0.3–1,108 ug N L^{-1} (Bruun et al., 2017; Hama-Aziz et al., 2017; Quesnel et al., 2019; Reay et al., 2003; 2004; 2009; Roper, 2008).

Data is lacking on the impact of N input form (synthetic fertilizers vs. manure) and timing on dissolved N_2O losses from agricultural fields. While several studies have examined dissolved N_2O losses in agricultural fields under manure inputs (Reay et al., 2009; Quesnel et al., 2019), none have compared different manure/N application treatments. Furthermore, the timing of manure application to agricultural fields is known to impact NO_3 leaching, with fall manure applications elevating leaching risk relative to spring (van Es et al., 2006). It is unknown whether this also applies to dissolved N_2O losses. Currently, there is limited measured data documenting N_2O concentrations and loss from tile drainage systems, particularly during the winter period. The effect of soil management, such as various cropping systems and fertilizer applications, on N_2O losses via tile drainage systems also needs more study. The quantification of N_2O production during the non-growing period and its transport from the soil profile into the tile drainage water are needed to provide a more complete picture of the impacts of agricultural management on indirect N_2O emissions and identify opportunities for mitigation. Furthermore, to date only one study has considered the relative magnitude of dissolved N_2O loss compared to surface N_2O emissions and NO_3 leaching (Quesnel et al., 2019).

This paper investigates N_2O losses in agricultural tile drainage water from a 3-year potato cropping rotation in PEI, Canada. Objectives of the study were to 1) quantify and compare the annual temporal variation in N_2O and NO_3^- concentrations in tile drainage systems and surface N_2O emissions in PEI 2) determine the impact of swine manure treatment form (solid and liquid) and timing (fall and spring application) on dissolved N_2O losses in tile drainage water and 3) evaluate the EF_5 for predicting N_2O emitted from nitrogen lost through leaching in PEI.

Materials and methods

Study site

The field experiment was initiated in 2000 at Agriculture and Agri-Food Canada's Harrington Research Farm, situated 14 km north of Charlottetown, PE (46° N lat, 63° W long). The research site covers an area of 2.9-ha with a gentle slope of 1%–3%. Between 1986 and 1989 the site was divided into 13 subsurface drainage plots, each with dimensions ranging from 0.21 to 0.28 ha (Milburn et al., 1997). Tile drainage systems were installed to account for individual plot size and drainage capacity. Each plot contained two tile drains within the plot, and individual plots were separated by buffer drains to limit cross-contamination from adjacent plots due to subsurface or surface flow crossing plot boundaries. Three shorter tile drains were installed in plots 8, 9 and 10 to accommodate the irregular shape of the field. The tile drains were spaced at an interval of 12 m in plots 8, 9 and 10, and 15 m in the remaining plots. The tiles were placed at an average depth of 0.80 m and the drains discharged into tipping buckets housed in a heated discharge building.

The soils at the experimental site are Charlottetown sandy loam (Orthic Humo-Ferric Podzol), with a Malpeque sandy loam (Gleyed Eluviated Drystic Brunisol) occurring in plots 7, 8, 10, and 11 in the lower portions of the field, and a soil pH of 6.6 (Milburn et al., 1997). Charlottetown soils tend to be well drained, while Malpeque soils are imperfectly drained (MacDougall et al., 1988). Daily precipitation and soil temperature was recorded at the Harrington research farm meteorological station, located less than 1 km from the experimental site.

Nitrogen fertility treatments and cropping practices

The agronomic treatments consisted of 4 N fertility treatments applied prior to potato phase of the potato-barley-red clover rotation. The N treatments were: solid and liquid swine manure applied in the spring prior to planting of potatoes; solid manure applied in the fall prior to the potato year and NH_4NO_3 applied in the spring. Each treatment was replicated three times and the rate of application adjusted to supply 120 kg N ha^{-1}. Swine manure was generated in an adjacent facility that produced both solid and liquid manure (Campbell et al., 2003). During fall 2000 and 2003, solid swine manure was applied, while in spring 2001 and 2004 solid swine manure, liquid swine manure and ammonium nitrate were applied (Table 1). The experimental site was cropped to potato (Solanum tuberosum (L.) var. Shepody) in 2001 and 2004, to barley (Harem vulgare (L.) var. Iona) under-seeded to red clover (Trifolium pretense (L.) var. Marino) in 2002, and to red clover in 2003. In the spring of the barley year all plots received 60 kg N ha^{-1} as NH_4NO_3.

Water sampling and analysis

Water sampling for dissolved N_2O

The concentration of N_2O dissolved in tile drainage water was measured by collecting grab samples at the outlet of the drainage tiles during flow events in 2002, 2003 and 2004 (see supplementary for details on sample collection process). Samples were collected on a weekly basis or when drainage events were occurring. The diurnal pattern of N_2O emissions was examined by collecting samples every 4 hours over a 3-day flow event on April 27–29, 2004.

The NO_3^- and NH_4^+ content and temperature of tile water discharge was determined from water samples collected as part of a parallel study using ISCO 6712 automatic samplers (Teledyne ISCO Inc., Lincoln, NB) (Jiang et al., 2011) (see supplementary for details on sample collection process).

During the 2002 to 2004 observation period the frequency of sampling depended upon tile flow. During flow events samples were collected between 0800 and 0900 h. The flow rate for each tile drain was calculated by multiplying the total number of tips of the tipping bucket by the amount of water each bucket holds. The tipping buckets were wired to a data logger (Campbell Scientific, Logan, UT). Tile drainage water N_2O emissions were calculated by accounting for individual plot flow rate on each sampling date. Cumulative N_2O emissions were calculated by linear interpolation of N_2O concentrations over the sampling dates for each flow event

TABLE 1 Management practices for the experimental site from 2000 to 2004.

Year	Management practices
2000	Red clover
	Oct. 2 - Fall application of solid manure treatment at a rate to supply 120 kg N ha^{-1} Oct. 16 - Incorporation of manure and plow down of red clover crop
2001	Potato
	May 16 - Spring application and incorporation of ammonium nitrate, liquid manure, and solid manure treatments at a rate to supply 120 kg N ha^{-1} May 21 - Planting of potato crop Oct 10 - Harvesting of potato crop
2002	Barley
	May 28 – Planting of barley under-seeded with red clover May 28 – Application and incorporation of ammonium nitrate at 40 kg N ha^{-1} Sept. 4 - Harvest of barley crop
2003	Red clover
	July 9 - Red clover 1st cut Oct. 2 - Fall application of solid manure treatment at a rate to supply 120 kg N ha^{-1} Oct. 16 - Incorporation of manure and plow down of red clover crop Oct. 31 – Herbicide (Transorb @ 3 L ha^{-1}) application
2004	Potato
	May 17 – Spring application of ammonium nitrate, liquid manure, and solid manure treatments at a rate to supply 120 kg N ha^{-1}

and these concentrations applied to daily water flow as measured by the tipping bucket flow meters.

There is uncertainty as to the degree of degassing of N_2O that occurs as water runs along the tile drainage pipes. The influence of tile length on N_2O concentration was evaluated by sampling the three in-field tile drainage systems at plot #8, which was in addition to the 12 experimental plots where the agronomic treatments were replicated. Plot eight received the treatment of 120 kg N ha^{-1} NH_4NO_3. The total length of each tile drain in this plot was 81.5 m (see supplementary for details on sample collection process).

Stream and spring water sampling

On 28 May 2004, water samples were collected from streams and springs to compare their dissolved N_2O concentration with that of subsurface drainage water. The stream was situated adjacent to the research site, with subsurface drainage water flowing into it. Spring samples were also collected at a nearby location. Stream and spring water samples were collected by 5 mL disposable syringe (Luer-lok tip, latex free, Becton-Dickinson, Franklin Lakes, NJ), injected immediately in an exetainer (12 mL) with sodium azide and sealed with silica sealant.

Water sample analysis

Vials containing water samples for N_2O analysis were equilibrated at room temperature (25°C) before being analyzed for headspace N_2O concentration. N_2O analysis was performed using a Varian Star 3,800 Ga Chromatograph (Varian, Mississauga, ON) fitted with an electron capture detector with a Combi-PAL autosampler (CTC Analytics, Zwingen, Switzerland). The autosampler removes a 2.5 mL volume from the sample tube and injects this into a sample valve that delivers 0.1 mL to the ECD. The ECD was operated at 300°C, 90% Ar, 10% CH_4 carrier gas at 20 mL min^{-1}, Haysep N 80/100 pre-column (0.32 cm diameter x 50 cm length) and Haysep D 80/100 mesh analytical columns (0.32 cm diameter x 200 cm length) in a column oven operated at 70°C. Pre-column was used in combination with a four-port valve to remove water from the sample. Operational conditions and data handling was performed with Varian Star software. In each analytical run of 147 samples a single replicate of three concentrations of standard gas mixtures were included for standardization of the instrument. The lab temperature was recorded during the analysis of dissolved N_2O concentration. Total N_2O dissolved in the water sample is the sum of N_2O in the headspace and N_2O dissolved in water. The molar mass of N_2O in the headspace was calculated from the Ideal gas law (Equation 1).

$$M_{N_2O_g} = \frac{\left(P_{N_2O} * 10^{-6}\right) \times V_{N_2O}}{R \times T} \quad (1)$$

Where: M_{N2Og} = moles of N_2O in vial headspace (mol); P_{N2O} = partial pressure of gas in the headspace (atm); V_{HS} = Volume of headspace (L); R = Gas constant (0.08214 atm/mol k); and T = lab temperature (°K).

Henry's law (Equation 2) describes the partitioning of a compound between a dilute aqueous and the gas phase:

$$C_{N_2O} = H_{N_2O} \times P_{N_2O} \quad (2)$$

Where: C_{N2O} = Nitrous oxide concentration in the aqueous solution (moles/L); H_{N2O} = Henry's law constant for nitrous oxide (2.5×10^{-2} M/atm), and P_{N2O} = partial pressure of gas in the headspace (atm).

M_{N2Ol} (Equation 3) is caclulated from C_{N2O} present in V (5 mL) of the aqueous solution (1 mL of sodium azide and 4 mL of water sample).

$$M_{N_2O_l} = C_{N_2O} \times V \quad (3)$$

Where: M_{N2Ol} = Moles of the nitrous oxide in dissolved in water (moles); V = Volume of the aqueous solution in the vial (L).

Therefore, the total number of moles of nitrous oxide in the vial (Equation 4), less the estimated contribution of nitrogen by sodium azide (5.3×10^{-8} mol) is,

$$T_{N_2O} = \left(M_{N_2O_g} + M_{N_2O_l}\right) - \left(5.3 \times 10^{-8}\right) \quad (4)$$

Where: T_{N2O} = Total moles of nitrous oxide in head space and aqueous solution (moles).

The flux of dissolved N_2O (g N ha^{-1} d^{-1}) was calculated by multiplying the dissolved N_2O concentration by the volume of tile drainage discharge per unit area (L ha^{-1}) as measured by the tipping bucket gauges and the area of the plot drained by the tile system.

Nitrate and ammonium concentration of the water samples were determined colorimetrically using a TRAACS 800 analyzer (Milburn et al., 1997). Dissolved organic carbon was analyzed by Formacs TOC analyzer (Hasegawa et al., 2000).

Nitrous oxide production from sodium azide

An experiment was carried out to determine if the sodium azide produced any N_2O during storage. Sodium azide solution was prepared at the same concentration as used in the exetainers for dissolved N_2O sample collection (0.1 M). One mL of NaN_3 was injected into a 12 mL exetainers using a 1 mL syringe (Luer-lok tip, latex free, Becton-Dickinson, Franklin Lakes, NJ), followed by flushing with helium and evacuation. After evacuation, 4 mL of nano pure water was transferred to the exetainer by means of a syringe (5 mL, Luer-lok tip, latex free, Becton-Dickinson, Franklin Lakes, NJ), ensuring a positive pressure inside the exetainer. Some vials were analyzed immediately for head space N_2O concentration, while others were kept at lab temperature and analyzed after 1 month to determine the extent of N_2O production from the sodium azide. Sodium azide was found to contribute background levels of N_2O of approximately 5.3×10^{-8} mol of N_2O.

Nitrous oxide flux at the soil surface

N_2O flux measurements were made using a non-flow-through, non-steady-state (NFT-NSS) chamber with a total volume of 1.6 L covering a soil area of 315 cm^2. Deployment times were kept to 30 min with samples being collected at 0, 10, 20 and 30 min. Replicate (5) samples of the atmosphere at chamber height at the time of deployment were used to estimate the ambient (time zero) concentrations. Samples were collected by removing 20 mL of gas from the headspace of the chamber and injecting into previously evacuated (to 500 millitorr) 12 mL Exetainers (Labco, UK), each containing 4 mg of Magnesium Perchlorate-a desiccant to remove water from the gas samples. Five replicates of two standard gases were collected on each sampling occasion and were used to confirm the integrity of sample storage and handling.

N_2O flux measurements were made from 9 May to 26 September 2001, 14 May to 28 August 2002 and 16 May to 27 November 2003, and 10 March to 27 May 2004. Flux sampling conducted during the snow cover period (March 10 and 25, 2004), was carried out by inserting chambers into the snow (2–3 cm depth), and with samples collected in a similar manner as in the snow free period described. Two chambers were inserted in each plot. In 2001, when cropped to potato, these two chambers were separated by location: One chamber was installed in the hill and one in the furrow row locations within each plot. The hill and furrow locations were measured separately due to the distinctly different soil, nutrient and crop growth environments within these two locations. The chambers were removed and replaced to accommodate any management practices in the experimental site.

N_2O flux (F_{N2O}) was calculated by the following Equation 5 (Hutchinson and Livingston, 1993):

$$F_c = \left(\frac{dC}{dt}\right)\left(\frac{V_c * Mmol}{A * Vmol}\right) \quad (5)$$

Where, dC/dt is the rate of change of N_2O concentration inside the chamber (g N h^{-1}), A is the surface area of the chamber (0.0315 m^2), V_c is the total volume of the chamber (1.62 L), M_{mol} is molar mass of N_2O (44 g/mol) and V_{mol} is the volume of a mole of N_2O inside the chamber calculated from the ideal gas law based on temperature and pressure. The relative change in N_2O concentration with time (dC/dt), inside the chamber, was calculated by simple linear regression. Cumulative N_2O-N losses were calculated by linear interpolation between sampling dates.

N_2O analysis was performed using a Varian Star 3,800 Ga Chromatograph using the same method as for headspace N_2O concentration of the water samples.

Statistical analysis

An ANOVA on dissolved N_2O concentration was performed as a randomized complete block (RCB) design, according to treatment for each sampling date. Correlation analysis was done between dissolved N_2O concentration and NO_3^-, surface N_2O flux, dissolved organic carbon, tile flow, water temperature, and plot area. Correlation analysis was also done between cumulative N_2O loss and tile length of the experimental plots. Regression analysis was performed between cumulative N_2O and NO_3^- loss in subsurface tile drainage water. All statistical analysis was conducted using Statistical Analysis System (SAS institute, 1990).

Results and discussion

Climatic data

Two of the three non-growing periods examined had lower than normal precipitation (Table 2). Cumulative non-growing season precipitation (November to May) for 2001–2002 and 2003–2004 was 531 and 380 mm respectively significantly lower than the long-term (1971–2000) average of 701 mm (Table 2) (Government of Canada, 2019). In 2002–2003 higher than average rainfall resulted from four high rainfall events including a 90 mm precipitation event (Table 2; Figure 1B). The duration and extent of soil freezing varied considerably between years (Figure 1) despite the average non-growing season air temperature being similar over the three winter periods. In 2001–2002 the lowest soil temperature at 5 cm was - 0.2°C and the soil was only frozen for 24 days (March 6 to March 30; Figure 1A). In contrast, in 2002–2003, the soil was frozen to a depth of 5 cm for 119 days (November 27 to April 29) and was frozen to 10 cm for 93 days (January 16 to April 19; Figure 1B). In 2003–2004, the soil at 5-cm depth was frozen for 41 days (January 5 to February 15) and at 10-cm depth for 22 days (January 13 to February 4; Figure 1C). Differences in soil freezing despite small differences in average air temperatures reflect differences in snow cover with the 2002–2003 period having relatively little precipitation in the early part of the winter and therefore having little or no snow accumulation. The tile flow for the observation period ranged between <1 and 54.5 mm per day (data not shown). The cumulative tile flow for the 2002, 2003 and 2004 calendar years was 156, 99, and 68 mm respectively. The greater cumulative tile flow in 2002 corresponded to the milder temperatures during the 2001–2002 overwinter period. Peak tile flow was observed during spring thaw and following precipitation events.

TABLE 2 Mean temperature and total precipitation at the experimental site during the growing (May–October) and non-growing (November–April) periods.

		Mean temperature (°C)	Total precipitation (mm)
2001	Growing	15.4	394
	Non-Growing	−2.4	531
2002	Growing	13.5	643
	Non-Growing	−2.2	746
2003	Growing	14.7	503
	Non-Growing	−3.3	380
2004	Growing	13.9	363
	Non-Growing	−3.3	470

Dissolved N_2O emissions

Effect N treatments on dissolved N_2O

Dissolved N_2O concentrations in tile water discharge exhibited significant differences between sampling dates (p = 0.001) but were not significantly affected by nitrogen source (NH_4NO_3, solid manure and liquid manure) or timing (spring and fall application) of N application to the potato rotation (Table 3A; Table 3B; Figure 2). There are several possible explanations for this. In their meta-analysis examining the impact of manure applications on surface N_2O emissions in agricultural soils, Xia et al. (2020) found that the application of manure and synthetic fertilizers induced similar magnitude N_2O emissions when applied at the same N rate. While the overall emission factor following manure application (1.11%) is slightly lower than that of synthetic N fertilizer (1.25%), manure N_2O emissions were also impacted by factors such as C:N ratio and C content (Xia et al., 2020), which resulted in similar levels of emissions produced. It is reasonable to assume that this would also apply to dissolved N_2O below the soil surface. Additionally, while N fertilizer application has been found to be associated with elevated concentrations of dissolved N_2O and NO_3^- in water draining from agricultural fields (Hasegawa et al., 2000), since the processes responsible for producing dissolved N_2O in drainage water are spatially and temporally complex, the relationship between dissolved N_2O and N application rate may not be straightforward (Reay et al., 2004; Quesnel et al., 2019). For example, fertilizers and manures are applied and measured at or near the soil surface and can subsequently be transported by leaching and surface runoff. In contrast, N_2O can be produced throughout the soil profile; therefore, even after NO_3^- has been depleted from the soil surface, N_2O can still be being produced in the soil, resulting in a temporal disconnect in the presence of these substances due to spatial differences in where they are measured and/or produced. It is possible that these same processes could make it difficult to detect differences in N source treatments. Failure to detect differences in treatments may have also resulted from differences in the length of drainage pipe from the plot to the collection station. We noted an inverse relationship between the lengths of the tile lines and averaged observed dissolved N_2O concentrations (Figure 3). To confirm this observation air and water sampling access ports were inserted at three locations along the perforated portion of the tile line and at one location just outside the plot on an adjacent site. Average dissolved N_2O concentrations over ten sampling events were observed to decrease from 1.1 mg N_2O-N L^{-1} to 0.3 mg N_2O-N L^{-1} (Figure 4). These observations suggest that degassing of N_2O was occurring in the tile line and that concentrations measured at the sampling hut may underestimate total N_2O leaving the field. Normalizing all results for length of tile line did not, however, reveal significant N treatment effects. For the remainder of the discussion, we will consider trends observed across all 12 experimental units independent of N treatment.

Cumulative dissolved and surface N_2O losses

Annual cumulative dissolved N_2O emissions ranged from 0.01 to 5.69 kg N ha^{-1} (mean 0.83 kg N ha^{-1}) which were slightly higher than annual cumulative N_2O emissions occurring from the soil surface of 0.09–1.16 kg N ha^{-1} (mean 0.33 kg N ha^{-1}) (Table 3A). The dissolved N_2O-N loss through subsurface drainage water was an order of magnitude less than NO_3^--N, which ranged from 0.26 to 29.3 kg N ha^{-1} (mean 8.7 kg N ha^{-1}; Table 3A). The dissolved N_2O results in our study are higher than other values of dissolved N_2O in tile drains reported in the literature, which ranged from 0.03–0.38 kg N_2O-N $ha^{-1}yr^{-1}$ (Dowdell et al., 1979; Hack and Kaupenjohann, 2002; Reay et al., 2004; 2009; Quesnel et al., 2019). Similarly, Reay et al. (2009), observed annual dissolved losses of N_2O in agricultural drainage that were higher than the amount being emitted at the soil surface. In contrast, Bruun et al. (2017) found that the main export pathway was dissolved N_2O, with negligible N_2O produced at the soil surface, and both Dowdell et al. (1979) and Hack & Kaupenjohann, (2002) concluded that N_2O loss in agricultural drainage water was a minor component of the soil N balance. However, Quesnel et al. (2019) found that cumulative annual soil surface N_2O emissions (13.8 kg N_2O-N ha^{-1}) were much higher than dissolved N_2O losses (0.03 kg N_2O-N ha^{-1}) in tile drainage systems. Hama-Aziz et al. (2016) observed concentrations of dissolved N_2O in agricultural tile drainage systems were comparable to NO_3 concentrations. Our results indicate that dissolved N_2O emissions from potato cropping systems can be a major source of agricultural N_2O emissions in PEI–comparable or higher than surface N_2O emissions. This is likely because the majority of precipitation occurs in the non-cropping season in PEI, when conditions at the soil surface may be less favorable for denitrification and may prevent the release of N_2O produced in deeper soil layers to the atmosphere. However, large amounts of NO_3^- are still lost from these tile drainage systems.

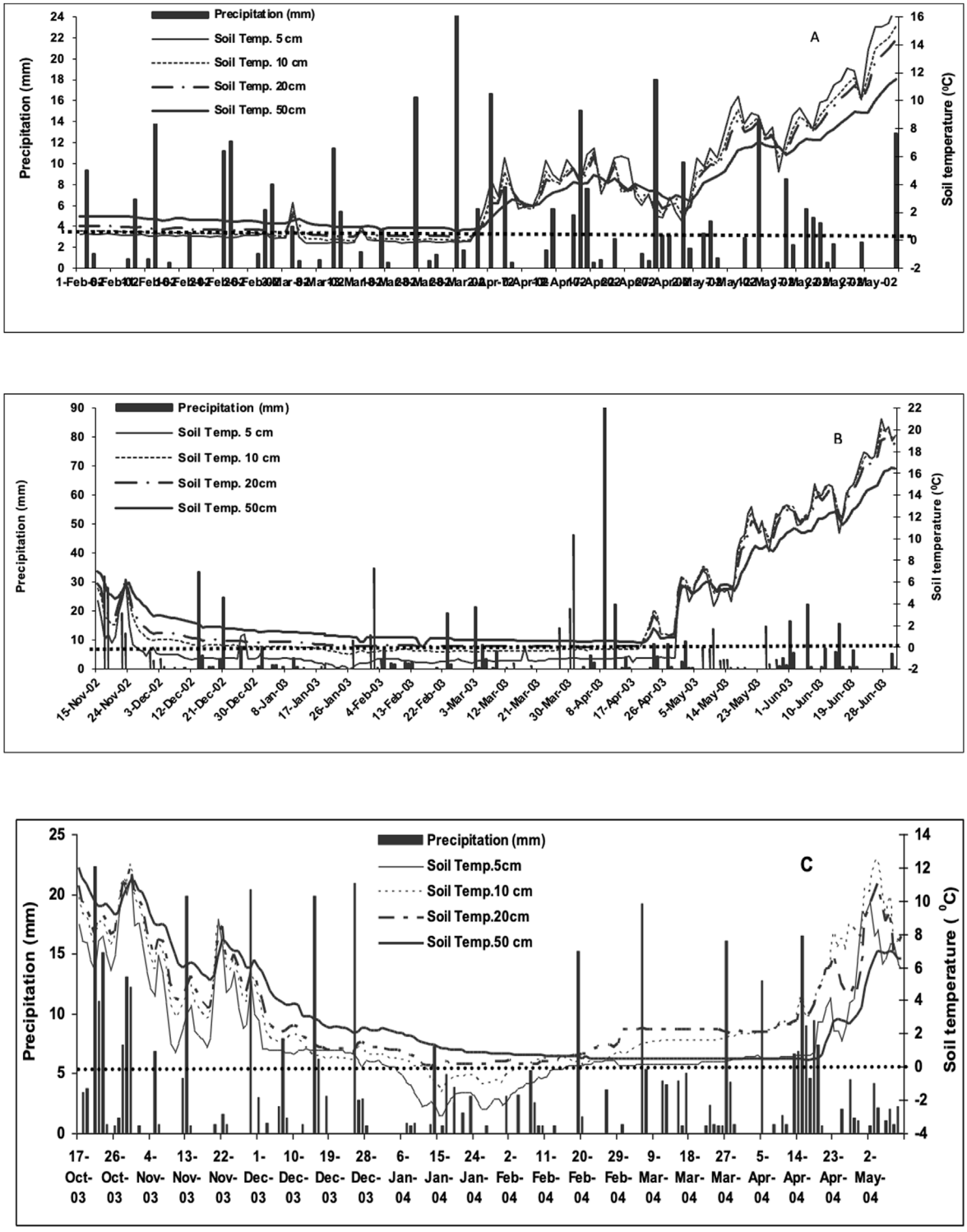


FIGURE 1
Precipitation and soil temperature during fall to spring periods at the Harrington Research station from **(A)** February - May 2002, **(B)** November 2002 to June 2003 and **(C)** October 2003 to May 2004.

Temporal variation in dissolved N_2O

N_2O loss in tile drainage water was strongly influenced by season with up to 62% of N_2O emissions occurred during the non-growing season (Figure 2A). One or two high N_2O emission events can contribute a significant amount for that particular year (Figure 2B). Dissolved N_2O concentrations exhibited high temporal variability and were independent of the volume of tile flow (data not shown). For instance, in 2003, the highest and lowest dissolved N_2O concentrations (3.8 mg N L^{-1}, 0.01 mg N L^{-1}) were observed within a timespan of several days during the same flow event. A study of dissolved N_2O

TABLE 3 (Panel A) Mean and range of values (12 plots) for cumulative annual N_2O and NO_3 dissolved in drainage water and surface N_2O flux from research plots as measured during the 2002, 2003 and 2004 monitoring periods and (Panel B) mean and range of values (3 replicates) for cumulative annual N_2O dissolved in drainage water from each N treatment as measured during the 2002, 2003 and 2004 monitoring periods.

Year	N_2O surface flux	N_2O dissolved in drainage water	Drainage as % of total N_2O loss	NO_3 dissolved in drainage water
		(kg N ha^{-1})		
Potato	0.46 (0.16–1.16)			
Winter 2002		0.54 (0.01–1.82)†	54%	16.9 (1.0–29.3)
Barley	0.15 (0.09–0.23)			
Winter 2003		1.73 (0.02–5.69)	82%	4.5 (0.14–12.6)
Red Clover	0.37 (0.18–0.48)			
Winter 2004		0.23 (0.02–0.42)	38%	4.8 (0.26–11.1)

Year	NH_4NO_3	Spring liquid manure	Spring solid manure	Fall solid manure
		(kg N ha^{-1})		
Potato				
Winter 2002	0.30 (0.17–0.53)	0.25 (0.01–0.67)	0.97 (0.01–1.82)	0.63 (0.06–1.3)
Barley				
Winter 2003	1.67 (1.22–2.13)	0.96 (0.02–1.47)	1.32 (0.13–2.34)	3.00 (0.54–5.69)
Red Clover				
Winter 2004	0.19 (0.11–0.24)	0.19 (0.01–0.31)	0.27 (0.03–.42)	0.26 (0.10–0.41)

†Mean (range of value) for 12 plots.
†Mean (range of value) for 3 replications.

emissions over a 36-h monitoring period observed a mean concentration of 0.48 mg N L^{-1}, a coefficient of variation of 46%, with values ranging from 0.13 to 0.81 mg N L^{-1}. Reay et al. (2003) have observed similar variation in dissolved N_2O in agricultural drainage waters. Peak dissolved N_2O concentrations (4.2 mg N L^{-1}) recorded in this study were higher than those reported by others (Dowdell et al., 1979; Hack and Kaupenjohann, 2002; Hasegawa et al., 2000; Minami and Fukushi, 1984; Minami and Oshawa, 1990; Reay et al., 2003; Sawamoto et al., 2002; Sawamoto et al., 2003).

Over the monitoring period dissolved N_2O concentrations of water collected from tile lines ranged from less than 0.01 mg N L^{-1}–4.2 mg N L^{-1} (Figure 2B). The highest dissolved N_2O concentrations occurred during winter 2003 (Figure 2B). A continuous frozen layer was present from 27 November 2002 to 29 April 2003, which may have prevented gas phase transport of N_2O to the soil surface and resulted in an accumulation of N_2O in the atmosphere of subsurface layers (Burton and Beauchamp, 1994). Elevated N_2O concentrations in the soil atmosphere would result in greater N_2O dissolution in soil water and a supersaturated soil solution. As N_2O is highly soluble in cold water, there is a high probability that the water draining through the soil profile at this time would contain a high concentration of dissolved N_2O (Goodroad and Keeney, 1984). In the tile flow of 2001–2002 and 2003–2004, N_2O emissions were much lower than 2002–2003. The winter pattern is similar for both years, with the soil at 5 cm depth freezing only for a few days at a time. Furthermore, there was precipitation at regular intervals from November to March in both 2001–2002 and 2003–2004 (Figures 1A, C). The lack of a continuous frozen layer and regular precipitation would favor more rapid NO_3^- leaching, reducing the opportunity for N_2O production and accumulation in the subsurface. The relative contribution of surface and sub-surface pathways appears to site-specific and may vary significantly from year to year.

Relationship between dissolved NO_3 and dissolved N_2O

During the observation period, dissolved NO_3^- emissions from tile lines fluctuated between 0.09 and 39 mg N L^{-1} (Figure 2B). In general, the NO_3^- concentrations observed in this study are comparable to previous studies conducted at this site (Milburn et al., 1997) and to values reported by others (Dowdell et al., 1979; Hack and Kaupenjohann, 2002; Hasegawa et al., 2000; Minami and Fukushi, 1984; Minami and Oshawa, 1990; Quesnel et al., 2019; Reay et al., 2003; Sawamoto et al., 2002; Sawamoto et al., 2003). The timing of manure and fertilizer applications to the potato crop (fall 2000, spring 2001, fall 2003, spring 2004) influenced the magnitude of NO_3^- loss in tile water. After the potato harvest in 2001, the research plots were left fallow. The NO_3^- not utilized by the potato crop and accumulating in the soil increased the loss of NO_3^- in the tile flow during 2001–2002 non-growing period (Figure 2B). Low rates of nitrogen fertilizer (40 kg N ha^{-1}) were applied to barley crop across all N treatments in 2002, reducing fall NO_3^- accumulation in the soil and the loss of NO_3^- via tile drainage flow during the 2002–2003 non-growing period (Figure 2B).

There was a significant ($p < 0.01$) negative correlation between dissolved N_2O-N and NO_3^--N concentration for individual

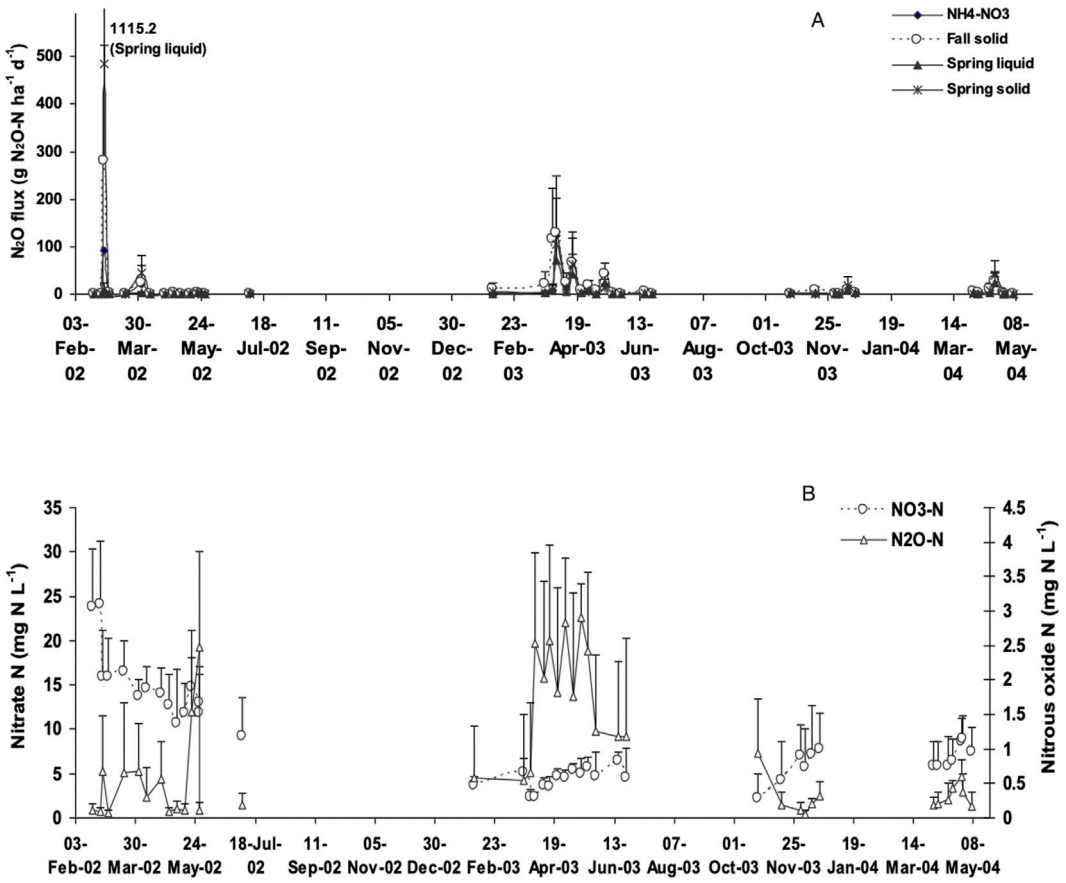


FIGURE 2
(A) Treatment effect on N2O flux from agricultural drainage water, and **(B)** N2O-N and NO3-N concentration in weekly samples of agricultural drainage water.

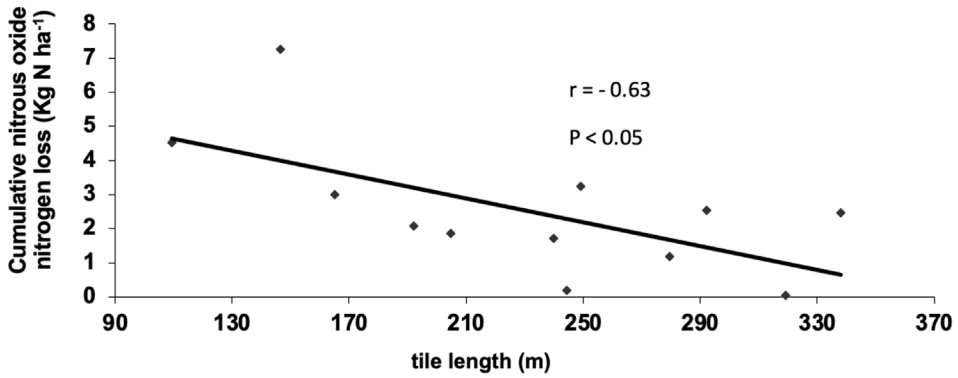


FIGURE 3
Relationship between cumulative N2O-N loss and tile length.

observations, but this accounted for less than 10% of the total variation in the data (R^2 = 0.05; Figure 5A). These results are similar to Sawamoto et al. (2003) and Reay et al. (2004), who both found little or no relation between N_2O-N and NO_3^--N concentration in agricultural drainage water. In contrast others have observed a positive relationship between dissolved N_2O-N and NO_3^--N in agricultural drainage waters (Hack and Kaupenjohann, 2002; Minami and Oshawa, 1990; Reay et al., 2003). Dowdell et al. (1979) and Hack and Kaupenjohann (2002) have noted NO_3^- concentrations are typically one to three orders of magnitude higher than N_2O concentrations. In our study N_2O and NO_3^- concentration were one to two orders of magnitude greater than dissolved N_2O concentrations, depending on season (Table 3A).

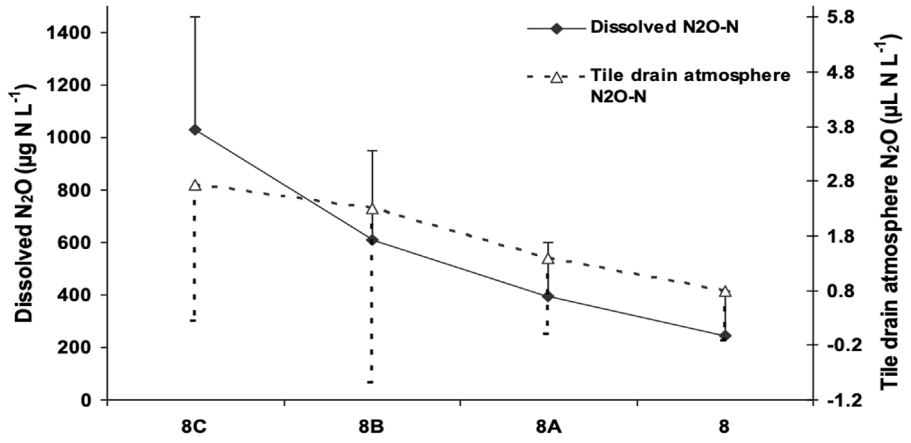


FIGURE 4
Dissolved N2O and tile drain atmosphere N2O concentration at three locations along a tile drain in plot# 8 (8A, 8B, 8C) and at the tile drain outlet of plot# 8 (8). Error bars represent the standard deviation of the 12 water and air samples taken during different days (between November 14 to 19 Dec 2003 and April 1 to 6 May 2004). Error bars are presented in opposite directions for the clarity of the figure.

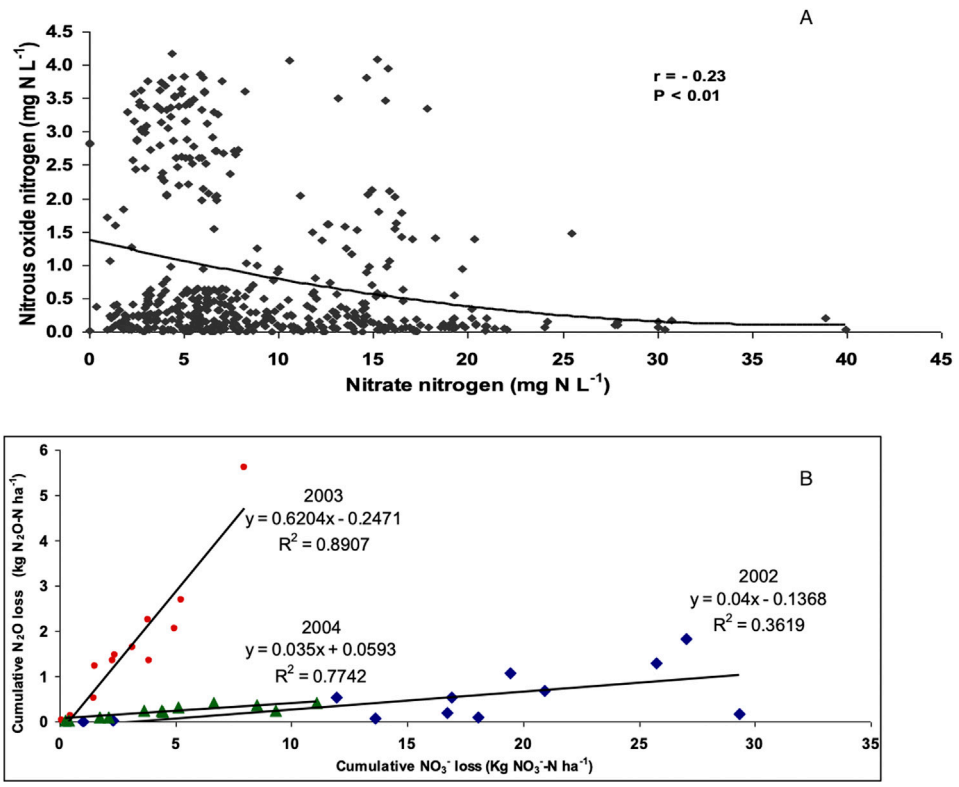


FIGURE 5
(A) Daily N2O-N loss vs. NO3-N loss in tile drainage water from a potato - barley - red clover rotation for 2002, 2003 and 2004, and **(B)** Cumulative N2O-N loss vs. cumulative NO3-N loss for 2002, 2003 and 2004.

The strength of the relationship between dissolved N_2O-N and NO_3^--N was much greater when cumulative losses were examined. A significant ($p < 0.001$) positive relationship existed between cumulative annual N_2O-N and NO_3^--N losses (Figure 5B). The slope of this relationship was significantly greater in 2003 than in the other 2 years of study. The relationships within individual years accounted for a much greater percentage of the total variation ranging from 36% to 89% of the total variation (Figure 5B).

The difference in the relationship between N_2O and NO_3^- concentrations in drainage water for individual sampling events (Figure 5A) vs. cumulative annual N losses (Figure 5B) provides an interesting contrast. The rather weak negative relationship in the weekly samples indicates that the processes resulting in these losses are

TABLE 4 Mean and range of values of N_2O concentrations in tile drainage water, stream water and spring water.

Water system	N_2O concentration
($\mu g\ N\ L^{-1}$)	
Tile drainage water	372 (4.0–778.2)†
Stream water	18.23 (8.4–33.1)‡
Spring water	36.08 (9.3–67.1)‡

†Mean (range of value) for 12 samples.
‡Mean (range of value) for 3 samples.

independent at this time scale or that these processes are occurring at different location and are thus exposed to different environmental conditions. However, the positive relationship between N_2O and NO_3^- for each year of observation indicates that over this longer timeframe both processes appear to be responding to similar controls. In essence the leakiness of the system with respect to nitrogen is similarly expressed in terms of both of NO_3^- and N_2O losses. These losses simply are not observed at the same time at the end of the tile drain. These results are similar to Quesnel et al. (2019), who observed a significant positive relationship between mean dissolved N_2O-N and NO_3^--N concentrations during the growing season, however they found that the relationship became weaker in the non growing season. They attributed this to the greater complexity of N_2O production and transport in the non-growing season. Overall, our results indicate that a positive relationship exists between NO_3^- and N_2O, but that these processes are spatially and/or temporally separate.

IPCC coefficient and dissolved N_2O emissions

Currently the IPCC coefficients for N_2O emissions from agricultural drainage is calculated as a fixed fraction of the NO_3^--N estimated to be lost from the soil profile (EF_5 = 0.0075 kg N_2O-N kg^{-1} N leached). Here, on an annual basis the ratio of kg N_2O-N lost per kg NO_3^--N leached ranged from 0.035 to 0.62 kg N_2O-N kg^{-1} N leached. These values are significantly higher than the IPCC coefficient for this site in these years and therefore would underestimate the actual N_2O emissions at this site.

Dissolved N_2O concentration in different water systems

To determine whether the water being discharged from the agricultural fields was enriched relative to the adjacent streams, water samples were collected on 28 May 2004 from subsurface tile drainage, stream and spring water. These samples displayed significant variation in dissolved N_2O concentrations (Table 4). Dissolved N_2O concentrations in stream and spring water were 8.4–33.1 $\mu g\ N\ L^{-1}$ (mean 18.2 $\mu g\ N\ L^{-1}$) and 9.0–67.1 $\mu g\ N\ L^{-1}$ (mean 36.1 $\mu g\ N\ L^{-1}$), respectively, while N_2O concentrations of water being discharged from the tile drainage system ranged from 4.0 to 778 $\mu g\ N\ L^{-1}$(mean 372 $\mu g\ N\ L^{-1}$). This indicates that the tile drainage water was enriched in dissolved N_2O prior to being released into the waterway. Low N_2O concentrations in stream water were likely reflect the degassing of dissolved N_2O degassing to the atmosphere following discharge, as was observed over the length of the tile line. This suggests that large amounts of indirect N2O loss can occur after the tile drain water enters the stream.

Conclusions

Annual tile drainage losses of dissolved N_2O from this site were substantive, approaching that of surface N_2O emissions. The nature of the winter period had important implications for the magnitude and timing of dissolved N_2O emissions. The presence of a continuous period of sub-zero soil and air temperatures resulted in greater dissolved N_2O emissions than occurred under more moderate winter temperatures. There was significant spatial and temporal complexity in the nature of dissolved N_2O emissions that complicated their characterization at a field scale.

Nitrogen application treatments, source and timing had no effect on the magnitude of dissolved N_2O loss. On an event basis, dissolved N_2O emissions were not correlated with NO_3^- concentrations. Dissolved N_2O and NO_3^- losses appeared to be occurring at different times, however, examined on a seasonal basis, plots with high NO_3^- losses also exhibited high dissolved N_2O loss.

Subsurface tile length influenced N_2O discharge from subsurface tile drainage water, indicating the presence of a sink within the system. Consequently, our results likely underestimate N_2O produced at the field level. More study is needed to understand the magnitude and fate of these N_2O losses.

Data availability statement

The raw data supporting the conclusions of this article will be made available by the authors, without undue reservation.

Author contributions

DB: Conceptualization, Formal Analysis, Funding acquisition, Investigation, Methodology, Project administration, Resources, Supervision, Writing–original draft, Writing–review and editing. HW: Data curation, Formal Analysis, Visualization, Writing–original draft, Writing–review and editing. JM: Conceptualization, Investigation, Methodology, Supervision, Writing–original draft, Writing–review and editing.

Funding

The author(s) declare that financial support was received for the research, authorship, and/or publication of this article. We would also like to acknowledge Agriculture and Agri-Food Canada's Biological Greenhouse Gas Sources and Sinks program, Nova Scotia Department of Agriculture, and Natural Sciences and Engineering Research Council for funding this research.

Acknowledgments

We would like to acknowledge the technical assistance of Balakumar Thangaraj, Brian Murray, and Drucie Janes in the collection and analysis of NO_3^- and N_2O concentration of tile water samples.

Conflict of interest

The authors declare that the research was conducted in the absence of any commercial or financial relationships that could be construed as a potential conflict of interest.

Publisher's note

All claims expressed in this article are solely those of the authors and do not necessarily represent those of their affiliated organizations, or those of the publisher, the editors and the reviewers. Any product that may be evaluated in this article, or claim that may be made by its manufacturer, is not guaranteed or endorsed by the publisher.

Supplementary material

The Supplementary Material for this article can be found online at: https://www.frontiersin.org/articles/10.3389/fenvs.2024.1479754/full#supplementary-material

References

Aulakh, M. S., Rennie, D. A., and Paul, E. A. (1984). Gaseous nitrogen losses from soils under zero-till as compared with conventional-till management systems. *J. Environ. Qual.* 13 (1), 130–136. doi:10.2134/jeq1984.00472425001300010024x

Baggs, E. M. (2011). Soil microbial sources of nitrous oxide: recent advances in knowledge, emerging challenges and future direction. *Curr. Opin. Environ. Sustain.* 3 (5), 321–327. doi:10.1016/j.cosust.2011.08.011

Bruun, J., Hoffmann, C. C., and Kjaergaard, C. (2017). Convective transport of dissolved gases determines the fate of the greenhouse gases produced in reactive drainage filters. *Ecol. Eng.* 98, 1–10. doi:10.1016/j.ecoleng.2016.10.027

Burton, D. L., and Beauchamp, E. G. (1985). Denitrification rate relationships with soil parameters in the field. *Commun. Soil Sci. Plant Anal.* 16, 539–549. doi:10.1080/00103628509367626

Burton, D. L., and Beauchamp, E. G. (1994). Profile nitrous oxide and carbon dioxide concentrations in a soil subject to freezing. *Soil Sci. Soc. Am. J.* 58, 115–122. doi:10.2136/sssaj1994.03615995005800010016x

Campbell, A. J., Van Lunen, T. A., MacLeod, J. A., Hurnik, D., and Linkletter, G. (2003). Design and performance of a swine finishing barn for production and manure research. *Can. Biosyst. Eng.* 45, 5.1–5.6.

Chapuis-Lardy, L. Y. D. I. E., Wrage, N., Metay, A., Chotte, J. L., and Bernoux, M. (2007). Soils, a sink for N2O? A review. *Glob. Change Biol.* 13 (1), 1–17. doi:10.1111/j.1365-2486.2006.01280.x

Choudhary, M. A., Akramkhanov, A., and Saggar, S. (2002). Nitrous oxide emissions from a New Zealand cropped soil: tillage effects, spatial and seasonal variability. *Agric. Ecosyst. Environ.* 93, 33–43. doi:10.1016/s0167-8809(02)00005-1

DelVecchia, A. G., Rhea, S., Aho, K. S., Stanley, E. H., Hotchkiss, E. R., Carter, A., et al. (2023). Variability and drivers of CO2, CH4, and N2O concentrations in streams across the United States. *Limnol. & Oceanogr.* 68 (2), 394–408. doi:10.1002/lno.12281

Dowdell, R. J., Burford, J. R., and Crees, R. (1979). Losses of nitrous oxide dissolved in drainage water from agricultural land. *Nature* 278, 342–343. doi:10.1038/278342a0

Drury, C. F., McKenney, D. J., Findlay, W. I., and Gaynor, J. D. (1993). Influence of tillage on nitrate loss in surface runoff and tile drainage. *Soil Sci. Soc. Am. J.* 57, 797–802. doi:10.2136/sssaj1993.03615995005700030028x

ECCC (Environment and Climate Change Canada) (2022). *National inventory Report 1990-2020: Greenhouse gas sources and sinks in Canada*. Canada: Ottawa.

Flessa, H., Ruser, R., Schilling, R., Loftfield, N., Munch, J. C., Kaiser, E. A., et al. (2002). N_2O and CH4 fluxes in potato fields: automated measurement, management effects and temporal variation. *Geoder* 105, 307–325. doi:10.1016/s0016-7061(01)00110-0

Gauder, M., Butterbach-Bahl, K., Graeff-Hnninger, S., Claupein, W., and Wiegel, R. (2012). *Soil-derived trace gas fluxes from different energy crops - results from a field experiment in southwest Germany*. Great Britain: Blackwell Publishing Ltd.

Gillam, K. M., Zebarth, B. J., and Burton, D. L. (2007). Nitrous oxide emissions from denitrification and the partitioning of gaseous losses as affected by nitrate and carbon addition and soil aeration. *Can. J. Soil Sci.* 88, 133–143. (in press). doi:10.4141/cjss06005

Goodroad, L. L., and Keeney, D. R. (1984). Nitrous oxide emissions from soils during thawing. *Can. J. Soil Sci.* 64, 187–194. doi:10.4141/cjss84-020

Government of Canada (2019). Canadian climate normals 1981-2010 station data. Available at: https://climate.weather.gc.ca/climate_normals/results_1981_2010_e.html?searchType=stnProv&lstProvince=PE&txtCentralLatMin=0&txtCentralLatSec=0&txtCentralLongMin=0&txtCentralLongSec=0&stnID=6526&dispBack=0 (Accessed December 1, 2023).

Granli, T., and Bøckman, O. C. (1994). Nitrous oxide from agriculture. *Norw J. Agric. Sci. Suppl.* 12, 128.

Hack, J., and Kaupenjohann, M. (2002). "N_2O discharge with drain water from agricultural soils of the upper Neckar region in southern Germany," in *Proc. Third int. Symp. Non-CO_2 Greenhouse gases: scientific understanding, control options and policy aspects, maastricht, Netherlands. 21-23 january 2002*. Editors J. Van Ham, A. P. M. Baede, R. Guicherit, and J. G. F. M. Williams-Jacobse (Millipress, Rotterdam, Netherlands), 185–190.

Hama-Aziz, Z. Q., Hiscock, K. M., and Cooper, R. J. (2016). Indirect nitrous oxide emission factors for agricultural field drains and headwater streams. *Environ. Sci. & Technol.* 51 (1), 301–307. doi:10.1021/acs.est.6b05094

Hama-Aziz, Z. Q., Hiscock, K. M., and Cooper, R. J. (2017). Dissolved nitrous oxide (N2O) dynamics in agricultural field drains and headwater streams in an intensive arable catchment. *Hydrol. Process.* 31 (6), 1371–1381. doi:10.1002/hyp.11111

Hasegawa, K., Hanaki, K., Matsuo, T., and Hidaka, S. (2000). Nitrous oxide from the agricultural water system contaminated with high nitrogen. *Chemosphere Glob. Change Sci.* 2, 335–345. doi:10.1016/s1465-9972(00)00009-x

Heincke, M., and Kaupenjohann, M. (1999). Effects of soil solution on the dynamics of N_2O emissions: a review. *Nutr. Cycl. Agroecosys.* 55, 133–157. doi:10.1023/a:1009842011599

Hutchinson, G., and Livingston, G. (1993). "Use of chamber systems to measure trace gas fluxes. Pages 63–78," in *Agricultural ecosystem effects on trace gases and global climate change*. Editors L. A. Harper, A. R. Mosier, J. M. Duxbury, and D. E. Rolston (Madison, WI: ASA, CSSA, SSSA). Special Publication No 55.

IPCC (2019). in *2019 refinement to the 2006 IPCC guidelines for national Greenhouse gas inventories. Volume 4 agriculture, forestry and other land use*. Editors Calvo Buendia, E., Tanabe, K., Kranjc, A., Baasansuren, J., Fukuda, M., Ngarize, S., et al. Published: IPCC, Switzerland.

IPCC (2021). in *Climate change 2021: the physical science basis. Contribution of working group I to the sixth assessment Report of the intergovernmental panel on climate change*. Editors Masson-Delmotte, V., Zhai, P., Pirani, A., Connors, S. L., Péan, C., Berger, S., et al. (Cambridge, United Kingdom and New York, NY, USA: Cambridge University Press). In press. doi:10.1017/9781009157896

IPCC (2022). in *Climate change 2022: mitigation of climate change. Contribution of working group III to the sixth assessment Report of the intergovernmental panel on climate change*. Editors Shukla, P. R., Skea, J., Slade, R., Al Khourdajie, A., van Diemen, R., McCollum, D., et al. (Cambridge, UK and New York, NY, USA: Cambridge University Press). doi:10.1017/9781009157926

IPCC (2023). "Climate change 2023: synthesis Report," in *Contribution of working groups I, II and III to the sixth assessment Report of the intergovernmental panel on climate change core writing team*. Editors Lee, H., and Romero, J. (Geneva, Switzerland: IPCC), 35–115. doi:10.59327/IPCC/AR6-9789291691647

Janzen, H. H., Desjardins, R. L., Asselin, J. M. R., and Grace, B. (1999). *The health of our air: toward a sustainable agriculture in Canada*. Ottawa, Canada: Agriculture and Agri Food Canada Publication# 1981/E. Available at: https://publications.gc.ca/site/eng/9.686880/publication.html

Jiang, Y., Zebarth, B., and Love, J. (2011). Long-term simulations of nitrate leaching from potato production systems in Prince Edward Island, Canada. *Nutrient Cycl. Agroecosyst. Former. Fertilizer Res.* 91 (3), 307–325. doi:10.1007/s10705-011-9463-z

Jiang, Y., Zebarth, B. J., Somers, G. H., MacLeod, J. A., and Savard, M. M. (2012). Nitrate leaching from potato production in eastern Canada. *Sustain. Potato Prod. Glob. Case Stud.*, 233–250. doi:10.1007/978-94-007-4104-1_13

Kavdir, Y., Hellebrand, H. J., and Kern, J. (2008). Seasonal variations of nitrous oxide emission in relation to nitrogen fertilization and energy crop types in sandy soil. *Soil & Tillage Res.* 98, 175–186. doi:10.1016/j.still.2007.11.002

Klavidko, E. J., Van Scoyoc, G. E., Monke, E. J., Oates, K. M., and Pask, W. (1991). Pesticide and nutrient movement into subsurface tile drains on a silt loam soil in Indiana. *J. Environ. Qual.* 20, 264–270. doi:10.2134/jeq1991.00472425002000010043x

Maag, M., and Vinther, F. (1996). Nitrous oxide emission by nitrification and denitrification in different soil types and at different soil moisture contents and temperatures. *Appl. Soil Ecol.* 4, 5–14. doi:10.1016/0929-1393(96)00106-0

MacDougall, J. I., Veer, C., and Wilson, F. (1988). *Soils of Prince Edward Island: Prince Edward Island soil sur vey. Research Branch*. Agriculture Canada.

Milburn, P., Macleod, J. A., and Sanderson, B. (1997). Control of nitrate leaching from early harvested potatoes on Prince Edward Island. *Can. Agri. Eng.* 39, 263–271.

Minami, K., and Fukushi, S. (1984). Methods for measurement N_2O flux from water surface and N_2O dissolved in water from agricultural land. *Soil Sci. Plant Nutr.* 30, 495–502. doi:10.1080/00380768.1984.10434716

Minami, K., and Oshawa, A. (1990). "Emission of nitrous oxide dissolved in drainage water from agricultural land," in *Soils and the Greenhouse effect*. Editor A. F. Bouman (Chichester, UK: John Wiley & Sons), 503–509.

Nangia, V., Gowda, P. H., Mulla, D. J., and Sands, G. R. (2010). Modeling impacts of tile drain spacing and depth on nitrate-nitrogen losses. *Artif. Drain.* 9 (1), 61–72. doi:10.2136/vzj2008.0158

Nevison, C. (2000). Review of the IPCC methodology for estimating nitrous oxide emissions associated with agricultural leaching and runoff. *Chemosphere Glob. Change Sci.* 2, 493–500. doi:10.1016/s1465-9972(00)00013-1

Quesnel, J., VanderZaag, A., Crolla, A., Kinsley, C., Gregorich, E., and Wagner-Riddle, C. (2019). Surface and subsurface N2O losses from dairy cropping systems. *Nutr. Cycl. Agroecosyst* 114, 277–293. doi:10.1007/s10705-019-10004-5

Randall, G. W., Huggins, D. R., Russelle, M. P., Fuchs, D. J., Nelson, W. W., and Anderson, J. L. (1997). Nitrate losses through subsurface tile drainage in conservation reserve program, alfalfa and row crop systems. *J. Environ. Qual.* 26, 1240–1247. doi:10.2134/jeq1997.00472425002600050007x

Reay, D., Edwards, A., and Smith, K. (2004). Nitrous oxide in agricultural drainage waters following field fertilisation. *Water Air Soil Pollut. Focus* 4, 437–451. doi:10.1023/b:wafo.0000028370.68472.d2

Reay, D. S., Edwards, A. C., and Smith, K. A. (2009). Importance of indirect nitrous oxide emissions at the field, farm and catchment scale. *Agric. Ecosyst. & Environ.* 133 (3/4), 163–169. doi:10.1016/j.agee.2009.04.019

Reay, S. D., Smith, K. A., and Edwards, C. A. (2003). Nitrous oxide emission from agricultural drainage waters. *Glob. Change Biol.* 9, 195–203. doi:10.1046/j.1365-2486.2003.00584.x

Risk, N., Snider, D., and Wagner-Riddle, C. (2013). Mechanisms leading to enhanced soil nitrous oxide fluxes induced by freeze-thaw cycles. *Can. J. Soil Sci.* 93 (4), 401–414. doi:10.4141/cjss2012-071

Risk, N., Wagner-Riddle, C., Furon, A., Warland, J., and Blodau, C. (2014). Comparison of simultaneous soil profile N_2O concentration and surface N_2O flux measurements overwinter and at spring thaw in an agricultural soil. *Soil Sci. Soc. Am. J.* 78 (1), 180–193. doi:10.2136/sssaj2013.06.0221

Rochette, P., and McGinn, S. M. (2008). N_2O emissions from agricultural soils in Canada (preface) can. *J. Soil Sci.* 88 (2), 131–132. doi:10.4141/cjss07301

Roper, J. (2008). *Influence of tillage practices on surface and subsurface nitrogen emissions from agricultural soils*. Halifax, NS: Dalhousie University. MSc thesis.

Roper, J., Burton, D., Madani, A., and Stratton, G. (2013). A simple method for quantifying dissolved nitrous oxide in tile drainage water. *Can. J. Soil Sci.* 93 (1), 59–64. doi:10.4141/cjss2012-021

Sawamoto, T., Kusa, K., Hu, R., and Hatano, R. (2002). Dissolved N_2O, CH4 and CO_2 in pipe drainage, seepage and stream water in a livestock farm in Hokkaido, Japan. *Soil Sci. Plant Nutr.* 48, 433–439. doi:10.1080/00380768.2002.10409222

Sawamoto, T., Kusa, K., Hu, R., and Hatano, R. (2003). Dissolved N_2O, CH4 and CO_2 emissions from subsurface drainage in a structured clay soil cultivated with onion in central Hokkaido, Japan. *Soil Sci. Plant Nutr.* 49, 31–38. doi:10.1080/00380768.2003.10409976

Shakoor, A., Shakoor, S., Rehman, A., Ashraf, F., Abdullah, M., Shahzad, S. M., et al. (2021). Effect of animal manure, crop type, climate zone, and soil attributes on greenhouse gas emissions from agricultural soils-A global meta-analysis. *J. Clean. Prod.* 278, 1–13. doi:10.1016/j.jclepro.2020.124019

Syakila, A., and Kroeze, C. (2011). The global nitrous oxide budget revisited. *Greehn. Gas. Meas. Manage.* 1, 17–26. doi:10.3763/ghgmm.2010.0007

Tian, L., Cai, Y., and Akiyama, H. (2019). A review of indirect N_2O emission factors from agricultural nitrogen leaching and runoff to update of the default IPCC values. *Environ. Pollut.* 245, 300–306. doi:10.1016/j.envpol.2018.11.016

Valayamkunnath, P., Gochis, D. J., Chen, F., Barlage, M., and Franz, K. J. (2022). Modeling the hydrologic influence of subsurface tile drainage using the national water model. *Water Resour. Res.* 58 (4). doi:10.1029/2021WR031242

van Es, H. M., Sogbedji, J. M., and Schindelbeck, R. R. (2006). Effect of manure application timing, crop, and soil type on nitrate leaching. *J. Environ. Qual.* 35 (2), 670–679. doi:10.2134/jeq2005.0143

Venterea, R., Bijesh, M., and Dolan, M. (2011). Fertilizer source and tillage effects on yield-scaled nitrous oxide emissions in a corn cropping system. *J. Environ. Qual.* 40 (5), 1521–1531. doi:10.2134/jeq2011.0039

Wagner-Riddle, C., Congreves, K., Abalos, D., Berg, A., Brown, S., Ambadan, J., et al. (2017). Globally important nitrous oxide emissions from croplands induced by freeze-thaw cycles. *Nat. Geosci.* 10, 279–283. doi:10.1038/ngeo2907

World Meteorological Organization (2014). *Scientific assessment of oxone depletion: 2014 global ozone research and monitoring project-rep*, 56. Geneva, Switzerland: World Meteorological Organization.

Xia, F., Mei, K., Zhang, C., Xu, Y., Dahlgren, R. A., and Zhang, M. (2020). Response of N2O emission to manure application in field trials of agricultural soils across the globe. *Sci. Total Environ.* 733, 139390. doi:10.1016/j.scitotenv.2020.139390

frontiers | Frontiers in Environmental Science

TYPE Original Research
PUBLISHED 28 February 2025
DOI 10.3389/fenvs.2025.1513704

Check for updates

OPEN ACCESS

EDITED BY
Jana Levison,
School of Engineering, University of Guelph, Canada

REVIEWED BY
Doru Stelian Banaduc,
Lucian Blaga University of Sibiu, Romania
Henrique J. O. Pinho,
Polytechnic Institute of Tomar (IPT), Portugal

*CORRESPONDENCE
Kerry T. B. MacQuarrie,
ktm@unb.ca

RECEIVED 18 October 2024
ACCEPTED 10 February 2025
PUBLISHED 28 February 2025

CITATION
Crossley LM, MacQuarrie KTB and Danielescu S (2025) Agricultural nitrate attenuation in a small groundwater-influenced wetland system. *Front. Environ. Sci.* 13:1513704. doi: 10.3389/fenvs.2025.1513704

COPYRIGHT
© 2025 Crossley, MacQuarrie and Danielescu. This is an open-access article distributed under the terms of the Creative Commons Attribution License (CC BY). The use, distribution or reproduction in other forums is permitted, provided the original author(s) and the copyright owner(s) are credited and that the original publication in this journal is cited, in accordance with accepted academic practice. No use, distribution or reproduction is permitted which does not comply with these terms.

Agricultural nitrate attenuation in a small groundwater-influenced wetland system

Leah M. Crossley[1], Kerry T. B. MacQuarrie[1,2]* and Serban Danielescu[3,4]

[1]Department of Civil Engineering, University of New Brunswick, Fredericton, NB, Canada, [2]Canadian Rivers Institute, University of New Brunswick, Fredericton, NB, Canada, [3]Fredericton Research and Development Centre, Agriculture and Agri-Food Canada, Fredericton, NB, Canada, [4]Canada Centre for Inland Waters, Environment and Climate Canada, Burlington, ON, Canada

Nitrate contamination of freshwater systems is common in agricultural watersheds, leading to human and environmental health concerns. The Bells Creek watershed, located in central Prince Edward Island (PEI), Canada, is dominated by agricultural land use and has elevated nitrate concentrations in groundwater and surface water. Beneficial Management Practices (BMPs), such as constructed wetlands, may provide a means of mitigating such contamination; however, the significance of small wetlands in regulating or attenuating nitrate in PEI has yet to be investigated. In this year-long (August 2023 – July 2024) study, the nitrate loads delivered to a small (1.2 ha) groundwater-influenced, stream-wetland system were quantified using high-frequency monitoring techniques. Results indicate that discharge variability is the primary control on the observed variability of surface and subsurface nitrate loads. The total annual nitrate load to the wetland was approximately 30,000 kg NO_3-N/yr. Groundwater discharge, which bypasses the wetland riparian zone, contributed approximately 67% of the total load to the wetland. Weekly flux calculations revealed that the wetland behaved as a nitrate sink for 49 out of 52 weeks of the year. Overall, the wetland attenuated 39% of the imported annual nitrate load which, on a wetland catchment area basis, is equivalent to 21.1 kg NO_3-N/ha catchment/yr. A positive, non-linear trend between the imported nitrate load and the percent change in nitrate load revealed that the wetland attenuated disproportionately more nitrate during periods of high imported loads. These findings indicate that small, constructed wetlands may be an effective component of BMPs aimed at reducing nitrate loads in agriculturally dominated watersheds like those in Prince Edward Island.

KEYWORDS

nitrate attenuation, constructed wetland, agricultural watershed, nitrate load pathways, beneficial management practices, high-frequency data

1 Introduction

Agricultural activities may produce excess nutrients, such as nitrogen (N) and phosphorus (P), and pesticides, that can enter freshwater systems via surface and subsurface transport pathways (Dunn et al., 2011; Mackie et al., 2021; Crawford and Alexander, 2024). Nitrate-nitrogen (NO_3-N) contamination of freshwater systems is of increasing concern within agriculturally dominated watersheds, such as those in the province of Prince Edward Island (PEI), Canada, where elevated nitrate levels in

groundwater and surface water have been linked to areas of intense agricultural land use (e.g., Benson et al., 2006; Danielescu and MacQuarrie, 2011; Liang et al., 2019; Crawford and Alexander, 2024). PEI's fractured sandstone aquifer, the province's sole source of potable water, is susceptible to contamination due to its unconfined (locally semi-confined) nature (Zebarth et al., 2015). Despite the presence of glacial till overburden, Lamb et al. (2019) demonstrated that infiltrating water and dissolved contaminants primarily move downward toward the aquifer, where contaminants such as nitrate can reside for several decades (Jiang and Somers, 2009; Critchley et al., 2014). Groundwater also contributes between 65% and 85% of annual stream discharge in PEI and, as such, the groundwater contribution to streams can have a major impact on surface water quality (Danielescu et al., 2009; Savard et al., 2010; Crawford and Alexander, 2024). Nitrate entering surface water bodies can put aquatic ecosystems at risk, as excess concentrations increase the likelihood of algal blooms, potentially causing anoxic conditions that, in addition to other factors such as the presence of agricultural pesticides and increasing water temperatures, have been linked to fish kills in PEI (Crawford and Alexander, 2024).

In working towards a sustainable balance between agriculture and freshwater systems, Beneficial Management Practices (BMPs), such as crop rotation, spring tillage, and buffer zones (Dunn et al., 2011; Zebarth et al., 2015), have been introduced to mitigate the amount of nutrients entering surface waters and aquifers. As discussed by Zebarth et al. (2015), agricultural systems are very complex, and in order to alleviate the perceived economic risk that farmers have with adopting BMPs, financial compensation or subsidies are typically required. Besides economic considerations, additional field investigations are required to demonstrate the effectiveness of BMPs for N reduction in connected groundwater-surface water-wetland systems, where multiple transport pathways may exist for delivery of N to riparian lowlands, streams or wetlands (e.g., Conant et al., 2016; Steiness et al., 2021).

The role of wetlands as nitrate sinks in agricultural catchments has been the subject of a number of studies within North America, with most showing the potential for significant removal. Cheng et al. (2020) used an empirical nitrate removal model to estimate, on a continental US-scale, that a 10% increase in strategically placed wetlands would result in a 54% decrease in N loads to surface water. A study conducted within the Minnesota River Basin by Hansen et al. (2018) found that wetland restoration would be five times more effective in reducing nitrate loads compared to other agricultural land management strategies. Hansen et al. (2021) used an integrated model of a subwatershed of the Minnesota River Basin to show that small (<2 ha) and shallow (<1.1 m deep) fluvial wetlands (i.e., wide, slowing, vegetated water bodies within a riverine corridor) were the most cost-effective nitrate management action in agricultural watersheds. Cheng and Basu (2017) found, through a meta-analysis of a global data base, that wetlands <0.03 ha in area accounted for 50% of N removal due to the larger sediment area to water volume ratio in small wetlands, emphasizing the disproportion role small wetlands play in nutrient processing within a landscape. A field-based study by Botrel et al. (2022) over six summers within the St. Lawrence River, in Québec, Canada found an aquatic vegetation meadow, located at the confluence of two agriculturally impacted tributaries, reduced NO_3-N loads by 47%–87%. Steiness et al. (2021) found that a riparian wetland in Denmark attenuated between 45% and 83% of the annual NO_3-N load, with the variability arising because of the uncertainty in the surface and subsurface pathways of nitrate delivery to the stream. While these results emphasize the potential of wetlands to be used as an adaptive BMP down-gradient of agriculturally intensive areas, studies are generally lacking with respect to small, groundwater-influenced, wetlands; wetlands <2 ha in area are relatively common in PEI, comprising 67% of the wetlands in the province (Dibblee, 2000). In addition, the influence of seasonal climate variability on nitrate loads and wetland attenuation capacity has seldom been investigated.

Although multi-year investigations of nitrate transport in freshwater systems in PEI have been conducted through discrete sampling (e.g., Savard et al. (2010), where samples were collected once per season over two years; Danielescu and MacQuarrie (2013), where no samples were collected between December and February), the sampling frequencies do not provide a comprehensive understanding of the variability of nitrate transport and attenuation in connected groundwater-surface water systems. Bowes et al. (2009) concluded that weekly sampling for N would be the minimum interval required to accurately represent nutrient dynamics in a riverine setting. A weekly sampling frequency was also adopted in a two year study by Beltran et al. (2021), where they assessed the seasonality within NO_3-N loads exported from a stream impacted by urbanization and channelization, finding that the stream reach that was disconnected from groundwater interactions was always a NO_3-N source, while the groundwater-connected reach oscillated seasonally between a source and sink. Miller et al. (2016) employed a 15-min sampling frequency, averaged daily in post-processing, at three sites within a watershed in a year long study and used hydrograph separation and daily NO_3-N concentrations to estimate the NO_3-N load via baseflow and runoff. In a PEI-based study conducted by Pavlovskii et al. (2023), high-frequency (i.e., 15-min interval) NO_3-N concentration data were collected at a single stream location for the month of September, revealing that heavy rainfall caused a sustained increase in groundwater nitrate load via baseflow up to 10 days following a storm event; however, the limited spatial and temporal extent of the data collection were not amenable to assessing attenuation or long-term trends. Climate projections for PEI indicate that while storm events may become less frequent, they will become more intense (Bhatti et al., 2022), potentially having implications for N transport and monitoring in agricultural watersheds, as high NO_3-N concentrations in the shallow portion of the PEI aquifer can be quickly discharged to surface water during heavy rainfall (Pavlovskii et al., 2023). As such, to better resolve nitrate loads delivered to small wetlands via surface and subsurface transport pathways, and potential nitrate attenuation within small wetlands, high-frequency (e.g., ≥2 measurements per day) and relatively long-term (e.g., ≥1 year) time series are required.

Given the need for an improved understanding of nitrate transport and attenuation within small, groundwater-influenced, wetlands, the objectives of this study were to: 1) collect high-frequency data for a small constructed wetland (<2 ha) to enable quantification of short-term (e.g., daily) and seasonal trends in nitrate loads; 2) to establish the contributions of surface water

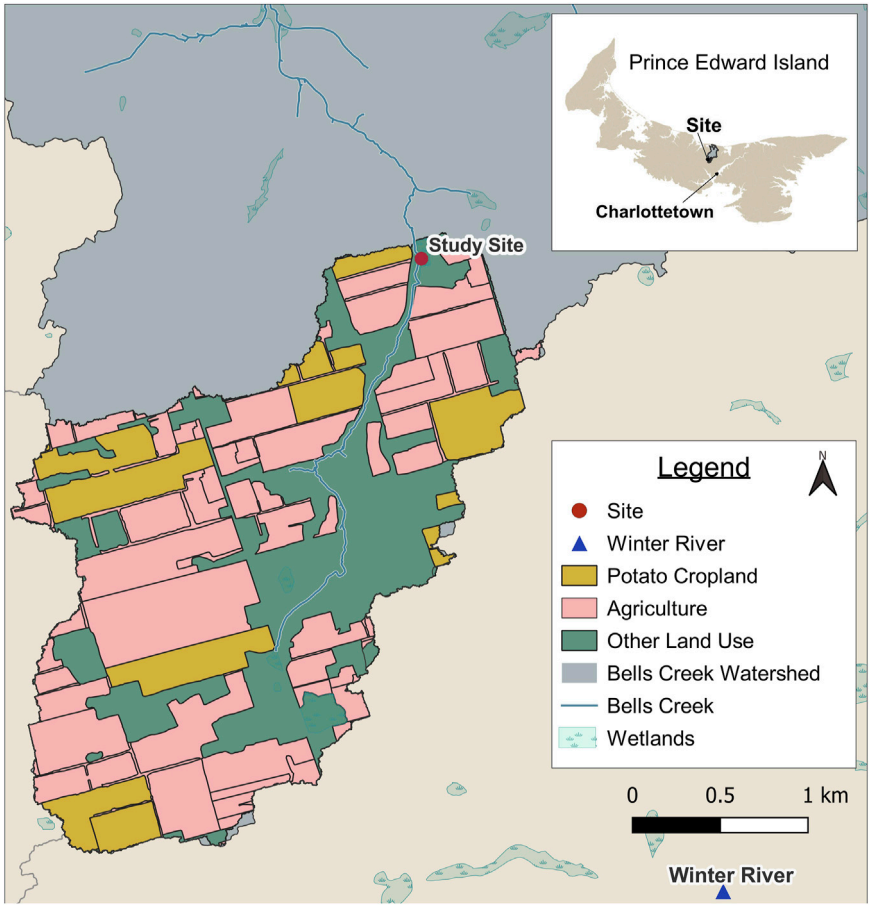


FIGURE 1
Location of the study site within the Bells Creek watershed. The map inset shows the site location within the province of PEI. Land use within the study site catchment area for the year 2010 is denoted in the legend. Winter River is the location of a Water Survey of Canada hydrometric station (01CC010).

and groundwater transport pathways to the nitrate loads; and, 3) to quantify the short-term and annual efficiency of nitrate load reduction within the wetland system. While this study is important in the context of nitrate contamination in PEI, as it is the first high-frequency and year-long groundwater-surface water-wetland study to be conducted in the region, this work can potentially translate to other groundwater-influenced systems within agricultural watersheds located in similar climates or hydrogeological settings. Investigating nitrate transport and attenuation in relatively small wetlands also offers the opportunity to better constrain nitrate loads and provide greater confidence in estimating nitrate load variations, which has proved challenging for many groundwater-influenced riparian systems (e.g., Steiness et al., 2021).

2 Site description

The study site is located 11 km north of the City of Charlottetown, adjacent to the Agriculture and Agri-Food Canada (AAFC) Experimental Farm in Harrington, PEI, within the Bells Creek watershed (Figure 1). Bells Creek, a 2 m wide second-order stream, flows northward through an open water wetland area known as Mill Pond, ultimately discharging to Covehead Bay estuary along the northern PEI coastline.

Mill Pond is a small (1.2 ha) wetland constructed in the 1950s with a single, well-defined outflow location (Outlet, Figure 2). The constructed wetland occupies a topographically low area and has an average water depth of approximately 2 m. Multiple underwater springs occur along the western shoreline where groundwater discharge can be observed year-round (Springs, Figure 2). A buffer of mature riparian vegetation surrounds the wetland, varying in width from approximately 18 m–250 m (Figure 2). Although an aquatic vegetation survey was not conducted as part of this work, a previous PEI-based study by Stevens et al. (2003) noted flora such as cattails (*Typha* spp.), common duckweed (*Lemna minor*), water-starwort (*Callitriche* spp.), water lilies (*Nuphar luteum* and *Nymphaea odorata*), pondweeds (*Potamogeton* spp.), algae (*Chara* spp.), and northern wild rice (*Zizania palustris*) in similar open water wetlands. Filamentous green algae, likely a form of *Cladophora* (Cynthia Crane, personal communication, 17 April 2024) has been observed growing loosely attached to the bottom sediments and, seasonally, a portion of the wetland surface is covered with floating green algae mats (see Supplementary Figure S1).

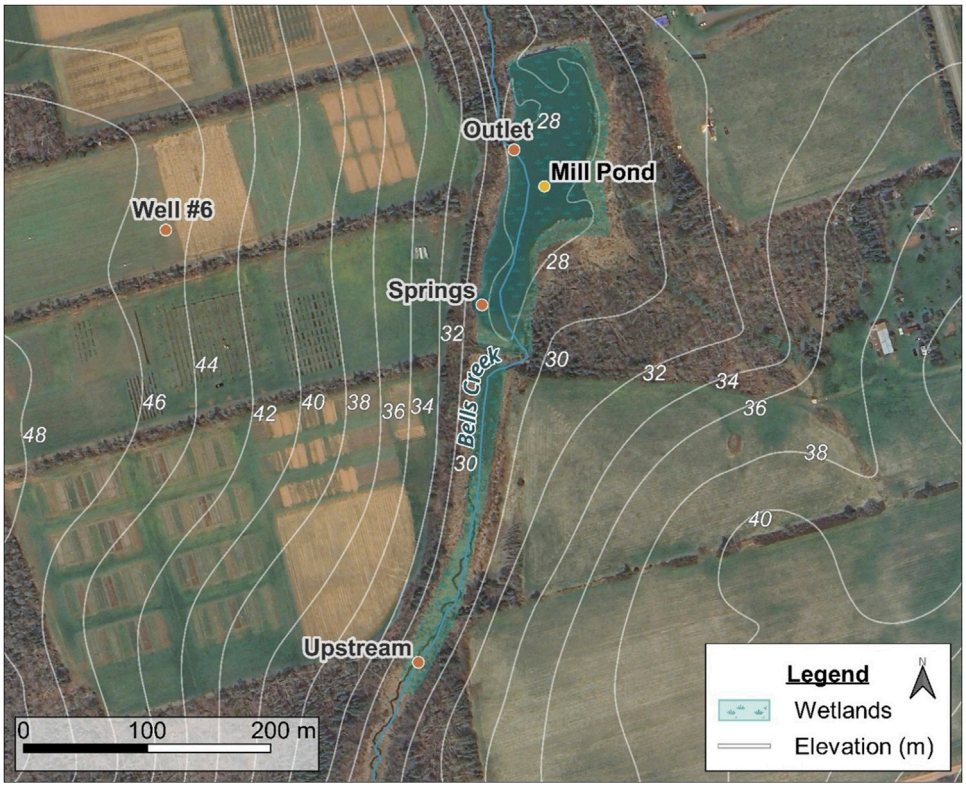


FIGURE 2
Sampling locations, including an upgradient groundwater monitoring well, Well #6, located on the AAFC Harrington Experimental Farm property.

The wetland catchment area is approximately 555 ha. Figure 1 shows the land usage upgradient of the study site for 2010; for the period of 2013–2023 the catchment land use was predominantly agricultural (67% on average) (Agriculture and Agri-Food Canada, 2024), with fields used for potato production at some time within the minimum 3-year crop rotation representing 13% of the total catchment area (Government of Prince Edward Island, 2019). As per the classification used in Crawford and Alexander (2024), having more than 50% of land use attributed to agriculture would imply that surface water quality may be severely impacted. In addition to agricultural sources of N, homes and businesses within the catchment area rely on septic systems for wastewater treatment. Using the typical septic system load of 1.6 kg NO_3-N/yr proposed for rural PEI by Grizard (2013), and given that there are approximately 40 residences within the catchment area that have septic systems, the total NO_3-N load from the wetland catchment area due to wastewater is approximately 0.12 kg NO_3-N/ha catchment/yr.

The climate in PEI is humid-continental, with long and mild winters and moderately warm summers (Zebarth et al., 2015; Bhatti et al., 2021). The Harrington Experimental Farm climate station recorded 1,035 mm of precipitation for the period of August 2023 to July 2024, and average monthly temperatures ranging from −4.4°C in February 2024 to 20.7°C in July 2024 (Environment and Climate Change Canada, 2024).

The geology of PEI consists of Carboniferous-aged, highly fractured sandstone intermixed with shale bedrock overlain by a thin mantle of glacial till with depths up to 15 m (Somers, 1992; Zebarth et al., 2015). Zebarth et al. (2015) have previously reported on the geology and aquifer conditions at the AAFC Harrington Experimental Farm site, where they indicate intensely to very intensely fractured sandstone bedrock overlain by argillaceous sandstone with intense horizontal to subvertical fractures, and sandy loam surface soils approximately 1 m deep that allow for rapid infiltration of rainfall and snowmelt. Groundwater flow in the fractured sandstone aquifer is controlled primarily by the extensive fractures, resulting in rapid movement of water and dissolved contaminants in the saturated zone with flow velocity estimates of 0.25–0.76 m/day (Zebarth et al., 2015). However, Malenica (2015) found that the majority of the NO_3-N mass within the aquifer underlying the AAFC Harrington Experimental Farm was stored within the bedrock matrix, rather than the fractures, with the highest NO_3-N concentrations primarily occurring within the vadose and shallow saturated bedrock zone. Malenica (2015) also found conditions within the aquifer to be unsuitable for microbial denitrification due to high dissolved oxygen concentrations and limited electron donors (i.e., organic carbon and/or mineral).

3 Methods

3.1 Wetland discharges

The total inflow of water to the constructed wetland is assumed to consist of the upstream surface water inflow (i.e., generated from the Bells Creek catchment area upgradient of the Upstream location, Figure 2), direct overland flow from the immediate wetland

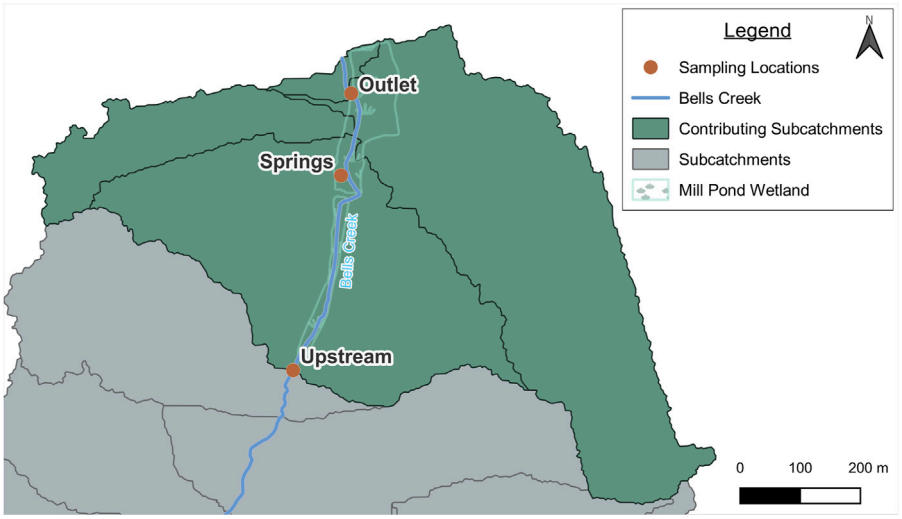


FIGURE 3
Catchment area for the Outlet location located within the Bells Creek watershed. The subcatchments contributing directly to the Mill Pond wetland are highlighted in green, with key monitoring locations indicated.

catchment area, and direct groundwater discharge. As has been visually confirmed, all outflow from the wetland occurs via surface water discharge at the Outlet location (Figure 2).

3.1.1 Surface water inflows and outflows

To obtain times series for surface water inflow and outflow, stage-discharge relationships were developed over the study period (August 2023-July 2024) for both the Upstream and Outlet locations. Discharge (Q) was measured at these locations near-monthly using FlowTracker 1 or FlowTracker 2 Acoustic Doppler Velocimeters (Sontek, Ohio, United States of America) and the velocity-area method; two measurements of Q were completed on all occasions at each location. Stilling wells equipped with Levelogger Model 5 pressure transducers (Solinst Canada Ltd.) were deployed to record water levels at 1-h intervals for the duration of the study period. While the Upstream stilling well was installed next to the Upstream stream-gauging location, the water level control for the Outlet location was a log that spanned the width of the Outlet channel and effectively functioned as a weir. The water head for the wetland was found to correlate well with the Outlet discharge and thus the water level was monitored in a stilling well located within the wetland. To provide barometric compensation of the pressure transducer readings, a Barologger Model 5 barometric pressure logger (Solinst Canada Ltd.) was installed near the Outlet. The developed stage-discharge relationships were used to calculate discharge at 1-h intervals using the 1-h water stage records. To ensure the pressure transducer water level and discharge time series were reasonable, the data collected at the Upstream and Outlet locations were compared to the discharge record at the nearby Water Survey of Canada winter River hydrometric station (01CC010; Figure 1).

3.1.2 Direct overland flow

Direct overland flow (i.e., runoff) from the area adjacent to the wetland was modelled using the Green-Ampt infiltration method in PCSWMM (Computational Hydraulics Inc.). The sandy loam surface soils observed at the AAFC Harrington site (Zebarth et al., 2015) were assumed to be consistent across the catchment. The Green-Ampt soil properties for sandy loam and other relevant inputs are presented in Supplementary Table S1A. The potential monthly evapotranspiration was calculated using the Thornthwaite method and adjusted for latitude (Supplementary Table S1B). A time series for direct runoff to the wetland, between the Upstream and Outlet locations, was found by summing the runoff from the four delineated subcatchments highlighted in Figure 3.

3.1.3 Direct groundwater discharge

Although direct groundwater discharge to the wetland was apparent as a series of underwater springs visible along the western shoreline (Figure 2), it was not feasible to instrument this area to quantify this discharge. Instead, groundwater discharge to the wetland was computed using Equation 1, under the assumption that the only other inflows to the wetland were those measured at the Upstream location and the computed runoff.

$$Q_{springs} = Q_{out} - Q_{us} - Q_{run} \quad (1)$$

where $Q_{springs}$ is the groundwater discharge (L^3/T), Q_{out} is the Outlet discharge (L^3/T), Q_{us} is the Upstream discharge (L^3/T), and Q_{run} is the runoff from the catchment area that contributes to the wetland (L^3/T) (Figure 3).

3.2 Water quality data collection

Samples were collected for water quality analyses approximately monthly between May 2023 and July 2024 at the Upstream, Outlet, and Springs locations (Figure 2). Samples from the Springs area were collected using a peristaltic pump and a dedicated drive-point

piezometer penetrating ~0.6 m into the fractured sandstone bedrock below the wetland. All samples were passed through a 0.45 μm filter and were refrigerated until analysis. Samples for cation analysis were acidified using 67%–70% nitric acid. Anions were analyzed using a Metrohm ion chromatograph (761 Compact IC equipped with a Metrosep A Supp 5 column, Switzerland), and cations were analyzed using an inductively coupled plasma-optical emission spectrometer (Varian Vista MPX, Australia) at the University of New Brunswick, Department of Civil Engineering Water Quality Laboratory. Field parameters including pH, temperature, specific conductivity, and dissolved oxygen (DO) were measured using a portable water quality meter (Thermo-Scientific Orion Star A329 Portable Meter). Field alkalinity values were obtained using a HACH digital titrator (Hach, Canada). Charge balance errors were calculated for all samples and a Piper plot of the major ion results was used to assess the hydrochemical facies of the water.

To obtain high-frequency data for NO_3-N, the dominant form of nitrogen in PEI freshwaters (Somers et al., 1999; Danielescu and MacQuarrie, 2011), Submersible Ultra-Violet Nitrate Analyzers (SUNA V2, Seabird Scientific, United States), were installed at the Outlet, Upstream, and in Well #6 (Figure 2). NO_3-N concentrations were recorded at 6-h intervals. The SUNAs were powered using 40 W solar panels and 12 V batteries protected inside large plastic bins (Supplementary Figure S2). The SUNAs at the Upstream and Outlet sites were secured inside stainless-steel cages, which were then fixed within the middle of the channel by driving rebar through the gaps in the cage and into the streambed. Between August 2023-March 2024, the Upstream SUNA was equipped with a copper biofouling guard while awaiting a SUNA equipped with a wiper that would clean the optical window prior to every sampling event. The Upstream SUNA was replaced by a SUNA with a wiper in March 2024. The Outlet SUNA was equipped with a wiper for the entirety of the study period. The sensor performance was verified using SUNA's internal diagnostics and concentration standards (i.e., 0, 0.5, 1, 2.5, 5, and 10 mg NO_3-N/L) before field deployment and on all field visits where the air temperature was above freezing to avoid damaging the optical lens. SUNA readings were also compared to concentrations measured in discrete NO_3-N samples collected at each of the locations (Supplementary Figure S3). As discussed by Miller et al. (2016), SUNAs do not explicitly account for absorbance by nitrite in the range of 210–220 nm; however, at the study site the concentration of nitrite is known to be less than laboratory detection limits.

To assess whether the NO_3-N concentrations from the Springs location were representative of the concentrations within the aquifer, and to provide groundwater NO_3-N data between the times of manual sampling, concentrations from the Springs location were compared to continuous nitrate concentrations obtained from Well #6, located approximately 400 m upgradient from the Springs location (Figure 2). To account for the lag time arising for groundwater to travel from Well #6 to the Springs sampling location, the Well #6 nitrate concentration time series was shifted forward by 748 days, which was found to provide the best correlation with the discrete samples collected from the Springs. This time shift falls within the range of travel times (519–1,600 days) estimated using the groundwater velocity range of 0.25–0.76 m/d previously estimated for the aquifer underlying Harrington Experimental Farm (Zebarth et al., 2015).

3.3 Loads

The results for dissolved chloride and NO_3-N from the manual water sampling were used with the corresponding stream discharge values, obtained on the same day as the water samples, to determine discrete (i.e., approximately monthly) loads. Chloride was used in this study as a conservative tracer as it is unlikely to be affected by biogeochemical reactions in either the subsurface or surface water system. The discrete Upstream and Outlet loads for both chloride and NO_3-N were computed using Equation 2.

$$\boldsymbol{LD = CQ} \tag{2}$$

where LD is the load (M/T), C is the concentration (M/L^3), and Q is the corresponding discharge (L^3/T).

To produce a time series of NO_3-N loads, linear interpolation was used between the SUNA concentration data (i.e., obtained at 6-h intervals) to estimate NO_3-N concentrations at 1-h intervals for all surface water monitoring locations. The NO_3-N load was then calculated at 1-h intervals for the duration of the study period using Equation 2. Equation 3 was used to calculate the cumulative NO_3-N load over a particular time interval (e.g., week, month).

$$\boldsymbol{LD_{\Delta t} = \sum_{i=1}^{n} C_i Q_i \Delta t} \tag{3}$$

where Δt is the time interval used in the concentration and discharge time series [T] and n is the number of observations within the interval.

During the study there were several periods when the SUNA at the Upstream site did not record NO_3-N concentrations (equivalent to 119 days of missing data or ~33% of the study period), and thus the Upstream NO_3-N loads could not be directly computed. For the first nine months of the study the Upstream SUNA did not have a wiper, and it appears that periods of missing data were related to high sediment loads in Bells Creek. Also, on one occasion, the power cable to the SUNA was damaged by animals. To estimate the missing NO_3-N load values, scikit-learn's implementation of gradient boosting regression was used (Pedregosa et al., 2011). Based on the results of a manual feature selection process, six features were used as input to the model: Upstream discharge, Upstream water temperature, Outlet NO_3-N load, atmospheric pressure, wetland water temperature, and air temperature. To evaluate the performance of the regressor, a 10-fold cross validation approach was taken whereby 90% of the data were used for training and the other 10% for testing. To explain the output of the model, Shapley Additive exPlantations (SHAP) values (Lundberg and Lee, 2017) were determined, which indicate the impact each model feature had on the predicted Upstream NO_3-N load time series.

3.4 Statistical analysis

The NO_3-N removal efficiency of the wetland was assessed on a weekly basis. A paired two-sample t-test for means was run on weekly subsets of the data for the duration of the study period (52 weeks), allowing for 168 observations per t-test (i.e., 168 h per week). A statistical significance level of $p < 0.05$ was used.

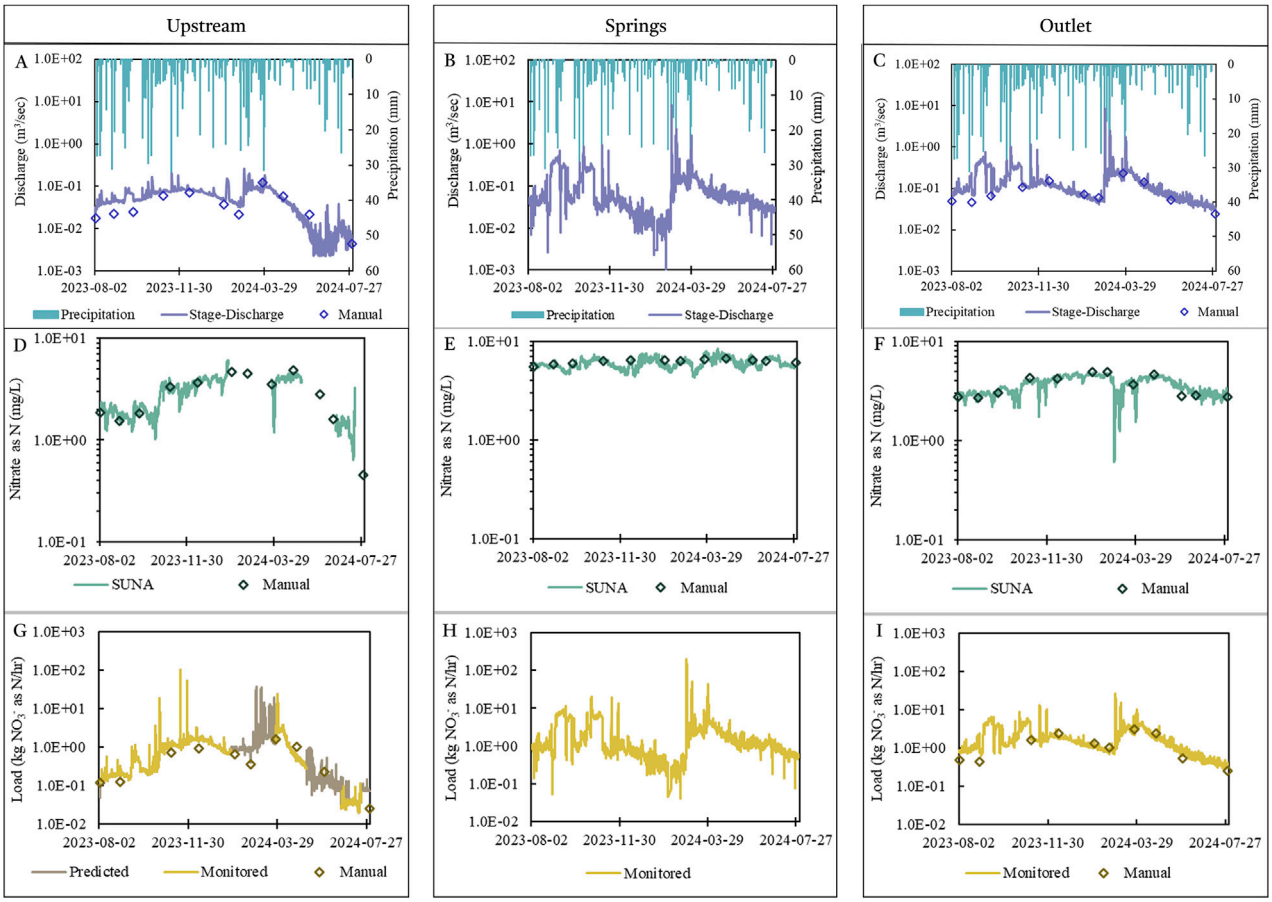


FIGURE 4
Plots of daily precipitation and discharge **(A–C)**; NO_3-N concentrations **(D–F)**; and NO_3-N loads **(G–I)** for each monitoring location. The Upstream plot for load **(G)** also shows the predicted values using the regression model during periods where the Upstream SUNA did not record concentration (Section 4.3.2).

4 Results

4.1 Discharge

Discharge results showed good agreement between the measured stream discharge values and the values obtained from the stage-discharge relationships (i.e., rating curves) (Figures 4A–C). The best-fit rating curve for the Upstream stage-discharge relationship was a linear function (R^2 = 0.86, n = 21), while the best-fit rating curve for the Outlet location was a power function (R^2 = 0.78, n = 24).

Stream discharge at the Upstream and Outlet surface water sites was seasonally variable (Figures 4A, C; Table 1), with the highest discharge observed in the late winter-early spring and the lowest discharge observed in the early summer months. The computed groundwater discharge to the wetland also exhibited seasonal variability (Figure 4B; Table 1), with the highest discharge coinciding with the two primary groundwater recharge periods (late fall and early spring). The average discharge from the wetland (0.160 m^3/s) was consistently higher than the average Upstream (surface water) inflow (0.055 m^3/s) due to the direct groundwater discharge to the wetland (0.110 m^3/s average). The cumulative direct overland flow simulated from the four subcatchments adjacent to the wetland (Figure 3) was only 1.04% of the cumulative Upstream flow, therefore, for subsequent computation of NO_3-N loads the load due to direct runoff was assumed negligible. Stream discharge at the Upstream and Outlet locations shows good correspondence (e.g., similar response to short-term precipitation events, and long-term seasonal trends) with the Winter River hydrometric station data (Supplementary Figure S4).

4.2 General water quality

The results of the major ion analyses exhibited little variability, with all surface water and groundwater samples being calcium-bicarbonate-type waters (Figure 5). The similarity of the major ion chemistry results indicates that groundwater has a strong influence on surface water quality at the study site. The pH of the surface water ranged from 7.1–9.4, and the average pH of the groundwater was 7.1. The dissolved oxygen (DO) concentration of surface water ranged from 7.2–17.0 mg/L, while the average DO of the groundwater was 9.5 mg/L (see also Supplementary Table S2).

TABLE 1 Cumulative groundwater inflow, surface water inflow, overland inflow, and surface water outflow to/from the constructed wetland, along with the relative groundwater contribution (BFI) for the year and seasonally where: winter (Dec-Feb), spring (Mar-May), summer (Jun-Aug), and fall (Sep-Nov).

	Winter	Spring	Summer	Fall	Total
Cumulative Groundwater Inflow (m^3/sec)	136.9	297.8	94.6	387.9	917.2
Cumulative Surface Water Inflow (m^3/sec)	150.1	141.2	40.1	147.8	479.2
Cumulative Direct Overland Inflow (m^3/sec)	0.8	1.2	1.4	1.6	5.0
Cumulative Surface Water Outflow (m^3/sec)	281.5	440.1	135.9	537.3	1,394.8
Relative Groundwater Contribution (BFI)	48%	68%	70%	72%	66%

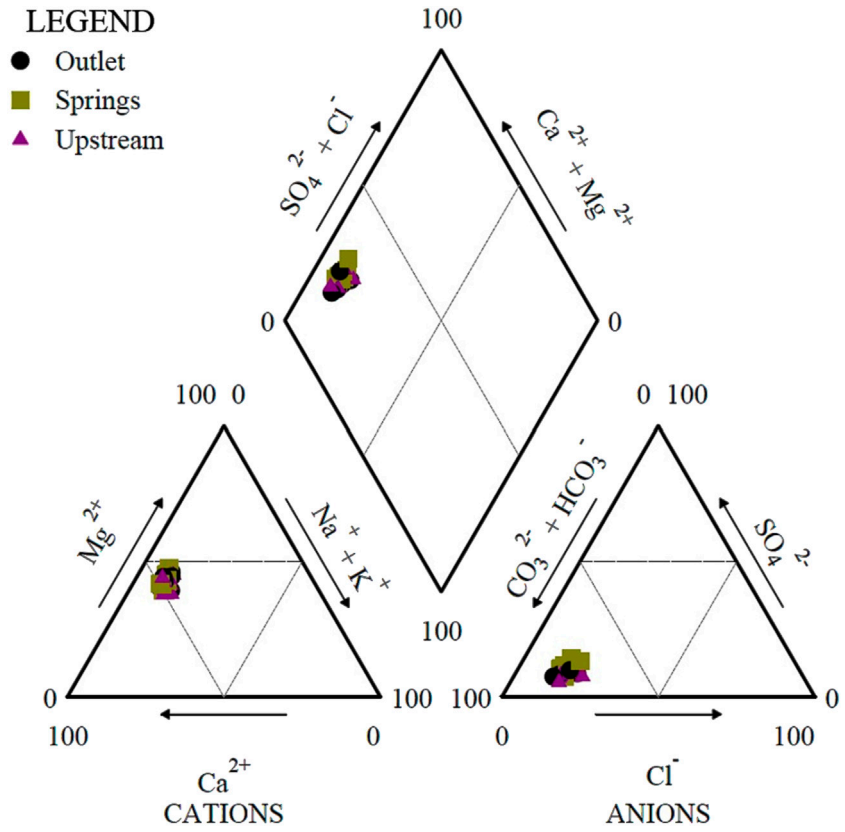


FIGURE 5
Piper plot for surface water (Outlet and Upstream) and groundwater (Springs) facies classification.

4.3 Loads

4.3.1 Chloride load

Chloride concentrations ranged from 12.7 to 15.5 mg/L at the Upstream location, 13.6–15.7 mg/L at the Outlet location, and 14.1–16.1 mg/L at the Springs groundwater discharge location. The chloride load delivered to the wetland ranged from 33 kg/day in July 2024 to 296 kg/day in March 2024 (see Supplementary Figure S5). The chloride load variations are therefore primarily related to changes in discharge, not changes in chloride concentrations.

For the year-long investigation groundwater contributed 53% (~21,000 kg/yr) of the total chloride load (~40,000 kg/yr) to the wetland. The average change in chloride load through the wetland was −0.5% (Supplementary Figure S5), indicating that chloride is transported conservatively in the groundwater-surface water-wetland system. Although chloride may be subject to uptake by wetland plants (e.g., Schück and Greger, 2022), that does not appear to be a significant sink in this wetland. The small mass balance difference for chloride provides confidence in the methods employed to quantify discharge and solute loads for this system.

4.3.2 Regression model for missing Upstream nitrate load data

The results of the ten-fold model cross-validation for the training and testing data revealed average R^2 values of 0.997 and 0.927, respectively, therefore validating that the approach is a good predictor of the Upstream NO_3-N load. SHAP values for features within the regression model are presented in Figure 6, where a larger

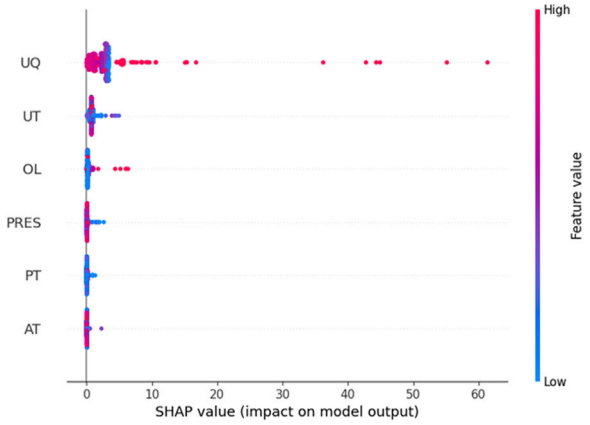


FIGURE 6
SHAP values determined for the gradient boosting regression model used to compute missing Upstream NO_3-N loads. Features included in model were: Upstream discharge (UQ), Upstream water temperature (UT), Outlet load (OL), atmospheric pressure (PRES), wetland water temperature (PT), and air temperature (AT).

SHAP value indicates a more significant impact on the model prediction. Overall, the Upstream discharge (UQ, Figure 6) data points have the greatest SHAP values and thus the greatest impact on the model output. It is also observed that the highest SHAP values for Upstream discharge occur when the magnitude of these points is greatest.

4.3.3 Nitrate loads

The average Upstream NO_3-N concentration (Figure 4D) for the study period was 2.8 mg/L, while for the Outlet it was 3.6 mg/L. Continuous groundwater NO_3-N concentrations from Well #6 (Figure 4E), and the NO_3-N concentrations from manual sampling at the Springs were consistently elevated (>4.3 mg/L). NO_3-N concentrations in the Outlet surface water are seasonally variable, but less so than at the Upstream location, exhibiting peak concentrations in the late fall-early winter (Figure 4F). The NO_3-N loads at all three locations have trends that closely follow the discharge data at each respective location, indicating that, like chloride, load variations are primarily related to changes in discharge, not NO_3-N concentrations (Figures 4G–I).

There is a strong correlation between the discrete load results, based on manual measurements, and the continuous NO_3-N loads recorded at the corresponding times for both the Upstream and Outlet locations, with R^2 values of 0.92 and 0.89, respectively (Figures 4G, I, respectively). This suggests that the methods employed to obtain the continuous time series for NO_3-N loads have produced reliable results.

The cumulative groundwater and surface water NO_3-N loads to the wetland for the 363-day study period were 20,000 kg and 10,000 kg, respectively, giving a relative contribution of groundwater to the total imported NO_3-N load of 67%. Seasonally, the relative contribution of groundwater to the total imported NO_3-N load for the winter (Dec-Feb), spring (Mar-May), summer (Jun-Aug), and fall (Sep-Nov) was 50%, 61%, 89%, and 77%, respectively. The estimated contribution of NO_3-N from septic system wastewater (64 kg NO_3-N/yr) was approximately 0.2% of the total load, indicating that agricultural sources dominate.

4.4 Wetland nitrate attenuation

To assess whether the Mill Pond wetland was functioning as a nitrate sink or source, the weekly NO_3-N loads imported and exported to the wetland during the 52-week study period were compared. As shown in Figure 7, the imported NO_3-N load exceeded the exported NO_3-N load during 50 of 52 weeks. The t-test results indicated that 51 out of 52 weeks had statistically significant differences ($p < 0.05$) between the imported and exported loads. The wetland had the greatest imported and exported loads in late winter and early spring; however, it also had the greatest removal rate during this time, with a maximum weekly removal rate of 82% in February-March 2024. The lowest imported and exported loads were observed in July 2024. During the two weeks when the wetland behaved as a nitrate source, the maximum increase in NO_3-N load was 8%.

5 Discussion

5.1 Using machine learning to fill data gaps

Unfortunately, missing data within long-term, high-frequency monitoring studies is a common hindrance to compiling a continuous data set (e.g., Pavlovskii et al., 2023). As such, using machine learning models to fill data gaps within datasets is an emerging sub-field of water quality studies. Sierra-Porta (2024) recently evaluated the suitability of ten machine learning models for filling water quality data gaps, finding that the gradient boosting model was among the most effective and accurate in predicting missing values. In the current study the gradient boosting model was also found to be effective at predicting the NO_3-N loads at the Upstream monitoring location, as shown by the results of the model cross-validation (see Section 4.3.2). Given the increased use of *in situ* nitrate monitoring instruments, such as SUNAs, and the continual challenges related to long-term field deployment, it is likely that the gradient boosting model, or other machine learning models, will become commonplace in water quality studies.

5.2 Groundwater-surface water connectivity

Throughout the study period, groundwater contributed 66% of the total freshwater discharge to the wetland; however, as seen in Table 1, the groundwater contribution varied seasonally. The maximum relative contribution occurred in the fall (72%), while the minimum occurred in the winter (48%).

In PEI, groundwater recharge typically occurs in late October due to reduced evapotranspiration, and again in March to early May due to snowmelt/rainfall (Jiang et al., 2015; Danielescu et al., 2022). These recharge periods correspond to peak groundwater baseflow periods and, consequently, peak groundwater nitrate contributions to the wetland (Figures 4B, H). Figure 8 shows the groundwater level measured in Well #6, upgradient of the wetland, and the computed

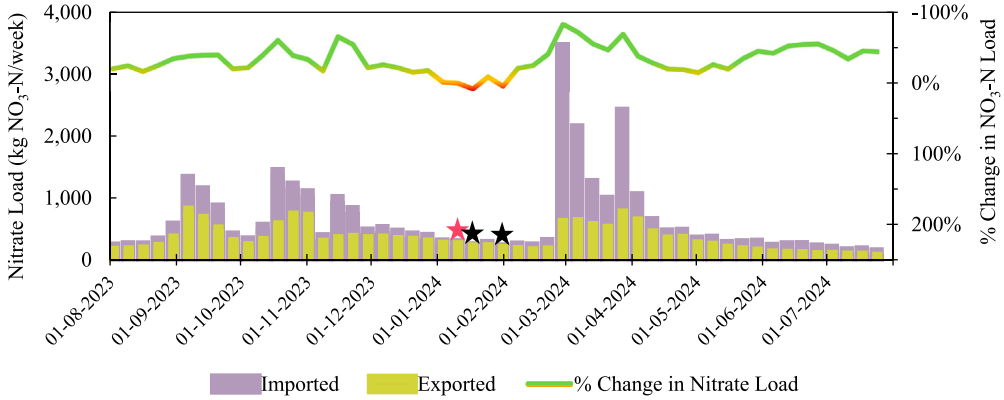


FIGURE 7
Weekly NO_3-N loads imported and exported from the wetland. The two weeks where the wetland behaves as a NO_3-N source are indicated with a black star above the bar. The week when there was no significant difference ($p > 0.05$) between the imported and exported loads is indicated with a pink star. The secondary axis shows the change in NO_3-N load (as %) using a gradient line with green indicating the highest removal rates. When the % change in load is negative, the wetland is a NO_3-N sink, whereas a positive value indicates that the wetland is a NO_3-N source.

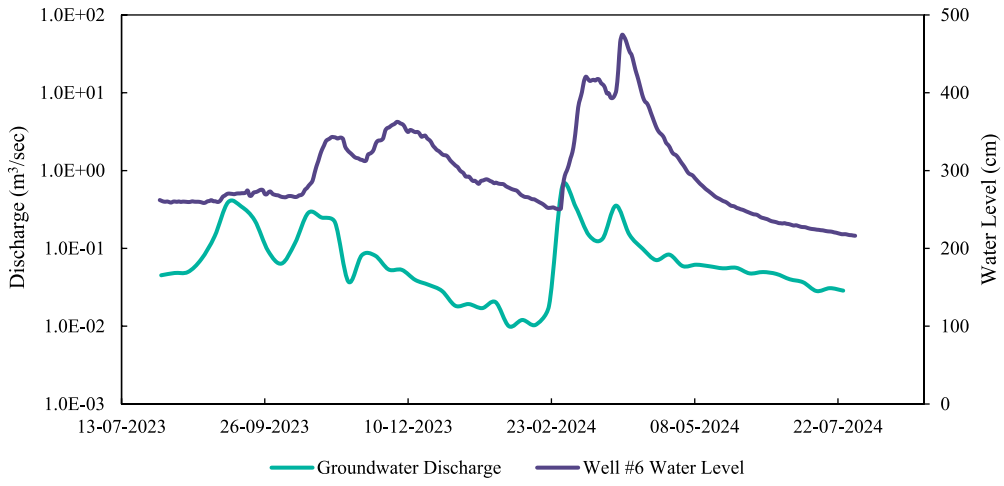


FIGURE 8
Weekly groundwater discharge to the wetland compared to the water level monitored in Well #6 over the study period.

groundwater discharge to the wetland. The occurrence of two principal recharge periods is reflected in both time series. The earlier increase observed in groundwater discharge at the Springs location may be explained by shorter flow paths adjacent to the wetland discharge area, whereas the water level in Well #6 shows a slower response due to the presence of a thick unsaturated zone (approximately ~16 m) (Figure 8).

5.3 Short and long-term trends in NO_3-N loads

As seen in Figure 4G, in late November 2023, the NO_3-N load at the Upstream location reached a maximum; however, as seen in Figure 4D, the NO_3-N concentrations decreased due to a dilution effect caused by heavy rain events (Figure 4A), indicating that the increases in surface water NO_3-N loads were driven by discharge. Moreover, the groundwater nitrate concentrations remained relatively constant throughout the study period (Figure 4E), whereas the groundwater NO_3-N load (Figure 4H) trended with the groundwater discharge (Figure 4B). Hence, as mentioned previously, discharge variability is the dominant control on nitrate loads delivered to the wetland via surface and subsurface pathways. This is further confirmed by the SHAP values obtained from application of the machine learning model, which indicated that the Upstream discharge had the greatest impact on the NO_3-N load at that location (Figure 6).

As seen in Figure 7, the NO_3-N load to the wetland was high in the fall, then again in March and April, corresponding to the periods with the highest groundwater discharge rates (Figure 4B). These findings are consistent with a study by Miller et al. (2016), which found a positive relationship between base flow index (BFI) and in-stream NO_3-N loads. Therefore, estimating BFI over short periods (i.e., monthly) within PEI watersheds could aid in understanding NO_3-N load dynamics within groundwater-influenced systems. The

seasonal trends and magnitude of loads in this study should be interpreted with caution due to the inter-annual variability in weather patterns (e.g., precipitation and temperature) that can significantly impact local and regional hydrological processes (Danielescu, 2023; Pavlovskii et al., 2023). For example, Oliver et al. (2024), using a PEI-based hydrologic model and future climate projections, showed that the fall peak in nitrate loads may shift from late fall to early December, while the spring peak may occur earlier in the season. Furthermore, Oliver et al. (2024) found that baseflow may increase during the winter and early spring as a result of increased precipitation as rainfall, more mid-winter thaws, and an earlier spring melt period, and a projected five-fold increase in February by the end of the century (2070–2100). In the current study the groundwater contribution to the Mill Pond wetland bypasses the riparian zone and enters the wetland via underwater springs, which allows for nitrate-rich groundwater to directly enter the receiving water body. As such, a potential five-fold increase in bypass flows during colder months (January and February), when the removal of NO_3-N within the wetland is at a minimum (Figure 7), could significantly increase the impact of nitrate in these freshwater systems.

5.4 The wetland response to nitrate loads

Danielescu et al. (2024) simulated a 3-year potato-barley-clover crop rotation for a field at the Harrington Experimental Farm and found that ~90 kg NO_3-N/ha/yr leached below the root zone in the potato year, while the barley and red clover (catch crops) years leached ~29 kg NO_3-N/ha/yr each. Interestingly, the load data from this study results in a catchment-based loading rate of 54.1 kg NO_3-N/ha catchment/yr (i.e., using the catchment area upgradient of the study site, Figure 1), which falls within the simulated leaching loads for potatoes and catch crops. In 2023 only 5.5% of the upgradient catchment was cropland in potato phase (Agriculture and Agri-Food Canada, 2024), which suggests that the NO_3-N loads we have determined are related to agricultural land use in previous years (i.e., legacy NO_3-N). For the study period the total NO_3-N load to the wetland was approximately 30,000 kg NO_3-N/yr. Steiness et al. (2021) estimated that a 1.3 ha wetland within an agricultural landscape in Denmark received an average annual NO_3-N load of 1,033 kg NO_3-N/yr (41 kg NO_3-N/ha catchment/yr) between 1990 and 2008, noting that these loads were, at the time, on the high end of reported values. A recent study by Oliver et al. (2024) in the Basin Head Lagoon, located in northeastern PEI, found that the annual NO_3-N load to the lagoon between 1990–2020 was 7 kg NO_3-N/ha catchment/yr, where groundwater contributed 83% of the load. The annual NO_3-N load we have determined for the Mill Pond wetland (54.1 kg NO_3-N/ha catchment/yr) is thus relatively high in comparison.

The small (1.2 ha) groundwater-influenced wetland investigated here attenuated approximately 39% of the total annual NO_3-N load (30,000 kg NO_3-N/yr); on catchment area basis this is equivalent to 21.1 kg NO_3-N/ha catchment/yr. The wetland behaved as a NO_3-N sink for approximately 94% of the study period, or 49 out of 52 weeks, a NO_3-N source for two weeks during January and February, and neither a NO_3-N source nor sink for one week in January (Figure 7). As seen in Figure 9, there is notable seasonal variability in the NO_3-N attenuation capacity of the wetland, with the winter (Dec-Feb) having removal rates in the range of 8 to −41% (where the data point in late February-early March with a removal rate of −82% is excluded), the spring (Mar-May) having removal rates in the range of −15% to −71%, the summer (Jun-Aug) having removal rates in the range of −15% to −55%, and the fall (Sep-Nov) having removal rates in the range of −17% to −65%, where negative values indicate a net reduction in load. Although previous studies did not report nitrate removal rates on a seasonal basis, Steiness et al. (2021) found that a 1.3 ha wetland attenuated between 43% and 83% of the annual NO_3-N load, while Cheng et al. (2020) found that strategically placed wetlands could reduce NO_3-N loads by 54%. The ranges of removal rates observed in the Mill Pond wetland are similar to previously reported values; however, they also highlight the significant seasonal variability in NO_3-N dynamics which may be missed with low-frequency monitoring.

As shown in a previous study in a constructed wetland (Kuschk et al., 2003), seasonal variation in nitrate attenuation within wetlands in temperate climates should be expected, given that lower water temperatures would reduce the amount of vegetative uptake and biological activity. However, as seen in Figure 9, the NO_3-N load reductions for all four seasons generally overlap in the range of −15% to −55%, indicating that the wetland investigated here may attenuate nitrate regardless of season. Figure 9 reveals a positive, non-linear trend between the imported NO_3-N load and the change in NO_3-N load and, by extension, the impact of increased discharge to the wetland. These results suggest that the wetland attenuates disproportionately more nitrate during high imported loads, especially during the spring and fall periods. Veraart et al. (2011) found that temperature disproportionately increases denitrification rates within constructed wetlands, which could be a potential factor producing the trend observed in the Mill Pond wetland.

As discussed in Mitsch and Wilson (1996), constructed wetlands could take 15–20 years to reach their full biologically viability and sustainability. The Mill Pond wetland was constructed in the 1950s and is considered well established. However, wetlands continuously evolve over time, notably due to sediment accumulation driven by factors such as geomorphology and hydrology (Anderson and Mitsch, 2006). The findings reported here provide a one-year snapshot of the wetland functioning, but it is possible that the nitrate attenuation capacity may change over longer time periods due to changes in wetland vegetation, land use and climate.

5.5 Potential nitrate removal processes

Previous studies by Jiang and Somers (2009) and Malenica (2015) have found that denitrification is not significant in attenuating nitrate within the PEI sandstone aquifer. This finding, combined with groundwater flow paths that apparently bypass the riparian zone, indicates that nitrate in groundwater is likely not attenuated before entering the Mill Pond wetland. This is also supported by the significant DO concentrations (>8.0 mg/L) determined at all locations, including the groundwater springs within the wetland (see Supplementary Table S2). While it was beyond the scope of the current study to identify specific NO_3-N

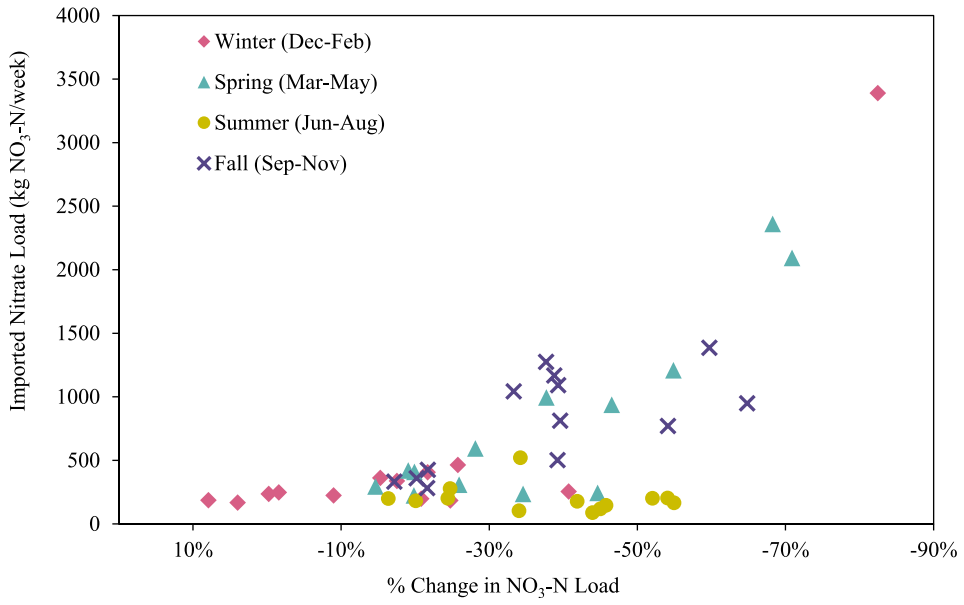


FIGURE 9
The imported NO_3-N load and the % change in NO_3-N load by season, where a negative % change in NO_3-N load indicates the wetland is a NO_3-N sink.

removal mechanisms, and there is limited evidence of denitrification (Crossley et al., 2024), it is possible that denitrification may be occurring in regions of the wetland bottom sediments not influenced by groundwater discharge, where low DO levels (i.e., <0.5 mg/L; Savard et al., 2010) may exist. In addition, the role of wetland vegetation, such as filamentous green algae, which proliferates during the summer months (e.g., Supplementary Figure S1) and is commonly observed in PEI freshwater wetlands (Cynthia Crane, personal communication, 17 April 2024), is not well understood. Additionally, it is understood that wetlands may remove other contaminants such as phosphorus and pesticides that were not investigated in this study (e.g., Kennedy and Mayer, 2002; Nowell, 2000). In future work, a multi-year study investigating the attenuation of various agricultural contaminants within a constructed wetland may provide greater insight into the removal potential of small wetlands as they evolve.

6 Conclusion

This study has assessed the surface and subsurface nitrate loads delivered to a small (1.2 ha) groundwater-influenced constructed wetland using high-frequency NO_3-N concentration and discharge data. Because NO_3-N concentrations in groundwater and surface water were relatively constant during the year-long investigation, variations in discharge rates were the dominant factor affecting the variation in nitrate loads delivered to the wetland. Groundwater discharge, bypassing the riparian zone, had higher NO_3-N concentrations than surface water inflows and contributed 67% of the total nitrate load to the wetland. The total nitrate load to the wetland from the 555 ha catchment area was approximately 30,000 kg NO_3-N/yr, (i.e., 54.1 kg NO_3-N/ha catchment/yr) which is substantial in comparison to other studies.

The constructed wetland behaved as a nitrate sink for 94% of the year-long study period, attenuating approximately 11,600 kg NO_3-N/yr or 39% of the total annual NO_3-N load. The average weekly NO_3-N removal rate was 33%, with variations depending on the time of year; weekly removal rates were in the range of 8%–41% during colder months and 16%–71% during the warmer months. These removal rates highlight the potential of small, constructed wetlands to be used as effective year-round nitrate attenuation systems within agricultural watersheds in PEI. Furthermore, a positive non-linear trend between the imported NO_3-N load and the change in NO_3-N reduction was identified, which is an important finding given that PEI climate change projections indicate higher intensity storms may result in larger event-based groundwater nitrate loads to surface waters.

As the first high-frequency, and four-season, groundwater-surface water-wetland nitrate study to be conducted in the region, these findings highlight not only the substantial NO_3-N loads within a typical rural watershed, but also the potential for small, constructed wetlands to be used as an effective component of nitrate BMP strategies.

Data availability statement

The raw data supporting the conclusions of this article will be made available by the authors, without undue reservation.

Author contributions

LC: Conceptualization, Data curation, Formal Analysis, Investigation, Methodology, Visualization, Writing–original draft.

KM: Conceptualization, Data curation, Funding acquisition, Investigation, Methodology, Resources, Supervision, Validation, Writing–review and editing. SD: Conceptualization, Data curation, Resources, Supervision, Validation, Writing–review and editing.

Funding

The author(s) declare that financial support was received for the research, authorship, and/or publication of this article. Funding for this research is provided by the Natural Sciences and Engineering Council of Canada (Discovery Grant held by K. T. B MacQuarrie) with support from Agriculture and Agri-Food Canada's Living Labs program.

Acknowledgments

We thank Dennis Connor (UNB), Mona Levesque (AAFC), Jared Wright (AAFC), and the Harrington Experimental Farm staff for valuable field and/or laboratory assistance. We acknowledge Ethan Eddy (UNB and E^2 Analytics) for his expertise in machine learning models and Sheldon Hann (AAFC) for his assistance in acquiring land use and GIS files. We acknowledge Megan Stone (CBCL) for her guidance in developing a surface water model in PCSWMM, and Computational Hydraulics Inc. (CHI) for providing a student license for PCSWMM for this study. Cynthia Crane, formerly with the PEI Department of Environment, Energy and Climate Action, provided insight regarding the algae occurrence within the study wetland. We thank the Holmes family, local landowners, for generously allowing access to the site and for providing historical information about the area.

Conflict of interest

The authors declare that the research was conducted in the absence of any commercial or financial relationships that could be construed as a potential conflict of interest.

Generative AI statement

The author(s) declare that no Generative AI was used in the creation of this manuscript.

Publisher's note

All claims expressed in this article are solely those of the authors and do not necessarily represent those of their affiliated organizations, or those of the publisher, the editors and the reviewers. Any product that may be evaluated in this article, or claim that may be made by its manufacturer, is not guaranteed or endorsed by the publisher.

Supplementary material

The Supplementary Material for this article can be found online at: https://www.frontiersin.org/articles/10.3389/fenvs.2025.1513704/full#supplementary-material

References

Agriculture and Agri-Food Canada (2024). Annual crop inventory. Available at: https://agriculture.canada.ca/atlas/apps/aef/main/index_en.html?AGRIAPP=23.

Anderson, C. J., and Mitsch, W. J. (2006). Sediment, carbon, and nutrient accumulation at two 10-year-old created riverine marshes. *Wetlands* 26 (3), 779–792. doi:10.1672/0277-5212(2006)26[779:SCANAA]2.0.CO;2

Beltran, J., Lautz, L. K., and Slosson, J. R. (2021). The impact of stream-groundwater exchange on seasonal nitrate loads in an urban stream. *Hydrol. Process.* 35 (8), e14324. doi:10.1002/hyp.14324

Benson, V. S., VanLeeuwen, J. A., Sanchez, J., Dohoo, I. R., and Somers, G. H. (2006). Spatial analysis of land use impact on ground water nitrate concentrations. *J. Environ. Qual.* 35 (2), 421–432. doi:10.2134/jeq2005.0115

Bhatti, A. Z., Farooque, A. A., Krouglicof, N., Peters, W., Acharya, B., Li, Q., et al. (2021). Climate change impacts on precipitation and temperature in Prince Edward Island, Canada. *World Water Policy* 7 (1), 9–29. doi:10.1002/wwp2.12046

Bhatti, A. Z., Farooque, A. A., Krouglicof, N., Peters, W., Li, Q., and Acharya, B. (2022). Prospective climates, and water availabilities under different projections of environmental changes in Prince Edward Island, Canada. *Water* 14 (5), 740. doi:10.3390/w14050740

Botrel, M., Hudon, C., Heffernan, J. B., Biron, P. M., and Maranger, R. (2022). Climate-driven variations in nitrogen retention from a riverine submerged aquatic vegetation meadow. *Water Resour. Res.* 58 (10), e2022WR032678. doi:10.1029/2022WR032678

Bowes, M. J., Smith, J. T., and Neal, C. (2009). The value of high-resolution nutrient monitoring: a case study of the River Frome, Dorset, UK. *J. Hydrology* 378 (1), 82–96. doi:10.1016/j.jhydrol.2009.09.015

Cheng, F. Y., and Basu, N. B. (2017). Biogeochemical hotspots: role of small water bodies in landscape nutrient processing. *Water Resour. Res.* 53 (6), 5038–5056. doi:10.1002/2016WR020102

Cheng, F. Y., Van Meter, K. J., Byrnes, D. K., and Basu, N. B. (2020). Maximizing US nitrate removal through wetland protection and restoration. *Nature* 588 (7839), 625–630. Article 7839. doi:10.1038/s41586-020-03042-5

Conant, B., Danielescu, S., Reeves, H., and Coulibaly, P. (2016). "Groundwater/surface water interaction. Chapt. 2," in *Groundwater science relevant to the great lakes water quality agreement: a status report*. Editors G. Grannemann, and D. Van Stempvoort (Environment and Climate Change Canada and U.S. Environmental Protection Agency).

Crawford, M., and Alexander, A. C. (2024). Fish kills and insecticides: historical water quality patterns in 10 agricultural watersheds in Prince Edward Island, Canada (2002–2022). *Front. Sustain. Food Syst.* 8. doi:10.3389/fsufs.2024.1356579

Critchley, K., Rudolph, D. L., Devlin, J. F., and Schillig, P. C. (2014). Stimulating *in situ* denitrification in an aerobic, highly permeable municipal drinking water aquifer. *J. Contam. Hydrology* 171, 66–80. doi:10.1016/j.jconhyd.2014.10.008

Crossley, L. M., MacQuarrie, K. T. B., and Danielescu, S. (2024). "Agricultural nitrate attenuation in a small groundwater-influenced wetland system," in *[conference paper], GeoMontreal: CGS/IAH-CNC groundwater conference* (Montreal, Quebec).

Danielescu, S. (2023). Development and application of ETCalc, a unique online tool for estimation of daily evapotranspiration. *Atmosphere-Ocean* 61 (3), 135–147. doi:10.1080/07055900.2022.2154191

Danielescu, S., and MacQuarrie, K. T. (2013). Nitrogen and oxygen isotopes in nitrate in the groundwater and surface water discharge from two rural catchments: implications for nitrogen loading to coastal waters. *Biogeochemistry* 115 (1), 111–127. doi:10.1007/s10533-012-9823-z

Danielescu, S., MacQuarrie, K. T., Zebarth, B., Nyiraneza, J., Grimmett, M., and Levesque, M. (2022). Crop water deficit and supplemental irrigation requirements for potato production in a temperate humid region (Prince Edward Island, Canada). *Water* 14 (17), 2748. doi:10.3390/w14172748

Danielescu, S., and MacQuarrie, K. T. B. (2011). Nitrogen loadings to two small estuaries, Prince Edward Island, Canada: a 2-year investigation of precipitation, surface water and groundwater contributions. *Hydrol. Process.* 25 (6), 945–957. doi:10.1002/hyp.7881

Danielescu, S., MacQuarrie, K. T. B., and Faux, R. N. (2009). The integration of thermal infrared imaging, discharge measurements and numerical simulation to

quantify the relative contributions of freshwater inflows to small estuaries in Atlantic Canada. *Hydrol. Process.* 23 (20), 2847–2859. doi:10.1002/hyp.7383

Danielescu, S., MacQuarrie, K. T. B., Nyiraneza, J., Zebarth, B., Sharifi-Mood, N., Grimmett, M., et al. (2024). Development and validation of a crop and nitrate leaching model for potato cropping systems in a temperate–humid region. *Water* 16 (3), 475. doi:10.3390/w16030475

Dibblee, R. (2000). PEI Wetlands [Vector digital data]. Available at: www.gov.pe/gis.

Dunn, A. M., Julien, G., Ernst, W. R., Cook, A., Doe, K. G., and Jackman, P. M. (2011). Evaluation of buffer zone effectiveness in mitigating the risks associated with agricultural runoff in Prince Edward Island. *Sci. Total Environ.* 409 (5), 868–882. doi:10.1016/j.scitotenv.2010.11.011

Environment and Climate Change Canada (2024). Historical data—climate. Available at: https://climate.weather.gc.ca/historical_data/search_historic_data_e.html.

Government of Prince Edward Island (2019). Corporate landuse inventory 2010. Available at: https://data.princeedwardisland.ca/.

Grizard, P. (2013). Modelling nitrate loading from watersheds to coastal waters of the northumberland strait. *[master's thesis]*. Canada: The University of New Brunswick.

Hansen, A. T., Campbell, T., Cho, S. J., Czuba, J. A., Dalzell, B. J., Dolph, C. L., et al. (2021). Integrated assessment modeling reveals near-channel management as cost-effective to improve water quality in agricultural watersheds. *Proc. Natl. Acad. Sci.* 118 (28), e2024912118. doi:10.1073/pnas.2024912118

Hansen, A. T., Dolph, C. L., Foufoula-Georgiou, E., and Finlay, J. C. (2018). Contribution of wetlands to nitrate removal at the watershed scale. *Nat. Geosci.* 11 (2), 127–132. doi:10.1038/s41561-017-0056-6

Jiang, Y., Nishimura, P., van den Heuvel, M. R., MacQuarrie, K. T. B., Crane, C. S., Xing, Z., et al. (2015). Modeling land-based nitrogen loads from groundwater-dominated agricultural watersheds to estuaries to inform nutrient reduction planning. *J. Hydrology* 529, 213–230. doi:10.1016/j.jhydrol.2015.07.033

Jiang, Y., and Somers, G. (2009). Modeling effects of nitrate from non-point sources on groundwater quality in an agricultural watershed in Prince Edward Island, Canada. *Hydrogeology J.* 17 (3), 707–724. doi:10.1007/s10040-008-0390-2

Kennedy, G., and Mayer, T. (2002). Natural and constructed wetlands in Canada: an overview. *Water Qual. Res. J.* 37 (2), 295–325. doi:10.2166/wqrj.2002.020

Kuschk, P., Wiessner, A., Kappelmeyer, U., Weissbrodt, E., Kästner, M., and Stottmeister, U. (2003). Annual cycle of nitrogen removal by a pilot-scale subsurface horizontal flow in a constructed wetland under moderate climate. *Water Res.* 37 (17), 4236–4242. doi:10.1016/S0043-1354(03)00163-5

Lamb, K. J., MacQuarrie, K. T. B., Butler, K. E., Danielescu, S., Mott, E., Grimmet, M., et al. (2019). Hydrogeophysical monitoring reveals primarily vertical movement of an applied tracer across a shallow, sloping low-permeability till interface: implications for agricultural nitrate transport. *J. Hydrology* 573, 616–630. doi:10.1016/j.jhydrol.2019.03.075

Liang, K., Jiang, Y., Nyiraneza, J., Fuller, K., Murnaghan, D., and Meng, F.-R. (2019). Nitrogen dynamics and leaching potential under conventional and alternative potato rotations in Atlantic Canada. *Field Crops Res.* 242, 107603. doi:10.1016/j.fcr.2019.107603

Lundberg, S. M., and Lee, S.-I. (2017). "A unified approach to interpreting model predictions," in *[conference paper], 31st conference on neural information processing systems* (Long Beach, CA, USA).

Mackie, C., Levison, J., Binns, A., and O'Halloran, I. (2021). Groundwater-surface water interactions and agricultural nutrient transport in a Great Lakes clay plain system. *J. Gt. Lakes. Res.* 47 (1), 145–159. doi:10.1016/j.jglr.2020.11.008

Malencia, A. (2015). Evaluation of nitrate distribution and matrix storage effects in a dual permeability fractured bedrock aquifer with heterogeneous hydrochemistry *[master's thesis]*. Canada: The University of Guelph.

Miller, M. P., Tesoriero, A. J., Capel, P. D., Pellerin, B. A., Hyer, K. E., and Burns, D. A. (2016). Quantifying watershed-scale groundwater loading and in-stream fate of nitrate using high-frequency water quality data. *Water Resour. Res.* 52 (1), 330–347. doi:10.1002/2015WR017753

Mitsch, W. J., and Wilson, R. F. (1996). Improving the success of wetland creation and restoration with know-how, time, and self-design. *Ecol. Appl.* 6 (1), 77–83. doi:10.2307/2269554

Nowell, L. H. (2000). *Pesticides in stream sediments and aquatic biota (pesticides in stream sediment and aquatic biota) [fact sheet]*. Sacramento, CA: USGS Publications. Available at: https://pubs.usgs.gov/fs/2000/0092/fs20000092.pdf.

Oliver, A. C., Kurylyk, B. L., Johnston, L. H., LeRoux, N. K., Somers, L. D., and Jamieson, R. C. (2024). Impacts of climate change and best management practices on nitrate loading to a eutrophic coastal lagoon. *Front. Environ. Sci.* 12. doi:10.3389/fenvs.2024.1468869

Pavlovskii, I., Jiang, Y., Danielescu, S., and Kurylyk, B. L. (2023). Influence of precipitation event magnitude on baseflow and coastal nitrate export for Prince Edward Island, Canada. *Hydrol. Process.* 37 (5), e14892. doi:10.1002/hyp.14892

Pedregosa, F., Varoquaux, G., Gramfort, A., Michel, V., Thirion, B., Grisel, O., et al. (2011). Scikit-learn: machine learning in Python. *J. Mach. Learn. Res.* 12, 2825–2830. doi:10.48550/arXiv.1201.0490

Savard, M. M., Somers, G., Smirnoff, A., Paradis, D., Bochove, E. van, and Liao, S. (2010). Nitrate isotopes unveil distinct seasonal N-sources and the critical role of crop residues in groundwater contamination. *J. Hydrology* 381 (1), 134–141. doi:10.1016/j.jhydrol.2009.11.033

Schück, M., and Greger, M. (2022). Chloride removal capacity and salinity tolerance in wetland plants. *J. Environ. Manag.* 308, 114553. doi:10.1016/j.jenvman.2022.114553

Sierra-Porta, D. (2024). Assessing the impact of missing data on water quality index estimation: a machine learning approach. *Discov. Water* 4 (1), 11. doi:10.1007/s43832-024-00068-y

Somers, G. (1992). "*Agricultural impacts on water quality—a P.E.I. perspective* [national workshop proceedings]," in *Agricultural impacts on water quality* (Ottawa, Ontario).

Somers, G., Raymond, B., and Uhlman, W. (1999). P.E.I. Water quality interpretive report. doi:10.13140/RG.2.1.1872.9442

Steiness, M., Jessen, S., van't Veen, S. G. M., Kofod, T., Højberg, A. L., and Engesgaard, P. (2021). Nitrogen-loads to streams: importance of bypass flow and nitrate removal processes. *J. Geophys. Res. Biogeosciences* 126 (5), e2020JG006111. doi:10.1029/2020JG006111

Stevens, C. E., Gabor, T. S., and Diamond, A. W. (2003). Use of restored small wetlands by breeding waterfowl in Prince Edward Island, Canada. *Restor. Ecol.* 11 (1), 3–12. doi:10.1046/j.1526-100X.2003.00107.x

Veraart, A. J., de Klein, J. J. M., and Scheffer, M. (2011). Warming can boost denitrification disproportionately due to altered oxygen dynamics. *PLoS ONE* 6 (3), e18508. doi:10.1371/journal.pone.0018508

Zebarth, B. J., Danielescu, S., Nyiraneza, J., Ryan, M. C., Jiang, Y., Grimmett, M., et al. (2015). Controls on nitrate loading and implications for BMPs under intensive potato production systems in Prince Edward Island, Canada. *Groundw. Monit. and Remediat.* 35 (1), 30–42. doi:10.1111/gwmr.12088

frontiers | Frontiers in Environmental Science

TYPE Original Research
PUBLISHED 21 October 2024
DOI 10.3389/fenvs.2024.1416018

Check for updates

OPEN ACCESS

EDITED BY
Carl Mitchell,
University of Toronto Scarborough, Canada

REVIEWED BY
Joseph Delesantro,
The Pennsylvania State University (PSU), United States
Tim Duval,
University of Toronto Mississauga, Canada

*CORRESPONDENCE
Keith E. Schilling,
keith-schilling@uiowa.edu

RECEIVED 11 April 2024
ACCEPTED 07 October 2024
PUBLISHED 21 October 2024

CITATION
Anderson E, Schilling KE, Just CL and Seo BC (2024) Quantifying the impact of a constructed wetland on downstream nitrate concentrations and loads in the U.S. Midwest.
Front. Environ. Sci. 12:1416018.
doi: 10.3389/fenvs.2024.1416018

COPYRIGHT
© 2024 Anderson, Schilling, Just and Seo. This is an open-access article distributed under the terms of the Creative Commons Attribution License (CC BY). The use, distribution or reproduction in other forums is permitted, provided the original author(s) and the copyright owner(s) are credited and that the original publication in this journal is cited, in accordance with accepted academic practice. No use, distribution or reproduction is permitted which does not comply with these terms.

Quantifying the impact of a constructed wetland on downstream nitrate concentrations and loads in the U.S. Midwest

Elliot Anderson[1], Keith E. Schilling[1]*, Craig L. Just[2] and Bong Chul Seo[3]

[1]Iowa Geological Survey, University of Iowa, Iowa City, IA, United States, [2]Department of Civil and Environmental Engineering, University of Iowa, Iowa City, IA, United States, [3]Department of Civil, Architectural, and Environmental Engineering, Missouri University of Science and Technology, Rolla, MO, United States

Constructed wetlands are standard conservation practices used to reduce nitrate loads in agricultural watersheds. Many studies have examined the efficiency of denitrification in wetlands under various scenarios, but quantifying the watershed-scale impact of wetlands on downstream nitrate levels is rarely done using field observations. In this study, we estimated nitrate removal in a constructed wetland in the headwaters of Mud Creek, a HUC12 watershed in eastern Iowa, from May–September 2022 and May–September 2023 (a ten-month period). We also measured nitrate loads at four successive downstream sites, three along Mud Creek and one below its confluence with the larger Cedar River. The wetland removed 6,200 kg of nitrate (74% of total inputs). At the three downstream locations in Mud Creek, the percentage of each site's total nitrate load removed by the wetland decreased to 19, 8.6, and 4.1%—this latter value represents the wetland's influence on nitrate removal in the entire Mud Creek basin. The wetland's impact of nitrate loads in the Cedar River was negligible (reduction of 0.02%). The percentage of a site's drainage area treated by the wetland approximately followed a 1:1 relationship to that site's percent reduction in nitrate. Profiles of nitrate concentrations in Mud Creek notably varied pre- and post-wetland. Concentrations before the installation steadily decreased along the waterway, while post-wetland concentrations rapidly decreased directly downstream of the wetland and steadily increased at each succeeding site. Our results demonstrate that while the wetland successfully lowered local nitrate levels, its effect on the basin's overall nitrate loads was minimal. Achieving nutrient reduction goals at the watershed scale solely using constructed wetlands appears infeasible given that the required number of practices greatly exceeds current efforts.

KEYWORDS

nitrate, wetland, scaling, remediation, monitoring, eutrophication

1 Introduction

Waterborne nitrate-nitrogen (nitrate) is a major pollutant of concern in the U.S. Corn Belt (Chambers et al., 2008; Schilling et al., 2012). Its presence drives stream and lake eutrophication at local and regional scales (Smith and Schindler, 2009), and downstream export has contributed to widespread hypoxic conditions in the Gulf of Mexico (Burkart and James, 1999; Rabalais et al., 2002). These eutrophic conditions have detrimental impacts on aquatic ecological health (Singh et al., 2022) and episodically spur harmful algal blooms, which present acute risks for humans and animals upon contact (Hallegraeff, 2003). Nitrate concentrations in drinking water also present an acute threat to human health (Fewtrell, 2004), and they may be carcinogenic under prolonged periods of exposure (Ward et al., 2018).

Nitrate delivery to waterbodies has been linked to agricultural activities (Syswerda et al., 2012), especially intensive row crop production (Randall and Mulla, 2001). Nitrate loss in the U.S. Corn Belt is among the highest per unit area in the nation (Aulenbach et al., 2007; Schilling and Libra, 2000). Specific states, such as Iowa (Jones et al., 2018b), contribute disproportionate amounts of nitrate to downstream waterbodies (Goolsby et al., 2001). In many watersheds, stream nitrate concentrations repeatedly exceed drinking water standards and threaten water suppliers using surface intakes (Jha et al., 2010; Jones et al., 2020). Municipal water suppliers must ensure nitrate levels in their finished drinking water are below the maximum contaminant level of 10 mg/L, and the expenses and labor associated with these treatment processes place financial burdens on numerous Midwest communities (Christianson et al., 2013; Vedachalam et al., 2019). Furthermore, surface water nitrate concentrations are often far greater than levels suggested by nutrient criteria meant to benefit ecological health (Dodds and Welch, 2000; Jones et al., 2018c).

In light of this situation, considerable effort has gone into lowering nitrate levels in Midwestern rivers and streams. Many states have initiatives with explicit nutrient reduction goals (Anderson et al., 2016; David et al., 2013; Scavia et al., 2017). In Iowa, efforts are guided by the Iowa Nutrient Reduction Strategy (Iowa State University, 2012). Additionally, specific waterbodies often have limits on allowable nutrient levels, which are defined through the creation of total maximum daily loads (TMDLs). Iowa has approximately 20 TMDLs for nutrients. Some of the most prominent TMDLs for nitrate include those created for the Cedar (Hutchinson and Christiansen, 2013), Des Moines (Schilling and Wolter, 2009), and Raccoon Rivers (Jha et al., 2010).

Conservation plays a large role in all of these reduction efforts, and numerous conservation strategies have been developed to reduce nitrate loads (Butt and Brown, 2000; Conley, 1999). Constructed wetlands have been shown to be among the most effective nitrate reduction practices (Crumpton, 2001; Haas et al., 2017), especially in strategies utilizing conservation planning tools (Scavia et al., 2017; Weber et al., 2018). Constructed wetlands are engineered systems designed and built to take advantage of natural processes typically found within the vegetation, soils, and microbiomes of the wetlands (Vymazal, 2007). Herein, all mention of wetlands refers specifically to constructed wetlands built for the purpose of improving water quality.

Although wetlands can treat a variety of waterborne pollutants, most have proven effective at fostering denitrification and removing large quantities of nitrate (Spieles and Mitsch, 1999). Not all nitrate removal in constructed wetlands occurs via denitrification (Martin and Reddy, 1997). Some nitrate is assimilated into dissolved or particulate organic nitrogen, which can be discharged downstream or retained in the wetland (Lee et al., 2009).

In agricultural landscapes, wetlands are usually located along the main channel of a stream or at major tile drainage outlets draining farmland catchments (Crumpton et al., 2006). Inflow water is slowed within the wetland, and the submerged vegetation and soils produce a subaqueous environment conducive to denitrification (Vymazal, 2007). The specific rate at which denitrification occurs depends on many factors, including incoming nitrate concentrations, water temperatures, flow rates, vegetation species or maturity, and residence time (Collins and Gillies, 2014; Lee et al., 2009; Lin et al., 2008).

A great deal of study has been conducted on maximizing wetland removal efficiency (Cheng et al., 2020; Crumpton et al., 2020; Singh et al., 2019). In many instances, wetlands have removed substantial portions (>50%) of their nitrate inputs (Crumpton et al., 2006; Hunt et al., 1999; Maxwell et al., 2017), leading to large reductions in local nitrate concentrations (Drake et al., 2018). While these nitrate reductions are a positive outcome, the benefits of a particular wetland on downstream water quality become increasingly hard to measure as more untreated water reaches the stream from larger drainage areas and dilutes the treated water containing fewer nitrates (Ikenberry et al., 2014; Kovacic et al., 2000). Loads removed by a wetland often become minuscule compared to loads in larger downstream waterbodies. For example, Drake et al. (2018) reported nitrate removal of 66,800 kg from 2014–2016 (a reduction of 49%) in a constructed wetland near the headwaters of the Cedar River in eastern Iowa. Compared to the nitrate flux of the entire Cedar River basin across the same timeframe (120 Gg; (Jones et al., 2018b)), this value represents a reduction of only 0.05%.

The downstream impacts of wetlands on river water quality have been estimated using load calculations (Drake et al., 2018) or watershed-scale models (Böhlke et al., 2009; Conan et al., 2003; Mitsch et al., 2005), but rarely have impacts been verified with field observations. Quantifying the spatial rate at which nitrate removal from a wetland diminishes with increasing watershed area remains largely unexplored. In this study, we evaluated the downstream impacts of a newly constructed wetland on nitrate levels in the highly agricultural Mud Creek watershed in east-central Iowa. After quantifying nitrate removal in the constructed wetland, we utilized high-resolution nitrate sensors in four downstream monitoring locations and in the larger receiving river system to document how the impacts of the wetland diminish with watershed scale. Specifically, our objectives were to: 1) calculate the nitrate removed by the wetland during May–Sep in 2022 and May–September 2023; 2) quantify nitrate loads in Mud Creek at four successive downstream locations to assess the impact of the wetland on downstream water quality, and 3) evaluate how the longitudinal profile of nitrate concentrations along Mud Creek varied before and after wetland installation.

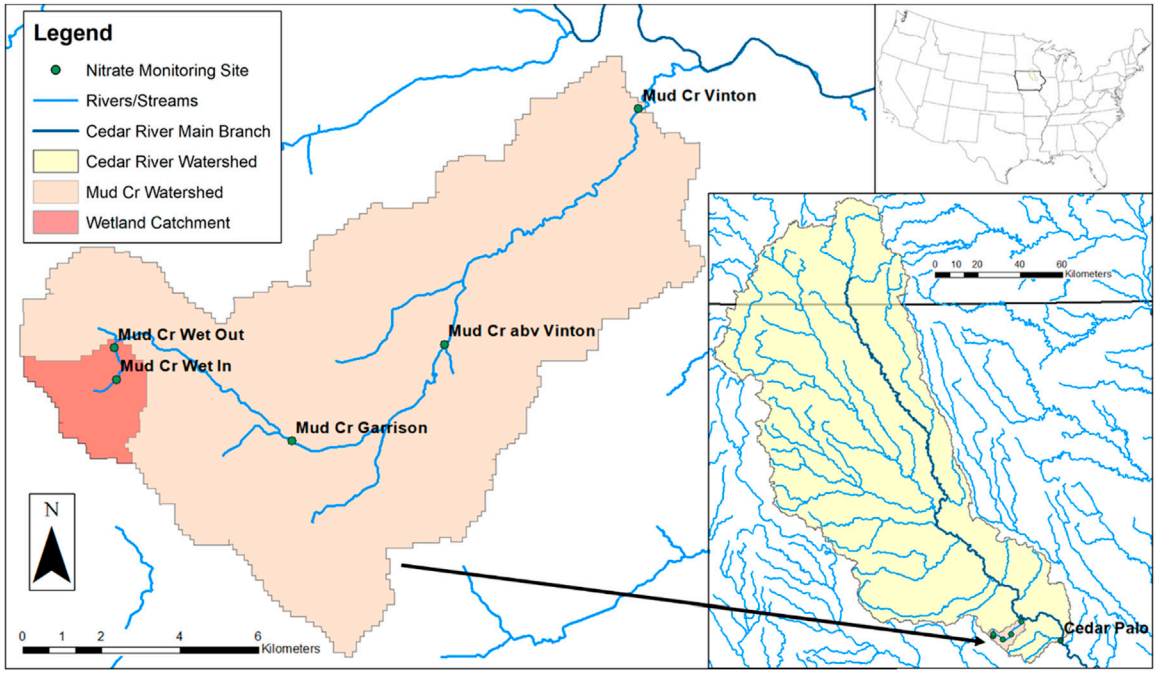


FIGURE 1
The nitrate monitoring sites and watersheds for the Cedar River, Mud Creek, and wetland. The main stem of the Cedar River is displayed in dark blue.

2 Methods

2.1 Site description and setting

Mud Creek is a perennial stream draining a 115 km^2 watershed (HUC12 basin 070802051104) in Benton County, Iowa (Figure 1). Mud Creek outfalls into the Cedar River—a much larger waterway with 15,800 km^2 of drainage area at its confluence with Mud Creek (~five HUC08 basins). Mud Creek is located in the Iowan Surface landform region (Prior, 1991), an area marked by low-relief topography and poorly drained glacial till plains overlying shallow sedimentary bedrock (mainly limestone, dolomite, and shale (Witzke, 1998)). The Cedar River basin also predominantly lies within the Iowan Surface and contains hydrologic and geologic behavior similar to that of Mud Creek.

Land use in Mud Creek watershed is agricultural, consisting of approximately 80% of the land area in row crop production (corn and soybean), with small amounts (<5% of the total watershed) of urban land use near Mud Creek's outfall in the town of Vinton, IA (Iowa DNR NRGIS, 2009). Annual precipitation in Benton County is approximately 850 mm (annual average from 1895–2023), with a majority of rainfall (~2/3) occurring during the spring and summer (NOAA, 2024). Artificial tile drainage is widespread and contributes, along with groundwater movement, to perennial flows at Mud Creek's outlet. The combination of high agricultural intensity and artificial drainage has resulted in impairments to surface water quality in the region (Brendel and Soupir, 2017; Kalkhoff et al., 2000; Squillace and Engberg, 1988), with nitrate being a particular pollutant of concern (Jones et al., 2018c; Schilling and Libra, 2000). Hence, the processes driving nitrate transport in Mud Creek are found throughout the overall Cedar River watershed, and the eutrophication challenges and remediation strategies conducted in Mud Creek are likewise taking place throughout the Cedar River basin (Weber et al., 2018).

2.2 Wetland construction

In 2021, a wetland was constructed near the headwaters of Mud Creek (Figure 1). The wetland is located along Mud Creek's main channel and contains a surface area of 5.1 ha. The design and installation of the wetland was completed as part of the Iowa Watershed Approach, a large-scale initiative to improve water quality and reduce flooding in nine major watersheds (Weber et al., 2018). Funding for the Mud Creek wetland was provided by both the Iowa Watershed Approach (https://iowawatershedapproach.org/) and the Environmental Protection Agency (https://www.epa.gov/), with the goal of lowering local nitrate concentrations and reducing flood peaks.

A local engineering firm completed the wetland's technical design. The wetland was constructed in-stream, with the main channel of Mud Creek acting as its primary inlet and outlet. It was designed to have a maximum depth of 2.1 m and a storage capacity of 160,000 m^3. Primary and auxiliary spillways were constructed to contain the 24-h design storms for return periods of 25 and 50 years, respectively. With the cooperation of the local landowner, row crop lands adjacent to the Mud Creek channel were converted to grass and native vegetation and incorporated into the wetland's storage area. The wetland became fully operational in August 2021—requiring a few months to fill with water post-construction. The total cost of the wetland, including its design, construction, and permitting efforts, was approximately $600,000.

TABLE 1 Nitrate monitoring sites and corresponding sensor information.

Short name	Long name	Site order	Site station (km)	Area (km^2)	Sensor ID	IFC ID	Long	Lat
Mud Cr Wet In[a]	Mud Creek upstream of Wetland	1	1.15	3.37	WQS0101	MUDCR04	−92.1676	42.09411
Mud Cr Wet Out[a]	Mud Creek downstream of Wetland	2	2.04	5.18	WQS0112		−92.168	42.1014
Mud Cr Garrison[a]	Mud Creek near Garrison, IA	3	8.07	31.86	WQS0102	MUDCR03	−92.1138	42.07951
Mud Cr abv Vinton[a]	Mud Creek upstream of Vinton, IA	4	13.34	58.02	WQS0103	MUDCR02	−92.0664	42.10121
Mud Cr Vinton[a]	Mud Creek at Vinton, IA	5	22.29	113.18	WQS0071	MUDCR01	−92.0057	42.1547
Cedar Palo[b]	Cedar River at Blairs Ferry Road at Palo, IA	6	56.75	16425.70	05464420		−91.7852	42.06916

[a]operated and maintained by IWQIS.
[b]operated and maintained by the USGS.

Compared to the larger Mud Creek watershed, the tributary area of the wetland is overwhelmingly agricultural (>95%). Approximately 3.37 km^2 of catchment area drains to the wetland via Mud Creek's main channel, whereas an additional 1.76 km^2 of adjacent farmland drains to the wetland via nine tile lines and one ephemeral creek. In total, the wetland treats an area of 5.18 km^2, which is 4.58% of the Mud Creek watershed. Mud Creek produces consistent flow at the wetland's inlet and outlet under normal hydrologic conditions. However, flow can cease during extended dry periods, resulting in stagnant water in the main channel. Tile lines typically flow during the spring and early summer but can also dry out in the absence of wet weather. After discharging from the wetland's outlet, flow continues unimpounded along Mud Creek for 21.9 km until it reaches the Cedar River. Overall, the wetland was typical (in terms of its dimensions and location) of those commonly constructed along stream channels in agricultural watersheds (Crumpton et al., 2020; Lemke et al., 2022; Messer et al., 2021).

2.3 Monitoring and data collection

Streamflow and nitrate concentrations were monitored at five locations along Mud Creek to assess the wetland's impact on stream conditions. Table 1 contains each location's relevant metadata, including their abbreviated names. Two of the monitoring locations included the wetland inlet (Mud Cr Wet In) and outlet (Mud Cr Wet Out). The remaining three sites were evenly spaced along Mud Creek, with the final location (Mud Cr Vinton) 1.6 km upstream of its confluence with the Cedar River.

Nitrate concentrations were monitored using *in situ* probes (Hach Nitratax Plus SC, 5 mm path length). When deployed, these sensors record nitrate concentrations every 15 min using ultraviolet absorption. This sensor model has proven proficient in providing continuous unbiased measurements of riverine nitrate in Iowa (Cao et al., 2023; Drake et al., 2018; Jones et al., 2017; Jones et al., 2020). In early 2020, nitrate sensors were deployed at each site except Mud Cr Wet Out, which was installed in July 2021 following wetland construction. Several sensors were installed in 2020 to gauge Mud Creek's longitudinal nitrate profile pre-wetland. The nitrate sensors were removed during winter and thus followed a deployment schedule from approximately roughly May to November each year from 2020–2023. Supplementary Figure S1 summarizes the sensors' operational timeframes at each location.

Nitrate concentrations measured using the probes were validated by collecting 30 grab samples at four sensor locations during 2020 (R^2 = 0.91). Nitrate concentrations in the grab samples ranged from 2.1–17.6 mg/L and were measured by the State Hygienic Laboratory at the University of Iowa. A Bland-Altman analysis confirmed agreement between measurement techniques at all sites (Dewitte et al., 2002). Furthermore, all probes were shipped to their parent manufacturer following their retrieval each winter. The manufacturer inspected and recalibrated the equipment to ensure continued functionality before redeployment in the spring. Mud Creek's continuous nitrate concentrations are publicly available through the Iowa Water Quality Information System (IWQIS: https://iwqis.iowawis.org/app/), a web portal containing continuous, *in situ* water quality data across Iowa. We have also included the specific nitrate data from our analysis within this study's Supplementary Material.

Streamflow values were estimated using stage-discharge relationships at the five sites (Quintero et al., 2021). Topographic surveys were conducted to determine the channel's cross-sectional geometries. Stream stages were monitored at four locations using stream sensors developed by the Iowa Flood Center (IFC); these sensors were installed on roadway bridges and used ultrasonic technology to measure river levels every 15 min (Kruger et al., 2016). No overhead bridge is present near the Mud Cr Wet Out site, so a water level transducer (*In-Situ* Level TROLL 400 Data Logger) was used to monitor stage elevations.

During a preliminary analysis in 2022, we noticed biases occurring in the values reported by IFC sensors, whereby stage was overestimated during low-flow conditions. We subsequently installed water level transducers at three Mud Creek sites (Mud Cr Wet In, Mud Cr Garrison, and Mud Cr Vinton) in early 2023. The transducers recorded stage elevations alongside the IFC sensors in 2023. These new stage data were used to correct the biases reported by the IFC sensors in 2022. Consequently, 15-min stage records were obtained for the 2022–2023 measurement period. Stages were converted to corresponding streamflow values using the continuous slope-area method (Lee et al., 2017). Streamflow estimates were validated using an acoustic Doppler velocimeter (SonTek FlowTracker2 Handheld-ADV) to measure flow on-site

10–12 times at each monitoring location in 2020 and 2023. Measured streamflow values ranged between 0.02 and 4.4 m^3/s, and all on-site measurements were within 15% of estimated discharges. All flow values are publicly available through the Iowa Flood Information System (https://ifis.iowafloodcenter.org/ifis/app/), a web portal that contains continuous flow measurements collected by the IFC sensors (Krajewski et al., 2017). The specific water depth and streamflow datasets used in this study have also been included in the Supplementary Material.

The United States Geological Survey (USGS) also operates a stream gauge along the Cedar River 34.9 km downstream of Mud Creek's outfall near Palo (USGS gauge 05464420). Both streamflow and nitrate have been continuously monitored at this site since 2012 using standard USGS protocols (Lins and Slack, 1999; Pellerin et al., 2014). To estimate the wetland's nitrate inputs not captured by the main inlet, tile lines and a creek draining directly to the wetland were monitored throughout May–October 2023 using grab samples collected every 2 weeks. Flow rates were estimated during sample collection by simply timing the rate at which discharge filled a 19-L bucket. Upon collection, grab samples were returned to a laboratory and analyzed for nitrate using a probe identical to those deployed in the field.

2.4 Nitrate load calculations

Nitrate loads were calculated using nitrate concentrations and corresponding flow values at all six monitoring locations. Load calculations presented in this study describe five-month periods (May–September) in 2022 and 2023. This timeframe was constrained by the deployment schedules of the nitrate sensors, but it broadly aligns with typical seasonal patterns of nitrate loads in Iowa (Zhang and Schilling, 2005). Most wetland denitrification also occurs during this period due to the higher nitrate concentrations, greater streamflow, and warmer temperatures (Crumpton et al., 2020; Stein and Hook, 2005).

Daily values were calculated for nitrate concentrations and streamflow by taking arithmetic means of the 15-min data. Nitrate concentrations were interpolated during occasional instances of sensor fouling (<5% of days), as linear interpolation has proven effective for stream nitrate (Schilling et al., 2017). Daily loads were then found at each site by multiplying mean nitrate concentrations and flow values. This daily load calculation method was used due to short-term variabilities of river stage measurement documented in our bridge sensor equipment. Bridge sensor readings can occasionally contain aberrant values, but these largely balance out on a daily scale (Kruger et al., 2016; Quintero et al., 2021). Other researchers have successfully utilized this method when estimating nitrate loads over months or years (Jones et al., 2018a; Pellerin et al., 2014; Zimmer et al., 2019). During days with no streamflow (i.e., stagnant water), loads were set to 0. Loads were aggregated across the entire analysis period (Table 2; May–September 2022 and May–September 2023) and for each individual month (Table 3). Yields were also calculated by dividing a site's nitrate load by its drainage area.

Nitrate loads entering the wetland through the peripheral tile lines were correlated to those entering the wetland through the main channel. This relationship suggested that tile nitrate consistently accounted for 20% of the nitrate inflow from the main channel (Supplementary Figure S6). We thus multiplied the daily loads at Mud Cr Wet In by 1.2 to estimate the total nitrate load entering the wetland (Mud Cr Wet Total). The mass of nitrate removed by the wetland (Wetland Removal) was calculated by taking the difference between the total nitrate entering it (Mud Cr Wet Total) and the nitrate discharged at the outlet (Mud Cr Wet Out). More precisely, the Wetland Removal term refers to all nitrate transformed or retained within the wetland; therefore, this calculation represents a simple mass balance of the wetland's nitrate inputs and outputs. To contextualize the mass of nitrate removed by the wetland, we defined the metric % Reduction, which was calculated as

$$\%\,Reduction = \frac{Wetland\ Removal}{Nitrate\ Load + Wetland\ Removal} * 100\%$$

where Nitrate Load is a site's nitrate flux across the analysis period. This percentage is bounded between 0% and 100% and is the nitrate removed by the wetland divided by the sum of this removal and a location's observed nitrate load. % Reduction thus quantifies the wetland's nitrate loss in terms of a site's overall nitrate load.

We also calculated another metric termed Wetland% of Watershed (Table 2). This term refers to the percentage of a site's drainage area treated by the wetland. For instance, the Mud Cr Garrison site has a tributary area of 31.9 km^2. The wetland's tributary area is 5.18 km^2, which comprises 16.3% of the total drainage area of Mud Cr Garrison.

3 Results

3.1 Observed nitrate concentrations

Figure 2 displays the daily nitrate concentrations estimated at each monitoring. Continuous daily records of nitrate concentrations were available from May to Nov each year at most sites. Retrieval and storage of the equipment was necessitated during the winter and early spring, and occasional short-term gaps in the nitrate records occurred due to sensor fouling (4.3% of daily nitrate estimates) or low water levels (6.3% of daily nitrate estimates). In particular, low water levels observed during the July–September 2023 period at the Mud Cr Wet Out resulted in missing nitrate values.

Concentrations were highest at the Mud Cr Wet In (median of 11.5 mg/L) and lowest at the Mud Cr Wet Out (median of 1.94 mg/L). Of the remaining sites, Cedar Palo generally had lower nitrate levels (median of 4.06 mg/L) compared to Mud Cr Vinton (7.55 mg/L) and Mud Cr Garrison (5.56 mg/L). A wide range of nitrate concentrations were observed throughout Mud Creek, with minimum values near 0.10 mg/L and a maximum value measured at Mud Cr Wet In (19.5 mg/L). Maximum concentrations at the remaining sites ranged from 12.3 to 15.1 mg/L. Nitrate concentrations typically peaked in May and June before steadily declining throughout the rest of the summer. The lowest concentrations (0.10 mg/L) were routinely measured in Aug and Sep, followed by a rise in concentrations in late Sep and October (Figure 2). Average annual nitrate concentrations were highest in 2020—the only year with above-average precipitation.

We also utilized the monitoring data to investigate the spatial pattern of nitrate concentrations in Mud Creek before and after

TABLE 2 Nitrate loads (from May - September 2022 and May - September 2023) and the corresponding reductions caused by the wetland. "Wetland% of Watershed" column refers to the percentage of the site's drainage area that is treated by the wetland.

Mud creek sites	Station (km)	Area (km^2)	Wetland% of watershed (%)	Water yield (mm)	Nitrate load (kg)	Nitrate yield (kg/ha)	% reduction
Mud Cr Wet In	1.15	3.37		140	6,440	19.1	
Mud Cr Wet Total		5.18			8,370	16.1	
Wetland Removal					6,200		
Mud Cr Wet Out	2.04	5.18	100.00	131	2,160	4.17	74.2
Mud Cr Garrison	8.07	31.86	16.26	138	26,400	8.29	19.0
Mud Cr abv Vinton	13.34	58.02	8.93	142	66,300	11.4	8.55
Mud Cr Vinton	22.29	113.18	4.58	145	145,000	12.8	4.09
Cedar Palo	56.75	16425.70	0.03	200	25,500,000	15.5	0.0243

TABLE 3 % Reduction of nitrate loads by month. Wetland removal refers to the nitrate retained by the wetland during a given month, while the water yield refers to the monthly streamflow yield at Mud Cr Vinton.

Category	2022					2023				
	May	June	July	August	September	May	June	July	August	September
Wetland removal (kg)	1,520	1,870	1,120	230	65	738	479	161	27	2
Water yield (mm)	32.5	31.7	20.0	8.03	4.53	22.3	9.90	5.70	2.90	2.02
Mud Cr Wet Out	67%	78%	86%	96%	92%	57%	78%	91%	100%	100%
Mud Cr Garrison	23%	28%	32%	21%	10%	8.2%	14%	13%	6.8%	0.76%
Mud Cr abv Vinton	7.2%	9.2%	11%	13%	8.1%	6.2%	10%	10%	7.8%	2.7%
Mud Cr Vinton	3.7%	4.8%	5.5%	4.2%	1.8%	2.8%	5.0%	4.2%	1.7%	0.14%
Cedar Palo	0.02%	0.02%	0.03%	0.02%	0.02%	0.02%	0.07%	0.05%	0.07%	0.01%

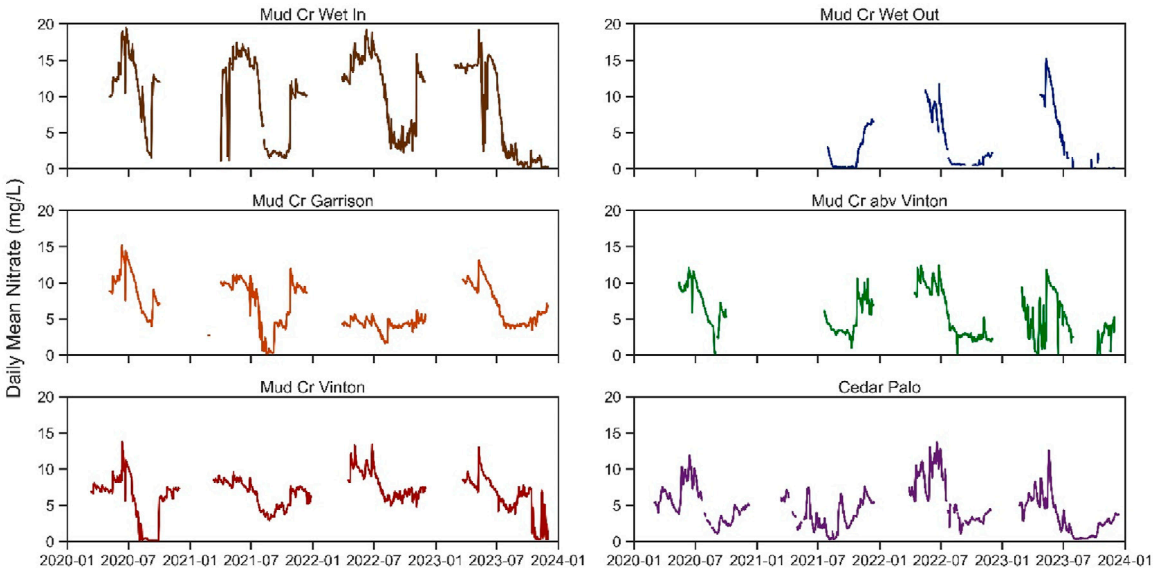


FIGURE 2
Daily mean nitrate concentrations at the six monitoring sites.

the wetland installation. Assessing the wetland's impact on local nitrate concentrations is of great interest to stakeholders, as nutrient concentrations portend eutrophic conditions. Lower nitrate concentrations in Mud Creek improve the water's drinkability and reduce the occurrence of algal blooms. The arithmetic mean of daily nitrate concentrations at each site in 2020 (pre-wetland) and 2022 (post-wetland) during the five-month analysis period (May–September) was evaluated. [Note that other years were not included in this analysis due to confounding factors: 2021 was the year the wetland was constructed, and 2023 was confounded by drought.] While 2020 and 2022 provide concise comparison points of the pre- and post-wetland conditions, this comparison does not capture differences in hydrologic conditions between these 2 years. These longitudinal profiles display local nutrient levels but do not describe the mass flux during these periods.

The longitudinal profiles of mean nitrate concentrations in Mud Creek in 2020 and 2022 show marked differences between these 2 years. In the pre-wetland condition, nitrate concentrations monotonically declined as water moved downstream. A steady decrease in stream nitrate concentrations is consistent with Peterson and Benning (2013) and Schilling et al. (2012), who reported nitrate concentrations highest in the headwaters of agricultural streams that gradually declined in downstream catchments with larger drainage areas. In contrast, the 2022 longitudinal profile shows a sharp drop in nitrate concentrations directly downgradient from the wetland—a clear sign of its efficacy in nitrate reduction. Following the sizable drop, concentrations rose at each subsequent site along Mud Creek, reaching levels near those measured in the Cedar River at Palo. This behavior was similar to the nitrate yields shown in Supplementary Figure S5.

3.2 Wetlands loads and nitrate removal

Daily nitrate loads were calculated at all six monitoring sites during the May–September timeframe in 2022 and 2023 (Figure 3). However, it is important to note that Eastern Iowa experienced significant drought conditions across the two-year monitoring period. Indeed, Palmer Drought Severity Index (PDSI) values dropped below −2 in 2022 and −4 in 2023 (Supplementary Figure S2), indicating moderate to severe drought periods. Nearby USGS gauges recorded annual streamflow totals far below average (Supplementary Figure S3). Consequently, the results from this study should not be viewed as representing the full range of hydrologic conditions but as a period marked by drier-than-average streamflow.

Daily nitrate loads into the wetland ranged from 0 to 151 kg (Figure 3). Loads exported from the wetland ranged from 0 to 48 kg. The days with the highest loads corresponded to the highest flow days, most of which took place in May, Jun, and Jul in 2022. Following a final wet weather event in July 2022, export loads gradually decreased through the remainder of the year. Two wet weather events occurred in May 2023, followed by the onset of significant drought conditions and diminished loads in Jun and Jul. By Aug, flows into and out of the wetland had completely dried up, resulting in days with 0 kg of nitrate load.

We estimated that 6,440 kg entered the wetland through the main channel across this ten-month period. When incorporating nitrate flux from the surrounding tile lines, estimated nitrate inputs to the wetland totaled 8,370 kg. Nitrate loads at the wetland outlet were 2,160 kg, indicating that the wetland removed 6,200 kg. This implied a % Reduction of 74.2%—meaning 74.2% of nitrate inputs were removed by the wetland. Nitrate yields, defined as a site's nitrate load from the ten-month analysis period divided by its tributary area, varied dramatically upstream (16.1 kg/ha) and downstream (4.17 kg/ha) of the wetland (Supplementary Figure S5).

3.3 Downstream loads and wetland impacts

Nitrate loads downstream of the wetland were much larger than the influx into the wetland (Supplementary Figure S4), which was expected given the increased drainage area for each successive monitoring location. Loads at the Mud Cr Garrison, Mud Cr abv Vinton, and Mud Cr Vinton sites were 26,400, 66,300, and 145,000 kg, respectively. The % Reduction declined monotonically from upstream to downstream (Figure 4), as the sites had reductions of 19.0% (Mud Cr Garrison), 8.55% (Mud Cr abv Vinton), and 4.09% (Mud Cr Vinton). This latter value effectively means the wetland reduced the nitrate load at the Mud Creek outlet by 4.09%. Loads at the Cedar Palo site were more than two orders of magnitude (25,500,000 kg) larger than Mud Creek, and the % Reduction due to the wetland was essentially negligible at the scale of the Cedar River (0.0243%).

Furthermore, we plotted each site's % Reduction value against its Wetland% of Watershed (Figure 5). The relation of % Reduction to Wetland% of Watershed was essentially linear and followed a 1:1 ratio, suggesting that the percentage of nitrate mass removed by a wetland was generally equivalent to the amount of tributary area treated by a wetland.

Nitrate yields spanning the ten-month analysis period were marked by a sharp decrease directly downstream of the wetland, followed by a steady rise at each successive monitoring location (Table 2). Downstream of the wetland, values were 4.20 (Mud Cr Wet Out), but they increased to 15.5 kg/ha at the Cedar Palo site. The yields within Mud Cr (4.20, 8.30, 11.4, and 12.8) were notably lower than those upstream of the wetland (16.1 kg/ha), but by the time the water had reached Cedar Palo, the yields were quite similar (15.5 kg/ha).

3.4 Monthly variations

Table 3 summarizes the nitrate load removed by the wetland and the subsequent % Reduction values for each of the 10 months included in our two-year analysis period. It also contains the monthly water yield at Mud Cr Vinton, which demonstrates Mud Creek's overall streamflow in that month. The 10 months encompass a range of hydrologic conditions ranging from 2.02 mm (September 2023) to 32.5 mm (May 2022). The nitrate load removed by the wetland was also highly variable, spanning 2 kg (September 2023) to 1,520 kg (May 2022).

The % Reduction values measured in the study experienced high variability by month. In the drier months (August–September 2023), the wetland removed 100% of the inflow nitrate. The % Reduction

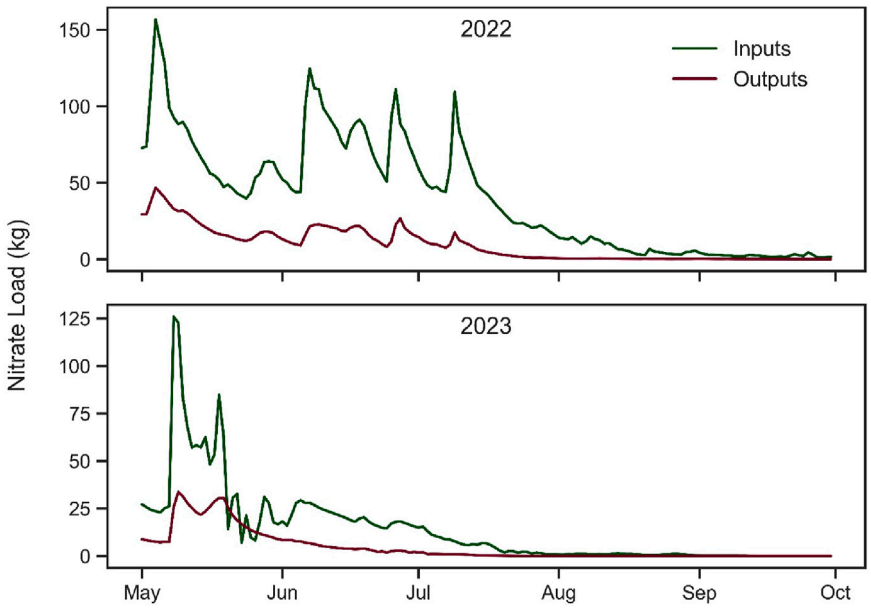


FIGURE 3
Estimated daily nitrate loads into and out of the wetland for 2022 (top) and 2023 (bottom).

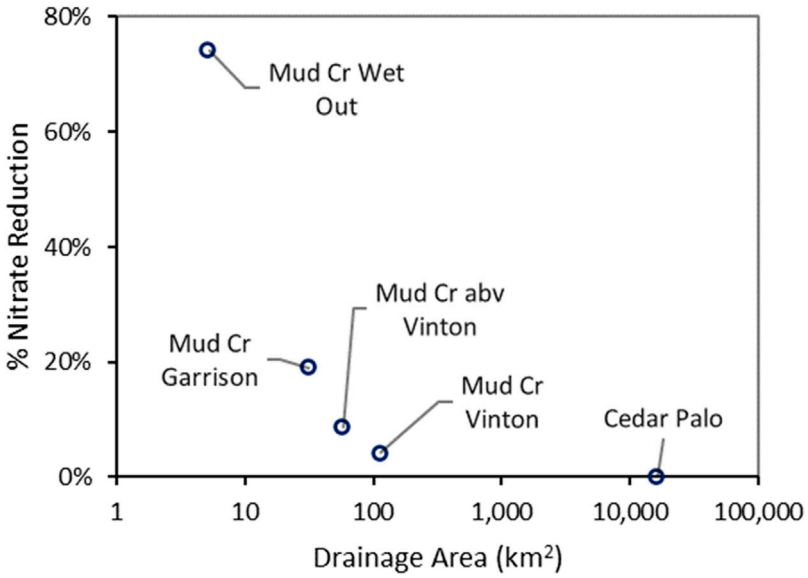


FIGURE 4
Percent nitrate reduction versus drainage area for the five nitrate sensor sites downstream of the wetland.

values were lower in wetter months, with a minimum % Reduction of 57% in May 2023. However, the % Reduction at the wetland was not well correlated with the % Reduction at downstream sites. Values ranged from 0.76%–32% at Mud Cr Garrison and 2.7%–14% at Mud Cr abv Vinton. The reduction for Mud Cr Vinton, which characterizes the entirety of the Mud Creek watershed, was lowest during the driest months (1.7% in August 2023 and 0.14% in September 2023). The maximum value was 5.5% in July 2022. In contrast, the reduction at Cedar Palo was never greater than 0.07%.

4 Discussion

4.1 Nitrate reduction in the wetland

Study results indicate that the constructed wetland in the upper Mud Creek watershed removed 6,200 kg of nitrate over a ten-month period occurring in 2022 and 2023, corresponding to a 74% reduction of input nitrate load. This nitrate load reduction is consistent with many studies documenting nitrate removal rates

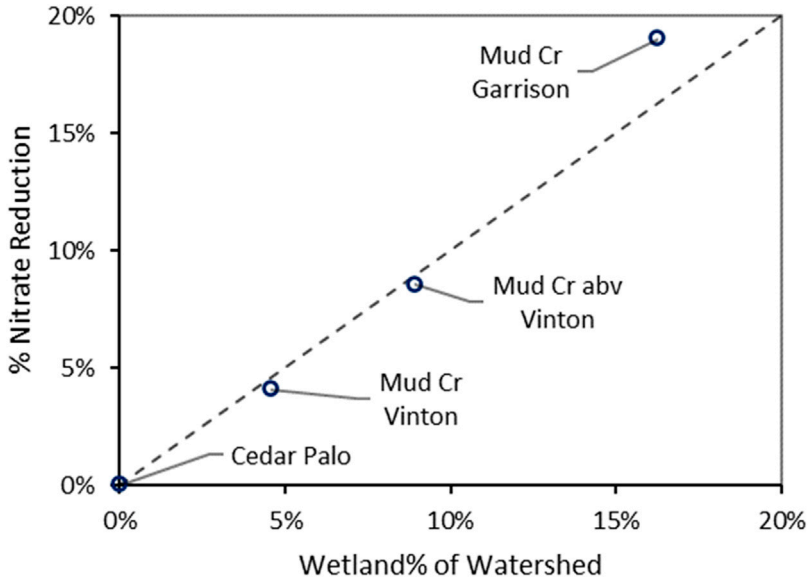


FIGURE 5
Percent nitrate reduction versus percentage of a site's drainage area treated by the wetland.

between 30% and 80% (Allred et al., 2014; Crumpton et al., 2006; Drake et al., 2018; Groh et al., 2015; Lemke et al., 2022). These results further suggest that this wetland is typical of those installed in Midwestern landscapes dominated by row crops. Although our monitoring data was insufficient to discern the processes responsible for nitrate removal in the wetland, denitrification, and assimilation are considered the dominant mechanisms at similar sites (Collins and Gillies, 2014; Crumpton, 2008; Crumpton et al., 2020; Drake et al., 2018; Lee et al., 2009; Lin et al., 2008). Overall, our results align with numerous studies highlighting constructed wetlands as an effective conservation practice for nitrate load reduction (Christianson et al., 2014; Crumpton et al., 2020; Gleason et al., 2011; Whigham, 1999).

Short-term variations in nitrate reductions were evident (Table 3) in the monitoring data, particularly related to streamflow and seasonality. Nitrate is mobilized following wet weather periods and delivered to the wetland through groundwater or tile line discharge (Schilling and Helmers, 2008; Spalding et al., 2001). During spring or summer wet weather events in agricultural basins, nitrate concentrations are typically diluted during peak flows but rise as streamflow recedes (i.e., during the falling limb of a hydrograph) due to the increased contributions of groundwater and tile drainage, which lag behind the surface runoff component (Speir et al., 2021; Tanner et al., 1999). Removal rates are often largest in the aftermath of rainfall events in the spring and summer when concentrations are the highest (Crumpton et al., 2020). These streamflow patterns influence the wetland residence time, complicating the relationship between flow rates and nitrate removal. Annual and monthly nitrate removal in wetlands typically decreases as the hydraulic loading rate increases because water residence times decrease with more water flux into the wetland (Crumpton, 2008; Drake et al., 2018). Longer residence time for water in a wetland means more time for nitrate reductions to occur via denitrification (Collins and Gillies, 2014; C; Lee et al., 2009; Lin et al., 2008). On the other hand, higher inflow rates lead to faster water flow through the wetland and less time for interactions between nitrate and the soil and plant media (Drake et al., 2018; Kadlec, 2010). For the Mud Creek wetland, the driest months contained the largest nitrate removal rates because of long residence times. In the months with severe drought conditions, nitrate removal reached 100% efficiency since no water exited the wetland. However, while the dry conditions resulted in high % Reduction values, nitrate mass removal was minimal due to low nitrate inputs into the wetland.

Furthermore, the location of the wetland in the headwater region of the Mud Creek watershed made it more susceptible to conditions with zero inflow during the drought. While the upper reaches of Mud Creek dried out during the later summer of 2023, perennial flow persisted in the downstream portions of the main channel due to the increased groundwater (baseflow) contributions present in a larger drainage area. Flow was perennial at the Mud Cr Garrison site and all downriver locations. During the 2023 dry period, the wetland was hydraulically disconnected from Mud Creek's main channel and did not provide measurable nitrate loss, but nitrate loads were still discharged into the Cedar River.

4.2 Downstream impacts of the wetland

While it is clear that the constructed wetland reduced nitrate loading at the scale of the wetland, our study's main objective was contextualizing the nitrate removal within the scale of a watershed. Calculating wetland nitrate removal efficiency is standard practice for wetlands, but rarely is it possible to measure the impact of the wetland on downstream nitrate loads. Most attempts at quantifying these impacts have used a model-based approach—simulating nitrate concentrations and loads at successive downstream locations (Arheimer and Wittgren, 2002; Böhlke et al., 2009;

Conan et al., 2003) and exploring the difference in nitrate levels before and after the wetland installation (Chavan and Dennett, 2008; Ham et al., 2010).

In our analysis, we used continuous monitoring of nitrate and streamflow at four downriver sites to quantify downstream loads using field measurements. Results showed the diminishing impact of the wetland at successive downstream monitoring locations and validated the general patterns described by nitrate-based watershed models (Arheimer and Wittgren, 2002; Böhlke et al., 2009; Conan et al., 2003). Empirical observations from our study demonstrated the spatial rate at which the wetland's impact on downstream water quality becomes indiscernible.

The landscape of the Mud Creek basin and much of the U.S. Corn Belt is dominated by intensive row crop agriculture, and measuring the impact of a singular practice on downstream water quality is often overwhelmed by untreated water from this landscape. Nitrate concentrations in Iowa rivers are significantly related to land cover; one can estimate mean annual nitrate concentrations in Iowa rivers by simply multiplying the row crop percentage in a watershed by 0.1 (Schilling and Libra, 2000). In this study, we showed that there is also a relationship between % Reduction and percentage of a watershed treated by a wetland (approximately 1:1). The portion of a watershed treated by a wetland was linearly related to the percentage of that watershed nitrate load removed by the wetland (Figure 5). This relationship presents a convenient rule of thumb for estimating the number of practices needed to achieve reduction goals. For example, if stakeholders in Mud Creek sought to reduce nitrate export by 20%, this could likely be achieved by installing four additional wetlands of similar volume and surface area. [6,200 kg * 5 = 31,000 kg, which is ~20% of 145,000 kg (the nitrate load at Mud Cr Vinton)] While many nuances surround wetland design and effectiveness, this calculation provides a first-order approximation of the investment level in conservation practices needed to achieve a nutrient reduction goal.

The nitrate concentrations in 2020 (pre-wetland) and 2022 (post-wetland) also revealed the wetland's impact on local nutrient levels (Figure 6). Although the difference between these profiles highlights the impacts of the wetland on local water quality conditions immediately below the outlet, this analysis is subject to a few limitations. First, this comparison of concentrations does not incorporate the overall nitrate mass removed by the wetland. It summarizes local nitrate conditions rather than explicitly denoting the wetland's impact on nitrate removal. Second, nitrate is also inherently variable and tied to recent hydrologic behavior, so these longitudinal profiles may vary considerably when examining short timeframes.

Figure 6 demonstrates how the wetland's influence predictably diminishes at downstream locations with greater tributary area. Nitrate concentrations increased in Mud Creek as more water from untreated landscapes entered the channel. By the time surface water in Mud Creek reached the confluence with the Cedar River, the wetland's influence was negligible. Hence, it is important to measure the impact of a conservation practice within a watershed at the appropriate scale. In a study of large-scale prairie restoration on watershed nitrate concentrations, Schilling and Spooner (2006) reported that the influence of headwater row crop areas on stream nitrate values overwhelmed the low-nitrate signal contributed from the restored prairie areas located in the core of the watershed, making it difficult to detect trends in the watershed over time. In both cases, water and nitrate derived from non-impacted areas confound the ability to measure conservation impacts at a watershed scale.

Although mean concentrations were higher at Mud Cr Vinton in the post-wetland condition than before its installation, this should not be viewed as a failure of the wetland since nitrate concentrations and loads can vary tremendously from year to year (Jones et al., 2018c), mainly due to hydrologic fluctuations (Ayers et al., 2021; Raymond et al., 2012). Sites often require several years (10+) of data to discern statistically significant differences in nitrate levels (Burt et al., 2010; Sprague et al., 2011), and many other factors may be at play, such as shifting conservation practices or land use, that could affect nitrate transport (Poor and McDonnell, 2007; Schilling and Libra, 2000).

4.3 Implications for nutrient reduction goals

The wetland's trivial impact on nitrate loads in the Cedar River also provides valuable context for meeting large-scale nutrient reduction goals. The State of Iowa explicitly aims to reduce its riverine nitrate export by 45%, which is guided by the Iowa Nutrient Reduction Strategy (Iowa State University, 2012). Many states in the U.S. Corn Belt draining to the Mississippi River and Gulf of Mexico have similar nutrient reduction goals (R. Christianson et al., 2018).

The Mud Creek wetland example sheds light on the degree of conservation practice implementation needed to achieve specific goals. This singular practice removed 0.02% of the nitrate at the Cedar Palo site. By extrapolating this removal rate, we estimate that over 1,850 constructed wetlands (with sizes similar to this study's wetland) would be needed to meet the 45% reduction goal in the Cedar River alone. It should be noted that this scaling exercise assumes a similar size, placement, and efficiency of the constructed practices. The footprint of these wetlands would comprise about 0.6% of the watershed's total area—a value aligned with what other studies have noted on wetland land use (Cheng et al., 2020; Crumpton, 2008). Installing 1,850 wetlands across five HUC08 basins (i.e., the Cedar watershed) is a level of investment far greater than any current water quality improvement efforts in the U.S. Corn Belt. Economic assessments have found the average design and construction cost for similar wetlands to be approximately $25,000/ha (Tyndall and Bowman, 2016); extrapolating this cost to 1,850 wetlands of similar size yields a dollar amount of $235 million. This value should be considered a minimum bound on wetland installation at this scale, as many local factors can further drive expenses. For instance, the cost of the Mud Creek wetland totaled $600,000—much greater than the simple estimate of $127,000 [5.1 ha * $25,000/ha]. Even the most successful initiatives have operated at a scale many orders of magnitude smaller (R. Christianson et al., 2018; Gleason et al., 2011; Weber et al., 2018). Given the political will in an agricultural state like Iowa, installing enough wetlands to meet the 45% reduction goal appears impractical and infeasible.

Consequently, it is essential to consider the issue of scale when evaluating the impact of any specific conservation practice. A constructed wetland can provide substantial water quality benefits

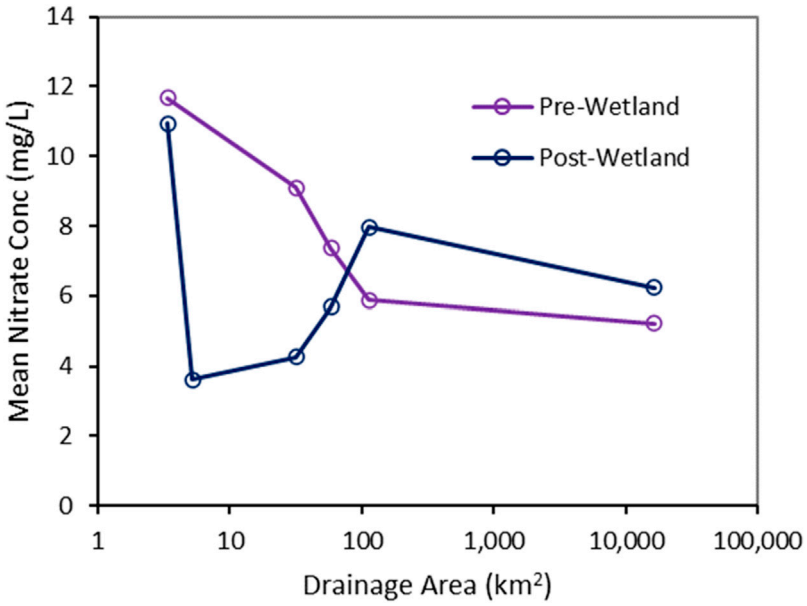


FIGURE 6
Mean nitrate concentrations (May - September) in Mud Creek pre-wetland (2020) and post-wetland (2022).

in the waters directly downstream of their outlets, yet its influence wanes at the HUC12 scale once water from untreated landscapes dominates a stream. At the HUC08 or state scale, wetlands alone are unlikely to curb eutrophication given the exorbitant number and cost needed. Nitrate pollution in the U.S. Corn Belt is so widespread that achieving the desired reductions will require a multi-faceted approach extending beyond implementing isolated conservation practices. Indeed, nearly all large-scale nutrient reduction efforts include components on limiting nitrate inputs and improving on-field retention on the landscape in addition to installing edge-of-field practices (Anderson et al., 2016; Hart et al., 1997; Scavia et al., 2017).

The wetland installed in Mud Creek was, by many metrics, a success; partnerships between funding agencies and landowners resulted in a practice that substantially reduced local nitrate concentrations and provided many ancillary benefits, including improved ecological health, recreation opportunities, and aesthetics. However, even successful practices have a downstream influence that quickly diminishes, and the impact of a single 5.1 ha wetland on nitrate load reduction was minor (<5%) at the HUC12 scale.

5 Conclusion

In this study, we evaluated the downstream impacts of a newly constructed wetland on nitrate levels during a ten-month period in 2022 and 2023 in the highly agricultural Mud Creek watershed located in east-central Iowa. High-resolution nitrate sensors deployed in four downstream monitoring locations and in the larger receiving river system documented the impacts of the wetland on watershed scale nitrate loads. Consistent with other wetland monitoring studies, the Mud Creek wetland was found to be an effective conservation practice, removing 74% of the nitrate that entered it. However, the impacts of the wetland on downstream water quality decreased considerably at downstream monitoring locations. At the outfall of Mud Creek into the Cedar River, the wetland was found to have reduced nitrate loads by 4.1%. Within the larger Cedar River basin, the single Mud Creek wetland reduced nitrate loads by 0.02%. Some variations in nitrate load reductions occurred primarily due to seasonal nitrate patterns and fluctuating streamflow levels. Study results suggest that the impact of any single conservation practice may be difficult to discern at the watershed scale and that a substantial number of practices will be needed to address nutrient reduction goals in larger watersheds.

Data availability statement

The data presented in this study are deposited in the IFIS (https://ifis.iowafloodcenter.org/ifis/), IWQIS (https://iwqis.iowawis.org), and USGS (https://waterdata.usgs.gov/nwis) repositories. Accession numbers can be found in the article/supplementary material. Further inquiries can be directed to the corresponding author.

Author contributions

EA: Conceptualization, Data curation, Formal Analysis, Investigation, Methodology, Writing–original draft, Writing–review and editing. KS: Conceptualization, Formal Analysis, Methodology, Writing–original draft. CJ: Conceptualization, Funding acquisition, Supervision, Writing–review and editing. B-CS: Investigation, Methodology, Writing–review and editing.

Funding

The author(s) declare that financial support was received for the research, authorship, and/or publication of this article. Funding for the project was provided by the Iowa Watershed Approach and the Environmental Protection Agency, Cooperative Agreement 00D86819.

Acknowledgments

The authors wish to thank Erin Elshoff, Cullen McDermott, Matthew Streeter, Thomas Stoeffler, and Jordan Barnett for their assistance in collecting field samples and maintaining *in-situ* equipment. We also thank the landowner for his willingness to construct this study's wetland on his property and his cooperation during the monitoring process.

Conflict of interest

The authors declare that the research was conducted in the absence of any commercial or financial relationships that could be construed as a potential conflict of interest.

Publisher's note

All claims expressed in this article are solely those of the authors and do not necessarily represent those of their affiliated organizations, or those of the publisher, the editors and the reviewers. Any product that may be evaluated in this article, or claim that may be made by its manufacturer, is not guaranteed or endorsed by the publisher.

Supplementary material

The Supplementary Material for this article can be found online at: https://www.frontiersin.org/articles/10.3389/fenvs.2024.1416018/full#supplementary-material

SUPPLEMENTAY FIGURE S1
Days on which nitrate measurements were collected at the Mud Creek monitoring sites.

SUPPLEMENTAY FIGURE S2
Weekly Palmer Drought Severity Index (PDSI) at the wetland.

SUPPLEMENTAY FIGURE S3
Annual water yield at three USGS gauges near Mud Creek. (Cedar Vinton: 05464315; Salt Cr: 05452000; Wolf Cr Dysart: 05464220).

SUPPLEMENTAY FIGURE S4
Nitrate loads versus drainage area at the six monitoring sites (May - Sep; 2022 and 2023).

SUPPLEMENTAY FIGURE S5
Nitrate yields versus drainage area at the six monitoring sites (May - Sep; 2022 and 2023).

SUPPLEMENTAY FIGURE S6
Comparison of nitrate loads entering the wetland through the peripheral tile lines (*y*-axis) and main channel (*x*-axis). The simple linear regression suggested a consistent relationship where tile loads were 20% of those in the main channel. Therefore, daily nitrate loads entering the wetland estimated as 1.2 times those measured at the main channel.

References

Allred, B. J., Gamble, D. L., Levison, P. W., Scarborough, R. L., Brown, L. C., and Fausey, N. R. (2014). Field test results for nitrogen removal by the constructed wetland component of an agricultural water recycling system. *Appl. Eng. Agric.* 30 (2), 163–177. doi:10.13031/aea.30.10061

Anderson, W. P., Wall, D., and Olson, J. L. (2016). "Minnesota nutrient reduction strategy," in Paper presented at the 2016 10th International Drainage Symposium Conference, Minneapolis, Minnesota, 6–9 September 2016, 1–9. doi:10.13031/ids.20162492032

Arheimer, B., and Wittgren, H. B. (2002). Modelling nitrogen removal in potential wetlands at the catchment scale. *Ecol. Eng.* 19 (1), 63–80. doi:10.1016/S0925-8574(02)00034-4

Aulenbach, B. T., Buxton, H. T., Battaglin, W. A., and Coupe, R. H. (2007). Streamflow and nutrient fluxes of the Mississippi-Atchafalaya River Basin and subbasins for the period of record through 2005 (2331-1258). Available at: https://pubs.usgs.gov/publication/ofr20071080 (March 20, 2024).

Ayers, J. R., Villarini, G., Schilling, K. E., and Jones, C. S. (2021). Development of statistical models for estimating daily nitrate load in Iowa. *Sci. Total Environ.* 782, 146643. doi:10.1016/j.scitotenv.2021.146643

Böhlke, J. K., Antweiler, R. C., Harvey, J. W., Laursen, A. E., Smith, L. K., Smith, R. L., et al. (2009). Multi-scale measurements and modeling of denitrification in streams with varying flow and nitrate concentration in the upper Mississippi River basin, USA. *Biogeochemistry* 93, 117–141. doi:10.1007/s10533-008-9282-8

Brendel, C., and Soupir, M. L. (2017). Relating watershed characteristics to elevated stream *Escherichia coli* levels in agriculturally dominated landscapes: an Iowa case study. *Water* 9 (3), 154. doi:10.3390/w9030154

Burkart, M. R., and James, D. E. (1999). Agricultural-nitrogen contributions to hypoxia in the Gulf of Mexico. *J. Environ. Qual.* 28 (3), 850–859. doi:10.2134/jeq1999.00472425002800030016x

Burt, T., Howden, N., Worrall, F., and Whelan, M. (2010). Long-term monitoring of river water nitrate: how much data do we need? *J. Environ. Monit.* 12 (1), 71–79. doi:10.1039/b913003a

Butt, A. J., and Brown, B. L. (2000). The cost of nutrient reduction: a case study of Chesapeake Bay. *Coast. Manag.* 28 (2), 175–185. doi:10.1080/089207500263585

Cao, P., Lu, C., Crumpton, W., Helmers, M., Green, D., and Stenback, G. (2023). Improving model capability in simulating spatiotemporal variations and flow contributions of nitrate export in tile-drained catchments. *Water Res.* 244, 120489. doi:10.1016/j.watres.2023.120489

Chambers, P. A., Vis, C., Brua, R. B., Guy, M., Culp, J. M., and Benoy, G. A. (2008). Eutrophication of agricultural streams: defining nutrient concentrations to protect ecological condition. *Water Sci. Technol.* 58 (11), 2203–2210. doi:10.2166/wst.2008.815

Chavan, P. V., and Dennett, K. E. (2008). Wetland simulation model for nitrogen, phosphorus, and sediments retention in constructed wetlands. *Water, air, soil Pollut.* 187, 109–118. doi:10.1007/s11270-007-9501-2

Cheng, F., Van Meter, K., Byrnes, D., and Basu, N. (2020). Maximizing US nitrate removal through wetland protection and restoration. *Nature* 588 (7839), 625–630. doi:10.1038/s41586-020-03042-5

Christianson, L., Knoot, T., Larsen, D., Tyndall, J., and Helmers, M. (2014). Adoption potential of nitrate mitigation practices: an ecosystem services approach. *Int. J. Agric. Sustain.* 12 (4), 407–424. doi:10.1080/14735903.2013.835604

Christianson, L., Tyndall, J., and Helmers, M. (2013). Financial comparison of seven nitrate reduction strategies for Midwestern agricultural drainage. *Water Resour. Econ.* 2, 30–56. doi:10.1016/j.wre.2013.09.001

Christianson, R., Christianson, L., Wong, C., Helmers, M., McIsaac, G., Mulla, D., et al. (2018). Beyond the nutrient strategies: common ground to accelerate agricultural water quality improvement in the upper Midwest. *J. Environ. Manag.* 206, 1072–1080. doi:10.1016/j.jenvman.2017.11.051

Collins, A. R., and Gillies, N. (2014). Constructed wetland treatment of nitrates: removal effectiveness and cost efficiency. *JAWRA J. Am. Water Resour. Assoc.* 50 (4), 898–908. doi:10.1111/jawr.12145

Conan, C., Bouraoui, F., Turpin, N., de Marsily, G., and Bidoglio, G. (2003). Modeling flow and nitrate fate at catchment scale in Brittany (France). *J. Environ. Qual.* 32 (6), 2026–2032. doi:10.2134/jeq2003.2026

Conley, D. J. (1999). Biogeochemical nutrient cycles and nutrient management strategies. *Man River Syst. Funct. River Syst. at Basin Scale*, 87–96. doi:10.1007/978-94-017-2163-9_10

Crumpton, W. G. (2001). Using wetlands for water quality improvement in agricultural watersheds; the importance of a watershed scale approach. *Water Sci. Technol.* 44 (11-12), 559–564. doi:10.2166/wst.2001.0880

Crumpton, W. G. (2008). 3. Potential of Restored and Constructed Wetlands to Reduce Nutrient Export from Agricultural Watersheds in the Corn Belt. ASABE. doi:10.13031/2013.24242

Crumpton, W. G., Stenback, G., Helmers, M., and Miller, B. (2006). Potential benefits of wetland filters for tile drainage systems: impact on nitrate loads to Mississippi River subbasins. Available at: https://www.fsa.usda.gov/Assets/USDA-FSA-Public/usdafiles/EPAS/PDF/fsa_final_report_crumpton_rhd.pdf (March 20, 2024).

Crumpton, W. G., Stenback, G. A., Fisher, S. W., Stenback, J. Z., and Green, D. I. S. (2020). Water quality performance of wetlands receiving nonpoint-source nitrogen loads: nitrate and total nitrogen removal efficiency and controlling factors. *J. Environ. Qual.* 49 (3), 735–744. doi:10.1002/jeq2.20061

David, M., McIsaac, G., Czapar, G., Schnitkey, G., and Mitchell, C. (2013). Science assessment to support an Illinois nutrient loss reduction strategy. *Urbana-Champaign, Coll. Agric. Consumer, Environ. Sci.*, 33–45.

Dewitte, K., Fierens, C., Stockl, D., and Thienpont, L. M. (2002). Application of the Bland–Altman plot for interpretation of method-comparison studies: a critical investigation of its practice. *Clin. Chem.* 48 (5), 799–801. doi:10.1093/clinchem/48.5.799

Dodds, W. K., and Welch, E. B. (2000). Establishing nutrient criteria in streams. *J. North Am. Benthol. Soc.* 19 (1), 186–196. doi:10.2307/1468291

Drake, C. W., Jones, C. S., Schilling, K. E., Amado, A. A., and Weber, L. J. (2018). Estimating nitrate-nitrogen retention in a large constructed wetland using high-frequency, continuous monitoring and hydrologic modeling. *Ecol. Eng.* 117, 69–83. doi:10.1016/j.ecoleng.2018.03.014

Fewtrell, L. (2004). Drinking-water nitrate, methemoglobinemia, and global burden of disease: a discussion. *Environ. health Perspect.* 112 (14), 1371–1374. doi:10.1289/ehp.7216

Gleason, R. A., Euliss Jr, N., Tangen, B., Laubhan, M., and Browne, B. (2011). USDA conservation program and practice effects on wetland ecosystem services in the Prairie Pothole Region. *Ecol. Appl.* 21 (sp1), S65–S81. doi:10.1890/09-0216.1

Goolsby, D. A., Battaglin, W. A., Aulenbach, B. T., and Hooper, R. P. (2001). Nitrogen input to the Gulf of Mexico. *J. Environ. Qual.* 30 (2), 329–336. doi:10.2134/jeq2001.302329x

Groh, T. A., Gentry, L. E., and David, M. B. (2015). Nitrogen removal and greenhouse gas emissions from constructed wetlands receiving tile drainage water. *J. Environ. Qual.* 44 (3), 1001–1010. doi:10.2134/jeq2014.10.0415

Haas, M. B., Guse, B., and Fohrer, N. (2017). Assessing the impacts of Best Management Practices on nitrate pollution in an agricultural dominated lowland catchment considering environmental protection versus economic development. *J. Environ. Manag.* 196, 347–364. doi:10.1016/j.jenvman.2017.02.060

Hallegraeff, G. (2003). Harmful algal blooms: a global overview. *Man. harmful Mar. microalgae* 33, 1–22.

Ham, J., Yoon, C. G., Kim, H.-J., and Kim, H.-C. (2010). Modeling the effects of constructed wetland on nonpoint source pollution control and reservoir water quality improvement. *J. Environ. Sci.* 22 (6), 834–839. doi:10.1016/s1001-0742(09)60185-6

Hart, J., Marx, E., Christensen, N., and Moore, J. (1997). Nutrient management strategies. *J. Dairy Sci.* 80 (10), 2659–2666. doi:10.3168/jds.s0022-0302(97)76225-8

Hunt, P. G., Stone, K. C., Humenik, F. J., Matheny, T. A., and Johnson, M. H. (1999). In-stream wetland mitigation of nitrogen contamination in a USA coastal plain stream. *J. Environ. Qual.* 28 (1), 249–256. doi:10.2134/jeq1999.00472425002800010030x

Hutchinson, K. J., and Christiansen, D. E. (2013). Use of the soil and water assessment tool (SWAT) for simulating hydrology and water quality in the Cedar River basin, Iowa 2000–10. *Sci. Investig. Rep. 2013–5002*, 36.

Ikenberry, C. D., Soupir, M. L., Schilling, K. E., Jones, C. S., and Seeman, A. (2014). Nitrate-nitrogen export: magnitude and patterns from drainage districts to downstream river basins. *J. Environ. Qual.* 43 (6), 2024–2033. doi:10.2134/jeq2014.05.0242

Iowa DNR NRGIS. (2009). High Resolution Land Cover Web Service. Iowa Geospatial Data Clearinghouse. Available at: https://geodata.iowa.gov/maps/05c7740a09304883bdae3b3945966c1a/about.

Iowa State University (2012). Iowa nutrient reduction strategy. Available at: https://www.nutrientstrategy.iastate.edu/ (March 20, 2024).

Jha, M. K., Wolter, C. F., Schilling, K. E., and Gassman, P. W. (2010). Assessment of total maximum daily load implementation strategies for nitrate impairment of the Raccoon River, Iowa. *J. Environ. Qual.* 39 (4), 1317–1327. doi:10.2134/jeq2009.0392

Jones, C. S., Davis, C. A., Drake, C. W., Schilling, K. E., Debionne, S. H., Gilles, D. W., et al. (2018a). Iowa statewide stream nitrate load calculated using *in situ* sensor network. *JAWRA J. Am. Water Resour. Assoc.* 54 (2), 471–486. doi:10.1111/1752-1688.12618

Jones, C. S., Kim, S.-W., and Schilling, K. (2017). Use of continuous monitoring to assess stream nitrate flux and transformation patterns. *Environ. Monit. Assess.* 189, 35–12. doi:10.1007/s10661-016-5749-6

Jones, C. S., Li, T., Sukalski, A., Thompson, D. A., and Cwiertny, D. M. (2020). Use of real-time sensors for compliance monitoring of nitrate in finished drinking water. *Water Sci. Technol.* 82 (12), 2725–2736. doi:10.2166/wst.2020.365

Jones, C. S., Nielsen, J. K., Schilling, K. E., and Weber, L. J. (2018b). Iowa stream nitrate and the Gulf of Mexico. *PloS one* 13 (4), e0195930. doi:10.1371/journal.pone.0195930

Jones, C. S., Schilling, K. E., Simpson, I. M., and Wolter, C. F. (2018c). Iowa stream nitrate, discharge and precipitation: 30-year perspective. *Environ. Manag.* 62 (4), 709–720. doi:10.1007/s00267-018-1074-x

Kadlec, R. H. (2010). Nitrate dynamics in event-driven wetlands. *Ecol. Eng.* 36 (4), 503–516. doi:10.1016/j.ecoleng.2009.11.020

Kalkhoff, S. J., Barnes, K. K., Becher, K., Savoca, M. E., Schnoebelen, D. J., Sadorf, E. M., et al. (2000). Water quality in the eastern Iowa basins, Iowa and Minnesota, 1996–98. Available at: https://pubs.usgs.gov/publication/cir1210.

Kovacic, D. A., David, M. B., Gentry, L. E., Starks, K. M., and Cooke, R. A. (2000). Effectiveness of constructed wetlands in reducing nitrogen and phosphorus export from agricultural tile drainage. *J. Environ. Qual.* 29 (4), 1262–1274. doi:10.2134/jeq2000.00472425002900040033x

Krajewski, W. F., Ceynar, D., Demir, I., Goska, R., Kruger, A., Langel, C., et al. (2017). Real-time flood forecasting and information system for the state of Iowa. *Bull. Am. Meteorological Soc.* 98 (3), 539–554. doi:10.1175/bams-d-15-00243.1

Kruger, A., Krajewski, W. F., Niemeier, J. J., Ceynar, D. L., and Goska, R. (2016). Bridge-mounted river stage sensors (BMRSS). *IEEE Access* 4, 8948–8966. doi:10.1109/access.2016.2631172

Lee, C., Fletcher, T. D., and Sun, G. (2009). Nitrogen removal in constructed wetland systems. *Eng. life Sci.* 9 (1), 11–22. doi:10.1002/elsc.200800049

Lee, K., Firoozfar, A. R., and Muste, M. (2017). Technical Note: monitoring of unsteady open channel flows using the continuous slope-area method. *Hydrology Earth Syst. Sci.* 21 (3), 1863–1874. doi:10.5194/hess-21-1863-2017

Lemke, A. M., Kirkham, K. G., Wallace, M. P., VanZomeren, C. M., Berkowitz, J. F., and Kovacic, D. A. (2022). Nitrogen and phosphorus removal using tile-treatment wetlands: a 12-year study from the midwestern United States. *J. Environ. Qual.* 51 (5), 797–810. doi:10.1002/jeq2.20316

Lin, Y.-F., Jing, S.-R., Lee, D.-Y., Chang, Y.-F., and Shih, K.-C. (2008). Nitrate removal from groundwater using constructed wetlands under various hydraulic loading rates. *Bioresour. Technol.* 99 (16), 7504–7513. doi:10.1016/j.biortech.2008.02.017

Lins, H. F., and Slack, J. R. (1999). Streamflow trends in the United States. *Geophys. Res. Lett.* 26 (2), 227–230. doi:10.1029/1998gl900291

Martin, J. F., and Reddy, K. (1997). Interaction and spatial distribution of wetland nitrogen processes. *Ecol. Model.* 105 (1), 1–21. doi:10.1016/s0304-3800(97)00122-1

Maxwell, E., Peterson, E. W., and O'Reilly, C. M. (2017). Enhanced nitrate reduction within a constructed wetland system: nitrate removal within groundwater flow. *Wetlands* 37, 413–422. doi:10.1007/s13157-017-0877-5

Messer, T. L., Trisha, L., Nelson, N., Ahiablame, L., Bean, E. Z., Boles, C., et al. (2021). Constructed wetlands for water quality improvement: a synthesis on nutrient reduction from agricultural effluents. *Trans. ASABE* 64 (2), 625–639. doi:10.13031/trans.13976

Mitsch, W. J., Day, J. W., Zhang, L., and Lane, R. R. (2005). Nitrate-nitrogen retention in wetlands in the Mississippi River basin. *Ecol. Eng.* 24 (4), 267–278. doi:10.1016/j.ecoleng.2005.02.005

NOAA. (2024). Precipitation Access Tools. National Centers for Environmental Information (NCEI). Available at: https://www.ncei.noaa.gov/products/precipitation.

Pellerin, B. A., Bergamaschi, B. A., Gilliom, R. J., Crawford, C. G., Saraceno, J., Frederick, C. P., et al. (2014). Mississippi River nitrate loads from high frequency sensor measurements and regression-based load estimation. *Environ. Sci. and Technol.* 48 (21), 12612–12619. doi:10.1021/es504029c

Peterson, E. W., and Benning, C. (2013). Factors influencing nitrate within a low-gradient agricultural stream. *Environ. Earth Sci.* 68, 1233–1245. doi:10.1007/s12665-012-1821-x

Poor, C. J., and McDonnell, J. J. (2007). The effects of land use on stream nitrate dynamics. *J. Hydrology* 332 (1-2), 54–68. doi:10.1016/j.jhydrol.2006.06.022

Prior, J. C. (1991). *Landforms of Iowa*. Iowa City, IA, United States: University of Iowa Press.

Quintero, F., Rojas, M., Muste, M., Krajewski, W. F., Perez, G., Johnson, S., et al. (2021). Development of synthetic rating curves: case study in Iowa. *J. hydrologic Eng.* 26 (1), 05020046. doi:10.1061/(asce)he.1943-5584.0002022

Rabalais, N. N., Turner, R. E., and Wiseman Jr, W. J. (2002). Gulf of Mexico hypoxia, aka "The dead zone". *Annu. Rev. Ecol. Syst.* 33 (1), 235–263. doi:10.1146/annurev.ecolsys.33.010802.150513

Randall, G. W., and Mulla, D. J. (2001). Nitrate nitrogen in surface waters as influenced by climatic conditions and agricultural practices. *J. Environ. Qual.* 30 (2), 337–344. doi:10.2134/jeq2001.302337x

Raymond, P. A., David, M. B., and Saiers, J. E. (2012). The impact of fertilization and hydrology on nitrate fluxes from Mississippi watersheds. *Curr. Opin. Environ. Sustain.* 4 (2), 212–218. doi:10.1016/j.cosust.2012.04.001

Scavia, D., Kalcic, M., Muenich, R. L., Read, J., Aloysius, N., Bertani, I., et al. (2017). Multiple models guide strategies for agricultural nutrient reductions. *Front. Ecol. Environ.* 15 (3), 126–132. doi:10.1002/fee.1472

Schilling, K. E., and Helmers, M. (2008). Effects of subsurface drainage tiles on streamflow in Iowa agricultural watersheds: exploratory hydrograph analysis. *Hydrological Process. An Int. J.* 22 (23), 4497–4506. doi:10.1002/hyp.7052

Schilling, K. E., Jones, C., Wolter, C., Liang, X., Zhang, Y.-K., Seeman, A., et al. (2017). Variability of nitrate-nitrogen load estimation results will make quantifying load reduction strategies difficult in Iowa. *J. Soil Water Conservation* 72 (4), 317–325. doi:10.2489/jswc.72.4.317

Schilling, K. E., Jones, C. S., Seeman, A., Bader, E., and Filipiak, J. (2012). Nitrate-nitrogen patterns in engineered catchments in the upper Mississippi River basin. *Ecol. Eng.* 42, 1–9. doi:10.1016/j.ecoleng.2012.01.026

Schilling, K. E., and Libra, R. D. (2000). The relationship of nitrate concentrations in streams to row crop land use in Iowa. *J. Environ. Qual.* 29 (6), 1846–1851. doi:10.2134/jeq2000.00472425002900060016x

Schilling, K. E., and Spooner, J. (2006). Effects of watershed-scale land use change on stream nitrate concentrations. *J. Environ. Qual.* 35 (6), 2132–2145. doi:10.2134/jeq2006.0157

Schilling, K. E., and Wolter, C. F. (2009). Modeling nitrate-nitrogen load reduction strategies for the Des Moines River, Iowa using SWAT. *Environ. Manag.* 44 (4), 671–682. doi:10.1007/s00267-009-9364-y

Singh, N. K., Gourevitch, J. D., Wemple, B. C., Watson, K. B., Rizzo, D. M., Polasky, S., et al. (2019). Optimizing wetland restoration to improve water quality at a regional scale. *Environ. Res. Lett.* 14 (6), 064006. doi:10.1088/1748-9326/ab1827

Singh, S., Anil, A. G., Kumar, V., Kapoor, D., Subramanian, S., Singh, J., et al. (2022). Nitrates in the environment: a critical review of their distribution, sensing techniques, ecological effects and remediation. *Chemosphere* 287, 131996. doi:10.1016/j.chemosphere.2021.131996

Smith, V. H., and Schindler, D. W. (2009). Eutrophication science: where do we go from here? *Trends Ecol. and Evol.* 24 (4), 201–207. doi:10.1016/j.tree.2008.11.009

Spalding, R. F., Watts, D. G., Schepers, J. S., Burbach, M. E., Exner, M. E., Poreda, R. J., et al. (2001). Controlling nitrate leaching in irrigated agriculture. *J. Environ. Qual.* 30 (4), 1184–1194. doi:10.2134/jeq2001.3041184x

Speir, S. L., Tank, J. L., Bieroza, M., Mahl, U. H., and Royer, T. V. (2021). Storm size and hydrologic modification influence nitrate mobilization and transport in agricultural watersheds. *Biogeochemistry* 156 (3), 319–334. doi:10.1007/s10533-021-00847-y

Spieles, D. J., and Mitsch, W. J. (1999). The effects of season and hydrologic and chemical loading on nitrate retention in constructed wetlands: a comparison of low-and high-nutrient riverine systems. *Ecol. Eng.* 14 (1-2), 77–91. doi:10.1016/s0925-8574(99)00021-x

Sprague, L. A., Hirsch, R. M., and Aulenbach, B. T. (2011). Nitrate in the Mississippi River and its tributaries, 1980 to 2008: are we making progress? *Environ. Sci. and Technol.* 45 (17), 7209–7216. doi:10.1021/es201221s

Squillace, P. J., and Engberg, R. A. (1988). Surface-water quality of the Cedar River basin, Iowa-Minnesota, with emphasis on the occurrence and transport of herbicides, may 1984 through No vember 1985. *Dep. Interior, US. Geol. Surv.* 88.

Stein, O. R., and Hook, P. B. (2005). Temperature, plants, and oxygen: how does season affect constructed wetland performance? *J. Environ. Sci. Health* 40 (6-7), 1331–1342. doi:10.1081/ese-200055840

Syswerda, S. P., Basso, B., Hamilton, S. K., Tausig, J. B., and Robertson, G. P. (2012). Long-term nitrate loss along an agricultural intensity gradient in the Upper Midwest USA. *Agric. Ecosyst. and Environ.* 149, 10–19. doi:10.1016/j.agee.2011.12.007

Tanner, C. C., D'Eugenio, J., McBride, G. B., Sukias, J. P. S., and Thompson, K. (1999). Effect of water level fluctuation on nitrogen removal from constructed wetland mesocosms. *Ecol. Eng.* 12 (1), 67–92. doi:10.1016/S0925-8574(98)00055-X

Tyndall, J., and Bowman, T. (2016). *Iowa nutrient reduction strategy best management practice cost overview series: constructed wetlands*. Ames, IA, USA: Department of Ecology and Natural Resource Management, Iowa State University.

Vedachalam, S., Mandelia, A. J., and Heath, E. A. (2019). The impact of source water quality on the cost of nitrate treatment. *AWWA Water Sci.* 1 (1), e1011. doi:10.1002/aws2.1011

Vymazal, J. (2007). Removal of nutrients in various types of constructed wetlands. *Sci. Total Environ.* 380 (1), 48–65. doi:10.1016/j.scitotenv.2006.09.014

Ward, M. H., Jones, R. R., Brender, J. D., De Kok, T. M., Weyer, P. J., Nolan, B. T., et al. (2018). Drinking water nitrate and human health: an updated review. *Int. J. Environ. Res. public health* 15 (7), 1557. doi:10.3390/ijerph15071557

Weber, L. J., Muste, M., Bradley, A. A., Amado, A. A., Demir, I., Drake, C. W., et al. (2018). The Iowa Watersheds Project: Iowa's prototype for engaging communities and professionals in watershed hazard mitigation. *Int. J. river basin Manag.* 16 (3), 315–328. doi:10.1080/15715124.2017.1387127

Whigham, D. F. (1999). Ecological issues related to wetland preservation, restoration, creation and assessment. *Sci. Total Environ.* 240 (1-3), 31–40. doi:10.1016/s0048-9697(99)00321-6

Witzke, B. (1998). *Bedrock geologic map of northeast Iowa*. Trowbridge Hall Iowa City: Iowa DNR Geological Survey Bureau. Iowa Department of Natural Resources Iowa.

Zhang, Y.-K., and Schilling, K. E. (2005). Temporal variations and scaling of streamflow and baseflow and their nitrate-nitrogen concentrations and loads. *Adv. water Resour.* 28 (7), 701–710. doi:10.1016/j.advwatres.2004.12.014

Zimmer, M. A., Pellerin, B., Burns, D. A., and Petrochenkov, G. (2019). Temporal variability in nitrate-discharge relationships in large rivers as revealed by high-frequency data. *Water Resour. Res.* 55 (2), 973–989. doi:10.1029/2018wr023478

frontiers | Frontiers in Environmental Science

TYPE Original Research
PUBLISHED 27 January 2025
DOI 10.3389/fenvs.2024.1488925

Check for updates

OPEN ACCESS

EDITED BY
Keith Schilling,
The University of Iowa, United States

REVIEWED BY
Sergio Makrakis,
Western Parana State University, Brazil
Joseph Honings,
Iowa Geological Survey, United States

*CORRESPONDENCE
J. S. Strock,
jstrock@umn.edu

RECEIVED 30 August 2024
ACCEPTED 18 December 2024
PUBLISHED 27 January 2025

CITATION
Strock JS and Ranaivoson AZ (2025) Ditch management using low-grade weirs: an opportunity for mitigating water quality and quantity impacts.
Front. Environ. Sci. 12:1488925.
doi: 10.3389/fenvs.2024.1488925

COPYRIGHT
© 2025 Strock and Ranaivoson. This is an open-access article distributed under the terms of the Creative Commons Attribution License (CC BY). The use, distribution or reproduction in other forums is permitted, provided the original author(s) and the copyright owner(s) are credited and that the original publication in this journal is cited, in accordance with accepted academic practice. No use, distribution or reproduction is permitted which does not comply with these terms.

Ditch management using low-grade weirs: an opportunity for mitigating water quality and quantity impacts

J. S. Strock* and A. Z. Ranaivoson

Department Soil, Water and Climate and Southwest Research and Outreach Center, University of Minnesota, Lamberton, MN, United States

To improve productivity, extensive agricultural areas in the Midwest United States require drainage systems consisting of subsurface drainage (tile) and open ditches. Transport of sediment, pathogens, pesticides, and nutrients from runoff and drainage from crop fields contributes to eutrophication and degradation of surface waters. Solutions are needed to improve environmental quality and reduce the negative impacts from runoff and agricultural drainage systems. This study assessed the effect of low-grade weirs on discharge and nitrate-nitrogen concentration and loss from a pair of experimental drainage ditches. One control (without weirs) and one treatment (with weirs) ditch were studied from 2017 through 2023 at the University of Minnesota, Southwest Research and Outreach Center near Lamberton, MN, United States. This study was the first evaluation of agricultural ditches, with and without low-grade weirs, and their potential to mitigate discharge and nitrogen loss in a cold climate. Stage-discharge data were collected using a data logger and bubble level sensor. Water samples were collected for water quality analysis daily using automated samplers. Analysis of the data was conducted using paired t-tests and a paired analysis approach. Analysis of covariance and linear regression of the treatment ditch against the control ditch were highly significant for nitrate-nitrogen concentration and load. The ditch with the low-grade weir was found to significantly decrease nitrate-nitrogen concentration and load. More specifically, the treatment ditch reduced discharge, nitrate-nitrogen concentration and load by 51%, 22% and 58%, respectively. The greatest discharge from the ditches occurred in March while most nitrogen losses occurred between May and June. This study provides evidence and highlights the potential of ditches equipped with low-grade weirs to reduce nitrate-nitrogen losses when compared to ditches without low-grade weirs in a cold climate. In addition, the study also emphasizes the importance of climate as a driver of nitrate-nitrogen loss from crop lands and ditches which is amplified by monthly precipitation variability.

KEYWORDS

ditch, drainage, water quantity, water quality, weir

1 Introduction

The most recently published survey of agriculture estimates 22 million ha of subsurface drained land in the United States (US) (NASS, 2017). In the Midwest US, seasonal differences in the amount and timing of precipitation and crop water demand often result in surplus water early and late in the growing season and a water deficit in summer months (Reinhart et al., 2019).

Drainage is a critical year-round water management tool for enabling productive and profitable agricultural systems. Drainage is a natural process whereby water moves across, in, through, and out of the soil. Drainage systems permit or improve crop growth and productivity by removing non-capillary water from the soil. The benefits of drainage systems include prevention of flooding through the rapid removal of surface water and non-capillary soil water, lowering shallow ground water to prevent crop stress, and creation of suitable conditions for field operations (Kaur et al., 2017). For example, although excess rainfall induced crop yield loss in tile drained landscapes, it was determined that yield losses would have been worse without artificial drainage (Li et al., 2019). While drainage has multiple benefits it also has negative impacts, it alters the quantity and quality of water drained from agricultural lands (Williams et al., 2015). Surplus inorganic nitrogen (N) and other nutrients attributed to drainage within the Mississippi River watershed stimulate algal growth and eutrophication and ultimately contribute to the hypoxic zone in the Gulf of Mexico (Fennel and Laurent, 2018; Rabalais and Turner, 2019).

Solutions are needed to temporarily detain drainage water on the landscape and reduce nutrient losses to improve environmental quality and reduce negative impacts from drainage systems. Simultaneously, mitigation strategies are needed to supplement conventional agricultural best practices, for example, the 4R's of nutrient stewardship (Right source, Right rate, Right time, and Right place), to obtain reductions in non-point source agricultural nutrient loss. Technologies are needed to achieve peak flow reduction and removal of nutrients from agricultural drainage water without taking land out of production, they need to be low maintenance, and provide multiple ecosystem services. In watersheds where artificial drainage is practiced, surface and subsurface runoff from agricultural lands is often carried by a network of drainage ditches that function as headwater streams. Managing agricultural drainage ditches has potential for improving environmental quality benefits related to water quantity, quality, habitat, and biodiversity.

Ditch systems are typically small (1–2 m wide) historically natural streams that have been artificially deepened and straightened, or new channels, constructed to serve as an outlet for field drainage systems. Agricultural ditches are generally ephemeral aquatic ecosystems used to maintain optimal soil moisture in adjacent agricultural fields. Ditches act to transport not only water, but also nutrients, sediment, pathogens, and pesticides from agricultural fields to small streams and larger rivers (Olson, et al., 2016; Faust et al., 2018). These ditches have nominal hydraulic attenuation capacity, and minimal capacity for biogeochemical processing and natural retention of dissolved or particulate materials. Under low-flow conditions, ditches exhibit similar chemical and microbiological functions as wetlands (Moore et al., 2005; Martin et al., 2021) and appropriate management practices can be used to promote ecosystem services such as nutrient removal. Previous studies reported managed agricultural drainage ditches as potentially an efficient nutrient mitigation strategy (Kröger et al., 2008; Kröger et al., 2014). The challenge with many of these studies is that they were conducted in a warm climate, Mississippi, where the average annual temperature is 18°C and the mean minimum and maximum are −9°C and 32°C, respectively. It is important to know if managed drainage ditches have the same potential in cold northern climates like Minnesota, where the average annual temperature is 7°C and the mean minimum and maximum are −20°C and 27°C, respectively.

Traditionally, drainage ditch systems have been conveyance systems to eliminate water from the landscape as quickly as possible. Modifications to ditch systems have incorporated installation of different control measures including flashboard riser systems (Evans et al., 1995) and low-grade weirs (Kröger et al., 2008) to manage water flow in drainage ditch systems. Implementation of low-grade weirs has been shown to be effective in reducing N concentration and load to receiving waterbodies (Kröger et al., 2012). The N removal efficiency of microbial denitrification and denitrification rate depends on factors including the availability of carbon and adequate ambient temperature. In previous experiments, low-grade weirs were studied primarily in the southern United States and their performance in cold climates typical of northern latitudes remains unclear. Our approach consists of the installation of a low-grade weir within a ditch system in a cold climate. The purpose of the weir is to increase hydraulic retention time (HRT), decrease flow velocities, and create zones of inundation (Kröger et al., 2008), the cumulative effect of which is expected to be the establishment of conditions suitable for N cycle processes such as denitrification and bioaccumulation (Littlejohn et al., 2014; Kröger et al., 2014). Diverse vegetation communities grow in ditches and often promote biological nutrient uptake and removal (Faust et al., 2018). In addition, vegetation increases hydraulic friction in the ditch channel thereby promoting reduced flow velocity in the water column that increases HRT which further enhances the opportunity for nutrient removal (Faust et al., 2018; Nifong et al., 2019). A recent study in the Lower Mississippi River Basin demonstrated these beneficial effects of vegetative cover and residence time in a managed ditch system (Nifong et al., 2019).

The objective of this research was to evaluate the effectiveness of an agricultural drainage ditch management strategy in a cold climate to temporarily increase water storage and reduce nitrogen loading from agricultural runoff. Specifically, this field study evaluated the effectiveness of low-grade weirs on drainage discharge and nitrate-nitrogen concentration and loss from a pair of experimental drainage ditches in the upper Midwest, United States.

2 Materials and methods

2.1 Description of research site

A field experiment was conducted at the University of Minnesota, Southwest Research and Outreach Center (SWROC), near Lamberton, Minnesota (lat. N: 44°14′36″, lon. W: 95°18′20″) to study the potential of ditches equipped with low-grade weirs to

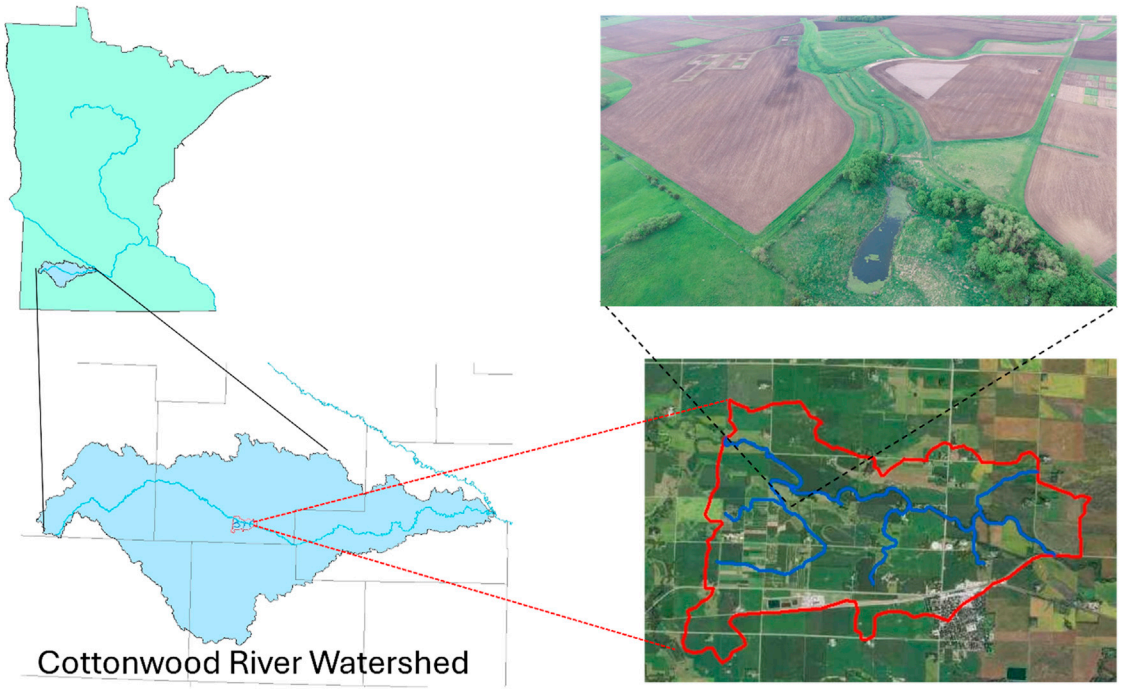


FIGURE 1
Location of ditch research facility in southwest Minnesota.

reduce nitrate-nitrogen (NO_3-N) losses when compared to ditches without low-grade weirs in a cold climate. The climate of the region is characterized as interior continental with cold winters and moderately hot summers with occasional cool periods. Average annual temperature is 7°C, with monthly extremes ranging from 32°C in July to −13°C in January. The long-term total annual precipitation at SWROC is 710 mm, considered adequate to grow crops without irrigation because most of it (69%) falls during the growing season from April to September.

The field research site was located in the Cottonwood River Major Watershed of southwest Minnesota. Farming is the principal segment of the economy in this watershed consisting primarily of row crop production of corn and soybeans. Land cover in the watershed consists of approximately 85% cultivated cropland, 8% grassland (including CRP land), 1% woodland, and 6% other land. The watershed landscape is characterized as having a complex mixture of gently sloping (2%–6% slope) well drained loamy soils and nearly level (0%–2% slope) poorly drained loamy soils formed in glacial till. Poorly drained soils are highly productive due to an extensive network of subsurface tile drainage and open-ditches.

2.2 Ditch features, design criteria, and management

This experimental site was established to identify the effectiveness of ditch management strategies to increase water storage and decrease nutrient discharge from an agricultural landscape. Strock et al. (2005) described the development of a vegetated ditch research facility in the glacial till plain within the Northern Corn Belt Plain region of southern Minnesota. Construction of the experimental channels was completed in late summer 2002. Briefly, two side-by-side, 200 m long, experimental vegetated ditch channels receive surface runoff and subsurface drain flow from the surrounding farmland (Figure 1). The drainage area consists of 132-ha section of the watershed. The area contributing water from surface runoff to the ditch facility is 73 ha, and the area contributing water from subsurface tile drainage is 59 ha. Of the total area contributing water from subsurface drainage, 21 ha lies outside the boundary of the total area contributing surface runoff.

The geometry of the experimental channels was typical of drainage channels in the region with bottom width of 1.5 m, height of 1.2 m, 2:1 side slopes (H:V), and bed slope of 0.1%. The peak discharge capacity of each experimental channel was 1.4 m^3s^{-1}. Water flows through 0.76 m (2.5 foot) H-flumes at the outlets of the experimental channels. A 1.5 m wide by 3.0 m long by 0.76 m deep polyvinylchloride (PVC) approach sections come before the H-flume in each channel. Water level in the treatment ditch is regulated using PVC weirs. Each weir was manufactured with a rubber seal to assure a tight fit to prevent leakage. Weirs measure a minimum of 0.15 m in height. Two weirs were stacked to achieve the desired water level control height, 0.3 m in this experiment. Once installed, the weirs were left in place continuously. The ditches consisted of mainly perennial vegetation, typical of the Midwest. Dominant species included *Poa palustris, Sagittaria latifolia, Phalaris arundinacea, and Bromus inermis.* Vegetation density was not quantified to determine if there were differences between the control and treatment channels.

The design for this project consisted of a control and treatment ditch and two time periods, a calibration and a treatment period (Figure 2). The calibration period was 2 years in length, 2004–2005.

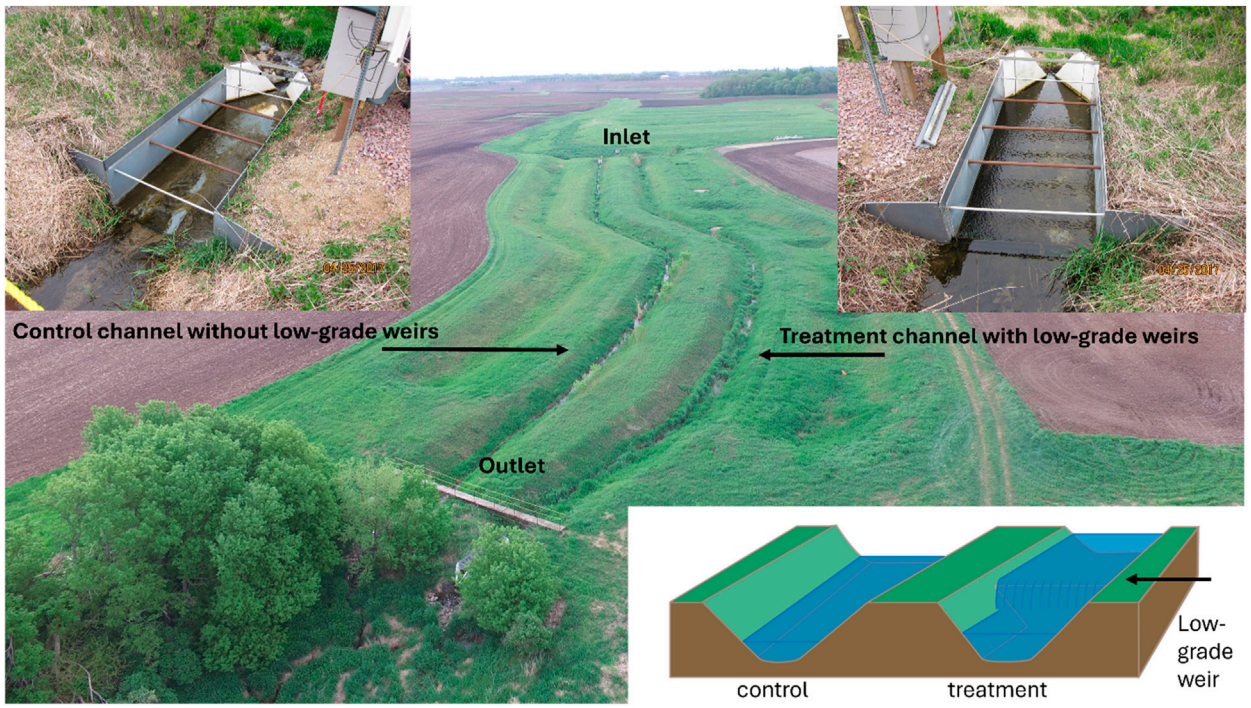


FIGURE 2
Experimental ditch facility showing inlet, outlet, treatment and control channels including a picture and drawing of the influence of the low-grade weir on water elevation in the treatment ditch.

In 2006, the treatment ditch received the prescribed experimental treatment, installation of a 0.3 m low-grade weir, while the control ditch remained unchanged. The control ditch served as a check for climatic and other variations during the year. The treatment period for this study ranged between 2017 and 2023. The treatment period was partitioned into three groups based on annual rainfall amounts: wet years: 2018–19, dry years 2021–2022, and normal/average years: 2017–2020–2023. In this project, the variables of interest were ditch discharge rate, m^3 d^{-1}, flow-weighted nitrate concentration (FWMNC), mg L^{-1}, and NO_3^--N load, kg.

2.3 Monitoring, water sampling and analysis

To study the effects of ditch management on surface and subsurface drainage discharge and water quality from the surrounding agricultural landscape, source water and ditch outflows were measured the watershed converges to a common equalization basin prior to being discharged to the two experimental ditch channels. This configuration helped minimize variability from surface runoff and subsurface drainage source water and was important to reduce high frequency fluctuations of water and nutrient inputs to the ditch channels and to promote complete mixing of source waters. After mixing water was equally distributed to each experimental channel. Source water flows and ditch outflows were measured from 2003 to 2009 and then again from 2017 to the present. The time gap between 2009 and 2017 was due to budget limitations. Inflow data was not collected between 2017 and 2020, due to equipment availability and budget limitations.

Daily mean values of drainage volume were calculated from continuously recorded stage data using stage-discharge relationships for the H-flumes. Each H-flume was instrumented with an OTT bubble level sensor (OTT Hydromet, Germany). An ISCO 3700C compact portable sampler (Teledyne ISCO, Inc., Lincoln, NE) was installed after each water metering H-flume. The ISCO 3700 samplers were used collect composite and discrete water samples from each experimental ditch based on base flow or storm flow hydrograph conditions. A Campbell Scientific CR1000 data logger (Campbell Scientific, Logan UT) was used to control the portable sampler and to collect the water level data.

A data logging program, using CRBasic programming language, was created to automatically record, store, and organize data from the bubble level sensor to the data logger for monitoring ditch hydrograph response to storm flow. The data logger program was also designed to collect a composite daily sample during base flow conditions and discrete samples during the rising, peak and recessional components of the hydrograph. Between 2017 and 2023 a total of 2,326 water samples were collected and analyzed. The distribution of samples by year was as follows, 290 in 2017, 449 in 2018, 781 in 2019, 283 in 2020, 190 in 2021, 178 in 2022, and 86 in 2023. The combination of water flow measurement and nutrient concentration allows for estimation of contaminant loading to surface water. Discharge was continuously measured, and water samples collected between ice-free periods in order to minimize potential damage to instrumentation.

Water samples were analyzed for NO_3^--N and dissolved reactive phosphorus (DRP) concentration. All chemical analyses were completed using Lachat 8500 Flow Injection Analyzer (Hach,

Loveland, CO). Samples were typically collected within 24 h of a storm event and either frozen or stored at 4° C for analysis within 24 h. Samples were filtered through a 0.45 µm nitrate-cellulose membrane before analysis of NO_3^--N and DRP. Dissolved reactive P was analyzed using colorimetric analysis by the molybdate-blue/ascorbic acid method (10-115-01-1-Q) at 880 nm. Nitrate-nitrogen was analyzed using colorimetric analysis by the cadmium reduction method (10-107-04-1-A) at 520 nm.

Nutrient concentration and water volume provided a nutrient load for respective baseflow and storm events. Drainage area was the total area of farm contributing surface and subsurface drainage to the experimental ditches. Nitrogen and phosphorus loads (kilograms and grams, respectively) were evaluated on a per hectare basis. Loads, which represent the actual nutrient load leaving a ditch at the outflow sampling station represented the daily load attained within a ditch as a result of the combination of surface and subsurface flow processes.

2.4 Statistical analysis

A paired watershed design was used to evaluate the impact of ditch management on water quantity and quality. Statistical tests on the experimental data were run on a JMP 15.0 Pro platform (JMP, 2019). The alpha value level of confidence was set at 0.10 for field experiment. The main data treatment for this set of ditch records was based on pairing all daily records from the control and the treatment ditch for the variables of interest. This data pairing extended to both the calibration (2004–2005) and the treatment periods (2017–2023). The partitioned data were then tested using analysis of covariance (ANCOVA) to compare linear relationships (slope and intercept) between the control and the treatment ditches over the calibration and treatment periods.

In addition to the paired watershed statistical method, two other methods were applied to assess significant differences between the parameters listed above: t-test and mean comparisons with Tukey HSD. A t-test was used in comparing discharge rate, $m^3\ d^{-1}$, FWMNC, mg L^{-1}, and NO_3-N load, kg over the entire length of the treatment period, 2017–2023, based on monthly average data. The Tukey HSD mean comparison handled relative contribution of monthly averages over the control and the treatment ditches.

3 Results

3.1 Precipitation characteristics

The study period, 2017–2023, provided an opportunity for evaluation of ditch management in a northern latitude under contrasting climatic conditions. Precipitation data was grouped in two ways. First, according to experimental interval, either the calibration or treatment period. Second, it was also organized into three bins representing dry, normal, and wet conditions. Annual precipitation averaged 838 mm over the calibration period and was 14% wetter than normal. During the treatment period, from 2017 to 2023, annual precipitation ranged from 511 mm (30% below normal) in 2022 to 1,010 mm (37% above normal) in 2019 (Table 1). Annual precipitation was highly variable during the treatment period, including two below-average years (2021 and 2022), three nearly normal/average years (2017, 2020, and 2023), and two above-average years (2018 and 2019).

3.2 Inflow and outflow

Water flow is seasonal, with higher flows normally from April through June when spring snowmelt combines with spring rainfall and seasonally high subsurface drainage flow. Based on annual observations over several decades, on average, subsurface drainage begins between the middle of March and the beginning of April, depending on air temperature, the presence or absence of snow and frost depth. During a typical year, drain flow ends in mid- to late-July. Soils in southern Minnesota are prone to snowmelt and/or rainfall runoff from early spring or early summer. Early-spring to early-summer are periods when the soil surface is relatively bare depending on the amount of residue leftover from primary and secondary tillage, if tillage is part of field management. In addition, normally annual row crops like corn and soybean are seedlings at this time with very small leaf areas leaving soil exposed to rain drop impacts.

Flow data collected during the calibration period is shown in Table 1. Annual discharge and N concentration varied between the 2 years due to differences in amount and timing of annual precipitation (Supplementary Figure S1). The discharge data represented a low flow year, 2004, and a high flow year, 2005. The mean discharge was 772 m^3.

Between 2021 and 2023 observed inflow to the ditches in the form of snowmelt runoff/surface runoff and subsurface drainage was highly variable and at times non-existent (Figure 3). Inflow was dominated by subsurface drainage which occurred in 16 months of this 3-year period. In contrast, snowmelt runoff/surface runoff occurred in 4 months over the same time span. Spring (March to May) inflow from subsurface drainage was usually the time when discharge was highest, with lower, secondary peaks of discharge occurring in summer and autumn. Continuous subsurface drainage between November 2021 and March 2022 was highly unusual. The greatest snowmelt runoff/surface runoff volume over this 3-year period, 63,736 m^3, was recorded during June 2023. As noted previously, precipitation during this year was slightly above average.

The first 6 months of 2021 were exceptionally dry, and no subsurface drainage was observed (Figure 3). Above average autumn precipitation from August through October, coupled with low evaporation and low to no transpiration, contributed to subsurface drain flow into the ditches. Frequent freeze/thaw cycles between November 2021 and March 2022 contributed to sustained subsurface drain flow into the ditches. Average to slightly above average precipitation between March and May 2022 resulted in the highest monthly subsurface drain flow recorded over this 3-year period, 99,623 m^3, in May. Subsurface drain flow in 2023 was much closer to normal with respect to timing and magnitude.

Hydraulic retention time was estimated in the spring of 2021 using a conservative bromide tracer. The HRT of the control channel was, on average, <30 min, whereas the HRT of the treatment channel was 11 h (data not shown). Between 2017 and 2023, implementation of the low-grade weir resulted in a 51% reduction in discharge from the control ditch, 1,057,530 m^3,

TABLE 1 Annual mean daily discharge rate, flow-weighted mean nitrate concentration (FWMNC), and mean nitrate loads for ditch parameters over the calibration and treatment periods.

Period	Year	Precipitation mm	Flow days	Control			Treatment		
				Discharge m^3	FWMNC mg L^{-1}	Load kg	Discharge m^3	FWMNC mg L^{-1}	Load kg
Calibration	2004	753	137	481	23.2	11.5	475	22.4	10.9
	2005	923	107	1,062	22.9	25.9	1,427	25.3	31.2
Treatment	2017	763	142	1,100	11.5	11.5	620	6.4	4.1
	2018	977	186	1,130	7.9	8.3	615	7.1	5.0
	2019	1,010	233	1,559	7.9	9.9	581	6.0	3.2
	2020	676	160	745	5.5	4.4	267	3.4	1.0
	2021	601	183	223	4.4	1.0	218	2.6	0.8
	2022	511	127	644	7.2	5.2	335	6.8	2.5
	2023	765	127	678	8.6	6.2	409	8.2	3.4

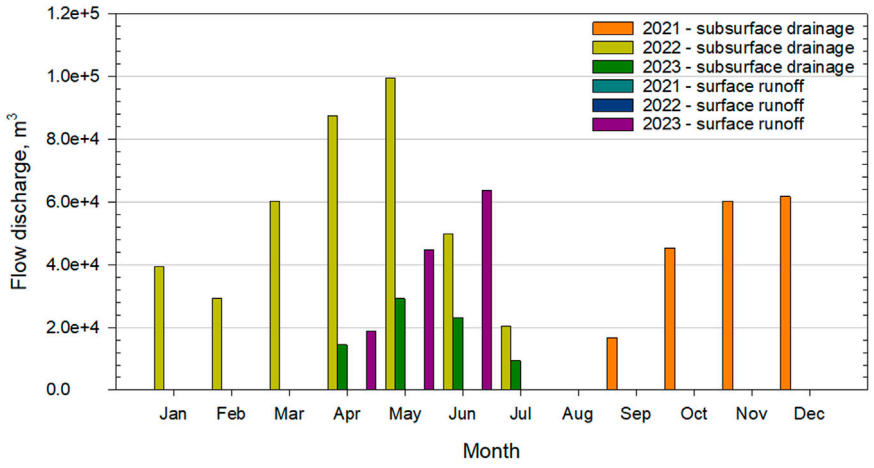


FIGURE 3
Monthly ditch inflow between 2021 and 2023.

TABLE 2 T-test for mean monthly discharge, flow-weighted mean nitrate concentration (FWMNC), and nitrate-nitrogen ($NO3^-N$) load between 2017 and 2023.

Years	Station[a]	Parameter	Units	n	Mean	Std Err	Difference	DF	Prob < t
2017–23	CTL	Discharge	$m^3\ d^{-1}$	43	976	183	−522	53	0.0049
2017–23	TRT	Discharge	$m^3\ d^{-1}$	43	454	66			
2017–23	CTL	FWMNC	mg L^{-1}	43	6.8	0.7	−2.1	82	0.0025
2017–23	TRT	FWMNC	mg L^{-1}	43	4.7	0.5			
2017–23	CTL	$NO3^-$-N Load	kg d^{-1}	43	7.1	0.6	−3.2	72	0.0001
2017–23	TRT	$NO3^-$-N Load	kg d^{-1}	43	3.9	0.5			

[a]Control, CTL; Treatment, TRT.

TABLE 3 Mean daily discharge, flow-weighted mean nitrate concentration (FWMNC), and mean nitrate load for paired ditch comparison during the calibration and treatment periods.

Variable	Calibration		Treatment		Change, %
	Control	Treatment	Control	Treatment	
Wet years, 2018–2019					
Discharge, m^3d^{-1}	362	451	1,370	596	-32
FWMNC, mg L^{-1}	22.9	22.1	7.9	6.5	71
Nitrate load, kg	8.3	9.7	9.2	4.0	59
Dry years, 2021–2022					
Discharge, m^3d^{-1}	362	451	246	123	73
FWMNC, mg L^{-1}	22.9	22.1	5.1	3.1	86
Nitrate load, kg	8.3	9.7	1.6	0.4	96
Average years, 2017, 2020, 2023					
Discharge, m^3d^{-1}	362	451	694	199	56
FWMNC, mg L^{-1}	22.9	22.1	7.0	3.0	86
Nitrate load, kg	8.3	9.7	4.8	0.7	93

compared to 514,905 m^3 from the treatment ditch. Discharge reduction from the ditches based on climate conditions (dry, average, wet) was linear. The smallest reduction in discharge between the control and treatment ditches occurred during the dry years, followed by the average years, with the greatest discharge reduction occurring during the wet years, 33%, 49%, and 56% respectively.

There was a statistically significant difference in mean daily discharge volume between the treatment and control ditch from 2017 through 2023 with the treatment ditch discharge being 53% lower than the control ditch, on average by 522 m^3 (Table 2). During the 2 years of below average precipitation, there were 183 days of flow in 2021 and 127 days in 2022 (Table 1). During the 2 years of above average precipitation, there were 186 days of flow in 2018 and 233 days of flow in 2019, respectively (Table 1). During the 3 years of average precipitation there were 142, 183, and 127 days of flow in 2017, 2020, and 2023, respectively (Table 1). It can be seen from these data that there were nearly the same number of days of ditch outflow during 2018, 2020, and 2021 representing a wet, average, and dry year, respectively. Thus, although snowmelt runoff and precipitation affected ditch outflow, the number of days of ditch outflow were not always consistent or predictable.

Under ideal circumstances, a calibration period would comprise the full range of expected conditions, dry, normal, and wet, but capturing the normal and wet end of the range helps quantify important hydrologic behavior and concomitant nutrient transport. Analysis of covariance was used to statistically analyze post treatment results between the control and treatment ditches. The results were grouped according to precipitation regimes as either wet, average, or dry conditions compared to the 30-year normal.

Using ANCOVA, there were differences in ditch discharge between calibration and treatment period regressions under wet, dry, and average conditions. Under wet conditions, the difference represented a shift in the regression toward lower discharge from the treatment ditch following implementation of the low-grade weir in relation to the unmanaged control ditch. During the treatment period, for wet years, discharge from the treatment ditch was negative indicating that discharge increase by 32% compared to the calibration period using the calibration equation and values observed during the treatment period (Table 3). Likewise, ANCOVA indicated that there were reductions in ditch discharge during dry and average years following the implementation of the low-grade weir. Using the calibration equations, this represented a reduction of 73% under dry conditions and 56% under average conditions (Table 3).

Monthly distribution and magnitude of mean daily outflow from 2017 to 2023 for the control ditch is found in Figure 4A. Overall, this figure shows that the majority of ditch outflow occurred during the 3-month period, March to May. In general, ditch outflow gradually declined between May and August as plant growth accelerated and rates of evaporation and transpiration increased. Ditch outflow began to increase in September and October in years when fall precipitation recharged the soil water content. No ditch outflow occurred in January and February when soil was continuously frozen. Major events that resulted in significant ditch outflow occurred in the early spring, March and April, of 2019 (Figure 4A). Other periods of high input that resulted in ditch outflow were early spring to mid-summer, April to July, and autumn, September and October, of 2018. There was a total absence of ditch outflow from April to September 2021 due to prolonged drought conditions (Figure 3).

Monthly distribution and magnitude of ditch mean daily outflow from 2017 to 2023 for the treatment ditch containing the low-grade weir is found in Figure 4B. Overall, this figure shows that monthly distribution of ditch outflow from the treatment ditch was similar to that of the control ditch. In contrast, the magnitude of the treatment ditch outflows for all months were lower than those from

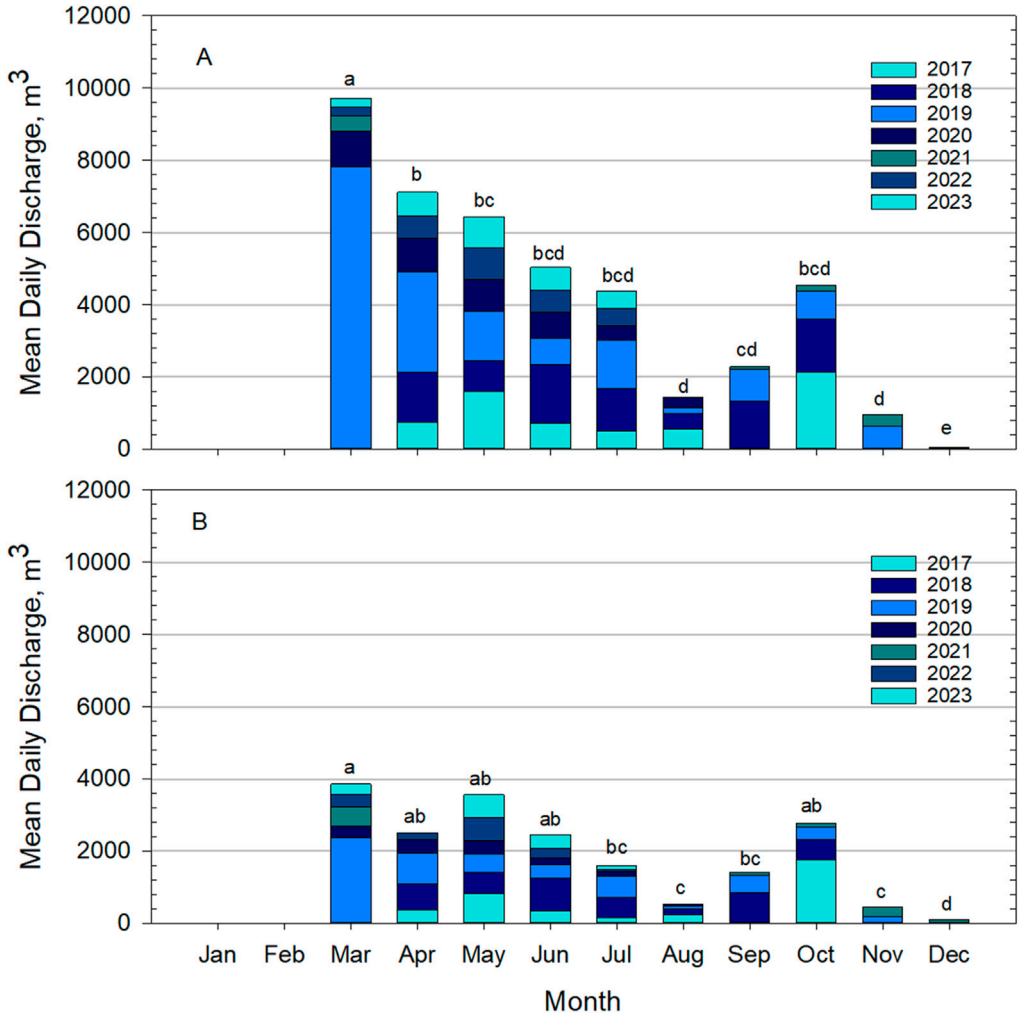


FIGURE 4
Monthly control **(A)** and treatment **(B)** ditch outflow between January and December. Means followed by the same lowercase letter are not significantly different at $P \leq 0.10$.

the control ditch. For the 3-month period between March and May, the mean monthly outflow for the treatment ditch was 56% lower than the treatment ditch. Between June and August, and September and November the outflow from the treatment ditch was reduced by 58% and 41%, respectively. This indicated that the low-grade weir was successful at increasing the water storage capacity of the control ditch.

3.3 Nitrogen concentration and loss

The processes that control nitrogen in aquatic environments include a combination of chemical and biological processes. Once in an aquatic ecosystem, such as a ditch, nitrogen is highly chemically and biologically active, undergoing numerous transformations and moving between benthic sediments and water column, and between the biotic and abiotic environment (Durand et al., 2011). In shallow flowing systems like ditches, biotic transformations of nitrogen are the dominant processes and include the autotrophic and heterotrophic uptake of nutrients from the water, assimilation into biomass, and release by excretion and microbial decomposition (Birgand et al., 2007). In addition, plants can take up nutrients from sediment pore water via roots or directly from the ditch water column. Under anaerobic conditions, denitrifying bacteria use nitrate as an electron acceptor to oxidize organic matter, thus reducing NO_3^--N to N_2O to N_2 during the process of denitrification.

3.3.1 Nitrogen concentration

Over the experimental period, from 2017 to 2023, implementation of the low-grade weir resulted in a 22% reduction in flow-weighted mean nitrate concentration (FWMNC) from the control ditch compared to the treatment ditch (Table 1). There was also a statistically significant difference in monthly FWMNC between the control and treatment ditch during the same period although the difference was small, on average 2.1 mg L^{-1} (Table 2). Between 2017 and 2023, the monthly FWMNC for the control ditch was 6.8 mg L^{-1} whereas the treatment ditch was 4.7 mg L^{-1}. This reduction in FWMNC is notable as it is somewhat uncommon to observe a significant

reduction in nitrate concentration. Kröger et al. (2012), studying ditches in Arkansas, showed no significant reduction in NO_3^--N concentration from ditch systems with and without weirs. When comparing the FWMNC based on climatic conditions, during the 2 years of below average precipitation (2021 and 2022) the daily FWMNC averaged 5.8 mg L^{-1} for the control ditch and the treatment ditch averaged 4.7 mg L^{-1} (Table 1). During the 2 years of above average precipitation (2018 and 2019) daily FWMNC averaged 7.9 mg L^{-1} and 6.6 mg L^{-1} for the control and treatment, respectively (Table 1). During the 3 years of average precipitation (2017, 2020, and 2023) daily FWMNC averaged 8.5 mg L^{-1} and 6.0 mg L^{-1} for the control and treatment ditches, respectively (Table 1). It was also apparent that the daily FWMNC for both ditches from the back-to-back dry years, 2021 and 2022, to 2023, increased on average by 1.6 mg L^{-1} and 0.7 mg L^{-1}. This rise coincided with an increase in mean daily discharge from 436 m^3 during 2021 and 2022 to 678 m^3 in 2023.

Statistical analysis using ANCOVA, showed that there were differences between calibration and treatment period regressions for daily FWMNC under wet, dry, and average conditions. Under wet conditions, the difference represented a shift in the regression toward lower FWMNC from the treatment ditch following implementation of the low-grade weir in relation to the control ditch. Overall, the FWMNC of the treatment ditch was reduced by 71% using the calibration equation and values observed during the treatment period (Table 3). Likewise, ANCOVA indicated that there were reductions in daily FWMNC during dry and average years following the implementation of the low-grade weir. Using the calibration equations, this represented a reduction of 86% under dry and average conditions, respectively (Table 3).

3.3.2 Nitrate-nitrogen loss

Precipitation is the driving force for hydrologic relationships and in turn is a dominant factor in nutrient transport. Between 2017 and 2023, implementation of the low-grade weir resulted in a 58% reduction in NO_3^--N from the control ditch, 8,423 kg, compared to 3,314 kg from the treatment ditch (Table 1). Nitrate-nitrogen load reduction from the ditches based on climate conditions (wet, average, dry) was linear. In contrast to discharge, the smallest reduction in NO_3^--N load between the control and treatment ditches occurred during the wet years, followed by the average years, with the greatest load reduction occurring during the dry years, 56%, 62,% and 68% respectively.

There was a statistically significant difference in mean monthly NO_3^--N load from the control ditch compared to the treatment ditch between 2017 and 2023 (Table 2). The mean monthly NO_3^--N load from the control ditch was 7.1 kg while the treatment ditch averaged, 3.9 kg, a difference of 3.2 kg (Table 2). During the 2 years of below average precipitation (2021 and 2022) daily NO_3^--N load averaged 3.1 kg for the control ditch whereas the treatment ditch averaged 1.7 kg (Table 1). During the 2 years of above average precipitation (2018 and 2019) daily NO_3^--N load averaged 9.1 kg and 6.6 kg for the control and treatment, respectively (Table 1). During the 3 years of average precipitation (2017, 2020, and 2023) daily NO_3^--N averaged 8.5 kg and 6.0 kg for the control and treatment ditches, respectively (Table 1). These data showed that, regardless of the climatic cycle, the treatment ditch with the low-grade weir always attenuated NO_3^--N load. The data also indicated that NO_3^--N load from the treatment ditch was lowest under dry conditions, intermediate under average conditions, and highest under wet conditions.

There was a statistically significant monthly effect of NO_3^--N load primarily related to periods of high, intermediate, and low flow (Table 3). Monthly distribution and magnitude of control ditch NO_3^--N losses from 2017 to 2023 is found in Figure 5A. Over the this period, at no time was monthly NO_3^--N loss from the treatment channel greater than the control channel. Overall, this figure shows that the greatest NO_3^--N losses occurred during the 2-month period, April and May. Ditch NO_3^--N losses also steadily declined between June and August. Nitrate losses began to increase in September in years when autumn precipitation recharged soil water content.

Monthly distribution and magnitude of ditch NO_3^--N losses from 2017 to 2023 for the treatment ditch containing the low-grade weir appear in Figure 5B. Overall, this figure shows that monthly distribution of ditch NO_3^--N losses from the treatment ditch was similar to that of the control ditch. In contrast, the magnitude of the treatment ditch NO_3^--N losses for all months were lower than those from the control ditch. Nitrate losses were lowest on average in August. A combination of lower flows and higher temperatures during summer is generally conducive to higher rates of microbial activity, including denitrification. These data suggest that use of weirs can provide enhanced hydrological residence time in these systems, and thus promote conditions conducive for nitrogen removal via denitrification to occur.

Above average annual precipitation resulted in greater NO_3^--N loads during to two wet years, 2018 and 2019. Nitrate-N losses were recorded in every month between April and October during 2018. On an annual basis, NO_3^--N loss was greater for the control channel, 1,544 kg compared to 930 kg for the treatment channel during 2018. The implementation of the low-weir in the treatment channel resulted in an overall reduction in NO_3^--N loss of 40% for the treatment channel compared to the control channel.

Nitrate-N losses were recorded in every month between March and October during 2019. Similar to 2018, on an annual basis, NO_3^--N loss was greater for the control channel, 2,307 kg compared to the treatment channel, 746 kg, during 2019. The maximum monthly NO_3^--N load occurred during April 2019 in the control channel. Above-average precipitation in late August and September resulted in an increase in NO_3^--N loss for both channels although the magnitude of the increase was smaller for the treatment ditch (Figures 5A, B). During August, ditch channels reached their lowest observed NO_3^--N losses of the growing season. This result is not unexpected as corn and soybean were vigorously growing at this point actively taking up water and nutrients.

Below average annual precipitation resulted in the smallest NO_3^--N loads during 2021 and 2022. During 2021, the first dry year of consecutive dry years, NO_3^--N losses were recorded in March and then September to December. On an annual basis, NO_3^--N loss was greater for the control channel, 183 kg compared to 146 kg for the treatment channel during 2021. During 2022, the second year of consecutive dry years, NO_3^--N losses were recorded in March through July. On an annual basis, NO_3^--N loss was greater for the control channel, 660 kg compared to 318 kg for the treatment channel during 2022. The implementation of the low-grade weir in the treatment channel resulted in an overall reduction in NO_3^--N loss of 52% compared to the control channel.

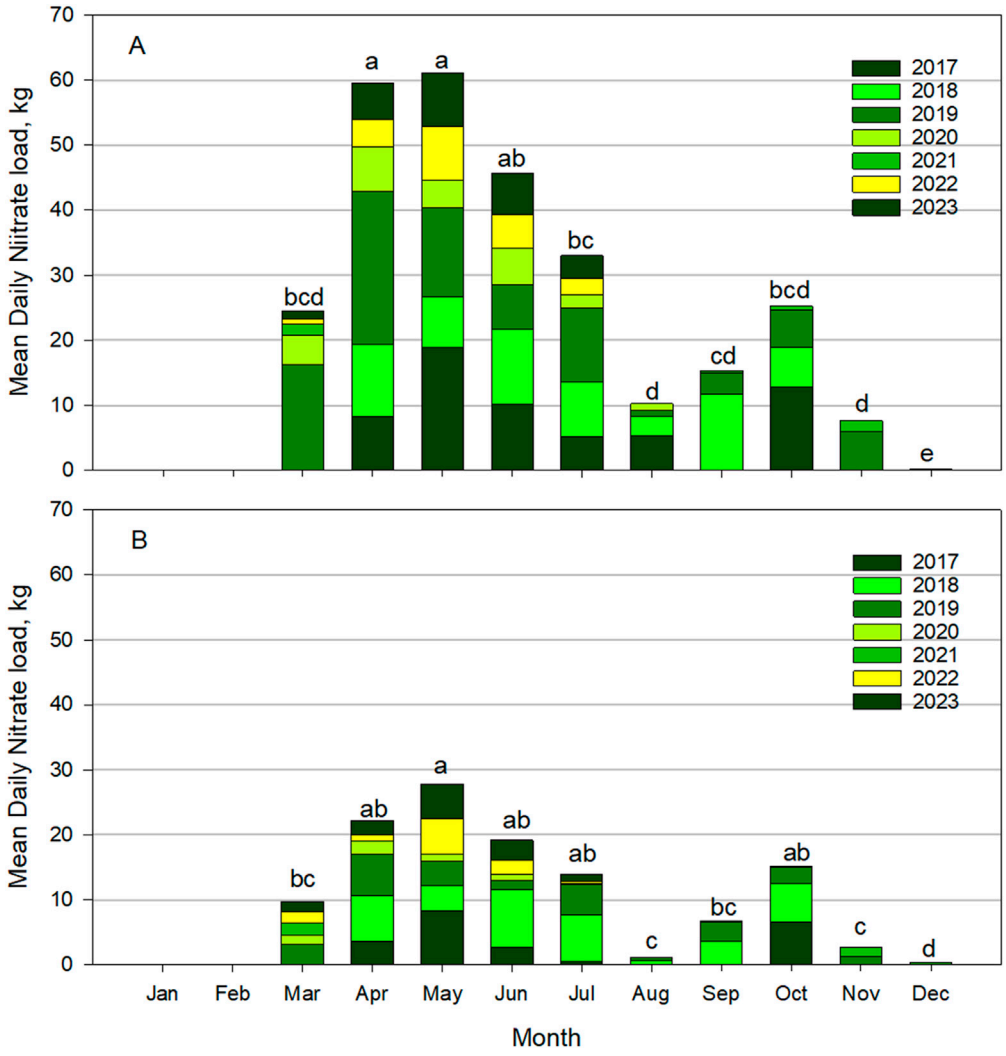


FIGURE 5
Monthly control **(A)** and treatment **(B)** ditch nitrate-load between January and December. Means followed by the same lowercase letter are not significantly different at $P \leq 0.10$.

The largest monthly loss of NO_3^--N in 2022 occurred during May when 245 kg was exported from the control ditch.

Average annual precipitation resulted in intermediate NO_3^--N loss during the 3 years, 2017, 2020 and 2023. On average, NO_3^--N loss was greater for the control channel, 1,041 kg compared to 391 kg for the treatment channel during these 3 years. The implementation of the low-grade weir in the treatment channel resulted in an overall reduction in NO_3^--N loss of 62% compared to the control channel.

4 Discussion

Annual variation in nutrient losses including NO_3^--N loss from drained agricultural landscapes has been primarily attributed to the volume of water exported through subsurface drainage (Gramlich et al., 2018). Subsurface drainage is influenced by the frequency, intensity, and distribution of precipitation over time and the amount of annual or monthly precipitation that occurs. Previous research has also shown that NO_3^--N concentration can be affected by dry and wet climatic conditions (Randall and Goss, 2008; Duncan et al., 2017). Based on the results from this experiment, it was evident that the presence of low-grade weirs in the treatment ditch affected NO_3^--N concentration.

The current experiment showed reductions in discharge and FWMNC from the treatment compared to the control ditch. In contrast, results reported from research conducted in the Lower Mississippi River Valley showed no difference in NO_3^--N concentration in systems with or without low-grade weirs (Kröger et al., 2012). Variations in ditch FWMNC observed in this study show that concentration does not depend solely on ditch discharge. Ditch NO_3^- concentrations are also an indication of nitrogen source, storage, and transport as well as biologically mediated processes such as microbial uptake, vegetation uptake, nitrification, and denitrification. Recent work on N dynamics in southern Manitoba demonstrated that high concentrations of inorganic N were associated with snowmelt runoff, while summer inorganic N concentrations remained consistently low, suggesting increased biological N transformation and N removal (Friesen-

Hughes et al., 2021). In addition, shifts in temperature across seasons, vegetation phenology, and subsurface drainage discharge periods could all impact FWMNC.

The overall reduction in NO_3^--N loss from the treatment channel indicated that the low-grade weir increased residence time in the ditch and this coupled with a larger wetted perimeter and deeper channel behind the low-grade weir likely resulted in denitrification. Recent studies have demonstrated the capacity of managed agricultural drainage ditches to mitigate N (Kröger et al., 2007; Kröger et al., 2012; Littlejohn et al., 2014). In these studies, the authors reported a wide range in NO_3^--N load reductions ranging from 14% to 66%. The authors ascribed the differences to shortened HRT attributed high flows. The current study demonstrated similar load reductions only under different climate conditions. Although not specifically measured, denitrification would be expected to be the main driver of NO_3^--N reduction in the treatment channel although uptake into emergent vegetation also likely occurred as air temperatures increased and vegetation matured. Increased HRT and increased area inundation under the ditch containing the low-grade weir system was hypothesized to have increased denitrification potential and as a result the potential for higher reductions in NO_3^--N load for treatment ditch compared to the control ditch.

Another possible explanation for NO_3^--N loss differences between the channels could be that one or both channels were influenced by shallow groundwater. Ditch channel-groundwater interactions in which a ditch channel gained water from shallow groundwater could appear to decrease NO_3^--N loss resulting result from a possible dilution effect of shallow groundwater with a lower NO_3^--N concentration than the ditch channel. In addition, seepage losses from a ditch channel to shallow groundwater could result in an apparent decrease in NO_3^--N loss from ditch channels. This phenomenon was observed by researchers in southern France (Dagès et al., 2008). The authors suggested that contaminants such as NO_3^--N would be confined to the wetted perimeter of ditches, and that its transmission to the deeper groundwater would occur very slowly or that it would return in some measure to the ditch flow if the water table were to rise above the water level in the ditch during a runoff event. The authors further suggested that groundwater contamination in catchments with dense ditch networks would be difficult to monitor both spatially and temporally (Dagès et al., 2008).

Excess water and droughts create *hot moments* and *hot spots* as distinct temporal and spatial components of biogeochemical responses. Excess water has a dominating effect on the export of dissolved nutrients from agricultural landscapes. Nitrate-nitrogen retention efficiency decreases with increasing flow (Wollheim et al., 2017). High flows generated by seasonal snowmelt or rainfall events mobilize large pulses of nutrients (e.g., Pellerin et al., 2012). Increased water depth and velocity during high flows reduces reactive capacity by decreasing HRT available for biogeochemical processing (Basu et al., 2011).

In contrast, low-flow periods such as droughts are potentially dominant control points for biogeochemical processing, enhancing variation in nutrient concentrations, metabolism, and nutrient uptake. For example, shifts in environmental conditions because of hydrologic pulsing could have an impact on ditch microorganism presence, abundance, and function. In a recent study, a ditch with low-grade weirs achieved 60% higher NO_3-N removal compared to an unmanaged ditch during low flow conditions (Wang et al., 2024). The authors attributed the reduction most likely to N removal by denitrification or another anerobic N removal process.

Low-grade weirs should be considered as BMPs for nitrogen removal in source agricultural landscapes, as they promote conditions conducive for NO_3-N reduction through denitrification (Kröger et al., 2014). Evaluation of weirs in this study under cold climate conditions and other research suggests that ditches managed with low-grade weirs increase HRT (Kröger et al., 2008) as well as decrease NO_3^--N concentrations and loads over drainage ditches that do not have any water management structures (Kröger et al., 2011). The process of nitrogen removal from agricultural drainage is dependent on microbial denitrification (Tank et al., 2021). Denitrification has been studied in systems used to treat agricultural drainage. In a study in Minnesota, the researchers found a significantly greater abundance of 16S rRNA gene and genes associated with denitrification (nirK, nirS, norB, and nosZ) in a ditch managed with a low-grade weir compared to an unmanaged ditch (Wang et al., 2024). In contrast, in a 3-year study aimed at understanding the effects of low-grade weirs on soil microbial communities in agricultural drainage ditches in Mississippi the researchers found no significant differences between sites with and without low-grade weirs (Baker et al., 2018). These disparities with the current study could be in part due to differences in ditch geometry, characteristics, management, and duration of treatment. For example, in the Mississippi study the researchers used rip-rap weirs which were only in place for 3 years. We hypothesize that ditch conditions may not have stabilized under this short length of time, thus the microbiome may not have had sufficient time for ditch conditions to come to the same level of stability as those in the present study (i.e. 17 years).

Nitrate removal performance within drainage ditches equipped with low-grade weirs has been shown to be effective at reducing NO_3-N load by 25%–67% with greater reductions observed under low-flow conditions (Littlejohn et al., 2014). Previous research in Indiana showed that two-stage ditches offer the potential to reduce NO_3-N concentrations, but NO_3-N load was observed to increase by 2% (Hodaj et al., 2017). In contrast, two-stage ditch research in Minnesota showed a NO_3-N load reduction range between 14% and 34% (Krider et al., 2022). In a review of the performance of denitrifying bioreactors for treatment of NO_3-N from agricultural drainage water the authors reported a mean (± standard deviation) NO_3-N load reduction of 40% ± 26% (Christianson et al., 2021). In a review of the performance of saturated buffers for treatment of NO_3-N from agricultural drainage water the authors reported a mean (± standard deviation) NO_3-N load reduction of 46% ± 24% (Johnson et al., 2023).

Our research demonstrated the potential benefits of using low-grade weirs as a management tool in drainage ditches at cold latitudes. However, the potential benefit of managing ditches with low-grade weirs is variable dependent on growing season precipitation. In addition, this experiment was conducted with only one weir in place over the entire length of the ditch as well as only two inflow sources of water. Along the length of public and private ditches there are many inflow sources of drainage water. The water quality and quantity impact of multiple inflow sources of water and their occurrence at irregular intervals is a knowledge gap. Moreover, low-grade weirs are currently manually operated.

Frequently adjusting low-grade weirs during the flow season is not practical unless the management process is automated. A more responsive management of low-grade is necessary for adjusting the drainage intensity during periods of low flow to high flow depending on timing and amount of precipitation, and subsequently optimizing the benefits of low-grade weirs. With the recent advances in sensor technologies, weather forecast, data acquisition, transmission, and analytics, the automation of low-grade weirs seems feasible.

5 Conclusion

The purpose of this research was to advance fundamental changes in agricultural drainage ditch management from the existing paradigm of ditch management that focuses on water conveyance, requiring periodic ditch maintenance (clean out) which shortens HRT and removes valuable carbon supplies (vegetation), drastically limiting nutrient cycling, especially N; to a new paradigm where ditches are managed using minimally invasive low-grade weirs to temporarily store water on the landscape to help mitigate peak flows and reduce nutrient losses from agricultural landscapes. Ditches are a common means of conveying excess drainage water from agricultural land in in the Midwest. These ditches are necessary for maintaining strong agricultural production, but they have the potential to lead to loading of excess nutrients to surface waters. Agricultural best management practices such as filter strips, conservation tillage and nutrient and residue management planning are currently practiced to minimizing agricultural impacts on water quantity and quality. However, other approaches such as minimally invasive ditch management of water flow, vegetation, and/or management of the ditch geometry have the potential to further help agricultural and environmental managers protect our nations water resources.

Overall ditch management was quite effective in mitigating discharge and nitrogen loss from runoff and drainage water. State and federal mandates for nitrogen reduction to the Gulf of Mexico for Minnesota are the same, a 45% reduction by 2045. To meet this goal practices like low-grade weirs in drainage ditches should be considered given that this experiment, with significant variation in annual precipitation amounts, indicates that on average, the installation of low-grade weirs in drainage ditches can reduce nitrate loss by 61%, 16% above the current mandate level. In addition, this style of management of ditch drainage water is minimally invasive and does not require additional agricultural land be taken out of production. Although two-stage ditches have been shown to have positive impacts on mitigating nutrients from agricultural production they are expensive to build and take valuable crop land out of production.

Ditches are complex systems with characteristics of headwater streams and wetlands. Designing and applying ditch management practices that address nonpoint source agricultural pollution problems will be beneficial in the implementation of water quality protection programs and achieving state and federal nutrient reduction goals.

Data availability statement

The raw data supporting the conclusions of this article will be made available by the authors, without undue reservation.

Author contributions

JS: Conceptualization, Data curation, Formal Analysis, Funding acquisition, Investigation, Methodology, Project administration, Resources, Supervision, Writing–original draft, Writing–review and editing. AR: Data curation, Formal Analysis, Writing–review and editing.

Funding

The author(s) declare that financial support was received for the research, authorship, and/or publication of this article. The researcher's time was supported in part by the Hatch capacity grant program, from the U.S. Department of Agriculture's National Institute of Food and Agriculture.

Conflict of interest

The authors declare that the research was conducted in the absence of any commercial or financial relationships that could be construed as a potential conflict of interest.

Publisher's note

All claims expressed in this article are solely those of the authors and do not necessarily represent those of their affiliated organizations, or those of the publisher, the editors and the reviewers. Any product that may be evaluated in this article, or claim that may be made by its manufacturer, is not guaranteed or endorsed by the publisher.

References

Baker, B. H., Brooks, J. P., Deng, D. D., Smith, R. K., Kröger, R., and Czarnecki, J. M. P. (2018). Effects of low-grade weirs on soil microbial communities in agricultural drainage ditches. *J. Environ. Qual.* 47, 1155–1162. doi:10.2134/jeq2017.12.0489

Basu, N. B., Thompson, S. E., and Rao, P. S. C. (2011). Hydrologic and biogeochemical functioning of intensively managed catchments: A synthesis of top-down analyses. *Water. Resour. Res.* 47 (10). doi:10.1029/2011wr010800

Birgand, F., Skaggs, R. W., Chescheir, G. M., and Gilliam, J. W. (2007). Nitrogen removal in streams of agricultural catchments—a literature review. *Crit. Rev. Environ. Sci. Technol.* 37 (5), 381–487. doi:10.1080/10643380600966426

Christianson, L. E., Cooke, R. A., Hay, C. H., Helmers, M. J., Feyereisen, G. W., Ranaivoson, A. Z., et al. (2021). Effectiveness of denitrifying bioreactors on water pollutant reduction from agricultural areas. *Trans. Am. Soc. Agric. Biol. Eng.* 64 (2), 641–658. doi:10.13031/trans.14011

Dagès, C., Voltz, M., Lacas, J., Huttel, O., Negro, S., and Louchart, X. (2008). An experimental study of water table recharge by seepage losses from a ditch with intermittent flow. *Hydrol. Process.* 22 (18), 3555–3563. doi:10.1002/hyp.6958

Duncan, J. M., Welty, C., Kemper, J. T., Groffman, P. M., and Band, L. E. (2017). Dynamics of nitrate concentration discharge patterns in an urban watershed. *Water Resour. Res.* 53, 7349–7365. doi:10.1002/2017WR020500

Durand, P., Breuer, L., Johnes, P. J., Billen, G., Butturini, A., Pinay, G., et al. (2011). "Nitrogen processes in aquatic ecosystems," in *European nitrogen assessment* M. A. Sutton and C. M. Erisman Cambridge: Cambridge University Press, 126–146. Available at: https://centaur.reading.ac.uk/20855/.

Evans, R., Skaggs, R. W., and Gilliam, J. W. (1995). Controlled versus conventional drainage effects on water quality. *J. Irrigation Drainage Eng.* 121 (4), 271–276. doi:10.1061/(asce)0733-9437(1995)121:4(271)

Faust, D., Kröger, R., Moore, M., and Rush, S. (2018). Management practices used in agricultural drainage ditches to reduce Gulf of Mexico hypoxia. *Bull. Environ. Contam. Toxicol.* 100, 32–40. doi:10.1007/s00128-017-2231-2

Fennel, K., and Laurent, A. (2018). N and P as ultimate and proximate limiting nutrients in the northern Gulf of Mexico: implications for hypoxia reduction strategies. *Biogeosciences* 15 (10), 3121–3131. doi:10.5194/bg-15-3121-2018

Friesen-Hughes, K., Casson, N., and Wilson, H. (2021). Nitrogen dynamics and nitrogen-to-phosphorus stoichiometry in cold region agricultural streams. *J. Environ. Qual.* 50 (3), 653–666. doi:10.1002/jeq2.20234

Gramlich, A., Stoll, S., Stamm, C., Walter, T., and Prasuhn, V. (2018). Effects of artificial land drainage on hydrology, nutrient and pesticide fluxes from agricultural fields–A review. *Agric. Ecosyst. and Environ.* 266, 84–99. doi:10.1016/j.agee.2018.04.005

Hodaj, A., Bowling, L. C., Frankenberger, J. R., and Chaubey, I. (2017). Impact of a two-stage ditch on channel water quality. *Agric. Water Manag.* 192, 126–137. doi:10.1016/j.agwat.2017.07.006

JMP (2019). *JMP, Version 15.0.* Cary, NC: SAS Institute Inc.

Johnson, G., Christianson, L., Christianson, R., Davis, M., Díaz-García, C., Groh, T., et al. (2023). Effectiveness of saturated buffers on water pollutant reduction from agricultural drainage. *J. Nat. Resour. Agric. Ecosyst.* 1 (1), 49–62. doi:10.13031/jnrae.15516

Kaur, G., Zurweller, B. A., Nelson, K. A., Motavalli, P. P., and Dudenhoeffer, C. J. (2017). Soil waterlogging and nitrogen fertilizer management effects on corn and soybean yields. *Agron. J.* 109, 97–106. doi:10.2134/agronj2016.07.0411

Krider, L., Kramer, G., Wilson, B., Magner, J., Lazarus, W., Hansen, B., et al. (2022). Alternative agricultural ditch designs, NO3-N treatment, construction costs, and benefits—mower county, Minnesota, USA. *J. Environ. Sci. Eng. B* 11, 229–240. doi:10.17265/2162-5263/2022.06.002

Kröger, R., Cooper, C., and Moore, M. (2007). A preliminary study of an alternative controlled drainage strategy in surface drainage ditches: low-grade weirs. *Agric. Water Manag.* 95, 678–684. doi:10.1016/j.agwat.2008.01.006

Kröger, R., Cooper, C., and Moore, M. (2008). A preliminary study of an alternative controlled drainage strategy in surface drainage ditches: low-grade weirs. *Agric. Water Manag.* 95, 678–684. doi:10.1016/j.agwat.2008.01.006

Kröger, R., Moore, M., Farris, J., and Gopalan, M. (2011). Evidence for the use of low-grade weirs in drainage ditches to improve nutrient reductions from agriculture. *Water Air Soil Pollut.* 221, 223–234. doi:10.1007/s11270-011-0785-x

Kröger, R., Pierce, S. C., Littlejohn, K. A., Moore, M. T., and Farris, J. L. (2012). Decreasing nitrate-N loads to coastal ecosystems with innovative drainage management strategies in agricultural landscapes: an experimental approach. *Agric. Water Manag.* 103, 162–166. doi:10.1016/j.agwat.2011.11.009

Kröger, R., Scott, J., and Prince Czarnecki, J. (2014). Denitrification potential of low-grade weirs and agricultural drainage ditch sediments in the lower Mississippi Alluvial Valley. *Ecol. Eng.* 73, 168–175. doi:10.1016/j.ecoleng.2014.09.019

Li, Y., Guan, K., Schnitkey, G. D., DeLucia, E., and Peng, B. (2019). Excessive rainfall leads to maize yield loss of a comparable magnitude to extreme drought in the United States. *Glob. change Biol.* 25 (7), 2325–2337. doi:10.1111/gcb.14628

Littlejohn, K., Poganski, B., Kröger, R., and Ramirez-Avila, J. (2014). Effectiveness of low-grade weirs for nutrient removal in an agricultural landscape in the Lower Mississippi Alluvial Valley. *Agric. Water Manag.* 131, 79–86. doi:10.1016/j.agwat.2013.09.001

Martin, E., Godwin, I., Cooper, R., Aryal, N., Reba, M., and Bouldin, J. (2021). Assessing the impact of vegetative cover within Northeast Arkansas agricultural ditches on sediment and nutrient loads. *Agric. Ecosyst. Environ.* 320, 107613. doi:10.1016/j.agee.2021.107613

Moore, M. T., Cooper, C. M., and Farris, J. L. (2005). "Drainage ditches," in *Water encyclopedia*. Editors J. Lehr, J. Keeley, J. Lehr, and T. B. Kingery (New York, NY: John Wiley and Sons, Inc.).

Nifong, R. L., Taylor, J. M., and Moore, M. T. (2019). Mulch-derived organic carbon stimulates high denitrification fluxes from agricultural ditch sediments. *J. Environ. Qual.* 48, 476–484. doi:10.2134/jeq2018.09.0341

Olson, K., Morton, L., and Speidel, D. (2016). Little river drainage district conversion of big swamp to fertile agricultural land. *J. Soil Water Conservation* 71 (2), 37a–43A. doi:10.2489/jswc.71.2.37a

Pellerin, B. A., Saraceno, J. F., Shanley, J. B., Sebestyen, S. D., Aiken, G. R., Wollheim, W. M., et al. (2012). Taking the pulse of snowmelt: in situ sensors reveal seasonal, event and diurnal patterns of nitrate and dissolved organic matter variability in an upland forest stream. *Biogeochemistry* 108, 183–198. doi:10.1007/s10533-011-9589-8

Rabalais, N. N., and Turner, R. E. (2019). Gulf of Mexico hypoxia: past, present, and future. *Limnol. Oceanogr. Bull.* 28 (4), 117–124. doi:10.1002/lob.10351

Randall, G. W., and Goss, M. J. (2008). "Nitrate losses to surface water through subsurface, tile drainage," in *Nitrogen in the environment: sources, problems, and management*. Editors J. L. Hatfield and R. F. Follett (Elsevier Inc).

Reinhart, B. D., Frankenberger, J. R., Hay, C. H., and Helmers, M. J. (2019). Simulated water quality and irrigation benefits from drainage water recycling at two tile-drained sites in the US Midwest. *Agric. Water Manag.* 223, 105699. doi:10.1016/j.agwat.2019.105699

Strock, J. S., Sands, G. R., Krebs, D. J., and Surprenant, C. (2005). Design and testing of a paired drainage channel research facility. *Appl. Eng. Agric.* 21 (1), 63–69. doi:10.13031/2013.17914

Tank, J. L., Speir, S. L., Sethna, L. R., and Royer, T. V. (2021). The case for studying highly modified agricultural streams: farming for biogeochemical insights. *Limnol. Oceanogr. Bull.* 30, 41–47. doi:10.1002/lob.10436

USDA National Agricultural Statistics Service (USDA-NASS) (2017). 2017 census of agriculture – United States data. Available at: https://www.nass.usda.gov/Publications/AgCensus/2017/Full_Report/Volume_1,_Chapter_1_US/st99_1_0047_0047.pdf.

Wang, H., Strock, J., Ranaivoson, A., and Ishii, S. (2024). Bioremediation of nitrate in agricultural drainage ditches: Impacts of low-grade weirs on microbiomes and nitrogen cycle gene abundance. *Sci. Total. Environ.* 955, 177070. doi:10.1016/j.scitotenv.2024.177070

Williams, M. R., King, K. W., and Fausey, N. R. (2015). Contribution of tile drains to basin discharge and nitrogen export in a headwater agricultural watershed. *Agric. Water Manag.* 158, 42–50. doi:10.1016/j.agwat.2015.04.009

Wollheim, W. M., Mulukutla, G. K., Cook, C., and Carey, R. O. (2017). Aquatic nitrate retention at river network scales across flow conditions determined using nested in situ sensors. *Resour. Res.* 53, 9740–9756. doi:10.1002/2017wr020644

frontiers | Frontiers in Environmental Science

TYPE Brief Research Report
PUBLISHED 16 September 2024
DOI 10.3389/fenvs.2024.1473726

Check for updates

OPEN ACCESS

EDITED BY
Keith Schilling,
The University of Iowa, United States

REVIEWED BY
Martin St. Clair,
The University of Iowa, United States
Robert Hirsch,
United States Department of the Interior, United States

*CORRESPONDENCE
Nick A. Chappell,
n.chappell@lancaster.ac.uk

RECEIVED 31 July 2024
ACCEPTED 02 September 2024
PUBLISHED 16 September 2024

CITATION
Chappell NA (2024) Quantifying rain-driven NO_3-N dynamics in headwater: value of applying SISO system identification to multiple variables monitored at the same high frequency.
Front. Environ. Sci. 12:1473726.
doi: 10.3389/fenvs.2024.1473726

COPYRIGHT
© 2024 Chappell. This is an open-access article distributed under the terms of the Creative Commons Attribution License (CC BY). The use, distribution or reproduction in other forums is permitted, provided the original author(s) and the copyright owner(s) are credited and that the original publication in this journal is cited, in accordance with accepted academic practice. No use, distribution or reproduction is permitted which does not comply with these terms.

Quantifying rain-driven NO_3-N dynamics in headwater: value of applying SISO system identification to multiple variables monitored at the same high frequency

Nick A. Chappell*

Lancaster Environment Centre, Lancaster University, Lancaster, United Kingdom

The nitrate–nitrogen (NO_3-N) concentration is a key variable affecting the ecosystem services supported by headwater streams. The availability of such data monitored continuously at a high frequency (in parallel to hydrometric and other water quality data) potentially permits a greater insight into the dynamics of this key variable. This study demonstrates how single-input single-output (SISO) system identification tools can make better use of these high-frequency data to identify a reduced number of numerical characteristics that support new explanatory hypotheses of rain-driven NO_3-N dynamics. A second-order watershed managed for commercial forestry in upland Wales (United Kingdom) provided the illustrative data. Fifteen-minute rainfall time series were used to simulate NO_3-N concentration dynamics and the potentially associated dynamics in dissolved organic carbon (DOC) and runoff, monitored at the same high resolution for two 30-day periods with a differing temperature regime. The approach identified robust, high-efficiency models needing few parameters. Comparison of only three derived dynamic response characteristics (DRCs) of *δ*, *TC*, and *SSG* for the three variables for the two different periods led to new hypotheses of rain-driven NO_3-N dynamics for further exploratory field investigation.

KEYWORDS

CAPTAIN Toolbox, dissolved organic carbon, high frequency, nitrate, stream, system identification, watershed

1 Introduction

With advances in sensor technology, more researchers and practitioners are continuously monitoring nitrate–nitrogen (NO_3-N) dynamics and other water quality variables at a high frequency, i.e., sub-daily or sub-hourly (Burns et al., 2019). For NO_3-N, this reveals the importance of diel and seasonal cycles (Halliday et al., 2013; Kermorvant et al., 2023) and complex short-term responses to rain events (Brunet et al., 2021). Time series of NO_3-N may also contain apparent interactions with other water quality variables, such as dissolved organic carbon (DOC) (Ledesma et al., 2022) or phosphate (Graeber et al., 2024).

As the accuracy and reliability of continuous in-field NO_3-N measurements have increased (Pellerin et al., 2013), so has the imperative to make the most of the information-rich time series that can now be collected (Burns et al., 2019). Improved evaluation of watershed models capable of simulating complex nitrate dynamics over wide time scales is possible with the higher-frequency data (Jiang et al., 2019). Where numerous water quality data streams are combined with synchronous data streams of potential controlling variables (e.g., solar radiation and rainfall), real-time "machine learning" can make rapid predictions of water quality changes for hazard mitigation (Tang et al., 2022; McGill and Ford, 2024). Similarly, numerical methods used for extracting 1) the dominant cycles and trends within NO_3-N time series; 2) quantifying the strength of dynamic relationships between a water quality variable and the controls on these dynamics; and 3) deriving dynamic response characteristics (DRCs) particular to the watershed, land use, or climate setting become credible. One such class of methods capable of extracting contained dynamics is system identification (SI) tools or models (Box et al., 2008). Typically, these methods differ from machine learning approaches or models built on biogeochemical–hydrological processes by the implicit goal of parsimony (Taylor et al., 2007). The goal is to simulate the dominant modes of behavior within a time series with the fewest number of model parameters in the least complex conceptual model structure. When the number of model parameters can be limited in this way (while still simulating outputs with high accuracy), uncertainty in the individual estimates of parameter values is constrained. The resultant reduced uncertainty may then lead to greater confidence in feasible interpretations of the process dynamics (Jones et al., 2014). Furthermore, by not "forcing" preconceived process dynamics to fit observed time series, new aspects of our perceptual understanding of water quality behavior may emerge from SI modeling (Burns et al., 2019).

Watercourses may have anthropogenically elevated concentrations of dissolved NO_3-N as a result of elevated nitrogen inputs to watersheds or through watershed disturbance. For example, in upland Wales (United Kingdom), soil and vegetation disturbances associated with commercial conifer forestry have been shown to lead to elevated NO_3-N losses to headwater streams (Neal et al., 2011; Halliday et al., 2013), risking acidification and eutrophication downstream. The instrumented headwater stream in upland Wales chosen for this illustrative study has been affected by such commercial forestry with its associated impacts on NO_3-N concentrations and other water quality variables (Ormerod and Durance, 2009; Jones and Chappell, 2014). This watershed is the 2-km^2 Trawsnant, with over 90% of its area covered by managed commercial conifer plantations. Lancaster University instrumented the watershed as part of the "Diversity of Upland Rivers for Ecosystem Service Sustainability" (DURESS) project within the Biodiversity and Ecosystem Service Sustainability (BESS) research program. The stream gauging station was installed at 52.12596° N, 3.74740° W, at a height of 322 m within the Welsh uplands. Approximately 44% of the watershed is covered by podzolic soil, 48% by histosol, and the remaining 9% by gleysol (Jones and Chappell, 2014). The geology comprises Ordovician sedimentary rocks (Cwmere and Yr Allt formations). A water quality station was located close to the stream gauge to collect parallel high-frequency time series of NO_3-N (dissolved and total), organic carbon (dissolved and total), water temperature, pH, and electrical conductivity. A network of automated rain gauges supported these stations. These parallel time series, all collected at a high frequency at every 15 min, permitted the comparison of rain-driven NO_3-N dynamics with those of DOC and hydrological dynamics. Previous studies have indicated that watershed hydrological responses to rainfall and DOC concentrations may help in understanding the rain-driven NO_3-N dynamics in similar low-order streams (Halliday et al., 2013; Koenig et al., 2017; Burns et al., 2019). A single-input single-output (SISO) form of system identification modeling (Taylor et al., 2007) was used in this study to quantify the rain-driven NO_3-N dynamics. The complexity of the accepted models was minimized (using numerical measures of efficiency and over-parameterization) to aid the hydrological/biogeochemical interpretation, as done by Jones and Chappell (2014), Jones et al. (2014), and Chappell et al. (2017a). The overall aim was to demonstrate the value of using a SISO system identification tool for quantifying rain-driven water quality dynamics, with the example of dissolved NO_3-N within a small stream emanating from a conifer plantation. The specific research objectives are to

1. Demonstrate the value of using SISO system identification to extract information from multiple water quality time series monitored at a high frequency along with parallel hydrometric data;
2. Quantify the degree of model complexity required to simulate rain-generated, dissolved NO_3-N concentration dynamics, along with reference dynamics of DOC concentration and streamflow; and
3. Gain consistent process interpretation (feasible hypotheses: following Beven and Chappell, 2021) from the identified values of SISO model parameters and their derivative DRCs from SISO model application to two periods differing in temperature.

2 Methods

The novelty of the approach illustrated comes from the combination of water quality and hydrometry monitored at a high frequency with SISO system identification modeling (Jones et al., 2014; Chappell et al., 2017a).

2.1 Monitoring dissolved NO_3-N and carbon plus hydrometric variables at a high frequency

A 430-L/s trapezoidal flume (Genesis Composites Ltd., Glenrothes) was used to generate the critical flow for discharge measurement. The water level was monitored at a tapping point installed within the throat of the flume using a CTWM82X5G4C3SUN pressure transmitter (Sensortechnics Ltd., Rugby). This was undertaken every 15-min and recorded using a CR1000 data logger (Campbell Scientific Ltd., Shepshed). Local deviation from the theoretical calibration was checked with salt dilution gauging. Rainfall was measured using two SBS500 rain

gauges (Environmental Measurements Limited, South Shields) connected to the same CR1000 data-logging systems.

The water quality station was located 60 m upstream of the flume. The dissolved NO_3-N and organic carbon were measured continuously in the field at the same 15-min intervals as the hydrometric measurements (rainfall and discharge) using an in-field "Spectrolyzer" (version 2) with an optical path length of 35 mm (s::can Messtechnik GmbH, Vienna). To prevent the voltage from dropping below 12 vDC, which would deactivate the unit, a 24-vDC power supply was used. The optical windows of the spectrolyzer were cleaned twice weekly with 10% hydrochloric acid applied to a small brush. Then, once per week, the measurement windows were soaked in the same solution for 5 min as a further cleaning step. The station incorporated an auto-sampler so that water samples could be taken for laboratory analysis for NO_3-N and DOC by the accredited analytical laboratories of UKCEH. These samples were used for the adjustment of the s::can RIVCOL global calibrations to the local Trawsnant water (e.g., Jones et al., 2014). The regular cleaning regime minimized the magnitude of steps in the concentration time series before and after each cleaning episode. To remove these small steps, exponential development of precipitates and algal growth on the windows over the exact 3–4-day periods between cleaning was assumed and removed using 15 lines of code in MATLAB (Jones et al., 2014). Stream temperature at the water quality station was monitored in parallel to the other variables using a CS547A probe (Campbell Scientific Ltd.).

2.2 SISO system identification modeling of rain-driven dynamics

The SISO system identification tool used to quantify the rainfall to NO_3-N dynamics through a series of storm events was the Refined Instrumental Variable Continuous-time Box–Jenkins IDentification (RIVCBJID) algorithm within the CAPTAIN Toolbox for MATLAB (Taylor et al., 2007). This continuous-time variant of this Refined Instrumental Variable (RIV) method describes the SISO system with differential equations (Young, 2015) rather than different equations of the discrete-time variant. RIV methods gain their skill in capturing dynamics by incorporating

(i) an initial pre-filtering stage to remove high-order noise (i.e., dynamics much shorter than the shortest time constant of the system) that affects the identification of the true model structure and
(ii) the covariance matrix (Box et al., 2008) that is used explicitly to find the most robust model with the least uncertainty.

2.2.1 Model structure

To reiterate, the form of the model identified by RIVCBJID may be expressed in ordinary differential equation terms. The simplest form of the dynamic model identified (i.e., with the least number of hydrological/biogeochemical components) is called a first-order model. With rain-driven nitrate concentration as an example, this model would be (ignoring initial conditions)

$$\frac{dC_{NO_3-N}(t)}{dt} + \alpha C_{NO_3-N}(t) = \beta r(t-\delta),$$

where C_{NO_3-N} is the stream nitrate–nitrogen concentration (mg/L monitored at a 15-min interval), r is the total rainfall per 15-min period (mm/15 min), δ is the pure time delay between rainfall and an initial C_{NO_3-N} response (number of 15-min periods in this study), α is the parameter capturing the rate of NO_3-N exhaustion (/15 min), β is the parameter capturing the magnitude of NO_3-N production or gain (mg/L 15-min/mm), and t is time in 15-min periods. The SISO data being modeled that contain more complex dynamics than higher-order models (e.g., second-order) may be defined (Jones et al., 2014). Prior to interpretation (see Section 2.2.3), these are typically decomposed by partial fraction expansion into multiple first-order components.

Similarly, the first-order SISO model illustrated may be expressed as a first-order transfer function in continuous time (sometimes abbreviated to CT-TF):

$$NO_3 - N = \frac{b}{s-a}e^{-s\delta}r; \quad s \sim \frac{d}{dt},$$

where s is the Laplace operator, $a = -\alpha$, and $b = \beta$. The structure of the CT-TF model identified (whether first-order or a higher order) is often shown in the form of a triad [*den num del*], where the number of denominators, *den* (i.e., number of *a* terms in the lower part of a transfer function), number of numerators, *num* (i.e., number of *b* terms in the upper part of a transfer function), and the number of time steps of pure time delay, *del* (where time-step length multiplied by $del = \delta$) are shown in square parentheses. For a first-order model, there is only one denominator (or *a* term), so the triad would take the form [1 *num del*]. Rain-driven runoff dynamics sometimes exhibit nonlinearity, where the magnitude of a nonlinearity term (p) is sometimes shown with a superscript outside the parentheses, e.g., $[den\ num\ del]^p$ (refer to Chappell et al., 2012 for example).

2.2.2 Application to high-frequency time series of NO_3-N, DOC, and runoff

RIVCBJID was applied to time series of dissolved NO_3-N concentration, DOC concentration, and stream discharge per unit area (i.e., runoff), with rainfall as the common input reference. A period of 234 days (09 January 2013 to 31 August 2013; in ISO 8601 ordinal date format 2012-374 to 2012-608) of synchronous 15-min time series was considered for analysis (Figures 1A, B).

Previous analysis of DOC time series from the Trawsnant watershed demonstrated differences in SISO chemograph responses between seasons (Jones et al., 2014). Thus, in this study with a NO_3-N focus, dynamics are quantified and compared between a 30-day period in late winter–spring (19 February–21 March; 2012-415 to 2012-445; Figure 1C) with those of a 30-day period in the early summer (27 May–26 June; 2012-512 to 2012-542; Figure 1D). The former had an average stream temperature of 2.8°C, and the latter, 9.4°C (see Figure 1B). The periods selected exhibit modest discharge responses but marked NO_3-N and DOC chemograph responses to rainfall (Figures 1A, C, D). The two periods also contrasted in their water balance. The discharge per unit area for the selected 30-day early-summer period was a much smaller proportion of the rainfall (i.e., 58 mm of 123 mm of rainfall) when compared with the late-winter–spring period (i.e., 49 mm of 51 mm of rainfall). The higher stream temperatures in the early-summer period are likely to have resulted from higher levels of net radiation (data available but not presented). These higher levels of net radiation are likely associated

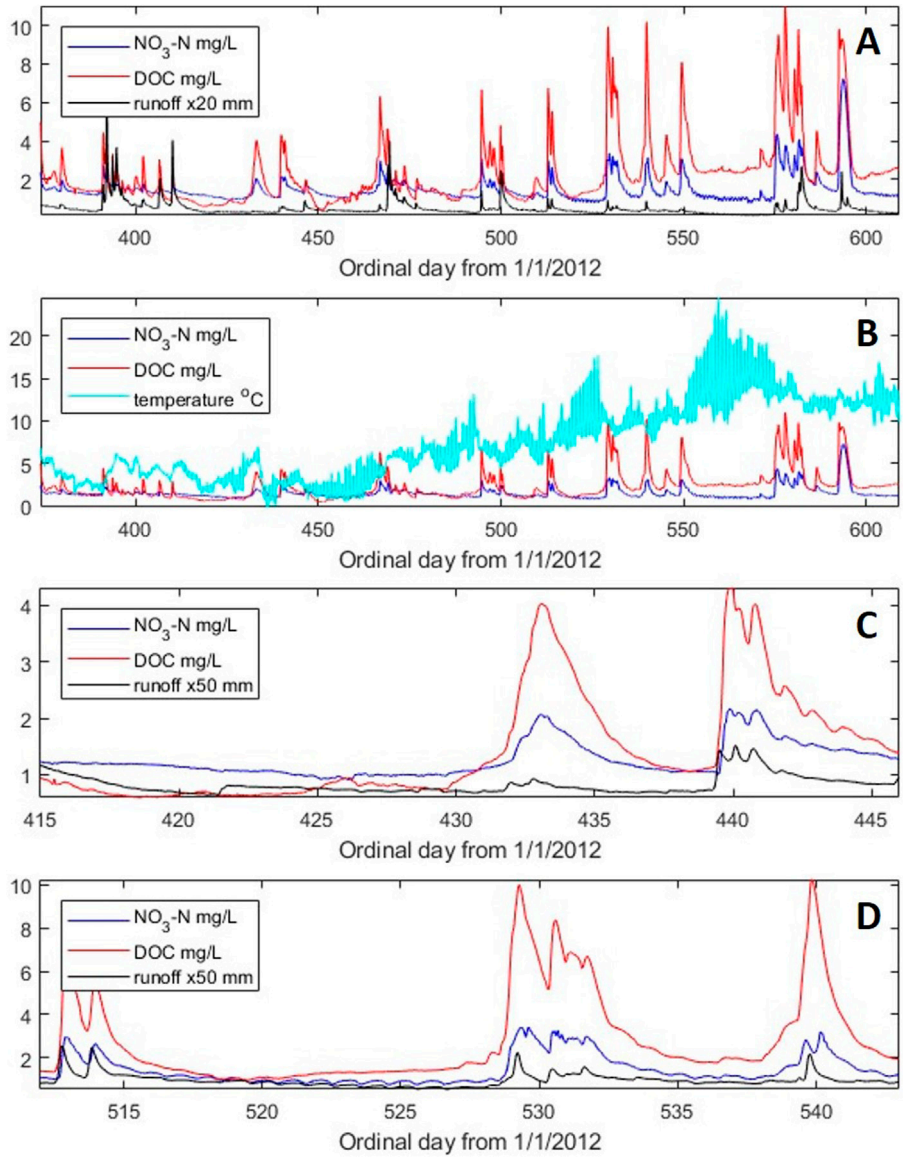


FIGURE 1
Time series of 234 days (09 January 2013 to 31 August 2013) at a 15-min resolution for the 2-km^2 Trawsnant stream in upland Wales (United Kingdom). Subplot **(A)** time series of dissolved NO_3-N concentration (mg/L), DOC concentration (mg/L), and unit area discharge (mm × 20); **(B)** time series of DOC concentration (mg/L) and stream temperature (°C); **(C)** 30-day "cold" (late winter–spring) period selected for SISO model identification; and **(D)** 30-day "warm" (early summer) period selected for SISO model identification.

with higher wet-canopy evaporation rates (and transpiration) from the upland conifers in the early-summer period (Page et al., 2020). These higher rates of evaporation may explain the observed reduced discharge per unit rainfall input in the summer period.

2.2.3 Process interpretation of rain-driven dynamics within the identified model structures

The process of interpretation of key terms within identified transfer functions may be described by three DRCs (Jakeman et al., 1993). These DRCs are i) the time constant or *TC*; ii) the steady-state gain or *SSG*; and iii) the already identified pure time delay or δ. A time constant is derived *directly* from an identified value of *a*:

$$TC = \frac{\Delta t}{a},$$

where Δt is the time step in the observations (15 min in this example). This derived *TC* is the *rate of exhaustion* (*or recession*) *of the concentration* (*or runoff*) *response* (*expressed as time*) *following the unit input of rainfall* (*mm*). The *SSG* is similarly derived *directly* from an identified value of *a* and *b*:

$$SSG = \frac{b}{a}.$$

This derived *SSG* is, for example, the *magnitude of the* NO_3*-N concentration increase* (*mg/L*) *for a unit input of rainfall* (*mm*). For a model of runoff where the input and output units are identical, the

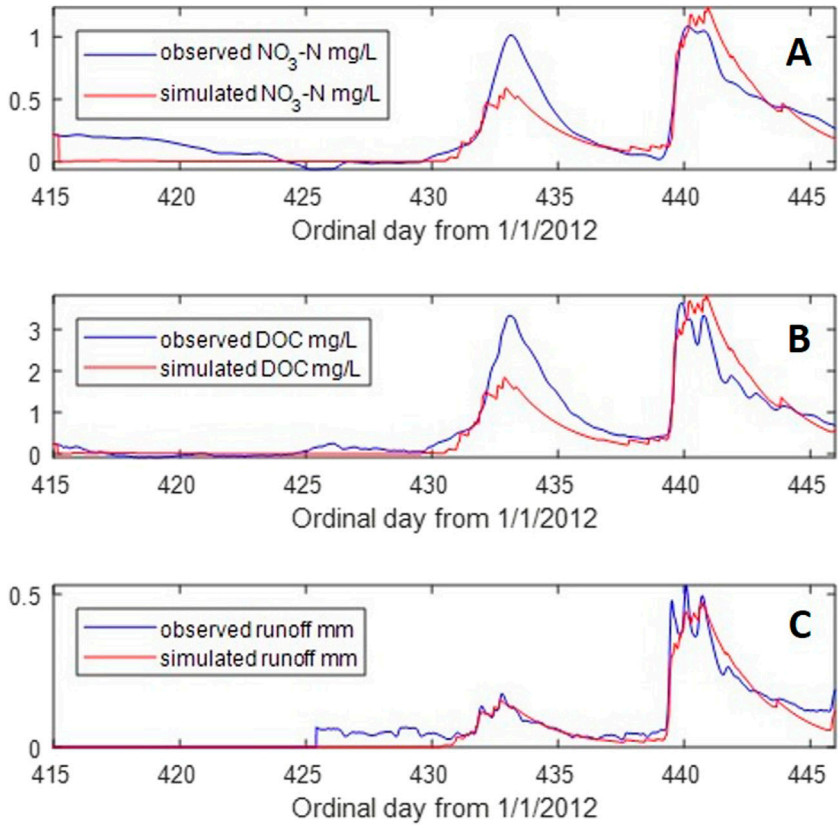


FIGURE 2
Observed and SISO-simulated time series for the 30-day "cold" period in late winter–spring (19 February–21 March 21 2013; ordinal date: 2012-415 to 2012-445). Subplot **(A)** NO_3-N concentration (mg/L); **(B)** DOC concentration (mg/L); and **(C)** runoff (mm, scaled by × 30 for model identification).

SSG is simply the simulated runoff coefficient (Chappell et al., 2006). The identified parameter of the pure time delay (δ) is the *delay between a unit input of rainfall* (*mm*) *and a unit* NO_3*-N or DOC concentration* (*mg/L*) *response* (*or runoff response, mm*).

3 Results

First-order SISO models (applied to 15-min resolution data) could describe most of the dominant modes of dynamics between a rainfall input and an output of either NO_3-N, DOC, or runoff (for either 30-day period; Figures 2, 3). Higher-order SISO models (e.g., more complex second-order models that may represent two parallel pathways with their own dynamics) could be identified. All of these higher-order models, however, failed the Young Information Criterion (*YIC*), indicating that higher model complexity was not justified by the information content of the data (refer to Chappell et al., 2012 for example).

Table 1 shows the SISO transfer function parameters of the identified models and the derived estimates of the DRCs that may be interpreted in hydrological or biogeochemical terms (Jones et al., 2014). The efficiency of the identified models at capturing the output dynamics is given with the metric of R_t^2 (i.e., simplified Nash–Sutcliffe efficiency; Chappell et al., 2012). Although the models capture most of the dominant modes of rain-driven dynamics, they do not capture them all (i.e., $R_t^2 < 1.0$). Visual inspection of the simulated versus observed NO_3-N and DOC chemographs and runoff hydrographs (Figures 2, 3) provides the same finding. These apparent discrepancies provide additional insights beyond the interpretations gained from the DRCs and are therefore discussed.

4 Discussion

First, the interpretations of rain to NO_3-N concentration modeling are presented, followed by additional interpretations arising from parallel modeling of rain–DOC and rain–runoff dynamics.

4.1 Dissolved NO_3-N response to a unit input of rainfall in a cold versus warm period

A unit input of rainfall within the contiguous series of three early-summer storms delivered a similar unit increase in the dissolved NO_3-N concentration to that of the pair of contiguous winter–spring storms. In the early summer, a 16.3-mg/L increase in the NO_3-N concentration per mm rainfall (above the instantaneous response) was observed against a slightly smaller increase of

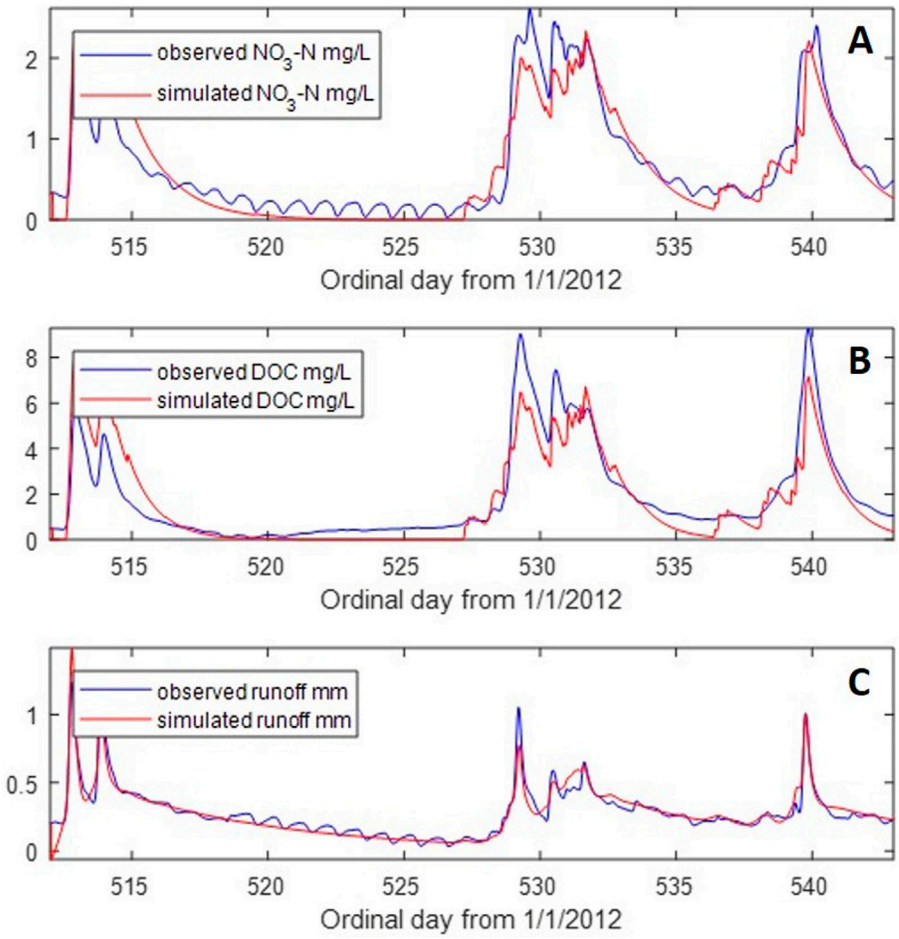


FIGURE 3
Observed and SISO-simulated time series for the 30-day "warm" period in the early summer (27 May–26 June 26 in 2023; ordinal date: 2012-512 to 2012-542). Subplot **(A)** NO_3-N concentration (mg/L); **(B)** DOC concentration (mg/L); and **(C)** runoff (mm, scaled by × 30 for model identification).

13.7 mg/L in the NO_3-N concentration per mm rainfall in the late winter–spring (Table 1). In some contrast, a large delay between the rainfall input and dominant mode of the concentration response of 5 h (i.e., 20 × 15-min time -steps) was observed in the case of late winter–spring storms. This was halved to 2.5 h (i.e., 10 × 15-min time steps) for the case of early-summer storms. With the storm pair in the winter period, the pulse of the NO_3-N concentration receded to two-thirds of its peak within 53.2 h (in the identified purely linear system). In contrast, in the summer period, the same rate of NO_3-N exhaustion was achieved in only 35.0 h, a 52% faster rate. Thus, the NO_3-N response per unit rainfall input appeared more quickly and depleted more quickly in the warmer, early-summer events than in the colder winter–spring events.

The antecedent runoff (a measure of catchment wetness: Chappell et al., 2017b) for the small events in the summer was slightly larger than that for the winter period (Figures 1C, D). This may have resulted in a reduced delay in developing a perched water table and, hence, lateral flow in the NO_3-N and DOC-rich organic surface layers of the forest floor (see Chappell et al., 1990; Winter et al., 2024) in these summer events. Drier antecedent conditions for the selected winter events may have additionally delayed the availability of NO_3-N in the upper soil through limits on mineralization and nitrification (Reynolds and Edwards, 1995; Rusjan et al., 2008; Koenig et al., 2017; Burns et al., 2019). Alternatively, the colder temperatures in the winter period may have limited the mineralization in the upper soil (Guntiñas et al., 2012). The faster exhaustion of the rain-driven NO_3-N signal at the water quality station in the headwater stream in the summer may be due to a higher rate of denitrification within the channel because of the higher temperatures (Figure 1B; Halliday et al., 2013; Kermorvant et al., 2023). Alternatively, if the size of the NO_3-N shallow source is limited and comparable for both periods, the faster responses in the summer period could have led to quicker exhaustion of the limited NO_3-N pool (e.g., Vaughan et al., 2017).

Clear diurnal cycles in the NO_3-N concentration time series emerge in the warmer period (Figures 1D, 3A). These have not been modeled with the SISO models utilized (negatively affecting model efficiency) but could be modeled using other SI models such as UCDHR (e.g., Halliday et al., 2013; Mindham et al., 2018). The greater sensitivity of the watershed to diurnal cycles in temperature (and its controlling net radiation) in the summer is interesting as it

TABLE 1 Structure and parameters of the identified SISO first-order models applied to NO_3-N concentration, DOC concentration, and runoff data given a rainfall input.

Relation	I	Model	R_t^2	*YIC*	*a*	*b*	*TC*	*SSG*
19 February–21 March ("cold period")								
Rain-NO_3-N	1.0	[1 1 20]	0.811	−9.51	0.0046959	0.064239	53.23	13.68
Rain-DOC	0.69	[1 1 15]	0.805	−9.37	0.0050423	0.20559	49.58	40.77
Rain-runoff	0.38	$[1\ 1\ 0]^{0.33}$	0.935	−11.33	0.0052678	0.022249	47.46	0.52
27 May–26 June("warm" period)								
Rain-NO_3-N	0.75	[1 1 10]	0.861	−10.37	0.0071362	0.11635	35.03	16.31
Rain-DOC	0.90	[1 1 9]	0.807	−9.48	0.010116	0.42726	24.71	42.24
Rain-runoff	0.30	$[1\ 2\ 3]^{0.99}$	0.910	−10.63	0.001662	1.3591 0.01311	150.42	0.56

The model structure is given in the form $[den\ num\ del]^p$. Term *den* is the number of transfer function denominators (i.e., recession or *a* parameters). Term *num* is the number of transfer function numerators (i.e., gain or *b* parameters). Term *del* is the number of time steps of pure time delay between input and output response (where time-step length multiplied by $del = \delta$), while *p* is the magnitude of the nonlinearity term within the Store Surrogate Sub-Model (Chappell et al., 2012). All models have an instantaneous component, *I* (without dynamics; Young, 2006), and its magnitude is in the units of the input variable. *YIC* is the Young Information Criterion, heuristic measure of model over-parameterization, and R_t^2 is the simplified Nash–Sutcliffe efficiency measure (Chappell et al., 2012). The DRCs are derived directly from the identified *a* and *b* model parameters. The *TC* is the transfer function time constant (h) and is derived from the value of the parameter *a*. The *SSG* is the steady-state gain (in units of the output variable/input variable) and is derived from the values of the *a* and *b* parameters used in combination. Note that the rain-runoff models were identified after first multiplying the runoff by 30 (thereby affecting the values of the *a* and *b* parameters in Table 1). Initial values of *SSG* for the rain-runoff models were consequently divided by 30 and then added to the instantaneous component (*I*), before presentation in the table.

parallels the SISO modeling finding of greater sensitivity of NO_3-N response ("flashiness") to rainfall inputs in this period.

4.2 Comparison with the DOC response

The dynamics of the rain-driven concentration response of DOC in the Trawsnant stream in the winter–spring and early-summer events was comparable to that of dissolved NO_3-N. The increase in the DOC concentration in the stream from the same unit input of rainfall was only marginally larger between the winter–spring and early-summer storms (i.e., an increase of 40.8–42.2 mg/L in the DOC concentration per mm rainfall). Similar to the NO_3-N response, the long delay before the initial response of the dominant DOC response of 3 h, 45 min in the winter–spring events reduced to 2 h, 15 min in the early-summer events (67% faster), and the storm-related pulse in the DOC concentration decreased more quickly in the summer months (i.e., *TC* 49.6 to 24.73 h: Table 1). This finding may imply that the dominant hydrological (i.e., antecedent conditions or water pathways) and/or biogeochemical controls affecting rain-driven NO_3-N dynamics between the two 30-day periods are the same for the DOC concentration.

Compared to NO_3-N, the magnitude of the response in the DOC concentration was considerably greater for the same unit input of rainfall. For example, in winter–spring, a 40.8 mg/L DOC increase per mm rainfall above the instantaneous response versus 13.7 mg/L increase per mm rainfall for the NO_3-N concentrations was observed. Thus, the Trawsnant watershed yielded more DOC than NO_3-N for the same rain event conditions. Figure 1B shows an increasing trend of the DOC concentration (starting on approximately day 2012-520), following the increase in stream temperature (starting approximately on day 2012-465). This may be caused by an increase in DOC production on the forest floor (Christ and David, 1996). Changing DOC:NO_3-N stoichiometry in the stream may have then given rise to the more rapid exhaustion of NO_3-N identified by the SISO modeling of the early-summer period (Ledesma et al., 2022). As a counter to this, the rate of exhaustion increased more with DOC than NO_3-N between the two periods (i.e., 50.1% reduction versus 34.2% reduction, respectively).

4.3 Comparison with streamflow generation

The SISO analyses yielded $[1\ 1\ 15]^{0.30}$ and $[1\ 2\ 3]^{0.99}$ rain-runoff models for the first and second periods, respectively (Table 1). This indicates that one hydrological pathway (or multiple paths combining to exhibit an apparent unitary behavior) dominates the Trawsnant hydrological response of the two studied periods with relatively small discharge events. The response, however, exhibited a marked increase in the residence time of the response from the winter–spring to the summer period, with the *TC* increasing by 217% from 47.5 to 150.4 h (Table 1). The dominant rainfall-runoff response had less than a 15-min initial delay (i.e., less than the time step of the data) in the winter–spring events, whereas the concentration responses had a pure time delay of 300 and 225 min for the NO_3-N and DOC, respectively (Table 1). These pure time delays in the dominant NO_3-N and DOC concentration response reduced to 150 and 135 min, respectively, while increasing to 45 min for the rainfall-runoff response in the early-summer period. These findings, using rainfall runoff as a reference, may support the idea that the changes in the dynamics between the two periods have a strong biogeochemistry control rather than a purely hydrological control.

It should be noted that the apparent diel cycle in the runoff between summer rainstorms (Figure 3C) has been experimentally measured to be an artifact of the pressure transmitters used (see also

Mindham et al., 2018) rather than a natural diel cycle in the stream discharge (that can be present in other local watersheds; Kirchner, 2009). This contrasts with the natural diurnal cycle in the NO_3-N concentration time series (Figures 1D, 3A).

5 Conclusion

The SISO system identification tool of RIVCBJID identified models of rain-NO_3-N, rain-DOC, and rain-runoff over 30-day periods (each including 2–3 rain events) that have a high simulation efficiency (R_t^2) of between 0.807 and 0.935 (Table 1). The water quality models comprised only four model parameters, namely, I (an instantaneous component with no dynamics; Young, 2006), δ, a, and b (Table 1). The runoff models required either five parameters, namely, p (a nonlinearity term), I, δ, a, and b or six parameters, namely, p, I, δ, a, and two b values (Table 1). The two b values provide a first-order model (i.e., one a parameter) in series. Water quality or hydrological models with such a small number of parameter values but high simulation efficiency are described as parsimonious (Chappell et al., 2017a). Slightly higher-order models (e.g., second-order models with two a values and two b values) were identified. These were, however, rejected as being "over-parameterized" (i.e., not justified by the dynamics in the data) for the selected Trawsnant events as the *YIC* values changed by more than +1 with higher model orders (Chappell et al., 2012).

Similarities and contrasts in behavior between rain-driven NO_3-N concentration dynamics between the two periods and with the other two variables (DOC concentration and runoff) were observed. For both water quality variables, the increase in the concentration per unit input of rainfall (*SSG*) remained similar in the cold and warm periods, as did the simulated runoff coefficient (i.e., *SSG* for the rain-runoff system). The *SSG* for the rain-DOC dynamics remained similar despite the increasing trend in the DOC concentration at times between storms (Figure 1B). In contrast, δ and *TC* for both water quality variables were much shorter (i.e., the system was more responsive) in the warmer period. This occurred as the hydrological system became more damped (i.e., δ and *TC* increased), perhaps highlighting the potential importance of the non-hydrological (e.g., biogeochemical) differences between the two periods.

The differences and similarities in the dynamics (between periods and variables) have feasible hydrological and biogeochemical interpretations based on the published findings of others. Whether these feasible interpretations *are* the dominant cause of the dynamics identified for the 2-km^2 Trawsnant stream (in upland Wales) , however, requires further field investigation (and subsequent numerical analysis). These further field investigations would benefit from high-frequency NO_3-N concentration time series at *distributed locations within the watershed* (Jones and Chappell, 2014; Burns et al., 2019), such as the litter layer, topsoil, upstream channels, and riparian zones. Similarly, improved rejection of feasible hypotheses would benefit from the *collection and analysis of a greater number of potentially controlling variables* at the watershed outlet (Burns et al., 2019; Li et al., 2022) and distributed throughout the watershed.

Additionally, the SISO models identified and interpreted in this study were for two 30-day periods with modest discharge responses but marked NO_3-N and DOC chemograph responses to rainfall. The robustness of the interpretations so far presented needs further evaluation by application to i) similar types of events in other years of record; ii) other seasons (e.g., autumn); iii) more complex storm periods with larger discharge responses; and iv) other water quality variables monitored in parallel (e.g., pH and electrical conductivity). These analyses are now planned.

Combining SISO system identification with high-frequency water quality and hydrometric data is, therefore, suggested as an approach to support more robust *experimental designs* of investigations into the rain-driven dynamics of NO_3-N and other important water quality variables.

Data availability statement

The original contributions presented in the study are included in the article/Supplementary Material; further inquiries can be directed to the corresponding author.

Author contributions

NC: conceptualization, data curation, formal analysis, funding acquisition, investigation, methodology, project administration, supervision, visualization, writing–original draft, and writing–review and editing.

Funding

The author(s) declare that financial support was received for the research, authorship, and/or publication of this article. This work was supported by the UKRI Natural Environment Research Council grant NE/J014826/1.

Acknowledgments

The author acknowledges the Natural Resources Wales and Scottish Woodland for providing access to the research watershed and Natural Resources Wales for permission to install the flume and conduct dilution gauging. The considerable assistance of Tim Jones with the installation and maintenance of field instruments and subsequent data quality assurance is greatly appreciated. The author would like to thank the two reviewers for their constructive comments.

Conflict of interest

The author declares that the research was conducted in the absence of any commercial or financial relationships that could be construed as a potential conflict of interest.

Publisher's note

All claims expressed in this article are solely those of the authors and do not necessarily represent those of their affiliated organizations, or those of the publisher, the editors, and the reviewers. Any product that may be evaluated in this article, or claim that may be made by its manufacturer, is not guaranteed or endorsed by the publisher.

References

Beven, K. J., and Chappell, N. A. (2021). Perceptual perplexity and parameter parsimony. *WIREs Water* 8 (4), e1530. doi:10.1002/wat2.1530

Box, G. E. P., Jenkins, G. M., and Reinsel, G. C. (2008). *Time series analysis: forecasting and control*. 4th Edn. Hoboken, NJ, USA: Wiley.

Brunet, C. E., Gemrich, E. R. C., Biedermann, S., Jacobson, P. J., Schilling, K. E., Jones, C. S., et al. (2021). Nutrient capture in an Iowa farm pond: insights from high-frequency observations. *J. Environ. Manag.* 299, 113647. doi:10.1016/j.jenvman.2021.113647

Burns, D. A., Pellerin, B. A., Miller, M. P., Capel, P. D., Tesoriero, A. J., and Duncan, J. M. (2019). Monitoring the riverine pulse: applying high-frequency nitrate data to advance integrative understanding of biogeochemical and hydrological processes. *WIREs Water* 6, e1348. doi:10.1002/wat2.1348

Chappell, N. A., Bonell, M., Barnes, C. J., and Tych, W. (2012). "Tropical cyclone effects on rapid runoff responses: quantifying with new continuous-time transfer function models," in *Revisiting experimental catchment studies in forest hydrology*. Editors A. A. Webb, M. Bonell, L. Bren, P. N. J. Lane, D. McGuire, D. G. Neary, et al. (Wallingford: IAHS Press IAHS Publ), 353, 82–93.

Chappell, N. A., Jones, T. D., and Tych, W. (2017a). Sampling frequency for water quality variables in streams: systems analysis to quantify minimum monitoring rates. *Water Res.* 123, 49–57. doi:10.1016/j.watres.2017.06.047

Chappell, N. A., Jones, T. D., Tych, W., and Krishnaswamy, J. (2017b). Role of rainstorm intensity underestimated by data-derived flood models: emerging global evidence from subsurface-dominated watersheds. *Environ. Model. Softw.* 88, 1–9. doi:10.1016/j.envsoft.2016.10.009

Chappell, N. A., Ternan, J. L., Williams, A. G., and Reynolds, B. (1990). Preliminary analysis of water and solute movement beneath a coniferous hillslope in mid-Wales, United Kingdom. *J. Hydrology* 116, 201–215. doi:10.1016/0022-1694(90)90123-f

Chappell, N. A., Tych, W., Chotai, A., Bidin, K., Sinun, W., and Thang, H. C. (2006). BARUMODEL: combined Data Based Mechanistic models of runoff response in a managed rainforest catchment. *For. Ecol. Manage.* 224, 58–80. doi:10.1016/j.foreco.2005.12.008

Christ, M. J., and David, M. B. (1996). Temperature and moisture effects on the production of dissolved organic carbon in a spodosol. *Soil Biol. biochem.* 28, 1191–1199. doi:10.1016/0038-0717(96)00120-4

Graeber, D., McCarthy, M. J., Shatwell, T., Borchardt, D., Jeppesen, E., Søndergaard, M., et al. (2024). Consistent stoichiometric long-term relationships between nutrients and chlorophyll-a across shallow lakes. *Nat. Commun.* 15, 809. doi:10.1038/s41467-024-45115-3

Guntiñas, M. E., Leiros, M. C., Trasar-Cepeda, C., and Gil-Sotres, F. (2012). Effects of moisture and temperature on net soil nitrogen mineralization: a laboratory study. *Eur. J. Soil Biol.* 48, 73–80. doi:10.1016/j.ejsobi.2011.07.015

Halliday, S. J., Skeffington, R. A., Wade, A. J., Neal, C., Reynolds, B., Norris, D., et al. (2013). Upland stream water nitrate dynamics across decadal to sub-daily timescales: a case study of Plynlimon, Wales. *Biogeosciences* 10, 8013–8038. doi:10.5194/bg-10-8013-2013

Jakeman, A. J., Littlewood, I. G., and Whitehead, P. G. (1993). An assessment of the dynamic response characteristics of streamflow in the Balquhidder catchments. *J. Hydrol.* 145, 337–355. doi:10.1016/0022-1694(93)90062-E

Jiang, S. Y., Zhang, Q., Werner, A. D., Wellen, C., Jomaa, S., Zhu, Q. D., et al. (2019). Effects of stream nitrate data frequency on watershed model performance and prediction uncertainty. *J. Hydrol.* 569, 22–36. doi:10.1016/j.jhydrol.2018.11.049

Jones, T. D., and Chappell, N. A. (2014). Streamflow and hydrogen ion interrelationships identified using Data-Based Mechanistic modelling of high frequency observations through contiguous storms. *Hydrology Res.* 45 (6), 868–892. doi:10.2166/nh.2014.155

Jones, T. D., Chappell, N. A., and Tych, W. (2014). First dynamic model of dissolved organic carbon derived directly from high frequency observations through contiguous storms. *Environ. Sci. Technol.* 48, 13289–13297. doi:10.1021/es503506m

Kermorvant, C., Liquet, B., Litt, G., Mengersen, K., Peterson, E. E., Hyndman, R. J., et al. (2023). Understanding links between water-quality variables and nitrate concentration in freshwater streams using high frequency sensor data. *PLoS ONE* 18 (6), e0287640. doi:10.1371/journal.pone.0287640

Kirchner, J. W. (2009). Catchments as simple dynamical systems: catchment characterization, rainfall-runoff modeling, and doing hydrology backward. *Water Resour. Res.* 45, W02429. doi:10.1029/2008WR006912

Koenig, L. E., Shattuck, M. D., Snyder, L. E., Potter, J. D., and McDowell, W. H. (2017). Deconstructing the effects of flow on DOC, nitrate, and major ion interactions using a high-frequency aquatic sensor network. *Water Resour. Res.* 53, 10655–10673. doi:10.1002/2017WR020739

Ledesma, J. L. J., Lupon, A., Martí, E., and Bernal, S. (2022). Hydrology and riparian forests drive carbon and nitrogen supply and DOC: NO_3^- stoichiometry along a headwater Mediterranean stream. *Hydrol. Earth Syst. Sci.* 26, 4209–4232. doi:10.5194/hess-26-4209-2022

Li, C., Yue, F.-J., Li, S.-L., Ge, J.-F., Chen, S.-N., and Qi, Y. (2022). Land use as a major factor of riverine nitrate in a semi-arid farming-pastoral ecotone: new insights from multiple environmental tracers and molecular signatures of DOM. *Front. Environ. Sci.* 10, 1061857. doi:10.3389/fenvs.2022.1061857

McGill, T., and Ford, W. I. (2024). Extreme learning machine predicts high-frequency stream flow and nitrate-N concentrations in a karst agricultural watershed. *J. ASABE* 67 (2), 305–319. doi:10.13031/ja.15747

Mindham, D. A., Tych, W., and Chappell, N. A. (2018). Extended State Dependent Parameter modelling with a Data-Based Mechanistic approach to non-linear model structure identification. *Environ. Model. Softw.* 104, 81–93. doi:10.1016/j.envsoft.2018.02.015

Neal, C., Reynolds, B., Norris, D., Kirchner, J. W., Neal, M., Rowland, P., et al. (2011). Three decades of water quality measurements from the Upper Severn experimental catchments at Plynlimon, Wales: an openly accessible data resource for research, modelling, environmental management and education. *Hydrol. Process.* 25 (24), 3818–3830. doi:10.1002/hyp.8191

Ormerod, S. J., and Durance, I. (2009). Restoration and recovery from acidification in upland Welsh streams over 25 years. *J. Appl. Ecol.* 46, 164–174. doi:10.1111/j.1365-2664.2008.01587.x

Page, T., Chappell, N. A., Beven, K. J., Hankin, B., and Kretzschmar, A. (2020). Assessing the significance of wet-canopy evaporation from forests during extreme rainfall events for flood mitigation in mountainous regions of the United Kingdom. *Hydrol. Process.* 34, 4740–4754. doi:10.1002/hyp.13895

Pellerin, B. A., Bergamaschi, B. A., Downing, B. D., Saraceno, J. F., Garrett, J. A., and Olsen, L. D. (2013). Optical techniques for the determination of nitrate in environmental waters: guidelines for instrument selection, operation, deployment, maintenance, quality-assurance, and data reporting. *U.S. Geol. Surv. Tech. Methods* 1–D5, 37. doi:10.3133/tm1D5

Reynolds, B., and Edwards, A. (1995). Factors influencing dissolved nitrogen concentrations and loadings in upland streams of the United Kingdom. *Agri. Water Manage.* 27, 181–202. doi:10.1016/0378-3774(95)01146-a

Rusjan, S., Brilly, M., and Mikoš, M. (2008). Flushing of nitrate from a forested watershed: an insight into hydrological nitrate mobilization mechanisms through seasonal high-frequency stream nitrate dynamics. *J. Hydrology* 354 (1–4), 187–202. doi:10.1016/j.jhydrol.2008.03.009

Tang, Y., Deng, J., Zang, C., and Wu, Q. (2022). Chaotic modeling of stream nitrate concentration and transportation via IFPA-ESN and Turning Point Analyses. *Front. Environ. Sci.* 10, 855694. doi:10.3389/fenvs.2022.855694

Taylor, C. J., Pedregal, D. J., Young, P. C., and Tych, W. (2007). Environmental time series analysis and forecasting with the Captain toolbox. *Environ. Modell. Softw.* 22, 797–814. doi:10.1016/j.envsoft.2006.03.002

Vaughan, M. C. H., Bowden, W. B., Shanley, J. B., Vermilyea, A., Sleeper, R., Gold, A. J., et al. (2017). High-frequency dissolved organic carbon and nitrate measurements reveal differences in storm hysteresis and loading in relation to land cover and seasonality. *Water Resour. Res.* 53, 5345–5363. doi:10.1002/2017WR020491

Winter, C., Jawitz, J. W., Ebeling, P., Cohen, M. J., and Musolff, A. (2024). Divergence between long-term and eventscale nitrate export patterns. *Geophys. Res. Lett.* 51, e2024GL108437. doi:10.1029/2024GL108437

Young, P. C. (2006). "Rainfall-runoff modeling: transfer function models," in *Encyclopedia of hydrological sciences*. Editors M. G. Anderson and J. J. McDonnell doi:10.1002/0470848944.hsa141a

Young, P. C. (2015). Refined instrumental variable estimation: maximum likelihood optimization of a unified Box-Jenkins model. *Automatica* 52, 35–46. doi:10.1016/j.automatica.2014.10.126

frontiers | Frontiers in Environmental Science

TYPE Original Research
PUBLISHED 25 September 2025
DOI 10.3389/fenvs.2025.1641345

Check for updates

OPEN ACCESS

EDITED BY
Krishnaswamy Jayachandran,
Florida International University, United States

REVIEWED BY
Peiyue Li,
Chang'an University, China
Nadeesha Ukwattage,
University of Colombo, Sri Lanka

*CORRESPONDENCE
Christina Zeuner,
✉ czeuner@uoguelph.ca

RECEIVED 04 June 2025
ACCEPTED 29 August 2025
PUBLISHED 25 September 2025

CITATION
Zeuner C, Levison J and Larocque M (2025) Insights on nitrate transport in a shallow, sandy aquifer at various temporal and spatial scales. *Front. Environ. Sci.* 13:1641345. doi: 10.3389/fenvs.2025.1641345

COPYRIGHT
© 2025 Zeuner, Levison and Larocque. This is an open-access article distributed under the terms of the Creative Commons Attribution License (CC BY). The use, distribution or reproduction in other forums is permitted, provided the original author(s) and the copyright owner(s) are credited and that the original publication in this journal is cited, in accordance with accepted academic practice. No use, distribution or reproduction is permitted which does not comply with these terms.

Insights on nitrate transport in a shallow, sandy aquifer at various temporal and spatial scales

Christina Zeuner[1]*, Jana Levison[1] and Marie Larocque[2]

[1]Department of Civil, Environmental and Water Resources Engineering, School of Engineering, Morwick G360 Groundwater Research Institute, University of Guelph, Guelph, ON, Canada, [2]Departement des sciences de la Terre et de l'atmosphere, Université du Québec à Montréal, Montreal, QC, Canada

Nitrogen is necessary for successful crop growth, but excess nitrogen in water has implications for both environmental and human health. The factors driving these impacts and their extent remain incompletely understood. In particular, how average nitrogen concentrations compare to concentrations following intense rain events is not well known, partly due to the challenges of building spatially and temporally realistic concentration datasets. Thus, the aim of this study was to investigate hydraulic and nutrient dynamics in a sand plain aquifer system in the Laurentian Great Lakes Basin (north of Lake Erie in Ontario, Canada) through monthly and sub-daily groundwater and surface water sampling to contextualize storm event responses. A study was conducted across the Lower Whitemans Creek (LWC) subcatchment and at a field scale site. Spatial and temporal variations in nitrate concentrations and field parameters were measured in groundwater and surface water monthly from October 2021 to November 2024. Event-based sampling campaigns were conducted using either an ISCO autosampler with a 2-hr interval (in November 2022 and March 2023) or SUNA/EXO monitoring stations with a monitoring interval of 15-60 min (at varying times during October 2022 to November 2024). The results showed that shallow groundwater loaded with NO3-N discharging to small creeks is apparently a notable contributor to elevated levels in Whitemans Creek. It was also observed that the high sampling frequency, carried out via in-situ monitoring equipment, provided marked advantages over automated grab sampling methods. The study highlights the benefits and limitations associated with the different sampling methods to guide future research related to nitrogen quantification, including enhancing the sampling procedures and dataset collection approaches.

KEYWORDS

nitrate, agricultural watershed, groundwater quality, surface water quality, storm event analysis

1 Introduction

Nutrients (e.g., nitrogen and phosphorous) are crucial for plant growth. However, when in excess, they can have negative impacts on the environment such as eutrophication of surface water bodies, and they can bring human health concerns. Chronic elevated nitrogen in the form of nitrate (NO_3-N) in drinking water represents a critical health concern given its link to methemoglobinemia, thyroid disease, and certain cancers (Ward et al., 2018). The World Health Organization suggests <50 mg NO_3^-/L in drinking water, while in Canada the drinking water standard is 45 mg NO_3^-/L (10 mg NO_3-N/L) (World Health Organization, 2021; Health Canada, 2013). Nitrate can enter drinking water through many pathways such

as biological fixation, wastewater treatment, and agricultural practices, with the latter being the most prevalent in groundwater resources (Health Canada, 2013). Nitrate concentrations generally are increasing across the globe with a noted common tie to agricultural fertilizers and pesticides (Abascal et al., 2022). Approximately half of the global population uses groundwater for domestic purposes (United Nations, 2022) while in Canada, 30% of people depend on groundwater to supply their needs, mostly in rural areas (ECCC, 2013).

Beyond regulations for drinking water for human health, aquatic environments and the species therein are also sensitive to long-term exposure to high NO_3-N concentrations. Recognizing and assessing the ecological risk alongside human health impacts from nonpoint source contamination, as is the case with NO_3-N from agricultural practices, have recently been highlighted as needing further consideration (Wang, et al., 2023). Additionally, there is growing recognition of the importance of groundwater as a biodiverse ecosystem (Saccò et al., 2024) and the lack of knowledge on how stressors, such as elevated NO_3-N, are impacting these systems (Castaño-Sánchez et al., 2020). Currently, it is recommended by the (CCME, 2012) that NO_3-N concentrations in freshwater do not exceed 3.0 mg/L (long-term exposure) and 124 mg/L (short-term <96 h) for the health of aquatic life (CCME, 2012).

While many studies have focused on nonpoint source loading to streams to understand the contamination sources and flow paths, and to determine the most suitable mitigation efforts for protecting available water resources (e.g., Rixon et al., 2024; Pohle et al., 2021; Zhi and Li, 2020), the complexity of groundwater-surface water systems require prioritizing different contaminants and pathways depending on region (Wang et al., 2023). Geological factors such as groundwater flow in sandy and fractured bedrock aquifers, in combination with fertilization practices result in the need for a site-by-site basis assessment approach (Gardner et al., 2020). Meteorological factors such as the intensity and frequency of precipitation events in areas with shallow groundwater can induce varying response times at different locations within the same watershed (Gootman and Hubbart, 2021). Seasonal events such as spring snow melts and those associated with agricultural land use (Irvine et al., 2019) or tile drain flow (Speir et al., 2021) can cause spatiotemporal spikes in NO_3-N. Other critical factors influencing NO_3-N concentrations and transport have been identified as site location and crop cover (Elsayed et al., 2025), slope and existence of preferential groundwater paths (Shabaga and Hill, 2010), variability in riparian buffer zones (Nsenga Kumwimba et al., 2023), or presence of wetlands (Crossley et al., 2025). Many studies have demonstrated the connection of algae blooms in lakes to the intensive agricultural practices surrounding the Great Lakes (Bosse et al., 2024; Crossman and Weisener, 2020; Watson et al., 2016). In rural Ontario (Canada), the concentrations of NO_3-N within the Grand River watershed have been recognized as an important issue for cold water salmonid species (Anderson, 2021; CCME, 2017; Ivey, 2024).

Additionally, the increasing variability in meteorological conditions leads to more intense storms and droughts, more frequent freeze and thaw events, and significant shifts in seasonal weather (Allan et al., 2020). Much of Canada is impacted by climate change in various ways including increased temperatures and more frequent extreme precipitation events. For the agricultural sector in southwestern Ontario specifically, the combination of extensive crop production, shallow aquifers, and changing groundwater recharge patterns can negatively impact potable water resources (Bhatti et al., 2021). In agricultural settings with shallow water tables, nitrate transport has been shown to increase in wet seasons as well as during and following large flow events (Williams et al., 2015). Potential nitrate contamination of groundwater and surface water can thus be exacerbated by rapid transport through sandy, overburden aquifers with intensive agriculture (Gardner et al., 2020; Saleem et al., 2020). As large hydrometeorological events become more frequent, increases in nitrate concentrations in surface water and groundwater are expected (Bhatti et al., 2021; Costa et al., 2022; Shephard et al., 2014). Measuring NO_3-N can be done on samples brought to a laboratory (off site), at the sampling location (on site), or directly in the waterbody of interest (*in situ*) through manual collection of grab samples at low frequency (e.g., monthly samples and short sampling campaigns; e.g., Venkiteswaran et al., 2019). The use of autosamplers provides a means for intermediate frequency (e.g., 4–8 h intervals, Biagi et al. (2022); rise-peak-fall of event hydrograph; May et al. (2023)). *In situ* sampling for NO_3-N can be done using spectrophotometry with submersible sensors (e.g., Crossley et al., 2025; Speir et al., 2021; Wollheim et al., 2017). Fouling issues are frequently reported as a limitation to this technique, but solutions have been reported (e.g., Liu et al., 2019). Solid-state potentiometric probes using *in situ* nitrate-selective electrodes provide an energy-efficient alternative (Cuartero and Crespo, 2018; Forrest et al., 2022). These techniques have different advantages and limitations which present specific challenges in the study of NO_3-N transport in agricultural watersheds, requiring further study to improve understanding.

The goal of this research was to better understand NO_3-N transport in an agriculturally intense, sandy aquifer at different spatial and temporal scales, using field instrumentation and a variety of sampling techniques, including examining responses from storm events. The specific objectives were to: (1) determine surface water and shallow groundwater quality trends across the subcatchment; (2) evaluate the influence of storm events on nitrate concentrations in groundwater and surface water; and (3) identify the strengths and weaknesses of different methods to optimize data collection approaches. This work was carried out using the Lower Whitemans Creek (LWC), a sub-catchment of the Grand River, as a field-based case study in a shallow, sandy aquifer system in southwester Ontario, Canada.

2 Site description

2.1 Land use

The Whitemans Creek subcatchment (Figure 1) was originally home to the Attiwandaronk First Nations (pop. 5,000) until conflict with the Iroquois in 1,653 (Dunham, 1945; Earthfx, 2018). In 1793, European settlers established the township of Burford as it was seen as ideal land for both plant and animal agriculture. Approximately 75% of the land was cleared to produce hay (20%), fall wheat (19%), pasture (16%), spring wheat (8.5%), oats (9.5%), corn (4%), and the remainder specialty crops (Reville, 1883). From the 1950s to the

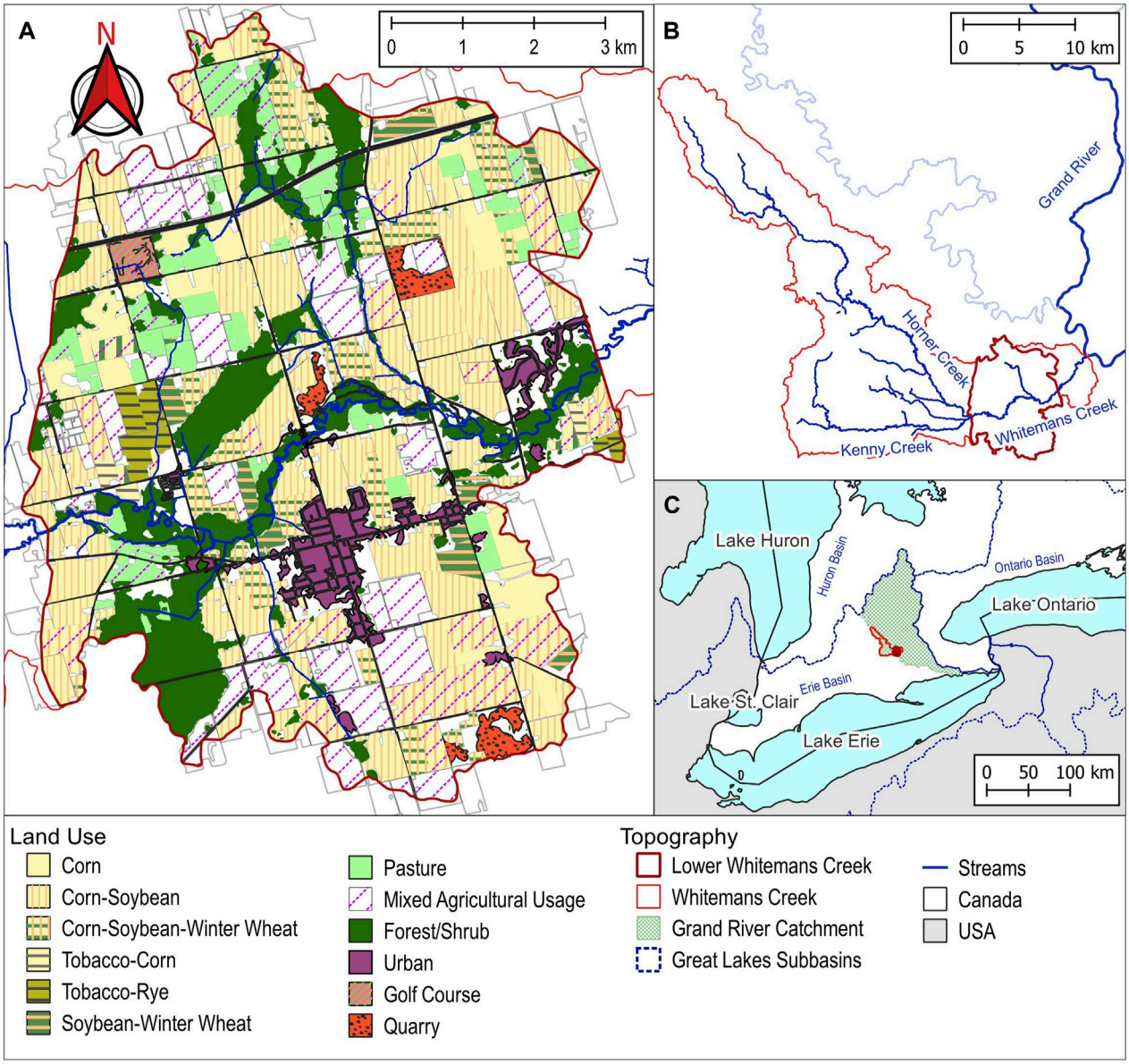


FIGURE 1
Map of the study area. **(A)** LWC catchment and land use (AAFC, 2023); **(B)** location of LWC within the larger Whitemans Creek catchment; and **(C)** location in southwestern Ontario, Canada.

1970s, across the entire Whitemans Creek sub-watershed, the main cash crop was corn, and the main specialty crop was tobacco. From 2011 to 2015, almost 30% of the area was used to grow corn, around 20% was used for soybeans. Overall, around 75% of the land was used for agricultural purposes (Earthfx, 2018). Most recently, LWC is intensively farmed for cash crops, hay, and specialty crops. From 2020 to 2023, in the Lower Whitemans Creek sub-catchment (64 km^2) land used for agriculture (46 km^2; Figure 1A) consists of mostly corn-soybean (36%), corn-soybean-winter wheat/rye (20%), and continual corn (10%) with the remaining 33% used for pasture and mixed crops such as potatoes, ginseng, tobacco, and rye (AAFC, 2023). Liu et al. (2021) showed legacy nitrogen stored in soils (82%–92%) and groundwater (6%–18%) to range from 705 to 1,071 kg N/ha. Historically, the nitrogen surplus in Whitemans Creek was between 40–50 kg/ha/yr (2000–2016) (Liu et al., 2021).

2.2 Hydrology

Whitemans Creek is a 6th order stream with many tributaries contributing to its flow within the LWC sub-catchment. Upstream of the inlet, the confluence of Horner Creek (5th order) and Kenny Creek (4th order) combine as the main surface water contributions (Figures 2A,B). Both locations have bridges near the confluence, providing an ideal location for stage and discharge measurements

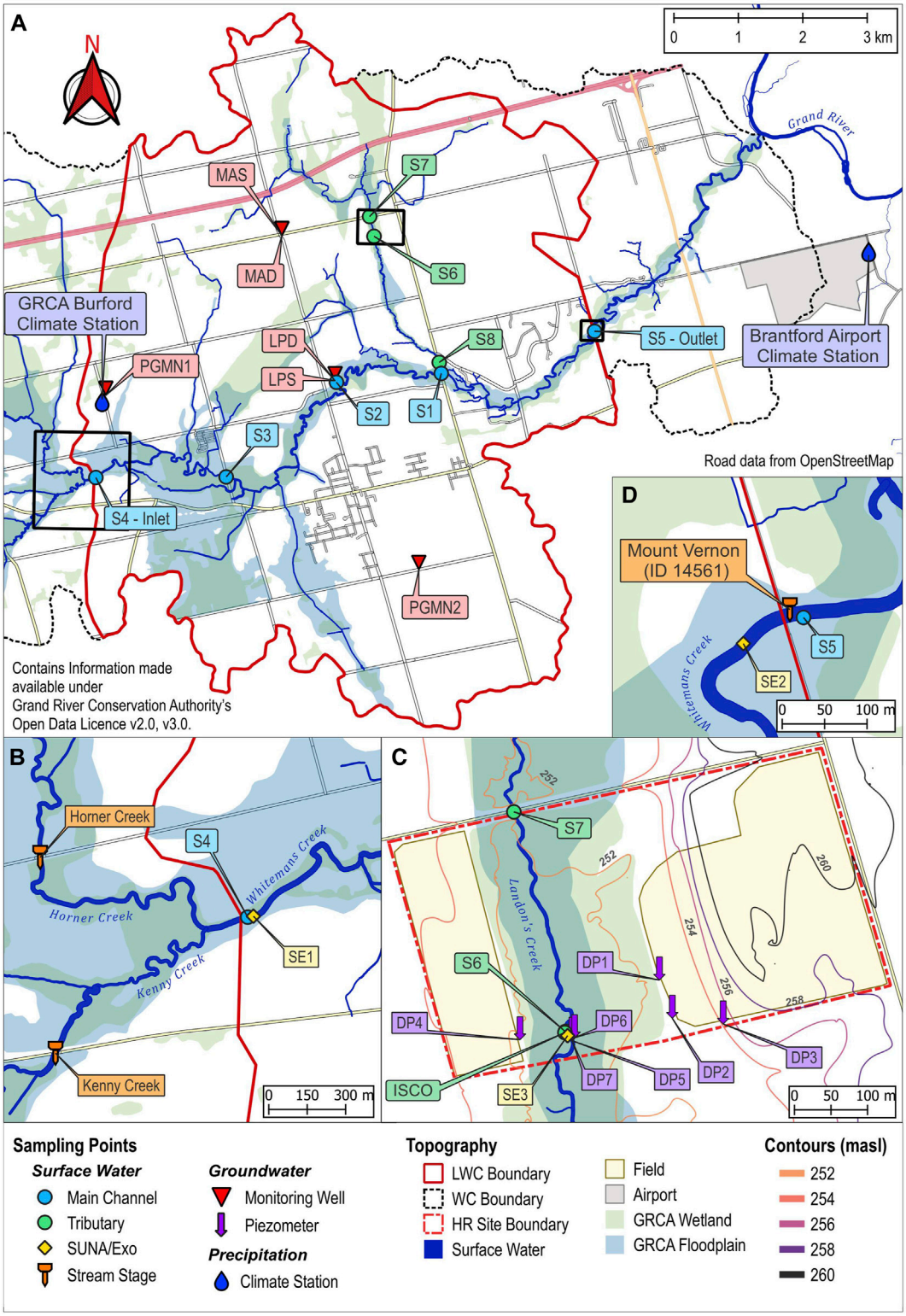


FIGURE 2
Sampling locations withing the Lower Whitemans Creek subcatchment **(A)** overview of the site with surface water and groundwater monitoring stations, **(B)** inlet location with upstream locations of the bridge-mounted ultrasonic sensors, **(C)** high resolution site, and **(D)** the outlet station.

for the study, as opposed to the inlet directly, where flooding over the banks is a common occurrence. There are one 3rd order stream, eight 2nd order and ten 1st order tributaries contributing to the surface water discharge measured at the Ontario Provincial (Stream) Water Quality Monitoring (PWQMN) water gauging station (Mt. Vernon, 02GB002; Figure 2D) (ECCC, 2024).

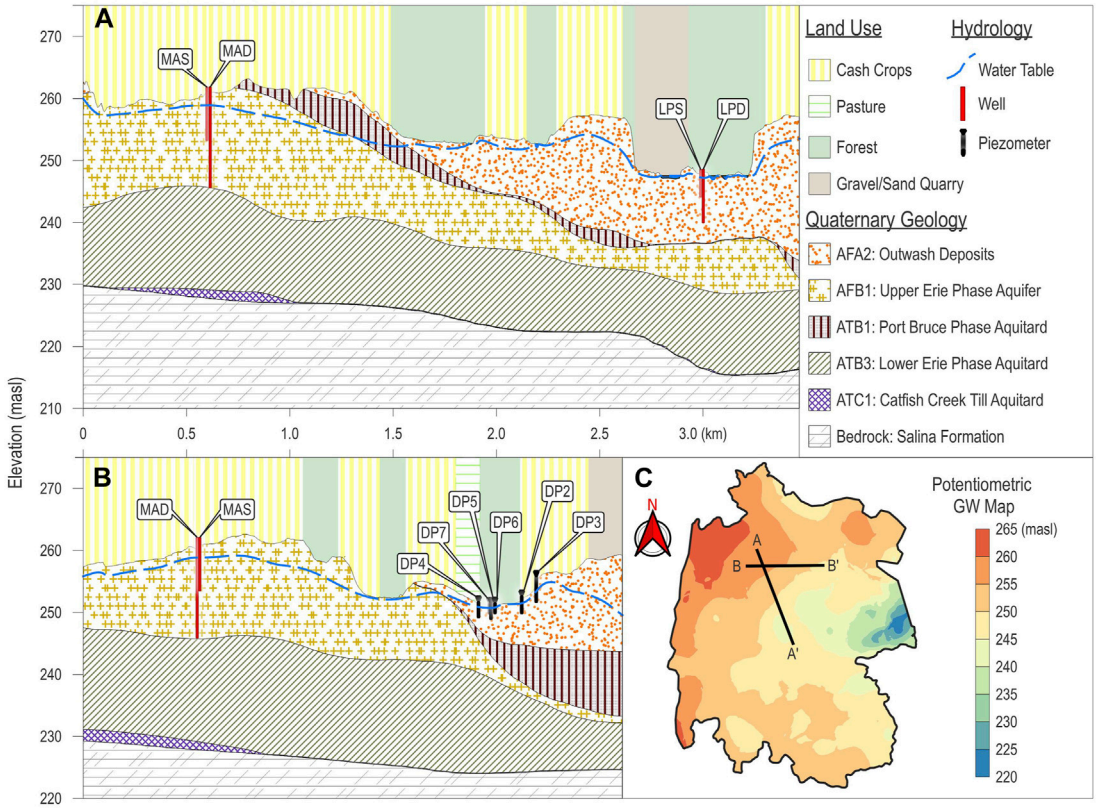


FIGURE 3
Geological cross sections **(A)** A-A′ cross-section, **(B)** B-B′ cross-section, and **(C)** piezometric map and location of cross-sections (Bajc and Dodge, 2011; Osman, 2017).

The PWQMN has a long-term monitoring station for water quality located at the outlet of LWC (Figure 2D, near S5) with records from 1980 covering a range of variables including nitrate, chloride, electrical conductivity, and pH (Kaltenecker, 2023). Stage and discharge are available for Whitemans Creek (Figure 2D, near S5; 02GB008) since 1961 (ECCC, 2024). Using daily discharge from the Mt. Vernon station the average discharge at the outlet was 4.28 m^3/s (maximum 41.60 m^3/s, minimum 0.35 m^3/s; Oct. 2021 to Nov. 2024). Discharge at the outlet was typically highest in winter and spring, relating to snow melt, while the lowest discharge consistently occurred in the early fall (ECCC, 2024). Larocque et al. (2019) estimated baseflow between 0.34 and 1.25 m^3/s from baseflow separation using a digital filter (Larocque et al., 2019) and 0.49 m^3/s using an integrated SWAT-MODFLOW model. Considering that a gain of surface discharge occurs between the inlet and outlet of 1.54 m^3/s (Osman, 2017), approximately 32% of Whitemans Creek surface water discharge occurring between the inlet and outlet is baseflow. Additionally, during the study period (Oct. 2021 to Nov. 2024), Whitemans Creek was found to only freeze over at the inlet (S4) and S3 while Landon's Creek was never frozen, indicating that Landon's Creek (Figure 2) is receiving groundwater during the winter season.

2.3 Geology and hydrogeology

The geology of LWC is characterized by the Norfolk Sand Plain–sandy soil, rapid infiltration, shallow water table–and the flatter southern part of the Horseshoe Moraines (Chapman and Putman, 1984; Chapman and Putnam, 2007). The Brunicolic gray-brown luvisol soil has been described as rapidly drained, loam to silt loam containing gravel in the first 20 cm, underlain by gravelly clay loam to 75 cm below ground level (bgl) (Acton, 1989; Janzen, 2018). Well drained (66%) and imperfectly drained (14%) soils comprise most of the cultivated fields while poor and very poorly drained soils (16%; 4% undefined) are in forested and riparian areas of the catchment (Acton et al., 1998; CanSIS, 2014). Tile drained fields in LWC make up just 5% of the total land used for plant agriculture (Ontario Ministry of Agriculture, 2025). Finally, within LWC, 85% of the land is classified as having predominantly nearly level/very gentle slopes (0.3°–3°), 10% as moderate (5°–8.5°), and 1.5% as strong slopes, with the steepest slope found on the north bank of Whitemans Creek at the outlet (S5, Figures 2D).

Surficial geology consists mainly of gravel and sand with small silt to sandy silt areas in the southwest and is underlain by Upper Silurian bedrock (Larocque et al., 2019; Chapman and Putnam, 2007; Osman, 2017). Geological cross-sections show an unconfined

aquifer (maximum thickness of 15 m in certain areas; Figure 3) characterized by the coarse sand and gravel of the Grand River valley outwash (AFA2) and the gravelly fine sand of the Upper Erie Phase aquifer (AFB1). Silty to clayey till (ATB1, ATB2) underlay the superficial aquifer (Bajc and Dodge, 2011).

Within the study area, two provincial monitoring wells are maintained by the Grand River Conservation Authority (GRCA), PGMN1 (Id: 477) since 2008 and PGMN2 (Id: 065) since 2001 (Roogojin, 2024). Four additional monitoring wells were dug for and used in previous studies in the area (LPS, LPD, MAS, and MAD; Figure 2) and are monitoring temperature and water level since 2016 (Larocque et al., 2019; Osman, 2017). The potentiometric map (Figure 3C), drawn using available data from well drillers logs, indicates groundwater flow from west to east north of the creek (Larocque et al., 2019; Osman, 2017). The LWC drains the aquifer all along the study area, indicating potential surface water–groundwater connections. Previous research suggested that groundwater is entering Whitemans Creek from different locations, either via the streambed or from the many small SW tributaries (Osman, 2017). Due to the high irrigation water consumption and Permits to Take Water (PTTWs, for users pumping more than 50,000 L/day) in the area, the Whitemans Creek subcatchment is a region of potential water conflict (Shifflett et al., 2014). In 2023, the Whitemans Creek had 102 PTTW, of which 40 were within the LWC study area (MECP, 2023). In addition to irrigation, groundwater from private wells is used as the only source of drinking water for the local population within Burford (urban area in Figure 1; population, 2021: 1,058) (Lake Erie Region Source Protection Committee, 2025; Statistics Canada, 2023).

2.4 Meteorological conditions

Hourly precipitation was measured at the GRCA Burford Climate Station located inside the LWC catchment area near the inlet (S4) (GRCA, 2024) and the temperature records were obtained from the Brantford Airport (BA) weather station (ID: 6140942) operated by Environment and Climate Change Canada since 2014 (CCCS, 2024). The Brantford Airport Climate station is located 4.4 km east of the outlet (S5) (Figure 2). At the nearby Brantford MOE (Ministry of the Environment) climate station (ID: 6140954, approx. 8 km east of Brantford Airport and in operation from 1960 to 2013), the mean annual precipitation from 1975 to 2005 was 861 mm (15% as snow water equivalent); mean daily air temperature was 7.6 °C; annual average minimum of −24.4 °C and maximum of 32.4 °C. Over the observation period (2021 and 2024), mean precipitation was 869 mm and the percentage of precipitation as snow varied between 6% and 25%. Mean daily air temperature was 9.2 °C with an annual average minimum of −19.7 °C and maximum of 32.4 °C.

3 Materials and methods

3.1 Instrumentation

The primary observation period extended from October 2021 to November 2023 and was supplemented with additional datasets collected from December 2023 to November 2024 (Arce-Rodriguez, 2024; Pattrick et al., 2024). Collected datasets included (1) groundwater level measurement (Van Essen Divers); (2) groundwater and surface water samples analyzed monthly for field parameters (EC: electrical conductivity, DO: dissolved oxygen, ORP: oxidation-reduction potential, pH, and water temperature), and major anions (i.e., fluoride, chloride, bromide, nitrite, nitrate, phosphate, and sulfate); (3) river stage measured with either pressure transducers or bridge-mounted ultrasonic level sensors; and (4) *in situ* water quality and nitrate sensing instrumentation during selected periods.

To complement the stage measurements at the Mt. Vernon station, three additional gauging stations were installed in 2022. Two are bridge-mounted ultrasonic level sensors on bridges over Horner Creek and Kenny Creek (Figure 2B) and one is a *Solinst* pressure transducer along Landon's Creek tributary.

3.1.1 Groundwater

A total of six monitoring wells were equipped with pressure and temperature transducers and were sampled monthly for major anions and field parameters. The provincial monitoring wells PGMN1 and PGMN2 were sampled monthly during the research while temperature and water table level were provided by the GRCA. The four pre-existing monitoring wells (LPS, LPD, MAS, and MAD), were reequipped in November 2021 with *Van Essen TD-Divers* (replacing *Solinst* transducers) for hourly monitoring of temperature and water level (well location on Figure 2, screened depth on Figure 5C).

A high resolution (HR) sampling location was selected for examining groundwater-surface water interaction and NO_3-N at a local scale on Landon's Creek (Figure 2C). The instruments were installed on either side of the stream (Figure 2A). HR was instrumented with six 25 mm-diameter *Solinst 615N Simple Well Point* piezometers with a screen length of 20 cm (i.e., drive point piezometers installed using a post hammer). Four piezometers (DP1-4; screen top 1.6,1.8,3.0, and 1.4 m bgs) were installed in July 2022, two of which (DP3 and DP4) were equipped with *Van Essen Micro-Divers* to monitor groundwater levels on opposing sides of the stream. In May 2023, three similar piezometers were installed at the tributary (DP5-7; screen top 1.0, 1.8, and 0.4 m bgs). When targeting storm events in 2022 and 2023, these sites were used for high-frequency sampling.

3.1.2 Surface water

Surface water instrumentation included an autosampler, pressure transducer, and *in situ* water quality stations. A Teledyne ISCO autosampler was use for targeting three storm events (Nov. 11–12, 2022; Mar. 22–23, 2023; Mar. 25, 2023). An in-stream *Solinst* pressure transducer, attached using aircraft cable to a steel fence post vertically hammered into the stream bed and protected with a perforated PVC pipe jacket, was used for temperature and stream stage measurements at 30 min intervals. Finally, three *in situ* water quality monitoring stations (labelled as SE, Figure 2) were used during the warm seasons at various sites from 2022 to 2024. These high-frequency monitoring stations were each equipped with a submersible *Seabird Scientific Ultraviolet Nitrate Analyzer V2* (SUNA) and a *YSI EXO Sonde* (EXO). The SUNA is an *in situ* spectrophotometer which uses a wavelength

TABLE 1 Sampling frequency and analysis methods—note measurement frequency in subsequent years was reduced from 15 min to 1 h for energy saving purposes.

	Manual grab	ISCO	SUNA/EXO		
Year	Oct. 2021 to Nov. 2024	Nov. 2022 and Mar. 2023	2022	2023	2024
Spatial Scale	Subcatchment	Field (HR site)	Local (Inlet)	Reach (Inlet, Outlet)	Local (Inlet, Outlet, HR)
Frequency	Monthly	2 h (3 events)	15 min	30 min	1 h
Water	Surface water and groundwater	Surface Water	Surface Water		
Analysis method					
NO_3-N	Laboratory — ion chromatography	Laboratory — ion chromatography	*In-situ* UV spectrometry (SUNA)		
Field Parameters	In-field portable meter (YSI ProPlus)	In-field portable meter (YSI ProPlus)	*In-situ* sensor (YSI EXO)		

range between 217–240 nm to measure NO_3-N concentrations in water (Johnson and Coletti, 2002; Seabird Scientific, 2024). Each EXO instrument was equipped with four probes for measuring electrical conductivity, temperature, pH, dissolved oxygen, and turbidity in stream water, but in the current project, only water temperature was used. The SUNA/EXO (SE) station SE1 (Figure 2B) was installed all 3 years (2022–2024) while SE2 (Figure 2D) at the outlet was in operation during 2023 and 2024. A third station, SE3 (Figure 2C), was used in 2024 for targeting storm events (Table 1).

3.2 Sampling and processing

Groundwater and surface water samples were collected monthly, during storm events, or for calibration purposes over the course of the study. All water samples were immediately stored in a cooler with ice until refrigeration at the laboratory, usually within 8 h from sampling. Samples to be analysed for major anions were filtered into 30 mL HDPE single-use bottles using 0.45 µm Fisherbrand Basix Syringe Filters, PVDF, non-sterile. Major anion analysis was conducted by the Morwick G360 Groundwater Research Institute laboratory using a Metrohm Eco IC Ion Chromatograph using Ion-Suppressed Chromatography (2.925.0020).

3.2.1 Monthly sampling

Groundwater sampling from wells and drive point piezometers were conducted using either a submersible pump (*Grundfos*), peristaltic pump (*GeoTech*), or hand pump foot tubing (*Waterra* HDPE tubing), depending on well diameter, screen depth, and equipment availability. Wells and piezometers were purged by pumping three well volumes or the amount of water required for stabilization of field parameters measured with a *YSI ProPlus* multiparameter (sensors included: specific conductivity, temperature, pH, dissolved oxygen, and oxidation-reduction potential). Clean 1 L HDPE sample bottles were rinsed three times with fresh sample water, filled with no headspace for all groundwater and surface water samples. Surface water grab samples were taken at all steam gauging stations approximately 2.5 m from the bank of the creek using an extendable dip pole at a depth between 0.25 and 0.5 m at five locations along the stream (Figure 2A; Supplementary Figures S1–S5). Grab samples in the tributary (Figure 2C; Supplementary Figures S6–S8) were collected in the center of the creek at approximately 0.25 m from the surface by hand.

3.2.2 Storm events

Three storm events (Nov. 11–12, 2022; Mar. 22–23, 2023; Mar. 25, 2023) were sampled with a *Teledyne ISCO* autosampler, which collected surface water samples every 2 hours and stored samples internally in 1 L HDPE bottles. Storm events assessed with the SUNA/EXO instruments were sampled at a frequency between 15 min and 1 hour depending on the sampling site and season (Table 1). Turbidity, sediment build-up, and sensor fouling impact the performance of the SUNA by impeding the UV light transmittance. The SUNA is designed to account for darker conditions by increasing the amount of time the sensor takes to scan its 256-channel spectrometer, but excessive fouling can still impact performance (Seabird Scientific, 2024). Throughout the deployment periods, sediments were manually removed from the sensors approximately once per month, with the 2024 season seeing cleaning occur every 2 weeks. Calibration with deionized water was conducted monthly for the SUNA and NO_3-N grab samples analyzed using ion chromatography were taken for comparison. The EXOs were also calibrated monthly following the procedures outlined by the YSI EXO user manual (Revision K; Xylem, 2020).

4 Results

4.1 Surface water and groundwater monthly sampling

Between November 2021 and November 2024, there were 890 continuous precipitation events (consecutive hours recording precipitation >0.1 mm) recorded at the Brantford Airport Weather station. A total of 76% of these events had intensities below 1 mm/hr with an average duration of 2.1 h (Figure 4A). Storm events with intensities above 2 mm/hr (red marks on Figure 4A) accounted for 11% during the study period with the most intense storm recording 22.4 mm/hr in a single hour (1 h duration, August 2022).

4.1.1 Flowrates and groundwater levels

Seasonal patterns in discharge at the Mt. Vernon station (S5) are readily evident, such as the significant increase during the spring snow melt, starting around February 15th in 2022, March 15th in 2023, and February 1st in 2024 (Figure 4A). Maximum spring season flow rates then reached 33.3, 39.5 and 38.5 m^3/s in 2022, 2023, and 2024, respectively. The extreme peak in discharge in August 2024,

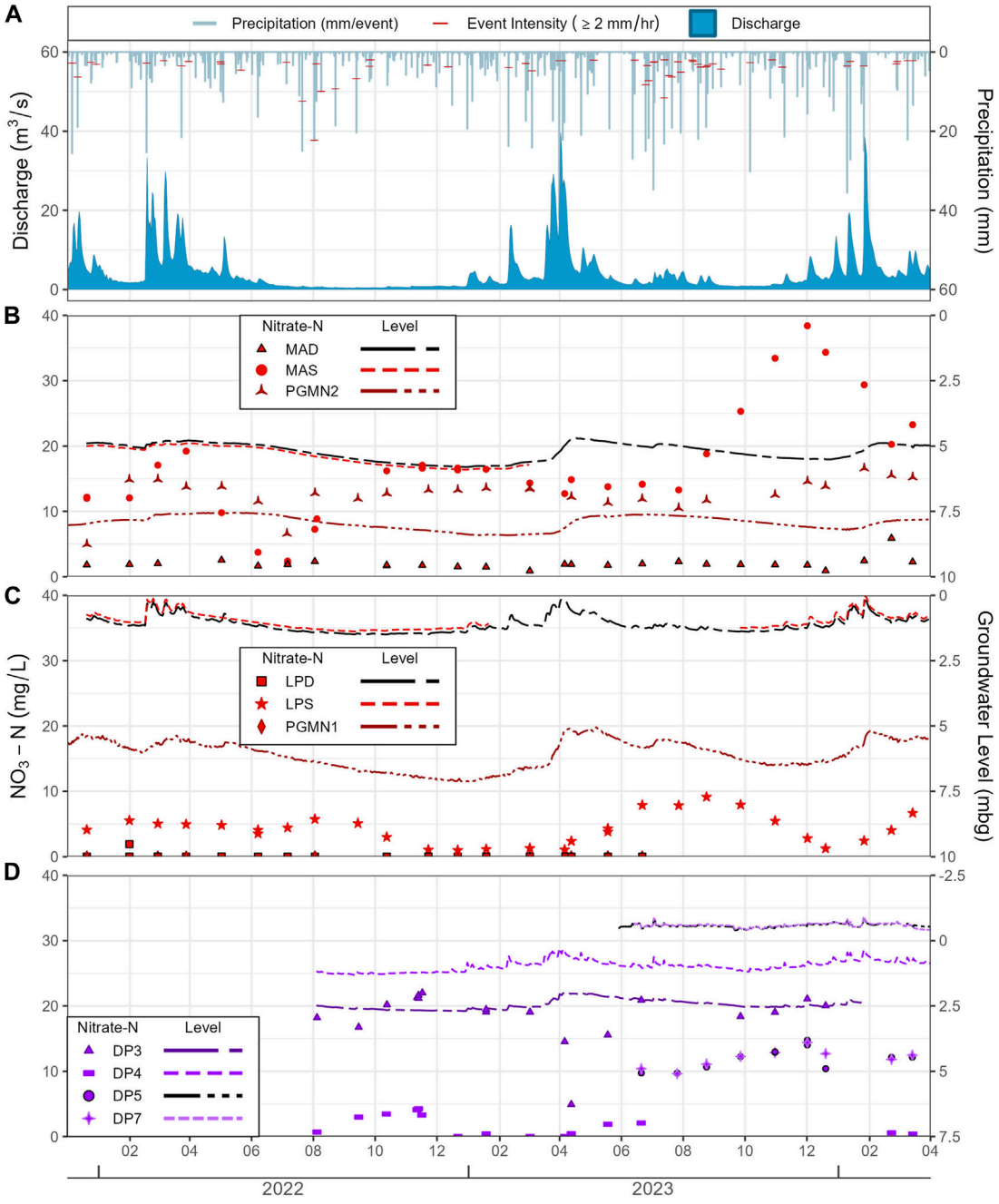


FIGURE 4
(A) Daily precipitation and stream discharge at the outlet; **(B–D)** groundwater NO_3-N concentrations and groundwater levels for different monitoring stations during the study period. PGMN1 was excluded from graph due to NO_3-N concentrations consistently below detection limit.

was linked to the tail of Hurricane Debby. Summer daily averages in discharge range between 1.3 and 3.5 m^3/s, reaching 0.4 m^3/s in the relatively dry summer and fall of 2022 while minimum discharge in summer/fall 2023 and 2024 was 0.8 and 0.7 m^3/s, respectively.

Groundwater levels in the sand aquifer (Figure 5C) responded to seasonal changes in inputs from precipitation and snowmelt (Figure 4). The maximum difference in groundwater levels was seen in PGMN1 (2.1 m; Figure 5C). The two in-stream drive points located at the HR site (DP5 and DP7) showed the least total change in water level (0.65 and 0.61 m respectively, Figure 5C). LPD, LPS, DP3, and DP4 were more sensitive to precipitation, as noted by the noisier data (Figures 4C,D), than MAD, MAS, and PGMN2 (Figure 4B).

4.1.2 Water chemistry

For major anions across all groundwater and surface water sampling locations throughout the study period, only NO_3-N, Cl^-, and $SO4^{2-}$ had measurable concentrations (Table 2; Supplementary Material). Nitrite (NO_2^-), bromide (Br^-), and phosphate (PO^{4-}) were always below the minimum detection

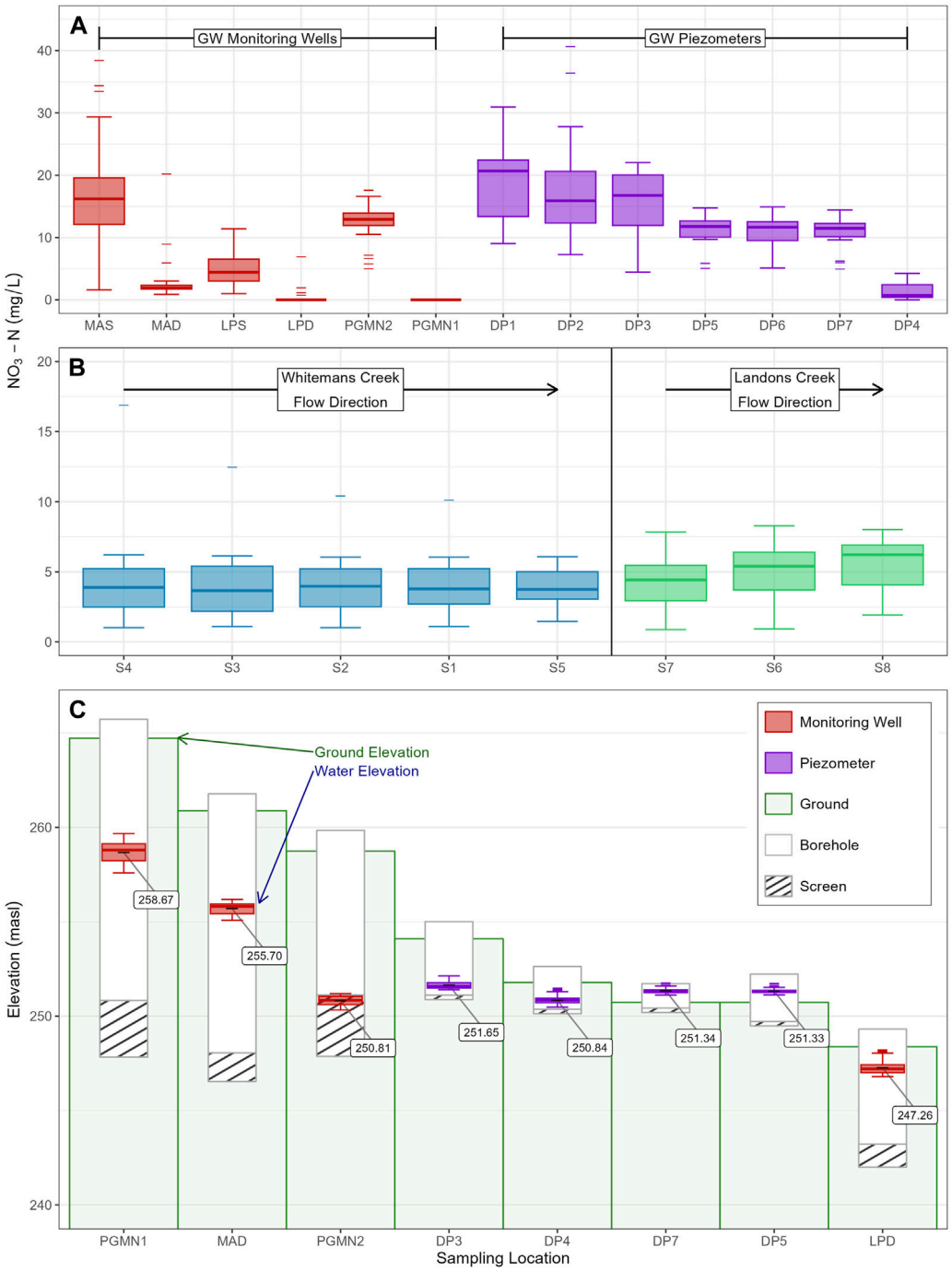


FIGURE 5
Trends in monthly NO3-N concentrations over the study period: **(A)** measurements from the six monitoring wells (red) and drivepoint piezometers at the HR Site (purple), **(B)** surface water concentrations ordered in downstream direction for Whitemans Creek (blue) and Landon's Creek (green), **(C)** average GW level over the course of the study period as compared to the ground elevation and screened depth of each well (in meters above sea level).

limit (MDL) at all sites (0.10 mg/L). Across all groundwater samples, only 25% had fluoride (Fl^-) concentrations above the MDL (mean = 0.7 mg/L; maximum = 3.2 mg/L) while surface water above the MDL occurred in 46% of samples (mean = 0.6 mg/L; maximum = 3.6 mg/L). Other field parameters measured over the study period were specific conductivity, pH, dissolved oxygen, and oxidation-reduction potential. Groundwater and surface water mean, minimum, and maximum values for the field parameters are summarized in Table 2 (timeseries graphs for each sampling location and field parameter are in the Supplementary Figures S1–S5).

NO_3-N concentrations in the shallow monitoring wells MAS and LPS averaged 17.2 and 5.0 mg/L NO_3-N with maximum values 38.4 and 11.4, respectively (Figure 5A). The deeper wells, MAD and LPD, had averages of 2.8 and 0.4 mg NO_3-N/L, and maximum values 20.2 and 6.9, respectively. Samples from the PGMN1 well

TABLE 2 Summary table of field parameters during study for groundwater and surface water samples [mean (minimum-maximum)]. See Supplementary Material for averages per location.

	Parameter		Groundwater (n = 319)	Surface Water (n = 238)
Major Anions	NO_3-N	(mg/L)	9.6 (0–40.7)	4.3 (0.9–16.9)
	Cl^-	(mg/L)	60.3 (1.5–346.5)	53.4 (11.4–814.2)
	SO_4^{2-}	(mg/L)	29.2 (0–109.6)	60.6 (12–136.0)
Field Parameters	SPC	(µS/cm)	771.8 (10–1772)	756.3 (8–2652)
	pH		7.4 (6.3–8.7)	7.6 (−68.4–8.7)
	DO	(mg/L)	8.2 (0.1–97.2)	23.7 (4.8–806.4)
	ORP	(mV)	47 (−281.1–498.2)	68.5 (−280.3–306.8)

TABLE 3 Summary of captured storm event characteristics.

Method	Event			Total precip.	Duration	Intensity
	Year	Month	Day	(mm)	(hours)	(mm/hr)
ISCO	2022	November	11–12	6.4	6	1.07
	2023	March	22–23	3.6	8	0.45
				4.4	4	1.10
			25	17.4	9	1.93
SUNA/EXO	2024	May	17	12	8	1.50
		June	29	18.2	6	3.03
		August	2	5.8	2	2.90
			5	13.6	1	13.60
			6	8.6	6	1.43
				4.6	2	2.30
			7	0.2	1	0.20
			9	4.8	3	1.60

never exceeded the NO_3-N detection limit while the PGMN2 samples averaged 12.5, peaking at 17.6 mg/L. Mean NO_3-N concentrations in the shallow drive point piezometers (DP1 to DP7) ranged between 21.4 (DP1) and 1.0 (DP4) mg/L NO_3-N, with a maximum value of 40.7 mg/L occurring in DP2 (Figure 5A).

Average NO_3-N concentrations at the five sampling locations on the main creek (S1-S5) varied between 4.1 (Inlet) and 3.9 (S2) mg/L (Figure 5B). Results from the tributary sampling sites (S6-S8) had NO_3-N concentrations between 4.3 (S7) and 5.6 (S8) mg/L, but the point nearest the outlet (S8) having a higher average concentration than the inlet (S7) (Figure 5A).

4.2 Event-based sampling

Two approaches for capturing responses of the study area to precipitation events were used and are referred to as the "ISCO" and "SUNA/EXO" methods. The three events captured using the ISCO method saw precipitation intensity ranging from 0.45 to 1.93 mm/hr, with the highest precipitation event and most intense event both occurring on 25 March 2023 (Table 3). A total of seven events captured by the SUNA/EXO method were analysed further, at times when most sensors were functioning properly. The intensity of six of these seven events were within the top 11% of most intense events recorded during the study period (see Section 4.2). Difference in the scale of storm events which were captured (i.e., intensity and timing of events) between the two methods were due to resource availability and difficulties in predicting when it was ideal to initiate ISCO sampling.

4.2.1 ISCO method

The ISCO method captured storm event responses at a single location on Landon's Creek tributary (S6). During the storm events (Figure 6), the NO_3-N concentrations varied between 5.5 and 6.5 mg/L (November 11–12, 2022), 1.1 and 1.9 mg/L (March 22–23, 2023), and 0.90 and 2.0 mg/L (25 March 2023). For the three events, NO_3-N concentrations decreased between 0.8 and 1.1 mg/L during the storm. Figures 6B,C were consecutive events, with the second occurring 41 h after the first. The sampling gap

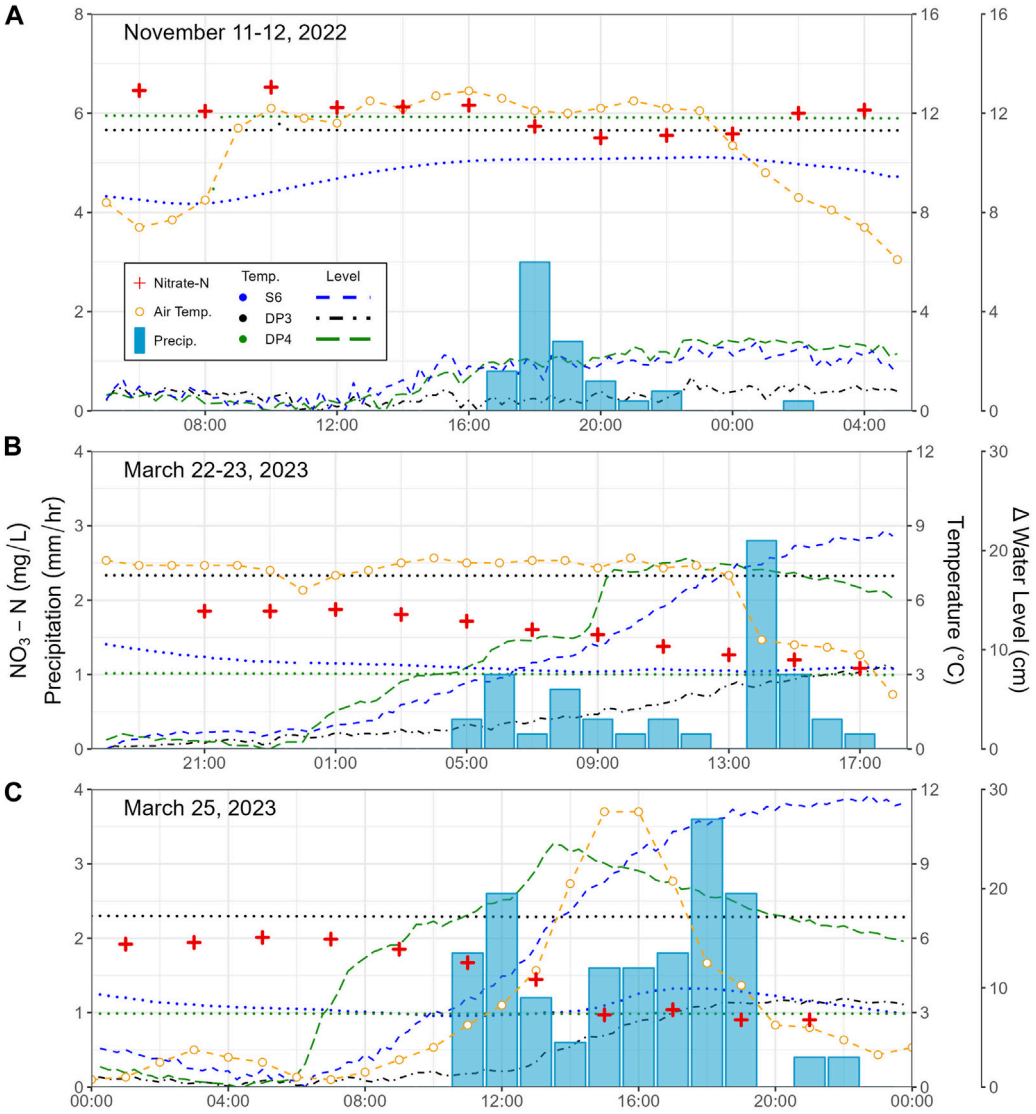


FIGURE 6
NO_3-N concentrations and water temperature in the stream during storm events from the ISCO meter, along with hourly precipitation and variation in stream stage during three storm events **(A)** November 11–12, 2022, **(B)** March 22–23, 2023, and **(C)** 25 March 2023.

between the two events was 30 h, after which the NO_3-N returned to the pre-storm high of ~2 mg/L before dropping again during the following event.

Stream temperature varied slightly throughout the course of each storm. When compared to change in atmospheric temperature, surface water temperature changed by 1.9 °C (8.4–10.2) and air temperature by 6.8 °C (6.1–12.9) (Nov.11), 1.1 °C (3.1–4.2) and air temperature by 5.5 °C (2.2–7.7) (Mar. 22), and 1.1 °C (2.9–4.0) and air temperature by 10.8 °C (0.3–11.1) (Mar. 25). Shallow groundwater temperature (DP3, DP4) did not change during any of the three storms.

Change in water level for both surface water (S6) and shallow groundwater (DP3, DP4) varied over the course of each storm. S6 and DP4 showed similar changes the water level magnitude 2.8 vs. 2.9 cm (Nov. 11), 22.0 vs. 19.2 cm (Mar. 22), and 29.4 vs. 24.5 cm (Mar. 25) while DP3 saw changes of 1.4, 8.4, and 9.0 cm, respectively.

4.2.2 SUNA/EXO method

High resolution temporal data were captured at specific locations using the SUNA/EXO stations. All data collected with the SUNAs were filtered by removing measurements for which the difference between the light spectrum absorbance (up to 20,000 counts) and the dark spectrum absorbance (thermal noise; typically between 500–600 counts) readings was less than 1,500. It was found that values below this range indicated significant sediment build-up on the sensor, resulting in unreliable readings. Validation of the sampling method was done through comparing grab sample concentrations measured in lab with ion chromatography to SUNA readings (Figure 7). The SUNA consistently recorded higher concentrations of NO_3-N than the grab samples, averaging +0.75 mg/L [±0.77] (max.: 2.87 mg/L; min.: 0.28 mg/L).

Daily average NO_3-N concentration and water temperature were compared to daily precipitation. During the fall of 2022, a SUNA-EXO (SE) station was set up at the inlet (S4) and recorded a

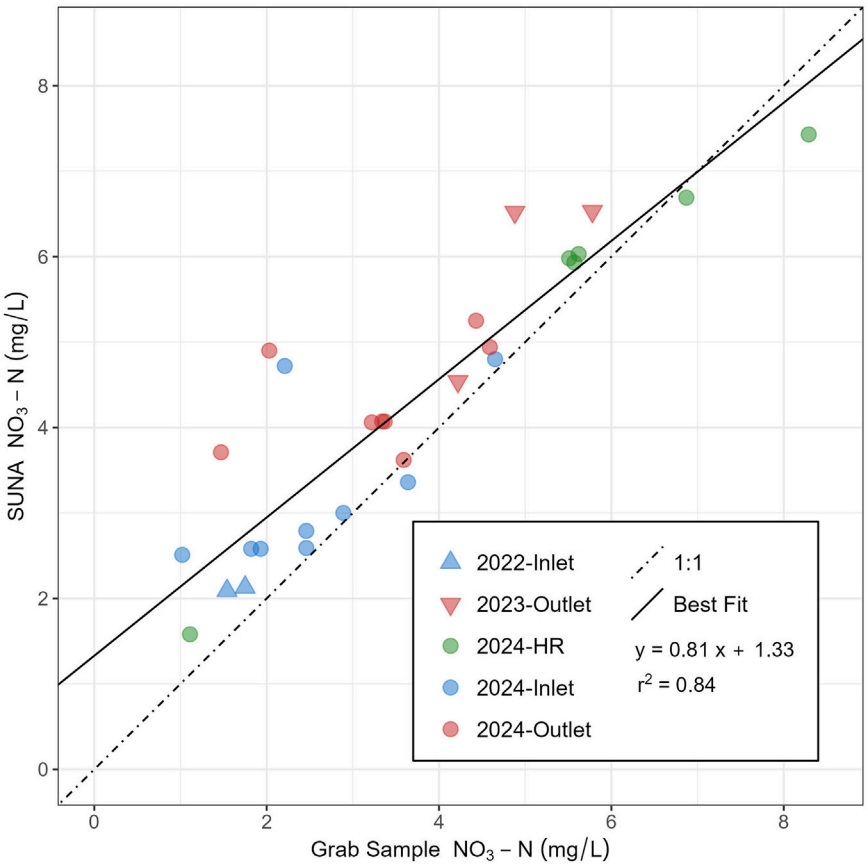


FIGURE 7
Comparison of NO_3-N concentrations recorded using the SUNA with grab samples taken near the same time at inlet, outlet and high resolution (HR) sites.

NO_3-N range of 1.24–2.28 mg/L. In 2023, the SE station at the outlet (S5) varied between 3.68 and 8.32 mg/L. During the 2024 sampling season, when all three SE stations were operational, NO_3-N concentrations varied between 2.18–5.65 (Inlet), 2.76–5.55 (Outlet), and 2.09–8.47 mg/L (HR). Daily averages of NO_3-N (considering only days with at least 8 h of measurements) had noisier readings from mid-April (DoY 100) to early August (DoY 220). When compared with the second part of the season, the noisier period corresponded to days with more daily precipitation (Figures 8A,C). Additionally, cooler temperatures in the tributary (S6) corresponded with higher concentrations of NO_3-N (Figures 8B,C).

During the 2024 sampling period, NO_3-N concentrations were compared to precipitation, water temperature, and change in stream level (i.e., stage height). The inlet and outlet SE stations were compared for two events, May 17 and 29 June 2024 (Figures 9A,B). NO_3-N peaked 5 days after the May event while it peaked just under 2 days after the June event at the inlet. The outlet peak for both events occurred after an additional 12 h. Peak values for the change in water level occurred approximately 12 h prior to all four peak values in NO_3-N.

For the first 10 days in August 2024 (DoY 213–222), three SE stations were compared (Inlet, Outlet, HR). NO_3-N notably dropped promptly over the course of a storm event at the HR site, also corresponding with an increase in water level (Figure 10). Such a relationship was not observed at the inlet and outlet SE stations during the same period (note: water level measurements at the inlet were lost during this period and NO_3-N concentrations are only available during daylight hours).

5 Discussion

To assess the transport pathways of NO_3-N in groundwater and surface water in connection to storm events in the study area, combinations of spatiotemporal sampling methods targeting different parameters were assessed. Concurrent methods for NO_3-N sampling were defined by low frequency high spatial coverage (monthly sampling on the entire LWC) or high frequency local scale (storm event sampling at a small number of specific locations). Water level and temperature measurements were sampled at high frequency (hourly) and at both reginal scale (monitoring wells distributed over the LWC) and local scale (high-resolution site instrumented with drive-point piezometers).

5.1 Interpretation of lower resolution data

On the monthly scale over the study period (Oct. 2021 to Nov. 2024), assessment of groundwater NO_3-N concentrations showed

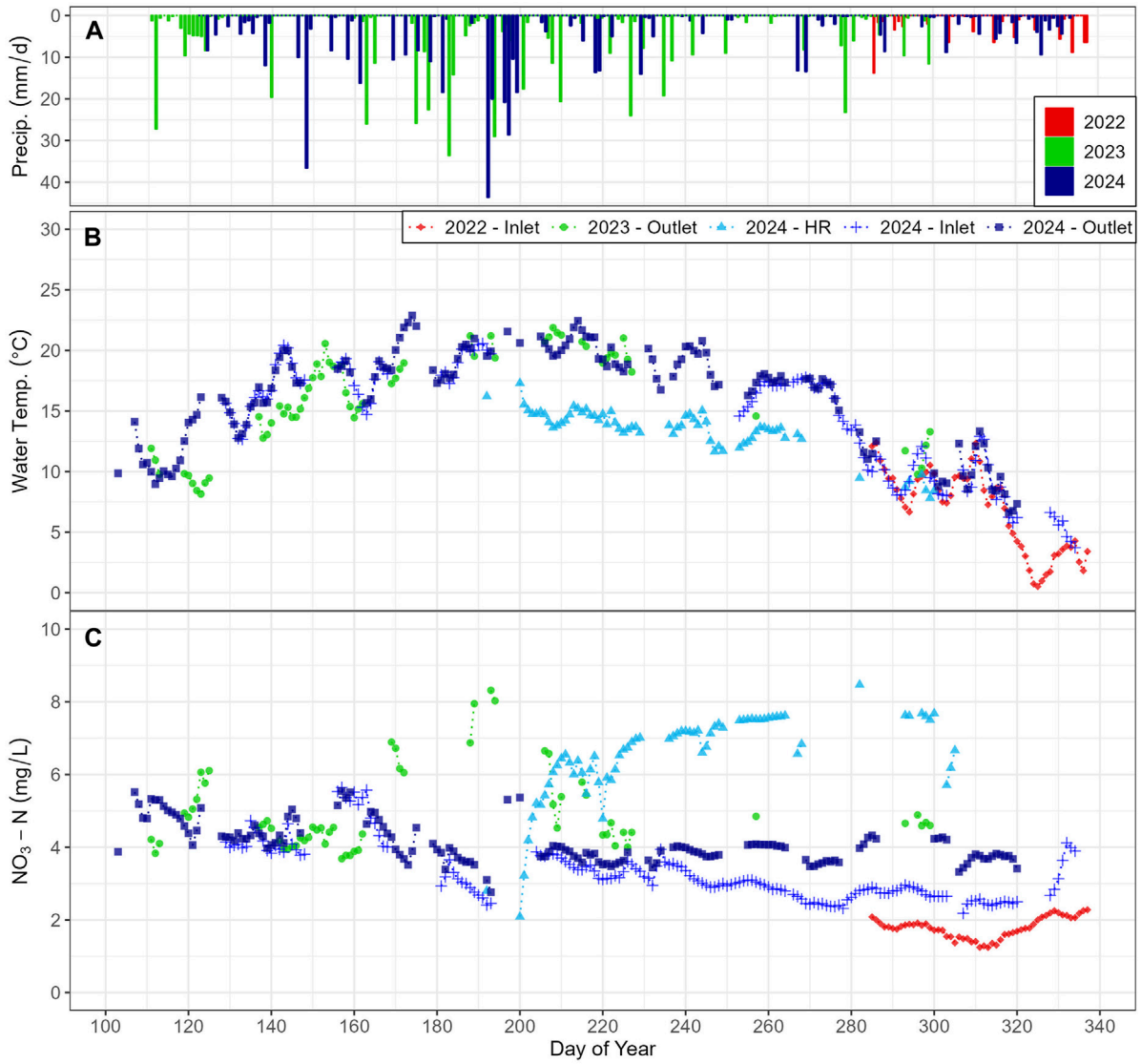


FIGURE 8
Comparison of **(A)** daily precipitation to **(B)** daily average stream temperature, and **(C)** NO_3-N concentrations in the stream from the SUNA and EXO at inlet, outlet and high resolution (HR) sites. Daily precipitation shown for full operating period each year.

distinct differences at the varying locations and depths. Average measurements from shallow wells MAS and LPS (17.2 and 5.0 mg/L) were markedly higher than in their paired deeper wells MAD and LPD (2.8 and 0.4 mg/L). The other two deep monitoring wells studied were PGMN1 (undetectable NO_3-N), and PGMN2 which consistently recorded some of the highest concentrations of NO_3-N. Wells screened at similar depths, but different locations, e.g., MAD (12.8–14.3 m bgs) vs. PGMN1 (13.9–16.9 m bgs), had notable differences in the average concentrations (2.2 mg/L in MAD and not detected in PGMN1). Finally, wells screened closer to the average water table level had higher NO_3-N concentrations than wells screened deeper, while still being in the overburden aquifer (screened near water table: MAS, LPS, PGMN2; screened relatively deeper than water table: PGMN1, MAD, LPD). Many factors can be contributing to this. For example, the vadose zone has been identified as an overlooked yet significant store of NO_3-N impacting groundwater quality, especially in agricultural areas where the vadose zone is thick (Ascott et al., 2017a), thicker than in the LWC where it varies between 0–7 m.

5.1.1 Hydrogeologic factors

Sensitivity of the water table to precipitation (Figure 4) was assessed by comparing stream discharge at the outlet (Mt. Vernon) to the water levels recorded in the monitoring wells. The frequency of fluctuations for each well hydrograph was highest for MAD and MAS, followed by PGMN2, then LPD, LPS, and then PGMN1. The fluctuations in groundwater levels in LPD and LPS notably follow changes in discharge closely, perhaps due to the proximity of these wells to the main creek, which contrasts with PGMN1, a well significantly further from the creek, that followed a smooth seasonal pattern with lowest levels during summer. Given the fluctuations in LPD/S following stream discharge, it is possible that WC is either a losing or gaining stream at this location, depending on season and storm event, which could be affecting

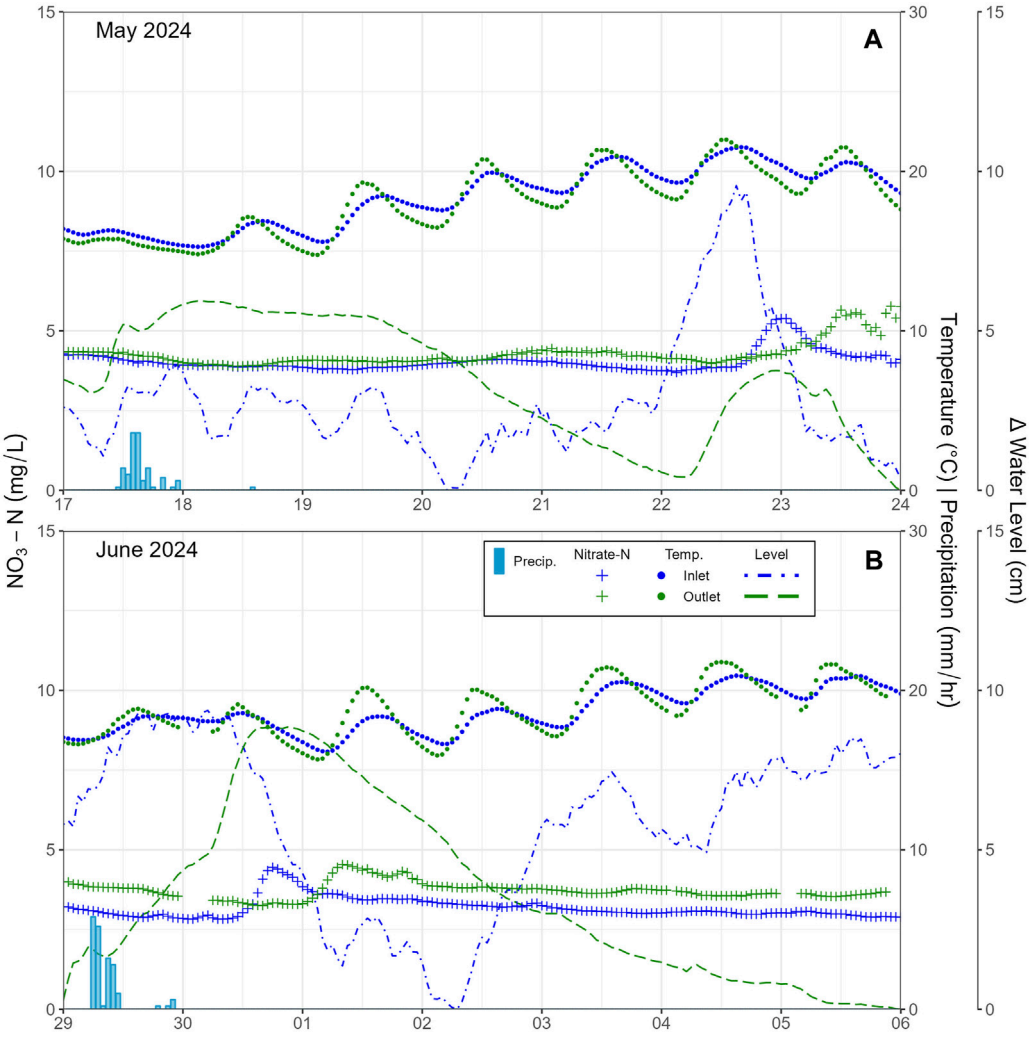


FIGURE 9
Comparison of stream NO_3-N concentrations and water temperature in the stream as a response to precipitation events **(A)** in May 2024 and **(B)** in June 2024 at inlet and outlet sites.

GW NO_3-N in LPS/D. For example, if WC is losing during high flows in the spring, the shallow groundwater would reflect NO_3-N concentrations in WC. During low flows, when WC is gaining, NO_3-N in LPS/D would be expected to reflect a different source, such as upgradient GW NO_3-N. While the pattern appears to reflect concentrations in LPS, it is not seen in LPD (see S1-5, Figure 5; Supplementary Figure S6). Therefore, LPD/S having lower relative NO_3-N as compared to MAD/S is likely caused by other factors, such as anthropogenic or biogenic factors discussed below.

On the south side of Whitemans Creek, only one well, PGMN2, was studied. It is screened at a depth comparable to that of MAD and PGMN1, yet it had a comparable average NO_3-N to MAS (15 and 17 mg/L). PGMN2 has a relatively deeper average GW level (~8 m bgs) compared to PGMN1 (~6 m bgs) and MAD/MAS (~5.5 m bgs) and had smoother (less variable) well hydrographs which could imply less connection to surface. This could also imply a higher storativity, i.e., the aquifer at this location can store more water and effectively buffer impacts from surface inputs. Differences in storativity may impact response times and thus NO_3-N concentrations. Although both MAD/MAS and PGMN2 are screened into similar overburden material, coarse sand (Osman, 2017) and gravelly sand (Government of Ontario, 2017) respectively, the quaternary hydrostratigraphic units are different, with MAD/MAS in the Upper Erie phase aquifer (AFB1) and PGMN2 in outwash deposits (ATA2) (Bajc and Dodge, 2011). Further testing using pumping tests would help determine the extent to which storativity may be impacting responses.

5.1.2 Anthropogenic factors

Land use (Table 4) likely also impacted the results, since the MAD and MAS wells (2.8 and 17.2 mg NO_3-N/L) were surrounded by cash crops which are fertilized with nitrogen during the corn rotation. PGMN2 (12.68 mg NO_3-N/L) was similar in that nearby fields are corn or potatoes, whereas PGMN1 (n.d.) is in a tree nursery and the LPD and LPS wells (0.4 and 5.0 mg NO_3-N/L) are in a forested park (Figure 2).

Land use surrounding the PGMN2 well is notably different than other wells monitored. Moreover, PGMN2 is located less than 1 km

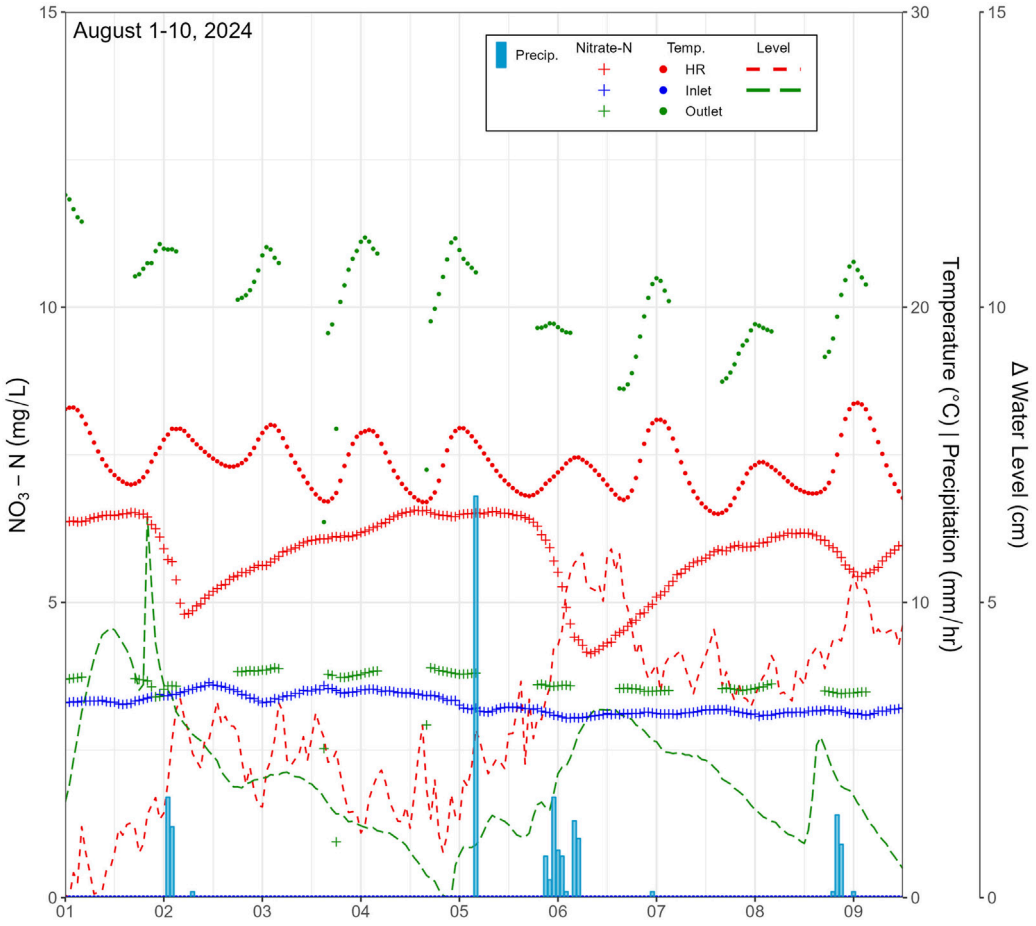


FIGURE 10
Comparison of stream NO_3-N concentrations and water temperature as a response to precipitation in August 2024 at inlet, outlet, and high resolution (HR) tributary site.

TABLE 4 Summary of conditions surrounding monitoring wells during the study period. Land use data from Annual Crop Inventory (AAFC, 2023). Coloured rotation legend corresponds to land use map (Figure 1).

Well ID	Sampling	Surrounding land use				Rotation
	Start date	2020	2021	2022	2023	
LPD, LPS	2021–10–25	Corn	Soybeans	Corn	Soybeans	
MAD, MAS		Corn				
PGMN1		Forest				
PGMN2	2021–11–22	Potatoes	Winter Wheat	Corn	Other Veg.	
DP1, DP2, DP3	2022–08–04	Pasture	Corn	Soybeans	Winter Wheat	
DP4		Soybeans		Pasture		
DP5, DP6, DP7	2023–06–20	Forested Wetland				

from a housing subdivision in the Township of Burford, where residences use septic systems for wastewater treatment (County of Brant, 2023; Maxwell, 2020). The PGMN2 well is screened near a similar elevation (~250 m asl) as the potentiometric surface located under the nearby houses (250–245 masl, Figure 3), from which elevated NO_3-N may be related, due to the septic systems which are

known to contribute NO_3-N, along with many other contaminants, to groundwater systems globally (Gyimah et al., 2024; Robertson, 2021). Monthly sampling data for specific conductivity and chloride was notably higher in PGMN2 (1,348 μS/cm and 253 mg Cl^-/L) than all other groundwater samples taken during the study (See Supplementary Table S1; Supplementary Figures S1, S2 for comparison). Additionally, the mixed agricultural land use (Figure 1) has recently consisted of potatoes and other vegetables along with corn and winter wheat (Table 4) on fields equipped with irrigation capabilities. These high concentrations measured at depths further below ground surface than the other wells (MAS, LPS) also screened near the water table may be indicative of legacy NO_3-N build up due to the relatively thicker vadose zone (Ascott et al., 2017a) or different antecedent GW geochemistry coming from the west, among other factors.

A comparable well to PGMN2 from Gardner et al. (2020) had high NO_3-N concentrations (average 13.5 mg NO_3-N/L) in Norfolk County, just south of LWC and in a sand plain aquifer, where proximity to residences on septic systems were identified as the likely source via timeseries patterns and isotopic signatures. However, not enough data was taken on the south side of the LWC catchment to be able to determine conclusively the sources of NO_3-N and its relationships to precipitation in PGMN2. Further study of NO_3-N isotopes could help identify sources of NO_3-N (Nikolenko et al., 2018). Some samplings of NO_3-N isotopes were conducted in 2023 at the site (for collection and processing methods see Arce-Rodriguez (2024); Supplementary Material), but PGMN2 did not show notable signatures for septic waste.

5.1.3 Geochemical and biogenic factors

Heterotrophic denitrification, a redox transformation, in groundwater can occur under specific conditions, typically when NO_3-N concentrations are greater than 1 mg/L, dissolved oxygen is below 2 mg/L, pH is between 5.5 and 8.0, and chloride is below 500 mg/L (Rivett et al., 2008). Presence of electron acceptors (e.g., dissolved organic carbon) are also typically needed. To determine redox state of natural waters, methods such as cross-referencing dissolved oxygen (DO), manganese (Mn), iron (Fe), and NO_3-N to field measured oxidation-reduction potential (ORP), categorized into anoxic (−300 to 0 mV), suboxic (0–50 mV), and oxic (50–300 mV) (Gardner et al., 2020; Kehew, 2001; Stumm and Morgan, 1996). As the transformation of NO_3-N requires anoxic environments, when the redox potential is moderate-to-low, NO_3-N is not expected to be present (Grant Ferris et al., 2021; Kehew, 2001).

When comparing monthly groundwater samples over the course of the study the deeper wells averaged between 2.7 and 4.1 mg DO/L (MAD, LPD, PGMN1) while the shallow ranged from 6.7 to 11.2 mg DO/L (MAS, LPS, PGMN2, DP1-7). Only wells LPD and PGMN1 had, on average, reducing conditions with ORPs of −35.34 and −19.49 mV respectively. However, all groundwater samples recorded ORP values below zero at varying points in the study (See Supplementary Table S2; Supplementary Figures S3, S4 for further detail). Chloride concentrations never exceeded 350 mg/L in any groundwater samples and pH consistently ranged between 6.2 and 8.5 (Supplementary Tables S1, S2). Considering these factors, it seems unlikely that denitrification contributed to the noted lower concentrations of NO_3-N with depth between MAS and MAD. A stronger argument may be made for denitrification potentially occurring at LPS and LPD during times when DO fell below 2 mg/L. For PGMN2 and DP1-7 favorable conditions for denitrification were less likely, since all these monitoring points are screened just below the average water table depth and have relatively high DO and ORP values. However, sampling these wells required the use of foot valve hand pumping, which prevented a flowthrough cell from being used when sampling, thus may have artificially increased the measured DO values. PGMN1 had the strongest evidence for denitrification contributing to NO_3-N rarely being detected in the well, as the DO was consistently low (2.7 mg DO/L) and ORP averaged below 0 mV.

The 2023 NO_3-N isotopes samples from Arce-Rodriguez (2024) show indications of denitrification in only three of the 75 samples taken, all three originating from the MAD well. Further delineation of sources was not possible due to most samples falling within the Soil-N range, where sources of NO_3-N range from possible mineral fertilizers, naturally occurring in soil, manure, or septic sources (+3‰ to +8‰; Nikolenko et al., 2018).

5.2 Interpretation of higher resolution data

5.2.1 Hydrogeologic factors

During all storm events, water elevations in streams and groundwater level both rose within a short timeframe, within a day on Landon's Creek (Figures 6, 10) or within two to 5 days in Whitemans Creek (Figure 9). Deeper monitoring wells further away from the tributary and creek (MAD/S, PGMN2) did not appear to respond in the same rapid fashion as seen at the high resolution site (DP3, DP4) or the shallow well near the main creek (LPD/S), which can be seen in the relative smoothness of water level measurements in Figure 4B as compared to Figures 4C,D. When linked with NO_3-N concentrations, the rapid response in the tributary to storm events initially lowered the NO_3-N concentration but was followed within a day by a return to pre-storm levels (e.g., 1.1 mg/L at the end of March 23 and 2.1 mg/L beginning 24 March 2023; Figure 6). In the LWC, no noticeable NO_3-N dilution was seen due to the storm events and, on the contrary, a noticeable increase occurred slightly delayed from the peak in discharge. Additionally, the outlet for both May and June/July lagged about half a day behind the peak in concentration occurring at the inlet (Figure 9). The August 1–10, 2024 rain event was the most thoroughly captured event using the methods attempted. Decreasing NO_3-N concentrations were observed at the HR site, followed by a rapid rise to pre-storm levels (e.g., ~6.5 mg/L pre Aug. 6th storm, ~5.5 mg/L mid storm, and return to ~6.3 mg/L by Aug. 8th, 2024; Figure 10), while no notable drop in NO_3-N was recorded during the same period at the Inlet and Outlet stations (Figure 10).

This can be interpreted as the small tributary likely acting as a conduit for NO_3-N entering the main creek. From the research conducted at the HR site, Landon's Creek appears to be a gaining stream, which could explain why it has particularly high NO_3-N concentrations. The creek supports coldwater species of brook, brown, and rainbow trout (personal communication with Trout Unlimited Canada [now Freshwater Conservation Canada) – Middle Grand Chapter, 2024; (OMNR, 2025)]. It maintains a higher temperature relative to LWC during the winter (min.: 2.3 °C–4 °C at S6 vs. 0 °C–0.2 °C at S1) and lower

during the summer (max.: 16.4 °C–20 °C at S6 vs. 20.7 °C–22.5 °C at S1) (Supplementary Table S2), did not freeze over in the winter (both the inlet and S3 froze at times), and did not go dry in the summer. A similar study on the larger Bazile Creek in Nebraska (1958 km^2) highlighted the higher impact of some groundwater-fed tributaries in conducting NO_3-N to the main creek, emphasizing the need for sampling lower-order streams (Richards et al., 2021).

5.2.2 Anthropogenic factors

On the field scale at the HR site, DP4 has the lowest average NO_3-N concentration (1.40 mg/L) and is located on an alfalfa field only receiving potash (potassium) as fertilizer. Highest concentrations are on the cash crop field (Corn-Soybean-Winter Wheat) (DP1:19.8 mg/L, DP2:17.8, DP3: 15.4) and in between are the bank/bed DPs (DP5:11.0 mg/L, DP6: 10.6, DP7: 10.6 (Figure 5A). Elevated levels of NO_3-N in shallow groundwater can be linked to fertilization under high water inputs, such as the case with irrigation (Su et al., 2022). While the HR site fields are not irrigated, as is the case with the majority of operations within the LWC catchment, the associated shallow GW levels also appear to correspond to surface inputs from precipitation (rain and snow), as highlighted by the increase in apparent noise of the timeseries where the water table is nearer to the surface (Figure 4). The delay time difference between stream stage (S6) and GW levels at the HR Site, where DP4 responds before S6 and DP3 responds after, may, in-part, be due to different land usage. Rapid (sub-daily delay) shallow groundwater verses stream response to precipitation events have been shown to vary in a small subcatchment, with GW responding before or after depending on land use (Gootman and Hubbart, 2021). The implication being that local land use can notably change response to precipitation and should be considered for assessing response to non-point source contaminants. However, more events than those captured in this study would be needed to draw a stronger connection to land use specifically, as differences in slope and relative location to S6 are present.

The shallow groundwater below a corn-soybean-winter wheat rotational field (Figure 1) averaged between 15–19 mg/L (DP1-3) and the groundwater in the nearby stream between 10–11 mg/L (DP5,7), while the tributary (S6) averaged 5 mg NO_3-N/L (Figure 5B). The difference between the average groundwater and surface water at the HR Site may be the result of water contributions from the shallow GW on the alfalfa field (1.40 mg/L at DP4) or deeper groundwater from further away (e.g., MAD averaging 2.2 mg/L) discharging to Landon's Creek, causing a dilution. Alternatively, the difference may, in part, be due to the shallow GW and SW being transported through a wetland area (Figure 3C), as retention in the hyporheic zone via denitrification is a possibility (Boulton et al., 2010; Lefebvre et al., 2024).

5.2.3 Geochemical and biogenic factors

Over the course of the study, it was noted that Landon's Creek had a pattern of downstream increase of NO_3-N, implying the ability of the stream to retain nitrogen is less than the overall contribution, a common situation in groundwater fed streams near cropped fields (Hill, 2023). As the water travels downstream in Landon's Creek the average concentration increases from 4.0 to 5.5 mg/L. In contrast, Whitemans Creek holds a relatively constant average of 4.1 mg/L between the inlet and the outlet (S1-5, Figure 5). Since the discharge also increases, either groundwater or surface water necessarily contributes to the stream flow. If the surface water from other small streams act similarly to Landon's Creek, then Whitemans Creek must either be retaining NO_3-N, receiving discharge from the lower parts of the aquifer (i.e., PGMN1, MAD, LPD), or some combination to maintain a constant NO_3-N at the outlet when contributing SW is higher.

The scientific literature shows that the presence of wetlands can contribute to reduce non-point source pollutant loading to groundwater and surface water (Nsenga Kumwimba et al., 2023; Ranalli and Macalady, 2010; Walton et al., 2020). Natural attenuation of NO_3-N occurs mainly via denitrification, but plant assimilation, and microbial immobilization can also play a role, all of which can vary with location, season, hydrogeology. Some recent studies focused on small groundwater-fed wetlands used 222Rn as a natural tracer to delineate water source (Lefebvre et al., 2024), or in-stream high-frequency NO_3-N sampling (Crossley et al., 2025). They demonstrate both the potential for retention and the many simultaneous factors (e.g., temporal changes in geochemical conditions for denitrification or storm intensity) affecting this retention. Lefebvre et al. (2024) found that 80% of groundwater entering a small stream was via the wetland flow, where denitrification and plant assimilation can occur. In the current study, beavers were observed to create dams which flooded the HR site, something which potentially can decrease NO_3-N downstream transport and increase nutrient storage (Larsen et al., 2021). Here, the experimental methods were not designed to highlight these effects, but the presence of a riparian wetland inhabited by beavers in the HR site may decrease NO_3-N concentrations in the shallow groundwater of DP5-7 and in Landon's Creek (S6-8). However, beaver activity on Landon's Creek may also negatively impact nearby farms through flooding and the coldwater species through water temperature increase associated with stream bank deterioration.

5.3 Advantages and limitations of the sampling methods addressing various spatiotemporal scales

Each of the three methods used for characterizing NO_3-N in the LWC watershed under varying conditions had advantages and limitations, as described below (see summary in Table 5). The monthly sampling methods allowed for a regional spatial scale assessment and a low-frequency temporal scale assessment of NO_3-N concentrations within the subcatchment. Some visible seasonal trends and relationships to land use can be assessed with these methods (Figure 4), but the low frequency does not allow for event-based assessment. However, this method is important for contextualizing water dynamics when using higher frequency methods such as the ISCO or SUNA/EXO. Supplementation of the monthly NO_3-N samples with groundwater level, precipitation, and discharge at the outlet helped to highlight seasonal trends (Figure 4). Use of discharge was restricted to the outlet due to complications creating stage-discharge rating curves with stream levels recorded at the inlet and HR site. These difficulties stemmed from beavers damming the creek (downstream of S6 and upstream of Inlet) and subsequent clearing by farmers whose fields were being flooded.

TABLE 5 Comparison of sampling methods conducted during the research period.

Method	Monthly sampling	ISCO	SUNA/EXO
Situation	Contextualizing the broader catchment over longer periods of time. Surface water and groundwater	Storm events Surface water only	Storm events Surface water only
Reliability	Conditions on collection day and related impacts difficult to quantify.	Not measured *in-situ* (delay between collection and processing)	Fouling and technical failure, expensive and large equipment may be targets for vandalism.
Temporal	Very coarse (once per month but continually over 3 years)	Can be very fine but limited in number of total samples that can be taken (24)	Very fine (15–60 min intervals)
Spatial	Throughout the 65 km^2 subcatchment at 8 SW and 13 GW sites.	Immediate – only one location was possible per storm event as only one ISCO was available	Coarse distribution with only 3 stations – inlet, outlet, and one centrally located on a tributary
Cost	High cost per sample but distributed over a long period of time.	High cost per sample over a short period of time – over 1–2 days of a storm event.	Very high upfront costs for complex equipment but low operational and post-processing cost.
Collection	Significant manual effort requiring 12 h of fieldwork by two researchers, but only occurring monthly.	Significant manual effort requiring one research in the field multiple days in a row to conduct set up, sample collection, and in-field post processing. The need for repeated storm event capture increases the associated effort with this method.	Very low manual effort when sampling, requiring only initial installations and monthly checks and calibrations.
Analysis	Smaller datasets cannot differentiate between outliers and typical variation due to antecedent conditions without many years of data, inter-year trends may be deducible if long enough study period taken place.	Reasonable quantity of data per storm and prompt assessment of sampling errors (i.e., equipment failure can be noted when samples are collected) allows for data reliability to be assessed quickly for each event.	Very large datasets, difficult to "clean" for unknown facts as sensors are not monitored throughout storm events (e.g., sediment build-up, equipment failures)

Semi-automatic sampling of events, using the ISCO autosampler, were more reliable for capturing a whole precipitation event (i.e., less susceptible to sediment fouling than the SUNA/EXO station), but the total number of samples that could be taken was limited and the time invested for each storm event campaign was significantly greater than the SUNA/EXO station. In this study, 24 samples were taken at 2-h intervals over the storm and collected at a later point, rather than *in situ*. Potential for negative impacts using the method (e.g., biofilm build-up in the intake line; Koopman et al., 1989) can be a concern but a recent report showed that this study offered optimal conditions for its use (i.e., small watershed, targeted event, short duration etc.) (Wilson et al., 2024). Nevertheless, time invested for each storm event campaign was significantly greater than the SUNA/EXO station.

The SUNA/EXO stations provided high frequency data, allowing for many paths of inquiry into the stream and, when paired with groundwater logger data, shallow groundwater dynamics. However, in the stream environments in which the SUNAs and EXOs were installed two distinct issues arose: 1) power failure and 2) impacts of sediment transport. Firstly, all three riparian locations available for installation of the sites were forested which reduced the efficiency of the solar panels while at the HR site the battery to be manually recharged and changed frequently. Additionally, failure of the batteries themselves was common (e.g., Figure 10: the inlet instruments during this period failed to record stream temperature while the outlet instrument was only operational during daylight hours, due to internal battery failure and solar panel charging failures respectively). Secondly, sediment transport in the stream was found to be important, rendering readings from the sensors unreliable at times. In particular, storm events fouled the equipment quickly, playing a role in the number of usable events captured (e.g., Figure 9A: NO_3-N signal measured by the SUNA degrade following peak in stream level after a storm in May 2024). Both issues can be addressed by either 1) increasing the manual effort or 2) increasing costs. Manually cleaning sediment once every 2 weeks and after significant storm events reduced long periods of lost data. Installation of wipers and back-up power systems would increase system costs but reduce manual efforts. The benefits of high-frequency sampling to capture storm events are increasingly being discussed (Pellerin et al., 2016; Rozemeijer et al., 2025). These challenges are known and reported in the literature (e.g., power loss/ice, Wollheim et al., 2017; sediment build-up; Crossley et al., 2025; Miller et al., 2017).

5.4 Study limitations

The study focused on varying temporal and spatial sampling scales for NO_3-N within an agricultural subcatchment with a focus on understanding storm events. Monthly grab sampling and ISCO sampling targeted water quality parameters and major anions. If the study had been conducted for a longer period, an index-based method, such as the one suggested by Ascott et al. (2017b) to associate precipitation events with groundwater flooding, could be potentially used for shallow groundwater NO_3-N concentrations and precipitation. Also, tracer methods using isotopes (e.g., stable isotopes of water, radon) were not assessed, but have been shown in other studies to provide valuable information regarding NO_3-N transport and should be considered in more detail for future studies (Jafari et al., 2021; Lefebvre et al., 2013; Nikolenko et al., 2018; Sukanya et al., 2022). The role of wetlands as nature-based solutions that contribute to the natural attenuation of nitrate needs to be investigated further.

The importance of tributary contribution of NO_3-N to the main creek were drawn from sampling focused on a single tributary, Landon's Creek. In the subcatchment, there are many smaller

tributaries and two larger tributaries (Schofield Drain and Lewis Drain, northwest and southwest respectively) of similar scale to Landon's Creek (Figure 2). The scope of the project did not include assessing multiple tributaries. However, differences in each due to location, soils, and topography would likely reveal differences in response and comparative studies would likely provide additional depth to conclusions. Additionally, the south side of the catchment, while showing similar hydrogeological characteristics (i.e., water table depth and material), would require further investigation since limited spatial groundwater sampling was done there.

Finally, the large datasets from high frequency sampling have the potential to reveal useful patterns in transport dynamics but can demand complex data analysis methods for cleaning and interpretation. Here, visual interpretation of spatiotemporal trends was performed. Further applications of such high frequency chemical datasets, such as with stream baseflow separation with a focus on nutrient transport (Miller et al., 2017), could better inform the relationship of loading to storm events. Significant gaps in datasets complicate such efforts, but methods for filling in gaps using predictive machine learning models could be investigated further to address the shortcomings (Crossley et al., 2025; Elsayed et al., 2024; Jones et al., 2022). Numerical models, such as SWAT-MODLFOW-RT3D (e.g., Wei et al., 2019) or HydroGeoSphere (e.g., Saleem et al., 2020), can be developed for specific sites and calibrated, using what data has been collected, to model spatiotemporal variability and test the watershed under controlled conditions.

6 Conclusion

This study has assessed NO_3-N transport in a sandy sub-catchment of an agriculturally intense region in southwestern Ontario through monthly and storm event sampling while evaluating data collection methods. The field-based study in the Lower Whitemans Creek sub-catchment used three water quality monitoring methods (monthly sampling, 2-h autosampling, and *in situ* multiparameter instruments) varying at different spatial scales and frequency between October 2021 and November 2024 and compared these parameters with hourly records of precipitation, discharge, GW and SW water levels, as well as water and atmospheric temperature.

The results showed that groundwater-fed streams can contribute NO_3-N to the main creek, indicating the need to find ways to reduce loading. The results also show that targeted storm sampling of NO_3-N and water level monitoring may be helpful to quantify this NO_3-N loading. High frequency sampling using autosamplers (such as the ISCO or SUNA/EXO) has been shown to be useful to capture storm-related transport of NO_3-N, but some issues were identified with data collection. ISCO sampling is more time intensive but, due to the nature of collection and relative simplicity of method, the technology was found to be more reliable. In contrast, the complexity of the SUNA/EXO systems can readily collect the extensive datasets needed to assess many storm events; however, this can lead to noisy data and frequent maintenance issues, causing assessment of results to be difficult.

Bringing to the forefront some of the complications associated with sampling in an open system is a major implication of this study. This showcasing of methods for targeted storm event sampling, highlighting the advantages and disadvantages of the different approaches, needs to be emphasized for greater explanatory power of results to be achieved. The best sampling technique necessarily depends on study objective, but also depends on land use, geology, and meteorology, among other factors presenting unique conditions. Using data collection methods best suited to assess NO_3-N concentration in surface and groundwater in rural areas, especially related to high-intensity rain events, should be a crucial component of any study to optimize field sampling campaigns, post treatment of datasets, and accounting for data uncertainty. Ultimately, more adapted techniques will lead to better understanding of the factors impacting NO_3-N mitigation in agricultural settings. These techniques will thus contribute to identifying approaches to reduce loading and enhance natural attenuation to the advantage of the human population and of the ecosystems.

Data availability statement

The datasets presented in this article are not readily available because the raw data supporting the conclusions of this article will be made available by the authors, without undue reservation. Requests to access the datasets should be directed to czeuner@uoguelph.ca.

Author contributions

CZ: Writing – original draft, Writing – review and editing, Formal Analysis, Methodology, Conceptualization, Investigation, Data curation. JL: Project administration, Validation, Supervision, Writing – review and editing, Funding acquisition, Conceptualization, Resources. ML: Supervision, Writing – review and editing, Funding acquisition, Project administration, Validation, Resources, Conceptualization.

Funding

The author(s) declare that financial support was received for the research and/or publication of this article. Ontario Agri-Food Innovation Alliance, Ontario Graduate Scholarship.

Acknowledgments

The authors would like to thank the Grand River Conservation Authority, specifically Sonja Strynatka, Jeff Pitcher, and Tim Patterson, who helped significantly with data access and collection, and Ryan Smith and Joanne Rykes from the School of Engineering, University of Guelph, for problem solving and laboratory support. And a special thank you to Floyd and Kim Davis for the invaluable support throughout the whole project. The authors wish to explicitly thank ClimateData.ca for providing the climate information used in this paper. ClimateData.ca was created through a collaboration between the Pacific Climate Impacts Consortium (PCIC), Ouranos Inc., the Prairie Climate Centre

(PCC), Environment and Climate Change Canada (ECCC) Centre de Recherche Informatique de Montréal (CRIM) and Habitat7.

Conflict of interest

The authors declare that the research was conducted in the absence of any commercial or financial relationships that could be construed as a potential conflict of interest.

Generative AI statement

The author(s) declare that no Generative AI was used in the creation of this manuscript.

Any alternative text (alt text) provided alongside figures in this article has been generated by Frontiers with the support of artificial intelligence and reasonable efforts have been made to ensure accuracy, including review by the authors wherever possible. If you identify any issues, please contact us.

Publisher's note

All claims expressed in this article are solely those of the authors and do not necessarily represent those of their affiliated organizations, or those of the publisher, the editors and the reviewers. Any product that may be evaluated in this article, or claim that may be made by its manufacturer, is not guaranteed or endorsed by the publisher.

Supplementary material

The Supplementary Material for this article can be found online at: https://www.frontiersin.org/articles/10.3389/fenvs.2025.1641345/full#supplementary-material

References

Abascal, E., Gómez-Coma, L., Ortiz, I., and Ortiz, A. (2022). Global diagnosis of nitrate pollution in groundwater and review of removal technologies. *Sci. total Environ.* 810, 152233. doi:10.1016/j.scitotenv.2021.152233

Acton, C. J. (1989). *The soils of brant county*. Guelph: Ontario Institute of Pedology.

Acton, D. F., Alley, N. F., Baril, R., Day, J. H., Fulton, R. J., Heringa, P. K., et al. (1998). "Landform classification," in *The Canadian system of soil classification*. Editor R. H. Haynes Third Edition (Ottawa, ON: NRC Research Press) 161–178.

Agriculture and Agri-Food Canada (AAFC) (2023). *Data from: annual crop inventory, 2023*. Ottawa, ON, Canada: Government of Canada. Available online at: https://open.canada.ca/data/en/dataset/ba2645d5-4458-414d-b196-6303ac06c1c9 (Accessed September 17, 2023).

Allan, R. P., Barlow, M., Byrne, M. P., Cherchi, A., Douville, H., Fowler, H. J., et al. (2020). Advances in understanding large-scale responses of the water cycle to climate change. *Annals of the New York Academy of Sciences*, 1472 (1), 49–75. doi:10.1111/nyas.14337

Anderson, M. (2021). Water quality board report GM-01-21-04. Available online at: https://www.grandriver.ca/our-watershed/water/surface-water-resources/surface-water-quality/ (Accessed February 26, 2025).

Arce-Rodriguez, J. (2024). *Nitrogen dynamics conceptualization in a sand plain aquifer in the Lake Erie Basin*. Guelph (ON): University of Guelph.

Ascott, M. J., Gooddy, D. C., Wang, L., Stuart, M. E., Lewis, R. S., Ward, R. S., et al. (2017a). Global patterns of nitrate storage in the vadose zone. *Nat. Commun.* 8, 1416. doi:10.1038/s41467-017-01321-w

Ascott, M. J., Marchant, B. P., Macdonald, D., McKenzie, A., and Bloomfield, J. (2017b). Improved understanding of spatio-temporal controls on regional scale groundwater flooding using hydrograph analysis and impulse response functions. *Hydrol. Process.* 31 (25), 4586–4599. doi:10.1002/hyp.11380

Bajc, A. F., and Dodge, J. E. P. (2011). Three-dimensional mapping of surficial deposits in the Brantford– Woodstock area, southwestern Ontario. *Groundw. Resour. Study* 10. Available online at: https://www.geologyontario.mines.gov.on.ca/publication/GRS010 (Accessed September 11, 2023).

Bhatti, A. Z., Farooque, A. A., Li, Q., Abbas, F., and Acharya, B. (2021). Spatial distribution and sustainability implications of the Canadian groundwater resources under changing climate. *Sustainability* 13 (17), 9778. doi:10.3390/su13179778

Biagi, K. M., Ross, C. A., Oswald, C. J., Sorichetti, R. J., Thomas, J. L., and Wellen, C. C. (2022). Novel predictors related to hysteresis and baseflow improve predictions of watershed nutrient loads: an example from Ontario's lower Great Lakes basin. *Sci. Total Environ.* 826, 154023. doi:10.1016/j.scitotenv.2022.154023

Bosse, K. R., Fahnenstiel, G. L., Buelo, C. D., Pawlowski, M. B., Scofield, A. E., Hinchey, E. K., et al. (2024). Are harmful algal blooms increasing in the Great lakes? *Water (Basel)* 16 (14), 1944. doi:10.3390/w16141944

Boulton, A. J., Datry, T., Kasahara, T., Mutz, M., and Stanford, J. A. (2010). Ecology and management of the hyporheic zone: stream-groundwater interactions of running waters and their floodplains. *J. North Am. Benthol. Soc.* 29 (1), 26–40. doi:10.1899/08-017.1

Canadian Centre for Climate Services (CCCS) (2024). *Data from: climate data extraction tool*. Ottawa, ON, Canada: Government of Canada. Available online at: https://climate-change.canada.ca/climate-data/#/ (Accessed September 30, 2024).

Canadian Council of Ministers of the Environment (CCME) (2012). "Nitrate ion," in *Canadian water quality guidelines for the protection of aquatic life* (Winnipeg: Canadian Council of Ministers of the Environment). Available online at: https://www.ccme.ca/en/resources/canadian_environmental_quality_guidelines#.

Canadian Council of Ministers of the Environment (CCME) (2017). "CCME water quality index, user's manual – 2017 update," in *Canadian environmental quality guidelines, 1999* (Winnipeg: Canadian Council of Ministers of the Environment). Available online at: https://www.ccme.ca/en/resources/canadian_environmental_quality_guidelines#.

Canadian Soil Information Service (CanSIS) (2014). *Data from: detailed soil survey (DSS) compilations*. Ottawa, ON, Canada: Government of Canada. Available online at: https://sis.agr.gc.ca/cansis/nsdb/dss/v3/index.html (Accessed May 8, 2025).

Castaño-Sánchez, A., Hose, G. C., and Reboleira, A. S. P. (2020). Ecotoxicological effects of anthropogenic stressors in subterranean organisms: a review. *Chemosphere* 244, 125422. doi:10.1016/j.chemosphere.2019.125422

Chapman, L. J., and Putman, D. F. (1984). The physiography of southern Ontario; Ontario geological survey, special volume 2. Toronto, ON: Ontario Ministry of natural resources. Available online at: https://www.geologyontario.mines.gov.on.ca/publication/SV02.

Chapman, L. J., and Putnam, D. F. (2007). Data from: physiography of southern Ontario MRD228. Ontario.ca. Available online at: https://www.geologyontario.mines.gov.on.ca/publication/MRD228 (Accessed February 19, 2025).

Costa, D., Sutter, C., Shepherd, A., Jarvie, H., Wilson, H., Elliott, J., et al. (2022). Impact of climate change on catchment nutrient dynamics: insights from around the world. *Environ. Rev.* 31, 4–25. doi:10.1139/er-2021-0109

County of Brant (2023). A Simple Grand plan: the official plan for the country of brant. Available online at: https://www.brant.ca/en/planning-and-Development/official-plan.aspx (Accessed June 3, 2025).

Crossley, L. M., MacQuarrie, K. T. B., and Danielescu, S. (2025). Agricultural nitrate attenuation in a small groundwater-influenced wetland system. *Front. Environ. Sci.* 13, 1513704. doi:10.3389/fenvs.2025.1513704

Crossman, J., and Weisener, C. (2020). "Contaminants of the Great lakes," in *The handbook of environmental chemistry*. Editors D. Barceló and A. G. Kostianoy (Springer Chem), 101. doi:10.1007/978-3-030-57874-9

Cuartero, M., and Crespo, G. A. (2018). All-solid-state potentiometric sensors: a new wave for *in situ* aquatic research. *Curr. Opin. Electrochem* 10, 98–106. doi:10.1016/j.coelec.2018.04.004

Dunham, M. (1945). *Grand River*. Toronto, ON: McClelland and Stewart.

Earthfx (2018). Whitemans creek tier three local area water budget and risk assessment: risk assessment report. Available online at: https://www.sourcewater.ca/source-protection-areas/grand-river-source-protection-area/grand-river-water-budget-studies/whitemans-creek-tier-3/ (Accessed July 30, 2024).

Elsayed, A., Rixon, S., Levison, J., Binns, A., and Goel, P. (2024). Machine learning models for prediction of nutrient concentrations in surface water in an agricultural watershed. *J. Environ. Manage.* 372, 123305. doi:10.1016/j.jenvman.2024.123305

Elsayed, A., Levison, J., Binns, A., Larocque, M., and Goel, P. (2025). Regression-based machine learning models for nitrate and chloride prediction in surface water in a small

agricultural Sand Plain sub-watershed in southwestern Ontario, Canada. *Front. Environ. Sci.* 13, 1543852. doi:10.3389/fenvs.2025.1543852

Environment and Climate Change Canada (ECCC) (2013). *Water sources: groundwater*. Gatineau, QC, Canada: Government of Canada. Available online at: https://www.canada.ca/en/environment-climate-change/services/water-overview/sources/groundwater.html#sub5 (Accessed December 4, 2021).

Environment and Climate Change Canada (ECCC) (2024). *Water level and flow*. Gatineau, QC, Canada: Government of Canada. Available online at: https://wateroffice.ec.gc.ca/mainmenu/historical_data_index_e.html [Accessed April 30, 2024].

Forrest, T., Cherubini, T., Jeanneret, S., Zdrachek, E., Damala, P., and Bakker, E. (2022). A submersible probe with in-line calibration and a symmetrical reference element for continuous direct nitrate concentration measurements. *Environ. Sci. Process Impacts* 25, 519–530. doi:10.1039/d2em00341d

Gardner, S. G., Levison, J., Parker, B. L., and Martin, R. C. (2020). Groundwater nitrate in three distinct hydrogeologic and land-use settings in southwestern Ontario, Canada. *Hydrogeol. J.* 28, 1891–1908. doi:10.1007/s10040-020-02156-4

Gootman, K. S., and Hubbart, J. A. (2021). Rainfall, runoff and shallow groundwater response in a mixed-use, agro-forested watershed of the northeast, USA. *Hydrol. Process* 35 (8), e14312. doi:10.1002/HYP.14312

Government of Ontario (2017). Data from: well records. Available online at: https://www.ontario.ca/page/well-records (Accessed September 30, 2024).

Grant Ferris, F., Szponar, N., and Edwards, B. A. (2021). "Groundwater microbiology," in *Guelph, ON: the groundwater project*.

Grand River Conservation Authority (GRCA) (2024). Data from: Grand River information network: monitoring data download. *GRCA Open Data License v2.0*. Available online at: https://data.grandriver.ca/downloads.html.

Gyimah, R., Lebu, S., Owusu-Frimpong, I., Semiyaga, S., Salzberg, A., and Manga, M. (2024). Effluents from septic systems and impact on groundwater contamination: a systematic review. *Environ. Sci. Pollut. Res.* 31, 62655–62675. doi:10.1007/s11356-024-35385-1

Health Canada (2013). "Guidelines for Canadian drinking water quality: guideline technical document — nitrate and nitrite," in *Water and air quality bureau, healthy environments and consumer safety branch*. Ottawa, Ontario: Health Canada.

Hill, A. R. (2023). Patterns of nitrate retention in agriculturally influenced streams and rivers. *Biogeochemistry* 163, 155–183. doi:10.1007/s10533-023-01027-w

Irvine, C., Macrae, M., Morison, M., and Petrone, R. (2019). Seasonal nutrient export dynamics in a mixed land use subwatershed of the Grand River, Ontario, Canada. *J. Gt. Lakes. Res.* 45, 1171–1181. doi:10.1016/j.jglr.2019.10.005

Ivey, J. (2024). "GM-06-24-52 water quality in the Grand River watershed-update on nitrates," in *Hybrid meeting of the general membership - general meeting 28 June 2024. Grand River Conservation authority* (Cambridge (ON): GRCA Administration Centre/Zoom Virtual Meeting).

Jafari, T., Kiem, A. S., Javadi, S., Nakamura, T., and Nishida, K. (2021). Using insights from water isotopes to improve simulation of surface water-groundwater interactions. *Sci. Total Environ.* 798, 149253. doi:10.1016/j.scitotenv.2021.149253

Janzen, B. (2018). Geology of the Grand River watershed: an overview of bedrock and quaternary geological interpretations in the Grand River watershed. Available online at: https://www.grandriver.ca/media/vb4p5t0i/watershed-geology_march272019.pdf (Accessed March 7, 2024).

Johnson, K. S., and Coletti, L. J. (2002). *In situ* ultraviolet spectrophotometry for high resolution and long-term monitoring of nitrate, bromide and bisulfide in the ocean. *Deep-Sea Res. I* 49 (7), 1291–1305. doi:10.1016/S0967-0637(02)00020-1

Jones, A. S., Jones, T. L., and Horsburgh, J. S. (2022). Toward automating post processing of aquatic sensor data. *Environ. Model. and Softw.*, 151:105364. doi:10.1016/j.envsoft.2022.105364

Kaltenecker, G. (2023). Data from: provincial (stream) water quality monitoring network (PWQMN). Available online at: https://data.ontario.ca/dataset/provincial-stream-water-quality-monitoring-network.

Kehew, A. E. (2001). "Redox reactions and processes," in *Applied chemical hydrogeology* (Upper Saddle River, N.J.: Prentice Hall), 129–165.

Koopman, B., Stevens, C. M., Logue, C. L., Karney, P., and Bitton, G. (1989). Automatic sampling equipment and bod test nitrification. *Water Res.* 23(12), 1555–1561. doi:10.1016/0043-1354(89)90121-8

Lake Erie Region Source Protection Committee (2025). "County of brant," in *Grand River source protection area approved assessment report* (Cambridge, ON). Available online at: https://www.sourcewater.ca/source-protection-areas/grand-river-source-protection-area/grand-river-assessment-report/ (Accessed June 3, 2025).

Larocque, M., Levison, J., Gagne, S., and Saleem, S. (2019). Groundwater use for agricultural production - current water budget and expected trends under climate change. Final technical report for Quebec-Ontario Cooperation for Agri-Food Research Competition. Guelph, ON: OMAFRA and Québec City, QC: MAPAQ. Available online at: https://www.ouranos.ca/en/projects-publications (Accessed November 29, 2021).

Larsen, A., Larsen, J. R., and Lane, S. N. (2021). Dam builders and their works: beaver influences on the structure and function of river corridor hydrology, geomorphology, biogeochemistry and ecosystems. *Earth-Science Rev.* 218, 103623. doi:10.1016/j.earscirev.2021.103623

Lefebvre, K., Barbecot, F., Ghaleb, B., Larocque, M., and Gagné, S. (2013). Full range determination of ^{222}Rn at the watershed scale by liquid scintillation counting. *Appl. Radiat. Isotopes* 75, 71–76. doi:10.1016/j.apradiso.2013.01.027

Lefebvre, K., Barbecot, F., Larocque, M., Gibert-Brunet, E., Gillon, M., Noret, A., et al. (2024). Using 222Rn to quantify wetlands interflow volume and quality discharging to headwater streams. *Appl. Geochem.* 169, 106037. doi:10.1016/j.apgeochem.2024.106037

Liu, W., Maxwell, B., Birgand, F., Youssef, M., Chescheir, G., and Tian, S. (2019). Multipoint high-frequency sampling system to gain deeper insights on the fate of nitrate in artificially drained fields. *J. Irrigation Drainage Eng.* 146 (1), 06019012. doi:10.1061/(ASCE)IR.1943-4774.0001438

Liu, J., Van Meter, K. J., McLeod, M. M., and Basu, N. B. (2021). Checkered landscapes: hydrologic and biogeochemical nitrogen legacies along the river continuum. *Environ. Res. Lett.* 16 (11), 115006. doi:10.1088/1748-9326/ac243c

Maxwell, M. (2020). PW-20-06 Burford water and wastewater servicing and drainage master plan. Available online at: https://engagebrant.ca/burford-servicing?tool=qanda (Accessed May 5, 2025).

May, H., Rixon, S., Gardner, S., Goel, P., Levison, J., and Binns, A. (2023). Investigating relationships between climate controls and nutrient flux in surface waters, sediments, and subsurface pathways in an agricultural clay catchment of the Great Lakes Basin. *Sci. Total Environ.* 864, 160979. doi:10.1016/j.scitotenv.2022.160979

Miller, M. P., Tesoriero, A. J., Hood, K., Terziotti, S., and Wolock, D. M. (2017). Estimating discharge and nonpoint source nitrate loading to streams from three end-member pathways using high-frequency water quality data. *Water Resour. Res.* 53, 10201–10216. doi:10.1002/2017WR021654

Ministry of the Environment, Conservation and Parks (MECP) (2023). Source protection information atlas. Available online at: https://www.lioapplications.lrc.gov.on.ca/SourceWaterProtection/index.html?viewer=SourceWaterProtection.SWPViewer&locale=en-CA (Accessed April 30, 2023).

Nikolenko, O., Jurado, A., Borges, A. V., Knöller, K., and Brouyère, S. (2018). Isotopic composition of nitrogen species in groundwater under agricultural areas: a review. *Sci. Total Environ.* 621, 1415–1432. doi:10.1016/j.scitotenv.2017.10.086

Nsenga Kumwimba, M., Huang, J., Dzakpasu, M., De Silva, K., Ohore, O. E., Ajibade, F. O., et al. (2023). An updated review of the efficacy of buffer zones in warm/temperate and cold climates: insights into processes and drivers of nutrient retention. *J. Environ. Manage.* 336, 117646. doi:10.1016/j.jenvman.2023.117646

Ontario Ministry of Agriculture, Food and Rural Affairs (2025). Data from: tile drainage area. Ontario GeoHub. Available online at: https://geohub.lio.gov.on.ca/search?tags=agriculture.

Ontario Ministry of Natural Resources (OMNR) (2025). *Aquatic resource area survey point: fisheries section, fish and wildlife branch, natural resources management division. Natural resources values information system*. Peterborough, ON, Canada: Ontario GeoHub. Available online at: https://geohub.lio.gov.on.ca/datasets/lio::aquatic-resource-area-survey-point/about (Accessed May 2, 2025).

Osman, A. R. M. (2017). "Water use conflict: a characterization and water quantity study in an agriculturally stressed subcatchment in Southwestern Ontario,". Guelph (ON): University of Guelph.

Pattrick, E., Levison, J., Binns, A., Larocque, M., and Goel, P. (2024). "Examining phosphorous transport and groundwater-surface water interactions in a Great Lakes Basin setting," in *GeoMontreal 2024 - 77th Canadian geotechnical conference and the 16th joint CGS/IAH-CNC groundwater conference. Hotel bonaventure, 15-18 september* (Montreal, QC: Karma-Link Management Services Ltd. and X-CD Technologies Inc).

Pellerin, B. A., Stauffer, B. A., Young, D. A., Sullivan, D. J., Bricker, S. B., Walbridge, M. R., et al. (2016). Emerging tools for continuous nutrient monitoring networks: Sensors advancing science and water resources protection. *J. Am. Water Resour. Assoc.* 52 (4), 993–1008. doi:10.1111/1752-1688.12386

Pohle, I., Baggaley, N., Palarea-Albaladejo, J., Stutter, M., and Glendell, M. (2021). A framework for assessing concentration-discharge catchment behavior from low-frequency water quality data. *Water Resour. Res.* 57, e2021WR029692. doi:10.1029/2021WR029692

Ranalli, A. J., and Macalady, D. L. (2010). The importance of the riparian zone and in-stream processes in nitrate attenuation in undisturbed and agricultural watersheds - a review of the scientific literature. *J. Hydrol.* 389, 406–415. doi:10.1016/j.jhydrol.2010.05.045

Reville, F. D. (1883). "Part III: county of brant," in *The history of the county of brant, Ontario* (Toronto, ON: Warner, Beers, and Co), 147–249.

Richards, G., Gilmore, T. E., Mittelstet, A. R., Messer, T. L., and Snow, D. D. (2021). Baseflow nitrate dynamics within nested watersheds of an agricultural stream in Nebraska, USA. *Agric. Ecosyst. Environ.* 308, 107223. doi:10.1016/j.agee.2020.107223

Rivett, M. O., Buss, S. R., Morgan, P., Smith, J. W. N., and Bemment, C. D. (2008). Nitrate attenuation in groundwater: a review of biogeochemical controlling processes. *Water Res.* 42 (16), 4215–4232. doi:10.1016/j.watres.2008.07.020

Rixon, S., May, H., Persaud, E., Elsayed, A., Levison, J., Binns, A., et al. (2024). Subsurface influences on watershed nutrient concentrations and loading in a clay

dominated agricultural system. *J. Hydrol.* 645, 132140. doi:10.1016/j.jhydrol.2024.132140

Robertson, W. (2021). Septic system impacts on groundwater quality. *Guelph, Groundw. Proj.*

Rozemeijer, J., Jordan, P., Hooijboer, A., Kronvang, B., Glendell, M., Hensley, R., et al. (2025). Best practice in high-frequency water quality monitoring for improved management and assessment; a novel decision workflow. *Environ. Monit. Assess.* 197, 353. doi:10.1007/s10661-025-13795-z

Saccò, M., Mammola, S., Altermatt, F., Alther, R., Bolpagni, R., Brancelj, A., et al. (2024). Groundwater is a hidden global keystone ecosystem. *Glob. change Biol.* 30 (1), 17066. doi:10.1111/gcb.17066

Saleem, S., Levison, J., Parker, B., Martin, R., and Persaud, E. (2020). Impacts of climate change and different crop rotation scenarios on groundwater nitrate concentrations in a sandy aquifer. *Sustainability* 12 (3), 1153. doi:10.3390/SU12031153

Seabird Scientific (2024). User manual SUNA V2 submersible ultraviolet nitrate analyzer - revision J. Available online at: https://www.seabird.com/nutrient-sensors/suna-v2-nitrate-sensor/family-downloads?productCategoryId=54627869922 (Accessed July 7, 2024).

Shabaga, J. A., and Hill, A. R. (2010). Groundwater-fed surface flow path hydrodynamics and nitrate removal in three riparian zones in southern Ontario, Canada. *J. Hydrol.* 388, 52–64. doi:10.1016/j.jhydrol.2010.04.028

Shephard, M. W., Mekis, E., Morris, R. J., Feng, Y., Zhang, X., Kilcup, K., et al. (2014). Trends in Canadian short-duration extreme rainfall: including an intensity–duration–frequency perspective. *Atmosphere-Ocean* 52 (5), 398–417. doi:10.1080/07055900.2014.969677

Shifflett, S., Kovacs, H., and Wong, A. (2014). Agricultural irrigation: forecasts for future water needs. *Grand River Watershed Water Manag. Plan. Camb. Grand River Conservation Auth.* Available online at: https://www.grandriver.ca/our-watershed/water/water-management-plan/studies-and-reports/.

Speir, S. L., Tank, J. L., Bieroza, M., Mahl, U. H., and Royer, T. V. (2021). Storm size and hydrologic modification influence nitrate mobilization and transport in agricultural watersheds. *Biogeochemistry* 156, 319–334. doi:10.1007/s10533-021-00847-y

Statistics Canada (2023). Data from: census profile, 2021 census of population. *Stat. Can. Cat. No. 98-316-X2021001*. Available online at: https://www12.statcan.gc.ca/census-recensement/2021/dp-pd/prof/index.cfm?Lang=E (Accessed August 12, 2025).

Stumm, W., and Morgan, J. J. (1996). "Oxidation and reduction; equilibria and microbial mediation," in *Aquatic chemistry: chemical equilibria and rates in natural waters, environmental science and technology* (New York, NY: Wiley), 425–515.

Su, F., Wu, J., Wang, D., Zhao, H., Wang, Y., and He, X. (2022). Moisture movement, soil salt migration, and nitrogen transformation under different irrigation conditions: field experimental research. *Chemosphere* 300, 134569. doi:10.1016/j.chemosphere.2022.134569

Sukanya, S., Noble, J., and Joseph, S. (2022). Application of radon (222Rn) as an environmental tracer in hydrogeological and geological investigations: an overview. *Chemosphere* 303 (3), 135141. doi:10.1016/j.chemosphere.2022.135141

United Nations (2022). *The united Nations world water development report 2022: groundwater: making the invisible visible*. Paris: UNESCO.

Venkiteswaran, J. J., Schiff, S. L., and Ingalls, B. P. (2019). Quantifying the fate of wastewater nitrogen discharged to a Canadian river. *Facets* 4 (1), 315–335. doi:10.1139/facets-2018-0028

Walton, C. R., Zak, D., Audet, J., Petersen, R. J., Lange, J., Oehmke, C., et al. (2020). Wetland buffer zones for nitrogen and phosphorus retention: impacts of soil type, hydrology and vegetation. *Sci. Total Environ.* 727, 138709. doi:10.1016/j.scitotenv.2020.138709

Wang, Y., Yuan, S., Shi, J., Ma, T., Xie, X., Deng, Y., et al. (2023). Groundwater quality and health: making the invisible visible. *Environ. Sci. and Technol.* 57 (13), 5125–5136. doi:10.1021/acs.est.2c08061

Ward, M. H., Jones, R. R., Brender, J. D., de Kok, T. M., Weyer, P. J., Nolan, B. T., et al. (2018). Drinking water nitrate and human health: an updated review. *Int. J. Environ. Res. Public Health* 15 (7), 1557. doi:10.3390/IJERPH15071557

Watson, S. B., Miller, C., Arhonditsis, G., Boyer, G. L., Carmichael, W., Charlton, M. N., et al. (2016). The re-eutrophication of Lake Erie: harmful algal blooms and hypoxia. *Harmful Algae* 56, 44–66. doi:10.1016/j.hal.2016.04.010

Wei, X., Bailey, R. T., Records, R. M., Wible, T. C., and Arabi, M. (2019). Comprehensive simulation of nitrate transport in coupled surface-subsurface hydrologic systems using the linked SWAT-MODFLOW-RT3D model. *Environmental Modelling & Software* 122, 104242. doi:10.1016/j.envsoft.2018.06.012

Williams, M. R., King, K. W., and Fausey, N. R. (2015). Contribution of tile drains to basin discharge and nitrogen export in a headwater agricultural watershed. *Agric. Water Manag.* 158, 42–50. doi:10.1016/J.AGWAT.2015.04.009

Wilson, T. P., Miller, C. V., Lechner, E. A., and Survey, U. S. G. (2024). "Guidelines for the use of automatic samplers in collecting surface-water quality and sediment data," in *Techniques and methods 1-D12* (Reston, VA: U.S. Geological Society). doi:10.3133/tm1D12

Wollheim, W. M., Mulukutla, G. K., Cook, C., and Carey, R. O. (2017). Aquatic nitrate retention at river network scales across flow conditions determined using nested *in situ* sensors. *Water Resour. Res.* 53 (11), 9740–9756. doi:10.1002/2017WR020644

World Health Organization (2021). *A global overview of national regulations and standards for drinking-water quality*. second edition. Geneva: Licence: CC BY-NC-SA 3.0 IGO. Available online at: https://www.who.int/publications/i/item/9789240023642 (Accessed July 25, 2025).

Xylem, Y. S. I. (2020). EXO user manual: advanced water quality monitoring platform. *YSI, a Xylem brand. 603789REF Revis. K.*

Zhi, W., and Li, L. (2020). The shallow and deep hypothesis: subsurface vertical chemical contrasts shape nitrate export patterns from different land uses. *Environ. Sci. Technol.* 54 (19), 11915–11928. doi:10.1021/acs.est.0c01340

frontiers | Frontiers in Environmental Science

TYPE Original Research
PUBLISHED 28 March 2025
DOI 10.3389/fenvs.2025.1543852

Check for updates

OPEN ACCESS

EDITED BY
Hossein Tabari,
University of Antwerp, Belgium

REVIEWED BY
Balaji Etikala,
Yogi Vemana University, India
Paweł Tomczyk,
Wroclaw University of Environmental and Life Sciences, Poland

*CORRESPONDENCE
Ahmed Elsayed,
aelsay03@uoguelph.ca

RECEIVED 12 December 2024
ACCEPTED 17 March 2025
PUBLISHED 28 March 2025

CITATION
Elsayed A, Levison J, Binns A, Larocque M and Goel P (2025) Regression-based machine learning models for nitrate and chloride prediction in surface water in a small agricultural sand plain sub-watershed in southwestern Ontario, Canada.
Front. Environ. Sci. 13:1543852.
doi: 10.3389/fenvs.2025.1543852

COPYRIGHT
© 2025 Elsayed, Levison, Binns, Larocque and Goel. This is an open-access article distributed under the terms of the Creative Commons Attribution License (CC BY). The use, distribution or reproduction in other forums is permitted, provided the original author(s) and the copyright owner(s) are credited and that the original publication in this journal is cited, in accordance with accepted academic practice. No use, distribution or reproduction is permitted which does not comply with these terms.

Regression-based machine learning models for nitrate and chloride prediction in surface water in a small agricultural sand plain sub-watershed in southwestern Ontario, Canada

Ahmed Elsayed[1,2]*, Jana Levison[1], Andrew Binns[1], Marie Larocque[3] and Pradeep Goel[4]

[1]School of Engineering, Morwick G360 Groundwater Research Institute, University of Guelph, Guelph, ON, Canada, [2]Irrigation and Hydraulics Department, Faculty of Engineering, Cairo University, Giza, Egypt, [3]Department of Earth and Atmospheric Sciences, Université du Québec à Montréal, Montreal, QC, Canada, [4]Ministry of the Environment, Conservation and Parks, Etobicoke, ON, Canada

Machine learning (ML) models have proven to be an efficient technique for better understanding and quantification of surface water quality, especially in agricultural watersheds where considerable anthropogenic activities occur. However, there is a lack of systematic investigations that can examine the application of different ML regression models in agricultural settings to predict the surface water quality using a group of input variables, including hydrological (e.g., surface flow), meteorological (e.g., precipitation), and field (e.g., crop cover) conditions. In this study, multiple ML regression models, including support vector machine (SVM) and regression trees (RT), were employed on a 2-year dataset collected from a sand plain agricultural sub-watershed in southwestern Ontario, Canada (i.e., Lower Whitemans Creek) to predict the nitrate and chloride concentrations in surface water at nine sampling sites within the sub-watershed. The prediction capabilities of these ML models were determined using a group of evaluation metrics including the coefficient of determination (R^2) and root-mean squared error (RMSE). In general, the Gaussian Process Regression (GPR) model was the optimal algorithm to predict the nitrate and chloride concentrations in surface water (R^2 was 0.99 and 0.98 respectively for training and testing). According to the results of a feature importance analysis, it was found that the field conditions (specifically the location of sampling site (main channel or tributary site) and crop cover) were the most crucial model input variables for accurate predictions of the output variables. This study underscores that ML regression models can be implemented to effectively quantify the water quality properties of surface water in agricultural watersheds using easily measurable parameters. These models can assist decision makers in advancing successful actions and steps towards protecting the available surface water resources.

KEYWORDS

machine learning, nitrate, chloride, surface water quality, agricultural watersheds

1 Introduction

Surface water bodies (e.g., rivers, lakes, and streams) act as primary water resources for many communities, ecosystems, and activities including agriculture, fishing, and recreation (Gorgoglione et al., 2021). However, these systems are highly vulnerable to contamination from multiple natural contributors, including soil erosion, rock weathering, and decomposition of organic matter, and anthropogenic sources such as industrial discharge, urban stormwater, agricultural activities, and untreated wastewater (Akhtar et al., 2021; Marshall et al., 2022; Rixon et al., 2024). In addition, surface runoff from agricultural fields can elevate the concentration of nutrients (i.e., nitrogen and phosphorus species) in surface water due to the application of synthetic and manure-based fertilizers (Ha et al., 2020; Liang et al., 2020). These nutrients can degrade the surface water quality, leading to serious environmental problems such as algal blooms, oxygen depletion and eutrophication (Ahmed and Lin, 2021; Elsayed et al., 2021; Elsayed et al., 2022a). Such degradation of surface water quality has raised global concerns, leading to the establishment of national and international agreements and policies that aim to safeguard the available water resources. For example, the Canadian-U.S. Great Lakes Water Quality Agreement and Canada-Ontario Agreement on Great Lakes Water Quality and Ecosystem Health were issued to highlight the importance of considering the role of nutrient transport and dynamics on the water quality of the Great Lakes (Environment and Climate Change Canada, 2017; Environment and Climate Change Canada, 2021; Ministry of the EnvironmentConservation and Parks, 2021). In general, the obligations from different frameworks and policies are a crucial component of sustainable water resources management and environmental protection, emphasizing the importance of continuous water quality monitoring in watersheds.

Nitrate (NO_3^-) is frequently reported to be exported from agricultural watersheds to surface water because it is highly soluble and mobile in water (Gardner et al., 2020; Elsayed et al., 2023a). Also, it can be easily leached from the soil matrix because it is highly stable and cannot be combined with other pollutants in water (Arabgol et al., 2016; Bedi et al., 2020). In addition, there are multiple contributors of chloride (Cl^-) in agricultural watersheds including both natural (e.g., salts in rocks and soils, and atmospheric deposition) and anthropogenic (e.g., road de-icing salts, and soil fertilizers) sources. High Cl^- levels in agricultural watersheds can adversely affect plant health and soil quality, negatively impacting agricultural yield and long-term soil productivity (Mackie et al., 2022; Syeed et al., 2023). Moreover, elevated Cl^- concentrations in surface water can cause ecological imbalances in aquatic systems such as osmotic stress, acute and chronic toxicity for aquatic organisms (Castiblanco et al., 2023). Thus, NO_3^- and Cl^- concentrations serve as critical indicators for assessing the health of surface water in agricultural watersheds, magnifying the necessity of effective and continuous water quality monitoring of surface water bodies.

Continuous monitoring of these surface water quality parameters is crucial to effectively manage pollution sources and prevent the disruption of biodiversity and surface water quality. By collecting and maintaining advanced datasets on water quality parameters (e.g., NO_3^- and Cl^-), decision makers can implement evidence-based policies and facilitate timely interventions to safeguard water resources (Chow et al., 2020; Persaud et al., 2023). However, conventional monitoring methods, especially in agricultural watersheds, are often limited by multiple challenges associated with sampling and logistical constraints (Bhattarai et al., 2021). For example, regular sampling across large and diverse regions is costly, time-consuming, and labor-intensive. In addition, logistical constraints often limit access to certain areas, especially during winter, heavy rainfall, and snowfall events, resulting in spatial and temporal gaps in water quality datasets. Most water quality parameters (e.g., nutrient and solid concentrations) also require standard laboratory measurement procedures to obtain the final concentrations which are costly, resource-intensive, and time-consuming for obtaining continuous time-series in agricultural watersheds. Such challenges and the need for vigilant water quality management has led to increased attention to innovative monitoring and predictive approaches aided by data-driven techniques using machine learning (ML) models.

Recently, ML models have emerged as a powerful tool to tackle the limitations of traditional surface water sampling and monitoring methods (Pandey et al., 2023). ML regression models can offer a scalable solution to predict water quality parameters using a variety of environmental predictors, such as climatological and hydrological conditions (Kim et al., 2021; Varadharajan et al., 2022). ML models can also effectively compensate for the lack of comprehensive sampling data and offer predictions that support realistic decision-making by imitating complex patterns from historical observations (Imani et al., 2021; Portuguez-Maurtua et al., 2022; Wang X. et al., 2022). Unlike typical mechanistic models, ML models can process extensive and complex datasets with diverse parameters, allowing for high-resolution predictions across both time and space (Elsayed et al., 2022b; Elsayed et al., 2023b). ML models are particularly well adapted to agricultural watersheds where contaminant concentrations are highly variable and influenced by multiple environmental factors.

Previous studies applied different ML regression models (e.g., support vector machine and ensemble models) to predict general surface water quality parameters such as ammoniacal nitrogen and suspended solids concentration (Ahmed et al., 2019), total dissolved solids (Shah et al., 2021), and Carlson's Trophic State Index (i.e., a reservoir water quality index) (Chou et al., 2018). However, few studies reported ML investigations that focused on specific surface water quality parameters, such as NO_3^- and Cl^-, within the unique context of agricultural watersheds under different meteorological, hydrological, and field conditions. Limited studies have focused on engaging ML regression models to describe and predict the water quality conditions in different agricultural watersheds (Jung et al., 2021; Wang S. et al., 2022). Other studies employed multiple ML classification and regression models to quantify nutrient concentrations in surface water in clay agricultural settings (Elsayed et al., 2023b; Elsayed et al., 2024a). Few studies have compared the ability of different individual ML regression models to reproduce field datasets of NO_3^- and Cl^- concentrations from sand plain agricultural watersheds using a range of environmental predictors (e.g., meteorological and field conditions).

Furthermore, many of the previous studies predicted or simulated only a single surface water quality parameter. For

example, multiple ML regression models were employed to only predict the water quality index (WQI) (Asadollah et al., 2021; Kouadri et al., 2021; Khoi et al., 2022), concentration of chlorophyll a (Chang et al., 2021), and total phosphorus (Qiao et al., 2021). Other previous studies used only 1 ML algorithm to predict water quality datasets without considering other potential candidates of ML models for higher prediction accuracy. For example, some previous employed the multiple linear regression (MLR) (Ha et al., 2020; Qun'ou et al., 2021), artificial neural network (ANN) (Imani et al., 2021; Gorgoglione et al., 2021; Balson and Ward, 2022), self-organizing map (Yu et al., 2021), random forest (Wang et al., 2021; Behrouz et al., 2022), and ensemble models (Melesse et al., 2020; Zhang et al., 2022) to predict nutrient concentrations in surface water. This reflects a major knowledge gap about the applicability of different ML regression models and further the selection of optimal models to predict multiple water quality parameters based on systematic comparisons about the performance of these models. Ultimately, limited studies have explored the adaptability of ML models to seasonal and spatial variability in contaminant levels, which is particularly pronounced in agricultural landscapes.

The main objectives of this study are to: (1) examine the interdependence and correlations between different process parameters (e.g., meteorological conditions) and surface water quality (i.e., nitrate-nitrogen (NO_3^--N) and Cl^- concentrations); (2) compare the ability of different ML regression models to predict NO_3^--N and Cl^- concentrations in surface water given a group of input variables (e.g., field conditions); and (3) perform a feature importance analysis on the model input variables to assess their significance on the prediction accuracy of the optimal ML models.

2 Study area and data collection

2.1 Site description

The available dataset was obtained from the Lower Whitemans Creek study area (LWC) which is an agricultural sub-watershed in southwestern Ontario, Canada (Figure 1). The sub-watershed is located near Burford, Ontario in the lower portion of the Whitemans Creek watershed (404 km^2 with a stream order of 6.0). The Whitemans Creek watershed is a tributary of the Grand River watershed (6,700 km^2) in southwestern Ontario. The LWC sub-watershed has an approximate area of 63.5 km^2, and it is dominated by agricultural activities (73% of the total watershed area) including pasture and forages. The main crops in the sub-watershed include corn (36%), soybeans (17%), pasture/forages (15%), and winter wheat (6%) (AAFC, 2023). It should be noted that these percentages of crop cover are determined based on the total watershed area. Elevations in LWC range between 254 and 360 m with an average slope of 3.4% over the entire sub-watershed. The sub-watershed is considered the most water-stressed region with the highest agricultural irrigation demand in the entire Grand River watershed (Wong, 2011; Larocque et al., 2019). The surficial geology is mainly comprised of gravel and sand with limited silt to sandy silt areas in the southwest region. Further details about the site description can be found in previous investigations that intensively studied the sub-watershed (Osman, 2017; Larocque et al., 2019; Arce-Rodriguez, 2024; Zeuner et al., 2025).

2.2 Dataset collection and description

In the current study, the available dataset was collected from five main observation sites that are located along the main channel (S1 to S5, S4 and S5 represents the sub-watershed inlet and outlet) (Figure 1). Also, the dataset was gathered from four observation sites (i.e., TF1 to TF4) that are located on tributaries (Figure 1). More details about the sampling sites, such as distance to the watershed outlet and geographic coordinates, are tabulated in Supplementary Table S1. The sampling campaign extended from October 2021 until the end of December 2023 for the main channel observation sites while the observation period of the tributary sampling sites ranged from August 2022 until the end of December 2023. Surface water was monitored monthly and sampled for water physico-chemical and quality parameters at these nine observation sites. These water physico-chemical parameters included the water temperature, dissolved oxygen (DO), pH, electrical conductivity (EC), and oxidation-reduction potential (ORP). The major surface water quality parameters were also monitored including the NO_3^--N and Cl^-. Daily precipitation was monitored at the Brantford Airport Station that is close to the watershed outlet (approximately 5 km) (ECCC, 2021). The land use and crop cover were obtained from the actual agricultural activities during the observation period within the sub-watershed (AAFC, 2023).

The physico-chemical water parameters (e.g., water temperature and pH) were measured using a handheld multi-parameter instrument (i.e., YSI ProPlus). The surface water samples were collected from the center of the stream at a depth of approximately 0.40 m below the water surface for quantifying the water quality parameters. These water samples were gathered using clean high density polyethylene bottles which were stored on ice and then sent for analysis within a day of sampling. During the analysis of water quality parameters, the samples were filtered using 0.45 µm Fisherbrand Basix Syringe Filters then they were analyzed using a Metrohm Eco IC Ion Chromatograph at the Morwick G360 Groundwater Research Institute laboratory in the University of Guelph. The detection range of NO_3^--N was 0.01–100 mg NO_3^--N/L while the measurement error/detection accuracy was ±0.1 mg NO_3^--N/L. For the Cl^- measurements, the detection range and accuracy were 1–500 mg/L and ±1.0 mg/L, respectively. Precipitation was monitored in the Brantford Airport Station, that is operated by the Environment and Climate Change Canada - Meteorological Service of Canada, using an OTT-Pluvio^2 rain gauge that can measure both the rain- and snow-fall depth and intensity with a detection range of 0.1–200 mm/day and detection accuracy of ±0.2 mm (ECCC, 2021). The air temperature and water levels were measured using FTS THS-3 and Sutron Accubar Bubbler pressure sensors, respectively. The detection range varied between −50°C and 50°C for the air temperature and 0–5 m for the water level. The detection accuracy was ±0.1°C for the air temperature and ±0.5 cm for the water level. More details about the data collection can be obtained from other studies that investigated this sub-watershed (Arce-Rodriguez, 2024; Zeuner et al., 2025).

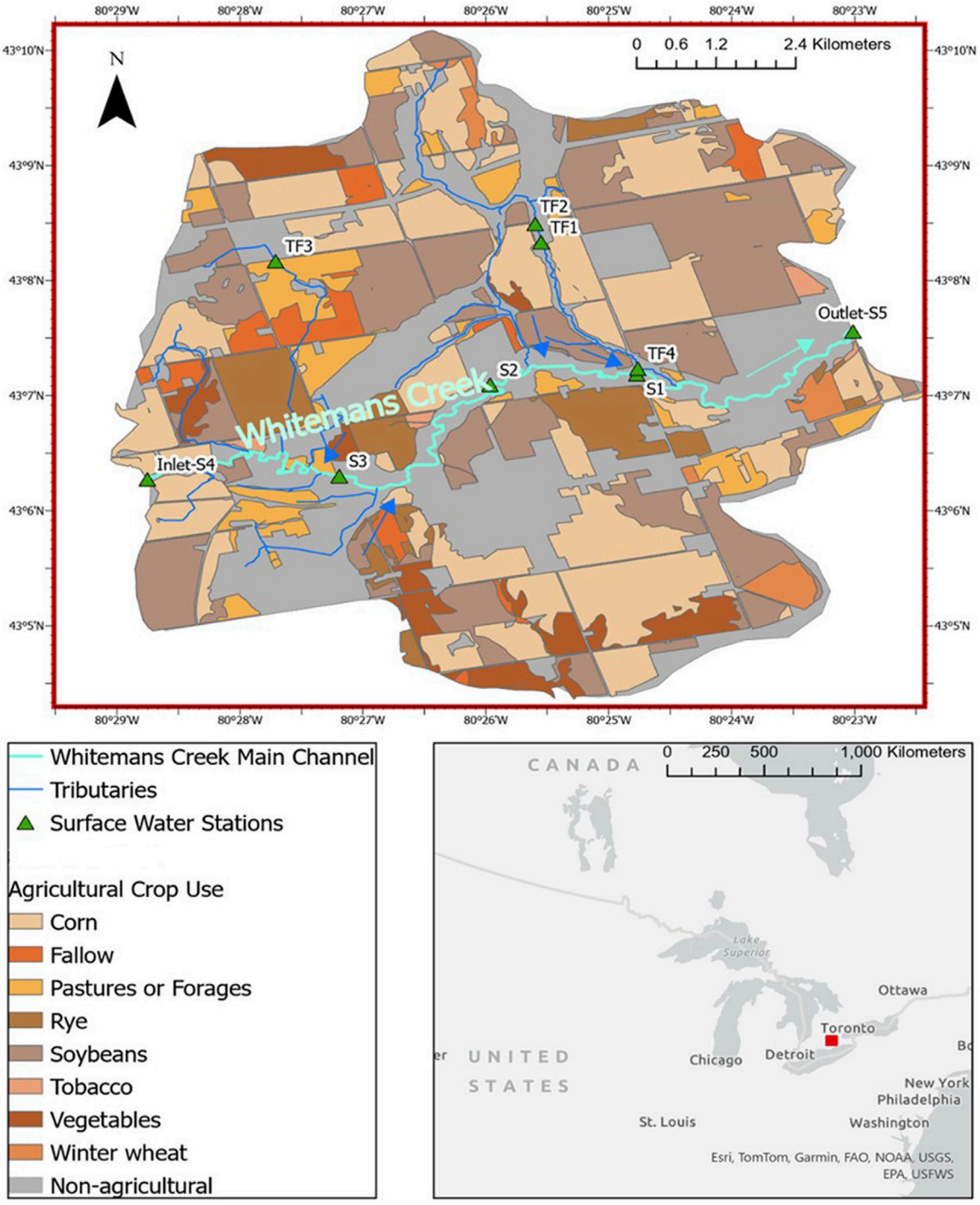


FIGURE 1
The Lower Whitemans Creek (LWC) sub-watershed in southwestern Ontario (Canada) with the five main observation sites on the main water course within the sub-watershed (i.e., S1 to S5) and four tributary observation sites (i.e., TF1 to TF4). The map shows the main river within the sub-catchment (i.e., Whitemans Creek). The background map, spatial data, and crop use were adopted from OpenStreetMap and Agriculture and Agri-Food Canada (AAFC) - Annual Crop Inventory (AAFC, 2023).

2.3 Hydrological and meteorological conditions

During the observation period (i.e., 1 October 2021 to 31 December 2023), the average daily stream flow ranged from 0.35 to 39.5 m^3/s where the average daily stream flow over the observation period was 4.15 m^3/s. The peaks of the stream flow were corresponding to snow-melt events in the winter and/or early spring over the entire observation period (Figure 2). For example, the highest stream flow (i.e., 39.5 m^3/s) was recorded in early spring of 2023 (i.e., the first week of April). Other peak stream flows were observed in March 2022 and 2023, corresponding to snow-melt

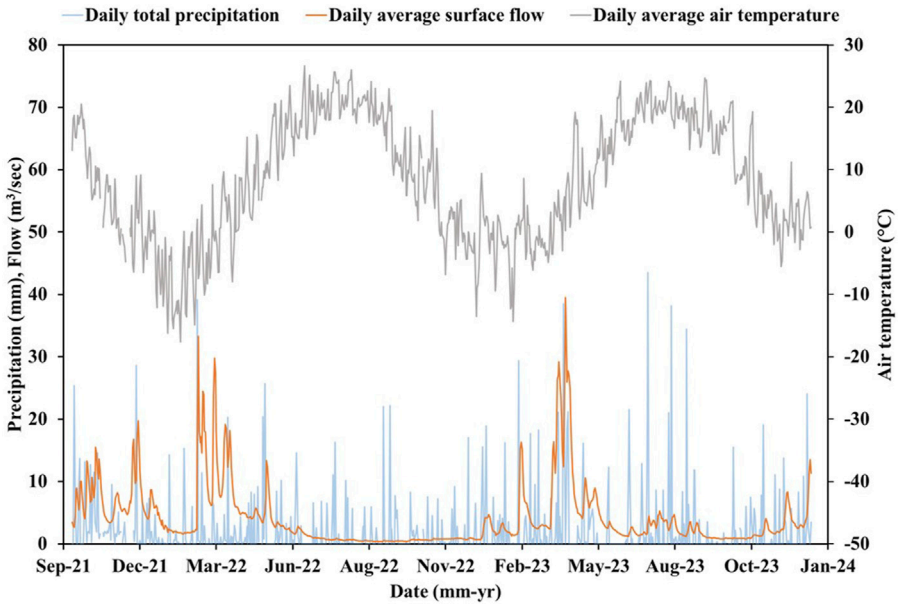


FIGURE 2
Daily average stream flow, total precipitation, and average air temperature during the observation period (1 October 2021 – 31 December 2023).

events. In addition, the daily average stream flow was high during the winter of 2022 and 2023 where it reached to approximately 16.3 m^3/s in February 2023 (Figure 2). Over the observation period, the total precipitation was 1763 mm while the average of the total annual precipitation amount was approximately 785 mm. In general, the total rainfall depth was the highest in the fall of 2021 with a total depth of 311.3 mm while the fall of 2022 was the driest season over the observation period with a total rainfall depth of 108.3 mm (Figure 2). The highest daily total rainfall depth was recorded in the Summer of 2023 (i.e., July 2023) with a total depth of 43.5 mm. Following to this rainfall event, the second highest rainfall depths were 39.2 and 38.5 mm that were measured in February 2022 and April 2023, respectively, resulting in the highest stream flow records during the observation period. The average daily air temperature ranged between −17.6°C and 26.7°C over the observation period where the minimum and maximum air temperatures were observed in January and June 2022, respectively. In addition, there was no major variability in the annual pattern of the air temperature (similar to the sinusoidal wave) where the maximal and minimal air temperatures were approximately 24 and -14°C during the summer and winter, respectively (Figure 2).

2.4 Surface water quality parameters

In the current study, the selection and classification of the measured water quality parameters followed established environmental standards and guidelines such as those outlined by the Canadian Water Quality Guidelines, the U.S. Environmental Protection Agency, and the World Health Organization. For example, the standard reference/acceptable limit of NO_3^--N concentration in surface water was marked at 2.95 mg NO_3^--N/L according to the Canadian Water Quality Guideline for the Protection of Aquatic Life (CWQGPAL) (Steele and Veliz, 2007; Canadian Council of Ministers of the Environment, 2011; Canadian Council of Ministers of the Environment, 2012). For the Cl^- concentration in surface water, the standard reference was selected based on the guidelines determined by the Canadian Council of Ministers of the Environment (CCME) (CCME, 2011). According to the CCME, the aesthetic guidelines for drinking water was chosen to be 250 mg/L which was determined based on numerous considerations towards human health, Cl^- taste thresholds, and the corrosion possibilities of the drinking water distribution networks and systems (Health Canada, 1987). The guidelines for the Cl^- concentration in surface water were then revised to consider the protection of freshwater aquatic life, setting guidelines of 120 mg/L and 640 mg/L for chronic (short-term) and acute (long-term) toxicological effects, respectively (Health Canada, 1999; CCME, 2011). In general, these environmental standards and guidelines define the acceptable limits for water quality parameters in surface water and groundwater systems.

NO_3^--N concentration in surface water at the five main observation locations along the main water course (i.e., S1 to S5) ranged from 1.10 to 6.05 mg NO_3^--N/L with an average of 3.78 mg NO_3^--N/L (Figure 3a). These observations are consistent with the NO_3^--N concentrations reported in other sand and silt plain agricultural watersheds (Tian et al., 2016; Sigler et al., 2018; Stelzer and Scott, 2018; Richards et al., 2021; Wang X. et al., 2022). However, they are relatively lower than the reported NO_3^--N concentrations in surface water in a clay agricultural watershed in southern Ontario (Rixon et al., 2020; Mackie et al., 2021; May et al., 2023). This is mainly because clay soils have lower soil permeability, leading to slow water infiltration rate into the soil which increases the surface runoff that carry NO_3^--N from fertilizers

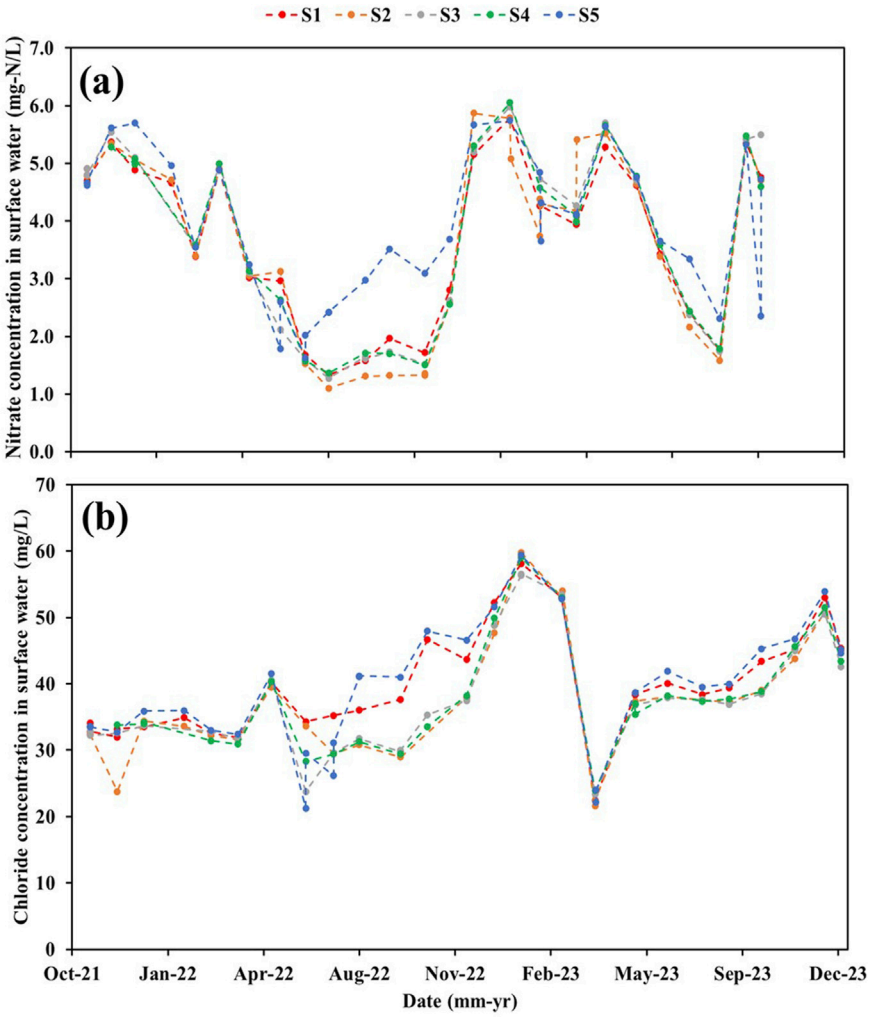


FIGURE 3
Surface water quality parameters at the five main observation sites (i.e., from S1 to S5) over the observation period (1 October 2021–31 December 2023): **(a)** NO_3^--N, and **(b)** Cl^- concentrations. Water quality datasets were collected by Arce-Rodriguez, 2024; Zeuner et al., 2025.

directly into surface water, leading to higher NO_3^--N concentrations in surface water. In addition, tile drains, that are common in clay agricultural watersheds, represent a major source of NO_3^--N transport into surface water (Rixon et al., 2020; May et al., 2023).

Moreover, the average NO_3^--N concentration in surface water in the sub-watershed (i.e., 3.78 mg NO_3^--N/L) is greater than the CWQGPAL limit (i.e., 2.95 mg NO_3^--N/L) (Canadian Council of Ministers of the Environment, 2011; Canadian Council of Ministers of the Environment, 2012), emphasizing a considerable level of contamination in the surface water within LWC (Figure 3a). The NO_3^--N concentrations in surface water at the five observation sites were consistent where the peak concentrations took place in November and December 2021 March 2022 as well as January, March, and December 2023, following snow-melt events during winter and early spring. Also, one NO_3^--N concentration peak was observed in June 2023 following a rainfall and runoff event during the summer (Figure 3a). Such snow-melt and rainfall events are governing controllers on NO_3^--N transport because it is highly mobile and dissolvable in water where it can be rapidly transported from the soil matrix to the main water course with high surface runoff conditions. These observations are comparable with the main outcomes of previous NO_3^--N transport investigations in agricultural watersheds (Miller et al., 2015; Singh and Craswell, 2021; D'Haene et al., 2022; Yang et al., 2024).

Cl^- concentration in the surface water at the five observation sites on the main channel varied from 21.25 to 59.76 mg/L with an average of 38.40 mg/L (Figure 3b). These Cl^- concentrations are comparable with those concentrations reported specifically in Ontario, Canada, and generally across North America (Steele and Aitkenhead-Peterson, 2011; Stets et al., 2018; Sorichetti et al., 2022; Castiblanco et al., 2023). In addition, the range of the Cl^- concentration in the LWC sub-watershed is below the limits of the aesthetic guidelines for drinking water (i.e., 250 mg/L) and both the short- and long-term guidelines for aquatic life (i.e., 120 and 640 mg/L, respectively). For the five observation locations along the main channel, the Cl^- concentrations were consistent where the peak concentrations were observed in January, March, and December 2023 when snow-melt events during winter and early spring took place (Figure 3b). These high concentrations of Cl^- are probably linked to the winter since the application of road salt is

commonly used in the sub-watershed during the snowfall events. In addition, salts from applying synthetic and manure-based fertilizers can contribute to the high Cl^- concentrations in surface water in the sub-watershed (David et al., 2016; Merchán et al., 2018; Park et al., 2018). These observations are generally consistent with the main observations of previous studies pertaining to Cl^- transport in stream water in different watersheds (Mullaney et al., 2009; Perera et al., 2013; Granato et al., 2015). This is also compatible with the fact that road salt is considered the main source of Cl^- transport in different watersheds in north America especially the Great Lakes Basin (Chapra et al., 2009; Oswald et al., 2019; Mackie et al., 2022). Further observations about the NO_3^--N and Cl^- concentrations in surface water at the tributary observation sites be found in the Supplementary Material Section (Supplementary Figure S1).

3 Methods

3.1 Machine learning (ML) regression models

In the current study, 8 ML regression algorithms were trained and tested to predict the NO_3^--N and Cl^- concentrations in surface water in the sub-watershed using a group of input variables including meteorological, hydrological, field, and water physico-chemical parameters. These ML algorithms were the linear regression (LR) (Chou et al., 2018; El Bilali and Taleb, 2020), regression trees (RT) (Kuzmanovski et al., 2015; Qun'ou et al., 2021), support vector machine (SVM) (Cervantes et al., 2020; Xu et al., 2020), artificial neural network (ANN) (Hafeez et al., 2019; Kim et al., 2021), Gaussian process regression (GPR) (Richardson et al., 2017; Daemi et al., 2019), ensemble bagged trees (Zhang et al., 2022), ensemble boosted trees (Melesse et al., 2020), and random forest (Zhou et al., 2019) models. These models were selected because they are commonly used in the literature with a demonstrated history of accurate prediction capabilities and robust performance especially for small-sized datasets (Ashari et al., 2013; Aggarwal, 2016; Gondia et al., 2022). Each model relies on specific methodologies to predict the output variables where the suitability of each model depends mainly on the nature of the dataset and the possible detection of the interplay relationships between the model input and output variables. The main methodologies, applicability, advantages, and limitations of the employed ML regression models are briefly explained in the Supplementary Material Section.

3.2 Evaluation metrics of ML regression models

Five different evaluation metrics were applied to assess the performance of the 8 ML regression models in predicting the NO_3^--N and Cl^- concentration in surface water within the LWC sub-watershed. These evaluation metrics are the coefficient of determination (R^2) (Equation 1), root mean squared error (RMSE) (Equation 2), mean absolute error (MAE) (Equation 3), mean absolute percentage error (MAPE) (Equation 4), and variance of errors (σ^2) (Equation 5). These evaluation metrics were chosen for measuring the performance of the predictive models as they are commonly employed in previous ML regression studies (Kovacs et al., 2022; Sajib et al., 2023; Sajib et al., 2024). Further details about the definition and rational behind these evaluation metrics can be found in the Supplementary Material Section.

$$R^2 = \left[\frac{\sum_{i=1}^{n}(Y_i - \bar{Y})(\hat{Y}_i - \tilde{Y})}{\sqrt{\sum_{i=1}^{n}(Y_i - \bar{Y})^2}\sqrt{\sum_{i=1}^{n}(\hat{Y}_i - \tilde{Y})^2}}\right]^2 \quad (1)$$

$$RMSE = \sqrt{\frac{\sum_{i=1}^{n}(Y_i - \hat{Y}_i)^2}{n}} \quad (2)$$

$$MAE = \frac{\sum_{i=1}^{n}|Y_i - \hat{Y}_i|}{n} \quad (3)$$

$$MAPE = \frac{1}{n}\sum_{i=1}^{n}\left|\frac{Y_i - \hat{Y}_i}{Y_i}\right| \quad (4)$$

$$\sigma^2 = \frac{1}{n}\sum_{i=1}^{n}(e_i - \bar{e})^2 \quad (5)$$

Where: Y_i = observed (actual) output variable, $\hat{Y}_i$ = predicted (modelled) output variable, $\bar{Y}$ = mean of the observed values of the output variable, $\tilde{Y}$ = mean of the predicted values of the output variable, e_i = error (difference between observed and predicted output variable), $\bar{e}$ = average error between observed and predicted output, and n = total number of observations.

3.3 Data analysis and pre-processing

In the current study, 200 observations were obtained from the main channel and tributary observation sites. Some of these observations were eliminated from the dataset because some parameters, such as water physico-chemical parameters, were not measured within these observations. Additional data pre-processing was applied on the observations to statistically remove the outliers of the model variables by employing the box and whiskers method through developing a box plot for each of the ML regression model input and output variables at the main channel (Figure 4a) and tributary (Figure 4b) observation sites. There were 121 remaining observations from the main channel and 40 remaining observations for the tributary sites. The total number of observations (161 observations) is of the same order of magnitude with those reported in other studies, ranging from 40 to 300 data points (Najah Ahmed et al., 2019; Bedi et al., 2020; Elsayed et al., 2023b; Sakizadeh et al., 2024; Subbarayan et al., 2024).

The parameters of the available dataset were divided into four categories based on their relevancy and application in the ML regression models (Table 1). The first category includes the hydrological and meteorological conditions such as the daily flow rate and the daily precipitation on the day prior to the sampling. The second category contains field conditions such as the location of sampling sites (main channel or tributary) and the crop cover with a percentage of the three primary crops (i.e., corn, soybeans, and pasture) in the sub-watershed. The third category consists of field measured physico-chemical parameters including the water temperature, pH, DO, EC, and ORP. These three categories represented the input variables (i.e., features) of the ML regression models. These categories can enhance the ML model performance and predictive accuracy by accounting for

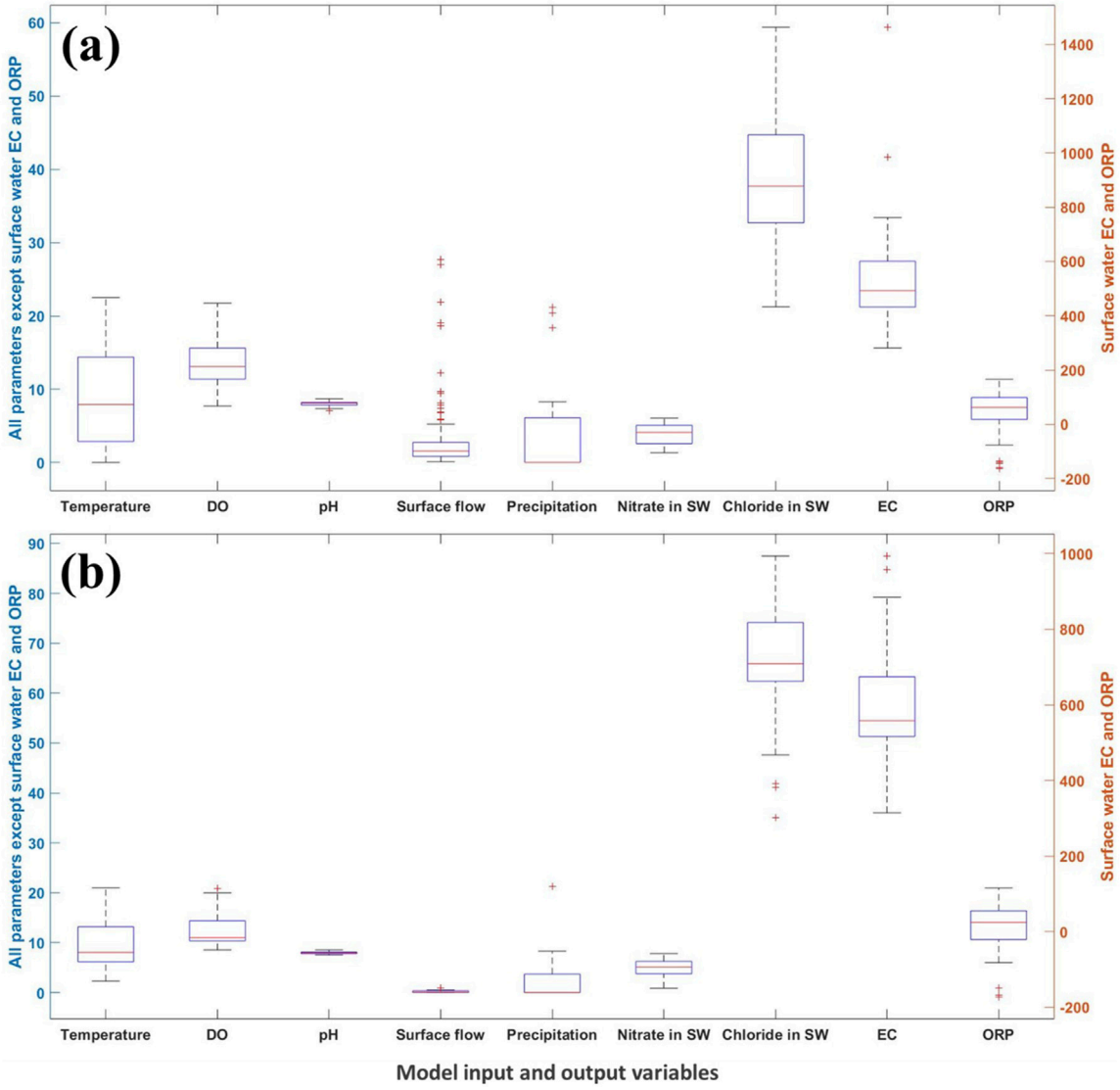


FIGURE 4
Box plot diagram for the surface water parameters using box and whisker approach for the: **(a)** main channel and **(b)** tributary sampling sites. * The units of surface water parameters are °C for temperature, mg/L for DO, m^3/s for daily surface flow, mm for 24-h precipitation, mg NO_3^--N/L for NO_3^--N concentration, mg/L for Cl^- concentration, µS/cm for EC, and mV for ORP.

hydrological, meteorological, and physico-chemical interactions influencing surface water quality. The fourth category involves the surface water quality parameters including NO_3^--N and Cl^- concentrations. In the current study, nitrate concentration represents nitrate-nitrogen (NO_3^--N) concentration in mg NO_3^--N/L. The fourth category was chosen to be the model output variables to describe the most important and prevalent parameters that can reflect the surface water quality in the sub-watershed. NO_3^--N and Cl^- are key indicators of agricultural and anthropogenic influences on surface water quality. NO_3^--N is a major contaminant associated with agricultural runoff and groundwater contamination while Cl^- serves as a conservative tracer to reflect the natural sources (e.g., atmospheric deposition and salts in rocks and soils) and anthropogenic activities such as application of soil fertilizers and road salts.

The total number of model variables used for the application of ML regression algorithms was 13 variables which is comparable with those reported in previous ML regression studies (between10 and 20 variables) (Knoll et al., 2019; Chang et al., 2021; Mosavi et al., 2021; Wang et al., 2021; Wells et al., 2021; Elsayed et al., 2022b). Here, the selected features are those listed in Table 1, including meteorological and hydrological, field, physico-chemical parameters as input variables, and water quality parameters as output variables. The observation period covered more than 2 years of monthly and event-based sampling where the temporal and spatial variations in the model features were measured. The sampling campaigns covered three successive non-growing and two successive growing seasons (from October 2021 to December 2023). This observation period is comparable with those reported in other ML investigations (Wagh et al., 2018; Islam et al., 2021; Perović et al., 2021; Yang et al., 2021).

TABLE 1 Description of the main categories and parameters within the available dataset.

Category definition	Input/output variables	Main parameters in the group	Data sources
Hydrological and meteorological conditions	Input variables	• Average daily surface flow • 24-h precipitation prior to the sampling time	Weather station (i.e., Brantford Airport) and Environment Canada ECCC (2021)
Field conditions	Input variables	• Location of sampling site (i.e., main channel or tributary site) • Crop cover o Corn o Soybeans o Pasture	Field observations and remote sensing (i.e., Agriculture and Agri-Food Canada -Annual Crop Inventory) AAFC (2023)
Physico-chemical water parameters	Input variables	• Temperature • pH • Dissolved oxygen • Oxidation-reduction potential • Electrical conductivity	On-site field measurements
Water quality parameters	Output variables	• Nitrate-nitrogen concentration in surface water • Chloride concentration in surface water	Field sampling and laboratory analysis

TABLE 2 Main statistical parameters of the model input and output variables.

Parameter (Unit)	$X_{Min.}$	$X_{Max.}$	$\bar{X}$	σ	C_V (%)	C_S
DO (mg/L)	7.7	21.7	13.3	3.0	22.7	0.56
Temperature (°C)	0	22.5	9.0	6.5	72.9	0.56
EC (µS/cm)	281	1,464	540	159	29.4	1.58
ORP (mV)	−173	166	40.2	68.9	151.3	−0.98
pH (−)	7.03	8.69	8.01	0.29	3.6	−0.36
Daily average surface flow (m^3/s)	0.017	27.7	2.6	4.9	188.1	3.63
24-h precipitation (mm)	0	21.2	3.7	6.0	163.8	1.94
Nitrate-nitrogen (mg NO_3^--N/L)	0.85	7.8	4.1	1.6	39.1	−0.18
Chloride (mg/L)	21.2	87.5	45.4	15.3	33.8	0.81

* $X_{Min.}$: Minimum, $X_{Max.}$: Maximum, $\bar{X}$: Average, σ: Standard deviation, C_V: Coefficient of variation, and C_S: coefficient of skewness.

The minimum ($X_{Min.}$), maximum($X_{Max.}$), average (mean) ($\bar{X}$), standard deviation (σ), coefficient of variation (C_V) and coefficient of skewness (C_S) were estimated for the model input and output variables (Table 2). Based on the statistical analysis, the highest coefficients of variation and skewness were corresponding to the daily average stream flow (188.1 and 3.63) and 24-h precipitation before sampling time (163.8 and 1.94), respectively. This is mainly due to the high variability in the meteorological and hydrological conditions in the LWC sub-watershed. Such variability was observed in other previous studies that investigated the hydrological response of watersheds in the Great Lakes Basin (Elsayed et al., 2023a; Elsayed et al., 2024a).

3.4 Modeling approach

Additional analysis was performed on some of the model input variables to prepare these features for the ML modeling. For example, the 24-h total precipitation prior to the sampling time was assumed to be uniform across the sampling locations (i.e., S1 to S5 and TF1 to TF4) within the sub-watershed for each observation. This assumption is based on the observations and local knowledge of the sub-watershed, which indicated no reported variations in snowfall or rainfall events that could disrupt the uniformity of precipitation across the nine observation locations. In addition, LWC is considered a small-sized catchment with minimal spatial variability in the meteorological conditions including the total precipitation. The stream flow rate at the observation sites was estimated using the watershed area ratio method (Gianfagna et al., 2015) since there was a lack of stage data at these observations locations which hindered the determination of surface flow rate by standard stage and rating curve techniques.

One of the key concerns in hydrological and water quality modeling is the potential collinearity between input variables which can lead to redundancy and affect the model performance. In particular, precipitation and stream flow are often correlated as precipitation serves since a primary driver of stream flow. However, in the current study, both variables were retained in the application

of ML models because they capture distinct hydrological processes that contribute to water quality variability. Precipitation represents direct meteorological inputs while stream flow integrates multiple watershed responses, including antecedent soil moisture conditions, groundwater contributions, land use impacts, snow-melt events, and flow routing processes. Excluding stream flow from candidate model input variables can disregard its role as an aggregated hydrological response to various environmental drivers. In addition, most ML models (e.g., tree- and kernel-based models) are inherently more robust against multi-collinearity compared to simple ML models. By keeping both precipitation and stream flow in the analysis, it is ensured that ML models can learn from the full spectrum of hydrological variability, improving their predictive accuracy for the output variables.

For the crop cover, it was assumed to be uniform at all the sampling sites for each growing season, since the agricultural fields dominate the sub-watershed (approximately 73%) with similar crop patterns and distributions. For example, all sampling sites had a crop cover of 38, 37, and 11% for the soybeans, corn, and pasture, respectively, during the growing season of 2022 (i.e., from May to September 2022). For the growing season of 2023, the crop cover changed for all sampling locations to be 36, 17, and 15% for corn, soybeans, and pasture, respectively. During the non-growing seasons, the crop cover and percentage of each crop within the sub-watershed was considered to be zero where there were no agricultural activities in LWC during this period.

The previously mentioned model input variables, in Table 1, were employed to train the ML regression models to predict the output variables. The available dataset was divided into two sets where 70% and 30% of the dataset were used for the training and testing processes, respectively. Training process is used to familiarize the ML regression models with the input and output variables while considering the interplay between these model variables which assists in increasing the robustness of the ML regression models. Testing process is applied to determine the prediction accuracy of the ML model to estimate the output variables given new set of input variables.

Each ML regression model was used to predict a single output variable at a time (i.e., separate models for predicting NO_3^--N and Cl^- concentrations), considering the previously mentioned inputs variables in Table 1. For each ML regression model, the effect of the model hyper parameters was assessed to obtain the highest model prediction accuracy for each output variable. For example, the learner parameters, number of neurons, hidden layers, ensemble parameters were changed for the models to achieve the maximum model prediction capabilities expressed by the optimal evaluation metrics including R^2 and error indicators (e.g., RMSE and MAPE).

The main criteria of selecting the major research points relied on including a variety of input variables related to hydrological, meteorological, field conditions beside the physico-chemical water parameters to predict the NO_3^--N and Cl^- concentrations in surface water. The model input variables were chosen to be easily measured and quantified with minimal effort and time. In addition, the sampling locations were selected to capture the hydrological responses and nutrient dynamics in both the main and tributary sites, evaluating the spatial variability of nitrate and Cl^- concentrations in surface water. These sampling locations were also chosen to examine the changes in NO_3^--N and Cl^- concentrations along the flow path in surface water, considering potential pollutant accumulation or dilution effects. Moreover, the observation period was more than 2 years with monthly sampling to identify the temporal variation of water quality parameters during the growing and non-growing seasons within the sub-watershed. For the model output variables, NO_3^--N and Cl^- were chosen due to their strong correlations with hydrological and field parameters while other water quality parameters (e.g., organic matter and microbial contamination) may not exhibit similar relationships with the selected input variables such as crop cover and management practices. Non-linear interactions and complex biogeochemical processes may require alternative modeling strategies beyond regression-based ML such as deep learning techniques and/or hybrid models (i.e., combination of process-based and data-driven models). In general, the selection of the model inputs and outputs was determined based on a combination of hydrological, geographical, and physico-chemical factors to ensure a comprehensive assessment of NO_3^--N and Cl^- concentrations across the sub-watershed.

3.5 Interdependence analysis

An interdependence analysis was performed by developing a correlation matrix between the model input and output variables to examine the degree of linearity and strength in relationships between the model variables. The correlation matrix, or correlation plot, serves as a key tool for identifying the relationships between different pairs of the model variables. Interdependence analysis is essential in complex processes, such as NO_3^--N and Cl^- transport to surface water, because the behaviour of each process parameter might be influenced by other parameters. In general, interdependence and correlation analyses aid in understanding the underlying mechanisms and relationships within the contaminant transport process and determining the crucial factors of the process which can enhance the prediction accuracy of ML models by eliminating the redundant variables. In these analyses, a high positive correlation between two model variables indicates a strong direct relationship, meaning that as one variable increases, the other also increases, and the reverse is correct when they decrease. On the other hand, a negative correlation reflects an inverse relationship, where a decrease in one variable is associated with an increase in the other. The interpretation of the correlation strength was determined based on commonly accepted limits and ranges in previous studies (Evans, 1996; Mukaka, 2012). Weak correlation can be defined when the correlation coefficient between a pair of model variables is less than 0.39. For moderate correlation, the correlation coefficient is ranged between 0.40 and 0.59 while strong correlation can be found when the correlation coefficient is greater than 0.60.

In the current study, the interdependence analysis was separately carried out on the main channel and tributary observation sites. In other words, the interdependence between the model variables was determined for each group of sites to examine the possible correlations between the process variables at different sampling locations. Thus, the process variables from the five main observation sites along the main water course (i.e., S1 to S5) were investigated to determine the potential correlation among

TABLE 3 The proposed feature importance scenarios using the optimal regression model and their corresponding model input variables.

Scenario ID	Model input variables (Features)
Base scenario	Temperature, DO, EC, pH, ORP, surface flow, 24-h precipitation, location of sampling site (main or tributary), crop cover
Scenario 1	DO, EC, pH, ORP, surface flow, 24-h precipitation, location of sampling site (main or tributary), crop cover
Scenario 2	Temperature, EC, pH, ORP, surface flow, 24-h precipitation, location of sampling site (main or tributary), crop cover
Scenario 3	Temperature, DO, pH, ORP, surface flow, 24-h precipitation, location of sampling site (main or tributary), crop cover
Scenario 4	Temperature, DO, EC, ORP, surface flow, 24-h precipitation, location of sampling site (main or tributary), crop cover
Scenario 5	Temperature, DO, EC, pH, surface flow, 24-h precipitation, location of sampling site (main or tributary), crop cover
Scenario 6	Temperature, DO, EC, pH, ORP, 24-h precipitation, location of sampling site (main or tributary), crop cover
Scenario 7	Temperature, DO, EC, pH, ORP, surface flow, location of sampling site (main or tributary), crop cover
Scenario 8	Temperature, DO, EC, pH, ORP, surface flow, 24-h precipitation, crop cover
Scenario 9	Temperature, DO, EC, pH, ORP, surface flow, 24-h precipitation, location of sampling site (main or tributary)
Scenario 10	Surface flow, 24-h precipitation, location of sampling site (main or tributary), crop cover
Scenario 11	Temperature, DO, EC, pH, ORP, location of sampling site (main or tributary), crop cover
Scenario 12	Temperature, DO, EC, pH, ORP, surface flow, 24-h precipitation

DO: Dissolved oxygen.
EC: Electrical conductivity.
ORP: Oxidation-reduction potential.

these variables within the LWC sub-watershed. In another interdependence analysis, the process variables from the four tributary sites (i.e., TF1 to TF4) were examined and used for quantifying their possible correlations. For the interdependence and correlation analyses, the Pearson correlation coefficient was used to evaluate the strength and direction of the relationships between the model input and output variables. Pearson correlation is suitable for dealing with the water quality datasets that often exhibit linear relationships with other parameters such as hydrological and meteorological conditions. In addition, it was successfully adopted in multiple nutrient transport studies in the literature (Wagh et al., 2018; Elsayed et al., 2023b; Sajib et al., 2024). It is also commonly used for decision-making and water resources management because of its straightforward interpretation and practical applications (Sajib et al., 2023; Elsayed et al., 2024b; Uddin et al., 2024). In comparison to other correlation approaches (e.g., Spearman correlation), Pearson correlation can provide valuable insights about the magnitude of linear dependence between the model variables.

3.6 Feature importance analysis

In the current study, all candidate model input variables were initially included in the ML models, followed by a feature importance analysis (i.e., interpretability analysis) for these variables to assess their significance on the prediction accuracy of NO_3^--N and Cl^- in surface water using the optimal ML regression model. This approach can provide a more objective and comprehensive assessment of input variable contributions rather than relying solely on feature pre-selection based on prior assumptions (Knoll et al., 2019; Islam et al., 2021). Although some regression-based studies employ manual or stepwise selection methods before developing models, these methods can be sometimes subjective and biased. Also, such methods lack the consideration of the hidden patterns and nonlinear interactions among the environmental variables that can be unique to each dataset and watershed system. By first including a broad set of hydrological, meteorological, and field parameters, the ML models were exposed to all potential explanatory factors. Then, the subsequent feature importance analysis can aid in systematically ranking the input variables based on their predictive power, refining the model's input selection (Wheeler et al., 2015; Harrison et al., 2021). This method enhances the interpretability of ML models and provides valuable insights into key drivers of water quality, which can be utilized in future monitoring and management strategies by stakeholders and decision makers (Messier et al., 2019).

This analysis was initially performed by omitting one input variable at a time to measure the influence of each input variable on the prediction accuracy of the optimal ML regression model (Table 3). These analyses were represented by scenarios from #1 to #9 in Table 3. Then, each group of input variables (i.e., hydrological and meteorological conditions, water physico-chemical parameters, field conditions) was removed to assess the impact of this group on the performance of the optimal ML

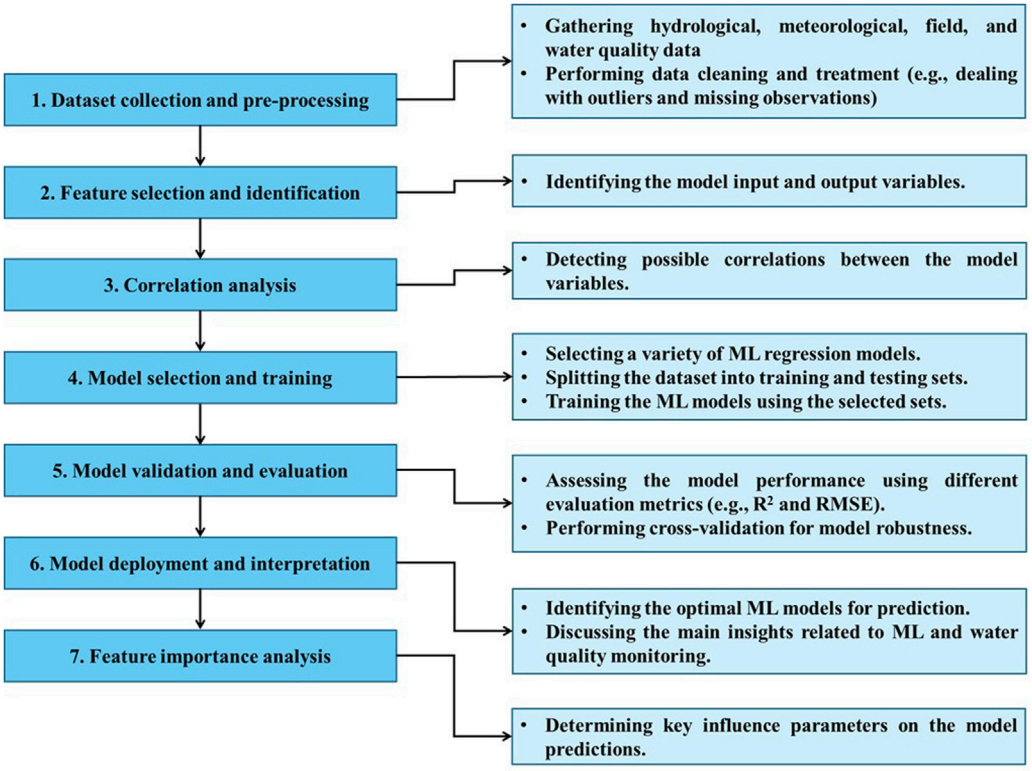


FIGURE 5
A flowchart for the individual methodological steps of applying the ML models.

regression models in predicting the output variables (Tables 1, 3). This group of simulations were referred as scenarios from #10 to #12 (Table 3). The feature importance analysis can generally assist in determining the governing factors on the accuracy of model predictions, recommending the superiority of specific input variables within the NO_3^--N and Cl^- transport processes.

Ultimately, the individual methodological steps of developing and validating the applied ML models for predicting NO_3^--N and Cl^- concentrations in surface water were described in a Figure 5. These steps included the dataset collection and pre-processing, identification of model parameters, correlation analysis, model selection, training, validation, and interpretation as well as the feature importance analysis. The details associated with each methodological step are highlighted in Figure 5.

4 Results and discussion

4.1 Interdependence analysis

For the five main observation sites along the main channel, there was no strong correlation between the Cl^- concentration in surface water and the model input variables including the meteorological, hydrological, water physico-chemical, and field conditions (Figure 6). The range of correlation coefficients between measured Cl^- concentration and model input variables was −0.42 to 0.22, indicating low interdependence between the Cl^- concentration and the meteorological, hydrological, and field conditions in the LWC sub-watershed. This finding is comparable to the main outcomes of previous Cl^- studies where it was found that the pathways of Cl^- transport was controlled by anthropogenic drivers (e.g., road salt application) rather than meteorological variables and field conditions (Kaushal et al., 2005; Perera et al., 2013; Overbo et al., 2021). For example, some previous studies demonstrated that the degree of urbanization, ubiquity of septic systems in the watershed, presence of wastewater treatment facilities and land use type are the governing factors on the Cl^- concentration in surface water (Betts et al., 2015; Lax et al., 2017; Overbo et al., 2021).

Similarly to Cl^- concentrations, NO_3^--N concentrations at the five main channel observation sites were also not strongly correlated with the model input variables (Figure 6). The correlation coefficient between the NO_3^--N concentration in surface water and other model input variables ranged from −0.32 to 0.38, indicating weak interdependence between NO_3^--N concentration and these features. This observation is consistent with the outcomes of previous NO_3^--N transport investigations where it was demonstrated that there were no clear relationships between NO_3^--N concentrations in surface water and meteorological conditions, hydrological conditions, and field parameters (Wagh et al., 2018; Gorgoglione et al., 2021; Perović et al., 2021; Elsayed et al., 2023b; Elsayed et al., 2024a). However, some previous studies emphasized that the NO_3^--N concentration in surface water is highly affected by the timing and amount of fertilizer application in agricultural fields (Rixon et al., 2020; Mackie et al., 2021; Singh and Craswell, 2021; D'Haene et al., 2022; Yang et al., 2024). In

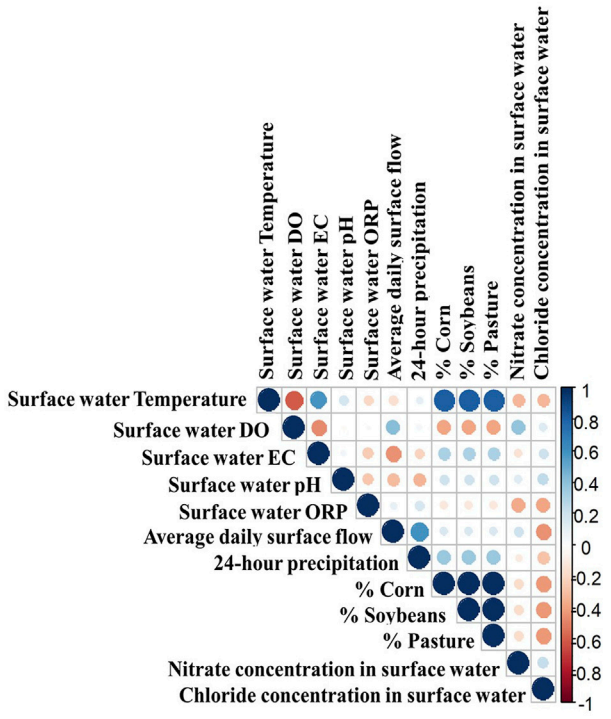


FIGURE 6
Correlation plot for the model input and output variables for the five main channel observation sites (i.e., S1 to S5).

addition, the interplay between the different model variables and NO_3^--N concentration in surface water might not be easily captured by the correlation matrix because these relationships are not strictly linear nor involve high interactions between the model variables. In other words, the relationships between the model variables are highly non-linear with multi-variable interactions.

For the model input variables, there was a strong positive correlation between the crop cover (i.e., percentage of the three primary crops in the sub-watershed) and surface water temperature with a correlation coefficient of approximately 0.82 (Figure 6). This is because the growing season in the LWC sub-watershed takes place mainly during the summer (i.e., starting from May to September) where the water temperature is relatively high. This observation is consistent with the outcomes from other studies that analyzed the interdependence between process variables in agricultural watersheds (Elsayed et al., 2023a; Elsayed et al., 2024a). Also, the 24-h precipitation prior to sampling time had a strong positive correlation (0.61) with the average surface flow because of the influence of rainfall and snowfall events on increasing the stream flow rate (Figure 2). In addition, the surface water temperature was inversely correlated with the surface water DO (−0.60) and directly correlated with EC (0.58). Ultimately, there were no strong correlations between the rest of the model input variables for which the correlation coefficients ranged from −0.44 to 0.46.

In general, there were no strong correlations between the model output variables, especially the NO_3^--N concentration in surface water, and the model inputs as well as between the model inputs themselves, including the hydrological and meteorological conditions, and the field conditions. These unclear relationships between the model variables magnifies the importance of introducing ML regression models to describe the multi-dimensional interdependence between the process variables which enhance the understanding of the NO_3^--N and Cl^- transport processes.

4.2 ML regression models and the optimal models

Gaussian process regression (GPR) was found to be the optimal ML regression model to predict the NO_3^--N concentration in surface water (Table 4; Figures 7a, b). The evaluation metrics of the GPR model were 0.99 for R^2, 0.30 mg NO_3^--N/L for RMSE, 0.08 mg NO_3^--N/L for σ^2, 0.21 mg NO_3^--N/L for MAE, and 7.8% for MAPE during the training process. As for typical ML regression models, the model performance slightly decreased during the testing process where the evaluation metrics became 0.96 for R^2, 0.83 mg NO_3^--N/L for RMSE, 0.68 mg NO_3^--N/L for σ^2, 0.60 mg NO_3^--N/L for MAE, and 17.1% for MAPE, albeit with an acceptable model prediction accuracy. The performance of the GPR model is comparable with the findings of other previous ML studies where $R^2 \geq 0.9$ and MAPE $\leq$ 20% reflected high prediction accuracy and robustness in the model performance (Bedi et al., 2020; Yang et al., 2021; Kovacs et al., 2022; Elsayed et al., 2024b).

The ensemble boosted trees and random forest models yielded high prediction accuracy for the NO_3^--N concentration in surface water (Table 4; Figures 7a, b). The evaluation metrics of the ensemble boosted trees were 0.99 for R^2, 0.51 mg NO_3^--N/L for RMSE, 0.24 mg NO_3^--N/L for σ^2, 0.40 mg NO_3^--N/L for MAE, and 11.5% for MAPE for the training purposes while they decreased to 0.96 for R^2, 0.90 mg NO_3^--N/L for RMSE, 0.72 mg NO_3^--N/L for σ^2, 0.71 mg NO_3^--N/L for MAE, and 17.9% for MAPE during the model testing. For the random forest model, the training and testing evaluation metrics were 0.98 and 0.97 for R^2, 0.54 and 0.78 mg NO_3^--N/L for RMSE, 0.30 and 0.61 mg NO_3^--N/L for σ^2, 0.42 and 0.60 mg NO_3^--N/L for MAE, and 15.3% and 17.1% for MAPE, respectively. In multiple previous studies, the ensemble boosted tree and random forest models showed strong prediction capabilities in predicting the water quality parameters such as NO_3^--N and phosphorus concentrations (Harrison et al., 2021; Aldrees et al., 2022; Farazan et al., 2024; Zheng et al., 2024), confirming their robustness in predicting the output variables in the current study. The ensemble boosted trees and random forest models generally gave close descriptive accuracy to the one of the GPR model for predicting the output variables. However, the GPR model showed higher superiority and a more robust performance especially in the training process.

The rest of adopted ML regression models showed high prediction capabilities of NO_3^--N concentrations during the training process where the range of evaluation metrics was 0.92–0.97 for R^2, 0.82–1.33 mg NO_3^--N/L for RMSE, 0.68–1.78 mg NO_3^--N/L for σ^2, 0.56–1.10 mg NO_3^--N/L for MAE, and 18.5%–38.2% for MAPE (Table 4). During testing, the performance of these models declined in predicting the NO_3^--N concentrations where the evaluation metrics ranged from 0.54 to 0.96 for R^2, 1.27–4.46 mg NO_3^--N/L for RMSE, 1.61–19.78 mg NO_3^--N/L for σ^2, 0.95–1.69 mg NO_3^--N/L for MAE, and 28.1%–

TABLE 4 Evaluation metrics of NO_3^--N concentration in surface water using different ML regression models.

Model	Training					Testing				
	R^2	*RMSE* (mg NO_3^--N/L)	σ^2 (mg NO_3^--N/L)	*MAE* (mg NO_3^--N/L)	*MAPE* (%)	R^2	*RMSE* (mg NO_3^--N/L)	σ^2 (mg NO_3^--N/L)	*MAE* (mg NO_3^--N/L)	*MAPE* (%)
Linear regression	0.92	1.33	1.78	1.10	38.2	0.54	4.46	19.78	1.69	48.4
Regression trees	0.97	0.82	0.68	0.61	18.5	0.92	1.27	1.61	0.95	28.1
Support vector machine	0.97	0.91	0.83	0.56	20.6	0.89	1.41	1.95	1.04	28.5
Gaussian process regression	0.99	0.30	0.08	0.21	7.8	0.96	0.83	0.68	0.60	17.1
Artificial neural network	0.96	1.26	1.59	0.98	34.6	0.93	1.84	3.39	1.57	43.8
Ensemble bagged trees	0.96	1.03	1.07	0.82	30.4	0.95	2.91	8.46	1.36	40.3
Ensemble boosted trees	0.99	0.51	0.24	0.40	11.5	0.96	0.90	0.72	0.71	17.9
Random forest	0.98	0.54	0.30	0.42	15.3	0.97	0.78	0.61	0.60	17.1

* The evaluation metrics are the coefficient of determination (R^2), root mean square error (*RMSE*), variance of errors (σ^2), mean absolute error (*MAE*), and mean absolute percentage error (*MAPE*).

48.4% for MAPE (Table 4). The linear regression model had the least good performance among the applied ML regression models. This is mainly because the linear regression model was not completely compatible with the nature of dataset where the model did not have the capabilities to capture the complex relationships between the model variables. Also, the linear regression model is a simple regression approach which is not suitable for the LWC dataset that has many parameters with high non-linearity and uncertainty.

The GPR, ensemble boosted trees, and random forest also gave the best performance in predicting the Cl^- concentrations (Table 5; Figures 7c, d). The optimal ML regression algorithm was the GPR model where the evaluation metrics were 0.99 for R^2, 0.44 mg/L for RMSE, 0.19 mg/L for σ^2, 0.26 mg/L for MAE, and 0.7% for MAPE during the model training while they were reduced to 0.98 for R^2, 5.51 mg/L for RMSE, 31.08 mg/L for σ^2, 3.73 mg/L for MAE, and 8.4% for MAPE for the testing process. During the model training, the evaluation metrics of the random forest and ensemble boosted tree models were 0.99 for R^2, 3.12 and 4.14 mg NO_3^--N/L for RMSE, 9.84 and 13.62 mg/L for σ^2, 2.01 and 2.83 mg NO_3^--N/L for MAE, and 4.8% and 6.1% for MAPE, respectively. These values decreased during the model testing for the random forest and ensemble boosted trees to be 0.99 and 0.98 for R^2, 4.51 and 6.72 mg NO_3^--N/L for RMSE, 20.8 and 38.96 mg/L for σ^2, 3.61 and 4.96 mg NO_3^--N/L for MAE, and 8.4% and 10.3% for MAPE, respectively. The three models were common for yielding the best prediction accuracy of NO_3^--N and Cl^- concentrations because they were trained using the same input variables which were compatible with the nature of the dataset and the involved process variables.

Similar to the prediction of NO_3^--N concentration in surface water, the linear regression was the least good model for predicting the Cl^- concentrations especially during the model testing where the evaluation metrics were 0.66 for R^2, 38.47 mg/L for RMSE, 1,473 mg/L for σ^2, 11.95 mg/L for MAE, and 28.7% for MAPE. The remaining ML regression model gave good prediction accuracy during the training process where the range of evaluation metrics was 0.99 for R^2, 5.10–6.02 mg/L for RMSE, 26.04–36.5 mg/L for σ^2, 3.02–4.71 mg/L for MAE, and 7.2%–9.3% for MAPE (Table 5). For the model testing, the performance of these models slightly decreased where the evaluation metrics ranged from 0.96 to 0.98 for R^2, 5.51–9.67 mg/L for RMSE, 31.08–95.66 mg/L for σ^2, 3.73–5.95 mg/L for MAE, and 10.9%–12.8% for MAPE.

The selected 3 ML regression models (i.e., GPR, ensemble boosted trees, and random forest) showed a high prediction accuracy of the output variables where the predicted NO_3^--N and Cl^- concentration were well-scattered around the 45°-line in the regression plot especially for the training process (Figure 7). It should be mentioned that the GPR model was the most accurate model in predicting the output variables especially during the model training which was reflected on the evaluation metrics and the regression between the observed and predicted NO_3^--N and Cl^- concentrations. The GPR model also showed the least deviation of the 45°-line regression line compared to the rest of potential models (Figure 7). However, for the model training using NO_3^--N concentrations as the model output, the ensemble boosted tree and random forest models tended to underestimate the NO_3^--N concentration up to 4.0 mg NO_3^--N/L while they overestimated the NO_3^--N concentrations higher than 4.0 mg NO_3^--N/L (Figure 7). A similar trend was observed during the model training using Cl^- concentrations where the ensemble booted tree and random forest models overestimated the Cl^- concentrations larger than 70 mg/L. Such underestimations and overestimations decreased the R^2 values and increased the error metrics of the two models compared to GPR during the training processes, confirming that the GPR algorithm was the optimal ML regression model for predicting the two output variables.

Such underestimations and overestimations are clear at either extremely low or high NO_3^--N and Cl^- concentrations where these

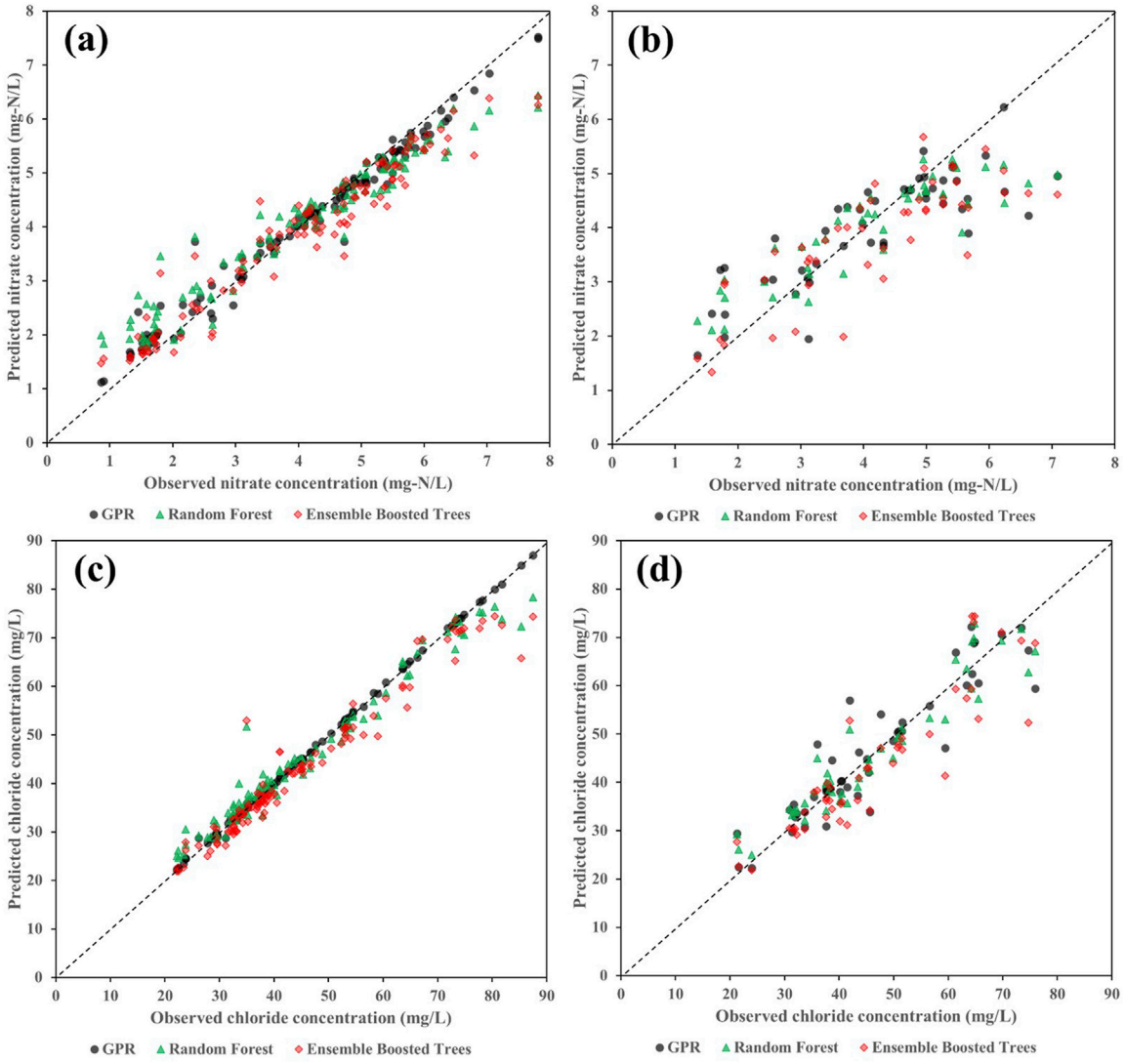


FIGURE 7
Regression plots for the optimal three algorithms for predicting the output variables: **(a)** training for NO_3^--N concentration, **(b)** testing for NO_3^--N concentration, **(c)** training for Cl^- concentration, and **(d)** testing for Cl^- concentration in surface water.

values represented the two ends of the normal distribution of the dataset (i.e., 5% end of the distribution). These extreme data points were relatively limited and less present in the model training process compared to the concentrations near the median of the normal distribution. Moreover, most of the ML regression techniques inclined towards predicting the output variables closer to the mean of the target distribution which lowers the model prediction accuracy at the extremely high values. In addition, these models can sacrifice the variance to achieve high prediction accuracy as well as low RMSE value (Li et al., 2020). Moreover, the relationships between model inputs and outputs are different at the extremes compared to those near the mean values in many cases, deteriorating the model prediction accuracy at the extremes. To overcome these challenges associated with the extremes, more observations of these values can be collected and included in the training datasets which can improve the training capabilities of the ML models at the extremes.

Although the evaluation metrics of the ensemble boosted tree and random forest models were comparable with those obtained by the GPR model, they were not able to completely capture the actual variabilities in the NO_3^--N and Cl^- concentrations especially during the training process (Figure 7). The GPR model was able to perfectly capture the variability in NO_3^--N and Cl^- concentrations with the input variables over the observation period at the five main and four tributary observation locations where the predicted and observed concentrations were aligned on the 45°-line of the regression plot (Figure 7). This indicates the robustness of the GPR model in tracing the variations in the output variables under different conditions of the input variables.

4.3 Feature importance analysis

The GPR model was selected for the feature importance analysis since it was the optimal model for predicting the NO_3^--N and Cl^- concentrations in surface water. Accordingly, it was found that the R^2 value was not changed across the proposed scenarios during the

TABLE 5 Evaluation metrics of Cl^- concentration in surface water using different ML regression models.

Model	Training					Testing				
	R^2	*RMSE* (mg/L)	σ^2 (mg/L)	*MAE* (mg/L)	*MAPE* (%)	R^2	*RMSE* (mg/L)	σ^2 (mg/L)	*MAE* (mg/L)	*MAPE* (%)
Linear regression	0.98	7.71	60.10	5.17	11.7	0.66	38.47	1,473	11.95	28.7
Regression trees	0.99	5.10	26.04	3.11	7.2	0.98	6.16	38.80	4.47	9.8
Support vector machine	0.99	5.30	28.28	3.02	7.2	0.96	9.67	95.66	5.95	12.8
Gaussian process regression	0.99	0.44	0.19	0.26	0.7	0.98	5.51	31.08	3.73	8.4
Artificial neural network	0.99	5.78	33.41	4.71	9.3	0.97	7.86	61.78	5.23	11.6
Ensemble bagged trees	0.99	6.02	36.5	3.90	9.2	0.98	5.74	32.25	4.83	10.9
Ensemble boosted trees	0.99	4.14	13.62	2.83	6.1	0.98	6.72	38.96	4.96	10.3
Random forest	0.99	3.12	9.84	2.01	4.8	0.98	4.51	20.80	3.61	8.4

TABLE 6 Feature importance analysis of the evaluation metrics for the prediction of NO_3^--N and Cl^- in surface water for the testing dataset according to the proposed simulation scenarios (Table 3).

Model	Testing – Nitrate-nitrogen (NO_3^--N)					Testing – Chloride (Cl^-)				
	R^2	*RMSE* (mg NO_3^--N/L)	σ^2 (mg NO_3^--N/L)	*MAE* (mg NO_3^--N/L)	*MAPE* (%)	R^2	*RMSE* (mg/L)	σ^2 (mg/L)	*MAE* (mg/L)	*MAPE* (%)
Base scenario	0.96	0.83	0.68	0.60	17.1	0.98	5.51	31.08	3.73	8.37
Scenario 1	0.96	0.85	0.73	0.62	17.3	0.98	5.75	33.74	3.96	8.84
Scenario 2	0.96	0.87	0.75	0.62	17.7	0.98	5.16	26.22	3.25	7.25
Scenario 3	0.96	0.82	0.66	0.59	15.7	0.97	6.88	48.42	4.83	10.31
Scenario 4	0.96	0.83	0.70	0.58	16.5	0.98	5.91	35.54	3.91	8.58
Scenario 5	0.96	0.79	0.62	0.60	17.2	0.98	5.56	31.61	3.85	8.54
Scenario 6	0.96	0.87	0.77	0.63	18.3	0.98	5.48	30.57	3.56	7.96
Scenario 7	0.96	0.83	0.70	0.62	17.6	0.98	5.74	33.64	4.02	8.91
Scenario 8	0.94	1.02	1.04	0.72	20.9	0.97	7.41	55.65	4.97	10.56
Scenario 9	0.96	0.82	0.67	0.60	17.2	0.98	5.53	31.23	3.83	8.61
Scenario 10	0.96	0.83	0.70	0.66	19.3	0.98	6.33	40.95	4.96	11.15
Scenario 11	0.95	0.91	0.83	0.68	20.1	0.98	5.60	31.85	3.85	8.45
Scenario 12	0.94	1.07	1.14	0.77	21.3	0.97	7.53	57.98	4.98	10.83

testing process except for Scenario #8, 11, and 12 when the location of the sampling site (i.e., main channel or tributary), hydrological and meteorological conditions (i.e., average flow rate and 24-h precipitation), and field conditions (i.e., location of the sampling site and crop cover) were omitted from the input variables, respectively (Table 6). The R^2 value slightly decreased from 0.96 for the base scenario (i.e., including all the input variables) to 0.94 for Scenario #8 and 12 and 0.95 for Scenario #11 (Table 6). In addition, the error metrics (e.g., RMSE and MAPE) corresponding to these scenarios were relatively larger than those of the base scenario. For example, the MAPE value increased to 20.9% for Scenario #8, 20.1% for Scenario # 11, and 21.3% for Scenario #12 compared to the base scenario that had a MAPE value of 17.1% (Table 6). This highlights the importance of including the location of sampling site as one of the input variables for training and validating the ML models. In the main channel, the flow rate is relatively higher than that in tributary sites with a significant in-stream processes and hydrological dynamics such as mixing and

dispersion. In addition, the contributing areas to the main channel and tributary sites are different and this can change the nitrogen and Cl^- loading rate. It should also be noted that omitting the surface water EC (in Scenario #3) and pH (in Scenario #4) relatively decreased the MAPE value to 15.7% and 16.5% compared to the base scenario while the R^2 values did not change with removing these input variables (R^2 = 0.96) (Table 6).

Similar results were observed in the training scenarios where the sensitivity of model predictions to the location of sampling sites, hydrological, and field conditions in Scenario #8, 11, and 12 was higher than that of the testing dataset. Although there was no significant change in R^2 values, that ranged from 0.98 to 0.99, the MAPE values significantly decreased when the previously mentioned input variables were eliminated. The MAPE values were 10.9% for Scenario #8, 13.6% for Scenario #11, and 17.5% for Scenario #12 compared to the base scenario with an MAPE value of 7.8% (Supplementary Table S2). Similarly, the other error metrics of these scenarios were relatively higher than those of the base scenario.

For the prediction of Cl^- concentration in surface water, the R^2 value of the proposed scenarios was not significantly changed compared to the base scenario (R^2 = 0.98) during the model testing where it ranged from 0.97 to 0.98 (Table 6). However, the MAPE value of Scenarios #3, 8,10, and 12 were slightly increased to be 10.31, 10.56, 11.15, and 10.83%, respectively, compared to the base scenario that had MAPE value of 8.37%. This reflects that the surface water EC, location of the sampling site, water physico-chemical parameters (e.g., surface water temperature), and the field conditions can affect the prediction accuracy of the GPR model in predicting the Cl^- concentration in surface water. On the other hand, the MAPE value decreased in Scenarios #2 (7.25%) and 6 (7.96%) when the surface water DO, and average flow rate were excluded from the input variables during the model testing (Table 6).

In the training dataset, the R^2 was determined to be 0.99 for all the proposed scenarios, including the base scenario, except for Scenario #10 where the R^2 became 0.98 when the water chemistry and physics parameters were eliminated from the training dataset (Supplementary Table S2). This decrease in R^2 value was reflected on the error metrics where the MAPE significantly increased from 0.70% for the base scenario to 9.32% for Scenario #10, highlighting the importance of including the physico-chemical water parameters.

4.4 Overall insights about the ML models

4.4.1 Selection of ML regression models

Based on the results of the ML regression model, it was emphasized that the GPR algorithm was the optimal model for predicting the NO_3^--N and Cl^- concentrations in surface water in the LWC sub-watershed over the observation period. This model resulted in the highest R^2 value and the least error metrics among the 8 ML regression models employed in the current study. The R^2 value was 0.99 for predicting the output variables during the model training while it slightly decreased to 0.98 and 0.96 during the model testing of the Cl^- and NO_3^--N concentrations, respectively. Such high prediction accuracy reflects the robustness of the GPR model in capturing the variations in the output variables over more than 2 years of observations.

In general, the GPR model was the optimal model for predicting the output variables because it is extremely suitable for small and medium-sized datasets (i.e., total number of observations = 161) (Richardson et al., 2017). In addition, GPR is an effective technique for dealing with the model input and output variables with high non-linearity and uncertainty which is common in the nutrient and Cl^- transport processes (Elsayed et al., 2024a). GPR techniques also consider the distributions over function instead of a single function, presenting a distribution of likely outcomes rather than predicting a single point estimate (the approach that followed in simple regression models) which can reduce the uncertainty of output variables (Daemi et al., 2019).

Ensemble boosted tree and random forest were the next best models after the GPR model. They yielded relatively high prediction accuracy where the range of R^2 was 0.98–0.99 for the training dataset and 0.96–0.98 for the testing dataset during the prediction of Cl^- and NO_3^--N concentrations in surface water. This is mainly because these models can enhance the prediction accuracy by reducing the mis-prediction rates in model variables with the minimal number of iterations (Zhou et al., 2019). They also can develop robust models by avoiding the weak models involved in the ensemble models and increase the contribution of potential candidates for better prediction of the output variables. Moreover, they can capture the complex relationships between the model variables which is common in the nutrient transport applications in surface water. Ultimately, they can effectively deal with noisy datasets with multiple non-linear and uncertain parameters which is appropriate and compatible with the dataset of the LWC sub-watershed (Melesse et al., 2020).

On the other hand, some ML regression models, such as linear regression, were not optimal choices for predicting the output variables using the given input variables. This is mainly because the linear regression model is a simple algorithm to detect the complicated correlations and interdependences between the model variables (Chou et al., 2018). The linear regression model is not suitable for high-dimensional datasets with high uncertainty and non-linearity (Qun'ou et al., 2021). Thus, it is highly recommended to implement more complex models, such as the GPR, ensemble boosted trees, and random forest algorithms, over the linear regression for accurate prediction of NO_3^--N and Cl^- concentrations in surface water in the LWC sub-watershed. These outcomes are consistent with the major findings of previous ML investigations in a clay agricultural watershed (Elsayed et al., 2023b; Elsayed et al., 2024a), highlighting the complexity of contaminant transport processes in different agricultural settings which requires complex ML algorithms (e.g., ensemble models) than simple models (e.g., linear regression) for better prediction of surface water quality parameters. These models can be employed by stakeholders and decision makers for better quantification of Cl^- and NO_3^--N levels in the main watercourse within the sub-watershed. Furthermore, additional investigations on different agricultural settings are required to generalize and confirm the applicability of such complex ML models in predicting numerous water quality parameters not only in surface water but also in groundwater and tile drains.

4.4.2 Applicability and transferability of ML models

ML regression models can be used to predict water quality parameters in both surface and groundwater across any agricultural watershed. These output variables may include nitrogen, phosphorus, and Cl^- concentrations while incorporating various input variables specific to each watershed, such as hydrological, meteorological, and field conditions. However, the effectiveness and reliability of different ML regression models can vary depending on the environmental characteristics of the watershed. For example, the optimal ML regression models could have strong predictive abilities in other agricultural watersheds with features similar to those of the LWC sub-watershed, such as meteorological conditions (e.g., precipitation), geology (e.g., sandy soils), and geography (e.g., within the Great Lakes Basin). The quality, resolution, and frequency of available datasets also significantly impact the development of reliable and practical models.

Also, diverse monitoring datasets are needed to develop, train, validate, and analyze the ML regression models. These models can potentially be employed by decision makers and stakeholders to assess the risk of nutrient and Cl^- transport from agricultural fields to surface water. In addition, these ML models can be used to predict the water quality at unmonitored locations, fill the missing observations of water quality parameters, and identify the governing parameters of the water quality. By monitoring and using the easily observable input variables, such as field conditions, ML models can quantify the contamination levels in surface water. For example, well-trained ML models coupled with continuous monitoring of the physico-chemical water parameters (e.g., temperature and pH) using real-time sensors can assist in obtaining continuous time-series of water quality parameters at the location of these sensors. Accordingly, these models can overcome the challenges of quantifying water quality concentrations using the standard sampling methods, reducing the time, effort, and cost associated with these typical sampling methods.

In this study, a comprehensive dataset with a wide range of variables, including meteorological, hydrological, and field conditions, was used to evaluate the potential of ML regression models in predicting NO_3^--N and Cl^- concentrations in surface water. Such high-quality, diverse datasets may not be available in other agricultural watersheds. For example, in some watersheds, the number of relevant features may be insufficient for accurate predictions, and the frequency or resolution of data collection may limit the effectiveness of the ML models. These challenges are key limitations in applying ML models as predictive tools for estimating water quality parameters in surface water. Therefore, it is essential to apply these optimal models across various agricultural watersheds, using comprehensive datasets that cover hydrological, meteorological, and field conditions, in order to extend their applicability and overcome the limitations of ML models.

The application of the optimal ML regression models employed in the current study can be extended to include additional datasets from other agricultural watersheds with distinct input and output variables. Moreover, the scope of ML models can be expanded to cover the prediction of groundwater quality parameters. Also, the importance and interpretability analyses can be extended to other datasets that were collected from different agricultural catchments. The proposed ML regression models can be re-trained using new datasets to predict the Cl^- and NO_3^--N concentrations in surface water, assisting in better understanding of the mechanisms of contaminant transport in surface water. Also, the applicability of these models can be extended to consider additional output variables if these models got exposed to larger dataset with multiple water quality parameters. This should enhance the generalization of the adopted ML regression models to different datasets pertaining to water quality monitoring in surface water.

4.4.3 Major contributions, limitations, and future research steps

In the current study, unlike previous ML studies that focused on a single water quality parameter or a single monitoring site, an integrated multi-site and multi-variable approach was adopted to predict both NO_3^--N and Cl^- concentrations in surface water across nine distinct observation sites within an agricultural watershed. Such approach enhanced the robustness of the ML models and the corresponding outcomes which can provide a more comprehensive description of the spatial variability of water quality parameters in agricultural watersheds. In addition, our study was capable of bridging the data-driven modeling and water quality interpretation. In other words, while most of regression-based ML studies focus mainly on model performance, our study included conducting a feature importance analysis to identify the most influential factors that can contribute to water quality predictions in surface water. This allowed better understanding of the underlying hydrological and land-use processes driving water quality changes, demonstrating meaningful insights in both ML advancements and practical watershed management. The scope of the current study also covered addressing some challenges associated with agricultural watersheds which are highly dynamic systems influenced by seasonal variability, fertilizer applications, and hydrometeorological conditions. By incorporating a diverse set of input variables (e.g., hydrological and meteorological conditions), the outcomes of this study were more oriented towards investigating the prediction capabilities of regression-based ML models in agricultural watersheds. This can aid in more precise forecasting of water quality parameters in agricultural watersheds, providing critical insights for pollution mitigation and sustainable land management practices.

Although the optimal ML models demonstrated high predictive performance in the Lower Whitemans Creek sub-watershed, their generalization to other watersheds with different hydrological and meteorological conditions remains one of the most critical challenges associated with employing these models in water quality prediction. This is mainly because these ML models are highly dependent on the quality of the training datasets, and their performance may decline when applied to other regions with limited, biased, or inconsistent datasets. Moreover, watersheds with different pollutant transport mechanisms (e.g., wetlands) may require additional and/or different input variables as well as model re-validation and adjustment.

Such limitations create remarkable room for multiple research directions and attempts for further investigation into water quality prediction. For example, future studies can explore the applicability of ML models on a broader range of water quality parameters such as phosphorus concentration in surface water. In addition, the scope of these ML models can be expanded to monitor the water quality

parameters in groundwater. Moreover, larger datasets covering multiple hydrological cycles, spatial and seasonal variations should be incorporated to assess model effectiveness over longer observation periods. Also, hybrid modeling approaches that combine ML with process-based hydrological models can offer more interpretable and physically meaningful predictions, bridging the gap between data-driven models and well-established water quality modeling frameworks. Such future research directions formulate more comprehensive assessment of the robustness of ML models in different water quality contexts.

5 Conclusion

In the current study, different groups of ML regression models were systematically employed on a 2-year dataset obtained from a sand plain agricultural sub-watershed in southwestern Ontario, Canada to predict the NO_3^--N and Cl^- concentrations in surface water in five main channel and four tributary sampling sites using a group of input variables such as hydrological, meteorological, and field conditions. Based on various evaluation metrics, it was demonstrated that the GPR algorithm was the optimal model for predicting the two output variables. The R^2 value of the GPR model for the NO_3^--N concentration in surface water was 0.99 (for training) and 0.96 (for testing) while it was 0.99 (for training) and 0.98 (for testing) for Cl^- concentration. In addition, the ensemble bagged tree and random forest models gave high prediction accuracy that was comparable to that obtained by the GPR model especially for the testing datasets. Moreover, a feature importance analysis was conducted to determine the significance of model input variables on the prediction accuracy of the two output variables. Accordingly, it was found that the field conditions, especially the location of sampling sites (main channel and tributary sites), are the governing input variables of accurate prediction of the NO_3^--N and Cl^- concentrations in surface water. This study provides meaningful insights into the practical benefits of using ML models to complement traditional field monitoring in agricultural watersheds, offering more efficient and precise predictions of water quality parameters in surface water. The major findings of this study underscore that ML regression models can significantly enhance the accuracy and responsiveness of environmental decision-making processes to avoid the deterioration of surface water quality.

Data availability statement

The original contributions presented in the study are included in the article/Supplementary Material, further inquiries can be directed to the corresponding author.

Author contributions

AE: Conceptualization, Data curation, Formal Analysis, Investigation, Methodology, Software, Visualization, Writing–original draft. JL: Conceptualization, Funding acquisition, Project administration, Resources, Supervision, Validation, Writing–review and editing. AB: Conceptualization, Funding acquisition, Project administration, Resources, Supervision, Validation, Writing–review and editing. ML: Funding acquisition, Project administration, Resources, Supervision, Validation, Writing–review and editing, Conceptualization. PG: Funding acquisition, Project administration, Resources, Supervision, Validation, Writing–review and editing, Conceptualization.

Funding

The author(s) declare that financial support was received for the research and/or publication of this article. This work was supported by the Ontario Ministry of the Environment, Conservation and Parks (MECP) and Natural Sciences and Engineering Research Council of Canada (NSERC–Alliance; Grant # 401934).

Acknowledgments

The authors would like to acknowledge Grand River Conservation Authority (GRCA) for access to data and land. The authors would like to thank Floyd Davis for access to the land and support during the field sampling.

Conflict of interest

The authors declare that the research was conducted in the absence of any commercial or financial relationships that could be construed as a potential conflict of interest.

Generative AI statement

The author(s) declare that no Generative AI was used in the creation of this manuscript.

Publisher's note

All claims expressed in this article are solely those of the authors and do not necessarily represent those of their affiliated organizations, or those of the publisher, the editors and the reviewers. Any product that may be evaluated in this article, or claim that may be made by its manufacturer, is not guaranteed or endorsed by the publisher.

Supplementary material

The Supplementary Material for this article can be found online at: https://www.frontiersin.org/articles/10.3389/fenvs.2025.1543852/full#supplementary-material

References

Aggarwal, C. C. (2016). *Data mining: the textbook*. Berlin: Springer, 285–426.

Agriculture and Agri-Food Canada (AAFC) (2023). Annual crop inventory 2022. Available online at: https://open.canada.ca/data/en/dataset/199e4ab6-832b-4434-ac39-e4887d7cc4e5.

Ahmed, A. N., Othman, F. B., Afan, H. A., Elsha, A., Ming Fai, C., Shabbir Hossain, M., et al. (2019). Machine learning methods for better water quality prediction. *J. Hydrology* 578, 124084. doi:10.1016/j.jhydrol.2019.124084

Ahmed, M. H., and Lin, L. S. (2021). Dissolved oxygen concentration predictions for running waters with different land use land cover using a quantile regression forest machine learning technique. *J. Hydrology* 597, 126213. doi:10.1016/j.jhydrol.2021.126213

Akhtar, N., Izzuddin, M., Ishak, S., Bhawani, S. A., and Umar, K. (2021). Various natural and anthropogenic factors responsible for water quality degradation: a review. *Water* 13 (19), 2660. doi:10.3390/w13192660

Aldrees, A., Hassan, H., Faisal, M., and Mohamed, A. M. (2022). Prediction of water quality indexes with ensemble learners: bagging and boosting. *Process Saf. Environ. Prot.* 168 (August), 344–361. doi:10.1016/j.psep.2022.10.005

Arabgol, R., Sartaj, M., and Asghari, K. (2016). Predicting nitrate concentration and its spatial distribution in groundwater resources using support vector machines (SVMs) model. *Environ. Model. Assess.* 21 (1), 71–82. doi:10.1007/s10666-015-9468-0

Arce-Rodriguez, J. (2024). *Nitrate transport in a sand plain aquifer in the Lake Erie Basin*. MASc thesis. University of Guelph, 190. Available online at: https://hdl.handle.net/10214/28354.

Asadollah, S. B. H. S. H., Sharafati, A., Motta, D., and Yaseen, Z. M. (2021). River water quality index prediction and uncertainty analysis: a comparative study of machine learning models. *J. Environ. Chem. Eng.* 9 (1), 104599. doi:10.1016/j.jece.2020.104599

Ashari, A., Paryudi, I., and Tjoa, A. M. (2013). Performance comparison between naïve bayes, decision tree and k-nearest neighbor in searching alternative design in an energy simulation tool. *Int. J. Adv. Comput. Sci. Appl.* 4 (11), 33–39. doi:10.14569/ijacsa.2013.041105

Balson, T., and Ward, A. S. (2022). A machine learning approach to water quality forecasts and sensor network expansion: case study in the Wabash River Basin, United States. *Hydrol. Process.* 36 (6), 1–15. doi:10.1002/hyp.14619

Bedi, S., Samal, A., Ray, C., and Snow, D. (2020). Comparative evaluation of machine learning models for groundwater quality assessment. *Environ. Monit. Assess.* 192 (12), 776. doi:10.1007/s10661-020-08695-3

Behrouz, M. S., Yazdi, M. N., and Sample, D. J. (2022). Using Random Forest, a machine learning approach to predict nitrogen, phosphorus, and sediment event mean concentrations in urban runoff. *J. Environ. Manag.* 317, 115412. doi:10.1016/j.jenvman.2022.115412

Betts, A., Gharabaghi, B., McBean, E. d., Levison, J., and Parker, B. (2015). Salt vulnerability assessment methodology for municipal supply wells. *J. Hydrol.* 531, 523–533. doi:10.1016/j.jhydrol.2015.11.004

Bhattarai, A., Dhakal, S., Gautam, Y., and Bhattarai, R. (2021). Prediction of nitrate and phosphorus concentrations using machine learning algorithms in watersheds with different land use. *Water* 13 (21), 3096. doi:10.3390/w13213096

Canadian Council of Ministers of the Environment (2011). Selected tools to evaluate water monitoring networks for climate change adaptation.

Canadian Council of Ministers of the Environment (2012). Canadian water quality guidelines for the protection of aquatic life: nitrate. *Can. Counc. Minist. Environ.* Available online at: http://ceqg-rcqe.ccme.ca/download/en/197.

Castiblanco, E. S., Groffman, P. M., Duncan, J., Band, L. E., Doheny, E., Emma, T. F., et al. (2023). Long-term trends in nitrate and chloride in streams in an exurban watershed. *Urban Ecosyst.* 26, 831–844. doi:10.1007/s11252-023-01340-0

Cervantes, J., Garcia-Lamont, F., Rodríguez-Mazahua, L., and Lopez, A. (2020). A comprehensive survey on support vector machine classification: applications, challenges and trends. *Neurocomputing* 408, 189–215. doi:10.1016/j.neucom.2019.10.118

Chang, C. F., Garcia, V., Tang, C., Vlahos, P., Wanik, D., Yan, J., et al. (2021). Linking multi-media modeling with machine learning to assess and predict lake chlorophyll a concentrations. *J. Gt. Lakes. Res.* 47 (6), 1656–1670. doi:10.1016/j.jglr.2021.09.011

Chapra, S. C., Dove, A., and Rockwell, D. C. (2009). Great Lakes chloride trends: long-term mass balance and loading analysis. *J. Gt. Lakes. Res.* 35 (2), 272–284. doi:10.1016/j.jglr.2008.11.013

Chou, J., Ho, C., and Hoang, H. (2018). Determining quality of water in reservoir using machine learning. *Ecol. Inf.* 44, 57–75. doi:10.1016/j.ecoinf.2018.01.005

Chow, R., Scheidegger, R., Doppler, T., Dietzel, A., Fenicia, F., and Stamm, C. (2020). A review of long-term pesticide monitoring studies to assess surface water quality trends. *Water Res. X* 9, 100064. doi:10.1016/j.wroa.2020.100064

Daemi, A., Kodamana, H., and Huang, B. (2019). Gaussian process modelling with Gaussian mixture likelihood. *J. Process Control* 81, 209–220. doi:10.1016/j.jprocont.2019.06.007

David, M. B., Mitchell, C. A., Gentry, L. E., and Salemme, R. K. (2016). Chloride sources and losses in two tile-drained agricultural watersheds. *J. Environ. Qual.* 45, 341–348. doi:10.2134/jeq2015.06.0302

D'Haene, K., Waele, J. D., Neve, S. D., and Hofman, G. (2022). Agriculture, Ecosystems and Environment Spatial distribution of the relationship between nitrate residues in soil and surface water quality revealed through attenuation factors. *Agric. Ecosyst. Environ.* 330 (January), 107889. doi:10.1016/j.agee.2022.107889

El Bilali, A., and Taleb, A. (2020). Prediction of irrigation water quality parameters using machine learning models in a semi-arid environment. *J. Saudi Soc. Agric. Sci.* 19 (7), 439–451. doi:10.1016/j.jssas.2020.08.001

Elsayed, A., Ghaith, M., Yosri, A., Li, Z., and El-Dakhakhni, W. (2024b). Genetic programming expressions for effluent quality prediction: towards AI-driven monitoring and management of wastewater treatment plants. *J. Environ. Manag.* 356 (October 2023), 120510. doi:10.1016/j.jenvman.2024.120510

Elsayed, A., Hurdle, M., and Kim, Y. (2021). Comprehensive model applications for better understanding of pilot-scale membrane-aerated biofilm reactor performance. *J. Water Process Eng.* 40, 101894. doi:10.1016/j.jwpe.2020.101894

Elsayed, A., Rixon, S., Levison, J., Binns, A., and Goel, P. (2023b). Application of classification machine learning algorithms for characterizing nutrient transport in a clay plain agricultural watershed. *J. Environ. Manage.* 345, 118924. doi:10.1016/j.jenvman.2023.118924

Elsayed, A., Rixon, S., Levison, J., Binns, A., and Goel, P. (2024a). Machine learning models for prediction of nutrient concentrations in surface water in an agricultural watershed. *J. Environ. Manag.* 372, 123305. doi:10.1016/j.jenvman.2024.123305

Elsayed, A., Rixon, S., Zeuner, C., Levison, J., Binns, A., and Goel, P. (2023a). Text mining-aided meta-research on nutrient dynamics in surface water and groundwater: popular topics and perceived gaps. *J. Hydrology* 626 (PB), 130338. doi:10.1016/j.jhydrol.2023.130338

Elsayed, A., Siam, A., and El-Dakhakhni, W. (2022b). Machine learning classification algorithms for inadequate wastewater treatment risk mitigation. *Process Saf. Environ. Prot.* 159, 1224–1235. doi:10.1016/j.psep.2022.01.065

Elsayed, A., Yu, J., Lee, T., and Kim, Y. (2022a). Model study on real-time aeration based on nitrite for effective operation of single-stage anammox. *Environ. Res.* 212, 113554. doi:10.1016/j.envres.2022.113554

Environment and Climate Change Canada (2021). *Canada-US Great Lakes water quality agreement*. Government of Canada. Available online at: https://www.canada.ca/en/environment-climate-change/services/great-lakes-protection/canada-united-states-water-quality-agreement.html.

Environment and Climate Change Canada (ECCC) (2017). Phosphorus and excess algal growth.

Evans, J. D. (1996). *Straightforward statistics for the behavioral sciences*. Pacific Grove: Thomson Brooks/Cole Publishing Co.

Farazan, S. Z., Paudyal, D., Chadalavada, S., and Alam, M. J. (2024). Temporal dynamics and predictive modelling of streamflow and water quality using advanced statistical and ensemble machine learning techniques. *Water* 16 (15), 2107. doi:10.3390/w16152107

Gardner, S. G., Levison, J., Parker, B. L., and Martin, R. C. (2020). Groundwater nitrate in three distinct hydrogeologic and land-use settings in southwestern Ontario, Canada. *Hydrogeology J.* 28, 1891–1908. doi:10.1007/s10040-020-02156-4

Gianfagna, C. C., Johnson, C. E., Chandler, D. G., and Hofmann, C. (2015). Watershed area ratio accurately predicts daily streamflow in nested catchments in the Catskills, New York. *J. Hydrology Regional Stud.* 4, 583–594. doi:10.1016/j.ejrh.2015.09.002

Gondia, A., Ezzeldin, M., and El-dakhakhni, W. (2022). Machine learning – based decision support framework for construction injury severity prediction and risk mitigation. *ASCE-ASME J. Risk Uncertain. Eng. Syst. Part A Civ. Eng.* 8 (3), 1–17. doi:10.1061/AJRUA6.0001239

Gorgoglione, A., Castro, A., Iacobellis, V., and Gioia, A. (2021). A comparison of linear and non-linear machine learning techniques (PCA and SOM) for characterizing urban nutrient runoff. *Sustainability* 13 (4), 2054–2119. doi:10.3390/su13042054

Granato, G. E., DeSimone, L. A., Barbaro, J. R., and Jeznach, L. C. (2015). *Methods for evaluating potential sources of chloride in surface waters and groundwaters of the conterminous United States*. US Geological Survey.

Ha, N. T., Nguyen, H. Q., Truong, N. C. Q., Le, T. L., Thai, V. N., and Pham, T. L. (2020). Estimation of nitrogen and phosphorus concentrations from water quality surrogates using machine learning in the Tri an Reservoir, Vietnam. *Environ. Monit. Assess.* 192 (12), 789. doi:10.1007/s10661-020-08731-2

Hafeez, S., Wong, M. S., Ho, H. C., Nazeer, M., Nichol, J., Abbas, S., et al. (2019). Comparison of machine learning algorithms for retrieval of water quality indicators in case-II waters: a case study of Hong Kong. *Remote Sens.* 11, 617. doi:10.3390/rs11060617

Harrison, J. W., Lucius, M. A., Farrell, J. L., Eichler, L. W., and Relyea, R. A. (2021). Prediction of stream nitrogen and phosphorus concentrations from high-frequency

sensors using Random Forests Regression. *Sci. Total Environ.* 763, 143005. doi:10.1016/j.scitotenv.2020.143005

Health Canada (1987). *Guidelines for Canadian drinking water quality: guideline technical document*. Chloride.

Health Canada (1999). *Guidelines for Canadian drinking water quality: guideline technical document*. Chloride.

Imani, M., Hasan, M. M., Bittencourt, L. F., McClymont, K., and Kapelan, Z. (2021). A novel machine learning application: water quality resilience prediction Model. *Sci. Total Environ.* 768, 144459. doi:10.1016/j.scitotenv.2020.144459

Islam, A. R. M. T., Chandra, S., Chowdhuri, I., Salam, R., Islam, S., Zahid, A., et al. (2021). Application of novel framework approach for prediction of nitrate concentration susceptibility in coastal multi-aquifers, Bangladesh. *Sci. Total Environ.* 801, 149811. doi:10.1016/j.scitotenv.2021.149811

Jung, C., Ahn, S., Sheng, Z., Ayana, E. K., Srinivasan, R., and Yeganantham, D. (2021). Evaluate river water salinity in a semi-arid agricultural watershed by coupling ensemble machine learning technique with SWAT model. *J. Am. Water Resour. Assoc.* 58, 1175–1188. doi:10.1111/1752-1688.12958

Kaushal, S. S., Groffman, P. M., Likens, G. E., Belt, K. T., Stack, W. P., Kelly, V. R., et al. (2005). Increased salinization of fresh water in the northeastern United States. *Proc. Natl. Acad. Sci. U.S.A.* 102, 13517–13520. doi:10.1073/pnas.0506414102

Khoi, D. N., Quan, N. T., Linh, D. Q., Nhi, P. T. T., and Thuy, N. T. D. (2022). Using machine learning models for predicting the water quality index in the La buong river, vietnam. *Water* 14, 1552–1612. doi:10.3390/w14101552

Kim, T., Yang, T., Gao, S., Zhang, L., Ding, Z., Wen, X., et al. (2021). Can artificial intelligence and data-driven machine learning models match or even replace process-driven hydrologic models for streamflow simulation?a case study of four watersheds with different hydro-climatic regions across the CONUS. *J. Hydrology* 598, 126423. doi:10.1016/j.jhydrol.2021.126423

Knoll, L., Breuer, L., and Bach, M. (2019). Large scale prediction of groundwater nitrate concentrations from spatial data using machine learning. *Sci. Total Environ.* 668, 1317–1327. doi:10.1016/j.scitotenv.2019.03.045

Kouadri, S., Elbeltagi, A., Reza, A., Islam, T., and Kateb, S. (2021). Performance of machine learning methods in predicting water quality index based on irregular data set: application on Illizi region (Algerian southeast). *Appl. Water Sci.* 11 (12), 190–220. doi:10.1007/s13201-021-01528-9

Kovacs, D. J., Li, Z., Baetz, B. W., Hong, Y., Donnaz, S., Zhao, X., et al. (2022). Membrane fouling prediction and uncertainty analysis using machine learning: a wastewater treatment plant case study. *J. Membr. Sci.* 660, 120817. doi:10.1016/j.memsci.2022.120817

Kuzmanovski, V., Trajanov, A., Leprince, F., Džeroski, S., and Debeljak, M. (2015). Modeling water outflow from tile-drained agricultural fields. *Sci. Total Environ.* 505, 390–401. doi:10.1016/j.scitotenv.2014.10.009

Larocque, M., Levison, J., Gagné, S., and Saleem, S. (2019). "Groundwater use for agricultural production – current water budget and expected trends under climate change," in *Final report submitted to MAPAQ and OMAFRA. Université du Québec à Montréal and University of Guelph. Montréal (Québec) and Guelph (Ontario)*, 67.

Lax, S., Peterson, E., and Van der Hoven, S. (2017). Stream chloride concentrations as a function of land use: a comparison of an agricultural watershed to an urban agricultural watershed. *Environ. Earth Sci.* 76 (20), 708–712. doi:10.1007/s12665-017-7059-x

Li, X., Li, Z., Huang, W., and Zhou, P. (2020). Performance of statistical and machine learning ensembles for daily temperature downscaling. *Theor. Appl. Climatol.* 140, 571–588. doi:10.1007/s00704-020-03098-3

Liang, K., Jiang, Y., Qi, J., Fuller, K., Nyiraneza, J., and Meng, F. R. (2020). Characterizing the impacts of land use on nitrate load and water yield in an agricultural watershed in Atlantic Canada. *Sci. Total Environ.* 729, 138793. doi:10.1016/j.scitotenv.2020.138793

Mackie, C., Lackey, R., Levison, J., and Rodrigues, L. (2022). Groundwater as a source and pathway for road salt contamination of surface water in the Lake Ontario Basin: a review. *J. Gt. Lakes. Res.* 48 (1), 24–36. doi:10.1016/j.jglr.2021.11.015

Mackie, C., Levison, J., Binns, A., and O'Halloran, I. (2021). Groundwater-surface water interactions and agricultural nutrient transport in a Great Lakes clay plain system. *J. Gt. Lakes. Res.* 47 (1), 145–159. doi:10.1016/j.jglr.2020.11.008

Marshall, R., Levison, J., Parker, B., and Mcbean, E. (2022). Septic system impacts on source water: two novel field tracer experiments in fractured sedimentary bedrock. *Sustainability* 14, 1959. doi:10.3390/su14041959

May, H., Rixon, S., Gardner, S., Goel, P., Levison, J., and Binns, A. (2023). Investigating relationships between climate controls and nutrient flux in surface waters, sediments, and subsurface pathways in an agricultural clay catchment of the Great Lakes Basin. *Sci. Total Environ.* 864, 160979. doi:10.1016/j.scitotenv.2022.160979

Melesse, A. M., Khosravi, K., Tiefenbacher, J. P., Heddam, S., Kim, S., Mosavi, A., et al. (2020). River water salinity prediction using hybrid machine learning models. *Water* 12 (10), 2951–3021. doi:10.3390/w12102951

Merchán, D., Casalí, J., Valle, J. D., Lersundi, D., Campo-bescós, M. A., Giménez, R., et al. (2018). Runoff, nutrients, sediment and salt yields in an irrigated watershed in southern Navarre (Spain). *Agric. Water Manag.* 195, 120–132. doi:10.1016/j.agwat.2017.10.004

Messier, K. P., Wheeler, D. C., Flory, A. R., Jones, R. R., Patel, D., Nolan, B. T., et al. (2019). Modeling groundwater nitrate exposure in private wells of North Carolina for the Agricultural Health Study. *Sci. Total Environ.* 655, 512–519. doi:10.1016/j.scitotenv.2018.11.022

Miller, M. P., Tesoriero, A. J., Capel, P. D., Pellerin, B. A., Hyer, K. E., Burns, D. A., et al. (2015). Quantifying watershed-scale groundwater loading and in-stream fate of nitrate using high-frequency water quality data. *Water Resour. Res.* 52, 330–347. doi:10.1002/2015WR017753

Ministry of the Environment, Conservation and Parks (2021). *Canada-ontario Great lakes agreement*. Government of Ontario. Available online at: https://www.ontario.ca/document/canada-ontario-great-lakes-agreement.

Mosavi, A., Hosseini, F. S., Choubin, B., Goodarzi, M., Dineva, A. A., and Sardooi, E. R. (2021). Ensemble boosting and bagging based machine learning models for groundwater potential prediction. *Water Resour. Manag.* 35 (1), 23–37. doi:10.1007/s11269-020-02704-3

Mukaka, M. M. (2012). A guide to appropriate use of correlation coefficient in medical research. *Malawi Med. J.* 24 (3), 69e71.

Mullaney, J. R., Lorenz, D. L., and Arnston, A. D. (2009). *Chloride in groundwater and surface water in areas underlain by the glacial aquifer system, northern United States*. Reston, VA: US Geological Survey.

Najah Ahmed, A., Binti Othman, F., Abdulmohsin Afan, H., Khaleel Ibrahim, R., Ming Fai, C., Shabbir Hossain, M., et al. (2019). Machine learning methods for better water quality prediction. *J. Hydrology* 578, 124084. doi:10.1016/j.jhydrol.2019.124084

Osman, A. R. M. (2017). Water use conflict: a characterization and water quantity study in an agriculturally stressed sub-catchment in Southern Ontario. *MASc thesis, Univ. Guelph*, 190. Available online at: http://hdl.handle.net/10214/12134.

Oswald, C. J., Giberson, G., Nicholls, E., Wellen, C., and Oni, S. (2019). Spatial distribution and extent of urban land cover control watershed-scale chloride retention. *Sci. Total Environ.* 652, 278–288. doi:10.1016/j.scitotenv.2018.10.242

Overbo, A., Heger, S., and Gulliver, J. (2021). Evaluation of chloride contributions from major point and nonpoint sources in a northern U.S. state. *Sci. Total Environ.* 764, 144179–179. doi:10.1016/j.scitotenv.2020.144179

Pandey, P., Gupta, A. P., Dutta, J., and Thakur, T. K. (2023). "Role of artificial intelligence in water conservation with special reference to India," in *Emerging technologies for water supply, conservation and management*. Editors E. Balaji, G. Veeraswamy, P. Mannala, and S. Madhav (Cham, Switzerland: Springer). doi:10.1007/978-3-031-35279-9_4

Park, Y., Kim, Y., Park, S., Shin, W., and Lee, K. (2018). Water quality impacts of irrigation return flow on stream and groundwater in an intensive agricultural watershed. *Sci. Total Environ.* 630, 859–868. doi:10.1016/j.scitotenv.2018.02.113

Perera, N., Gharabaghi, B., and Howard, K. (2013). Groundwater chloride response in the Highland Creek watershed due to road salt application: a re-assessment after 20 years. *J. Hydrol.* 479, 159–168. doi:10.1016/j.jhydrol.2012.11.057

Perović, M., Šenk, I., Tarjan, L., Obradović, V., and Dimkić, M. (2021). Machine learning models for predicting the ammonium concentration in alluvial groundwaters. *Environ. Model. Assess.* 1, 1–17. doi:10.1007/s10666-020-09731-9

Persaud, E., Levison, J., Ali, G., and Robinson, C. (2023). Using isotopic tracers to enhance routine watershed monitoring – insights from an intensively managed agricultural catchment. *J. Environ. Manag.* 344, 118364. doi:10.1016/j.jenvman.2023.118364

Portuguez-maurtua, M., Arumi, J. L., Lagos, O., Stehr, A., and Arquiñigo, N. M. (2022). Filling gaps in daily precipitation series using regression and machine learning in inter-andean watersheds. *Water* 14 (11), 1799. doi:10.3390/w14111799

Qiao, Z., Sun, S., Jiang, Q., Xiao, L., Wang, Y., and Yan, H. (2021). Retrieval of total phosphorus concentration in the surface water of miyun reservoir based on remote sensing data and machine learning algorithms. *Remote Sens.* 13 (22), 4662. doi:10.3390/rs13224662

Qun'ou, J., Lidan, X., Siyang, S., Meilin, W., and Huijie, X. (2021). Retrieval model for total nitrogen concentration based on UAV hyper spectral remote sensing data and machine learning algorithms – a case study in the Miyun Reservoir, China. *Ecol. Indic.* 124, 107356. doi:10.1016/j.ecolind.2021.107356

Richards, G., Gilmore, T. E., Mittelstet, A. R., Messer, T. L., and Snow, D. D. (2021). Baseflow nitrate dynamics within nested watersheds of an agricultural stream in Nebraska, USA. *Agric. Ecosyst. Environ.* 308 (June 2020), 107223. doi:10.1016/j.agee.2020.107223

Richardson, R. R., Osborne, M. A., and Howey, D. A. (2017). Gaussian process regression for forecasting battery state of health. *J. Power Sources* 357, 209–219. doi:10.1016/j.jpowsour.2017.05.004

Rixon, S., Levison, J., Binns, A., and Persaud, E. (2020). Spatiotemporal variations of nitrogen and phosphorus in a clay plain hydrological system in the Great Lakes Basin. *Sci. Total Environ.* 714, 136328. doi:10.1016/j.scitotenv.2019.136328

Rixon, S., May, H., Persaud, E., Elsayed, A., Levison, J., Binns, A., et al. (2024). Subsurface influences on watershed nutrient concentrations and loading in a clay dominated agricultural system. *J. Hydrology* 645, 132140. doi:10.1016/j.jhydrol.2024.132140

Sajib, A. M., Diganta, M. T. M., Moniruzzaman, M., Rahman, A., Dabrowski, A. I., Uddin, M. G., et al. (2024). Assessing water quality of an ecologically critical urban canal incorporating machine learning approaches. *Ecol. Inf.* 80, 102514. doi:10.1016/j.ecoinf.2024.102514

Sajib, A. M., Diganta, M. T. M., Rahman, A., Dabrowski, T., Olbert, A. I., and Uddin, M. G. (2023). Developing a novel tool for assessing the groundwater incorporating water quality index and machine learning approach. *Groundw. Sustain. Dev.* 23, 101049. doi:10.1016/j.gsd.2023.101049

Sakizadeh, M., Zhang, C., and Milewski, A. (2024). Spatial distribution pattern and health risk of groundwater contamination by cadmium, manganese, lead and nitrate in groundwater of an arid area. *Environ. Geochem. Health* 46 (3), 80–25. doi:10.1007/s10653-023-01845-9

Shah, M. I., Alaloul, W. S., Alqahtani, A., Aldrees, A., Musarat, M. A., and Javed, M. F. (2021). Predictive modeling approach for surface water quality: development and comparison of machine learning models. *Sustainability* 13, 7515. doi:10.3390/su13147515

Sigler, W. A., Ewing, S. A., Jones, C. A., Payn, R. A., Brookshire, E. N. J., Klassen, J. K., et al. (2018). Connections among soil, ground, and surface water chemistries characterize nitrogen loss from an agricultural landscape in the upper Missouri River Basin. *J. Hydrology* 556, 247–261. doi:10.1016/j.jhydrol.2017.10.018

Singh, B., and Craswell, E. (2021). Fertilizers and nitrate pollution of surface and ground water: an increasingly pervasive global problem. *SN Appl. Sci.* 3 (4), 1–24. doi:10.1007/s42452-021-04521-8

Sorichetti, R. J., Raby, M., Holeton, C., Benoit, N., Carson, L., Desellas, A., et al. (2022). Chloride trends in Ontario ' s surface and groundwaters. *J. Gt. Lakes.* 48, 512–525. doi:10.1016/j.jglr.2022.01.015

Steele, M. K., and Aitkenhead-Peteerson, R. (2011). Long-term sodium and chloride surface water exports from the Dallas/Fort Worth region. *Sci. Total Environ.* 409 (16), 3021–3032. doi:10.1016/j.scitotenv.2011.04.015

Steele, R., and Veliz, M. (2007). Water quality in the ausable bayfield maitland valley. Retrievedfrom. Available online at: http://www.sourcewaterinfo.on.ca/images/uploaded/uploadedDownloads/WC_Chap2_Mar_08.pdf.

Stelzer, R. S., and Scott, J. T. (2018). Predicting nitrate retention at the groundwater-surface water interface in sandplain streams. *J. Geophys. Res. Biogeosciences* 123 (9), 2824–2838. doi:10.1029/2018JG004423

Stets, E. G., Lee, C. J., Lytle, D. A., and Schock, M. R. (2018). Increasing chloride in rivers of the conterminous U . S. and linkages to potential corrosivity and lead action level exceedances in drinking water. *Sci. Total Environ.* 613–614, 1498–1509. doi:10.1016/j.scitotenv.2017.07.119

Subbarayan, S., Thiyagarajan, S., Karuppannan, S., and Panneerselvam, B. (2024). Enhancing groundwater vulnerability assessment: comparative study of three machine learning models and five classification schemes for Cuddalore district. *Environ. Res.* 242 (July 2023), 117769. doi:10.1016/j.envres.2023.117769

Syeed, M. M. M., Hossain, S., Karim, R., Faisal, M., Hasan, M., and Hayat, R. (2023). Surface water quality profiling using the water quality index, pollution index and statistical methods: a critical review. *Environ. Sustain. Indic.* 18 (January), 100247. doi:10.1016/j.indic.2023.100247

Tian, S., Youssef, M. A., Richards, R. P., Liu, J., Baker, D. B., and Liu, Y. (2016). Different seasonality of nitrate export from an agricultural watershed and an urbanized watershed in Midwestern USA. *J. Hydrology* 541, 1375–1384. doi:10.1016/j.jhydrol.2016.08.042

Uddin, G., Nash, S., Rahman, A., Dabrowski, T., and Olbert, A. I. (2024). Data-driven modelling for assessing trophic status in marine ecosystems using machine learning approaches. *Environ. Res.* 242 (July 2023), 117755. doi:10.1016/j.envres.2023.117755

Varadharajan, C., Appling, A. P., Arora, B., Christianson, D. S., Hendrix, V. C., Kumar, V., et al. (2022). Can machine learning accelerate process understanding and decision relevant predictions of river water quality? *Hydrol. Process.* 36 (4), 1–22. doi:10.1002/hyp.14565

Wagh, V., Panaskar, D., Muley, A., Mukate, S., and Gaikwad, S. (2018). Neural network modelling for nitrate concentration in groundwater of Kadava River basin, Nashik, Maharashtra, India. *Groundw. Sustain. Dev.* 7, 436–445. doi:10.1016/j.gsd.2017.12.012

Wang, R., Kim, J. H., and Li, M. H. (2021). Predicting stream water quality under different urban development pattern scenarios with an interpretable machine learning approach. *Sci. Total Environ.* 761, 144057. doi:10.1016/j.scitotenv.2020.144057

Wang, S., Wang, Y., Wang, Y., and Wang, Z. (2022a). Assessment of influencing factors on non-point source pollution critical source areas in an agricultural watershed. *Ecol. Indic.* 141 (35), 109084. doi:10.1016/j.ecolind.2022.109084

Wang, X., Xu, Y. J., and Zhang, L. (2022b). Watershed scale spatiotemporal nitrogen transport and source tracing using dual isotopes among surface water, sediments and groundwater in the Yiluo River Watershed, Middle of China. *Sci. Total Environ.* 833 (March), 155180. doi:10.1016/j.scitotenv.2022.155180

Wells, M. J., Gilmore, T. E., Nelson, N., Mittelstet, A., and Böhlke, J. K. (2021). Determination of vadose zone and saturated zone nitrate lag times using long-Term groundwater monitoring data and statistical machine learning. *Hydrology Earth Syst. Sci.* 25 (2), 811–829. doi:10.5194/hess-25-811-2021

Wheeler, D. C., Nolan, B. T., Flory, A. R., Dellavalle, C. T., and Ward, M. H. (2015). Modeling groundwater nitrate concentrations in private wells in Iowa. *Sci. Total Environ.* 536, 481–488. doi:10.1016/j.scitotenv.2015.07.080

Wong, A. (2011). *Water use inventory report for the Grand River watershed*. GRCA.

Xu, T., Coco, G., and Neale, M. (2020). A predictive model of recreational water quality based on adaptive synthetic sampling algorithms and machine learning. *Water Res.* 177, 115788. doi:10.1016/j.watres.2020.115788

Yang, Y., Shang, X., Chen, Z., Mei, K., Wang, Z., Dahlgren, R. A., et al. (2021). A support vector regression model to predict nitrate-nitrogen isotopic composition using hydro-chemical variables. *J. Environ. Manag.* 290 (November 2020), 112674. doi:10.1016/j.jenvman.2021.112674

Yang, Y., Yuan, Y., Xiong, G., Yin, Z., Guo, Y., Song, J., et al. (2024). Patterns of nitrate load variability under surface water-groundwater interactions in agriculturally intensive valley watersheds. *Water Res.* 267 (August), 122474. doi:10.1016/j.watres.2024.122474

Yu, J., Tian, Y., Wang, X., and Zheng, C. (2021). Using machine learning to reveal spatiotemporal complexity and driving forces of water quality changes in Hong Kong marine water. *J. Hydrology* 603, 126841. doi:10.1016/j.jhydrol.2021.126841

Zeuner, C., Levison, J., and Larocque, M. (2025). Insights on nitrate transport in a shallow, sandy aquifer at various temporal and spatial scales. *Front. Environ. Sci.*

Zhang, Z., Huang, J., Duan, S., Huang, Y., Cai, J., and Bian, J. (2022). Use of interpretable machine learning to identify the factors influencing the nonlinear linkage between land use and river water quality in the Chesapeake Bay watershed. *Ecol. Indic.* 140, 108977. doi:10.1016/j.ecolind.2022.108977

Zheng, Y., Wei, J., Zhang, W., Zhang, Y., Zhang, T., and Zhou, Y. (2024). An ensemble model for accurate prediction of key water quality parameters in river based on deep learning methods. *J. Environ. Manag.* 366 (July), 121932. doi:10.1016/j.jenvman.2024.121932

Zhou, P., Li, Z., Snowling, S., Baetz, B. W., Na, D., and Boyd, G. (2019). A random forest model for inflow prediction at wastewater treatment plants. *Stoch. Environ. Res. Risk Assess.* 33 (10), 1781–1792. doi:10.1007/s00477-019-01732-9

frontiers | Frontiers in Environmental Science

TYPE Original Research
PUBLISHED 07 March 2025
DOI 10.3389/fenvs.2025.1557004

Check for updates

OPEN ACCESS

EDITED BY
Paweł Tomczyk,
Wroclaw University of Environmental and Life Sciences, Poland

REVIEWED BY
Thomas Shahady,
University of Lynchburg, United States
Oleg Makhnin,
New Mexico Institute of Mining and Technology, United States

*CORRESPONDENCE
Kang Liang,
kliang800@gmail.com

RECEIVED 07 January 2025
ACCEPTED 13 February 2025
PUBLISHED 07 March 2025

CITATION
Liang K, Jiang Y, Fuller K, Cordeiro M, Zhang X, Qi J, Geng X, Liu T, Zhang Q, Azimi MA and Meng F-R (2025) Large variability of nitrate load estimated from sparse measurements by typical methods in Atlantic Canada.
Front. Environ. Sci. 13:1557004.
doi: 10.3389/fenvs.2025.1557004

COPYRIGHT
© 2025 Liang, Jiang, Fuller, Cordeiro, Zhang, Qi, Geng, Liu, Zhang, Azimi and Meng. This is an open-access article distributed under the terms of the Creative Commons Attribution License (CC BY). The use, distribution or reproduction in other forums is permitted, provided the original author(s) and the copyright owner(s) are credited and that the original publication in this journal is cited, in accordance with accepted academic practice. No use, distribution or reproduction is permitted which does not comply with these terms.

Large variability of nitrate load estimated from sparse measurements by typical methods in Atlantic Canada

Kang Liang[1,2]*, Yefang Jiang[3], Keith Fuller[4], Marcos Cordeiro[5], Xuesong Zhang[2], Junyu Qi[6], Xiaoyuan Geng[7], Tao Liu[8], Qian Zhang[9], Mohammad Amir Azimi[10] and Fan-Rui Meng[10]

[1]Oak Ridge Institute for Science and Education, Oak Ridge, TN, United States, [2]USDA-ARS Hydrology and Remote Sensing Laboratory, Beltsville, MD, United States, [3]Charlottetown Research and Development Center, Agriculture and Agri-Food Canada, Charlottetown, PE, Canada, [4]Kentville Research and Development Center, Agriculture and Agri-Food Canada, Kentville, NS, Canada, [5]Department of Animal Science, University of Manitoba, Winnipeg, MB, Canada, [6]Earth System Science Interdisciplinary Center, University of Maryland, College Park, MD, United States, [7]Canadian Soil Information Service (CanSIS), AER Ottawa, Agriculture and Agri-Food Canada, Ottawa, ON, Canada, [8]College of Forest Resources and Environmental Science, Michigan Technology University, Houghton, MI, United States, [9]University of Maryland Center for Environmental Science/U.S. Environmental Protection Agency Chesapeake Bay Program, Annapolis, MD, United States, [10]Faculty of Forestry and Environmental Management, University of New Brunswick, Fredericton, NB, Canada

Nitrogen pollution in aquatic ecosystems, primarily from agricultural sources, presents significant environmental challenges. At the land management decision level, reducing nitrate leaching requires knowledge of nitrate loading over time and location, the complexity of which is amplified by limited data availability, especially in poorly gauged watersheds. This issue is particularly pronounced in cold and humid regions where water quality data are often collected during the growing season only. Large data gaps result in systematic errors when estimating nitrogen load based on traditional regression methods. In this study, we explore the feasibility of using process-based hydrologic model to estimate nitrate loads from sparse temporal water quality data in a coastal agricultural watershed in Atlantic Canada and compared its performance with three regression methods. We found that the absence of the available 16% non-growing season data during the 10-year study period can lead to significant biases (as high as 21%) in load estimation by regression methods. In contrast, nitrate load estimates obtained with the Soil and Water Assessment Tool (SWAT) were less sensitive to systematic data gaps. The results suggest that process-based models like SWAT can be a viable alternative for nitrate load estimation when limited data is available. As agri-environmental water quality issues become more pressing, it is crucial to use appropriate methods based on data quality and availability to avoid misleading results.

KEYWORDS

nitrate load, sparse data, water quality, regression model, physical-based model

1 Introduction

Nitrogen (N) is one of the major pollutants in aquatic ecosystems. Agroecosystems receive approximately 75% of the reactive N generated by human activities to support agricultural productivity (Galloway et al., 2003). A significant proportion of this N (mainly in the form of nitrate) is lost to the environment, adversely affecting the health of aquatic ecosystems due to the limited utilization rate of N fertilizer by crops (Galloway et al., 2008; Odgaard et al., 2019). Reducing nitrate load in aquatic ecosystems has become a critical environmental challenge in many regions, especially those with intensive agricultural production (Milovanovic, 2007; Ongley et al., 2010; Hou et al., 2019).

Decision making at the land management level to reduce nitrogen losses requires detailed knowledge of nitrate loading over time and location. This accuracy is crucial for several reasons: (i) understanding the water quality of downstream environments, (ii) calibrating and validating watershed models, (ii) guiding policy-making for cost-effective pollution control programs, (iii) evaluating the effectiveness of these programs, (iv) assessing long-term N load trends, and (v) estimating riverine fluxes and identifying specific upstream sources (Stenback et al., 2011; Lee et al., 2016; Nguyen et al., 2017). One approach for quantifying nitrate load involves frequent water sampling or taking representative samples that capture the seasonality or major hydrological events at multiple locations. However, nitrate concentrations in such samples are known to be variable and dependent on the flow regime. In addition, the selection of representative samples can be subjective and sampling is often constrained by accessibility and safety concerns, potentially introducing significant uncertainties (Fu et al., 2017).

Nitrate load at the watershed scale results from complex surface and sub-surface biophysiochemical transport processes and can be estimated by integrating measured concentration and discharge data (Zamyadi et al., 2007). The dynamic nature of stream discharge adds to the challenge of accurately quantifying temporal nitrate loads. However, the availability of water quality and stream discharge data is a significant concern, as most watersheds worldwide are poorly gauged or ungauged (Hrachowitz et al., 2013). Estimating nitrate load is subject to various sources of error such as different sampling frequencies and estimation methods.

Significant efforts have been made to explore the optimal sampling frequencies for load estimation (Robertson and Roerish, 1999; Toor et al., 2008; Jiang et al., 2019; Zhang and Hirsch, 2019). It is widely agreed that high-frequency data significantly reduces the uncertainty in estimating constituent loads (Pellerin et al., 2014; Rode et al., 2016). For example, Birgand et al. (2010) suggested that the uncertainty of estimating nitrate flux using averaging or interpolation methods increases with longer sampling intervals, and considerable uncertainty arises when continuous flow data is not used. Zhang and Hirsch (2019) applied a modified version of the weighted regression method, WRTDS_K, to estimate constituent flux under five different sampling regimes, concluding that WRTDS_K performance improves with more available samples. Ideally, continuous measurement of discharge and constituent concentration data is required for accurate flux estimates (Verma et al., 2012). However, continuous measurement is rarely available due to the complexity of water quality measurement, the high cost of monitoring equipment, and the challenges in maintaining continuous monitoring equipment. The deployment and maintenance of continuous monitoring infrastructure/equipment requires ongoing funding and human resources and can be particularly challenging in remote areas or regions with extreme weather. Although daily or more frequent discharge measurements on streams and rivers are often available from environmental protection agencies or specific projects (Ullrich and Volk, 2010; Yang et al., 2019), commonly used sampling frequencies are monthly, bimonthly, event-based, or even less frequent (Zamyadi et al., 2007). Moatar and Meybeck (2005) pointed out that monthly sampling frequency has been the primary strategy of 80% of water quality surveys conducted in France since 1971. In an agricultural basin located in upstream of the Huaihe River, one of China's largest rivers, total N concentration and discharge data were collected monthly and bimonthly from 2006 to 2011 by the Bureau of Environmental Protection of Zhumadian City (Yang et al., 2016). In Thailand, water quality data was captured three to four times annually by Pollution Control of Thailand (Yadav et al., 2019). These studies indicated that discrete sampling regimes are still widely used. Globally, an accurate estimate of nitrate flux remains challenging due to limited data availability. Discrete sampling does not fully capture the concentration-discharge range, particularly during extreme wet or dry periods, when the concentration-discharge relationship varies significantly (Pellerin et al., 2014). Hirsch (2014) suggested that using a single method across a wide range of cases can result in a mixture of unbiased and severely biased results. Using the appropriate method, therefore, becomes a critical step in accurate load estimation.

Numerous approaches have been developed and applied for constituent load estimation (Verhoff et al., 1980; Ferguson, 1986; Preston et al., 1989; Mattikalli and Richards, 1996; Arnold et al., 1998; Runkel et al., 2004; Hirsch et al., 2010; Li et al., 2020). These approaches can be broadly classified into statistical methods, process-based models, and remote sensing/GIS methods. Statistical approaches explore certain statistical relationships between flow and constituent concentration and can be further categorized (Guo et al., 2002; Moatar and Meybeck, 2005; Verma et al., 2012) into averaging methods and interpolation/extrapolation methods, ratio estimators, regression-based methods, and data mining methods. Averaging methods calculate flux using mean concentration and mean flow. This approach is simple and straightforward but the calculated results can be substantially biased when insufficient data are used (Zamyadi et al., 2007). Interpolation/extrapolation approaches assumes that instantaneous concentration or flow data are representative of much longer periods (Moatar and Meybeck, 2005). Linear interpolation (LI) is a simple and straightforward approach that assumes the change of concentration between two adjacent data points follows a linear pattern. However, the accuracy of LI can be highly sensitive to the number and timing of samples. Ratio estimators use flow data as the independent variable and load as the dependent variable (Guo et al., 2002). Regression-based techniques utilize expected patterns of covariance between

concentrations and flow and/or time (Lee et al., 2016), while data mining methods are relatively user-friendly, given that they are not constrained by data assumptions or the number of parameters used (Li et al., 2020). LOADEST (Load Estimator) (Cohn et al., 1992; Runkel et al., 2004) and the WRTDS (Hirsch et al., 2010) are widely used regression methods for constituent load estimation. LOADEST applies multiple regression techniques that accounts for changes in streamflow, season, and time (Cohn et al., 1992). WRTDS uses weighted regressions that give more relevance to closer and more relevant data points, making it better at adapting to changing environmental conditions (Hirsch et al., 2010). Both methods are easy to apply and can handle larger datasets and incorporate effects like seasonality and flow conditions, which are critical for accurate load estimation. However, their accuracy is also dependent on high-frequency data. Process-based models incorporate the underlying biophysicochemical processes (e.g., plant growth, leaching, runoff, nitrification/denitrification, etc.), using mathematical equations to represent the movement of water and the transport and transformation of chemicals at the field or watershed scale (Brilli et al., 2017). A relatively complete suite of biogeochemical processes is generally embedded in these models. Additionally, many of these models incorporate watershed characteristics such as soil, topography, climate, land cover/land use, and/or management operations into models (Ator and Garcia, 2016; Molina-Navarro et al., 2018; Sorando et al., 2019; Liang et al., 2020; Cordeiro et al., 2022). The Soil and Water Assessment Tool (SWAT) is one of the most widely applied process-based watershed models for water quality and water quality estimation (Gassman et al., 2014; Fu et al., 2019) due to its relatively complete representation of biogeochemical processes of watershed (Neitsch et al., 2011; Gassman et al., 2014). While the model offers a detailed simulation of watershed processes, SWAT requires extensive data input and high computational resources, especially when applied over large watersheds.

Many studies have been conducted to evaluate commonly-used process-based models (Borah and Bera, 2003; Brilli et al., 2017; Fu et al., 2019), or the relative performance of different statistical methods in predicting constituent load (Preston et al., 1989; Cohn, 1995; Guo et al., 2002; Moatar and Meybeck, 2005; Lee et al., 2016; Lee et al., 2019; Li et al., 2020; Saha et al., 2024). No method appears to offer a consistent advantage over others under all circumstances, especially when dealing with sparsely collected data. Markus et al. (2014) pointed out that it is difficult to estimate load with regression methods for extreme dry or wet periods given that these periods typically are not well represented by historical records. Using linear interpolation to calculate nitrate loads from discrete samples can be particularly sensitive to the timing and number of discrete samples (Aulenbach and Hooper, 2006).

In this study, we applied the physically-based SWAT model and three statistical models—linear interpolation (LI), LOADEST, and WRTDS_K—to estimate nitrate loads in a typical agricultural region in Prince Edward Island (PEI), Canada. The primary goal is to examine the variability of different methods in nitrate load estimation when only sparse measurements are available and identify the most suitable load estimation method, which has broad relevance to nitrate load estimation in regions with a similar setting.

2 Materials and methods

2.1 Study area and data collection

In cold and humid regions such as Atlantic Canada, water samples are primarily collected during the growing season when the water is not frozen, and sites are more accessible. According to the public data from the Department of Environment of Prince Edward Island (PEI) (https://www.princeedwardisland.ca/en/service/view-surface-water-quality), 11 stations across the province consistently recorded water quality data from 2011 to 2020. On average, each station collected 7.3 nitrate concentration samples annually, with 6.1 (83.5%) of these samples taken during the growing season (May to October). Estimating nitrate load during the cold/wet seasons using data from the warm/dry seasons poses significant challenges, as historical studies indicate strong seasonality in stream discharge and nitrate loss in this region (Bugden et al., 2014; Liang et al., 2019a; Oliver et al., 2024). Previous research has shown that nitrate loss from croplands mainly occurs during the non-growing season (late fall, winter, and early spring) in PEI, when evapotranspiration is low and crop uptake is reduced, resulting in more water and nitrogen being lost to groundwater and surface water bodies (Bugden et al., 2014; Liang et al., 2019a). Therefore, identifying an appropriate method for estimating nitrogen load in regions such as PEI becomes critically important.

This study was conducted in the Dunk River Watershed (DRW) in the Atlantic Canada province Prince Edward Island (Figure 1). The drainage area of the watershed is approximately 143 km^2, 80% of which is under agricultural production with a long history of fertilizer application (Figure 1). Agricultural land use is dominated by potatoes in rotation with forages and grains. The climate in this region is characterized as humid with a cool to mild temperature regime (Köppen-Geiger Dfb, data from WorldClim.org). The annual (1999–2020) precipitation ranged from 951 mm (2001) to 1,488 mm (2009) with an average of 1,281 mm, approximately 24% of which was in the form of snow in the dormant season (Dec - Mar) based on data from the New Glasgow weather station (46.41N, 63.35W). Discharge and water quality data have been monitored by Environment and Climate Change Canada (ECCC) and the provincial Department of Environment through the DUNK RIVER AT WALL ROAD station (Station ID: 01CB002 and SSH 51; location: 46.35N, 63.63W) near the outlet of the watershed. Long-term daily streamflow data has been monitored, and water samples have been collected for water quality analysis at monthly or biweekly intervals mainly in the non-frozen season, which is generally between April and November. The analysis was carried out using data from the period of 2011–2020, during which about 6~10 water samples were collected for water chemistry analysis annually. Such a sampling strategy is a common approach in Canada (Quilbé et al., 2006) due to the challenge of sampling in the long and cold winter season. However, as illustrated in Figure 1, the discharge of Dunk River and other rivers in the region is variable, especially during the winter months because of the combined effects of low evapotranspiration, snow precipitation, and freeze-thaw events. This lack of water quality data and the large variation in discharge in the non-growing season make the estimation of nitrate load in the region challenging.

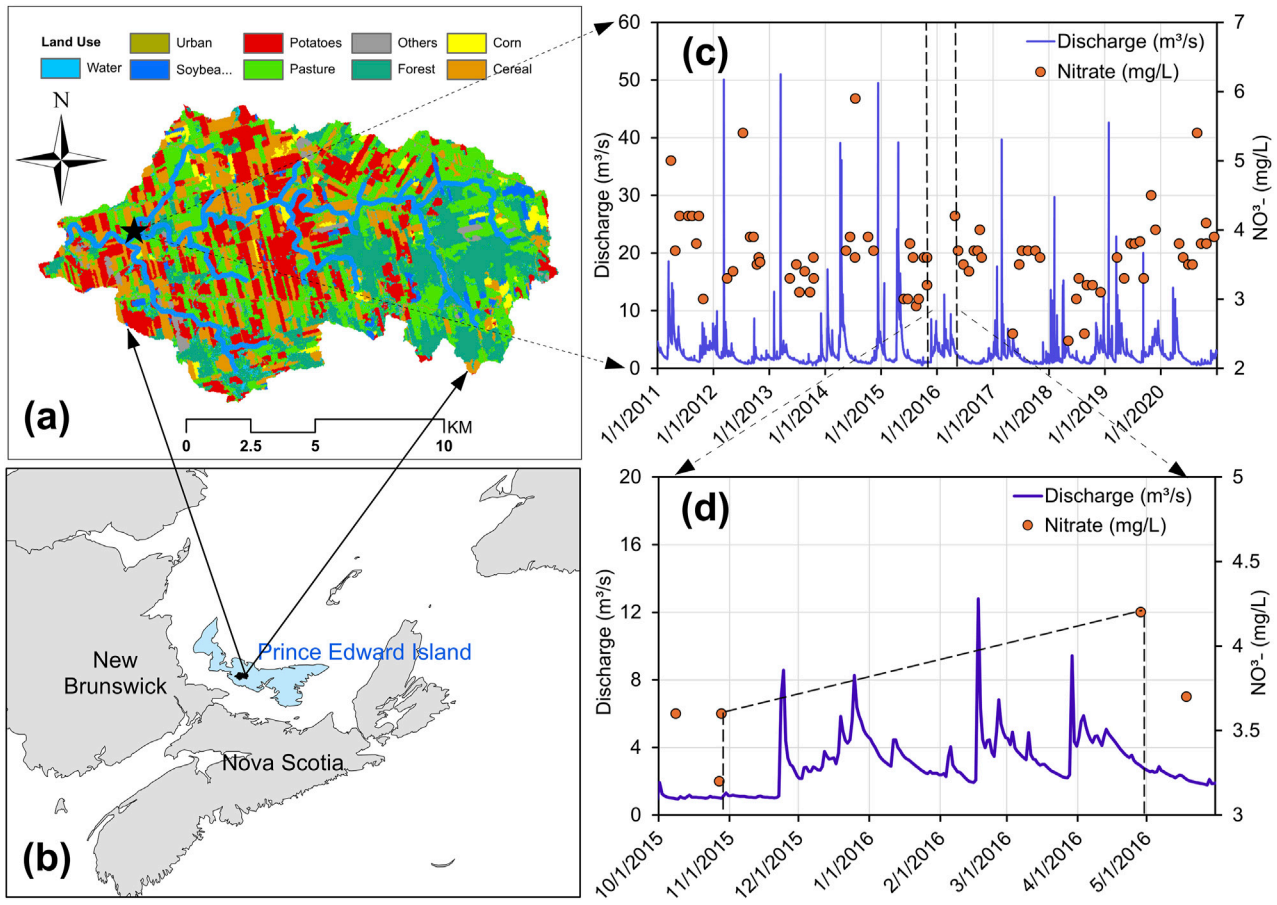


FIGURE 1
Discharge and nitrate concentration of the Dunk River Watershed **(A)** in central west Prince Edward Island **(B)**, Canada. Daily discharge data were available **(C)**, but water quality data were missing during the late fall–winter–early spring seasons (i.e., in 2015/2016) **(D)**.

2.2 Nitrate load estimation

The process-based watershed model SWAT2012 (Arnold et al., 1998), and three statistical methods including linear interpolation (LI), LOADEST (Runkel et al., 2004) and WRTDS_K (Hirsch et al., 2010; Zhang and Hirsch, 2019) were used to estimate the nitrate load of the Dunk River Watershed between 2011 and 2020.

2.2.1 Soil and water assessment tool

The SWAT model is a widely recognized watershed hydrological model developed to predict the impact of climate, land use, and management practices on water, sediment, and chemical yields in complex watersheds with varying soils, land use, landscape, and management conditions over long periods (Arnold et al., 1998; Gassman et al., 2014; Fu et al., 2019). Being a physically based model, SWAT requires detailed spatial data, including the Digital Elevation Model (DEM), soil properties, land use, and weather as model input. By dividing a watershed into multiple sub-basins and further into Hydrologic Response Units (HRUs), SWAT simulates the water cycle and associated nutrient flows. Due to its capacity and flexibility, SWAT has been broadly used for (1) evaluation of water resources or/and water quality status (Awotwi et al., 2019; Bauwe et al., 2019); (2) contaminant source analysis (Risal and Parajuli, 2019; Liang et al., 2020); (3) scenario analysis such as land use, management practices, climate variability, etc. (Yang and Best, 2015; Wagena et al., 2018; Chen et al., 2019; Wang et al., 2020); (4) evaluation of existing or inform future management practices (Moriasi et al., 2013; El-Khoury et al., 2015; Qi et al., 2018; Liang et al., 2019b; Liang et al., 2023); (5) and tracing drivers of water pollution (Li et al., 2009; Ouyang et al., 2018).

The SWAT model was setup using the ArcSWAT 2012 interface under ArcGIS 10.5.1. with detailed annual land use from 2011 to 2020 and calibrated and validated against daily streamflow, baseflow, and nitrate load for the study period using the SUFI-2 algorithm within the SWAT Calibration and Uncertainty Procedure (SWAT-CUP 2019) (Abbaspour et al., 2015). Soil data was derived from the National Soil DataBase (NSDB) of Canada. Annual land use data was obtained from the Annual Crop Inventory maps published by Agriculture and Agri-Food Canada from 2011 to 2020 (available at http://www.agr.gc.ca/atlas/aci/). Weather data including precipitation, maximum and minimum daily temperature, wind speed, solar radiation, and relative humidity were obtained from the New Glasgow station (46.41, −63.35) of ECCC. Gupta et al. (1999) proposed that logarithmic transformation enhances the sensitivity to changes in low-flow conditions by amplifying low flows and dampening high flows. Therefore, log-

transformed discharge and baseflow data were used for calibration. The model was calibrated for daily discharge and nitrate from 2011 to 2016 and validated from 2017 to 2020.

The goodness-of-fit of the SWAT simulations on streamflow and nitrate load was evaluated using the Nash-Sutcliffe Efficiency (NSE), percent bias (PBIAS) and the coefficient of determination (R^2). NSE is a widely used statistical parameter for assessing the goodness of fit of hydrologic models (Moriasi et al., 2007). The NSE ranges from -∞ to 1, where 1 indicates a perfect match between simulation and observation. PBIAS measures the average tendency of the simulated values to be larger or smaller than observations. Low magnitude PBIAS indicate better simulation with zero as the optimum value. Positive PBIAS values indicate model overestimation and negative PBIAS values indicate model underestimation (Gupta et al., 1999). The R^2 provides a measure of how well the observed data is explained by the model, with R^2 ranging from 0 to 1.

2.2.2 Linear interpolation

Linear interpolation uses concentration data to estimate the missing data, and it assumes a linear relationship between two adjacent concentration data points (Equation 1). Among flux estimation methods, the LI method is one of the simplest methods and has been broadly used to estimate constituent concentration/load in many studies, and there have been very few comparable evaluations of interpolation methods (Hirsch, 2014). However, the uncertainty of this method is that it ignores the influence of discharge and the fact that two adjacent data points may have been collected under vastly different hydrologic conditions.

$$C_s = C_i + \frac{D_s - D_i}{D_j - D_i} * \left(C_j - C_i\right) \quad (1)$$

where C_s is the estimated nitrate concentration of a specific data point at day s (D_s), which is between day i (D_i) and day j (D_i). C_i and C_j are the observed concentration data of two adjacent data points at day i (D_i) and day j (D_i), respectively.

2.2.3 Load estimator

The LOADEST is a regression-based model specifically designed for estimating constituent loads in rivers and streams by the US Geological Survey (USGS) (Cohn et al., 1992; Runkel et al., 2004). LOADEST has various levels of complexity depending on the use of fewer, or more, explanatory variables (Runkel et al., 2004). A complex form of LOADEST, the 7-parameter model was used in this study as it has been shown to perform well in relatively large watersheds (Cohn et al., 1992). The model uses multiple linear regression to fit the variables, including streamflow, streamflow squared, season (first-order Fourier series represented by sine and cosine terms), time, and time squared (Equation 2).

$$\ln(C_t) = \alpha_0 + \alpha_1 \ln Q + \alpha_2 (\ln Q)^2 + \alpha_3 \sin(2\pi T_t) + \alpha_4 \cos(2\pi T_t) + \alpha_5 T_t + \alpha_6 {T_t}^2 + \varepsilon \quad (2)$$

where $ln(C_t)$ is the natural logarithm of constituent concentration for period t; ln Q is the natural logarithm of mean daily discharge; T_t is adjusted decimal time in years, which equals decimal time minus center of decimal time; ε is a model residual; and α_k are model parameters to be estimated.

The LOADEST model requires nitrate concentration and stream discharge data as input to predict load. There are three statistical methods for estimating LOADEST regression model coefficients during calibration: Adjusted Maximum Likelihood Estimation (AMLE), Maximum Likelihood Estimation (MLE), and Least Absolute Deviation (LAD). The AMLE and MLE methods are used when the calibration model errors or residuals follow a normal distribution, while LAD is typically used when the errors are randomly distributed. LOADEST has been widely applied in the U.S. and beyond to estimate daily constituent load for a variety of water quality parameters under different sample sizes and sampling strategies (Park and Engel, 2015; Chen et al., 2022; Saha et al., 2024).

2.2.4 Weighted regression on time, discharge, and season

Similar to LOADEST, the WRTDS model was also developed by the USGS and is one of the commonly used regression methods for estimating constituent load (Hirsch et al., 2010). The WRTDS is an advanced regression-based approach, incorporating time, discharge, and season to predict constituent concentrations (Equation 3).

$$\ln(C_t) = \beta_0 + \beta_1 t + \beta_2 \ln Q + \beta_3 \sin(2\pi t) + \beta_4 \cos(2\pi t) + \varepsilon \quad (3)$$

where $ln(C_t)$ is the natural logarithm of constituent concentration for period t; ln Q is the natural logarithm of mean daily discharge; t is the time in years, ε is a model residual; and β_k are model parameters to be estimated.

WRTDS uses weighted regression to estimate the coefficients of Equation 3. Unlike LOADEST, the equation for WRTDS is estimated many times for a given dataset allowing the regression coefficients to vary across the time and discharge domain. The weight of each observation is based on the relevance of that observation to the estimation point. The relevance of each observation is defined by distances between the observation point and estimation point with respect to time, discharge, and season. And the weighted distance is measured through three dimensions, which are the time distance, seasonal distance and discharge distance (Hirsch et al., 2010). In this study, we applied the modified version of WRTDS, known as the WRTDS_Kalman Filter (WRTDS_K), which has shown improved performance over WRTDS due to the incorporation of autocorrelation information in model residuals on sampled days (Lee et al., 2019; Zhang and Hirsch, 2019). Hirsch et al. (2010) suggested using at least 100 observations with nonzero weight. To meet this data requirement, the nitrate and discharge datasets from 1999 to 2020 were used for nitrate load estimation by WRTDS_K.

2.3 Statistical analysis

Statistical analysis was carried out by using R 4.2.2. The WRTDS_K was implemented through an R package EGRET (Exploration and Graphics for RivEr Trends); a detailed description of the package is provided in Hirsch and De Cicco (2015). LOADEST was executed using the FORTRAN program available on the USGS website: https://water.usgs.gov/software/

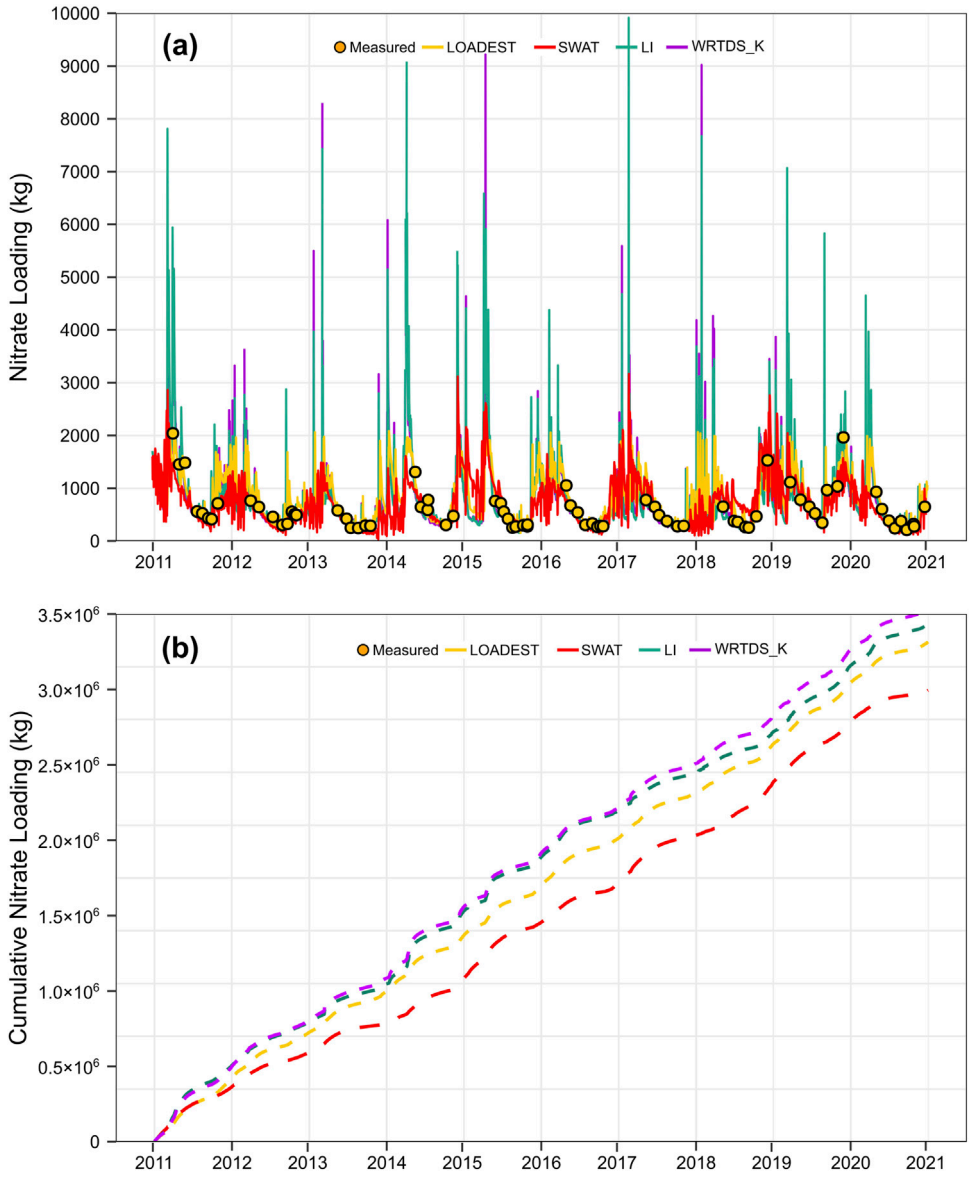


FIGURE 2
Daily **(A)** and accumulated nitrate load **(B)** of the Dunk River watershed estimated by LI (linear interpolation), LOADEST, WRTDS_K, and SWAT from 2011 to 2020.

loadest/download/. Linear interpolation was performed using the *approx* function in R. The mean, median, and standard deviation of daily nitrate load estimated by different methods was analyzed. Analysis of Variation (ANOVA) and correlation analysis was performed to explore the relationship between daily nitrate load estimated by different models, with $p < 0.05$ considered to be statistically significant.

3 Results

3.1 Model evaluation

We calibrated the SWAT model using measurements of streamflow, baseflow, and nitrate load from 2011 to 2017, and subsequently validated the model with data from 2018 to 2020. Moriasi et al. (2007) recommended that model performance can be considered satisfactory if $R^2 > 0.50$, PBIAS $\leq \pm 25\%$, and NS > 0.50 for monthly simulation. The model's performance in predicting flow and nitrate load met the recommended standard. During the calibration phase, the NSE, PBIAS, and R^2 values were 0.6, 17.4%, and 0.65 for streamflow, respectively. Comparable results were seen during the validation phase, with NSE, PBIAS, and R^2 values of 0.59, 11%, and 0.61. The baseflow predictions during calibration, the NSE, PBIAS, and R^2 values were 0.43, 8.6%, and 0.6. During the validation phase, with NSE, PBIAS, and R^2 values of 0.62, −5.6%, and 0.68, respectively. For nitrate load predictions, the calibration period saw NSE, PBIAS, and R^2 values of 0.71, 6.5%, and 0.70. During the validation period, similar values were recorded: NSE of 0.67, PBIAS of −5.5%, and R^2 of 0.68.

TABLE 1 Daily nitrate load (kg/day) estimated by LOADEST, SWAT, LI, and WRTDS_K between 2011 and 2020.

Metrics	LOADEST	SWAT	LI	WRTDS_K
Median	684	624	559	605
Mean	778 ± 424	703 ± 443	806 ± 910	829 ± 892
Range	148–2,083	17–3,149	163–15,383	178–14,702

3.2 Estimated daily nitrate load

Large differences in nitrate load estimation were found between the four methods during the 10-year study period (Figure 2). The variations in nitrate load were correlated with changes in discharge, with high flow often corresponding to high nitrate flux, and vice versa. Although nitrate concentration decreased due to the dilution effect of high flow, total nitrate exported from the watershed still increased as a result of the high flow. Overall, high flow was primarily observed from late autumn to spring. This finding is consistent with other studies conducted in similar climates (Devito et al., 1996; Devito et al., 2005; Tan and Zhang, 2011; Qi et al., 2016). Peak flows are mostly observed during late autumn to spring in response to diminished evapotranspiration, rainfall, and snowmelt. The variation in timing and magnitude of precipitation, evapotranspiration, and runoff are therefore important drivers of the seasonal variation in streamflow. Summer precipitation (June to August) accounted for only 20.4% of annual precipitation. Evapotranspiration tends to be in excess of precipitation only in the summer under cold and humid climates (Devito et al., 1996).

During the growing/low flow season, nitrate load estimates from the four methods provided reasonable approximations, compared with observed loads, which were calculated from the measured nitrate concentration and discharge data on specific days. The range of daily nitrate load for SWAT and LOADEST was 17–3,149 and 148–2,083 kg day^{-1}, respectively, compared with 163–15,383 and 178–14,702 kg day^{-1} for LI and WRTDS_K. The major differences among the four methods occurred primarily during high flow seasons when no observed nitrate concentration data were available. SWAT and LOADEST demonstrated relatively similar patterns in the range of estimated load and were substantially lower and narrower than those of LI and WRTDS_K. The average estimated daily nitrate loads during the 10 years are 703 ± 443, 778 ± 424, 806 ± 910, and 829 ± 892 kg day^{-1} for SWAT, LOADEST, LI, and WRTDS_K, respectively (Table 1). The lowest loads typically occurred in August or September, while the highest loads usually occurred in March or April. As also indicated in Figure 2, the accumulated nitrate load estimated by WRTDS_K and SWAT are consistently the highest and the lowest among the four methods. The discrepancies between different methods increases over time especially during high flow periods. For the entire 10-year period, accumulated nitrate flux estimated by LOADEST, LI, and WRTDS_K was 10.7%, 14.7%, and 18.0% higher than the SWAT model.

3.3 Nitrate load in the growing and non-growing season

Nitrate loads varied significantly between growing and non-growing season months across all methods (Figure 3). The daily nitrate load peaks in April, were 1,293, 1,024, 1,697, and 1,683 kg day^{-1} for LOADEST, SWAT, LI, and WRTDS_K, respectively. By contrast, during August and September, daily nitrate loads decrease to below 400 kg day^{-1} across all methods. Generally, the estimates from the four methods are similar during the growing season, when measured nitrate data are available. However, there are substantial differences among models for the non-growing season months (Figures 3, 4).

Results of ANOVA test indicate that daily nitrate load estimated by WRTDS_K and LI are significantly higher than that by SWAT ($p < 0.01$), while LI and LOADEST do not show a significant difference. Notably, the largest discrepancies between the regression methods and SWAT were found in 2014. Nitrate flux estimated by LI and WRTDS_K was higher than that estimated by SWAT by as much as 65.6% and 62.3%, respectively. Even though the difference of the average daily nitrate load for 2010–2020 was not obvious between SWAT and LOADEST, in some years the load estimated by LOADEST can be substantially higher than SWAT.

Mean growing season nitrate loads were lower and very similar, with values of 514 ± 288, 557 ± 293, 538 ± 365, and 537 ± 341 kg day^{-1} for SWAT, WRTDS_K, LI, and LOADEST, respectively (Figure 4; Table 2). In contrast, there were major differences in load estimation during the non-growing season. Mean nitrate loads in the non-growing season estimated by SWAT, LOADEST, LI, and WRTDS_K were 894 ± 488, 1,002 ± 419, 1,077 ± 1,178, and 1,126 ± 1,146 kg day^{-1}, respectively (Table 2).

Since nitrate loads were estimated primarily based on growing season data, the correlations between nitrate load estimates by different methods are stronger during the growing season than in the non-growing season. At a seasonal level, correlation analysis reveals that LOADEST, LI, and WRTDS_K exhibit a very strong correlation in both the growing and non-growing seasons (Figure 5), with correlation indices above 0.9. The strongest correlation is between LI and WRTDS_K, with indices exceeding 0.97 in both seasons. Although the nitrate load estimated by SWAT showed a weaker correlation with the regression methods, its strongest correlation was with LOADEST, with correlation indices of 0.77 in the growing season and 0.63 in the non-growing season.

3.4 Nitrate load estimation without non-growing season data

Over the 10-year period, there were 76 water quality data points, with 64 (or 84%) of them falling within the growing season. To assess the variability of nitrate load estimations by these four methods when non-growing season data are completely missing, we removed the 12 non-growing season data points. The removal of non-growing season data conversely led to significant variation in estimated nitrate load for the non-growing season by the regression methods. For instance, the average daily non-growing season nitrate load estimated by LOADEST decreased by 21%, from 1,002 kg day^{-1}–831 kg day^{-1}. Similarly, the average daily non-growing season nitrate load estimated by WRTDS_K decreased by 18%, from 1,126 kg day^{-1} –957 kg day^{-1}. A slight decrease was observed for LI, with the average daily nitrate load decreasing by 1.8%, from 1,076 kg day^{-1}–1,057 kg day^{-1}. The removal of non-growing season data had little to no impact on the estimation of growing season

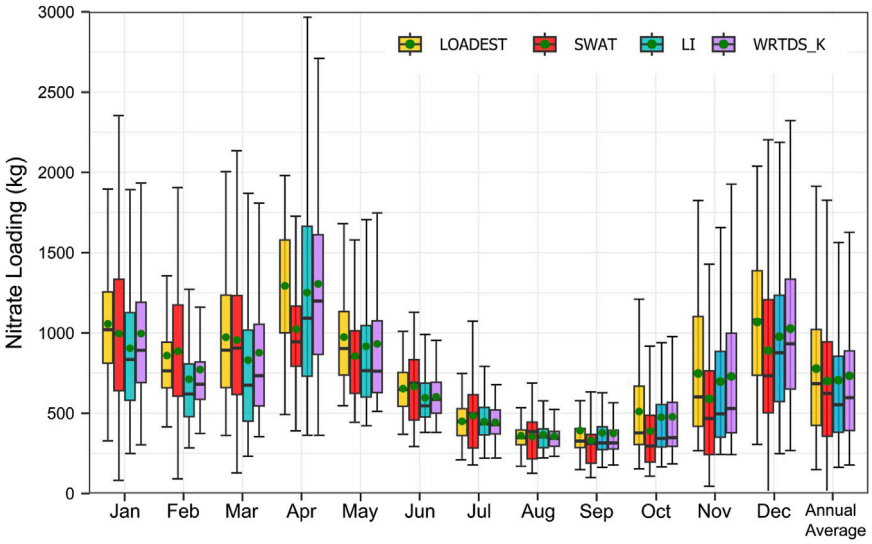


FIGURE 3
Boxplot of mean daily nitrate load by month, estimated for the study period by LOADEST, SWAT, LI, and WRTDS_K. The horizontal line inside boxes represents the median value of nitrate load. Red dots indicate the mean nitrate load estimated by each model.

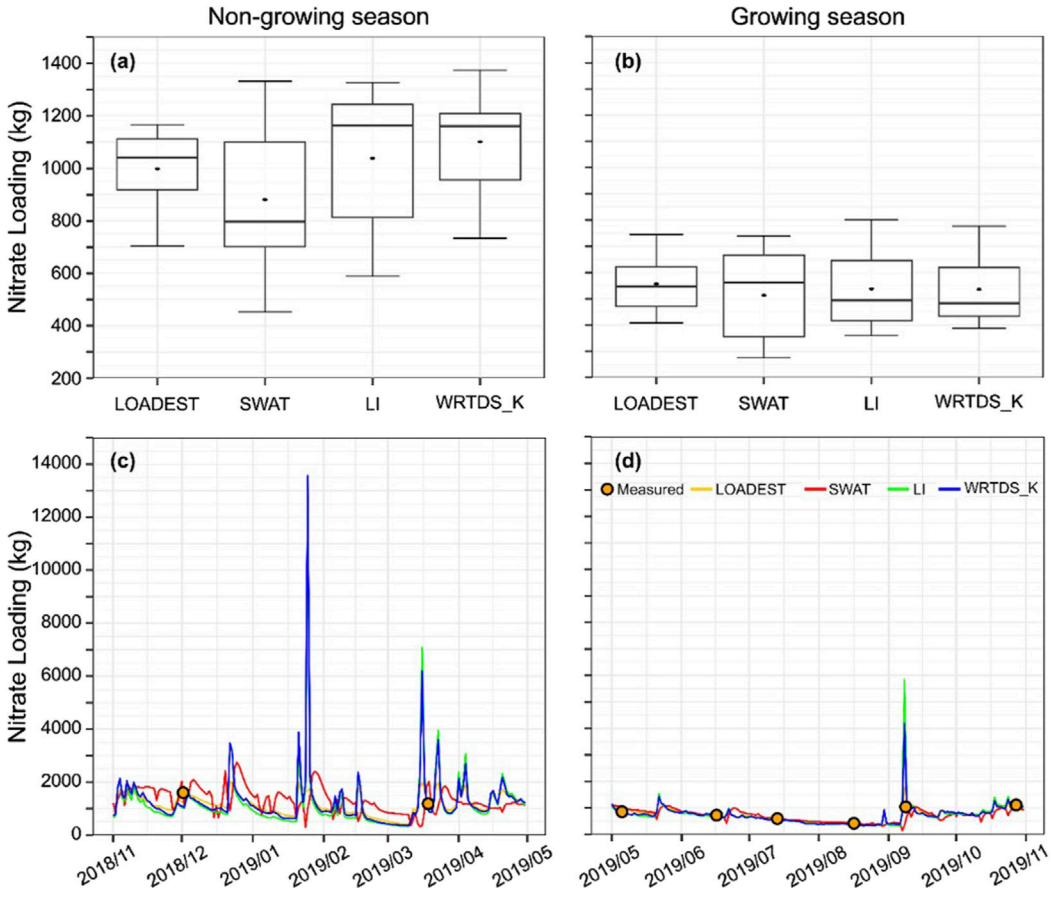


FIGURE 4
Non-growing season **(A)** and growing season **(B)** nitrate loads estimated by different methods. **(C, D)** show the in-season variation of daily nitrate load estimated by different methods.

TABLE 2 Growing season (GS) and non-growing season (NGS) daily nitrate load (kg/day) predicted by LOADEST, SWAT, LI, and WRTDS_K between 2011 and 2020.

Period	Metrics	LOADEST	SWAT	LI	WRTDS_K
GS	Median	472	452	451	443
	Mean	557 ± 293	514 ± 288	538 ± 365	537 ± 341
	Range	148–1,912	99–2,048	163–5,838	178–4,183
NGS	Median	951	850	770	833
	Mean	1,002 ± 419	894 ± 488	1,077 ± 1,178	1,126 ± 1,146
	Range	266–2,084	18–3,149	231–15,383	242–14,702

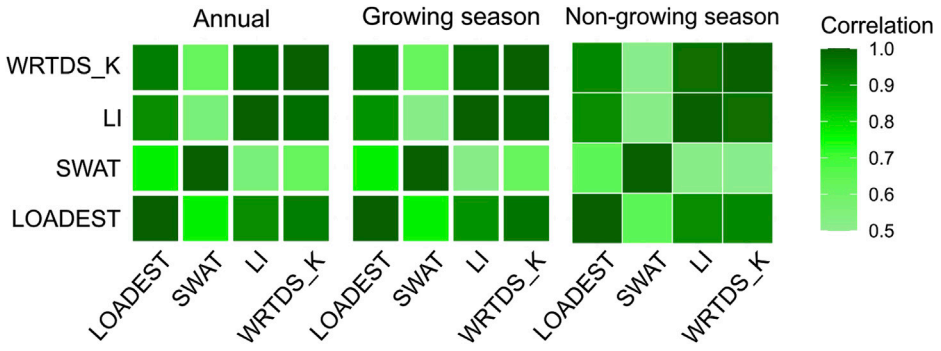


FIGURE 5
Correlation heatmap of nitrate load estimated by different methods.

nitrate load by regression methods. With LOADEST and WRTDS_K, the average daily nitrate load decreased by 6.5% and 0.4%, respectively. However, the removal of non-growing season data for calibration had minimal impact on SWAT, for both the growing and non-growing seasons.

4 Discussion

Discrete sampling has been a common strategy worldwide, particularly in cold and humid regions such as Atlantic Canada. In these areas, water samples are primarily collected during the warm seasons when the water is not frozen, and sites are more accessible. The highly dynamic nature and strong seasonal trends of water flow make estimating nitrate loads using sparsely measured water quality data a challenging task. Missing non-growing season data can lead to severe biases in load estimation by regression methods. These methods rely on existing data to establish the relationship between flow and constituent concentration and thus estimate load. Conversely, the process-based model SWAT, which is calibrated for flow and nitrogen, simulates the water and nitrogen cycling processes, and thus, can effectively represent the dilution effect of increased stream flow on nitrate mass in the wet seasons.

Nitrate concentrations were higher during the growing season and decreased during the non-growing season. Low nitrate concentrations often occur at times of high flow due to the dilution effect (Sith et al., 2019; Stutter et al., 2008). This observation is also consistent with the historical nitrate data from several watersheds in PEI, where low nitrate concentrations were frequently observed during wet seasons (Jiang et al., 2015). Regression methods generally overestimate nitrate loads during high-flow periods (Duan et al., 2014), which aligns with the results of our current study. This overestimation likely occurs because regression methods use concentration data from low flow periods to interpolate concentrations during high flow periods and cannot effectively account for the dilution effect, leading to an overestimation of both concentration and load. This bias can be amplified during years with significantly higher wet-season precipitation, resulting in high stream discharge during late winter or early spring when the snow melts. Out of the total 1,420 mm of precipitation, 267 mm was attributed to snowfall. Consequently, the nitrate load estimated by LOADEST was 28.2% higher than that estimated by SWAT.

The USGS estimated nitrate-N exported from the Mississippi River during 2004–2006 and found that LOADEST and a composite method estimated loads that were 9% and 16% higher than loads calculated using continuous *in situ* data (every 2–3 h) (Duan et al., 2014). Additionally, nitrate concentrations below the root zone are often highly variable during warmer months due to fertilizer application. As previously discussed, nitrate concentrations in rivers during the wet season can be significantly lower compared to the growing season. Accordingly, in our study, regression methods using concentration data from dry seasons to estimate concentrations during wet seasons, resulted in overestimation of

nitrate loads for wet seasons. Markus et al. (2014) pointed out that modeling loads with regression methods for extreme dry or wet periods is challenging because these periods are typically underrepresented in historical records. It is generally believed that LI has significant uncertainties because it ignores the influence of discharge and the possibility that two adjacent data points may have been collected under vastly different hydrologic conditions (Niedzielski and Halicki, 2023). Using LI to calculate nitrate loads from discrete samples can be particularly sensitive to the timing and number of discrete samples (Aulenbach and Hooper, 2006). Although LOADEST and WRTDS_K models account for seasonality and time, these methods still subject to substantial uncertainty in the non-growing season when there is no measured concentration data available. For example, the strong correlations between LI, LOADEST, and WRTDS_K in load estimations during the non-growing season likely suggest that the LOADEST and WRTDS_K might have also a problem to reliably establish discharge-concentration relationship during this period.

The SWAT model offers a detailed representation of N cycles and incorporates critical watershed input information such as land use, climate, soil properties, and topography data to simulate the hydrologic, chemical, or sediment cycles. In addition, N cycling, being one of the most common SWAT applications, is well represented in terms of processes in the model (Fu et al., 2019). The calibration of daily streamflow, baseflow, and nitrate load together with the detailed watershed information input, makes SWAT likely to provide more reliable nitrate load estimates under conditions of sparse water quality data, compared to other regression methods. However, the model also requires an extensive amount of data for model input and evaluation compared to regression methods, which require only time, discharge, and season of the collected samples.

Surface runoff and baseflow are the two primary processes driving nitrogen loads in PEI. Baseflow/groundwater flow has been reported as a major process that drives nitrogen to rivers, particularly during dry seasons, while runoff plays a more significant role during wet seasons (Jiang et al., 2004; Liang et al., 2020). For example, Liang et al. (2020) reported that in the Wilmot River watershed, which is adjacent to the Dunk River watershed, groundwater contributed 82.3%–99.0% nitrate load under different land uses during the growing season, whereas surface runoff contributed about 11.3%–43.3% of the total nitrate load during the non-growing season. Nitrate loads during the non-growing season were enhanced by runoff resulting from snowmelt events. The calibration of daily streamflow, baseflow, and nitrate load ensures a reasonable estimation of nitrogen transport through groundwater and runoff during both the growing and non-growing seasons. This likely explains the relatively small variation in SWAT's estimation of nitrogen load compared to regression models after the removal of 20% of the non-growing season data. The large bias of nitrate load estimation by regression models, especially during the non-growing season, results from a lack of fit between concentration and discharge data, coupled with substantial seasonal variability in their relationship. However, numerous studies have demonstrated the advantages of regression models such as LOADEST and WRTDS, especially when a reasonable amount of representative water quality data is available. They are favored for their ease of application and the relatively small effort required for model setup (Chanat et al., 2016; Lee et al., 2016). Our study suggests that caution is needed when applying regression models for constituent load estimation when there is insufficient water quality data to build a representative discharge-constituent concentration relationship. Process-based models such as SWAT could be a better alternative under such circumstances. While there is no universally agreed-upon method for calculating nitrate flux, the use of a more robust tool such as SWAT can help limit these errors. Without leveraging information from SWAT, regression methods may fail to provide reasonable estimates, particularly when the monitoring data are too limited to establish a reliable concentration-discharge relationship., This issue is especially prevalent in regions with high and variable precipitation weather patterns, such as Atlantic Canada.

5 Conclusion

Nitrate load estimation has been a challenge, particularly in cold and humid regions like Atlantic Canada where data availability is limited and seasonal variations in nitrate loss are pronounced. Our study examined different methods for estimating nitrate loads in the Dunk River watershed in PEI, aiming to identify the most suitable approach for load estimation when the available water quality data is predominantly (>84%) from the growing season. Our study highlights the complexities of nitrate load estimation with limited data availability and confirmed that the absence of the 16% available non-growing season data during the 10-year study period can lead to significant biases in load estimation by regression methods, with biases potentially reaching as high as 21%, while nitrate load estimates obtained with SWAT were found to be less sensitive to systematic data gaps. In such cases, process-based models like SWAT may offer more accurate estimates by incorporating detailed mathematical representations of flow and nitrogen cycles and watershed information calibrated for flow and nitrogen cycles under conditions of limited data availability. Additionally, process-based models also hold the benefits of scenario analysis (e.g., management/land use etc.), source identification, tracing of the drivers of water pollutants, etc. Policymakers and researchers should consider employing hydrological models for nitrate load estimation in situations with limited water quality measurement, despite their requirement for more expertise. However, the choice of estimation method should be dynamic and case-specific, considering the unique characteristics of each watershed and the available data. With agri-environmental water quality issues become increasingly pressing, it is crucial to employ data collection strategies that capture seasonal variations in streamflow and nitrate concentration effectively, especially in regions like Atlantic Canada. By doing so, we can improve our understanding of nitrate load dynamics and develop more effective strategies for mitigating N pollution in aquatic ecosystems.

Data availability statement

The raw data supporting the conclusions of this article will be made available by the authors, without undue reservation.

Author contributions

KL: Conceptualization, Data curation, Formal Analysis, Investigation, Methodology, Software, Visualization, Writing–original draft, Writing–review and editing. YJ: Conceptualization, Funding acquisition, Investigation, Methodology, Resources, Supervision, Writing–review and editing. KF: Investigation, Validation, Writing–review and editing. MC: Investigation, Validation, Writing–review and editing. XZ: Investigation, Resources, Writing–review and editing. JQ: Validation, Writing–review and editing. XG: Validation, Writing–review and editing. TL: Validation, Writing–review and editing. QZ: Methodology, Validation, Writing–review and editing. MA: Methodology, Software, Writing–review and editing. F-RM: Conceptualization, Investigation, Methodology, Supervision, Writing–review and editing.

Funding

The author(s) declare that financial support was received for the research, authorship, and/or publication of this article. This study was funded by the projects "Using Living Laboratory approach to develop and transfer innovative soil and water quality BMPs in Prince Edward Island" (Grant No. J-002269) and "Reducing sediment, N and P load from arable cropping systems to receiving waters in eastern Canada" (Grant No. J-001270) from Agriculture and Agri-Food Canada.

Acknowledgments

The authors would like to thank the Environment and Climate Change Canada, Agriculture and Agri-Food Canada, and the provincial government of Prince Edward Island for providing the data used in this study. U.S. Department of Agriculture (USDA) is an equal opportunity provider and employer. Mention of trade names or commercial products in this publication is solely for the purpose of providing specific information and does not imply recommendation or endorsement by the USDA.

Conflict of interest

The authors declare that the research was conducted in the absence of any commercial or financial relationships that could be construed as a potential conflict of interest.

The author(s) declared that they were an editorial board member of Frontiers, at the time of submission. This had no impact on the peer review process and the final decision.

Generative AI statement

The author(s) declare that no Generative AI was used in the creation of this manuscript.

Publisher's note

All claims expressed in this article are solely those of the authors and do not necessarily represent those of their affiliated organizations, or those of the publisher, the editors and the reviewers. Any product that may be evaluated in this article, or claim that may be made by its manufacturer, is not guaranteed or endorsed by the publisher.

References

Abbaspour, K. C., Rouholahnejad, E., Vaghefi, S., Srinivasan, R., Yang, H., and Kløve, B. (2015). A continental-scale hydrology and water quality model for Europe: calibration and uncertainty of a high-resolution large-scale SWAT model. *J. Hydrology* 524, 733–752. doi:10.1016/j.jhydrol.2015.03.027

Arnold, J. G., Srinivasan, R., Muttiah, R. S., and Williams, J. R. (1998). Large area hydrologic modeling and assessment part I: model development 1. *J. Am. Water Resour. Assoc.* 34 (1), 73–89. doi:10.1111/j.1752-1688.1998.tb05961.x

Ator, S. W., and Garcia, A. M. (2016). Application of SPARROW modeling to understanding contaminant fate and transport from uplands to streams. *JAWRA J. Am. Water Resour. Assoc.* 52 (3), 685–704. doi:10.1111/1752-1688.12419

Aulenbach, B. T., and Hooper, R. P. (2006). The composite method: an improved method for stream-water solute load estimation. *Hydrological Process. An Int. J.* 20 (14), 3029–3047. doi:10.1002/hyp.6147

Awotwi, A., Anornu, G. K., Quaye-Ballard, J. A., Annor, T., Forkuo, E. K., Harris, E., et al. (2019). Water balance responses to land-use/land-cover changes in the Pra River Basin of Ghana, 1986–2025. *Catena* 182, 104129. doi:10.1016/j.catena.2019.104129

Bauwe, A., Kahle, P., and Lennartz, B. (2019). Evaluating the SWAT model to predict streamflow, nitrate loadings and crop yields in a small agricultural catchment. *Adv. Geosciences* 48, 1–9. doi:10.5194/adgeo-48-1-2019

Birgand, F., Faucheux, C., Gruau, G., Augeard, B., Moatar, F., and Bordenave, P. (2010). Uncertainties in assessing annual nitrate loads and concentration indicators: Part 1. Impact of sampling frequency and load estimation algorithms. *Trans. ASABE* 53 (2), 437–446. doi:10.13031/2013.29584

Borah, D., and Bera, M. (2003). Watershed-scale hydrologic and nonpoint-source pollution models: review of mathematical bases. *Trans. ASAE* 46 (6), 1553–1566. doi:10.13031/2013.15644

Brilli, L., Bechini, L., Bindi, M., Carozzi, M., Cavalli, D., Conant, R., et al. (2017). Review and analysis of strengths and weaknesses of agro-ecosystem models for simulating C and N fluxes. *Sci. Total Environ.* 598, 445–470. doi:10.1016/j.scitotenv.2017.03.208

Bugden, G., Jiang, Y., van den Heuvel, M., Vandermeulen, H., MacQuarrie, K., Crane, C., et al. (2014). *Nitrogen loading criteria for estuaries in Prince edward Island.* Prince Edward Island, Canada: Government of Prince Edward Island.

Chanat, J. G., Moyer, D. L., Blomquist, J. D., Hyer, K. E., and Langland, M. J. (2016). *Application of a weighted regression model for reporting nutrient and sediment concentrations, fluxes, and trends in concentration and flux for the Chesapeake Bay Nontidal Water-Quality Monitoring Network, results through water year 2012.* Richmond, VA: United States Geological Survey.

Chen, J., Shi, W., and Jin, X. (2022). Pollutant flux estimation of the Lijiang River based on an improved prediction-correction method. *Front. Environ. Sci.* 10, 868404. doi:10.3389/fenvs.2022.868404

Chen, Y., Marek, G. W., Marek, T. H., Moorhead, J. E., Heflin, K. R., Brauer, D. K., et al. (2019). Simulating the impacts of climate change on hydrology and crop production in the Northern High Plains of Texas using an improved SWAT model. *Agric. Water Manag.* 221, 13–24. doi:10.1016/j.agwat.2019.04.021

Cohn, T. (1995). Recent advances in statistical methods for the estimation of sediment and nutrient transport in rivers. *Rev. Geophys.* 33 (S2), 1117–1123. doi:10.1029/95rg00292

Cohn, T., Cauldes, D., Gilroy, E., Zynjuk, L., and Summers, R. (1992). The validity of a simple longlinear model for estimating fluvial constituent loads entering Chesapeake Bay. *Water Resour. Res.* 28 (9), 2353–2363.

Cordeiro, M. R. C., Liang, K., Wilson, H. F., Vanrobaeys, J., Lobb, D. A., Fang, X., et al. (2022). Simulating the hydrological impacts of land use conversion from annual crop to perennial forage in the Canadian Prairies using the Cold Regions Hydrological Modelling platform. *Hydrology Earth Syst. Sci.* 26 (22), 5917–5931. doi:10.5194/hess-26-5917-2022

Devito, K. J., Creed, I. F., and Fraser, C. J. D. (2005). Controls on runoff from a partially harvested aspen-forested headwater catchment, Boreal Plain, Canada. *Hydrol. Process.* 19 (1), 3–25. doi:10.1002/hyp.5776

Devito, K. J., Hill, A., and Roulet, N. (1996). Groundwater-surface water interactions in headwater forested wetlands of the Canadian Shield. *J. Hydrology* 181 (1-4), 127–147. doi:10.1016/0022-1694(95)02912-5

Duan, S., Powell, R. T., and Bianchi, T. S. (2014). High frequency measurement of nitrate concentration in the Lower Mississippi River, USA. *J. Hydrology* 519 (Part A), 376–386. doi:10.1016/j.jhydrol.2014.07.030

El-Khoury, A., Seidou, O., Lapen, D. R., Que, Z., Mohammadian, M., Sunohara, M., et al. (2015). Combined impacts of future climate and land use changes on discharge, nitrogen and phosphorus loads for a Canadian river basin. *J. Environ. Manage* 151, 76–86. doi:10.1016/j.jenvman.2014.12.012

Ferguson, R. (1986). River loads underestimated by rating curves. *Water Resour. Res.* 22 (1), 74–76. doi:10.1029/wr022i001p00074

Fu, B., Li, Y., Wang, Y., Campbell, A., Zhang, B., Yin, S., et al. (2017). Evaluation of riparian condition of Songhua River by integration of remote sensing and field measurements. *Sci. Rep.* 7 (1), 2565–2616. doi:10.1038/s41598-017-02772-3

Fu, B., Merritt, W. S., Croke, B. F. W., Weber, T. R., and Jakeman, A. J. (2019). A review of catchment-scale water quality and erosion models and a synthesis of future prospects. *Environ. Model. and Softw.* 114, 75–97. doi:10.1016/j.envsoft.2018.12.008

Galloway, J. N., Aber, J. D., Erisman, J. W., Seitzinger, S. P., Howarth, R. W., Cowling, E. B., et al. (2003). The nitrogen cascade. *Bioscience* 53 (4), 341–356. doi:10.1641/0006-3568(2003)053[0341:tnc]2.0.co;2

Galloway, J. N., Townsend, A. R., Erisman, J. W., Bekunda, M., Cai, Z., Freney, J. R., et al. (2008). Transformation of the nitrogen cycle: recent trends, questions, and potential solutions. *Science* 320 (5878), 889–892. doi:10.1126/science.1136674

Gassman, P. W., Sadeghi, A. M., and Srinivasan, R. (2014). Applications of the SWAT model special section: overview and insights. *J. Environ. Qual.* 43 (1), 1–8. doi:10.2134/jeq2013.11.0466

Guo, Y., Markus, M., and Demissie, M. (2002). Uncertainty of nitrate-N load computations for agricultural watersheds. *Water Resour. Res.* 38 (10), 3-1-3–12. doi:10.1029/2001wr001149

Gupta, H. V., Sorooshian, S., and Yapo, P. O. (1999). Status of automatic calibration for hydrologic models: comparison with multilevel expert calibration. *J. Hydrologic Eng.* 4 (2), 135–143. doi:10.1061/(asce)1084-0699(1999)4:2(135)

Hirsch, R. M. (2014). Large biases in regression-based constituent flux estimates: causes and diagnostic tools. *JAWRA J. Am. Water Resour. Assoc.* 50 (6), 1401–1424. doi:10.1111/jawr.12195

Hirsch, R. M., and De Cicco, L. A. (2015). *User guide to Exploration and Graphics for RivEr Trends (EGRET) and dataRetrieval: R packages for hydrologic data*. Reston, VA: United States Geological Survey.

Hirsch, R. M., Moyer, D. L., and Archfield, S. A. (2010). Weighted regressions on time, discharge, and season (WRTDS), with an application to chesapeake bay river inputs. *J. Am. Water Resour. Assoc.* 46 (5), 857–880. doi:10.1111/j.1752-1688.2010.00482.x

Hou, C., Chu, M. L., Guzman, J. A., Triana, J. S. A., Moriasi, D. N., and Steiner, J. L. (2019). Field scale nitrogen load in surface runoff: impacts of management practices and changing climate. *J. Environ. Manag.* 249, 109327. doi:10.1016/j.jenvman.2019.109327

Hrachowitz, M., Savenije, H., Blöschl, G., McDonnell, J., Sivapalan, M., Pomeroy, J., et al. (2013). A decade of predictions in ungauged basins (PUB)—a review. *Hydrological Sci. J.* 58 (6), 1198–1255. doi:10.1080/02626667.2013.803183

Jiang, S. Y., Zhang, Q., Werner, A. D., Wellen, C., Jomaa, S., Zhu, Q. D., et al. (2019). Effects of stream nitrate data frequency on watershed model performance and prediction uncertainty. *J. Hydrology* 569, 22–36. doi:10.1016/j.jhydrol.2018.11.049

Jiang, Y., Nishimura, P., van den Heuvel, M. R., MacQuarrie, K. T. B., Crane, C. S., Xing, Z., et al. (2015). Modeling land-based nitrogen loads from groundwater-dominated agricultural watersheds to estuaries to inform nutrient reduction planning. *J. Hydrology* 529, 213–230. doi:10.1016/j.jhydrol.2015.07.033

Jiang, Y., Woodbury, A. D., and Painter, S. (2004). Full-Bayesian inversion of the Edwards aquifer. *Groundwater* 42 (5), 724–733.

Lee, C. J., Hirsch, R. M., and Crawford, C. G. (2019). An evaluation of methods for computing annual water-quality loads. *U. S. Geol. Surv.* doi:10.3133/sir20195084

Lee, C. J., Hirsch, R. M., Schwarz, G. E., Holtschlag, D. J., Preston, S. D., Crawford, C. G., et al. (2016). An evaluation of methods for estimating decadal stream loads. *J. Hydrology* 542, 185–203. doi:10.1016/j.jhydrol.2016.08.059

Li, S., Bhattarai, R., Cooke, R. A., Verma, S., Huang, X., Markus, M., et al. (2020). Relative performance of different data mining techniques for nitrate concentration and load estimation in different type of watersheds. *Environ. Pollut.* 263, 114618. doi:10.1016/j.envpol.2020.114618

Li, Z., Liu, W.-z., Zhang, X.-c., and Zheng, F.-l. (2009). Impacts of land use change and climate variability on hydrology in an agricultural catchment on the Loess Plateau of China. *J. Hydrology* 377 (1-2), 35–42. doi:10.1016/j.jhydrol.2009.08.007

Liang, K., Jiang, Y., Nyiraneza, J., Fuller, K., Murnaghan, D., and Meng, F.-R. (2019a). Nitrogen dynamics and leaching potential under conventional and alternative potato rotations in Atlantic Canada. *Field Crops Res.* 242, 107603. doi:10.1016/j.fcr.2019.107603

Liang, K., Jiang, Y., Qi, J., Fuller, K., Nyiraneza, J., and Meng, F.-R. (2020). Characterizing the impacts of land use on nitrate load and water yield in an agricultural watershed in Atlantic Canada. *Sci. Total Environ.* 729, 138793. doi:10.1016/j.scitotenv.2020.138793

Liang, K., Qi, J., Liu, E., Jiang, Y., Li, S., and Meng, F.-R. (2019b). Estimated potential impacts of soil and water conservation terraces on potato yields under different climate conditions. *J. Soil Water Conservation* 74 (3), 225–234. doi:10.2489/jswc.74.3.225

Liang, K., Zhang, X., Liang, X.-Z., Jin, V. L., Birru, G., Schmer, M. R., et al. (2023). Simulating agroecosystem soil inorganic nitrogen dynamics under long-term management with an improved SWAT-C model. *Sci. Total Environ.* 879, 162906. doi:10.1016/j.scitotenv.2023.162906

Markus, M., Demissie, M., Short, M. B., Verma, S., and Cooke, R. A. (2014). Sensitivity analysis of annual nitrate loads and the corresponding trends in the lower Illinois River. *J. Hydrologic Eng.* 19 (3), 533–543. doi:10.1061/(asce)he.1943-5584.0000831

Mattikalli, N. M., and Richards, K. S. (1996). Estimation of surface water quality changes in response to land use change: application of the export coefficient model using remote sensing and geographical information system. *J. Environ. Manag.* 48 (3), 263–282. doi:10.1006/jema.1996.0077

Milovanovic, M. (2007). Water quality assessment and determination of pollution sources along the Axios/Vardar River, Southeastern Europe. *Desalination* 213 (1-3), 159–173. doi:10.1016/j.desal.2006.06.022

Moatar, F., and Meybeck, M. (2005). Compared performances of different algorithms for estimating annual nutrient loads discharged by the eutrophic River Loire. *Hydrol. Process.* 19 (2), 429–444. doi:10.1002/hyp.5541

Molina-Navarro, E., Andersen, H. E., Nielsen, A., Thodsen, H., and Trolle, D. (2018). Quantifying the combined effects of land use and climate changes on stream flow and nutrient loads: a modelling approach in the Odense Fjord catchment (Denmark). *Sci. Total Environ.* 621, 253–264. doi:10.1016/j.scitotenv.2017.11.251

Moriasi, D. N., Arnold, J. G., Van Liew, M. W., Bingner, R. L., Harmel, R. D., and Veith, T. L. (2007). Model evaluation guidelines for systematic quantification of accuracy in watershed simulations. *Trans. ASABE* 50 (3), 885–900. doi:10.13031/2013.23153

Moriasi, D. N., Gowda, P. H., Arnold, J. G., Mulla, D. J., Ale, S., and Steiner, J. L. (2013). Modeling the impact of nitrogen fertilizer application and tile drain configuration on nitrate leaching using SWAT. *Agric. Water Manag.* 130, 36–43. doi:10.1016/j.agwat.2013.08.003

Neitsch, S. L., Arnold, J. G., Kiniry, J. R., and Williams, J. R. (2011). *Soil and water assessment tool theoretical documentation version 2009*. Temple, TX: U.S. Department of Agriculture - Agricultural Research Service.

Nguyen, H. H., Recknagel, F., Meyer, W., Frizenschaf, J., and Shrestha, M. K. (2017). Modelling the impacts of altered management practices, land use and climate changes on the water quality of the Millbrook catchment reservoir system in South Australia. *J. Environ. Manag.* 202 (Part 1), 1–11. doi:10.1016/j.jenvman.2017.07.014

Niedzielski, T., and Halicki, M. (2023). Improving linear interpolation of missing hydrological data by applying integrated autoregressive models. *Water Resour. Manag.* 37 (14), 5707–5724. doi:10.1007/s11269-023-03625-7

Odgaard, M. V., Olesen, J. E., Graversgaard, M., Borgesen, C. D., Svenning, J.-C., and Dalgaard, T. (2019). Targeted set-aside: benefits from reduced nitrogen loading in Danish aquatic environments. *J. Environ. Manag.* 247, 633–643. doi:10.1016/j.jenvman.2019.06.107

Oliver, A. C., Kurylyk, B. L., Johnston, L. H., LeRoux, N. K., Somers, L. D., and Jamieson, R. C. (2024). Impacts of climate change and best management practices on nitrate loading to a eutrophic coastal lagoon. *Front. Environ. Sci.* 12. doi:10.3389/fenvs.2024.1468869

Ongley, E. D., Xiaolan, Z., and Tao, Y. (2010). Current status of agricultural and rural non-point source Pollution assessment in China. *Environ. Pollut.* 158 (5), 1159–1168. doi:10.1016/j.envpol.2009.10.047

Ouyang, W., Yang, W., Tysklind, M., Xu, Y., Lin, C., Gao, X., et al. (2018). Using river sediments to analyze the driving force difference for non-point source pollution dynamics between two scales of watersheds. *Water Res.* 139, 311–320. doi:10.1016/j.watres.2018.04.020

Park, Y. S., and Engel, B. A. (2015). Analysis for regression model behavior by sampling strategy for annual pollutant load estimation. *J. Environ. Qual.* 44 (6), 1843–1851. doi:10.2134/jeq2015.03.0137

Pellerin, B. A., Bergamaschi, B. A., Gilliom, R. J., Crawford, C. G., Saraceno, J., Frederick, C. P., et al. (2014). Mississippi River nitrate loads from high frequency sensor measurements and regression-based load estimation. *Environ. Sci. and Technol.* 48 (21), 12612–12619. doi:10.1021/es504029c

Preston, S. D., Bierman Jr, V. J., and Silliman, S. E. (1989). An evaluation of methods for the estimation of tributary mass loads. *Water Resour. Res.* 25 (6), 1379–1389. doi:10.1029/wr025i006p01379

Qi, J., Li, S., Bourque, C. P. A., Xing, Z., and Meng, F.-R. (2018). Developing a decision support tool for assessing land use change and BMPs in ungauged watersheds based on

decision rules provided by SWAT simulation. *Hydrology Earth Syst. Sci.* 22 (7), 3789–3806. doi:10.5194/hess-22-3789-2018

Qi, J., Li, S., Li, Q., Xing, Z., Bourque, C. P. A., and Meng, F.-R. (2016). Assessing an enhanced version of SWAT on water quantity and quality simulation in regions with seasonal snow cover. *Water Resour. Manag.* 30 (14), 5021–5037. doi:10.1007/s11269-016-1466-8

Quilbé, R., Rousseau, A. N., Duchemin, M., Poulin, A., Gangbazo, G., and Villeneuve, J.-P. (2006). Selecting a calculation method to estimate sediment and nutrient loads in streams: application to the Beaurivage River (Québec, Canada). *J. Hydrology* 326 (1-4), 295–310. doi:10.1016/j.jhydrol.2005.11.008

Risal, A., and Parajuli, P. B. (2019). Quantification and simulation of nutrient sources at watershed scale in Mississippi. *Sci. Total Environ.* 670, 633–643. doi:10.1016/j.scitotenv.2019.03.233

Robertson, D. M., and Roerish, E. D. (1999). Influence of various water quality sampling strategies on load estimates for small streams. *Water Resour. Res.* 35 (12), 3747–3759. doi:10.1029/1999wr900277

Rode, M., Wade, A. J., Cohen, M. J., Hensley, R. T., Bowes, M. J., Kirchner, J. W., et al. (2016). Sensors in the stream: the high-frequency wave of the present. *Environ. Sci. Technol.* 50 (19), 10297–10307. doi:10.1021/acs.est.6b02155

Runkel, R. L., Crawford, C. G., and Cohn, T. A. (2004). "Load Estimator (LOADEST): a FORTRAN program for estimating constituent loads in streams and rivers".

Saha, G., Shen, C., Duncan, J., and Cibin, R. (2024). Performance evaluation of deep learning based stream nitrate concentration prediction model to fill stream nitrate data gaps at low-frequency nitrate monitoring basins. *J. Environ. Manage* 357, 120721. doi:10.1016/j.jenvman.2024.120721

Sith, R., Watanabe, A., Nakamura, T., Yamamoto, T., and Nadaoka, K. (2019). Assessment of water quality and evaluation of best management practices in a small agricultural watershed adjacent to Coral Reef area in Japan. *Agric. Water Manag.* 213, 659–673. doi:10.1016/j.agwat.2018.11.014

Sorando, R., Comin, F. A., Jimenez, J. J., Sanchez-Perez, J. M., and Sauvage, S. (2019). Water resources and nitrate discharges in relation to agricultural land uses in an intensively irrigated watershed. *Sci. Total Environ.* 659, 1293–1306. doi:10.1016/j.scitotenv.2018.12.023

Stenback, G. A., Crumpton, W. G., Schilling, K. E., and Helmers, M. J. (2011). Rating curve estimation of nutrient loads in Iowa rivers. *J. Hydrology* 396 (1-2), 158–169. doi:10.1016/j.jhydrol.2010.11.006

Stutter, M. I., Langan, S. J., and Cooper, R. J. (2008). Spatial contributions of diffuse inputs and within-channel processes to the form of stream water phosphorus over storm events. *J. Hydrol.* 350, 203–214. doi:10.1016/j.jhydrol.2007.10.045

Tan, C. S., and Zhang, T. Q. (2011). Surface runoff and sub-surface drainage phosphorus losses under regular free drainage and controlled drainage with sub-irrigation systems in southern Ontario. *Can. J. Soil Sci.* 91 (3), 349–359. doi:10.4141/cjss09086

Toor, G. S., Harmel, R. D., Haggard, B. E., and Schmidt, G. (2008). Evaluation of regression methodology with low-frequency water quality sampling to estimate constituent loads for ephemeral watersheds in Texas. *J. Environ. Qual.* 37 (5), 1847–1854. doi:10.2134/jeq2007.0232

Ullrich, A., and Volk, M. (2010). Influence of different nitrate-N monitoring strategies on load estimation as a base for model calibration and evaluation. *Environ. Monit. Assess.* 171 (1-4), 513–527. doi:10.1007/s10661-009-1296-8

Verhoff, F. H., Melfi, D. A., and Yaksich, S. M. (1980). River nutrient and chemical transport estimation. *J. Environ. Eng. Div.* 106 (3), 591–608. doi:10.1061/jeegav.0001047

Verma, S., Markus, M., and Cooke, R. A. (2012). Development of error correction techniques for nitrate-N load estimation methods. *J. Hydrology* 432-433, 12–25. doi:10.1016/j.jhydrol.2012.02.011

Wagena, M. B., Collick, A. S., Ross, A. C., Najjar, R. G., Rau, B., Sommerlot, A. R., et al. (2018). Impact of climate change and climate anomalies on hydrologic and biogeochemical processes in an agricultural catchment of the Chesapeake Bay watershed, USA. *Sci. Total Environ.* 637-638, 1443–1454. doi:10.1016/j.scitotenv.2018.05.116

Wang, Q., Qi, J., Li, J., Cole, J., Waldhoff, S. T., and Zhang, X. J. W. r. (2020). Nitrate loading projection is sensitive to freeze-thaw cycle representation. *Water Res.* 186, 116355. doi:10.1016/j.watres.2020.116355

Yadav, S., Babel, M. S., Shrestha, S., and Deb, P. (2019). Land use impact on the water quality of large tropical river: mun River Basin, Thailand. *Environ. Monit. Assess.* 191 (10), 614. doi:10.1007/s10661-019-7779-3

Yang, G., and Best, E. P. H. (2015). Spatial optimization of watershed management practices for nitrogen load reduction using a modeling-optimization framework. *J. Environ. Manag.* 161, 252–260. doi:10.1016/j.jenvman.2015.06.052

Yang, X., Jomaa, S., Buttner, O., and Rode, M. (2019). Autotrophic nitrate uptake in river networks: a modeling approach using continuous high-frequency data. *Water Res.* 157, 258–268. doi:10.1016/j.watres.2019.02.059

Yang, X., Liu, Q., Fu, G., He, Y., Luo, X., and Zheng, Z. (2016). Spatiotemporal patterns and source attribution of nitrogen load in a river basin with complex pollution sources. *Water Res.* 94, 187–199. doi:10.1016/j.watres.2016.02.040

Zamyadi, A., Gallichand, J., and Duchemin, M. (2007). Comparison of methods for estimating sediment and nitrogen loads from a small agricultural watershed. *Can. Biosyst. Eng.* 49, 1.

Zhang, Q., and Hirsch, R. M. (2019). River water-quality concentration and flux estimation can be improved by accounting for serial correlation through an autoregressive model. *Water Resour. Res.* 55 (11), 9705–9723. doi:10.1029/2019wr025338

frontiers | Frontiers in Environmental Science

TYPE Original Research
PUBLISHED 17 June 2025
DOI 10.3389/fenvs.2025.1549218

Check for updates

OPEN ACCESS

EDITED BY
Jana Levison,
University of Guelph, Canada

REVIEWED BY
Pradeep Goel,
Ontario Ministry of the Environment and Climate Change, Canada
Peter Smiley,
Agricultural Research Service (USDA), United States

*CORRESPONDENCE
Debabrata Sahoo,
dsahoo@clemson.edu

RECEIVED 20 December 2024
ACCEPTED 28 April 2025
PUBLISHED 17 June 2025

CITATION
Jordan EN, Sahoo D, Sawyer CB, Pike JW, Park DM, White SA and Haggard BE (2025) Nutrient dynamics in restored and unrestored urban streams in the Piedmont ecoregion of South Carolina.
Front. Environ. Sci. 13:1549218.
doi: 10.3389/fenvs.2025.1549218

COPYRIGHT
© 2025 Jordan, Sahoo, Sawyer, Pike, Park, White and Haggard. This is an open-access article distributed under the terms of the Creative Commons Attribution License (CC BY). The use, distribution or reproduction in other forums is permitted, provided the original author(s) and the copyright owner(s) are credited and that the original publication in this journal is cited, in accordance with accepted academic practice. No use, distribution or reproduction is permitted which does not comply with these terms.

Nutrient dynamics in restored and unrestored urban streams in the Piedmont ecoregion of South Carolina

Emily N. Jordan[1], Debabrata Sahoo[2]*, Calvin B. Sawyer[2], Jeremy W. Pike[2], Dara M. Park[1], Sarah A. White[1] and Brian E. Haggard[3]

[1]Plant and Environmental Sciences, Clemson University, Clemson, SC, United States, [2]Department of Agricultural Sciences, Clemson University, Clemson, SC, United States, [3]Department of Biological and Agricultural Engineering, University of Arkansas, Fayetteville, AR, United States

The United States invests billions of dollars annually to perform stream restoration projects, yet few studies have investigated the effects this ecosystem manipulation has on nutrient cycling and associated water quality. Water quality improvement remains a substantial motivation for mitigating catchment-scale disturbances, especially in urban streams. Various urban land use practices impact the transfer and transport of nutrients such as soluble reactive phosphorus, ammonium, and nitrate plus nitrite from land into the streams and rivers. The uptake length (S_w), or the distance a dissolved nutrient travels downstream within a stream reach, can be measured using short-term nutrient injections, where shorter uptake lengths suggest greater nutrient retention. This study evaluated the efficacy of using nutrient injection experiments as a monitoring tool to assess nutrient retention efficiency in first-order urban restored (RES) and urban unrestored (URE) stream reaches within the Piedmont ecoregion of South Carolina during the winter and summer seasons of 2022. Results suggested that the lack of fine sediment, such as silt and clay, may affect the nutrient cycling of phosphorus. The total nitrogen:total phosphorus ratio indicated the stream was phosphorus-limited during the experiments. The mean soluble reactive phosphorus uptake length throughout the study was shorter in RES than URE, suggesting that the restored reach was more efficient in retaining dissolved phosphorus. During summer injection, RES observed the shortest soluble reactive phosphorus uptake length of 77 m, while URE marked the longest uptake length of 3059 m during the same period. However, during winter injections, the URE segment had both the shortest and longest uptake lengths. In summer, RES exhibited noticeably shorter ammonium uptake lengths, while ammonium uptake lengths could not be calculated in URE. The presence of engineered pools in RES assisted in nutrient dynamics and helped trap nutrients, particularly soluble reactive phosphorus and ammonium, and could be prioritized in stream restoration

efforts. Preliminary results from this study could provide helpful insights into the effectiveness of stream restoration and in-stream structures on nutrient dynamics, although further research is needed.

KEYWORDS

nutrient cycling, nitrogen, phosphorus, uptake length, stream restoration, trapping efficiency

1 Introduction

Globally, stream ecosystems are experiencing a decline in water quality and biodiversity, primarily due to an excess of nutrients, such as nitrogen (N) and phosphorus (P), which have become more readily available due to significant land use changes and practices (Miserendino et al., 2011; Liao et al., 2018). In the United States, N and P are the most widespread and studied chemical stressors assessed in lotic ecosystems (EPA, 2022b). Nutrient contributions from both agriculture and urbanization exceed the intrinsic ability of freshwater ecosystems to process N and P enrichment (Nina and Jonathan, 1999; Cole et al., 1993; Manning et al., 2020; Caraco and Cole, 1999), causing poor water quality and reducing the quality of habitat for biota.

Depending on the watershed size and location, urban development generally encompasses a much smaller fraction of the total catchment area than agricultural development (Allan, 2004). However small these urban areas, their influence on watersheds is more pronounced because of impervious surfaces (Bledsoe and Watson, 2001; Paul and Meyer, 2001; Tranmer et al., 2022). The contrast between the geomorphology of riffles and pools, baseflows and stormflows, and hillslopes and in-stream dynamics is exacerbated by urbanization (Blaszczak et al., 2019). The urban land developmental process overwhelms the buffering capacity of streams through loss of riparian vegetation, increased stormwater drainage pipes, impervious surfaces, and runoff carrying various contaminants (Paul and Meyer, 2001). Together, these manipulations result in channel and geomorphic degradation from intense storm flows (Bledsoe and Watson, 2001; Russell et al., 2020), substantial loss of native biodiversity (Stranko et al., 2012), and increased nutrient export to downstream watersheds (Klocker et al., 2009).

The set of physical, biological, and chemical changes consistently observed within streams draining urban land is known as the urban stream syndrome (Walsh et al., 2005). The urban stream syndrome is rooted in rapidly urbanizing catchments that interrupt the natural organizational ability of streams to erode and deposit bed surface material in equilibrium (Wolman, 1967). While there are several explanations for channel modifications [e.g., channelization] due to changes in hydrology, on many occasions, the frequent hydraulic disturbance from storm flows leads to an unbalanced removal of sediment from the stream banks, causing channel enlargement and simplification (Russell et al., 2020). Advanced municipal infrastructure, like sanitary sewers and wastewater treatment plants, effectively reduces nitrogen waste from cities while potentially increasing diffuse nitrogen pollution across watersheds (Bernhardt et al., 2008; Howarth et al., 1996). It is well known that excess release of key contaminants such as N, P, and sediment/solids into stream water from stormwater runoff associated with watershed development deteriorates the physical environment and ecological processes within the stream (Brown et al., 2009; Kaushal et al., 2017; Kriech and Osborn, 2022; Paul and Meyer, 2001; Williams and Filoso, 2023).

The pressure from urban development has placed attention on reducing in-stream nutrient concentrations through a vast number of stream restoration projects (Lammers and Bledsoe, 2017). Stream restoration is a popular, multibillion-dollar investment practice implemented by state and federal agencies, non-government organizations (NGOs), and consultants to improve stream health, structure, and function (Bernhardt et al., 2005). Engineering design practices in the Southeastern United States traditionally follow the Rosgen's Natural Channel Design to restore the natural pattern, profile, and dimensions of a disturbed stream by emulating a stable channel within the same watershed (Rosgen, 2007). However, these restoration approaches do not address water quality, nutrient dynamics, and their fate and transport. One of the main drivers behind the widespread adoption of stream restoration initiatives in the United States can be explained by mitigation credits issued by regulatory agencies as a financial incentive for developers to invest in stream restoration to meet a waterbody's Total Maximum Daily Load requirement (Thompson et al., 2018; Williams et al., 2017).

Typically, urban stream restoration is an attempt to reduce the magnitude of flashiness produced by urbanization and reconnect the stream to the floodplain. Restoration involves installing native plant materials and constructing geomorphic complexity and channel stability with boulders, wood, and rock deflectors with the intention of dissipating water flow and increasing hydrologic residence time (Palmer et al., 2014). Previous studies of restored streams assume that once geomorphic complexity and hydrologic residence time are increased, then nutrient processing will be restored because water has more time to exchange back and forth between the surface water column and sediment (Ensign and Doyle, 2006; Craig et al., 2008; Bukaveckas, 2007; Roberts, Mulholland, and Houser, 2007; McMillan et al., 2014). Despite decades of stream restoration practice, factors that govern the responsiveness of in-stream nutrient dynamics to the restoration process are merely conceptual. Efforts to quantify the implications of N and P removal through stream monitoring research need more attention.

Current monitoring practices have focused on testing water quality improvement by analyzing nutrient cycling in post-restoration surface waters of streams (McMillan et al., 2014; Newcomer Johnson et al., 2016; Reisinger et al., 2016). Different stream features in a restored stream, such as riffle-pool sinuosity, change the interaction of the nutrients traveling downstream and potentially increase the retention of nutrient molecules within the stream by enhancing the timing and magnitude of downstream travel (Figure 1). Downstream transport of N and P in flowing water

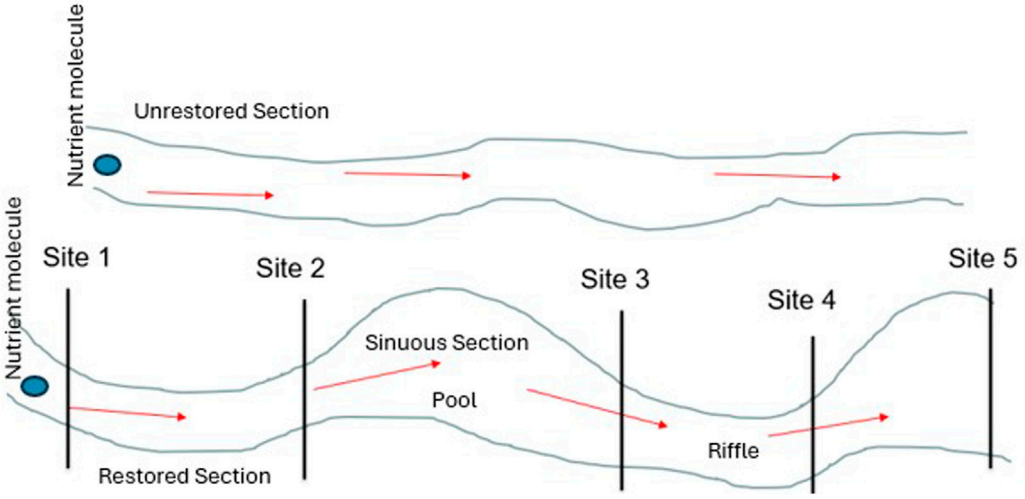


FIGURE 1
Conceptual diagram illustrating nutrient retention in a restored and unrestored first-order stream.

has been studied through short-term injections, where nutrient retention efficiency was measured as the spiraling length or downstream distance traveled before assimilation (Haggard et al., 2001; Chaubey et al., 2007). The rate at which aquatic ecosystems cycle nutrients from the dissolved state within the water column to the particulate state within the sediment or biota is defined as nutrient retention efficiency (Chaubey et al., 2007). This capture and release process influences the timing, magnitude, and form of nutrients that are transported downstream (Meyer et al., 1988).

The spiraling length of a nutrient molecule is the sum of the distance traveled in the particulate form (turnover length, S_p) and dissolved form (uptake length, S_w) (Stream Solute Workshop, 1990). Under baseflow conditions, S_w calculates the distance a dissolved nutrient travels downstream before it is removed from the water column, and nutrient S_w dominates the total spiraling length (Newbold et al., 1983). This transport (S_w) represents retention efficiency and varies by land use, anthropogenic disturbances (e.g., urbanization), and restoration design (Beechie et al., 2010; Haggard et al., 2005; Klocker et al., 2009; McMillan et al., 2014). Assessment of nutrient uptake ability can be performed using short-term nutrient injections within the restored reach (Stream Solute Workshop, 1990).

The overarching goal of this research was to analyze how nutrient injections could aid in monitoring in-stream nutrient dynamics in low-order urban restored (RES) and unrestored (URE) streams in the Piedmont ecoregion of South Carolina. The research question for this study focused on the controls of soluble reactive phosphorus (SRP), ammonium (NH_4-N), and nitrate plus nitrite (NO_3-N + NO_2-N) in two contrasting reaches of the same stream. The specific research questions of this study were to assess the influence of restoration design (e.g., riffle and pool geomorphology), reach length, season, discharge, and other background measurements on performance via estimated nutrient uptake lengths and nutrient trapping efficiencies. We hypothesized that unique spatial and temporal differences in nutrient retention would occur in RES and URE reaches.

To address these research questions, short-term nutrient injection techniques were used in restored and unrestored urban stream reaches to evaluate the spatial and temporal variations in N and P dynamics and understand nutrient retention, whole-stream nutrient trapping efficiency, and nutrient trapping efficiency in the engineered pools.

2 Materials and methods

2.1 Site description

The study was conducted in Richland Creek, a first-order urban stream in the southern inner piedmont ecoregion of South Carolina. For this study, reaches refer to the restored and unrestored locations, sites refer to sampling locations, and restored stream features refer to riffles and pools in RES and URE streams. Sampling occurred in winter (January–March) and summer (June–July) months of 2022. Two stream reaches were selected within Richland Creek in Greenville, South Carolina. The first stream reach was the RES reach in McPherson Park, and the second was the URE reach downstream, parallel to the E Park Ave highway (Figure 2). Richland Creek drains into the Saluda River basin (hydrological unit code 03050109) and is a tributary of the Reedy River with both reaches having approximately 1.8 km^2 of the watershed area that consists of less than 1% of pasture, mixed forest, and deciduous forest and approximately 99% urban land use (United States Geographical Survey, 2019).

Based on the information provided by the City of Greenville (*personal communication*), stream restoration was completed in December 2018 using Rosgen's Natural Channel Design that begins directly after a culvert in ~150 m of stream. The objective of this restoration effort was to stabilize the bank and reduce nutrient loading [e.g., total phosphorus (TP) and total nitrogen (TN)] generated by urban land use within the Richland Creek watershed. The stream restoration design plan can be obtained from the City of Greenville, South Carolina. Based on the design

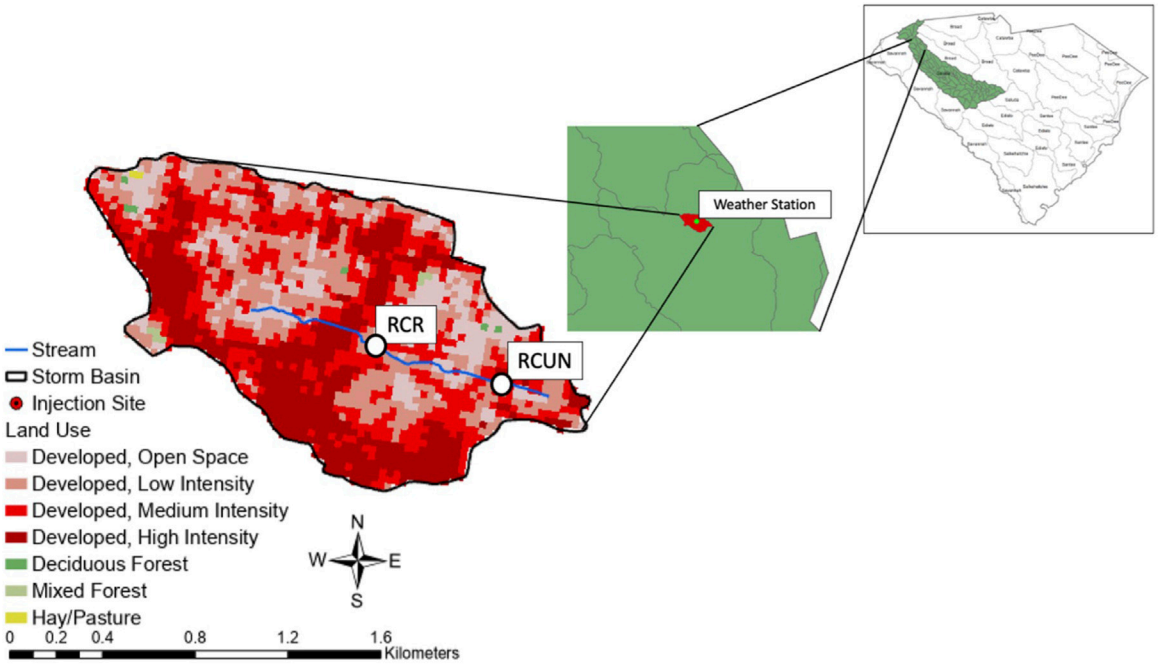


FIGURE 2
Richland Creek watershed and respective sites, Richland Creek—Restored (RES) and Richland Creek—Unrestored (URE), reside in the upper subwatershed of the Saluda River Basin in Greenville, South Carolina. The weather station is indicated by a green marker.

TABLE 1 Length (m) of each pool within the restored (RES) reach.

Site	Location	Pool length (m)
RES	POOL 1	8
Step pool begins	POOL A	6
	POOL B	4
	POOL C	5
	POOL D	5
Step pool ends	POOL E	5
	POOL 2	14
	POOL 3	12

plan, it was noticed that regenerative stormwater conveyances, native plants, and biodegradable materials were installed, and over-steepened bank sediment was removed. Detailed information on the installed pools, species of plants, type of plants, where they were planted, and type of biodegradable materials used can be referenced in the design plan. There are two types of stream features, one created step pool that is 25 m long, composed of five sub-pools ranging in length from 4 m to 6 m, and three constructed pools ranging in length from 8 m to 14 m (Table 1). The sequence of constructed step pools has a gradual decline in slope that dissipates energy from high stream discharge, controls erosion, enhances oxygenation, and improves downstream water quality; while the constructed pools provide diversity in stream discharge with a single, deeply excavated stream bed that impounds flow and captures sediment. The sequence of step pools and constructed pools was created during the stream restoration project. The study area focused on a restored reach of ~70 m length and an unrestored reach of ~80 m length, with injection experiments occurring at the top of the restored and unrestored reaches. The restored reach includes 11 sampling sites that were consistently sampled for each experiment. These sites contained three riffle and pool features and a step pool conveyance that was included in the sampling (Table 1). The study reach length was cut short due to an outlet pipe at the downstream boundary of the restored reach that continuously drains into the stream.

Approximately 0.5 km downstream of the RES (separated by a road culvert) section is the URE reach of Richland Creek (Figure 2). This reach is impacted by land uses similar to those of the RES reach. Anecdotal evidence and conversation with local residents within the project area indicated that the land was purchased around the 1930s, and the stream was channelized around the mid-1940s with a stone wall that currently runs parallel to the main road (East Park Ave.) along the entire stream reach. The stream bed is mainly composed of bedrock with remnant riffle-pool structures. Five sampling sites were consistently sampled for each experiment near these remnant riffle-pool structures. URE receives continuous discharge of the outlet pipe at the downstream boundary of the restored reach throughout the entire sampling period. Stormwater outlets recur throughout the reach but were not discharging during the sampling period.

The average width varied spatially (28%) between the RES and URE reaches where the RES reach (range: 2.4–2.7 m, average = 2.62 m ± 0.14) was wider than the URE reach (range: 1.8–2.6 m, average = 1.98 m ± 0.30) throughout the study period, likely due to stream features incorporated during restoration such as sinuosity from riffle and pool structures ($t = 4.35$, $p < 0.05$, $n = 6$) (Table 2).

TABLE 2 Depth, width, velocity, and discharge of sites within restored (RES) and unrestored (URE) reaches of Richland Creek during injections.

	Depth (cm)	Width (m)	Velocity (m/s)	Discharge (m^3/s)
Winter				
January				
RES	16	2.7	0.024	0.013
URE	21	1.8	0.053	0.013
February				
RES	19	2.7	0.018	0.003
URE	12	1.8	0.064	0.012
March				
RES	20	2.7	0.054	0.002
URE	23	1.8	0.030	0.003
Summer				
June				
RES	19	2.7	0.040	0.003
URE	23	1.8	0.039	0.005
Early July				
RES	19	2.4	0.034	0.002
URE	8	2.0	0.122	0.003
Late July				
RES	19	2.4	0.056	0.002
URE	8	2.6	0.090	0.003

TABLE 3 Average monthly precipitation (mm) recorded in Greenville County from 2022 to 2023 (AccuWeather, Inc., 2023) and by historical Greenville County weather stations over the last 30 years (National Oceanic and Atmospheric Administration, 2020).

	Winter precipitation (mm)				Summer precipitation (mm)		
County	January	February	March	Mean	June	July	Mean
Greenville data	96	119	142	119 ± 23	17	55	36 ± 27
Historic Greenville data	112	90	109	104 ± 12	112	117	115 ± 3.0

The average velocity and discharge between the RES and URE reaches were also similar and did not vary by season. The average discharge of both the RES and URE reaches was expected to increase during the winter season and decrease during the summer season (Table 2) (Dyer et al., 2022). The flow regime was affected by higher temperatures and lower precipitation in the summer season (Table 3). Summer flows are generally reduced due to water losses from evapotranspiration from the mixed deciduous forest vegetation (present in the RES and URE reaches) and infiltration along the stream channel (Lundquist and Cayan, 2002). The low-flow period in both sections persisted throughout the study period and may have been more affected by other processes because the stream carries such a low volume of water.

The impervious area in the watershed includes roads, bridges, and access areas in the park that potentially restrict the opportunity for organic matter to decompose into various particle sizes, consequently reducing the possibility of sediment transport into the stream. The dominant particle size of the creek was gravel. The creek contains minimal amounts of silt and clay particles, likely because they are typically found in pools where velocities decrease and allow them to settle (EPA, 2023). In general, the RES reach had 71% gravel, 29% sand, and less than 1% silt and clay, while the URE reach had 73% gravel, 27% sand, and less than 1% silt and clay as estimated during the sampling. [Advancing Standards Transforming Markets (2017)]

The average temperatures for the injection dates in winter were 10°C in January, 12°C in February, and 23°C in March. January and February average temperatures from the injection dates were within the 30-year minimum and maximum averages for Greenville County, where the study sites are located. However, March was 6°C higher than the historic average maximum temperature in the Greenville County area (National Oceanic and Atmospheric Administration, 2020). During the summer, the sampled sites collectively had an average temperature of 30°C in June and 28°C in July during the injection dates (Table 2), which was also within the 30-year minimum and maximum average temperature in Greenville County (National Oceanic and Atmospheric Administration, 2020). Given the overall weather data (Table 4), there were no atypical trends when compared with the long-range data. Therefore, there is a fair degree of confidence that the empirical findings from this study are representative of the seasonal conditions. The average monthly

TABLE 4 Date of each injection along with the weather station data and background total nitrogen and total phosphorus ratio (TN:TP) recorded on each day of an injection for restored (RES) and unrestored (URE) reaches of Richland Creek.

	Winter			Summer		
	January	February	March	June	Early July	Late July
RES	1/14/2022	2/26/2022	3/6/2022	6/21/2022	7/12/2022	7/25/2022
Time	2:29 p.m.	3:14 p.m.	12:49 p.m.	11:34 a.m.	11:24 a.m.	10:49 a.m.
Atm. temp (°C)	13	13	22	29	26	30
Dew point	−1	3	15	16	21	23
Humidity (%)	39	51	67	45	73	71
Wind speed (km/h)	2.1	0.6	2.9	1	0.5	1.4
Pressure (Pa)	14	15	15	15	15	15
Precipitation (mm)	0	0	0	0	0	0
Condition	Fair	Fair	Cloudy	Fair	Fair	Fair
TN:TP	72:1	74:1	43:1	34:1	24:1	27:1
URE	1/28/2022	2/20/2022	3/2/2022	6/22/2022	7/15/2022	7/21/2022
Time	11:49 a.m	5:39 p.m.	2:09 p.m.	11:09 a.m.	10:19 a.m.	11:53 a.m.
Atm. temp (°C)	6	12	24	31	29	27
Dew point	−2	−8	2	16	19	21
Humidity (%)	55	25	23	40	56	70
Wind speed (km/h)	2.1	1.3	4.2	2.9	0.5	2.6
Pressure (Pa)	15	15	15	15	15	14
Precipitation (mm)	0	0	0	0	0	0
Condition	Cloudy	Fair	Fair	Fair	Fair	Fair
TN:TP	79:1	67:1	39:1	35:1	28:1	27:1

precipitation from a Greenville weather station was compared with the 30-year average precipitation in Greenville County to understand how rainfall may have influenced the watersheds during the study period. Based on weather station data, higher than the 30-year average precipitation occurred in the winter, while 3× lower-than-normal precipitation occurred during the summer (Table 3) (National Oceanic and Atmospheric Administration, 2020). June was the driest month, with the lowest precipitation amounts that were below the historical precipitation levels for Greenville County (Table 3). This dry summer period may have been a result of ongoing climate warming in the rapidly growing state of South Carolina (Sanchez et al., 2020).

2.2 Nutrient injection experiments

All experiments were conducted under baseflow conditions between sunrise and sunset (Table 4). Field experiments avoided periods of storm events. Stream velocity measurements (Marsh-McBirney Inc., 1990) were conducted and discharge (Turnipseed and Sauer, 2010) was calculated during baseflow conditions, the day before each experiment, near the most upstream injection site of each study reach using a Flo-Mate 2000 flow meter (Hach Company, Frederick, Maryland, United States). Stream velocity measurements were taken using the midsection method (Young, 1950). Velocity measurements were taken at every 0.15 m within the transect at the standard 0.6 water depth using the top-setting wading rod near the injection site. Discharge was then calculated to estimate the amount of salt to be added to the Marriott bottle. One modified Marriott bottle (20 L polypropylene bottle) with a constant effusion velocity was used for injection. The target solute injection concentration was determined by the discharge of the stream, spike concentration, emitter rate, volume of the Mariotte bottle, and molecular weight of each solute for each experiment.

To quantify the in-stream uptake of N as ammonium (NH_4-N), nitrate plus nitrate (NO_3-N + NO_2-N), and soluble reactive phosphorus (SRP), 12 separate short-term solute addition experiments (six separate experiments per reach) were conducted during the winter season, January through March 2022, and the summer season, June through July 2022 (Table 4). Conductivity measurements were collected as part of the injection studies, and the measurements were also used to understand the spatial and temporal heterogeneity of stream flow and water quality. The duration of each injection depended on the discharge rate, but the plateau was generally reached over 1 h for the two selected reaches on all occasions. The plateau is the point in time when the

downstream concentration of salt reaches a steady state condition, which is observed through the conductivity measurements using YSI ProDSS. The solute solution varied for each experiment date because the concentration of each solute depends on the discharge of the stream reach. The solute solution, containing sodium phosphate monobasic monohydrate ($NaH_2PO_4{\cdot}H_2O$, as a phosphate source), ammonium nitrate (NH_4NO_3, as an ammonium and nitrate source), and sodium chloride (NaCl, as a conservative tracer source), was added at constant flow rate using a Mariotte bottle at the injection site (beginning of the reach) on each separate experiment. This was conducted according to the standard procedures outlined in the Stream Solute Workshop (1990). NaCl was used to correct for dilution in NH_4-N, NO_3-N + NO_2-N, and SRP concentrations within the reach because chloride concentration remains relatively constant as water moves downstream. Spike concentrations of SRP (0.03 mg/L), NH_4-N (0.1 mg/L), NO_3-N + NO_2-N (0.1 mg/L), and NaCl (3 mg/L) solutes were set on each sampling date based on previous studies [e.g., Stream Solute Workshop, 1990; Haggard et al., 2001; Chaubey et al., 2007; McMillan et al., 2014; where a small spike concentration is set according to the demand for the nutrient. Excess nutrient concentration is not prescribed to avoid oversaturation of nutrients in the stream reach.].

The discharge of the stream was again calculated at the injection site on the injection day. If the discharge was within a 10% difference from the previous reading taken the day before injection, no change was made to the Mariotte bottle's emitter rate. Weather conditions were recorded for reference.

The Mariotte bottle was placed ~1.5 m upstream of the first sampling site inside the tripod consistently for all the experiments. Before injection started, background water samples were collected using acid-washed 250-mL HDPE wide-mouth bottles at each sampling site. Samples were taken in constricted, well-mixed areas of the stream, or riffles. At the RES sites, sampling was conducted at distinguished riffles, specifically at the head and the tail, where there was free-flowing, mixing water.

Water samples were taken at each site using three 250-mL bottles at the right, middle, and left portions of the stream channel. All three samples were mixed, and one composite sample was collected and analyzed. Sampling at each site was conducted with minimal disturbance by sampling from downstream to upstream. Water samples were filtered with 0.45-μm pore size filters before the injection started. The conductivity sensors were completely submerged in the nearest rifle next to the Mariotte bottle and at the most downstream sampling site. The Mariotte bottle was turned on once the sensors were in place. The conductivity readings were recorded at the most upstream site and the downstream site. Surface water plateau samples were collected in a manner similar to that of background samples when the conductivity reached a plateau at the downstream site. Once the samples were collected, injection was stopped, and conductivity measurements were recorded until conductivity readings returned to background conditions.

All water samples were filtered and acidified, if needed, then stored at < 4°C until delivery to the Arkansas Water Resources Center's certified water quality lab (https://awrc.uada.edu/water-quality-lab/). Filtered water samples were analyzed for nitrate, sulfate, fluoride, and chloride using an ion chromatograph (EPA Method 300.0, Dionex System 1600). Filtered, acidified (pH < 2) water samples were analyzed for dissolved nutrients on a wet chemistry autoanalyzer (Skalar Sans++ System), including SRP (EPA Method 365.1, method detection limit of 0.004 mg/L), NH_4-N (EPA Method 351.2, method detection limit of 0.020 mg/L), and NO_3-N + NO_2-N (EPA Method 353.2, method detection limit of 0.017 mg/L) and used for analysis described in Section 2.4. Unfiltered water samples were digested using the persulfate, autoclave method (APHA 4500–P–J), and then the digested samples were analyzed on the wet chemistry autoanalyzer for SRP and NO_3-N + NO_2-N following previously described methods to get TP and TN concentrations in the unfiltered samples. These measurements were used to obtain the concentrations of the three nutrient variables listed. The SRP values obtained from the filtered, acidified samples were used for the current analysis.

2.3 Calculations for nutrient uptake variables

Nutrient uptake length, a measure to study nutrient dynamics in a stream, is the distance a nutrient molecule travels in dissolved form before being taken up from the water column. It is calculated using the nutrient spiraling approach (Stream Solute Workshop, 1990). The nutrient uptake length, S_w, is derived from k, which is the uptake rate constant (m^{-1}). A simple first-order rate equation was used to determine the length (m) a nutrient travels in the water column because the proportion of added nutrients generally decreases exponentially with distance and is expressed as follows:

$$C_x = C_o{*}e^{-kx}, \quad (1)$$

where C_x is the diluted corrected concentration at each of the sampling locations, x is the distance downstream from the injection point, C_o is the diluted corrected concentration at the most upstream sampling location below the injection point, and k is the uptake rate constant that is determined as the slope of a line representing the proportion of nutrients remaining in the water column versus distance downstream (Stream Solute Workshop, 1990). S_w is calculated as the inverse of k for each injection as follows:

$$S_w = -1/k. \quad (2)$$

S_w is corrected to the average of the background nutrient and tracer concentrations and the change in nutrient concentration with distance downstream. Variations in hydrological properties such as stream discharge affect the retention efficiency of a stream, which impacts S_w. When velocity is considered with S_w, the uptake rate coefficient, K_c (L/s), is used to account for such variation (Stream Solute Workshop, 1990). The greater the K_c, the shorter the S_w, resulting in increased nutrient processing within the stream. In cases where nutrient concentrations did not decrease after applying dilution correction, these data were not included in the analysis.

The nutrient trapping efficiency (TE%), which represents the percentage of nutrients trapped within a stream reach during the nutrient injection period, is calculated by the following

$$TE\% = [(US_C - DS_C)/US_C]{*}100, \quad (3)$$

TABLE 5 Nutrient uptake length, S_w (m), across all sampling sites for select nutrients, followed by the nutrient uptake rate, K_c (1/s), mass transfer coefficient, V_f (m/s), and *p*-value for the uptake length of each nutrient.

	SRP				NH_4-N				NO_3-N + NO_2-N			
	S_w	K_c	V_f	*p*-value	S_w	K_c	V_f	*p*-value	S_w	K_c	V_f	*p*-value
January												
RES	248	0.00009	0.00002	0.0009	310	0.0001	0.00002	0.006	1951	0.00001	0.000003	0.76
URE	32	0.001	0.0003	0.004	47	0.0009	0.0002	0.008	a	a	a	a
February												
RES	a	a	a	a	a	a	a	a	a	a	a	a
URE	a	a	a	a	429	0.0001	0.00002	0.393	89	0.0007	0.0001	0.09
March												
RES	a	a	a	a	779	0.0001	0.00001	0.733	a	a	a	a
URE	1140	0.00003	0.00001	0.72	218	0.0001	0.00003	0.656	a	a	a	a
June												
RES	77	0.0004	0.00005	0.000026	75	0.0004	0.0005	0.15	a	a	a	a
URE	3059	0.00001	0.000003	0.74	a	a	a	a	a	a	a	a
Early July												
RES	a	a	a	a	102	0.0003	0.00003	0.12	a	a	a	a
URE	253	0.0004	0.00008	0.09	a	a	a	a	a	a	a	a
Late July												
RES	a	a	a	a	a	a	a	a	a	a	a	a
URE	a	a	a	a	a	a	a	a	a	a	a	a

a Value not reported and excluded from analyses because a decrease in nutrient concentration was not observed.

where US_c is the plateau-corrected upstream concentration of the nutrient and DS_c is the plateau-corrected downstream concentration of the nutrient, meaning the plateau concentrations of the upstream and downstream locations are corrected by the average of all background concentration samples. The estimation of TE% can also be used as an indicator of nutrient dynamics in streams. A similar calculation method can be used to estimate the TE% of restored stream features [e.g., engineered pool] by using the data collected from the nutrient injection experiments. The water samples taken from the upstream and downstream sections of the pools in the RES reach during the plateau were collected, corrected to the background concentration of the sampling site, and used to calculate the TE% of the pools.

2.4 Statistical analysis

The same reaches, sites, and pools were repeatedly measured throughout the study, resulting in pseudoreplication within the dataset for statistical analysis. Nutrient uptake length was calculated based on Equation 1, which used $\alpha = 0.05$ for a regression analysis between background corrected nutrient concentration and distance from the injection site, with the associated *p*-value reported for significance. Section 3.1, In-stream nutrient retention, analyzes the difference between nutrient uptake length, discharge, and water temperature using Spearman's ρ test. Nutrient uptake lengths were compared across reaches ($n = 2$) using a t-test assuming unequal variances and seasons assuming equal variances. Reported statistics were determined to be significant at $\alpha = 0.05$. Section 3.2, Nutrient trapping efficiency, reports the means of measured values with corresponding standard deviations to represent error and uses a regression analysis to model the relationship between TE% (dependent variable) and pool length (independent variable) in the RES reach. Section 3.3, Background water chemistry measurements, reports the means of measured values with corresponding standard deviations to represent error. It uses t-tests to measure spatial and seasonal variation for reported variables and a regression analysis to examine the relationship between background conductivity for each reach (dependent variable) and water temperature (independent variable). Section 3.4, Conductivity analysis and anomalies, reports the means of measured values with corresponding standard deviations to represent error. It uses t-tests to measure seasonal variance of URE mean conductivity, assuming equal variance, and a regression analysis to examine the relationship between background conductivity (dependent variable), water temperature (independent variable), and discharge (independent variable). Box plots were used to understand the distribution of conductivity measurements during the injection. JMP Pro version 16.0 software was used for statistical data analysis (SAS Institute, Cary, North Carolina).

3 Results

3.1 In-stream nutrient retention

SRP uptake length was reported two of six times in the RES reach and three of six times in the URE reach (Table 5). The RES reach

TABLE 6 Whole-stream trapping efficiency (TE%) of plateau soluble reactive phosphorus (SRP), ammonia (NH_4), and nitrate plus nitrite nitrogen (NO_3-N + NO_2-N) concentrations at each site in restored (RES) and unrestored (URE) reaches of Richland Creek during injections.

	January	February	March	June	Early July	Late July
SRP						
RES	31	a	a	36	a	a
URE	55	a	a	a	29	a
NH_4-N						
RES	25	a	24	43	34	a
URE	23	a	a	0.4	a	a
NO_3-N + NO_2-N						
RES	7	a	a	a	a	a
URE	a	38	a	a	a	a

a Value not reported and excluded from analyses because a decrease in nutrient concentration was not observed.

showed shorter SRP uptake lengths and higher uptake rate and mass transfer coefficient in June (77 m), when compared to the URE reach, which showed shorter uptake lengths and higher uptake rate and mass transfer coefficient in January (32 m) and early July (253 m) injections (Table 5). Together, there was no strong correlation between the SRP uptake length and discharge for the RES and URE reaches ($\rho = 0.51$, $p > 0.05$, $n = 6$) nor was there a significant relationship between SRP uptake length and water temperature ($\rho = 0.21$, $p > 0.05$, $n = 6$) throughout the study period. The mean SRP uptake lengths of the RES (163 m) and URE (1121 m) reaches did not differ using a *t*-test assuming unequal variances ($t = 1.38$, $p > 0.05$, $n_{RES} = 2$, $n_{URE} = 4$). No seasonal variation was found between the combined SRP uptake lengths of the RES and URE reaches throughout the study, using a *t*-test assuming unequal variances ($t = 0.64$, $p > 0.05$, $n = 3$).

The NH_4-N uptake occurred more in the RES than in the URE reach. NH_4-N uptake occurred four of six times within the RES reach, and it occurred three of six times in the URE reach (Table 5). The RES reach had the shortest NH_4-N uptake length on two of six occasions in June (75 m), and early July (102 m) injections, while the URE reach had the shortest in January (47 m), February (429 m), and March (218 m) injections (Table 5). Together, the NH_4-N uptake lengths for the RES and URE reaches did not correlate with water temperature ($\rho = 1.0$, $p > 0.05$, $n = 7$) throughout the study, nor was there a correlation between NH_4-N uptake and discharge ($\rho = 0.57$, $p > 0.05$, $n = 7$).

The low number of samples limited the strength of these comparisons. Sample sizes were limited because results were excluded where a decrease in nutrients was not observed (Table 5) due to illicit pollutant discharge on the planned experimental date. The shortest NH_4-N uptake length at the URE reach in January (47 m) may reflect premature sampling (before the plateau was observed).

The mean NH_4-N uptake lengths between the RES (317 m) and URE (231 m) reaches had no statistical difference using a *t*-test assuming unequal variances ($t = 0.84$, $p > 0.05$, $n_{RES} = 3$, $n_{URE} = 4$). When the NH_4-N uptake lengths were combined from the RES and URE reaches for each season, the winter NH_4-N uptake lengths were longer than the summer, but the difference was not statistically significant using a *t*-test assuming unequal variances ($t = 2.17$, $p > 0.05$, $n_{winter} = 5$, $n_{summer} = 2$).

There were only two instances of NO_3-N + NO_2-N uptake with subsequent uptake rate and mass transfer coefficients calculations in January (1,951 m) in the RES reach and February (89 m) in the URE reach (Table 5). The Spearman's ρ test could not be used to assess the relationship between nutrient uptake length, discharge, and water temperature, and a *t*-test could not be used to differentiate nutrient uptake length between sites and seasons, due to a lack of NO_3-N + NO_2-N uptake observations.

3.2 Nutrient trapping efficiency

There were two occasions of whole-stream TE% of SRP in the RES (34% ± 4%) and URE (42% ± 18%) reaches. From these two occasions, the RES TE% was higher in the summer while the URE TE% was higher in the winter (Table 6). The RES reach performed well with four of six observations of whole-stream TE% of NH_4-N (32% ± 9%), with higher TE% in the summer. The TE% for NH_4-N in the URE reach was observed only two of six times (12% ± 16%), with higher TE% in the winter (Table 6). The whole-stream TE% of NO_3-N + NO_2-N in the RES and URE reaches both showed one occasion in the winter (Table 6). The average TE% of SRP in the step pool of the RES reach was similar in the winter (6% ± 4%) and summer (5% ± 5%). The average SRP TE% in the constructed pools in the winter (11% ± 6%) and summer (13% ± 14%) was similar (Table 7). The TE% of NH_4-N in the step pool of the RES reach was more than three times higher in the summer (45% ± 37%) than the winter season (13% ± 13%), and it was also higher in the constructed pools in the summer (52% ± 18%) than the winter season (16% ± 8%) (Table 7). The RES reach had a TE% for NO_3-N + NO_2-N in step pools (32% ± 32%) and constructed pools (22% ± 16%) in the winter, while the summer only had one instance of uptake (Table 7).

Trapping efficiency and pool length (i.e., the longitudinal distance of the pool) were compared to determine if a higher trapping efficiency could be associated with a longer pool length. The step pool and constructed pools in the RES reach showed a positive exponential response and a significant relationship between

TABLE 7 Trapping efficiency (TE%) in pools for the RES reach during injections.

		January	February	March	June	Early July	Late July
SRP							
	POOL 1	b	b	b	a	9	a
Step pool begins	POOL A	a	1	a	a	a	a
	POOL B	a	3	a	15	a	a
	POOL C	a	6	11	a	3	2
	POOL D	a	1	a	a	2	3
Step pool ends	POOL E	6	9	10	4	a	a
	POOL 2	18	a	a	9	a	a
	POOL 3	7	a	8	1	a	33
NH_4-N							
	POOL 1	b	b	b	25	66	a
Step pool begins	POOL A	a	a	a	a	a	92
	POOL B	a	9	31	a	a	a
	POOL C	a	a	36	67	67	a
	POOL D	a	12	4	10	a	16
Step pool ends	POOL E	2	4	4	a	a	19
	POOL 2	21	12	a	65	67	a
	POOL 3	6	a	23	35	52	a
NO_3-N + NO_2-N							
	POOL 1	b	b	b	a	52	a
Step pool begins	POOL A	a	a	a	a	a	a
	POOL B	a	67	a	a	a	a
	POOL C	a	a	a	a	a	a
	POOL D	a	a	a	a	a	a
Step pool ends	POOL E	6	a	22	a	a	a
	POOL 2	32	39	a	a	a	a
	POOL 3	3	15	a	a	a	a

a Value not reported and excluded from analyses because a decrease in nutrient concentration was not observed.
b Eliminated the first site because the samples were too close to the injection site and caused dilution.

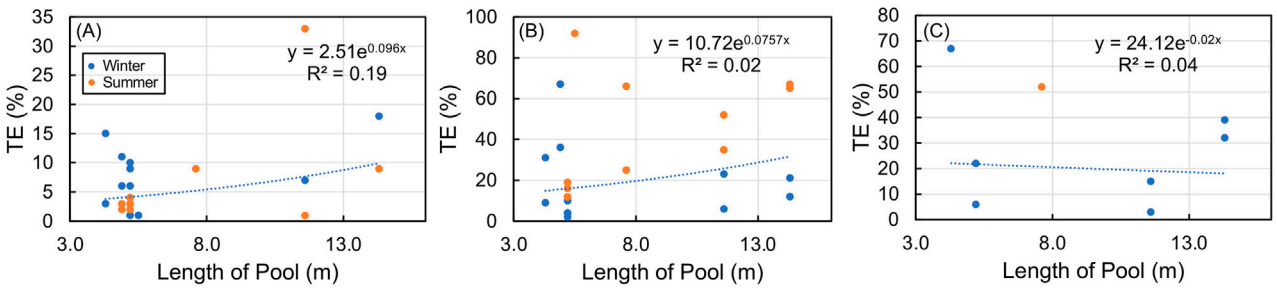


FIGURE 3
Whole-stream trapping efficiency (TE) in RES pools compared with each pool length for **(A)** soluble reactive phosphorus SRP, **(B)** NH_4-N, and **(C)** NO_3-N + NO_2-N in the summer (orange dot) and winter (blue dot).

the TE% of SRP and pool length (r = 0.44, $p < 0.05$, n = 21), while no relationship existed between the TE% of NH_4-N (r = 0.14, $p > 0.05$, n = 24) throughout both the winter and summer seasons (Figures 3A, B). The TE% of NO_3-N + NO_2-N also showed no relationship with pool length (r = 0.20, $p > 0.05$, n = 8) (Figure 3C). When considering all the pools in the RES reach, the highest average TE% for SRP and NH_4-N was in the summer, while the highest average TE% for NO_3-N + NO_2-N was in the winter.

3.3 Background water chemistry measurements

As expected, the water temperature increased from winter (average = 13 ± 3°C) to summer (average = 22 ± 1°C) in both sites (Table 5). The conductivity in the RES and URE reaches varied spatially between sites, likely because sampling was conducted on different dates (t = 2.68, $p < 0.05$, n = 6) (Table 2). The RES reach

TABLE 8 Event average of background water chemistry characteristics of restored (RES) and unrestored (URE) reaches of Richland Creek. Parameters include NH_4-N, NO_3-N + NO_2-N, DIN, SRP, TN, TP, F, Cl, SO_4, and DO in mg/L, water temperature (°C), conductivity (μS/cm), and pH.

	NH_4-N	NO_3-N + NO_2-N	DIN	SRP	TN	TP	F	Cl	SO_4	DO	Water Temp.	Conductivity	pH
Winter													
January													
RES	0.028	1.88	1.90	0.028	1.98	0.027	0.16	11.95	11.17	12	11.9	111	6.0
URE	0.026	1.96	1.98	0.022	2.07	0.026	0.17	14.19	10.14	12	9.3	100	5.9
February													
RES	0.025	1.80	1.83	0.028	1.86	0.025	0.16	12.69	13.34	12	14.4	122	6.3
URE	0.020	1.80	1.82	0.029	1.92	0.029	0.17	12.48	10.6	12	11.8	98	6.6
March													
RES	0.026	1.85	1.88	0.031	1.94	0.045	0.18	13.06	12.04	12	16.7	124	6.6
URE	0.022	1.90	1.93	0.036	1.98	0.051	0.19	12.25	10.21	11	15.9	110	6.6
Summer													
June													
RES	0.034	1.78	1.81	0.046	1.97	0.059	0.21	11.47	10.32	10	21.5	118	6.6
URE	0.032	2.07	2.10	0.041	2.10	0.060	0.18	11.79	8.93	10	21.7	114	6.7
Early July													
RES	0.033	1.66	1.69	0.051	1.87	0.079	0.25	11.09	10.95	9	22.4	131	6.5
URE	0.032	1.97	2.00	0.035	1.90	0.069	0.19	11.76	8.43	9	22.2	116	6.6
Late July													
RES	0.036	1.76	1.80	0.050	1.88	0.071	0.18	10.89	8.12	9	23.5	123	6.9
URE	0.042	1.81	1.86	0.055	2.05	0.076	0.24	11.66	9.73	9	22.8	120	6.7

lacked seasonal variation in background conductivity, while background conductivity in the URE reach increased in the summer ($t = 3.40$, $p < 0.05$, $n = 3$). Regression analysis confirmed that background conductivity increased as water temperature increased from winter to summer months for the URE reach ($r = 0.95$), but temperature and conductivity correlated poorly for the RES reach ($r = 0.61$).

Monthly averages of F, SO_4, and Cl in both sites did not exceed the EPA National Secondary Drinking Water Regulations (NSDWRs) recommendations (F: 2.0 mg/L, SO_4 and Cl: 250 mg/L) (Table 8) (Environmental Protection Agency, 2022a). Spatial differences in background concentration of NH_4-N were not observed between the RES and URE reaches (Table 8). The average background concentration of NH_4-N varied temporally for the RES ($t = 6.41$, $p < 0.05$, $n = 3$) and URE ($t = 3.36$, $p < 0.05$, $n = 3$) reaches, with the lowest concentrations occurring in the winter months in the RES (0.027 ± 0.001 mg/L) and URE (0.02 ± 0.003 mg/L) reaches. Higher average NH_4-N concentrations were measured in summer for the RES (0.035 ± 0.001 mg/L) and URE (0.04 ± 0.006 mg/L) reaches (Table 8). The average background concentration of NO_3-N + NO_2-N varied spatially between the RES and URE reaches throughout the study period ($t = 2.47$, $p < 0.05$, $n = 6$), with no difference associated with season (Table 8). The RES and URE reaches differed ($t = 2.16$, $p < 0.05$, $n = 6$) in the average background TN concentration, but TN was similar within each reach, regardless of season (Table 8). The background TN concentration is higher in the URE than in the RES reach.

TP concentration did not vary between the RES and URE reaches ($t = 0.07$, $p > 0.05$, $n = 6$) but did vary by season (both reaches reported $t = 2.13$, $p < 0.05$, $n = 3$), with higher background TP concentration in the RES reach in the summer (0.07 ± 0.01 mg/L) than the winter (0.03 ± 0.01 mg/L) and in the URE reach in the summer (0.07 ± 0.008 mg/L) than the winter (0.04 ± 0.01 mg/L) (Table 8). When comparing average background concentrations of SRP, both the RES and URE reaches concentration ranges were similar, from 0.02 mg/L to 0.05 mg/L (average = 0.04 ± 0.011) (Table 8). The SRP was significantly higher in the summer months than in winter months for the RES reach ($t = 10.95$, $p < 0.05$, $n = 3$), while the URE reach showed no significant seasonal difference (Table 8). In all the experiments, the TN:TP ratio exceeded the 16:1 baseline, making TN abundant and TP deficient (Table 4). The TN:TP ratio was similar between the RES and URE sites and seasons, with the RES reach ranging from 24:1 to 74:1 (46 ± 22) and the URE reach ranging from 27:1 to 79:1 (46 ± 22) throughout the study period (Table 4).

3.4 Conductivity analysis and anomalies

Conductivity readings in the RES reach took approximately 42 min (± 11) to observe a rise in conductivity, while the URE reach took an average of 30 min (± 7) throughout the experiments (Jordan, 2023). The average plateau time between the RES and URE reaches varied spatially by 60% on average throughout the sampled months. The RES reach plateaued after an average of 86 min (± 4), and the URE reach plateaued after an average of 47 min (± 6) during the experiments (Jordan, 2023). There was a distinct contrast in the mean conductivity between the winter months in the URE reach (Figure 4). The mean conductivity in March was 7% higher than in the other winter months. The summer months showed a significant

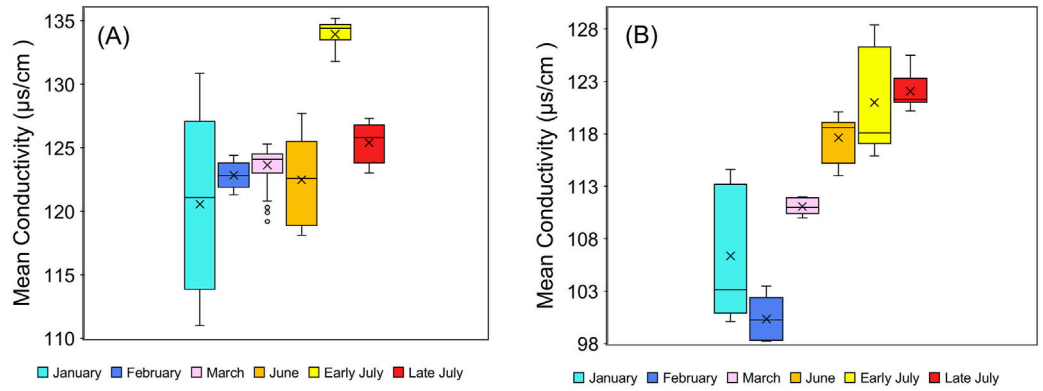


FIGURE 4
Boxplot of stream conductivity at **(A)** RES and **(B)** URE reaches of Richland Creek in the winter and summer seasons. The box plot shows conductivity between the upper and lower quantiles for monthly experiments. The line in the box represents the median of conductivity. The error bars show the maximum and minimum non-outliers of conductivity.

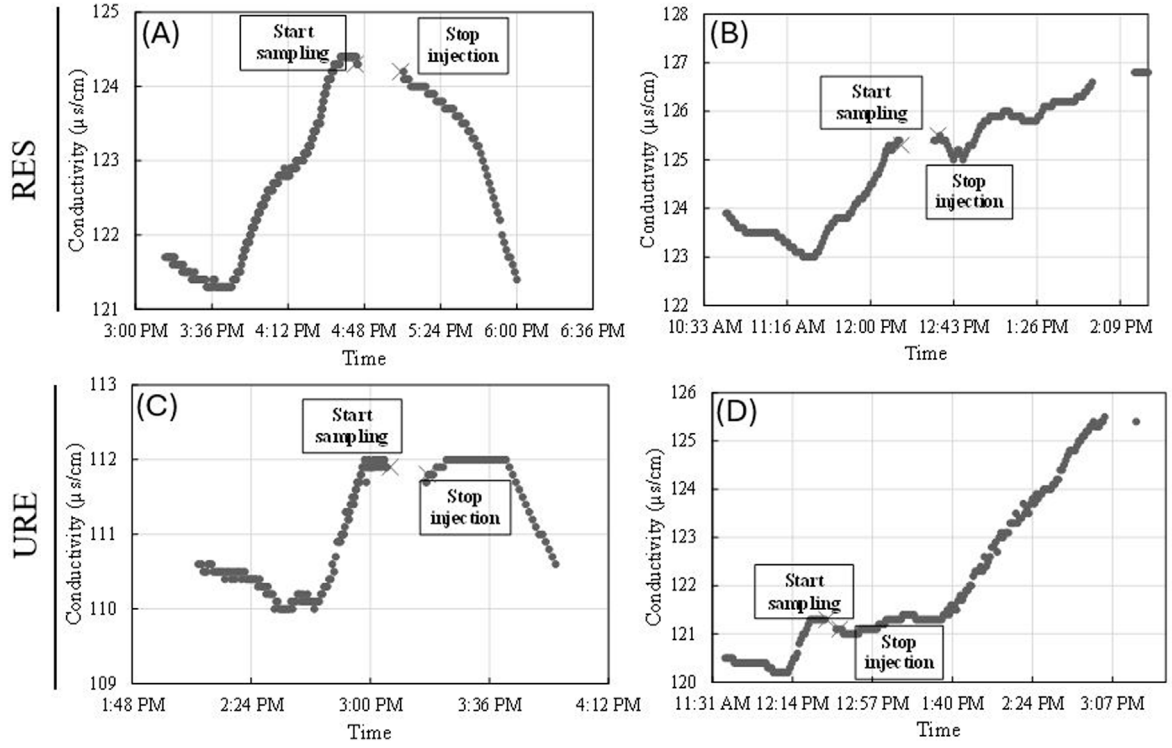


FIGURE 5
Conductivity curves representing **(A)** restored February injection, **(B)** restored late July injection, **(C)** unrestored March injection, and **(D)** unrestored late July injection.

increase (t = 3.40, $p < 0.05$, n = 3) in mean conductivity in the URE reach (Figure 4). The seasonal difference of 13% between winter and summer mean conductivity in the URE reach was likely due to the strong correlation of background conductivity with water temperature (r = 0.96, $p < 0.05$, n = 6) and discharge (r = 0.92, $p < 0.05$, n = 6).

Once samples were collected after the EC plateaued, the injection was terminated, and, in general, the conductivity levels gradually returned to the initial background levels. While conductivity measurement returned to background readings during the winter experiments in the RES and URE reaches (Figure 5), conductivity behaved differently for the RES and URE reaches in the summer season (Figure 5). The conductivity measurements began to rise after terminating the injection in the RES and URE reaches in the summer months (Figure 5). In late July, the RES reach had a gradual rise (slope = 0.012) in conductivity after presumed plateau of 125 µS/cm, which reached a final conductivity of 127 µS/cm; the URE reach had a steeper rise in conductivity

(slope = 0.27) after reaching a plateau of 121 μS/cm, which reached a final background conductivity of 125 μS/cm after the injection was terminated. Normally, conductivity should have returned to initial readings.

4 Discussion

4.1 In-stream nutrient retention

The SRP uptake in the RES and URE reaches was responsive during some of the sampled months, even though these sites consisted of predominantly gravel material. The lack of fine sediment due to rip rap in the RES reach and bedrock in the URE reach affects P cycling and reduces the amount of P sorption possible in the stream. More than 70% of the stream sediment at both sites was gravel, while less than 30% was sand. Restoration efforts typically focus on the removal of fine sediments from the natural gravel substrate (Morgan et al., 2019). The predominant small cobble and gravel bed in the RES and URE reaches may have resulted in fewer observations of SRP uptake. The lack of reported nutrient uptake lengths among the 12 experiments was possibly due to either significantly higher background nutrient concentration, likely from additional inputs from urban land use or not injecting a sufficiently high injection concentration of nutrients compared to the background concentration during the injection experiment (Table 5, explained under "a"). The RES reach maintained the shortest SRP uptake length in June; this could be attributed to higher rates of primary production during periods of higher light availability that exert a higher demand for P (Mulholland, 2004). The URE reach may have had the shortest SRP uptake in January because the TN:TP ratio was the highest (79:1, Table 4) in this sampled month, and therefore, the system was presumed to be phosphorus-limited with P in demand. The SRP uptake lengths in the RES reach were within the same range as five low-order restored urban streams in the Piedmont region of North Carolina (McMillan et al., 2014). Other streams had similar SRP uptake length; however, they were in low-order agricultural systems with a mixture of forest and pasture land uses (Marti and Sabater, 1996; Haggard et al., 2001; Chaubey et al., 2007).

Variation in discharge, previous rainfall events, weather conditions, and export of nutrients from the watershed could all assist in the complex interaction of nutrient availability in the water column and may influence the differences in NH_4-N uptake lengths for each site. The NH_4-N uptake in the RES reach was marked on more occasions than in the URE reach (Table 5), likely due to increased travel time attributable to transient storage and pools over the stream length. NH_4-N uptake may have been limited in the URE reach due to a lack of transient storage area, stream channelization, or disconnection to in-channel and riparian vegetation, all of which likely contribute to a decline in NH_4-N retention in small drainage streams (Bukaveckas, 2007; Le et al., 2018). These uptake lengths were within the range of other reported NH_4-N uptake length values in agricultural systems [e.g., forested and pasture land use] (Haggard et al., 2001; Simon and Benfield, 2002; Chaubey et al., 2007).

NO_3-N + NO_2-N was the dominant form of nitrogen for both sites (Table 5) and contributed to the high TN:TP ratio in the winter season (Table 2). When considering this high ratio, nitrogen was not limited during the winter sampling period. The discharge was high in January, which may have contributed to the detectable transport of this nutrient. A shorter uptake length is expected in this relatively slow-moving urban stream because other studies have documented longer nutrient uptake lengths with increasing discharge (Lautz and Siegel, 2007; Valett et al., 1996). However, the data were not consistent with expectations. Results from a previous study showed no retention of NO_3-N + NO_2-N and increased NO_3-N + NO_2-N concentration downstream of injection because of nitrification of injected NH_4-N (Chaubey et al., 2007).

4.2 Nutrient trapping efficiency

The overall mean TE% for all pools for SRP and NH_4-N was greater in the summer than in the winter, while the mean TE% for all pools for NO_3-N + NO_2-N was greater in the winter. Biotic activities are generally dominant during summer months. Pools play a crucial role in nutrient retention, with biotic activities in these areas aiding in the trapping and retention of nutrients. Higher TE% for NH_4-N may have been a result of restoration efforts in the RES reach. These TE% values could potentially be used for designing stream restoration projects and for nutrient crediting in such initiatives. Future research should investigate whether pool lengths exceeding 25 m are necessary to enhance the uptake of NH_4^+-N and NO_3^--N + NO_2^--N in urban headwater streams. To the best of the authors' knowledge, no previous studies have assessed nutrient TE% in different features within a restored site, particularly those with features like pools and step pools. The methodology and results obtained for pool length can also be applied when designing pools for restoration purposes.

4.3 Background water chemistry measurements

Observed discharges from stormwater pipes from winter to summer sampling dates in the RES reach (Table 2) may indicate that ecological processes that influence stream conductivity are less influenced by temperature. Inputs of ions through these stormwater pipes in the highly urban area of the RES and URE reaches may have impacted stream conductivity, which is a good indicator of human activity (O'Brien and Wehr, 2010; Wu et al., 2015; Köse et al., 2014). The higher background concentration of NH_4-N in the summer was most likely due to increased temperatures stimulating ammonification in water along with other co-occurring ecological processes (Racchetti et al., 2011). This could also be a result of impaired water quality from nitrogen enrichment from the surrounding urban watershed (Dodds and Smith, 2016). Visual observations indicated the presence of periphyton mats in the water column and on rip rap during the summer sampling period. Bacterially mediated reactions are sensitive to seasonal changes in stream water temperature, which affect the nitrate availability in the water column. The relationship between water temperature and nitrification within stream ecosystems is a well-researched topic. Studies show that temperature has a significant positive correlation with nitrate loss, meaning higher temperatures create more denitrification reactions within a stream system (Hill,

1988; Rasmussen et al., 2011). Processes involved in nitrate loss could be a consequence of a hydrologically disconnected floodplain, a lack of riparian area, or a result of the constant stormwater pipe discharge from upstream; however, Wolf et al. (2013) found that hydrological connectivity increases nitrate inputs. Additionally, excess TN and TP loads are common in developed areas, where stormwater runoff and soil-bound phosphorus are carried off impervious surfaces (Carpenter et al., 1998), potentially impacting nutrient cycling in stream systems.

The Redfield ratio is a well-established principle in ecology that describes the stoichiometric proportion of TN to TP in aquatic ecosystems, where a ratio of 16:1 is typically observed. This ratio is central to the principle of nutrient limitation, which states that the element in shortest supply relative to demand will limit biological productivity. However, the stoichiometric proportion of TN to TP in an urban stream can be highly variable due to increased nutrient inputs from anthropogenic sources, which can lead to an alteration of the typical Redfield ratio. A P-limited system is typical for surface waters. The RES and URE reaches exceeded the biological need for nitrogen for each sampled event (Table 5). This is common for urban streams because wastewater inputs and stormwater runoff have increased the downstream N exported in streams in recent years, which has influenced N demands (Reisinger et al., 2016). The lower ratio in the summer than winter in the RES and URE reaches could be due to the utilization of nutrients due to planktonic demand. Higher temperatures create a higher biological demand for nutrients. However, there is a higher concentration of TP in the water column, yet the TN:TP ratio shows that there is a demand for phosphorus. These unparalleled relationships could reflect the complex process during the growth and decay of algae when transitioning from summer to winter seasons.

4.4 Conductivity analysis and anomalies

The RES reach took the longest time to reach a plateau during early and late July (1 h 31 min and 1 h 30 min), most likely due to the combined effects of low discharge (Table 2), less rainfall (Table 3), stream restoration features such as riffles, pools, step pools, and higher temperatures in the summer month (Table 4). Conductivity is closely related to water temperature, and during the URE sampling period, March showed higher conductivity than other winter months. This is likely because the water temperature in March was seven degrees higher than in January and four degrees higher than in February (Table 5). The summer months showed a significant increase in mean conductivity (Figure 4), likely due to higher temperatures and lower discharge rates, which concentrated salts in the water column (Hayashi et al., 2012).

Diurnal fluctuation in conductivity has been documented in small or first-order streams in connection with enhanced photosynthetic processes, salt concentration via evaporation/evapotranspiration (evaporitic enrichment), or daily discharge variations from wastewater treatment plants during daylight hours (Hayashi et al., 2012; Calles, 1982). The elevated conductivity of the studied urban stream could be explained by these studies; however, the increase in conductivity over time in summer requires further examination, including evaluation of the influence of temperature on conductivity in urban environments. Additionally, the influence of groundwater discharge is believed to be greater during the dry season (summer) in perennial river systems (Le Maitre and Colvin, 2018). The RES and URE reaches experienced the lowest average precipitation in the summer (Table 3), making this period a dry season; however, the influence of groundwater on conductivity cannot be confirmed, only hypothesized.

5 Conclusion

The RES and URE urban streams retained SRP, although their streambed was predominantly small cobble and gravel. SRP retention likely occurred because Richland Creek is a P-limited system, reflected in the TN:TP ratio, with the slow-moving waters characteristic of a first-order watershed. In general, the summer results clearly indicated greater SRP and NH_4-N retention in the RES reach than in the URE reach, highlighting the effectiveness of restoration on nutrient retention. Significant retention of NO_3-N + NO_2-N was not observed in either the RES or the URE reaches, indicating that these sites may be a source of downstream NO_3-N + NO_2-N transport.

These whole-stream nutrient (e.g., SRP and NH_4-N) TE% experiments revealed that this stream traps more SRP and NH_4-N during the summer than winter. The RES reach was more effective than the URE reach when compared for nutrient TE%, suggesting that restoration has positive impacts on nutrient retention. The nutrient TE% in engineered pools at the RES reach indicated that SRP and NH_4-N uptake were more effective in the summer. Additionally, engineered pools in the RES reach were more efficient at assimilating NH_4-N than the other nutrients.

While the current study provides some guidance, initial data, and assessment of the method to quantify the effectiveness of stream restoration on nutrient dynamics, nutrient retention, whole-stream nutrient TE%, and nutrient TE% in engineered pools within streams, additional datasets in multiple restoration settings across different regions are required to make regulatory and policy recommendations. Additional research in multiple stream restoration settings [e.g., across different types and sizes] with analysis and interpretational data would be beneficial to creating such a regulatory practice. To assess the efficacy of stream restoration on nutrient dynamics, it is essential to account for the influence of periphyton, microbial activities, microhabitats, and microbiomes. The results from this study could be included when designing stream restoration features and nutrient reduction designs that could be linked to stream restoration credits. Therefore, conducting experiments during the summer, when these processes are most active, is likely to yield critical insights into their efficacy. When conducting nutrient injection studies to understand the efficacy of nutrient retention in stream restoration, it is important to ensure that the reach length adheres to the principles outlined in the Stream Solute Workshop (1990).

Data availability statement

The raw data supporting the conclusion of this article will be made available by the authors, without undue reservation. Should a

manuscript be developed based on this data, the authors and the data collectors request appropriate acknowledgment and authorship.

Author contributions

EJ: Conceptualization, Data curation, Formal analysis, Investigation, Methodology, Resources, Software, Visualization, Writing – original draft, and Writing – review and editing. DS: Conceptualization, Data curation, Formal analysis, Funding acquisition, Investigation, Methodology, Project administration, Resources, Software, Supervision, Validation, Visualization, and Writing – review and editing. CS: Formal analysis, Funding acquisition, Investigation, Methodology, Resources, Software, Supervision, Validation, Visualization, and Writing – review and editing. JP: Formal analysis, Funding acquisition, Investigation, Methodology, Project administration, Resources, Supervision, and Writing – review and editing. DP: Data curation, Formal analysis, Investigation, Methodology, Resources, Software, Supervision, Validation, Visualization, and Writing – review and editing. SW: Data curation, Formal analysis, Investigation, Methodology, Resources, Software, Supervision, Validation, Visualization, and Writing – review and editing. BH: Conceptualization, Data curation, Formal analysis, Investigation, Methodology, Resources, Software, Validation, Visualization, and Writing – review and editing.

Funding

The author(s) declare that financial support was received for the research and/or publication of this article. The water quality analysis was supported by the Arkansas Water Resources Center through 104B base funding and USDA Hatch funding. Funding and support were provided by CS, JP, DP, BH, and DS.

Acknowledgments

The authors would like to express their gratitude to Mr. Paul Dow, City Engineer, City of Greenville, for granting access to the sites, designs, plans, and history of the sites. The authors would also like to thank Michael Masters, shop technician, Department of Agricultural Sciences, Clemson University, for assisting in delivering the hardware required for the project. Our appreciation also extends to Ibrahim Busari, Morolake Fatunmbi, Meredith Brock, and Collin Kane for their assistance during the fieldwork.

Conflict of interest

The authors declare that the research was conducted in the absence of any commercial or financial relationships that could be construed as a potential conflict of interest.

Generative AI statement

The author(s) declare that no Generative AI was used in the creation of this manuscript.

Publisher's note

All claims expressed in this article are solely those of the authors and do not necessarily represent those of their affiliated organizations, or those of the publisher, the editors and the reviewers. Any product that may be evaluated in this article, or claim that may be made by its manufacturer, is not guaranteed or endorsed by the publisher.

References

Accuweather Inc (2023). *Accuweather Inc*. Available online at: https://www.accuweather.com/en/us/greenville/29601/weather-forecast/330681?city=greenville (Accessed April 13, 2023).

Advancing Standards Transforming Markets (2017). *Standard Test Methods for Particle-Size Distribution (Gradation) of Soils Using Sieve Analysis*. West Conshohocken, PA. Available online at: https://www.astm.org/d6913-04r09e01.html.

Allan, J. D. (2004). Landscapes and riverscapes: the influence of land use on stream ecosystems. *Annu. Rev. Ecol. Evol. Syst.* 35, 257–284. doi:10.1146/annurev.ecolsys.35.120202.110122

AWRC (2023). *Water Quality Lab: Certification and Quality Assurance*. Available online at: https://awrc.uada.edu/water-quality-lab/certification-and-quality-assurance/.

Beechie, T. J., Sear, D. A., Olden, J. D., Pess, G. R., Buffington, J. M., Moir, H., et al. (2010). Process-based principles for restoring river ecosystems. *BioScience* 60 (3), 209–222. doi:10.1525/bio.2010.60.3.7

Bernhardt, E. S., Band, L. E., Walsh, C. J., and Berke, P. E. (2008). Understanding, managing, and minimizing urban impacts on surface water nitrogen loading. *Ann. N. Y. Acad. Sci.* 1134 (1), 61–96. doi:10.1196/annals.1439.014

Bernhardt, E. S., Palmer, M. A., Allan, J. D., Alexander, G., Barnas, K., Brooks, S., et al. (2005). Synthesizing U.S. River restoration efforts. *Science* 308 (5722), 636–637. doi:10.1126/science.1109769

Blaszczak, J. R., Delesantro, J. M., Urban, D. L., Doyle, M. W., and Bernhardt, E. S. (2019). Scoured or suffocated: urban stream ecosystems oscillate between hydrologic and dissolved oxygen extremes. *Limnol. Oceanogr.* 64 (3), 877–894. doi:10.1002/lno.11081

Bledsoe, B. P., and Watson, C. C. (2001). Effects of urbanization on channel instability. *J. Am. Water Resour. Assoc.* 37 (2), 255–270. doi:10.1111/j.1752-1688.2001.tb00966.x

Brown, L. R., Cuffney, T. F., Coles, J. F., Fitzpatrick, F., McMahon, G., Steuer, J., et al. (2009). Urban streams across the USA: lessons learned from studies in 9 metropolitan areas. *J. North Am. Benthol. Soc.* 28 (4), 1051–1069. doi:10.1899/08-153.1

Bukaveckas, P. A. (2007). Effects of channel restoration on water velocity, transient storage, and nutrient uptake in a channelized stream. *Environ. Sci. Technol.* 41 (5), 1570–1576. doi:10.1021/es061618x

Calles, U. M. (1982). Diurnal variations in electrical conductivity of water in a small stream. *Nord. Hydrol.* 13, 157–164. doi:10.2166/nh.1982.0013

Caraco, N. F., and Cole, J. J. (1999). Human impact on nitrate export: An analysis using major world rivers. *Ambio,* 28 (2), 167–170. doi:10.2166/nh.1982.0013

Carpenter, S., Caraco, N., Correll, D., Howarth, R., Sharpley, A., and Smith, V. (1998). Nonpoint pollution of surface waters with phosphorus and nitrogen. *Ecol. Appl.* 8 (3), 559–568. doi:10.2307/2641247

Chaubey, I., Sahoo, D., Haggard, B. E., Matlock, A. D., and Costello, T. A. (2007). Nutrient retention, nutrient limitation, and sediment-nutrient interactions in a pasture-dominated stream. *Am. Soc. Agric. Biol. Eng.* 50 (1), 35–44. doi:10.13031/2013.22409

Cole, J. J., Peierls, B. L., Caraco, N. F., and Pace, M. L. (1993). "Nitrogen loading of rivers as a human-driven process," in *Humans as Components of Ecosystems* (New York, NY: Springer), 141–157. doi:10.1007/978-1-4612-0905-8_12

Craig, L. S., Palmer, M. A., Richardson, D. C., Filoso, S., Bernhardt, E. S., Bledsoe, B. P., et al. (2008). Stream restoration strategies for reducing river nitrogen loads. *Front. Ecol. Environ.* 6 (10), 529–538. doi:10.1890/070080

Dodds, W. K., and Smith, V. H. (2016). Nitrogen, phosphorus, and eutrophication in streams. *Inland Waters* 6 (2), 155–164. doi:10.5268/IW-6.2.909

Dyer, J., Mercer, A., and Raczyński, K. (2022). Identifying spatial patterns of hydrologic drought over the southeast US using retrospective national water model simulations. *Water* 14 (10), 1525. doi:10.3390/w14101525

Enironmental Protection Agency (2022a). *Drinking Water Regulations and Contaminants*. Available online at: https://www.epa.gov/sdwa/drinking-water-regulations-and-contaminants (Accessed April 13, 2023).

Ensign, S. H., and Doyle, M. W. (2006). Nutrient spiraling in streams and river networks. *J. Geophys. Res. Biogeosciences* 111 (G4). doi:10.1029/2005JG000114

Environmental Protection Agency (2022b). *How's My Waterway? Informing the Conversation About Your Waters*. Available online at: https://www.epa.gov/waterdata/hows-my-waterway (Accessed April 13, 2023).

Environmental Protection Agency (2023). Deposited and bedded sediment. Available online at: https://www.epa.gov/caddis/sediments (Accessed April 12, 2023).

Haggard, B. E., Stanley, E. H., and Storm, D. E. (2005). Nutrient retention in a point-source-enriched stream. *J. North Am. Benthol. Soc.* 24 (1), 29–47. doi:10.1899/0887-3593(2005)024<0029:NRIAPS>2.0.CO;2

Haggard, B. E., Storm, D. E., Tejral, R. D., Popova, Y. A., Keyworth, V. G., and Stanley, E. H. (2001). Stream nutrient retention in three northeastern Oklahoma agricultural catchments. *Trans. ASAE* 44 (3), 597–605. doi:10.13031/2013.6120

Hayashi, M., Vogt, T., Mächler, L., and Schirmer, M. (2012). Diurnal fluctuations of electrical conductivity in a pre-alpine river: effects of photosynthesis and groundwater exchange. *J. Hydrology* 450–451, 93–104. doi:10.1016/j.jhydrol.2012.05.020

Hill, A. R. (1988). Factors influencing nitrate depletion in a rural stream. *Hydrobiologia* 160, 111–122. doi:10.1007/BF00015474

Howarth, R. W., Billen, G., Swaney, D., Townsend, A., Jaworski, N., Lajtha, K., et al. (1996). "Regional nitrogen budgets and riverine N andamp; P fluxes for the drainages to the North Atlantic Ocean: natural and human influences," in *Nitrogen Cycling in the North Atlantic Ocean and its Watersheds* (Netherlands: Springer), 75–139. doi:10.1007/978-94-009-1776-7_3

Jordan, E. (2023). Nutrient dynamics in restored and unrestored urban streams: a study in the Southern Piedmont Ecoregion of South Carolina. Master's thesis. South Carolina, SC: Clemson University.

Kaushal, S. S., Duan, S., Doody, T. R., Haq, S., Smith, R. M., Newcomer, J., et al. (2017). Human-accelerated weathering increases salinization, major ions, and alkalinization in fresh water across land use. *Appl. Geochem.* 83, 121–135. doi:10.1016/j.apgeochem.2017.02.006

Klocker, C. A., Kaushal, S. S., Groffman, P. M., Mayer, P. M., and Morgan, R. P. (2009). Nitrogen uptake and denitrification in restored and unrestored streams in urban Maryland, USA. *Aquat. Sci.* 71 (4), 411–424. doi:10.1007/s00027-009-0118-y

Köse, E., Tokatli, C., and Çiçek, A. (2014). Monitoring stream water quality: a statistical evaluation. *Pol. J. Environ. Stud.* 23 (5), 1637–1647.

Kriech, A. J., and Osborn, L. V. (2022). Review of the impact of stormwater and leaching from pavements on the environment. *J. Environ. Manag.* 319, 115687. doi:10.1016/j.jenvman.2022.115687

Lammers, R. W., and Bledsoe, B. P. (2017). What role does stream restoration play in nutrient management? *Crit. Rev. Environ. Sci. Technol.* 47 (6), 335–371. doi:10.1080/10643389.2017.1318618

Lautz, L. K., and Siegel, D. I. (2007). The effect of transient storage on nitrate uptake lengths in streams: an inter-site comparison. *Hydrol. Process.* 21 (26), 3533–3548. doi:10.1002/hyp.6569

Le, A., Kasahara, T., and Vudhivanich, V. (2018). Seasonal variation and retention of ammonium in small agricultural streams in Central Thailand. *Environments* 5 (7), 78. doi:10.3390/environments5070078

le Maitre, D. C., and Colvin, C. A. (2018). Assessment of the contribution of groundwater discharges to rivers using monthly flow statistics and flow seasonality. *Water SA* 34 (5), 549. doi:10.4314/wsa.v34i5.180652

Liao, H., Sarver, E., and Krometis, L.-A. H. (2018). Interactive effects of water quality, physical habitat, and watershed anthropogenic activities on stream ecosystem health. *Water Res.* 130, 69–78. doi:10.1016/j.watres.2017.11.065

Lundquist, J. D., and Cayan, D. R. (2002). Seasonal and spatial patterns in diurnal cycles in streamflow in the western United States. *J. Hydrometeorol.* 3 (5), 591–603. doi:10.1175/1525-7541(2002)003<0591:SASPID>2.0.CO;2

Manning, D. W. P., Rosemond, A. D., Benstead, J. P., Bumpers, P. M., and Kominoski, J. S. (2020). Transport of N and P in U.S. streams and rivers differs with land use and between dissolved and particulate forms. *Ecol. Appl.* 30 (6), e02130. doi:10.1002/eap.2130

Marsh-McBirney Inc (1990). *Flow-Mate 200*. Available online at: https://www.fieldenvironmental.com/assets/files/Manuals/Marsh%20McBirney%20Flo-Mate%20Manual.pdf (Accessed December 3, 2021).

Marti, E., and Sabater, F. (1996). High variability in temporal and spatial nutrient retention in Mediterranean streams. *Ecology* 77 (3), 854–869. doi:10.2307/2265506

McMillan, S. K., Tuttle, A. K., Jennings, G. D., and Gardner, A. (2014). Influence of restoration age and riparian vegetation on reach-scale nutrient retention in restored urban streams. *JAWRA J. Am. Water Resour. Assoc.* 50 (3), 626–638. doi:10.1111/jawr.12205

Meyer, J. L., McDowell, W. H., Bott, T. L., Elwood, J. W., Ishizaki, C., Melack, J. M., et al. (2019). Elemental dynamics in streams. *Journal of the North American Benthological Society.* 7 (4), 410–432.

Miserendino, M. L., Casaux, R., Archangelsky, M., Di Prinzio, C. Y., Brand, C., and Kutschker, A. M. (2011). Assessing land-use effects on water quality, in-stream habitat, riparian ecosystems and biodiversity in Patagonian northwest streams. *Sci. Total Environ.* 409, 612–624. doi:10.1016/j.scitotenv.2010.10.034

Morgan, J. A., Royer, T. V., and White, J. R. (2019). Fine sediment removal influences biogeochemical processes in a gravel-bottomed stream. *Environ. Manag.* 64 (3), 258–271. doi:10.1007/s00267-019-01187-2

Mulholland, P. J. (2004). The importance of in-stream uptake for regulating stream concentrations and outputs of N and P from a forested watershed: evidence from long-term chemistry records for Walker Branch Watershed. *Biogeochemistry* 70 (3), 403–426. doi:10.1007/s10533-004-0364-y

National Oceanic and Atmospheric Administration (2020). *U.S. Climate Normals Quick Access*. Available online at: https://www.ncei.noaa.gov/access/us-climate-normals/#dataset=normals-annualseasonalandtimeframe=30andlocation=SCandstation=USC00383735 (Accessed April 13, 2023).

Newbold, J. D., Elwood, J. W., O'Neill, R. V., and Sheldon, A. L. (1983). Phosphorus dynamics in a woodland stream ecosystem: a study of nutrient spiralling. *Ecology* 64 (5), 1249–1265. doi:10.2307/1937833

Newcomer Johnson, T., Kaushal, S., Mayer, P., Smith, R., and Sivirichi, G. (2016). Nutrient retention in restored streams and rivers: a global review and synthesis. *Water* 8 (4), 116. doi:10.3390/w8040116

Nina, F. C., and Jonathan, J. C. (1999). Human impact on nitrate export: an analysis using major world rivers. *AMBIO* 28 (2), 167–170.

O'Brien, P. J., and Wehr, J. D. (2010). Periphyton biomass and ecological stoichiometry in streams within an urban to rural land-use gradient. *Hydrobiologia* 657 (1), 89–105. doi:10.1007/s10750-009-9984-5

Palmer, M. A., Hondula, K. L., and Koch, B. J. (2014). Ecological restoration of streams and rivers: shifting strategies and shifting goals. *Annu. Rev. Ecol. Evol. Syst.* 45 (1), 247–269. doi:10.1146/annurev-ecolsys-120213-091935

Paul, M. J., and Meyer, J. L. (2001). Streams in the urban landscape. *Annu. Rev. Ecol. Syst.* 32 (1), 333–365. doi:10.1146/annurev.ecolsys.32.081501.114040

Racchetti, E., Bartoli, M., Soana, E., Longhi, D., Christian, R. R., Pinardi, M., et al. (2011). Influence of hydrological connectivity of riverine wetlands on nitrogen removal via denitrification. *Biogeochemistry* 103 (1–3), 335–354. doi:10.1007/s10533-010-9477-7

Rasmussen, J. J., Baattrup-Pedersen, A., Riis, T., and Friberg, N. (2011). Stream ecosystem properties and processes along a temperature gradient. *Aquat. Ecol.* 45, 231–242. doi:10.1007/s10452-010-9349-1

Reisinger, A. J., Groffman, P. M., and Rosi-Marshall, E. J. (2016). Nitrogen-cycling process rates across urban ecosystems. *FEMS Microbiol. Ecol.* 92 (12), fiw198. doi:10.1093/femsec/fiw198

Roberts, B. J., Mulholland, P. J., and Houser, J. N. (2007). Effects of upland disturbance and instream restoration on hydrodynamics and ammonium uptake in headwater streams. *J. N. Am. Benthol. Soc.* 1 (26), 38–53. doi:10.1899/0887-3593(2007)26[38:eoudai]2.0.co;2

Rosgen, D. L. (2007). "Rosgen geomorphic channel design,"in *National Engineering Handbook Part 654 (210-VINEH)*. Editors J. Bernard, J. F. Fripp, and K. R. Robinson (Washington, D.C.: United States Department of Agriculture, Natural Resources Conservation Service), Chap. 11, 1–76.

Russell, K. L., Vietz, G. J., and Fletcher, T. D. (2020). How urban stormwater regimes drive geomorphic degradation of receiving streams. *Prog. Phys. Geogr. Earth Environ.* 44 (5), 746–778. doi:10.1177/0309133319893927

Sanchez, G. M., Terando, A., Smith, J. W., García, A. M., Wagner, C. R., and Meentemeyer, R. K. (2020). Forecasting water demand across a rapidly urbanizing region. *Sci. Total Environ.* 730, 139050. doi:10.1016/j.scitotenv.2020.139050

Simon, S. K., and Benfield, E. F. (2002). Ammonium retention and whole-stream metabolism in cave streams. *Hydrobiologia* 482, 31–39. doi:10.1023/a:1021257822591

Stranko, S. A., Hilderbrand, R. H., and Palmer, M. A. (2012). Comparing the fish and benthic macroinvertebrate diversity of restored urban streams to reference streams. *Restor. Ecol.* 20 (6), 747–755. doi:10.1111/j.1526-100X.2011.00824.x

Stream Solute Workshop (1990). Concepts and methods for assessing solute dynamics in stream ecosystems. *J. North Am. Benthol. Soc.* 9 (2), 95–119. doi:10.2307/1467445

Thompson, J., Pelc, C. E., Brogan, W. R., and Jordan, T. E. (2018). The multiscale effects of stream restoration on water quality. *Ecol. Eng.* 124, 7–18. doi:10.1016/j.ecoleng.2018.09.016

Tranmer, A. W., Caamaño, D., and Arteaga, A. E. (2022). Urban stream syndrome: quantifying topographic variation along an urban-rural gradient. *J. Environ. Manag.* 317, 115413. doi:10.1016/j.jenvman.2022.115413

Turnipseed, P., and Sauer, V. (2010). *Discharge Measurements at Gaging Stations: U.S. Geological Survey Techniques and Methods book 3*. United States Geological Survey (Reston, Virginia: USGS). Available online at: https://pubs.usgs.gov/tm/tm3-a8/tm3a8.pdf.

United States Geological Survey (2019). *NLCD 2019 Land Cover (CONUS)*. Available online at: https://www.mrlc.gov/data/nlcd-2019-land-cover-conus (Accessed December 10, 2021).

Valett, H. M., Morrice, J. A., Dahm, C. N., and Campana, M. E. (1996). Parent lithology, surface-groundwater exchange, and nitrate retention in headwater streams. *Limnol. Oceanogr.* 41 (2), 333–345. doi:10.4319/lo.1996.41.2.0333

Walsh, C. J., Roy, A. H., Feminella, J. W., Cottingham, P. D., Groffman, P. M., and Morgan, R. P. (2005). The urban stream syndrome: current knowledge and the search for a cure. *J. North Am. Benthol. Soc.* 24 (3), 706–723. doi:10.1899/04-028.1

Williams, M. R., Bhatt, G., Filoso, S., and Yactayo, G. (2017). Stream restoration performance and its contribution to the chesapeake bay TMDL: challenges posed by climate change in urban areas. *Estuaries Coasts* 40 (5), 1227–1246. doi:10.1007/s12237-017-0226-1

Williams, M. R., and Filoso, S. (2023). Changes in hydrology and pollutant loads from stream restoration in an urban headwater catchment. *J. Hydrology* 618, 129164. doi:10.1016/j.jhydrol.2023.129164

Wolf, K. L., Noe, G. B., and Ahn, C. (2013). Hydrologic connectivity to streams increases nitrogen and phosphorus inputs and cycling in soils of created and natural floodplain wetlands. *J. Environ. Qual.* 42 (4), 1245–1255. doi:10.2134/jeq2012.0466

Wolman, M. G. (1967). A cycle of sedimentation and erosion in urban river channels. *Geogr. Ann. Ser. A, Phys. Geogr.* 49 (2–4), 385–395. doi:10.1080/04353676.1967.11879766

Wu, J., Stewart, T. W., Thompson, J. R., Kolka, R. K., and Franz, K. J. (2015). Watershed features and stream water quality: Gaining insight through path analysis in a Midwest urban landscape, U.S.A. *Landsc. Urban Plan.* 143, 219–229. doi:10.1016/j.landurbplan.2015.08.001

Young, K. B. (1950). *A Comparative Study of Mean-Section and Mid-Section methods for computation of discharge measurements*, No. 53-277. US Geological Survey.

frontiers | Frontiers in Environmental Science

TYPE Original Research
PUBLISHED 27 August 2024
DOI 10.3389/fenvs.2024.1468869

Check for updates

OPEN ACCESS

EDITED BY
Yefang Jiang,
Agriculture and Agri-Food Canada (AAFC), Canada

REVIEWED BY
Kang Liang,
University of Maryland, College Park, United States
Yongbo Liu,
Environment and Climate Change Canada (ECCC), Canada

*CORRESPONDENCE
Rob. C. Jamieson,
jamiesrc@dal.ca

RECEIVED 22 July 2024
ACCEPTED 15 August 2024
PUBLISHED 27 August 2024

CITATION
Oliver AC, Kurylyk BL, Johnston LH, LeRoux NK, Somers LD and Jamieson RC (2024) Impacts of climate change and best management practices on nitrate loading to a eutrophic coastal lagoon.
Front. Environ. Sci. 12:1468869.
doi: 10.3389/fenvs.2024.1468869

COPYRIGHT
© 2024 Oliver, Kurylyk, Johnston, LeRoux, Somers and Jamieson. This is an open-access article distributed under the terms of the Creative Commons Attribution License (CC BY). The use, distribution or reproduction in other forums is permitted, provided the original author(s) and the copyright owner(s) are credited and that the original publication in this journal is cited, in accordance with accepted academic practice. No use, distribution or reproduction is permitted which does not comply with these terms.

Impacts of climate change and best management practices on nitrate loading to a eutrophic coastal lagoon

Alexandra C. Oliver, Barret L. Kurylyk, Lindsay H. Johnston, Nicole K. LeRoux, Lauren D. Somers and Rob. C. Jamieson*

Department of Civil and Resource Engineering and Centre for Water Resources Studies, Dalhousie University, Halifax, NS, Canada

Anthropogenic climate change and associated increasing nutrient loading to coasts will worsen coastal eutrophication on a global scale. Basin Head is a coastal lagoon located in northeastern Prince Edward Island, Canada, with a federally protected ecosystem. Nitrate-nitrogen (NO_3-N) is conveyed from agricultural fields in the watershed to the eutrophic lagoon via intertidal groundwater springs and groundwater-dominated tributaries. A field program focused on four main tributaries that discharge into the lagoon was conducted to measure year-round NO_3-N loading. These measurements were used to calibrate a SWAT+ hydrologic model capable of simulating hydrologic and NO_3-N loads to the lagoon. Several climate change scenarios incorporating different agricultural best management practices (BMPs) were simulated to better understand potential future NO_3-N loading dynamics. Results indicate that all climate change scenarios produced increased annual NO_3-N loading to the lagoon when comparing historical (1990–2020) to end of century time periods (2070–2100); however, only one climate scenario (MRI-ESM2-0 SSP5-8.5) resulted in a statistically significant (p-value <0.05) increase. Enlarged buffer strips and delayed tillage BMP simulations produced small (0%–8%) effects on loading, while changing the crop rotation from potato-barley-clover to potato-soybean-barley yielded a small reduction in NO_3-N loading between the historical period and the end of the century (26%–33%). Modeling revealed changes in seasonal loading dynamics under climate change where NO_3-N loads remained more consistent throughout the year as opposed to current conditions where the dominant load is in the spring. An increase in baseflow contributions to streamflow was also noted under climate change, with the largest change occurring in the winter (e.g., up to a five-fold increase in February). These findings have direct implications for coastal management in groundwater-dominated agricultural watersheds in a changing climate.

KEYWORDS

hydrologic model, SWAT+, climate change, best management practice, nitrate loading

Introduction

Rising water temperatures and increased export of freshwater and nutrients to the coast are expected to exacerbate coastal eutrophication in future years (Rabalais et al., 2009). Anthropogenic changes such as industrialization and increased population are responsible for accelerated climate change and increased nutrient loading to coastal water bodies (Howarth, 2008; Oppenheimer et al., 2019). In addition to the deleterious human and ecosystem health impacts of coastal eutrophication (Cloern, 2001; Sinha et al., 2019), the degradation of coastal waters impacts the ecosystem services provided by the water body such as recreation, tourism, and cultural value (Malone and Newton, 2020).

Agricultural activity and on-site domestic wastewater treatment systems can cause increased nitrate-nitrogen (NO_3-N) loading in rural watersheds. Soil nitrate can be derived from mineral fertilizers, manures, biological nitrogen fixation and soil organic matter (Zebarth et al., 2015). Since the advent of nitrogen fertilizer for agriculture in the 20th century, global usage has increased to approximately 10 times the rate of consumption in 1961 (Lu and Tian, 2017). Nitrogen in the form of ammonia is applied to agricultural fields through chemical fertilizer where it is readily converted to nitrite, then to nitrate by microorganisms in soil and groundwater (Fetter et al., 2017). Nitrate-nitrogen can be transported by runoff over agricultural fields or through groundwater flow once precipitation infiltrates into the aquifer (Spalding and Exner, 1993). Accordingly, the intensification in nitrogen use has resulted in accelerated coastal eutrophication due to non-point source, diffusive transport of soluble nitrate to the coast (Arhonditsis et al., 2000; Malone and Newton, 2020).

Climate change is expected to negatively affect agricultural activities across the globe (Bennett et al., 2021; Nelson et al., 2009), impacting moisture availability and plant physiology, and affecting agricultural productivity (Mahato, 2014) due to increasing air temperatures, shifting precipitation regimes, and increasing frequency and severity of extreme events (AghaKouchak et al., 2020; Rivera, 2014; Wang et al., 2022). These hydrometeorological changes could all contribute to changing agricultural practices and productivity. For example, increased temperatures are expected to prolong agricultural growing seasons (AAFC, 2020) and shift the source of irrigation from rainwater to groundwater (Paradis et al., 2016; Afzaal et al., 2020; Bhatti et al., 2022), further stressing vulnerable water resources. Agricultural best management practices (BMPs) have been developed to help confront, among other stressors, the impacts of future climate change (Lal et al., 2011; Wagena and Easton, 2018). While proactive agricultural practices like BMPs help to reduce nutrient losses from agricultural fields, the efficacy of BMPs in mitigating NO_3-N contamination in a changing climate is not well understood (Liu et al., 2017; Zebarth et el., 2015). Coastal agricultural watersheds are subject to additional stressors compared to inland watersheds, including the conversion of traditional nutrient sinks like wetlands and riparian zones to agricultural use (Boesch and Brinsfield, 2000) and other phenomena (e.g., seawater intrusion, coastal flooding, soil salinity) that impact agricultural sustainability (Gopalakrishnan et al., 2019; Tackley et al., 2023).

Understanding of nutrient transport dynamics from agricultural watersheds under a changing climate can be developed by using process-based simulation tools that incorporate changes in climate forcing and agricultural practices. The SWAT+ (Soil and Water Assessment Tool) hydrologic model is a time continuous, semi-distributed watershed model that simulates quality and quantity of surface water and groundwater over a three-dimensional domain (Arnold et al., 2012) with the input of land use, soil, elevation, and climate data. The model can simulate spatial and temporal dynamics of non-point source contaminant loading and has proven to be a valuable tool for environmental planning and management (Arnold et al., 2012). The goal of this study is to investigate the effects of climate change and alternative BMPs on NO_3-N loading to a shallow, coastal lagoon with a federally protected ecosystem. Projections from an ensemble of downscaled global climate model (GCM) runs were applied to a SWAT+ hydrologic model, and results were analyzed over three 30-year periods: historical (1990–2020), mid-century (2040–2070) and end of century (2070–2100). Buffer strips, delayed tillage of forage and alternative crop rotations were investigated in SWAT+ over these times periods to assess potential changes in NO_3-N loading resulting from the implementation of these common BMPs. As agricultural practices will also likely evolve with climate change to account for longer growing seasons, extended dry seasons, and shifting markets, a future agricultural scenario was also modeled in SWAT+ for which fertilizer amounts were increased, and the growing season was extended.

Methods

Study site

Eutrophic conditions in estuaries in the province of Prince Edward Island (PEI), Canada have been documented since 2002 with the implementation of the PEI Estuaries Survey (Bugden et al., 2014), although they have been anecdotally noted for decades prior. PEI is intensively cultivated for potatoes, accounting for 25% of Canadian potato exports (Government of Prince Edward Island, 2020). Potatoes require high fertilization rates but have poor nitrogen (N) uptake efficiency (Delgado et al., 2001), which causes significant leaching and runoff of N into surface and groundwater (De Notaris et al., 2018; Jiang et al., 2011; Zebarth et al., 2009). The island is characterized by well-drained soils and shallow aquifers that are highly susceptible to N contamination in the form of NO_3-N (Puckett et al., 2011). Rainfall, snowmelt, and associated recharge elevate water tables in PEI and drive discharge of N-rich groundwater to streams and, eventually, PEI coastal waters (Pavlovskii et al., 2023). Under current agricultural practices, groundwater NO_3-N concentrations in PEI are predicted to continue to increase as NO_3-N penetrates deeper into bedrock aquifers (Jiang and Somers, 2009; Zhang and Hiscock, 2011). This could deleteriously impact potable water quality in this province, which is fully dependent on groundwater for drinking water supply (Council of Canadian Academies, 2009), as well as the health of coastal ecosystems that receive contaminated groundwater.

Amidst growing public concern surrounding the health of PEI's environment, the province has implemented some mandatory

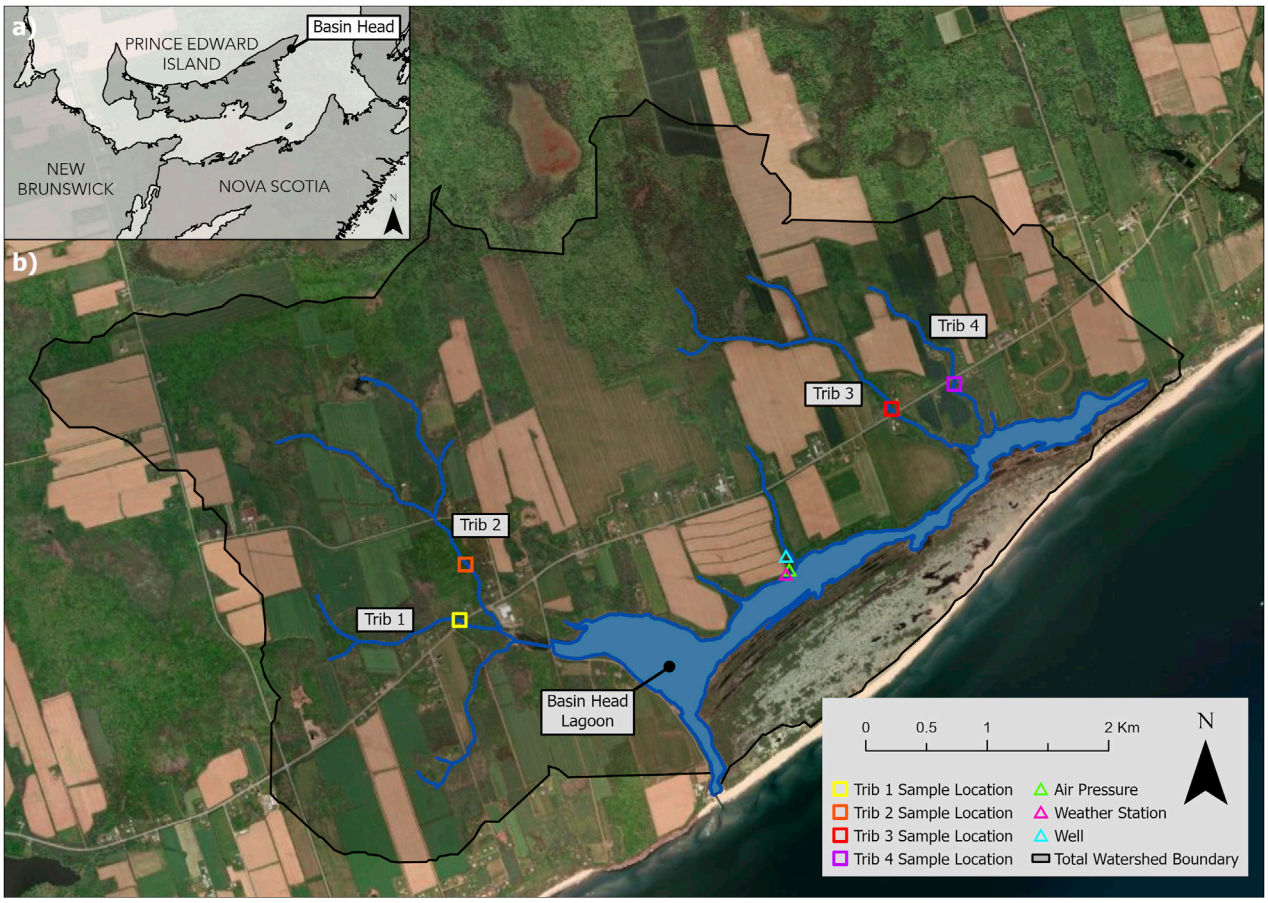


FIGURE 1
(A) Basin Head study site location on the northeastern shore of PEI in Atlantic Canada, **(B)** Basin Head lagoon, tributaries (Trib 1–4), sub-watersheds, and sampling and instrument locations [modified from Oliver et al. (2024)].

agricultural BMPs since the early 2000s. For example, 15 m buffer strips are required around any watercourse (Government of PEI, 2016), and the Agricultural Crop Rotation Act (Government of PEI, 2002) states that potatoes can only be grown on the same parcel of land once every 3 years. The Province of PEI also provides funding through the Agriculture Stewardship Program for farmers wishing to implement BMPs under the categories of manure and livestock management, agroforestry, water and supply management and integrated pest management (Sustainable CAP, 2023). Examples of BMPs currently employed in PEI are cover cropping, incorporating N-fixing plants into crop rotations, improving liquid manure application, implementing edge of field treatment systems such as buffer strips, constructed wetlands and vegetative swales. Research into the effects of alternative crop rotations to the traditional Potato-Barley-Clover (PBC) rotation on PEI has revealed that replacing red clover with soybeans, a legume, adds an additional cash crop, while reducing NO_3-N leaching and increasing potato tuber yield (Azimi et al., 2022; Liang et al., 2019).

Basin Head lagoon, located on the northeastern coast of PEI (Figure 1A), has been experiencing declining ecosystem health (Connolly, 2002). Accordingly, the lagoon was designated as a federal Marine Protected Area in 2005 with the goal of protecting the endemic giant Irish moss, a unique morphotype of Irish moss (*Chondrus crispus*), from declining ecosystem health and water quality (DFO, 2009). More prevalent and sustained hypoxic events have been noted over recent years, particularly in the shallower and more poorly mixed northeast arm of the lagoon throughout the spring and summer months (DFO, 2021). Hypoxic or anoxic conditions can result in irreversible changes to aquatic community structure (Coffin et al., 2018) and can threaten the health of the Irish moss in the Basin Head Marine Protected Area.

The Basin Head watershed is 14.6 km^2 (Figure 1B) with agriculture (41%) and forest (31%) comprising most of the land cover (KarisAllen et al., 2022). This study focuses on the four major tributaries that discharge into the lagoon with a collective drainage area of 7.2 km^2 (Figure 1B), and does not include direct runoff to the lagoon. The Charlottetown soil series is the most abundant throughout the entire province (MacDougall et al., 1988), and is the dominant soil type in the Basin Head watershed (95%). It is classified as a well-drained sandy loam located on gentle slopes (4%–9%) and is extremely well suited for agriculture (MacDougall et al., 1988). The porosity of the Charlottetown soil series varies from 30% in the till layer below 0.5 m (Francis, 1989; Heath, 1983; MacDougall et al., 1988) to approximately 50% in the upper, macroporous zone (Carter, 1987; MacDougall et al., 1988). Depth to bedrock, based on historical well data in the Kings County region, has been observed to

TABLE 1 Description, data sources and resolution for SWAT+ spatial inputs (topography, land use, and soil).

Watershed characteristic		Value	Source	Resolution (m)
Topography	Area	7.2 km^2	Province of PEI (2008)	10
	Elevation	Average 34.7 MASL (Minimum 6 MASL, Maximum 59 MASL)		
	Slope	0%–10%		
Land use		43% forest, 44% cropland, 7% shrubland, 3% wetland, 1% grassland, 1% barren, 1% transportation	Annual Crop Inventory (ACI) (AAFC, 2021)	30
Dominant soil type		Charlottetown series, USDA-SCS class C, Slope phase: 2%–5%, Dominant surface texture: sandy loam (<8% clay)	The National Soil Database (AAFC, 2022)	5

range from 0 to 6.2 m (Government of PEI, 2019; Joostema, 2015) and was measured to be 4.6 m at a shallow monitoring well in the watershed installed near the lagoon (KarisAllen et al., 2022) (Figure 1B). The bedrock aquifer that underlies PEI is primarily comprised of sandstone (80%–85%) and interbedded mudstone which is fractured, creating preferential flow paths (Francis, 1989). The fractured sandstone aquifer functions as a dual-porosity system, which presents challenges with characterization of aquifer effective porosity, specific yield, and hydraulic conductivity. However, equivalent porous medium approaches are commonly applied when modeling PEI groundwater systems (e.g., Stanic et al., 2024).

The climate of PEI is characterized as temperate and humid, with a mean annual precipitation of 1,173 mm at the Charlottetown weather station (1971–2000) and mean annual air temperature of 5.3°C (Paradis et al., 2016). Most precipitation (75%) falls as rain (Paradis et al., 2016), and precipitation is relatively uniformly distributed throughout the year, averaging between 80 and 120 mm per month (ECCC, 2023). Baseflow typically contributes 60%–70% of streamflow annually on PEI, and up to 100% in the summer months (Benson et al., 2007; DELJ, 2013); hence groundwater is critical to quantifying PEI water balances and nutrient transport. The fractured sandstone aquifer in the Basin Head watershed provides baseflow to the four tributaries that are the focus of this study (Figure 1) and provides flow for the 30+ intertidal springs that discharge directly into the lagoon (KarisAllen and Kurylyk, 2021; Oliver et al., 2024). The lagoon is tidally pumped and experiences mixing from waves, surges, and current during coastal storms (Bonnington et al., 2023).

Model inputs

The SWAT+ model (Arnold et al., 2012) requires climate variable inputs as well as GIS-based inputs for topography (i.e., Digital Elevation Model, DEM), land use and soils. A summary of the spatial data used to construct the SWAT+ model is presented in Table 1. Full maps of DEM, soil, and land use are provided in Supplementary Figures S1–S3. Figure 2 displays all soil types within the watershed boundaries; however, for simplicity in the model, the Charlottetown series was chosen to represent the entirety of the watershed due to its relative abundance (95%). Precipitation and maximum and minimum daily air temperature records were obtained from a weather station (Onset HOBO) installed at Basin Head (Figure 1B). This weather station did not provide accurate precipitation in winter months (December to March) as it did not possess a heated rain gauge; therefore, the record was supplemented with values from the nearest Environment and Climate Change Canada (ECCC) weather stations at East Point (ECCC ID 7177) and St. Peters (ECCC ID 7177), which are 12 km and 36 km from Basin Head. The East Point station was used to develop a local weather generator within the model (Neitsch et al., 2011) to simulate other variables such solar radiation, wind speed and relative humidity. The weather generator uses statistical monthly measures for air temperature, precipitation, solar radiation, dew point, and more to develop representative daily climate data for a subbasin.

SWAT+ models three major forms of nitrogen in the soil profile and shallow aquifer: (1) organic nitrogen associated with humus, (2) mineral forms of nitrogen held by soil colloids, and (3) mineral forms of nitrogen in solution. The movement of nitrogen between two 'pools' (i.e., valence states) of inorganic nitrogen, ammonium (NH_4^+) and nitrate (NO_3^-), and three pools of organic nitrogen is simulated. Nitrate transport in SWAT+ is simulated only in the mobile water layer, which includes water transported by surface runoff, lateral flow (i.e., groundwater flow within the soil profile) or percolation (i.e., water moving past the lowest soil profile layer and into the shallow aquifer). The mobile water layer nitrate concentration, $conc_{NO3,mobile}$, is multiplied by the flow from each pathway (surface runoff, lateral flow and percolation) to determine nitrate load from each source in the soil layer. Important parameters in these partitioning equations are θ_e, the fraction of porosity where anions are excluded, and SAT_{ly}, the saturated water content of the soil layer (mm H_2O), which determine nitrate load from each source in the soil layer, and δ_{gw}, the delay time associated with overlying geologic formations (days), which determines nitrate load in the shallow aquifer.

Another important input to the SWAT+ model is agricultural practices. Fertilizer amount, type, and application timing, as well as crop rotation timing influences the forcing of chemical leaching into soils and surface water runoff, and hence NO_3-N concentrations in receiving water bodies. Several groups with local knowledge of agricultural practices in Kings County, PEI, where Basin Head is located (i.e., Souris Wildlife, PEI Potato Board, and Fisheries and Oceans Canada) were contacted to develop representative agricultural practices for model inputs. Cropland in the

watershed is assumed to adhere to local industry standard crop rotations of potato, a grain (e.g., barley), and a forage (e.g., clover) on a 3-year rotation (herein PBC) as is mandated by the province (Azimi et al., 2022). Although in recent years clover has been replaced with a mix of legumes including alfalfa, sudangrass, pearl millet, and ryegrass, red clover was simulated to maintain consistency over the period of interest (1990–2100). Standard fertilizer application to potato crops in PEI is 155 kg N ha^{-1} (PEI Analytical Laboratories, Department of Agriculture and Fisheries, PEI). A 15-15-15 Nitrogen-Phosphorous-Potassium fertilizer was chosen based on availability in the SWAT+ interface and given the similarity to the 17-17-7 fertilizer employed by Liang et al. (2020) who studied N dynamics in PEI under different crop rotations. The application method of broadcast, which refers to fertilizer being spread uniformly over the entire field, was chosen based on local practices in the Basin Head watershed, Supplementary Table S1 provides a summary of the agricultural operations incorporated in SWAT+.

Data collection and model calibration

Discrete water samples were collected at the four main (i.e., highest flows) tributaries on 15 occasions covering diverse flow conditions from 11 November 2021, to 28 November 2023 (Figure 1B). Samples were analyzed for NO_3-N using the cadmium reduction colorimetric method-APHA Method 4500-E (APHA, 2022). These grab samples were also analyzed for total suspended solids (TSS) using Standard Method 2450D (APHA, 2022). Continuous stream stage measurements were recorded using Onset HOBO loggers at 15-min intervals. Stage was barometrically compensated with a HOBO air pressure logger (Figure 1B). Instantaneous stream discharge measurements were obtained using the velocity-area method (Turnipseed and Sauer, 2010) during the period of 26 June 2019, to 14 October 2023. Stage-discharge relationships were developed for each tributary (Supplementary Figure S4) and used to convert stage to flow. Monthly streamflow (Supplementary Figure S5) was used to calibrate the SWAT+ model hydrology, which is a standard interval for such SWAT+ applications (Ricci et al., 2023; Van Liew et al., 2012), while water quality measurements on a daily basis (i.e., sample concentration) were used to calibrate SWAT+ parameters for NO_3-N and TSS.

In groundwater-dominated watersheds, generally the most sensitive streamflow model parameters relate to groundwater and soil moisture. A literature review for SWAT+ modeling found the SCS curve number (cn2), baseflow recession constant (alpha), fraction of root zone percolation that reaches deep aquifer (perco), and soil evaporation compensation factor (esco) to be most sensitive (Ahmad et al., 2011; Liang et al., 2020; Spruill et al., 2000). These parameters, along with others identified in a sensitivity analysis conducted in SWAT+ Toolbox (Supplementary Table S2), were chosen to calibrate streamflow (James, 2022). Evaluation statistics used to assess model performance included the Nash-Sutcliffe efficiency (NSE), RMSE-observation standard deviation ratio (RSR), and percent bias (PBIAS) (Moriasi et al., 2007). Moriasi et al. (2007) states that for streamflow, an RSR less than 0.7 is satisfactory, an NSE over 0.4 is satisfactory, and PBIAS less than 10 is very good. The corresponding equations are presented below, where Y_i^{obs} is the observed streamflow and Y_i^{sim} is the simulated streamflow generated by SWAT+.

$$NSE = 1 - \left[\frac{\sum_{i=1}^{n}\left(Y_i^{obs} - Y_i^{sim}\right)^2}{\sum_{i=1}^{n}\left(Y_i^{obs} - Y_i^{mean}\right)^2}\right] \quad (1)$$

$$RSR = \left[\frac{\sqrt{\sum_{i=1}^{n}\left(Y_i^{obs} - Y_i^{sim}\right)^2}}{\sqrt{\sum_{i=1}^{n}\left(Y_i^{obs} - Y_i^{mean}\right)^2}}\right] \quad (2)$$

$$PBIAS = \left[\frac{\sum_{i=1}^{n}\left(Y_i^{obs} - Y_i^{sim}\right) \times 100}{\sum_{i=1}^{n} Y_i^{obs}}\right] \quad (3)$$

Grab sample concentrations (Supplementary Table S3) were used to calibrate NO_3-N outputs from SWAT+. Daily NO_3-N mass (kg/day) output from each tributary from SWAT+ were converted to a concentration (mg/L) by dividing the mass by the daily total flow. Modeled concentrations were compared to 11 grab sample concentrations from 11 November 2021, to 5 July 2023, and Root Mean Squared Error (RMSE) was calculated for the modeled vs. measured concentrations:

$$RMSE = \sqrt{\sum_{i=1}^{n}\frac{\left(\hat{y}_i - y_i\right)^2}{n}} \quad (4)$$

where $\hat{y_n}$ are predicted values, y_n are observed values, and n is the number of observations. RMSE was used as the statistical performance metric for NO_3-N and TSS calibration as continuous measurements were not available for these parameters. A SWAT study conducted on the relatively nearby Wilmont River watershed in southwestern PEI (Liang et al., 2020) was used as a reference for the calibration in the present study due to the similarity in study region and hydrologic conditions. Supplementary Table S4 shows the parameters used in the sensitivity analysis and calibration in Liang et al. (2020), which were chosen as a starting point for the calibration of NO_3-N at the study site.

Once the model is calibrated satisfactorily, projected results using climate change data can be analyzed to determine patterns in seasonality of flow and NO_3-N loading, and trends to baseflow index (BFI). BFI is calculated by dividing the total volume of baseflow by total streamflow for a period. The SWAT+ outputs of lateral flow (flo) and shallow groundwater flow (latQ) sum to determine baseflow, and total streamflow is the summation of water yield (wateryld) and lateral flow (flo) into the channel. The 'half-flow date', T50, is a measure of streamflow timing and is defined as the date by which 50% of streamflow for a given water-year (i.e., October 1 to September 30) has passed (Court, 1962). This measure has been used to characterize flow regimes in the neighboring province of Nova Scotia (Johnston et al., 2022), and was calculated in this study for the three model periods.

It should be noted that SWAT studies in other small (<10 km^2) watersheds have been noted to yield unsatisfactory results (Spruill et al., 2000), largely due to characteristically low times of concentration and a propensity toward 'flashiness' in peak runoff (Uzeika et al., 2012). Chu et al. (2004) noted that characterizing baseflow correctly can be more important in small watersheds. Bailey et al. (2020) outlines limitations to the current groundwater algorithms in SWAT+ and proposes an amendment

to the standard SWAT+ module to improve model accuracy, particularly in baseflow-dominated watersheds where model performance can be poor (Bosch et al., 2010; Luo et al., 2012). Despite the challenges in applying SWAT+ in small, baseflow-dominated systems, this model is widely used and still provides useful insight into the hydrology and transport dynamics in these environments.

Model scenarios

Climate change scenarios

Changes to climate forcing will drive changes in hydrologic processes and agricultural practices (Gordon et al., 2008), which can be represented in SWAT+. An analysis by the Pacific Climate Impacts Consortium [of 26 downscaled Coupled Model Intercomparison Project (CMIP) 6 Global Climate Models (GCMs)] (Eyring et al., 2016) and three Shared Socioeconomic Pathways (SSPs) (Riahi et al., 2017) was completed to select models projecting low, moderate, and high changes to precipitation and temperature. Climate data for these models were downloaded from the NASA Climate Data Services (NASA, 2023), and, for the sake of downscaling consistency, only models downscaled using Bias Correction/Constructed Analogues with Quantile Mapping Reordering (BCCAQv2) (Maurer et al., 2010; Cannon, 2015) were considered. The scenarios from the IPSL-CM6A-LR and EC-Earth3-veg GCMs were removed from consideration because they are deemed 'hot' models, projecting much greater warming than is generally expected (Rahimpour Asenjan et al., 2023). UKESM1-0-LL was removed for simplicity since it only represents a 360-day year, and BCC-CSM2-MR was missing from the NASA dataset. The remaining six models were compared based on their average annual precipitation for each modeled time period (1990-2020, 2040-2070 and 2070–2100) (Supplementary Table S5), and three representative models (INM-CM5-0, FGOALS-g3, and MRI-ESM2-0) were chosen for low, moderate, and high climate change scenarios (Figure 2). Two SSPs per climate model, SSP2-4.5 (RCP 4.5) and SSP5-8.5 (RCP 8.5), were chosen to represent mid-range and high emissions scenarios, yielding a total of six climate change scenarios with a wide range of possible climate outcomes. The climate data representing each scenario was entered in SWAT+, and the calibrated model was run from 1990 to 2100, with outputs from representative periods of historical (1990–2020), mid-century (2040–2070) and end of century (2070–2100) used for further analysis. The observation period GCM results for each climate scenario were used for the 1990-2020 comparison period rather than historic data in the watershed because the climate station in the watershed was only operational since 2018, and there is no nearby long-term climate station or one with very similar measurements to the Basin Head climate station (Figure 1B) during its operation. Therefore, the climate change analysis presented herein should be considered a sensitivity analysis to plausible future projections of climate change when compared to historic-period output for the same downscaled GCMs. A one-way ANOVA was conducted in Minitab (2021) to generate monthly pairwise comparisons of the NO_3-N loading between each period (N = 30) to determine if results were significantly different ($p < 0.0.5$) among scenarios.

Future agricultural practice scenario

It is important to consider societal changes that may arise due to climate change. Climate change will result in extended growing seasons in Atlantic Canada, defined by the number of days per year where the air temperature is over 5°C, with a projected increase in growing season length of 11% by 2050 and 18% by 2080 (Richards and Daigle, 2011) using climate data from the nearest station to Basin Head (East Baltic, 46.43N 62.17W). In SWAT+, these percentages were rounded to a 10% increase in growing season length for the mid-century period (2040–2070) and a 20% increase for the end of century period (2070–2100). To account for a longer growing season and potential loss in plant productivity, an additional percentage of fertilizer applied to crops was also incorporated. Arbitrarily, an increase in fertilizer application of 10% and 20% were applied for mid-century and end of century periods, respectively, to align with the projected increase in growing season length (Richards and Daigle, 2011). This future agricultural scenario was only run for the MRI-ESM2-0 SSP5-8.5 GCM to consider changing agricultural practices for a more extreme climate scenario. All model runs are listed in Supplementary Table S6 with corresponding weather inputs.

Best management practices

BMPs are implemented widely across PEI and include crop rotations, buffer strips, cover crops, farmable berms, and terraces. Three common BMPs were modeled in SWAT+ from 1990 to 2100 under the climate change scenario with the highest cumulative precipitation (MRI-ESM2-0 SSP5-8.5) to understand how NO_3-N loading could be mitigated in a 'worst-case' climate scenario. The BMP scenarios chosen to be simulated in SWAT+ were (1) buffer strips (60 m, 30 m), (2) delayed tillage of forage crop from fall to spring, and (3) alternative crop rotation of Potato-Soybean-Barley (PSB) from the default PBC rotation used for other SWAT+ runs.

Buffer strips refer to narrow strips of dense grass surrounding waterways on agricultural land (Helmers et al., 2006). They are known to slow down runoff velocity to control field erosion and trap particulate pollutants and have been shown to facilitate NO_3-N removal from shallow groundwater (Simpkins et al., 2002). A spatial analysis revealed that most agricultural fields in the watershed have a grassed buffer of 30 m between the field and waterways, which is double the provincially mandated width of 15 m. A scenario incorporating a 60 m buffer was simulated, which would be considered an extreme measure. The removal of NO_3-N in vegetative filter strips in SWAT+ is predicted based on the ratio between field area and filter strip area. It should be noted that the decrease in cropland associated with an increase in buffer size was not included in this simulation to isolate the effect of the buffer, thus, the total effect of an increased buffer width would be underestimated in these results.

Typically, on PEI, a forage crop (i.e., clover, timothy, rye) is grown in the year prior to potato planting. By delaying tillage of forage from fall to spring, just before planting, NO_3-N leaching in the winter months is reduced, and there is residual NO_3-N left in the

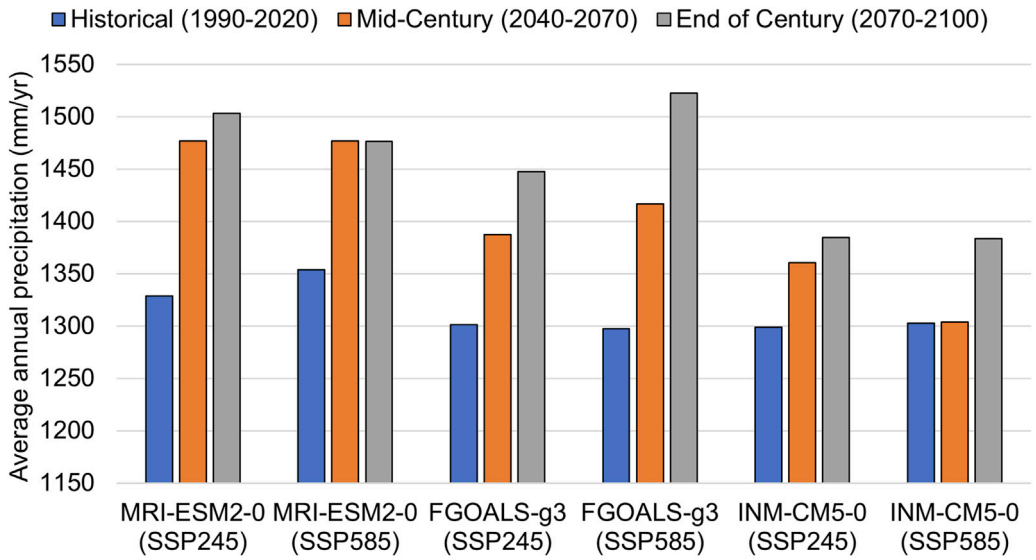


FIGURE 2
Representative climate models chosen based on average annual precipitation values for each modeled period. Distributions of the mean annual precipitation and air temperature for each scenario are presented in Supplementary Figures S8, S9.

soil in spring, reducing the need for fertilizer (Stuart, 2017). This effect was modeled in SWAT+ by editing the agricultural operations such that clover was plowed May 15th, prior to planting of potatoes, instead of on September 15th and by reducing fertilizer application by 25% (Stuart, 2017).

PBC is a representative crop rotation for PEI; however, recent studies have suggested that incorporating legumes may improve soil health, increase potato yields and reduce NO_3-N surplus leading to leaching due to the N fixing characteristics of legumes (Liang et al., 2019; Whittaker et al., 2023). A PSB crop rotation was modeled in SWAT+ (Supplementary Table S7) to test this hypothesis under the three periods, for which fertilizer application was reduced by 50% to account for the N fixing characteristics of soybeans. This reduction amount was chosen arbitrarily based on the results of Liang et al. (2019) that showed N efficiency (i.e., how well plants utilize available N) of PSB crop rotations were 1.6 times that of PBC rotations.

Results and discussion

Sampling results and model calibration

73 water samples from the Basin Head tributaries were analyzed for NO_3-N, of which 24 (33%) exceeded the Canadian Council of Ministers of the Environment (CCME) guideline for the protection of aquatic life in freshwater (3 mg L^{-1}, CCME, 2012). NO_3-N concentrations range from 0 to 6.2 mg/L, with tributary 1 having the highest average concentration (4.2 mg/L) compared to the other tributaries (1.3–1.9 mg/L). TSS concentrations ranged from 0 to 44.0 mg/L, with tributary 2 and 3 being higher on average (11.3–12.3 mg/L) than tributary 1 and 2 (6.1–7.2 mg/L). All grab sample measurements are summarized in Supplementary Table S3.

All sensitive model parameters for hydrology (Supplementary Table S8) were manually calibrated to the measured streamflow (Supplementary Figure S5) until the goodness of fit was satisfactory from April 1st to 1 September 2022, to represent hydrology in the growing season (Table 2). It should be noted that model results from winter months are not calibrated, thus one must take caution when drawing conclusions during these months. Also, snowmelt_min, snowmelt_max, and snowmelt_tmp are climate-related parameters, and would most likely be spatially uniform for a small watershed; they were manually changed to improve streamflow calibration. The sensitivity analysis revealed that simulated NO_3-N concentrations were sensitive to only six out of eight parameters: hlife_n, the half-life of nitrate in the shallow aquifer, nperco, the nitrate percolation coefficient, sdnco, the denitrification threshold water content, cdn, denitrification exponential rate coefficient, cmn, the rate factor for humus mineralization of active organic nutrients and n_updis, the nitrogen uptake distribution parameter. NO_3-N and TSS were calibrated from 11 November 2021, to 5 July 2023, and from 27 July 2022, to 5 July 2023, respectively. The graphical representation of NO_3-N calibration and RMSE (Equation 4) values between measured to simulated concentration are found in Supplementary Figure S6. Six parameters were calibrated for NO_3-N: hlife_n (600 for tributary 1, 200 for tributaries 2–4), nperco (0.15 for tributaries 1-3, 0.05 for tributary 4), sdnco (0.66), cdn (0.07), cmn (0.0029) and n_updis (66.7). RMSE (Equation 4) between measured NO_3-N load (i.e., concentration multiplied by flow) and simulated load were calculated to be 2.7, 7.6, 4.5 and 1.0 kg/day for tributaries 1 through 4.

The sediment calibration process in this study closely followed a previous SWAT study (Sinclair, 2014) by choosing sensitive starting parameters for calibration with a focus on in-channel processes. SWAT+ uses the Modified Universal Soil Loss Equation (MUSLE) to generate the landscape erosion contribution to channel TSS values. MULSE is a function of several factors, which were entered into SWAT+ as default values, except for the soil erodibility factor, which was calculated to be 0.49 based on soil

TABLE 2 Manually calibrated goodness of fit parameters for streamflow, NO_3-N and TSS for each tributary (trib, Figure 1B) for the calibration period April 1st to 1 September 2022.

	Goodness of fit parameter	Tributary 1	Tributary 2	Tributary 3	Tributary 4
Streamflow	NSE (Equation 1)	0.6	0.8	0.8	0.8
	RSR (Equation 2)	0.7	0.5	0.5	0.5
	PBIAS (Equation 3)	2.5	0.04	−20	−14
NO_3-N	RMSE (mg/L) (Equation 4)	2.1	1.1	1.3	1.3
TSS	RMSE (mg/L) (Equation 4)	9	19	21	15

information. High sediment loads in several PEI rivers have been documented, mainly citing sediment deposition resulting from intensive agricultural practices (Sirabahenda et al., 2020). Supplementary Figure S7 presents a graphical representation of TSS calibration and RMSE values between measured and simulated concentrations. Four parameters were calibrated for TSS: spexp (1), spcon (0.0001), cov fact (0.02 for tributaries 2 and 3, 0.005 for tributaries 1 and 4), and erod_fact (0.25 for tributaries 1 and 4, 0.75 for tributary 2 and 0.5 for tributary 3). RMSE between measured TSS load (i.e., concentration multiplied by flow) and simulated load were calculated to be 6.7, 34.7, 36.5, and 1.1 kg/day for tributaries 1 through 4. Final calibrated RSME values for NO_3-N, TSS, and streamflow for each tributary are found in Table 2. NO_3-N was successfully calibrated; however, RMSE values for TSS are significantly higher than 1–2 mg/L, indicating that it is only preliminarily calibrated for sediment transport.

Modelled conditions using MRI-ESM2-0 SSP5-8.5 from the historical period (1990–2020) generally aligned with expected water balance for PEI where an annual average of 1,100 mm of precipitation is partitioned into 440 mm evapotranspiration, 260 mm surface water runoff and 400 mm is groundwater flow (PEI Department of Fisheries and Environment, 1996). During this period SWAT+ simulates the average annual NO_3-N transported via surface runoff as 1 kg/ha, while average annual NO_3-N transported through groundwater is 6 kg/ha, which aligns with other PEI studies such as Grizard. (2013) that simulated an average NO_3-N load of 12 kg-N/ha watershed/yr for the period 1996-2012. Average annual sediment load via overland erosion was modelled to be 0.96 t/ha/yr, which aligns with a nearby previous study in Souris River, PEI that found overland erosion to occur at a rate of 1.5–1.8 t/ha/yr, attributing this high sediment load to row crop agriculture which is common across PEI (Alberto et al., 2016). SWAT+ models deposition of sediment in all tributaries in the watershed, meaning that all TSS at the channel outlets are originated from overland erosion.

Projected climate change impacts

Changes to moisture conditions and seasonality of precipitation events due to climate change could result in changes to the ratio of baseflow and surface runoff contributions in streamflow. The monthly averaged BFI was analyzed for each period in SWAT+, revealing shifts in the partitioning of streamflow over time (Figure 4B). Average BFI in the months of January to May increased from 0.39 in the historical (1990–2020) period to 0.74 and 0.78 in the mid-century (2020–2070) and end-of-century (2070–2100) periods. The largest BFI change occurred in February where monthly average BFI increased from 0.12 in the historical period to 0.63 and 0.68 in the two future periods (>five-fold increase). Average annual simulated BFI increased 22% from historical (1990–2020) to mid-century (2040–2070) periods, and only increased 1% between mid-century and end of century (2070–2100) periods. These baseflow changes could be attributed to increased precipitation as rainfall, more mid-winter thaws, and an earlier spring melt period, inducing recharge and subsequent flow through the shallow aquifer during the winter season.

The SWAT+ model projections also show suppressed summer flow, particularly in April and May, and increased winter flow between historical (1990–2020) and both future periods (2040-2070 and 2070–2100) and illustrate that projected changes in nitrate loading and streamflow follow similar seasonal patterns (Figures 4A, C). During the historical period in the months of January and February, the standard deviation in flow is much lower than the end-of-century period (average decrease of 74%). However, in the months of April to May, the standard deviations of the flow values in the end-of-century period are much lower than in the historical period (−72% on average). This indicates that in the winter months (January and February), there is more variance in flow in the end-of-century period, while in the spring months (April and May) there is more variance during the historical period. Standard deviations of flow between historical and both future periods were within 50% of each other from June to November and were highest from December to May. Increased flow variability in winter and early spring could reflect uncertainty in the effects of climate change on snowmelt processes. The historical period T50 (March 19), a measure of streamflow timing, was shifted earlier by 73 and 78 days respectively for the mid-century (January 7) and end of century (January 1) periods. Some studies (Mukundan et al., 2020; Shrestha et al., 2012) have proposed that earlier snowpack melt and an increase to annual rainfall due to climate change, both of which were modeled in this study, will increase the magnitude and shift the timing of nutrient loading. Average annual streamflow is simulated to increase 5% between historical (1990–2020) and mid-century (2040–2070) periods, and increase 4% between mid-century and end of century (2070–2100) periods. This could be attributed to increased precipitation expected in a future climate, or increased snowmelt due to higher temperatures. Higher streamflows with on average higher baseflow influence in future years (2040–2100) could result in a higher flux of NO_3-N to coastal waters.

Based on the SWAT+ simulations of future climate change impacts and the corresponding ANOVA analysis, only the

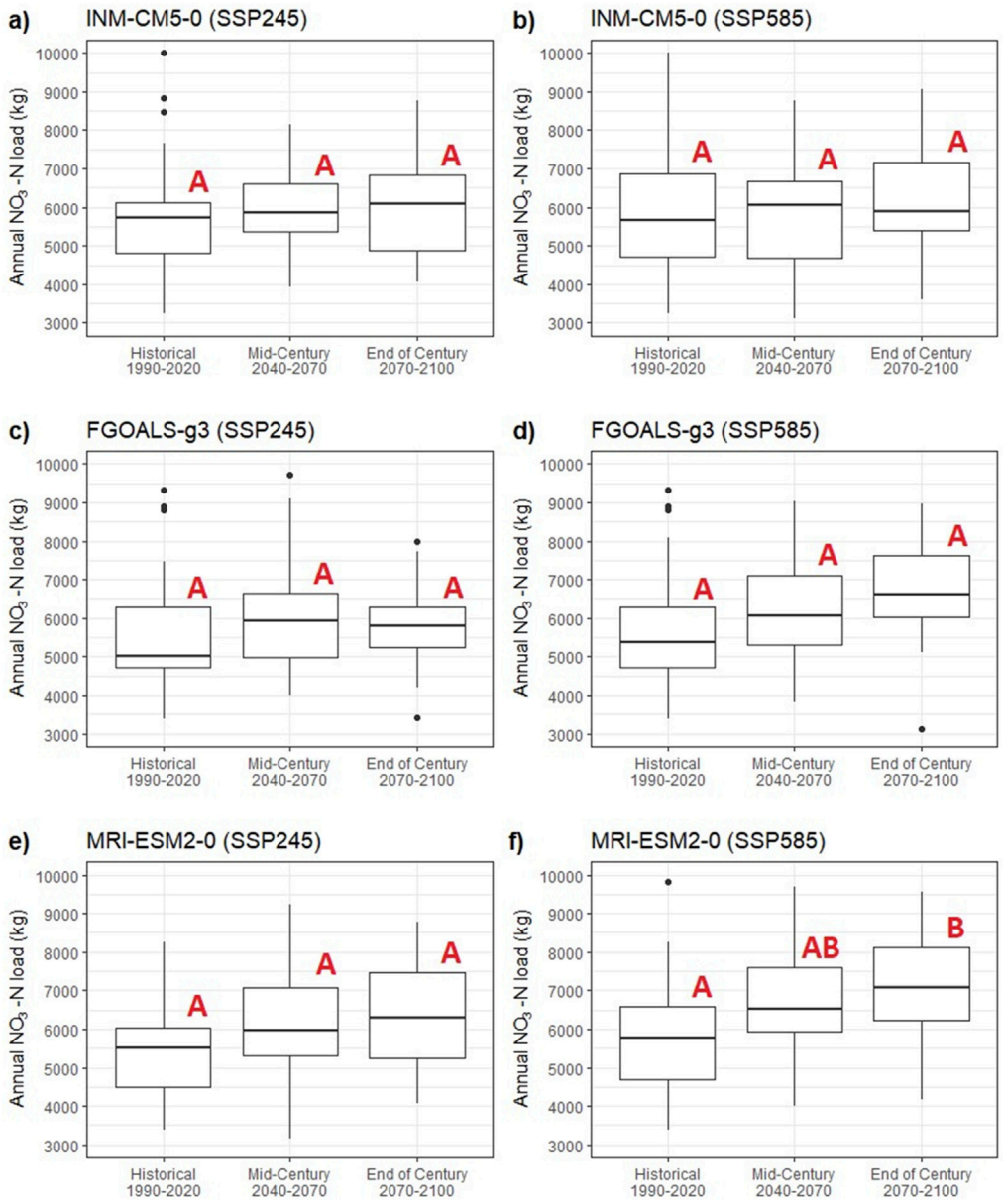


FIGURE 3
Annual NO_3-N load (box and whisker plots showing mean and quartiles) to lagoon from the four main tributaries (Figure 1B) for each climate model scenario (Figure 2), **(A)** INM-CM5-0 SSP2-4.5, **(B)** INM-CM5-0 SSP5-8.5, **(C)** FGOALS-g3 SSP2-4.5, **(D)** FGOALS-g3 SSP5-8.5, **(E)** MRI-ESM2-0 SSP2-4.5, **(F)** MRI-ESM2-0 SSP5-8.5. Distributions that do not share a letter are significantly statistically different.

scenario with the highest cumulative precipitation (MRI-ESM2-0 SSP5-8.5) resulted in statistically significant ($p < 0.05$) changes in NO_3-N loading to the lagoon, and only when comparing historical to end-of-century (1990-2020 to 2070–2100) time periods (Figure 3). Under this scenario, the median annual NO_3-N load increased from 5,752 to 7,239 kg (+26%). Among all climate scenarios considered, this scenario produced both the highest mean annual precipitation and the highest mean annual air temperature at the end of century (Supplementary Figures S8, S9).

The GCM scenarios with the lowest cumulative precipitation (INM-CM5-0 SSP2-4.5 and INM-CM5-0 SSP5-8.5) saw small changes in median NO_3-N load of less than 7% between consecutive model periods. The mid-range cumulative precipitation GCM scenario, FGOALS-g3 SSP2-4.5, yielded interesting results, as annual median NO_3-N load increased by 13% between historical (1990–2020) and mid-century (2040–2070) periods but decreased by 2% from mid-century (2040–2070) to end of century (2070–2100). The FGOALS-g3 SSP5-8.5 GCM yielded a 5% and 10% increase in annual median NO_3-N load between the same periods. In general, the simulations with higher cumulative precipitation resulted in larger increases in annual NO_3-N load (Figure 2). Between each subsequent modeled period, the MRI-ESM2-0 SSP2-4.5 GCM resulted in a 9% and 6% increase to median annual NO_3-N load, while MRI-ESM2-0 SSP5-8.5 resulted in an increase of 13% and 11%, respectively.

These NO_3-N load trends generally correspond to trends in cumulative precipitation (Figure 2) and suggest that the projected

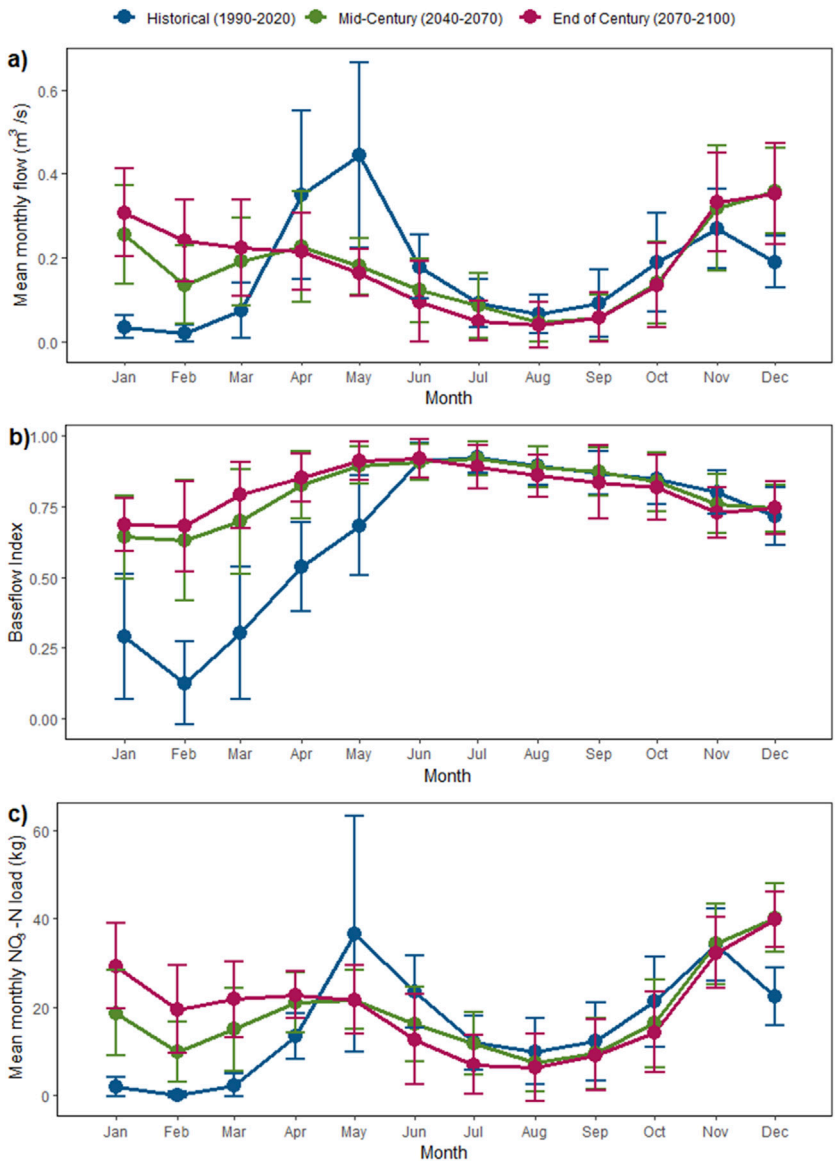


FIGURE 4
(A) Average monthly flow from all four tributaries for each 30-year period simulated in SWAT+, **(B)** Monthly average baseflow index at all four tributaries for each 30-year period simulated in SWAT+, **(C)** NO_3-N load (kg/day) averaged on monthly basis from all four tributaries for each 30-year period simulated in SWAT+. Error bars represent standard deviation of average annual values in each simulated period. The GCM plotted is the highest cumulative precipitation climate scenario MRI-ESM2-0 SSP5-8.5.

increased NO_3-N loading could be attributed to increased water yield and/or enhanced biogeochemical cycling of N (e.g., greater mineralization of organic N and nitrification of ammonia-N) (Pesce et al., 2018; Rabalais et al., 2009). The similarity in pattern of seasonal streamflow and NO_3-N (Figures 4A, C) indicates that increased water yield, rather than elevated concentration, is predominantly responsible for the projected increase in NO_3-N loading.

The effects of NO_3-N leaching through surface and groundwater pathways under future climate change scenarios is presently not well understood. However, it is known that climate change impacts groundwater recharge and discharge (Kurylyk et al., 2014), sea levels, soil conditions (i.e., soil moisture, organic carbon, alkalinity) and agricultural productivity (Stuart et al., 2011), all of which could impact nutrient loading and transport dynamics in coastal watersheds. Some studies investigating the effects of climate change on nutrient loading highlight the uncertainty of climate change models on a regional scale (Bürger et al., 2013; El-Khoury et al., 2015; Jeppesen et al., 2011). These have suggested that the use of different downscaling methods for GCMs can result in conflicting trends in directions and magnitudes of nutrient loading, which is likely partly related to the uncertainty in future trend directions and magnitudes for precipitation and groundwater recharge (Kurylyk and MacQuarrie, 2013). A few studies (e.g., Luo et al., 2020; Qi et al., 2009; Tong and Liu, 2006) have suggested that changes to hydrology have more influence on nutrient loading dynamics than changes in land use, while a local PEI study (De Jong et al., 2008) suggests land use is the more important factor. Pulido-Velazquez et al. (2015)

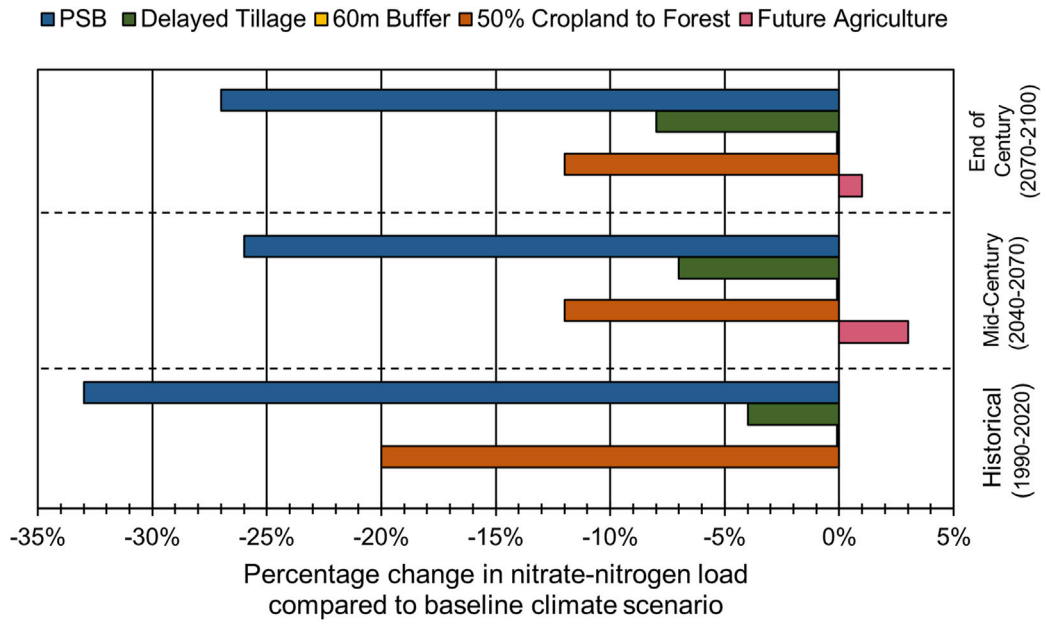


FIGURE 5
Percentage of NO_3-N load compared to baseline climate change scenario from all four modeled tributaries to the lagoon using a future agricultural scenario, altered land-use scenario where 50% of cropland is changed to forest, and BMPs (60 m Buffers, delayed tillage of cover crop from fall to spring, alternative crop rotation of Potato-Soybean-Barley, PSB). The GCM plotted is the highest cumulative precipitation climate scenario MRI-ESM2-0 SSP5-8.5.

noted the importance of analyzing the impacts of land use and hydrologic stressors together when considering nutrient loading patterns. The use of SWAT+ in this study addresses many of these concerns by incorporating future climate data and current land use and agricultural practices, with capability to simulate a wide range of future outcomes.

Seasonal trends in NO_3-N loading to the lagoon were also analyzed under the highest cumulative precipitation climate scenario, MRI-ESM2-0 SSP5-8.5 (Figure 4C). Simulations during the historical period (1990–2020) indicate that NO_3-N loading to the lagoon is highest during the months of May and November. These peaks likely correspond to NO_3-N availability due to recent fertilizer application in spring or harvest in fall and corresponding large precipitation events and snowmelt that typically occur in spring and fall in PEI. For the future climate scenarios, the overall average NO_3-N load increases, but the magnitudes of the May and November loads are damped. The increase in NO_3-N load in spring appears to occur earlier in the season, while the fall peak occurs later into December. The December peak is higher than the fall peak in the future scenarios; however, these are reversed in the historical period.

Impacts of best management practices

Agricultural practices were altered to represent conditions in a future climate by extending the growing season and increasing fertilizer application amounts by 10% and 20% for the mid-century and end-of-century periods respectfully. Model outputs indicated only small increases in NO_3-N load to the lagoon as a result of these changes. For the mid-century period, NO_3-N load was increased by 3%, and for the end of century period, it was increased 1% from the original climate change simulation. An additional scenario was simulated where 50% of crop land was converted to coniferous forest (Supplementary Table S9). Even with this drastic change in land use, NO_3-N load was only reduced by 20% in the historical period and by 12% for 2040 to 2100 when compared to the baseline climate change scenario (Figure 5). There results partially reflect the challenges in managing the 'legacy' effects of nitrate as aquifers can continue to pollute surface waters long after land-use practices change at the land surface (Tesoriero et al., 2013).

Model simulations incorporating BMPs revealed a small change (0%–8%) in NO_3-N loading when a 60 m buffer and delayed tillage were applied as conservation tools (Figure 5). Some studies in other watersheds have shown more pronounced benefits from the tested BMPs. For example, studies have identified grassed buffer strips as effective tools for reducing N export in surface runoff (Dunn et al., 2011; Heathwaite et al., 1998). Mankin et al. (2007) noted a strong reduction in total N concentration in field runoff and observed that infiltration accounted for >90% of total N removal. It is expected that grassed buffers have more impact on sediment, phosphorus, and pesticide transport where the main mode of transport is through surface runoff and soil erosion (Al-Wadaey et al., 2012; Sweeney and Newbold, 2014) rather than the groundwater-dominated transport in the Basin Head watershed. NO_3-N is soluble and once infiltrated into groundwater is generally unable to be reduced using BMPs that target surface water and soil erosion.

The SWAT+ model findings for Basin Head differ from results for other PEI studies. For example, delayed tillage of forage crops from fall to spring under a 3-year potato rotation on PEI has been shown to reduce N availability in soil and related leaching into the subsurface (Stuart, 2017), without negative effects on soil health or

potato yield (Carter et al., 1998). This practice aims to reduce mineralization of forage crops through the winter months to allow for more N carry-over into the growing season. However, in the modeled scenario, this practice should be paired with a reduction in fertilizer application to impact NO_3-N leaching. Sanderson et al. (1999) found that spring tillage improved potato tuber yields even at lower fertilization rates than late fall tillage. Model results did not indicate that this practice would significantly reduce NO_3-N loading over future decades, likely due to the large input of fertilizer still needed to cultivate potatoes and poor N utilization efficiency of the crop. The only appreciable reduction to NO_3-N loading in SWAT+ came from changing the crop rotation to PSB from PBC. Under the historical period, NO_3-N load is reduced by approximately 33% with this BMP; however, during the mid-century and end of century periods, this reduction is lowered to 26% and 27%, respectively (Figure 5). This indicates that crop rotation change for this watershed may yield reduced benefits as climate change intensifies. A future climate may experience competing phenomena where precipitation and hence hydrologic loads increase, yet high temperatures and low soil moisture decrease nutrient loading. These results are consistent with Liang et al. (2019) which found N surplus in soils to be significantly higher under a PBC rotation than a PSB rotation, hence leading to higher levels of N leaching. The N fixing properties of legumes in the PSB scenario allowed for a significant reduction in fertilizer application (50%), which is likely the cause of the reduction in NO_3-N leaching. It should be noted that this is a simplistic approach that does not consider exact N fixing characteristics of crop rotations at the site, and no *in situ* soil data was used to confirm the application rates.

Model limitations

A main limitation of the model results are that the findings cannot be generalized to watersheds outside the province of PEI due to the unique soil, crop and aquifer characteristics. Also, the climate change projections (GCMs) used were chosen solely based on cumulative precipitation, representing low, mid-range and high cumulative precipitation, thus, may not represent the full range of potential future conditions. Another limitation that should be noted is that the surface water watershed modeled map not necessarily align with the watershed of the aquifer. This is an assumption that is commonly employed in such studies (Fan, 2019). Based on validation efforts using additional streamflow records, high uncertainty exists in all modelled values currently produced. This model with a relatively short calibration period is used to simulate long-term climate impact, which enhances measurement uncertainty which affects the model confidence. Based on these limitations, such a model should primarily be used for exploratory purposes (Harmel et al., 2014), as in the present study. Streamflow rating curves may not account for high flow conditions properly due to most *in situ* measurements being collected at low flow (Supplementary Figure S4). Thus, extreme weather events cannot be accurately simulated. This introduces uncertainty in NO_3-N and TSS calibration, which uses streamflow to convert from load to concentration (Supplementary Figures S6, S7). Future work to reduce model uncertainty should include the collection of more flow with a higher range of hydrologic conditions, NO_3-N, and TSS data and watershed properties for model calibration and validation. Furthermore, it should also be emphasized that there is uncertainty in the prediction of NO_3-N transport because of the unknown secondary effects of climate change such as land use change, and changes to agricultural practices (i.e., fertilization rates and timing, growing season) (Howden et al., 2007; Jeppesen et al., 2011). For this reason, future studies are warranted that consider a broader range of future agricultural scenarios and seasonal shifts in hydrologic forcing.

Conclusion

This study evaluated the impacts of climate change and best management practice scenarios on NO_3-N loading to a threatened coastal lagoon in the Atlantic Canadian province of PEI. Model (SWAT+) results indicate that NO_3-N loading is expected to increase under climate change, further exacerbating eutrophic conditions and the related impacts on the protected ecosystem in this lagoon. However, only the highest cumulative precipitation climate model (MRI-ESM2-0 SSP5-8.5) resulted in statistically different (p-value <0.05) NO_3-N loading (+26%) between historical (1990–2020) and end-of-century (2070–2100) periods. Implementing buffer strips and delayed tillage had negligible (0%–8% reduction) effects on NO_3-N loading, while changing the crop rotation from potato-barley-clover to potato-soybean-barley yielded a decline (26%–33%) in NO_3-N loading compared to a climate change scenario without incorporation of best management practices. A future agricultural practice scenario was evaluated for mid-century (2040–2070) and end of century (2070–2100) to consider a longer growing season and higher fertilizer application amount. Simulated NO_3-N loading to the lagoon only increased by 3% and 1% respectively for these future time periods under this additional loading. To explore an extreme scenario where drastic measures were incorporated to limit agricultural contamination, a model scenario was run where 50% of cropland was converted to coniferous forest. This resulted in a reduction in NO_3-N loading of 12%–20%. Model analysis revealed changes to seasonal loading dynamics under climate change for which the effect of high spring and fall precipitation effects were subdued, and streamflow and related NO_3-N loads remained more seasonally consistent. Changes to streamflow partitioning were noted under climate change scenarios. Most notably, baseflow contributions increased in winter and early spring (January-May), with the largest change (5-fold increase) occurring in February. These results demonstrate the severity of nitrogen contamination within PEI aquifers and water bodies and the trajectory of NO_3-N loading to the province's coastal waters in a future climate. Although PEI remains a national leader in the implementation of best management practices and agricultural innovation, decades of agricultural activity and aquifer storage of NO_3-N will facilitate continual groundwater export of leached legacy nitrate to the coast. Extreme changes to land use and reduction to fertilizer application would be needed to appreciably reduce NO_3-N loading to the Basin Head watersheds and other PEI watersheds. Conservation tools such as crop rotation will likely become increasingly important to ensure agricultural practices remain resilient to the effects of climate change.

Data availability statement

The raw data supporting the conclusions of this article will be made available by the authors, without undue reservation.

Author contributions

AO: Conceptualization, Data curation, Formal Analysis, Investigation, Methodology, Validation, Visualization, Writing–original draft. BK: Conceptualization, Funding acquisition, Methodology, Project administration, Resources, Supervision, Writing–review and editing, Investigation. LJ: Investigation, Methodology, Writing–review and editing, Data curation. NL: Data curation, Formal Analysis, Methodology, Writing–review and editing. LS: Conceptualization, Methodology, Writing–review and editing. RJ: Conceptualization, Funding acquisition, Methodology, Project administration, Resources, Supervision, Writing–review and editing.

Funding

The author(s) declare that financial support was received for the research, authorship, and/or publication of this article. Research funding was provided by Environment and Climate Change Canada (Atlantic Ecosystems Initiatives Program, GCXE22P028), Fisheries and Oceans Canada (DFO Ocean Management Contribution Program), and the Canada Research Chairs Program.

Acknowledgments

We thank NL, LJ, and members of the Dalhousie University Centre for Water Resources Studies for field and modeling support, and Bailey Strong (Dalhousie University) for help with batch downloading and filtering the downscaled climate scenarios.

Conflict of interest

The authors declare that the research was conducted in the absence of any commercial or financial relationships that could be construed as a potential conflict of interest.

Publisher's note

All claims expressed in this article are solely those of the authors and do not necessarily represent those of their affiliated organizations, or those of the publisher, the editors and the reviewers. Any product that may be evaluated in this article, or claim that may be made by its manufacturer, is not guaranteed or endorsed by the publisher.

Supplementary material

The Supplementary Material for this article can be found online at: https://www.frontiersin.org/articles/10.3389/fenvs.2024.1468869/full#supplementary-material

References

Afzaal, H., Farooque, A. A., Abbas, F., Acharya, B., and Esau, T. (2020). Precision irrigation strategies for sustainable water budgeting of potato crop in Prince Edward Island. *Sustainability* 12 (6), 2419. doi:10.3390/su12062419

AghaKouchak, A., Chiang, F., Huning, L. S., Love, C. A., Mallakpour, I., Mazdiyasni, O., et al. (2020). Climate extremes and compound hazards in a warming world. *Annu. Rev. Earth Planet. Sci.* 48, 519–548. doi:10.1146/annurev-earth-071719-055228

Agriculture and Agri-food Canada (AAFC) (2020). Climate change impacts on agriculture. Available at: https://agriculture.canada.ca/en/environment/climate-change/climate-scenarios-agriculture#d.

Agriculture and Agri-food Canada (AAFC) (2021). Annual crop inventory (ACI). Available at: https://open.canada.ca/data/en/dataset/199e4ab6-832b-4434-ac39-e4887d7cc4e5.

Agri-food Canada (AAFC) (2022). *The national soil database*. Available at: https://sis.agr.gc.ca/cansis/nsdb/index.html.

Ahmad, H. M., Sinclair, A., Jamieson, R., Madani, A., Hebb, D., Havard, P., et al. (2011). Modeling sediment and nitrogen export from a rural watershed in Eastern Canada using the soil and water assessment tool. *J. Environ. Qual.* 40 (4), 1182–1194. doi:10.2134/jeq2010.0530

Alberto, A., St-Hilaire, A., Courtenay, S. C., and Van Den Heuvel, M. R. (2016). Monitoring stream sediment loads in response to agriculture in Prince Edward Island, Canada. *Environ. Monit. Assess.* 188, 415–15. doi:10.1007/s10661-016-5411-3

Al-Wadaey, A., Wortmann, C. S., Franti, T. G., Shapiro, C. A., and Eisenhauer, D. E. (2012). Effectiveness of grass filters in reducing phosphorus and sediment runoff. *Water, Air, & Soil Pollut.* 223, 5865–5875. doi:10.1007/s11270-012-1322-2

American Public Health Association (APHA) (2022). *Standard methods for examination of water and wastewater*. 23rd edition. Washington, DC: American Public Health Association, American Water Works Association, Water Environment Federation.

Arhonditsis, G., Tsirtsis, G., Angelidis, M. O., and Karydis, M. (2000). Quantification of the effects of nonpoint nutrient sources to coastal marine eutrophication: applications to a semi-enclosed gulf in the Mediterranean Sea. *Ecol. Model.* 129 (2-3), 209–227. doi:10.1016/S0304-3800(00)00239-8

Arnold, J. G., Moriasi, D. N., Gassman, P. W., Abbaspour, K. C., White, M. J., Srinivasan, R., et al. (2012). SWAT: model use, calibration, and validation. *Trans. ASABE* 55 (4), 1491–1508. doi:10.13031/2013.42256

Azimi, M. A., Jiang, Y., Meng, F. R., and Liang, K. (2022). Yield responses of four common potato cultivars to an industry standard and alternative rotation in Atlantic Canada. *Am. J. Potato Res.* 99 (3), 206–216. doi:10.1007/s12230-022-09873-4

Bailey, R. T., Bieger, K., Arnold, J. G., and Bosch, D. D. (2020). A new physically-based spatially-distributed groundwater flow module for SWAT+. *Hydrology* 7 (4), 75. doi:10.3390/hydrology7040075

Bennett, E. M., Baird, J., Baulch, H., Chaplin-Kramer, R., Fraser, E., Loring, P., et al. (2021). Ecosystem services and the resilience of agricultural landscapes. *Adv. Ecol. Res.* 64, 1–43. doi:10.1016/bs.aecr.2021.01.001

Benson, V. S., VanLeeuwen, J. A., Stryhn, H., and Somers, G. H. (2007). Temporal analysis of groundwater nitrate concentrations from wells in Prince Edward Island, Canada: application of a linear mixed effects model. *Hydrogeology J.* 15 (5), 1009–1019. doi:10.1007/s10040-006-0153-x

Bhatti, A. Z., Farooque, A. A., Krouglicof, N., Peters, W., Li, Q., and Acharya, B. (2022). Climate change impacts on rainfed agriculture and mitigation strategies for sustainable agricultural management: a case study of Prince Edward Island, Canada. *World Water Policy* 8 (2), 142–179. doi:10.1002/wwp2.12083

Boesch, D. F., and Brinsfield, R. B. (2000). Coastal eutrophication and agriculture: contributions and solutions. *Biol. Resour. Manag. Connecting Sci. Policy*, 93–115. doi:10.1007/978-3-662-04033-1_8

Bonnington, A. C., Jamieson, R. C., Smith, K. A., Oliver, A., Johnston, L. H., LeRoux, N. K., et al. (2023). Impacts of Extratropical Cyclone Fiona on a sensitive coastal lagoon ecosystem. *Limnol. Oceanogr.* 68 (12), 2703–2715. doi:10.1002/lno.12452

Bosch, D. D., Arnold, J. G., Volk, M., and Allen, P. M. (2010). Simulation of a low-gradient coastal plain watershed using the SWAT landscape model. *Trans. ASABE* 53 (5), 1445–1456. doi:10.13031/2013.34899

Bugden, G., Jiang, Y., van den Heuvel, M. R., Vandermeulen, H., MacQuarrie, K. T. B., Crane, C. J., et al. (2014) "Nitrogen loading criteria for estuaries in Prince edward island," in *Fisheries and Oceans Canada*, 3066. Ottawa, ON: Fisheries and Oceans Canada: Canadian Technical Report of Fisheries and Aquatic Sciences.

Bürger, G., Sobie, S. R., Cannon, A. J., Werner, A. T., and Murdock, T. Q. (2013). Downscaling extremes: an intercomparison of multiple methods for future climate. *J. Clim.* 26 (10), 3429–3449. doi:10.1175/JCLI-D-12-00249.1

Canadian Council of Ministers of the Environment (CCME) (2012). "Canadian water quality guidelines: nitrate ion," in *Scientific criteria document*. Winnipeg: Canadian Council of Ministers of the Environment.

Cannon, A. J. (2015). Selecting GCM scenarios that span the range of changes in a multimodel ensemble: application to CMIP5 climate extremes indices. *J. Clim.* 28 (3), 1260–1267. doi:10.1175/JCLI-D-14-00636.1

Carter, M. R. (1987). Physical properties of some Prince Edward Island soils in relation to their tillage requirement and suitability for direct drilling. *Can. J. Soil Sci.* 67 (3), 473–487. doi:10.4141/cjss87-045

Carter, M. R., Sanderson, J. B., and MacLeod, J. A. (1998). Influence of time of tillage on soil physical attributes in potato rotations in Prince Edward Island. *Soil Tillage Res.* 49 (1-2), 127–137. doi:10.1016/S0167-1987(98)00167-6

Chu, T. W., Shirmohammadi, A., Montas, H., and Sadeghi, A. (2004). Evaluation of the SWAT model's sediment and nutrient components in the piedmont physiographic region of Maryland. *Trans. ASABE* 47, 1523–1538.

Cloern, J. E. (2001). Our evolving conceptual model of the coastal eutrophication problem. *Mar. Ecol. Prog. Ser.* 210, 223–253. doi:10.3354/meps210223

Coffin, M. R. S., Courtenay, S. C., Knysh, K. M., Pater, C. C., and van den Heuvel, M. R. (2018). Impacts of hypoxia on estuarine macroinvertebrate assemblages across a regional nutrient gradient. *Facets* 3 (1), 23–44. doi:10.1139/facets-2017-0044

Connolly, K. (2002). *Baseline limnology and nutrient study of Basin Head lagoon, Prince edward island, with management implications*. Master's Thesis. Waterloo, ON: Wilfrid Laurier University. Available at: https://scholars.wlu.ca/etd/434/.

Council of Canadian Academies (2009). *The sustainable management of groundwater in Canada*. Ottawa, ON: Expert Panel Groundwater, Report to the Government of Canada.

Court, A. (1962). Measures of streamflow timing. *J. Geophys. Res.* 67 (11), 4335–4339. doi:10.1029/JZ067i011p04335

De Jong, R., Qian, B., and Yang, J. Y. (2008). Modelling nitrogen leaching in Prince Edward Island under climate change scenarios. *Can. J. Soil Sci.* 88 (1), 61–78. doi:10.4141/cjss07032

Delgado, J. A., Riggenbach, R. R., Sparks, R. T., Dillon, M. A., Kawanabe, L. M., and Ristau, R. J. (2001). Evaluation of nitrate-nitrogen transport in a potato–barley rotation. *Soil Sci. Soc. Am. J.* 65 (3), 878–883. doi:10.2136/sssaj2001.653878x

DELJ (2013). *Water extraction permitting policy*. Available at: https://www.princeedwardisland.ca/sites/default/files/publications/water_extraction_permitting_policy_2013.pdf.

De Notaris, C., Rasmussen, J., Sørensen, P., and Olesen, J. E. (2018). Nitrogen leaching: a crop rotation perspective on the effect of N surplus, field management and use of catch crops. *Agric. Ecosyst. & Environ.* 255, 1–11. doi:10.1016/j.agee.2017.12.009

Department of Fisheries and Oceans Canada (DFO) (2009). Ecological assessment of Irish moss (chondrus crispus) in Basin Head marine protected area (gulf region CSAS science advisory report 2008/059), Fisheries and Oceans Canada, moncton, Canada. Available at: https://waves-vagues.dfo-mpo.gc.ca/library-bibliotheque/335723.pdf.

Department of Fisheries and Oceans Canada (DFO) (2021). 2021-2026 Operational management plan Basin Head marine protected area. Available at: https://waves-vagues.dfo-mpo.gc.ca/library-bibliotheque/4104440x.pdf.

Dunn, A. M., Julien, G., Ernst, W. R., Cook, A., Doe, K. G., and Jackman, P. M. (2011). Evaluation of buffer zone effectiveness in mitigating the risks associated with agricultural runoff in Prince Edward Island. *Sci. Total Environ.* 409 (5), 868–882. doi:10.1016/j.scitotenv.2010.11.011

El-Khoury, A., Seidou, O., Lapen, D. R., Que, Z., Mohammadian, M., Sunohara, M., et al. (2015). Combined impacts of future climate and land use changes on discharge, nitrogen and phosphorus loads for a Canadian river basin. *J. Environ. Manag.* 151, 76–86. doi:10.1016/j.jenvman.2014.12.012

Environment and Climate Change Canada (ECCC) (2023). *Historical data, East Point*. Ottawa, ON: Prince Edward Island. [Station ID 7177; December 2022].

Eyring, V., Bony, S., Meehl, G. A., Senior, C. A., Stevens, B., Stouffer, R. J., et al. (2016). Overview of the coupled model intercomparison Project phase 6 (CMIP6) experimental design and organization. *Geosci. Model Dev.* 9 (5), 1937–1958. doi:10.5194/gmd-9-1937-2016

Fan, Y. (2019). Are catchments leaky? Wiley interdisciplinary reviews. *Water* 6 (6), e1386. doi:10.1002/wat2.1386

Fetter, C. W., Boving, T., and Kreamer, D. (2017). *Contaminant hydrogeology, Waveland Press*. Saddle River, NJ: Prentice Hall Press.

Francis, R. M. (1989). *Hydrogeology of the winter river basin, Prince edward island*. Charlottetown, PEI: PEI Department of Environment, PEI. Available at: http://www.gov.pe.ca/photos/original/cle_WinterR.pdf.

Gopalakrishnan, T., Hasan, M. K., Haque, A. S., Jayasinghe, S. L., and Kumar, L. (2019). Sustainability of coastal agriculture under climate change. *Sustainability* 11 (24), 7200. doi:10.3390/su11247200

Gordon, L. J., Peterson, G. D., and Bennett, E. M. (2008). Agricultural modifications of hydrological flows create ecological surprises. *Trends Ecol. & Evol.* 23 (4), 211–219. doi:10.1016/j.tree.2007.11.011

Government of PEI (2002). Agricultural crop rotation Act. Available at: https://www.princeedwardisland.ca/sites/default/files/legislation/a-08-01-agricultural_crop_rotation_act.pdf.

Government of PEI (2016). Watercourse, wetland and buffer zone activity regulations. Available at: https://www.princeedwardisland.ca/sites/default/files/publications/watercourse_wetland_and_buffer_zone_activity_guidelines_dec_2016.pdf.

Government of PEI (2019). *Water well information system [Kingsboro well logs from 1974 to 2012]*.

Government of Prince Edward Island (2020) "The Prince Edward Island potato sector: an economic impact analysis," in *Charlottetown, PE: strategic policy and evaluation division*. Charlottetown, PEI: PEI Department of Agriculture and Land. Available at: https://www.princeedwardisland.ca/sites/default/files/publications/af_potato_econ_impact_study.pdf.

Grizard, P. (2013). *Modeling nitrate loading from watersheds to coastal water of the Northumberland Strait*. Master's Thesis, Fredericton, NB: University of New Brunswick. Available at: https://unbscholar.lib.unb.ca/handle/1882/13636.

Harmel, R. D., Smith, P. K., Migliaccio, K. W., Chaubey, I., Douglas-Mankin, K. R., Benham, B., et al. (2014). Evaluating, interpreting, and communicating performance of hydrologic/water quality models considering intended use: a review and recommendations. *Environ. Model. & Softw.* 57, 40–51. doi:10.1016/j.envsoft.2014.02.013

Heath, R. C. (1983). *Basic ground-water hydrology (water supply paper 2220)*. Reston, VA: U.S. Geological Survey. Available at: https://pubs.er.usgs.gov/djvu/WSP/wsp_2220.pdf.

Heathwaite, A. L., Griffiths, P., and Parkinson, R. J. (1998). Nitrogen and phosphorus in runoff from grassland with buffer strips following application of fertilizers and manures. *Soil Use Manag.* 14 (3), 142–148. doi:10.1111/j.1475-2743.1998.tb00140.x

Helmers, M., Isenhart, T., Dosskey, M., Dabney, S., and Strock, J. (2006). Buffers and vegetative filter strips. Available at: https://www.epa.gov/sites/default/files/2015-07/documents/2006_8_24_msbasin_symposia_ia_session4-2.pdf.

Howarth, R. W. (2008). Coastal nitrogen pollution: a review of sources and trends globally and regionally. *Harmful Algae* 8 (1), 14–20. doi:10.1016/j.hal.2008.08.015

Howden, S. M., Soussana, J. F., Tubiello, F. N., Chhetri, N., Dunlop, M., and Meinke, H. (2007). Adapting agriculture to climate change. *Proc. Natl. Acad. Sci.* 104 (50), 19691–19696. doi:10.1073/pnas.0701890104

James, C. (2022). SWAT+ Toolbox. Available at: https://celray.github.io/docs/swatplus-toolbox/v1.0/index.html.

Jeppesen, E., Kronvang, B., Olesen, J. E., Audet, J., Søndergaard, M., Hoffmann, C. C., et al. (2011). Climate change effects on nitrogen loading from cultivated catchments in Europe: implications for nitrogen retention, ecological state of lakes and adaptation. *Hydrobiologia* 663, 1–21. doi:10.1007/s10750-010-0547-6

Jiang, Y., and Somers, G. (2009). Modeling effects of nitrate from non-point sources on groundwater quality in an agricultural watershed in Prince Edward Island, Canada. *Hydrogeology J.* 17 (3), 707–724. doi:10.1007/s10040-008-0390-2

Jiang, Y., Zebarth, B., and Love, J. (2011). Long-term simulations of nitrate leaching from potato production systems in Prince Edward Island, Canada. *Nutrient Cycl. Agroecosyst.* 91, 307–325. doi:10.1007/s10705-011-9463-z

Johnston, L. H., Dunnington, D. W., Greenwood, M. C., Kurylyk, B. L., and Jamieson, R. C. (2022). Identifying hydrologic regimes and drivers in Nova Scotia, Canada: catchment classification efforts for a data-limited region. *J. Hydrologic Eng.* 27 (11), 05022017. doi:10.1061/(ASCE)HE.1943-5584.0002200

Joostema, P. (2015). Site location plan: saltwater production well development [Well core log and pumping test data]. *Joost Environ.*

KarisAllen, J., and Kurylyk, B. L. (2021). Drone-based characterization of intertidal spring cold-water plume dynamics. *Hydrol. Process.* 35 (6), e14258. doi:10.1002/hyp.14258

KarisAllen, J. J., Mohammed, A. A., Tamborski, J. J., Jamieson, R. C., Danielescu, S., and Kurylyk, B. L. (2022). Present and future thermal regimes of intertidal groundwater springs in a threatened coastal ecosystem. *Hydrology Earth Syst. Sci.* 26 (18), 4721–4740. doi:10.5194/HESS-26-4721-2022

Kurylyk, B. L., and MacQuarrie, K. T. (2013). The uncertainty associated with estimating future groundwater recharge: a summary of recent research and an example from a small unconfined aquifer in a northern humid-continental climate. *J. hydrology* 492, 244–253. doi:10.1016/j.jhydrol.2013.03.043

Kurylyk, B. L., MacQuarrie, K. T., and Voss, C. I. (2014). Climate change impacts on the temperature and magnitude of groundwater discharge from shallow, unconfined aquifers. *Water Resour. Res.* 50 (4), 3253–3274. doi:10.1002/2013WR014588

Lal, R., Delgado, J. A., Groffman, P. M., Millar, N., Dell, C., and Rotz, A. (2011). Management to mitigate and adapt to climate change. *J. Soil Water Conservation* 66 (4), 276–285. doi:10.2489/jswc.66.4.276

Liang, K., Jiang, Y., Nyiraneza, J., Fuller, K., Murnaghan, D., and Meng, F. R. (2019). Nitrogen dynamics and leaching potential under conventional and alternative potato rotations in Atlantic Canada. *Field Crops Res.* 242, 107603. doi:10.1016/j.fcr.2019.107603

Liang, K., Jiang, Y., Qi, J., Fuller, K., Nyiraneza, J., and Meng, F. R. (2020). Characterizing the impacts of land use on nitrate load and water yield in an agricultural watershed in Atlantic Canada. *Sci. Total Environ.* 729, 138793. doi:10.1016/j.scitotenv.2020.138793

Liu, Y., Engel, B. A., Flanagan, D. C., Gitau, M. W., McMillan, S. K., and Chaubey, I. (2017). A review on effectiveness of best management practices in improving hydrology and water quality: needs and opportunities. *Sci. Total Environ.* 601, 580–593. doi:10.1016/j.scitotenv.2017.05.212

Lu, C., and Tian, H. (2017). Global nitrogen and phosphorus fertilizer use for agriculture production in the past half century: shifted hot spots and nutrient imbalance. *Earth Syst. Sci. Data* 9 (1), 181–192. doi:10.5194/essd-9-181-2017

Luo, C., Li, Z., Liu, H., Li, H., Wan, R., Pan, J., et al. (2020). Differences in the responses of flow and nutrient load to isolated and coupled future climate and land use changes. *J. Environ. Manag.* 256, 109918. doi:10.1016/j.jenvman.2019.109918

Luo, Y., Arnold, J., Allen, P., and Chen, X. (2012). Baseflow simulation using SWAT model in an inland river basin in Tianshan Mountains, Northwest China. *Hydrology Earth Syst. Sci.* 16 (4), 1259–1267. doi:10.5194/hess-16-1259-2012

MacDougall, J. I., Veer, C., and Wilson, F. (1988). *Soil of Prince edward island: Prince edward island soil survey*. Ottawa, ON: Agriculture Canada. Available at: https://sis.agr.gc.ca/cansis/publications/surveys/pe/pe83-54/index.html.

Mahato, A. (2014). Climate change and its impact on agriculture. *Int. J. Sci. Res. Publ.* 4 (4), 1–6.

Malone, T. C., and Newton, A. (2020). The globalization of cultural eutrophication in the coastal ocean: causes and consequences. *Front. Mar. Sci.* 7, 670. doi:10.3389/fmars.2020.00670

Mankin, K. R., Ngandu, D. M., Barden, C. J., Hutchinson, S. L., and Geyer, W. A. (2007). Grass shrub riparian buffer removal of sediment, phosphorus, and nitrogen from simulated runoff. *J. Am. Water Resour. Assoc.* 43 (5), 1108–1116. doi:10.1111/j.1752-1688.2007.00090.x

Maurer, E. P., Hidalgo, H. G., Das, T., Dettinger, M. D., and Cayan, D. R. (2010). The utility of daily large-scale climate data in the assessment of climate change impacts on daily streamflow in California. *Hydrology Earth Syst. Sci.* 14 (6), 1125–1138. doi:10.5194/hess-14-1125-2010

Minitab, L. L. C. (2021). Minitab. Available at: https://www.minitab.com.

Moriasi, D. N., Arnold, J. G., Van Liew, M. W., Bingner, R. L., Harmel, R. D., and Veith, T. L. (2007). Model evaluation guidelines for systematic quantification of accuracy in watershed simulations. *Trans. ASABE* 50 (3), 885–900. doi:10.13031/2013.23153

Mukundan, R., Hoang, L., Gelda, R. K., Yeo, M. H., and Owens, E. M. (2020). Climate change impact on nutrient loading in a water supply watershed. *J. Hydrology* 586, 124868. doi:10.1016/j.jhydrol.2020.124868

NASA (2023). Climate data services (CDS). Available at: https://www.nccs.nasa.gov/services/climate-data-services.

Neitsch, S. L., Arnold, J. G., Kiniry, J. R., and Williams, J. R. (2011). *Soil and water assessment tool theoretical documentation version 2009*. College Station, Texas: Texas Water Resources Institute, Texas A&M University. Available at: https://swat.tamu.edu/media/99192/swat2009-theory.pdf.

Nelson, G. C., Rosegrant, M. W., Koo, J., Robertson, R., Sulser, T., Zhu, T., et al. (2009). *Impact on agriculture and costs of adaptation. Food Policy Report*. Washington DC: International Food Policy Research Institute.

Oliver, A. C., Jamieson, R. C., Smith, K. A., Cantelon, J. A., and Kurylyk, B. L. (2024). Intertidal spring dynamics and coastal nutrient loading revealed through geophysics, drone surveys, and *in situ* monitoring. *Hydrol. Process.* 38 (5), e15144. doi:10.1002/hyp.15144

Oppenheimer, M., Glavovic, B. C., Hinkel, J., van de Wal, R., Magnan, A. K., Abd-Elgawad, A., et al. (2019). "Sea level rise and implications for low-lying islands, coasts and communities," in *IPCC special report on the ocean and cryosphere in a changing climate*. Editors H. O. PÖrtner, D. C. Roberts, V. Masson-Delmotte, P. Zhai, M. Tignor, E. Poloczanska, et al. (Cambridge, UK and New York, NY, USA: Cambridge University Press), 321–445. doi:10.1017/9781009157964.006

Paradis, D., Vigneault, H., Lefebvre, R., Savard, M. M., Ballard, J. M., and Qian, B. (2016). Groundwater nitrate concentration evolution under climate change and agricultural adaptation scenarios: Prince Edward Island, Canada. *Earth Syst. Dyn.* 7 (1), 183–202. doi:10.5194/esd-7-183-2016

Pavlovskii, I., Jiang, Y., Danielescu, S., and Kurylyk, B. L. (2023). Influence of precipitation event magnitude on baseflow and coastal nitrate export for Prince Edward Island, Canada. *Hydrol. Process.* 37, e14892. doi:10.1002/hyp.14892

PEI Department of Fisheries and Environment (1996). Water on Prince edward island: understanding the resource, knowing the issues. Available at: https://www.princeedwardisland.ca/sites/default/files/publications/water_on_prince_edward_island_understanding_the_resource_knowing_the_issues.pdf.

Pesce, M., Critto, A., Torresan, S., Giubilato, E., Santini, M., Zirino, A., et al. (2018). Modelling climate change impacts on nutrients and primary production in coastal waters. *Sci. Total Environ.* 628, 919–937. doi:10.1016/j.scitotenv.2018.02.131

Province of PEI (2008). *2 meter contours*. Available at: http://www.gov.pe.ca/gis/index.php3?number=1011267&lang=E#what.1.

Puckett, L. J., Tesoriero, A. J., and Dubrovsky, N. M. (2011). Nitrogen contamination of surficial aquifers-A growing legacy. *Environ. Sci. Technol.* 45 (3), 839–844. doi:10.1021/es1038358

Pulido-Velazquez, M., Peña-Haro, S., García-Prats, A., Mocholi-Almudever, A. F., Henríquez-Dole, L., Macian-Sorribes, H., et al. (2015). Integrated assessment of the impact of climate and land use changes on groundwater quantity and quality in the Mancha Oriental system (Spain). *Hydrology Earth Syst. Sci.* 19 (4), 1677–1693. doi:10.5194/hess-19-1677-2015

Qi, S., Sun, G., Wang, Y., McNulty, S. G., and Myers, J. M. (2009). Streamflow response to climate and landuse changes in a coastal watershed in North Carolina. *Trans. ASABE* 52 (3), 739–749. doi:10.13031/2013.27395

Rabalais, N. N., Turner, R. E., Díaz, R. J., and Justić, D. (2009). Global change and eutrophication of coastal waters. *ICES J. Mar. Sci.* 66 (7), 1528–1537. doi:10.1093/icesjms/fsp047

Rahimpour Asenjan, M., Brissette, F., Martel, J. L., and Arsenault, R. (2023). Understanding the influence of "hot" models in climate impact studies: a hydrological perspective. *Hydrology Earth Syst. Sci.* 27 (23), 4355–4367. doi:10.5194/hess-27-4355-2023

Riahi, K., Van Vuuren, D. P., Kriegler, E., Edmonds, J., O'neill, B. C., Fujimori, S., et al. (2017). The Shared Socioeconomic Pathways and their energy, land use, and greenhouse gas emissions implications: an overview. *Glob. Environ. change* 42, 153–168. doi:10.1016/j.gloenvcha.2016.05.009

Ricci, G. F., Centanni, M., DeGirolamo, A. M., and Gentile, F. (2023). Modelling daily streamflow in a temporary karst river system: comparing three approaches using the SWAT model. *Hydrological Sci. J.* 68 (3), 462–473. doi:10.1080/02626667.2023.2174027

Richards, W., and Daigle, R. (2011) "Scenarios and guidance for adaptation to climate change and sea level rise-NS and PEI municipalities," in *Atlantic climate adaptation solutions association*. Available at: https://www.novascotia.ca/nse/climate-change/docs/ScenariosGuidance_WilliamsDaigle.pdf.

Rivera, A. (2014). *Canada's groundwater Resources*. Markham, ON: Fitzhenry & Whiteside Limited. doi:10.4095/293431

Sanderson, J. B., MacLeod, J. A., and Kimpinski, J. (1999). Glyphosate application and timing of tillage of red clover affects potato response to N, soil N profile, and root and soil nematodes. *Can. J. Soil Sci.* 79 (1), 65–72. doi:10.4141/s98-028

Shrestha, R. R., Dibike, Y. B., and Prowse, T. D. (2012). Modeling climate change impacts on hydrology and nutrient loading in the Upper Assiniboine Catchment. *J. Am. Water Resour. Assoc.* 48 (1), 74–89. doi:10.1111/j.1752-1688.2011.00592.x

Simpkins, W. W., Wineland, T. R., Andress, R. J., Johnston, D. A., Caron, G. C., Isenhart, T. M., et al. (2002). Hydrogeological constraints on riparian buffers for reduction of diffuse pollution: examples from the Bear Creek Watershed in Iowa, USA. *Water Sci. Technol.* 45 (9), 61–68. doi:10.2166/wst.2002.0205

Sinclair, A. C. (2014). *An integrated modeling approach for the evaluation of phosphorus loading in rural Nova Scotia watersheds Doctoral Dissertation*. Halifax, NS: Dalhousie University.

Sinha, E., Michalak, A. M., Calvin, K. V., and Lawrence, P. J. (2019). Societal decisions about climate mitigation will have dramatic impacts on eutrophication in the 21st century. *Nat. Commun.* 10 (1), 939. doi:10.1038/s41467-019-08884-w

Sirabahenda, Z., St-Hilaire, A., Courtenay, S. C., and Van Den Heuvel, M. R. (2020). Assessment of the effective width of riparian buffer strips to reduce suspended sediment in an agricultural landscape using ANFIS and SWAT models. *Catena* 195, 104762. doi:10.1016/j.catena.2020.104762

Spalding, R. F., and Exner, M. E. (1993). Occurrence of nitrate in groundwater—a review. *J. Environ. Qual.* 22 (3), 392–402. doi:10.2134/jeq1993.00472425002200030002x

Spruill, C. A., Workman, S. R., and Taraba, J. L. (2000). Simulation of daily and monthly stream discharge from small watersheds using the SWAT model. *Trans. ASAE* 43 (6), 1431–1439. doi:10.13031/2013.3041

Stanic, S., LeRoux, N. K., Paldor, A., Mohammed, A. A., Michael, H. A., and Kurylyk, B. L. (2024). Saltwater intrusion into a confined island aquifer driven by erosion, changing recharge, sea-level rise, and coastal flooding. *Water Resour. Res.* 60 (1), e2023WR036394. doi:10.1029/2023WR036394

Stuart, M. E., Gooddy, D. C., Bloomfield, J. P., and Williams, A. T. (2011). A review of the impact of climate change on future nitrate concentrations in groundwater of the UK. *Sci. Total Environ.* 409 (15), 2859–2873. doi:10.1016/j.scitotenv.2011.04.016

Stuart, V. (2017). *Watershed evaluation of beneficial management practices (WEBs): managing our land and protecting our water through long-term watershed-scale research: final report (2004-2013)*. Ottawa. Ont: Agriculture and Agri-Food Canada.

Sustainable Canadian Agricultural Partnership (CAP) (2023). *Agriculture stewardship program*. Available at: https://www.princeedwardisland.ca/sites/default/files/publications/af_asp_guide.pdf.

Sweeney, B. W., and Newbold, J. D. (2014). Streamside forest buffer width needed to protect stream water quality, habitat, and organisms: a literature review. *J. Am. Water Resour. Assoc.* 50 (3), 560–584. doi:10.1111/jawr.12203

Tackley, H. A., Kurylyk, B. L., Lake, C. B., Lapen, D. R., and van Proosdij, D. (2023). Impacts of repeated coastal flooding on soil and groundwater following managed dike realignment. *Sci. Total Environ.* 893, 164957. doi:10.1016/j.scitotenv.2023.164957

Tesoriero, A. J., Duff, J. H., Saad, D. A., Spahr, N. E., and Wolock, D. M. (2013). Vulnerability of streams to legacy nitrate sources. *Environ. Sci. & Technol.* 47 (8), 3623–3629. doi:10.1021/es305026x

Tong, S. T., and Liu, A. J. (2006). Modelling the hydrologic effects of land-use and climate changes. *Int. J. Risk Assess. Manag.* 6 (4-6), 344–368. doi:10.1504/ijram.2006.009543

Turnipseed, D. P., and Sauer, V. B. (2010). *Discharge measurements at gaging stations (No. 3-A8)*. Reston, VA: US Geological Survey. doi:10.3133/tm3A8

Uzeika, T., Merten, G. H., Minella, J. P., and Moro, M. (2012). Use of the SWAT model for hydro-sedimentologic simulation in a small rural watershed. *Rev. Bras. Ciência do Solo* 36, 557–565. doi:10.1590/s0100-06832012000200025

Van Liew, M. W., Feng, S., and Pathak, T. B. (2012). Climate change impacts on streamflow, water quality, and best management practices for the Shell and Logan Creek Watersheds in Nebraska, USA. *Int. J. Agric. Biol. Eng.* 5 (1), 13–34. doi:10.3965/j.ijabe.20120501.003

Wagena, M. B., and Easton, Z. M. (2018). Agricultural conservation practices can help mitigate the impact of climate change. *Sci. Total Environ.* 635, 132–143. doi:10.1016/j.scitotenv.2018.04.110

Wang, X., Guo, J., Fenech, A., and Farooque, A. A. (2022). Future climate projections for Eastern Canada. *Clim. Dyn.* 59 (9-10), 2735–2750. doi:10.1007/s00382-022-06251-y

Whittaker, J., Nyiraneza, J., Zebarth, B. J., Jiang, Y., and Burton, D. L. (2023). The effects of forage grasses and legumes on subsequent potato yield, nitrogen cycling, and soil properties. *Field Crops Res.* 290, 108747. doi:10.1016/j.fcr.2022.108747

Zebarth, B. J., Danielescu, S., Nyiraneza, J., Ryan, M. C., Jiang, Y., Grimmett, M., et al. (2015). Controls on nitrate loading and implications for BMPs under intensive potato production systems in Prince Edward Island, Canada. *Groundw. Monit. Remediat.* 35 (1), 30–42. doi:10.1111/gwmr.12088

Zebarth, B. J., Drury, C. F., Tremblay, N., and Cambouris, A. N. (2009). Opportunities for improved fertilizer nitrogen management in production of arable crops in eastern Canada: a review. *Can. J. Soil Sci.* 89 (2), 113–132. doi:10.4141/cjss07102

Zhang, H., and Hiscock, K. M. (2011). Modelling the effect of forest cover in mitigating nitrate contamination of groundwater: a case study of the Sherwood Sandstone aquifer in the East Midlands, UK. *J. Hydrology* 399 (3-4), 212–225. doi:10.1016/j.jhydrol.2010.12.042

frontiers | Frontiers in Environmental Science

TYPE Original Research
PUBLISHED 27 March 2025
DOI 10.3389/fenvs.2025.1471213

Check for updates

OPEN ACCESS

EDITED BY
Hongbin Yin,
Chinese Academy of Sciences (CAS), China

REVIEWED BY
Bisrat Ayalew Yifru,
University of California, Davis, United States
Keith Schilling,
The University of Iowa, United States

*CORRESPONDENCE
Yefang Jiang,
Yefang.jiang@agr.gc.ca

RECEIVED 26 July 2024
ACCEPTED 10 March 2025
PUBLISHED 27 March 2025

CITATION
Jiang Y, Azimi MA, Meng F-R and Liang K (2025) The contribution of red clover to nitrate loading in an agricultural watershed.
Front. Environ. Sci. 13:1471213.
doi: 10.3389/fenvs.2025.1471213

COPYRIGHT
© 2025 Jiang, Azimi, Meng and Liang. This is an open-access article distributed under the terms of the Creative Commons Attribution License (CC BY). The use, distribution or reproduction in other forums is permitted, provided the original author(s) and the copyright owner(s) are credited and that the original publication in this journal is cited, in accordance with accepted academic practice. No use, distribution or reproduction is permitted which does not comply with these terms.

The contribution of red clover to nitrate loading in an agricultural watershed

Yefang Jiang[1]*, Mohammad Amir Azimi[2], Fan-Rui Meng[2] and Kang Liang[3]

[1]Charlottetown Research and Development Centre, Agriculture and Agri-Food Canada, Charlottetown, PE, Canada, [2]Faculty of Forestry and Environmental Management, University of New Brunswick, Fredericton, NB, Canada, [3]Earth Systems Science Interdisciplinary Center, University of Maryland College Park, College Park, MD, United States

Excessive nitrogen (N) input into the environment is a major contributor to the global contamination of drinking water sources and the eutrophication of aquatic ecosystems. This study investigated the impact of land use on nitrate loading in the Dunk River Watershed in Prince Edward Island, Canada, using the Soil and Water Assessment Tool (SWAT) by focusing on the role of red clover in potato rotation systems. Nitrogen uptake and accumulation of the main crops were refined using local measurements. The SWAT model estimated an annual average nitrate loading of 316 Mg N (or 22 kg N/ha) in the watershed. Although the potato–cereal–red clover (PBC) rotation land only accounted for 56% of the watershed, it contributed 90% of total nitrate loading, emphasizing the need to improve N-use efficiency. Annual nitrate loading varied with a coefficient of 24.8% but showed no significant long-term trend. Fluctuations were correlated with stream discharge and potato production area, as higher levels of both increased nitrate loading. Groundwater delivered approximately 98% of total nitrate loading. Red clover was estimated to accumulate 201 kg N/ha annually, comparable to the total N demand of potatoes in the region, contributing significant N to the crop rotation system. Substituting soybean for red clover in the PBC rotation resulted in a significant 16.7% reduction in nitrate loading. This reduction was driven by decreases in nitrate loading in potato (169.7–141.4 Mg N/yr.), cereal (77.3–70.5 Mg N/yr.), and red clover lands (36.8–0 Mg N/yr.), despite an increase in soybean land (5.9–26.5 Mg N/yr.). These findings highlight the importance of adequately accounting for N credits from red clover or substituting it with a crop that recycles less N, such as soybean, to enhance the sustainability of potato production. These findings also underscore the importance of properly modeling leguminous forages on nitrate loading estimations.

KEYWORDS

potatoes, crop rotation, nitrogen credits, SWAT, nitrate leaching, groundwater

1 Introduction

Nitrogen (N) is an important nutrient for crop growth and is utilized extensively worldwide to meet increasing food demand driven by population growth. However, excessive application and inefficient use of N fertilizer and/or leguminous green manure for crop production can result in significant nitrate leaching, leading to groundwater contamination (Meisinger and Delgado, 2002; Jiang et al., 2011). The discharge of nitrate-laden groundwater into receiving surface waters contributes to eutrophication worldwide

(Hua et al., 2018; Vörösmarty et al., 2010; De Notaris et al., 2018; Peralta and Stockle, 2002; Prunty and Greenland, 1997; Torstensson et al., 2006; Zebarth et al., 2009). For example, the estuaries of Prince Edward Island (PEI), Canada, part of the Gulf of St. Lawrence, have experienced eutrophication due to excessive nitrate loading, with several dozen anoxic events documented from 2016 to 2021 by the PEI Government (PEI government). Continuous freshwater quality monitoring in PEI has revealed a noticeable upward trend in nitrate levels (Jiang et al., 2015). This correlates with significant transformations in agricultural land use during the early to mid-1990s, with potato farmland expanding from 11,982 ha in 1951 to 43,770 ha in 1996 (Bugden et al., 2014; Grizard et al., 2020). Intensive potato production has been linked to elevated nitrate loadings in groundwater and down-gradient estuaries on the island (Benson et al., 2006; Savard et al., 2007; Zebarth et al., 2015; Jiang et al., 2015).

Forage legumes, such as red clover and alfalfa, are commonly planted as rotation crops to improve soil organic matter, break pest cycles, control weeds, and provide N for subsequent cash crops (Vos et al., 2012; Myrbeck, 2014; Jahanzad et al., 2017; Kelling et al., 2019). However, failing to account for their N contributions can increase the risk of nitrate leaching (Neeteson, 1989; Wyngaarden et al., 2015; Koropeckyj-Cox et al., 2021). In PEI, potatoes are typically grown in rotation with cereals underseeded with red clover, which is plowed down in the fall of the third year (Jiang et al., 2015). Depending on biomass growth, red clover can fix substantial N, ranging from 121 to 266 kg N/ha (Jiang et al., 2019; 2022). This N supply can fully meet potato N demands (Jiang et al., 2019; Liang et al., 2019). Fertilizing potatoes without properly considering this N source led to overfertilization, increasing nitrate leaching risks while reducing tuber yields (Jiang et al., 2022; Whittaker et al., 2023). Similarly, Yang et al. (2024) found that red clover accumulated up to 240 kg N/ha, supplying sufficient N to subsequent corn crops, which achieved yields comparable to fertilized corn in Ontario, Canada.

Although field experiments have consistently demonstrated that the substantial N contribution of red clover in crop production systems was an important source of nitrate leaching to groundwater, few studies have explored the contribution of red clover on nitrate loading to down-gradient water courses worldwide. Water quality in down-gradient water bodies is the product of a large spatial and temporal scale integration of land use in the watershed and the associated physical, chemical, and biological interactions occurring therein (Jorgensen, 2002; Bowen et al., 2007). As a result, reducing N loadings requires integrated land use management. The nitrate loading derived from one red clover crop field may not be able to create a serious off-site water quality problem. Still, the accumulated contribution of nitrate loadings from multiple red clover fields could be substantial and problematic. Understanding the integrated effect of red clover fields on nitrate loading across a broader agricultural landscape is important for developing effective watershed management strategies. However, conducting full-scale experiments to quantify red clover's influence on nitrate loading across watersheds is impractical due to the challenges of large-scale land management and potential long time lags between land use adjustments and water quality improvements (Jiang and Somers, 2009; Bouraoui and Grizzetti, 2014). The semi-distributed Soil and Water Assessment Tool (SWAT) simulates hydrological and water quality variables and crop growth at a watershed scale (Arnold and Fohrer, 2005; Arnold et al., 1998; Gassman et al., 2007), and can be used to evaluate the effects of land use on nitrate and other pollutant loadings (Akhavan et al., 2010; Cerro et al., 2014; Haas et al., 2017; Lee et al., 2017; Liang et al., 2020). SWAT requires intensive land use, crop growth, weather, field management, and topography data inputs. The uncertainties associated with model parameters and input data with SWAT can be translated into the predictions, compromising the quality of modeling results (Das et al., 2024; Tang et al., 2021). Using field measurements to constrain model parameters can reduce uncertainties (Salam et al., 2024). The objectives of this study were to: 1) develop a SWAT model in a representative agricultural watershed in PEI and 2) assess nitrate loadings in the watershed by focusing on the role of red clover in potato rotation systems.

2 Methods

2.1 Study site

The study was conducted in the Dunk River Watershed in PEI (Figure 1). The watershed has a total drainage area of 214 km^2. However, this research focused on the area above the tidal point in the watershed, which covers an area of 143 km^2. The area below the tidal point was excluded because there was no relevant stream flow or water quality data below this point. The topography is characterized by rolling hills, with slopes ranging from 2% to 10%, reaching a maximum elevation of 138 m above mean sea level in the eastern region. Geologically similar to other parts of the island, the watershed is entirely underlain by a sandstone formation consisting of a sequence of Permo-Carboniferous terrestrial red beds with a thickness of 1,200–1,600 m (van de Poll, 1989). The bedrock is covered by a layer of sandy glacial deposits ranging from 1 to 10 m in thickness. The uppermost portion (~150 m) of the formations constitutes an unconfined fractured aquifer, which serves as the primary source of drinking water for residents and contributes to over 60% of the annual stream flow (Jiang and Somers, 2009). The water table exhibits relatively rapid responses to precipitation and snowmelt events, with observations indicating a 5-day lag between an increase in groundwater level and precipitation events under similar geological conditions (Liao et al., 2005; Paradis et al., 2006). The climate of the region is characterized as humid, with cool to moderate temperatures. Precipitation varies from 810 mm in 2006 to 1,463 mm in 2002. The 20-year climate average (2002–2020) stands at 1,265 mm, with an average annual snowfall of 300 mm.

The Alberry and Charlottetown (Orthic Humo-Ferric Podzol) series soils dominate the watershed, comprising 72% and 14% of its area, respectively. The Charlottetown soil series is moderately well-drained with a moderately coarse texture, while the Alberry soil series is well-drained with a coarse texture. These soils originated from local glacial till deposits. More detailed information on soil types is available at http://sis.agr.gc.ca/cansis/soils/pe/soils.html. The watershed exemplifies a typical intensively farmed watershed in PEI, with agricultural land covering the majority of the total land area. The majority of the agricultural land is dedicated to potato cultivation, often rotated with cereals and forages (Jiang et al., 2015).

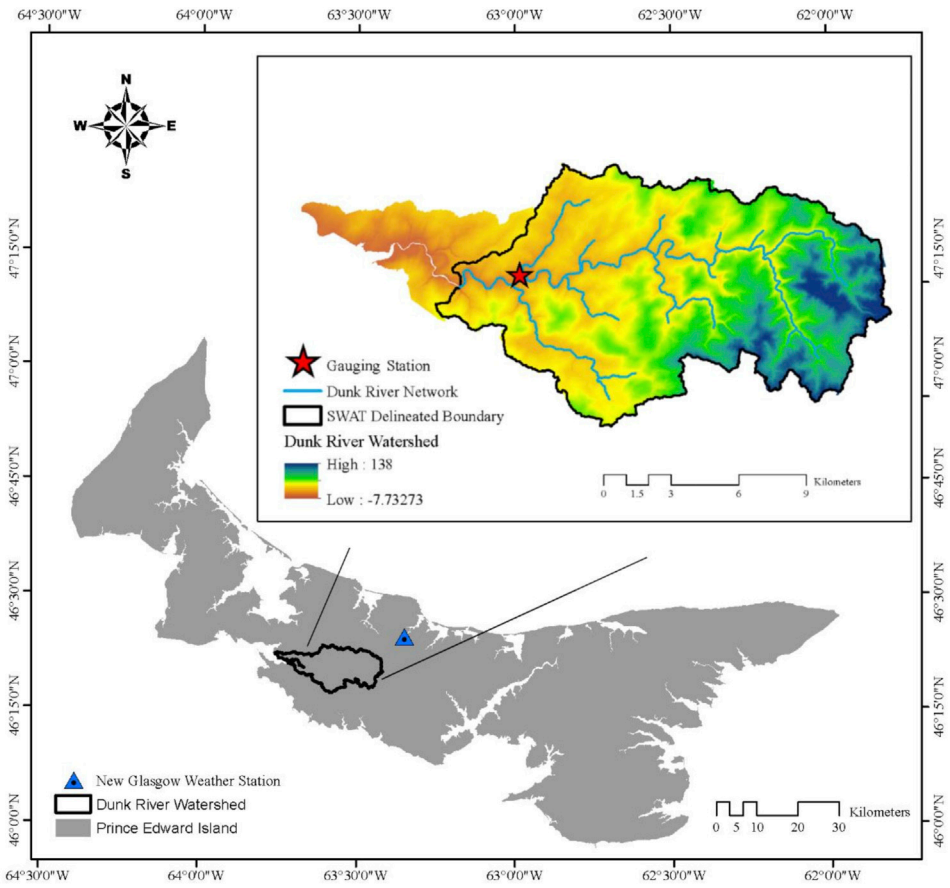


FIGURE 1
Location of the Dunk River Watershed.

The watershed is designated as one of four index basins in PEI due to its importance for environmental monitoring. Consequently, both Environment and Climate Change Canada (ECCC) and the Province share responsibility for monitoring activities in the area. ECCC has continuously monitored stream water levels and associated discharge since the 1960s. The gauging station, located approximately 3 km above the tidal point (Figure 1), covers a drainage area of about 112 km^2 upstream. Since the 1980s, the Province has been monitoring stream water quality, typically collecting 6–9 samples annually at the gauging station for water quality analysis, with 5–9 samples taken during the growing season (GS = May–Oct.) and 0–2 samples during the non-growing season (NGS = Nov.–Apr.). Agriculture and Agri-Food Canada (AAFC) has conducted crop cover inventories in PEI since 2011, providing valuable land use data for the watershed (Agriculture and Agri-Food Canada, 2010). With access to stream flow, water quality, and land use data since 2011, SWAT modeling was set to span the period from 2011 to 2020. Throughout the study period, a total of 75 water quality samples were collected, with 65 samples obtained during the GS and 12 during the NGS. The minimum daily nitrate concentration and loading were recorded at 2.4 mg N/L and 214 kg N/day, respectively, reaching a peak of 5.9 mg N/L and 1,310 kg N/day during the GS. During the NGS, the minimum nitrate concentration and loading were 3.1 mg N/L and 288 kg N/day, respectively, while the maximum nitrate concentration and loading were 5 mg N/L and 2043 kg N/day. The watershed has documented surface and groundwater nitrate enrichment issues (Bugden et al., 2014; Jiang et al., 2015; Grizard et al., 2020). Nitrate loading estimated using an integrated model was 23 kg N/ha in the watershed (Jiang et al., 2015), and a 30% reduction in nitrate loading is required to meet the estuarine N target set by the Province (Bugden et al., 2014).

2.2 SWAT modeling

2.2.1 SWAT model setup

The SWAT model requires various inputs, including weather, soil, land use, crop information, agricultural practices, and topography. For weather data, the weather records from the New Glasgow station (46.41°, 63.35°), located 13 km northeast of the watershed, were used. Soil data were obtained from the National Soil Database of Canada (NSDB), and annual land use data were obtained from the AAFC's 2011–2020 Annual Crop Inventory maps (Agriculture and Agri-Food Canada, 2010). Single-year land use datasets have been widely employed in SWAT modeling (El-Khoury et al., 2015; Sith et al., 2019; Yang et al., 2016). The reliability of model predictions is influenced by how well the model's land usage aligns with temporal changes in land use (Pai and Saraswat, 2011). Previous studies have shown that single-year

land use datasets, though widely used, compromised modeling accuracy while incorporating dynamic land use data improved predictions (Wang et al., 2018; Qi et al., 2015). The SWAT model spanned the 2011–2020 period. Because the dominance of agricultural and forested terrain, and nitrate loading from onsite septic systems was estimated to be as low as 2.4% of total nitrate loading in a previous study (Jiang et al., 2015), the impact of septic systems on nitrate loading was not explicitly simulated. Tile drains were not commonly adopted in PEI due to the well-drained sandy soils, and thus, were not simulated either.

The model divides a watershed into subbasins, which were then subdivided into hydrologic response units (HRUs) with homogeneous land use, soil, and slope characteristics (Ullrich and Volk, 2009). Hydrological and chemical parameters at the subbasin level are obtained by aggregating or calculating area-averaged values of the HRUs, serving as the primary calculation unit in SWAT. The main channel and watershed outputs are determined by implementing channel processes on the inputs to the channels. The fractured bedrock aquifer was conceptualized as a shallow unconfined layer and a deep confined layer and parameterized using the data in Jiang and Somers (2009). Model setup was performed using the ArcSWAT 2012 interface in ArcGIS 10.5.1. The watershed was divided into 29 subbasins by SWAT and further separated into 707 HRUs based on the homogeneity of land use, soil, and slope classes, using thresholds of 5%, 10%, and 15%, respectively.

2.2.2 Estimation of red clover coverage and crop N uptake parameters

In PEI red clover is commonly planted in rotation with potatoes as a green manure crop (Prince Edward Island Agricultural Insurance Corporation, 2022; Jiang et al., 2024). Red clover can accumulate a substantial amount of N through biological fixation and uptake (Liang et al., 2019; Jiang et al., 2022). Because red clover was widely planted as a rotation crop, accurately modeling N fixation, uptake, and transformation of red clover can have significant implications for overall N cycling within the watershed. While the annual crop inventory of land use has records of the most important crops, it did not explicitly map out the red clover crop coverage. Red clover is grouped along with other forages and pastures under the broad category of 'pasture'. Directly importing this land use data into SWAT precludes assessing the contribution of red clover to nitrate loading and misrepresents N cycling in the watershed. To address this issue, the temporal cropping sequence of the local industry standard potato–cereal–forage rotation was used to separate the red clover that was planted in rotation with potato from the broad pasture category. Red clover, when followed by potato, was reclassified as "red clover planted in rotation with potato". In some cases, the forages in the potato rotation were a mix of perennial grasses like timothies or ryes in addition to red clover. These forages were treated as "red clover" in SWAT modeling for simplification.

As the default plant N uptake parameters in SWAT may generate unrealistic plant N accumulations in the main crops (i.e., potato, barley, and red clover), measurements of crop biomass and N accumulation made in a field experiment conducted in the AAFC Harrington Research Farms (46.341°N and 63.3°W) from 2014 to 2017 were used to redefine the model parameters that control plant biomass and N uptake during model calibration. The experiment included the local industry standard potato–barley–red clover rotation (referred to as PBC rotation) and alternative potato–soybean–barley rotation (referred to as PSB rotation) as the main factor and four commonly planted potato cultivars (i.e., Russet Burbank, Shepody, Kennebec, and Gold Rush) in PEI as the second factor. The experiment details and results can be found in Liang et al. (2019) and Azimi et al. (2022). The parameters controlling plant biomass and N uptake including radiation-use efficiency or biomass-energy ratio (BIO_E), normal fraction of N in yield (CNYLD), normal fraction of N in plant biomass at emergence, 50% maturity, and maturity (PLTNFR_1, PLTNFR_2, PLTNFR_3) were adjusted to allow the crop N accumulation and biomass match the field measurements.

2.2.3 Model calibration and validation

Daily stream discharge and nitrate loadings were calibrated with the measured data using the SUFI-2 algorithm within the SWAT Calibration and Uncertainty Procedure (SWAT-CUP 2019; Abbaspour, 2015). The model was stabilized using a 3-year warm-up period (2008–2010), followed by calibration from 2011 to 2017, and subsequent validation from 2017 to 2020. To prioritize sensitive parameters, a Global Sensitivity Analysis approach was employed to analyze streamflow and N data (Abbaspour et al., 2004). The Global Sensitivity Analysis technique was utilized to assess the impact of individual parameter changes on the objective function (Nash-Sutcliffe efficiency) while keeping other parameters constant (Equation 1).

$$g = \alpha + \sum_{i=1}^{m} (\beta_i \times b_i) \quad (1)$$

This method involves the use of regression coefficients (α and β_i), a calibration parameter (b_i), and the number of parameters considered (m). The advantage of this method is its speed and relative sensitivity evaluation, as opposed to absolute sensitivity. The two statistical measures were used in SWAT-CUP to assess sensitivity are the t-stat index, which indicates the extent of parameter sensitivity (larger absolute values signify greater sensitivity), and the *p*-value, which determines the most sensitive parameters with $p < 0.05$ (Abbaspour et al., 2004; Brighenti et al., 2019).

The Nash-Sutcliffe efficiency (NS), percent bias (PBIAS), and coefficient of determination R^2 were employed to assess the goodness-of-fit of the SWAT model prediction for streamflow and nitrate N loading (Moriasi et al., 2007). The numeric scale of NS spans from -∞ to 1, with 1 signifying a perfect correspondence between simulation and observation. The PBIAS measures the average tendency of the model-predicted data to be higher or lower than their measured values. A low-magnitude PBIAS suggests superior simulation, with zero being the optimal value. Positive PBIAS values suggest model underestimation, while negative values imply model overestimation (Gupta et al., 1999). R^2 is a statistical measure representing the proportion of the variance in the dependent variable that is predictable from the independent variables. It is a value between 0 and 1, with a value of 1 indicating a perfect fit between the observed and predicted values (Neter et al., 1996).

R^2 and NS (Nash-Sutcliffe) stand out as two frequently employed statistical metrics for assessing the performance of hydrological models in simulating streamflow. However, these metrics are sensitive to extreme values, particularly peak flows resulting from runoff events, which could lead to an inaccurate assessment of model performance during low-flow periods (Krause et al., 2005; Pushpalatha et al., 2012). Consequently, their application in calibration may be biased towards high-flow periods, whereas this study primarily focuses on low-flow periods. A common method to alleviate the impact of runoff events on model calibration is the logarithmic transformation of streamflow values. Gupta et al. (1998) suggested that logarithmic transformation accentuates low flows and attenuates high flows, thereby enhancing sensitivity to changes in low-flow conditions. Therefore, log-transformed streamflow was employed in the calibration process.

2.2.4 Nitrate loading calculations

The validated SWAT model was employed to calculate the average annual nitrate loading rates for various land uses from 2011 to 2020. These loading rates were further partitioned into components representing surface water (SW), lateral flow (LF), and groundwater (GW) pathways within both the GS and NGS. Additionally, the model was utilized to compute the seasonal and yearly total nitrate loadings for each land use type over the same period (2011–2020). These comprehensive data sets were then used to characterize and assess the impact of different land uses on nitrate loading in the watershed.

Local field studies indicated that the majority of N from plowed-down red clover is released during the subsequent potato season, increasing the risk of excessive nitrate leaching and reduced potato tuber yield (Jiang et al., 2019; Azimi et al., 2022; Jiang et al., 2022). However, it remains uncertain whether the SWAT can accurately model this cross-year effect of red clover N cycling and the subsurface fate and transport of nitrate from the soil to the Dunk River. To address this question, the validated SWAT model was employed to forecast changes in nitrate loading when soybean replaced red clover in the PBC rotation. As soybean recycles significantly less N into the soil compared to red clover, this substitution effectively represents a reduction in red clover-derived N input. If the simulation demonstrates decreased nitrate loading during the potato and cereal phases, it would suggest that SWAT can capture the cross-year effect and subsurface processes; if not, it may indicate limitations in the model's capabilities. Furthermore, Liang et al. (2019) found that substituting soybean for red clover in potato rotations enhanced N use efficiency by up to 1.6 times and increased potato tuber yield by 13.4%. This finding suggests that soybean is a more environmentally and economically sustainable rotation crop. The simulation will illustrate the potential for nitrate loading reduction by adopting soybean as a rotation crop in the watershed, offering valuable insights into nitrate mitigation management strategies.

3 Results and discussion

3.1 Land use

From 2011 to 2020, agricultural land covered an average of 116 km^2 annually, representing 81.5% of the watershed area, with minor yearly variations (Figure 2). Each year, potato land occupied 16.7%–34.3% (average = 25.3%) of the watershed area. Potatoes were typically cultivated in a 3-year rotation with cereals and red clover. Cereals were mainly planted in rotation with potatoes, constituting 18.3% of the watershed area annually. The most common cereal was barley, with lesser amounts of rye and winter wheat. On average, 13.3% of the watershed was planted with red clover in rotation with potatoes each year. Red clover coverage peaked at 22.2% in 2014 and declined to a minimum of 16.6% in 2013. Due to the reclassification algorithm, which separated red clover from the perennial land use (pasture) category, the average proportion of "pasture" decreased from 35.3% to 22%. The annual average of potato rotation production land, which is approximately the total of potato, cereal, and red clover lands accounted for 57% of the area in the watershed. Potato rotation land area stayed relatively stable over time but the areas of potato, cereal, and red clover varied to some extent from year to year. Corn and soybeans were also planted in the watershed but occupied very small areas (Figure 2). General agricultural land refers to land where the annual crop cover inventory could not identify the agricultural products and covered relatively small areas (i.e., 0.1%). Buckwheat and brown mustard were planted in rotation with potatoes in the watershed to control the wireworm population (Jiang et al., 2022), but they were not identified in the crop inventory. These crops were likely grouped into other crop cover classes as they could not be accurately identified from satellite images. However, these crops typically require low N input, so the misclassifications are expected to have a minimal impact on overall nitrate loading estimations.

3.2 Model performance

3.2.1 Plant N accumulations

Using the default plant N uptake parameters (Table 1), the estimated plant N accumulations were 221 kg N/ha for potato, 110 kg N/ha for cereal (mainly barley), 829 kg N/ha for red clover, 44.8 kg N/ha for pasture, and 339 kg N/ha for soybean. While the default value for potato closely matched the expected N content, significant discrepancies were observed for red clover, soybean, and barley compared to reference plant N uptake values. Based on reference values (Azimi et al., 2022; Liang et al., 2019), the N accumulation estimates for cereal, red clover, pasture, and soybean were adjusted to 87.2, 201, 40, and 230 kg N/ha, respectively, while the value for potato remained unchanged. The default parameter for red clover resulted in a substantial overestimation of N accumulation, approximately 400% higher than the expected value. Similarly, the simulated N accumulation for soybeans exceeded the reference value (224 kg N/ha) by 51%. For barley, the model overpredicted N accumulation by 26% relative to the reference value of 87.5 kg N/ha. Note that N accumulation in the main crops varied by field and year due to differences in weather, management practices, and pressures from diseases, pests, and weeds. However, expected values were used in the model for simplification.

The default parameters yielded an annual plant N accumulation of 3,070 Mg N/yr. in the watershed. After adjusting the parameters, the annual plant N accumulation in the watershed decreased by 46%, to 1,642 Mg N/yr. The use of the default model parameters

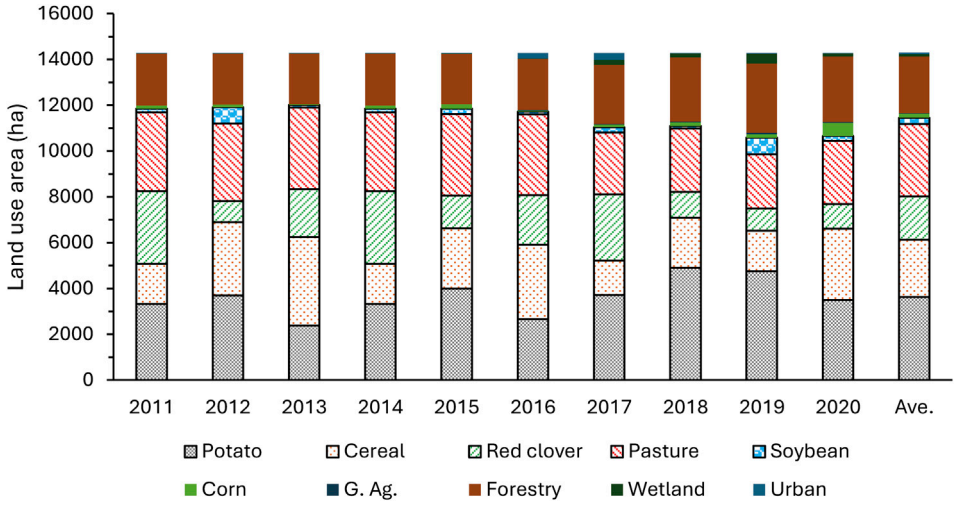


FIGURE 2
Land use in the Dunk River Watershed from 2011 to 2020, based on annual national crop cover inventory and land use reclassification analysis.

TABLE 1 Plant parameters for the main crops planted in rotation with potatoes.

Crop	Parameter	BIO_E	CNYLD	PLTNFR_1	PLTNFR_2	PLTNFR_3
Red clover	adjusted	8	0.025	0.025	0.025	0.025
	default	25	0.065	0.065	0.028	0.024
Barley	adjusted	15	0.021	0.059	0.0226	0.013
	default	35	0.021	0.059	0.0226	0.013
Soybean	adjusted	15	0.060	0.030	0.03	0.030
	default	25	0.065	0.524	0.265	0.258

substantially overestimated plant N accumulation by 87%. This overestimation can translate into an unrealistic overabundance of N input into the system along with crop residues recycled back into the soil, leading to unrealistic N leaching and loading estimates from plant residues. Various compensatory factors for excessive N input (e.g., excessive denitrification, decreasing automated fertilization operation, and ignoring legume N fixation) may cancel out the overestimation effect, creating a "good" model fit. However, these compensatory effects would inevitably lead to a misrepresentation of N cycling in the watershed, which could increase the risk of developing unreliable management strategies for reducing nitrate loading. This highlights the often-overlooked importance of constraining plant N uptake parameters using local field measurements.

3.2.2 Goodness-of-fit of SWAT modeling

Observed and simulated stream discharge and nitrate loading are shown in Figures 3, 4. The indicators of model performance are summarized in Table 2. During the calibration period, the model-predicted streamflow performance measured by NS, PBIAS, and R^2 values was 0.6%, 17.4%, and 0.65, respectively. Similar results were observed during the validation period, with NS, PBIAS, and R^2 values of 0.59%, 11%, and 0.61. For baseflow, the model showed a lower NS value of 0.43 during calibration, but PBIAS and R^2 values were 8.6% and 0.6, respectively, indicating relatively accurate baseflow estimation. Baseflow estimation performance improved during the validation period, with NS, PBIAS, and R^2 of 0.62%, −5.6%, and 0.68, respectively, which is comparable to the accuracy of surface flow estimation. Over the calibration period, the model accurately predicted nitrate loadings with NS, PBIAS, and R^2 of 0.71%, 6.5%, and 0.7, respectively. Similar measures were obtained during the validation period, with NS, PBIAS, and R^2 being 0.67%, −5.5%, and 0.68, respectively. Moriasi et al. (2007) suggested that a model is considered to have satisfactory performance if the monthly R^2 value is greater than 0.50, and the PBIAS is within the range of ±25%. However, when a model is calibrated using daily time steps, its performance may be lower than that of a monthly time step model (White and Chaubey, 2005). Wang et al. (2016) proposed that a model calibrated at a daily time step should have R^2 and NS values higher than 0.30 to be considered acceptable.

The lower NS value for predicted baseflow during calibration can be attributed to its smaller weight assigned in the objective function during model calibration compared to streamflow and total nitrate loading. However, small PBIAS values for baseflow estimation indicated that the model did not overestimate or underestimate streamflow during dry periods when baseflow was the sole nutrient delivery path. The inclusion of baseflow in model

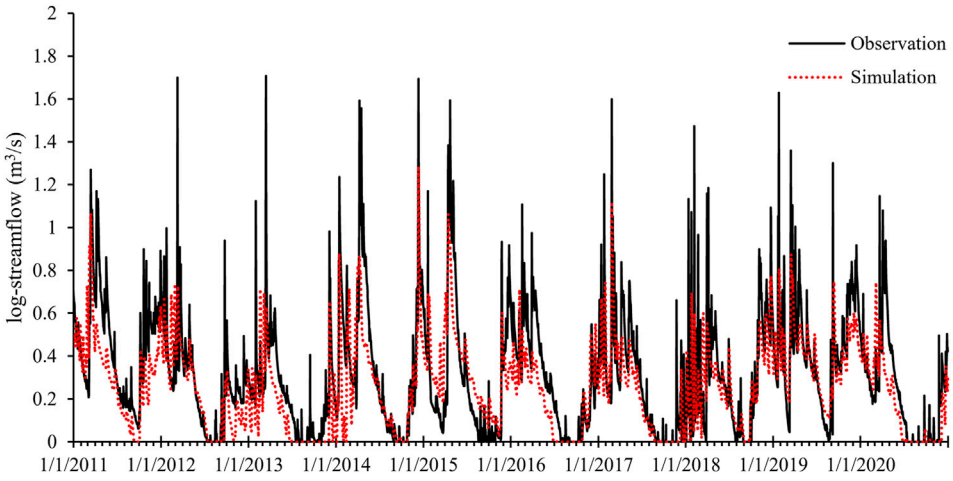


FIGURE 3
Comparison of observed and simulated daily streamflow in the Dunk River.

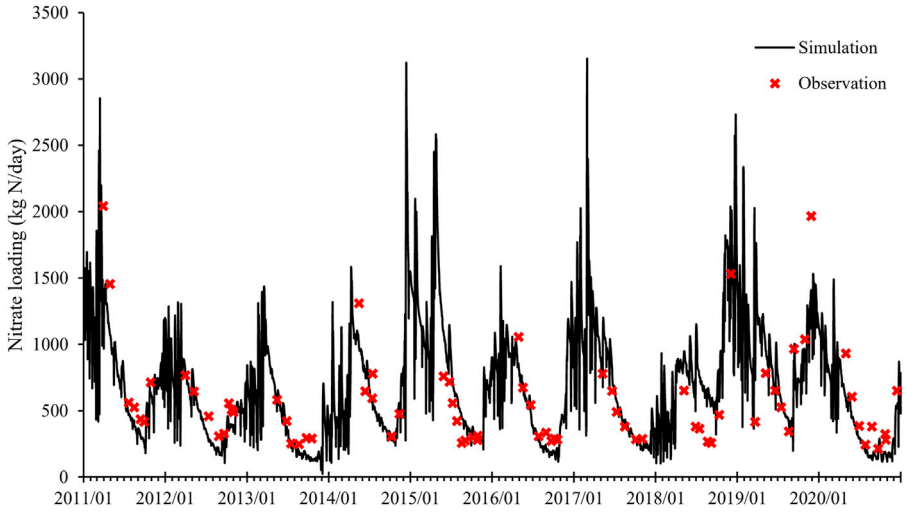


FIGURE 4
Comparison of observed and simulated daily nitrate loadings in the Dunk River.

TABLE 2 Goodness-of-fit of SWAT modeling.

	Period	R^2	NS	PBIAS (%)
Streamflow	calibration	0.65	0.60	17.4
	validation	0.61	0.59	11.0
Baseflow	calibration	0.56	0.43	8.6
	validation	0.68	0.62	−5.6
N loading	calibration	0.71	0.70	6.5
	validation	0.68	0.67	−5.5

calibration also prevented the model from compensating for any nitrate load underestimations through overestimating nitrate supply. Similar changes in PBIAS from the calibration to the validation period for both baseflow and nitrate loading may reflect the correlation between baseflow and nitrate load during dry periods. Overall, the SWAT model successfully predicted daily streamflow, nitrate loading, and baseflow based on the criteria outlined by Moriasi et al. (2007). The measurements of nitrate concentration during the NGS were limited, and increasing sampling points in the NGS could potentially enhance SWAT calibration.

TABLE 3 Land use-based nitrate loading rates in the Dunk River Watershed (averages of 2011–2020).

Land use	GS nitrate loading rate (kg N/ha/yr.)				NGS nitrate loading rate (kg N/ha/yr.)				Annual nitrate loading rate (kg N/ha/yr.)			
	SW	LF	GW	Total	SW	LF	GW	Total	SW	LF	GW	Total
Potato	0.007	0.684	14.8	15.5	0.001	0.154	31.2	31.3	0.008	0.838	46.0	46.8
Cereal	0.003	0.232	15.6	15.9	0.001	0.104	14.7	14.8	0.005	0.336	30.4	30.7
Red clover	0.001	0.058	6.3	6.4	0.004	0.364	12.6	12.9	0.006	0.421	18.9	19.3
Pasture	0.003	0.059	1.5	1.5	0.001	0.058	1.8	1.8	0.004	0.117	3.2	3.4
Soybean	0.000	0.052	10.0	10.0	0.015	0.336	10.5	10.8	0.015	0.389	20.5	20.9
Corn	0.009	0.561	15.8	16.4	0.007	0.162	15.7	15.8	0.016	0.723	31.5	32.2
G. Ag	0.026	0.427	8.5	9.0	0.010	0.478	11.9	12.4	0.037	0.904	20.4	21.4
Forestry	0.004	0.031	1.2	1.2	0.002	0.070	1.6	1.7	0.006	0.101	2.8	2.9
Wetland	0.020	0.013	1.0	1.0	0.006	0.030	1.0	1.1	0.027	0.042	2.0	2.1
Urban	0.035	0.269	21.7	22.0	0.037	0.353	17.2	17.6	0.072	0.623	38.9	39.6

Notes: SW, LF, and GW, refer to surface water, lateral flow, and groundwater, respectively; GS and NGS refer to growing season and non-growing season, respectively.

3.3 Land use-based nitrate loading rates

On an annual basis, average nitrate loading rates from potato, cereal, red clover, pasture, soybean, corn, and general agricultural lands were calculated to be 46.8, 30.7, 19.3, 3.4, 20.9, 32.2, and 21.4 kg N/ha, respectively (Table 3). Generally, agricultural lands had higher nitrate loading rates than forested land or wetlands. Urban land also had a high nitrate loading rate likely as a result of onsite sewage disposal. The variation in nitrate loading among different land uses underscores the importance of incorporating diverse land uses and preserving natural lands to maintain the ecological sustainability of agricultural watersheds. The GS nitrate loading rates of potato, cereal, and red clover lands were predicted to be 15.5, 15.9, and 6.4 kg N/ha, respectively, compared to 31.3, 14.8, and 12.9 kg N/ha during the NGS. The NGS nitrate loading rates of potato and red clover lands were 102% and 101% higher than the GS values (Table 3). The NGS nitrate loading rate from each land use was generally higher than the GS nitrate loading rate.

3.4 Watershed nitrate loading

Total nitrate loading into the Dunk River above the tidal point, which was defined as the sum of the nitrate loading from each HRU, was 316 Mg N/yr., equivalent to a global nitrate loading rate of 22 kg N/ha (Figures 5, 6). This rate is similar to the rate of 23 kg N/ha calculated using an integrated nitrate loading model (Jiang et al., 2015). The limitation of the integrated model is that it could not predict temporospatial variations of nitrate loading across the watershed as SWAT does. As the dominant crop, covering 25.3% of the watershed, potato land contributed 169.7 Mg N/yr. of nitrate loading, accounting for 53.7% of the total nitrate loading (Figure 5). The other major crops, including cereals, red clover, pasture, and soybean, contributed 77.3, 36.8, 10.6, and 5.9 Mg N/yr., respectively. Cereal land ranked as the second-highest contributor, accounting for 24.5%, followed by red clover land, contributing 11.6% of total nitrate loading. Other land uses collectively generated only 4.9% (i.e., 15.7 Mg N/yr.) nitrate loading. Nitrate loading from the onsite septic systems was estimated to be 8.1 Mg N/yr. (0.57 kg N/ha) in the watershed (Jiang et al., 2015). The nitrate loading from other land uses was assumed to include the nitrate loading from the septic systems. Although the PBC rotation land only occupied 56% of the watershed area, it contributed about 90% of the nitrate loading (Figure 5). The results emphasize the importance of improving N use efficiency of potato rotation production for mitigating nitrate loading in the Dunk River Watershed.

These results agree with the findings of Jiang et al. (2015), who estimated that 75%–98% of nitrate loading in receiving estuaries originated from potato-rotated lands in intensively farmed watersheds in PEI. This included potato land, the red clover, and cereal lands, which were in rotation with potatoes. These results also align with the widely accepted notion that agricultural land is the primary contributor to nitrate pollution in PEI's agricultural watersheds (Grizard et al., 2020; Jiang and Somers, 2009; Jiang et al., 2015; Liang et al., 2019). The fact that agricultural land has the most profound impact on water quality is consistent with Kersebaum et al. (2003) who indicated that agriculture is estimated to be responsible for 55% of non-point source pollution in the European Union. These findings support earlier studies by Haidary et al. (2013), revealing a significant negative correlation between water pollution and forest land coverage. Baker (1992) highlighted that undisturbed forests have a relatively minor impact on water quality compared to other land uses.

Surface runoff (SW), lateral flow (LF), and groundwater discharge (GW) paths delivered 0.03%, 1.8%, and 98.2% of the total nitrate loading, respectively, in the Dunk River Watershed (Figure 5), indicating that groundwater is the primary flow path of nitrate loading delivery. The results can be attributed to several factors. Firstly, nitrate loading is proportional to streamflow, and over 66% of annual streamflow and 100% of GS streamflow in PEI is derived from groundwater discharge (Figures 3, 4; Jiang et al., 2015). Secondly, fertilizer is commonly banded in the soil in PEI, reducing

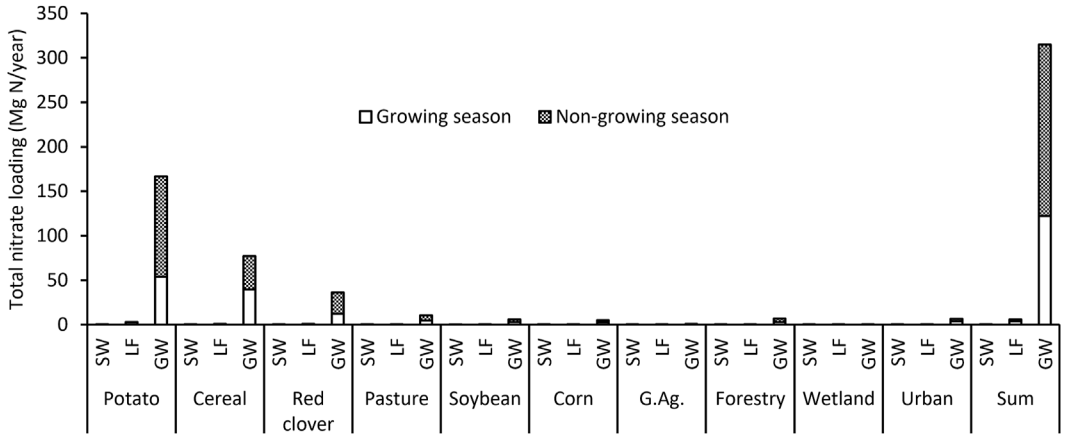


FIGURE 5
Average nitrate loadings from 2011 to 2020 in the Dunk River Watershed. (SW, LF, and GW represent surface water, lateral flow, and groundwater paths, respectively).

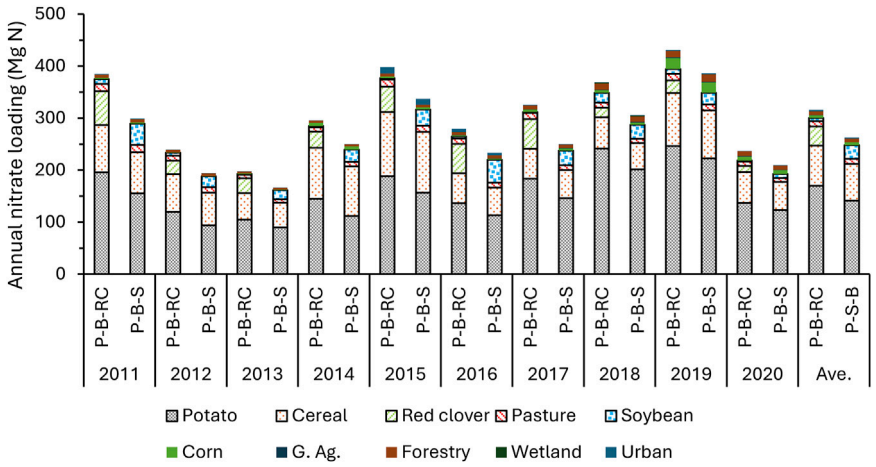


FIGURE 6
Comparison of annual nitrate loadings under different crop rotation scenarios in the Dunk River Watershed (PBC refers to potato production following the potato–barley–red clover rotation; PBS refers to potato production following the potato–barley–soybean rotation).

the risk of fertilizer being washed away by surface runoff (Jiang et al., 2015). When fertilizer is broadcast, it is normally applied when soils are not saturated. In this case, there is sufficient infiltrating water to carry the bulk of the nitrate to a depth where it is not vulnerable to surface runoff before the soils are saturated and runoff occurs, resulting in low nitrate levels in surface runoff (Baker, 2001). Thirdly, nitrate losses from manure runoff were negligible because manure applications were limited (Jiang et al., 2015). The finding about surface runoff contributing to low nitrate loadings aligns with field observations from former studies in PEI (Dunn et al., 2011; Jiang et al., 2015; Pavlovskii et al., 2023). Additionally, local field experiments have consistently demonstrated that nitrate leaching is the primary pathway of N losses from potato production systems (Jiang et al., 2019; 2022). Groundwater is the primary flow path of nitrate loading to surface water worldwide (Bachman et al., 1998; Schilling and Zhang, 2004; Steiness et al., 2021; Wherry et al., 2021).

Nitrate loadings in the main crops (potatoes, cereals, and red clovers) exhibited seasonal variations throughout the study period (Figure 7). The GS and NGS variation coefficients for nitrate loadings in these three primary croplands were 0.46, 0.41, and 0.5 for GS, and 0.26, 0.29, and 0.61 for NGS, respectively. However, neither GS nor NGS nitrate loadings demonstrated a significant long-term trend ($p > 0.2$). On average, nitrate loadings fluctuated seasonally, with 39% of the annual nitrate loading occurring during the GS and 61% during the NGS (Figure 5). Because the magnitude of nitrate loading is primarily governed by streamflow rate, NGS nitrate loading being higher than GS nitrate loading can be explained by NGS streamflow rate being higher than GS streamflow rate (Figure 3). On an annual basis, nitrate loadings varied from the highest of 431 Mg N in 2019 to the lowest of 197 Mg N in 2013 at a variation coefficient of 24.8%. The seasonal and yearly fluctuations were mainly driven by stream discharge and potato production area variations, with nitrate loading increasing

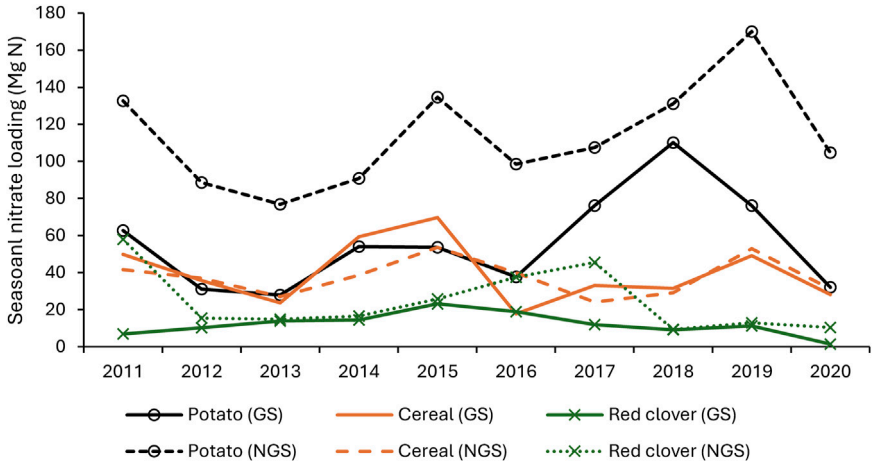


FIGURE 7
Seasonal nitrate loadings from the main crops in the Dunk River Watershed. (GS and NGS stand for growing season and non-growing season, respectively)

with higher stream discharge and potato production area (Figures 2–4). The annual potato production area explained 51% of the variation in nitrate loading (p = 0.02). The significant impact of annual land use changes underscores the necessity of accounting for temporal variations in land use when modeling nitrate loading dynamics. The relative rapid response of nitrate loading to land use change implies that most nitrate loadings were delivered via shallow groundwater in the fractured bedrock aquifer, which has a relatively short residence time (Jiang and Somers, 2009). The yearly nitrate loadings from 2011 to 2020 as shown in Figure 6 did not demonstrate a significant long-term temporal trend (p = 0.6). The absence of a long-term trend was attributed to the lack of systematic changes in key influential factors, such as land use and hydrology (Figures 2, 3), throughout the study period.

3.5 Nitrate loading changes from substituting red clover with soybean

Substituting red clover with soybean in the PBC rotation across the watershed significantly reduced nitrate loading by 16.8% in the Dunk River Watershed from 316 Mg N/yr. (i.e., 22 kg N/ha) to 263 Mg N/yr. (i.e., 18.4 kg N/ha) (paired t-test $p < 0.0001$) (Figure 6). This reduction alone contributed to over 50% of the total estuarine N loading reduction target of 30% set by the Province (Bugden et al., 2014). This reduction in nitrate loading was caused by nitrate loading reduction from the potato, cereal, and red clover lands from 169.7, 77.3, and 36.8 Mg N/yr. to 141.4, 70.5, and 0 Mg N/yr., respectively, increase in nitrate loading from the soybean land from 5.9 to 26.5 kg N/yr., and minor changes in nitrate loading from the other land uses. Because cereal, red clover, and soybean were planted in rotation with potatoes, the cereal, red clover, and soybean residues were recycled into the soil. The recycled crop residues were mineralized and then released nitrate, which could be transported to groundwater, used by the following crops, or denitrified. These subsurface processes can have annual effects on nitrate loading, contributing to nitrate loading changes not only in red clover and soybean lands but also in the potato and cereal lands. After SWAT calibration and validation, the red clover and soybean had annual N fixation rates of 134.5 kg N/ha and 193.2 kg N/ha, and similar plant N uptake of 229 kg N/ha and 201 kg N/ha, respectively. However, most of the soybean's N is harvested and removed from the field as soybean grains, while the red clover is commonly plowed down as green manure, being left in the soil. The lower level of N in the recycled soybean residues created less nitrate loading on a field and watershed scale. Although SWAT adopted simplified groundwater mass transport equations instead of classic advection-dispersion equations (Arnold and Fohrer, 2005), the simulations of changes in nitrate loading from replacing red clover with soybean respected the complicated pathways and subsurface processes to some extent.

Potato growers in PEI commonly followed the provincial government's recommendation of applying 185 kg N/ha to processing potatoes, with deductions of 17 kg N/ha for N credits from plowed-down red clover (where applicable) and an additional 17 kg N/ha for N credits from soil organic matter (PEI government, 2014; Jiang et al., 2024). However, several local studies (Jiang et al., 2019; 2022; Liang et al., 2019; Azimi et al., 2022; Whittaker et al., 2023) observed that N accumulation in red clover ranged from 121 to 266 kg N/ha. Because most of this N is expected to be released in the following potato-growing season (Wyngaarden et al., 2015; Masunga et al., 2016), adhering to the provincial recommendation of 17 kg N/ha would often result in excessive N application, significantly increasing the risk excessive of nitrate leaching and subsequent nitrate loading. The simulated changes in nitrate loading were compatible with these field observations. These findings highlight the need to adjust N inputs for potatoes by adequately accounting for N contributions from red clover, which is crucial for mitigating nitrate loading in the Dunk River Watershed.

4 Conclusion

The SWAT model estimated an average annual nitrate loading of 316 Mg N from 2011 to 2020 in the Dunk River Watershed,

corresponding to a loading rate of 22 kg N/ha. The PBC rotation, covering 56% of the watershed, contributed 90% of the total nitrate loading. Seasonal variations in nitrate loading were evident, with 39% occurring during the growing season and 61% during the non-growing season. Annual nitrate loading fluctuated between 197 Mg N in 2013 and 431 Mg N in 2019, with a coefficient of variation of 24.8%, but did not demonstrate a significant long-term temporal trend. These annual fluctuations correlated with stream discharge and potato production area, as higher values of both led to increased nitrate loading. Groundwater discharge accounted for approximately 98% of nitrate loading, highlighting the critical role of groundwater in delivering nitrate to the river.

Red clover was estimated to accumulate 201 kg N/ha annually, comparable to the total N demand of potatoes in the region, contributing significantly to the PBC rotation. Substituting red clover in the PBC rotation with soybean across the watershed significantly reduced nitrate loading by 16.7% while introducing soybean as a cash crop to increase farm profitability. This reduction in nitrate loading was mainly affected by decreases in potato (169.7–141.4 Mg N/yr.), cereal (77.3–70.5 Mg N/yr.), and red clover lands (36.8–0 Mg N/yr.), while nitrate loading in soybean land increased from 5.9 to 26.5 kg N/yr. These findings emphasize the importance of adequately accounting for N credits from red clover in the production system or substituting it with a crop that recycles less N into the production system for sustainable potato production in the watershed. These findings also underscore the importance of properly modeling leguminous forages on nitrate loading estimations.

Data availability statement

Publicly available datasets were analyzed in this study. This data can be found here: The sources are listed in the reference.

Author contributions

YJ: Conceptualization, Formal Analysis, Funding acquisition, Investigation, Methodology, Project administration, Resources, Supervision, Validation, Visualization, Writing–original draft, Writing–review and editing. MA: Formal Analysis, Investigation, Methodology, Validation, Visualization, Writing–original draft, Writing–review and editing. F-rM: Conceptualization, Formal Analysis, Investigation, Methodology, Project administration, Supervision, Validation, Visualization, Writing–original draft, Writing–review and editing, Resources. KL: Formal Analysis, Investigation, Methodology, Validation, Visualization, Writing–review and editing.

Funding

The author(s) declare that financial support was received for the research and/or publication of this article. This study was funded by the Agriculture and Agri-Food Canada Living Laboratories Initiative.

Acknowledgments

We would like to express our appreciation to Andrea McKenna, Executive Director at the East Prince Agri-Environment Association for her invaluable support throughout this project. The manuscript was improved thanks to comments from the two reviewers.

Conflict of interest

The authors declare that the research was conducted in the absence of any commercial or financial relationships that could be construed as a potential conflict of interest.

The author(s) declared that they were an editorial board member of Frontiers, at the time of submission. This had no impact on the peer review process and the final decision.

Publisher's note

All claims expressed in this article are solely those of the authors and do not necessarily represent those of their affiliated organizations, or those of the publisher, the editors and the reviewers. Any product that may be evaluated in this article, or claim that may be made by its manufacturer, is not guaranteed or endorsed by the publisher.

References

Abbaspour, K. C. (2015). "SWAT-CUP: SWAT calibration and uncertainty programs—a user manual," *Eawag Dübend.* 16–70.

Abbaspour, K. C., Johnson, C., and Van Genuchten, M. T. (2004). Estimating uncertain flow and transport parameters using a sequential uncertainty fitting procedure. *Vadose Zone J.* 3, 1340–1352. doi:10.2136/vzj2004.1340

Agriculture and Agri-Food Canada (AAFC) (2010). Available online at: https://open.canada.ca/data/en/dataset/ba2645d5-4458-414d-b196-6303ac06c1c9.

Akhavan, S., Abedi-Koupai, J., Mousavi, S.-F., Afyuni, M., Eslamian, S.-S., and Abbaspour, K. C. (2010). Application of SWAT model to investigate nitrate leaching in Hamadan–Bahar Watershed, Iran, *Agric. Ecosyst. Environ.* 139, 675–688. doi:10.1016/j.agee.2010.10.015

Arnold, J. G., and Fohrer, N. (2005). SWAT2000: current capabilities and research opportunities in applied watershed modelling. *Hydrol. Process.* 19, 563–572. doi:10.1002/hyp.5611

Arnold, J. G., Srinivasan, R., Muttiah, R. S., and Williams, J. R. (1998). Large area hydrologic modeling and assessment part I: model development 1. *JAWRA J. Am. Water Resour. Assoc.* 34, 73–89. doi:10.1111/j.1752-1688.1998.tb05961.x

Azimi, M. A., Jiang, Y., Meng, F.-R., and Liang, K. (2022). Yield responses of four common potato cultivars to an industry standard and alternative rotation in Atlantic Canada. *Am. J. Potato Res.* 99, 206–216. doi:10.1007/s12230-022-09873-4

Bachman, L. J., Lindsey, B. D., Brakebill, J. W., and Powars, D. S. (1998). *Ground-water discharge and base-flow nitrate loads of nontidal streams, and their relation to a hydrogeomorphic classification of the chesapeake bay watershed, middle atlantic coast.* Reston, Virginia: U.S. Geological Survey Water-Resources Investigations Report, 98–4059.

Baker, J. L. (2001). Limitations of improved nitrogen management to reduce nitrate leaching and increase use efficiency. *Sci. World J.* 1, 10–16. doi:10.1100/tsw.2001.457

Baker, L. A. (1992). Introduction to nonpoint source pollution in the United States and prospects for wetland use. *Ecol. Eng.* 1, 1–26. doi:10.1016/0925-8574(92)90023-u

Benson, V. S., VanLeeuwen, J. A., Sanchez, J., Dohoo, I. R., and Somers, G. H. (2006). Spatial analysis of land use impact on ground water nitrate concentrations. *J. Environ. Qual.* 35, 421–432. doi:10.2134/jeq2005.0115

Bouraoui, F., and Grizzetti, B. (2014). Modelling mitigation options to reduce diffuse nitrogen water pollution from agriculture. *Sci. Total Environ.* 468-469, 1267–1277. doi:10.1016/j.scitotenv.2013.07.066

Bowen, J. L., Kroeger, K. D., Tomasky, G., Pabich, W. J., Cole, M. L., Carmichael, R. H., et al. (2007). A review of land-sea coupling by groundwater discharge of nitrogen to New England estuaries: mechanisms and effects. *Appl. Geochem.* 22, 175–191. doi:10.1016/j.apgeochem.2006.09.002

Brighenti, T. M., Bonumá, N. B., Grison, F., de Almeida Mota, A., Kobiyama, M., and Chaffe, P. L. B. (2019). Two calibration methods for modeling streamflow and suspended sediment with the swat model. *Ecol. Eng.* 127, 103–113. doi:10.1016/j.ecoleng.2018.11.007

Bugden, G., Jiang, Y., van den Heuvel, M. R., Vandermeulen, H., MacQuarrie, K. T. B., Crane, C., et al. (2014). *Nitrogen loading criteria for estuaries in Prince edward island*. Canada: Canadian Technical Report of Fisheries and Aquatic Sciences 3066, Department of Fishery and Ocean.

Cerro, I., Antigüedad, I., Srinavasan, R., Sauvage, S., Volk, M., and Sanchez-Perez, J. M. (2014). Simulating land management options to reduce nitrate pollution in an agricultural watershed dominated by an alluvial aquifer. *J. Environ. Qual.* 43, 67–74. doi:10.2134/jeq2011.0393

Das, S. K., Ahsan, A., Khan, M. H. R. B., Yilmaz, A. G., Ahmed, S., Imteaz, M., et al. (2024). Calibration, validation and uncertainty analysis of a SWAT water quality model. *Appl. Water Sci.* 14, 86. doi:10.1007/s13201-024-02138-x

De Notaris, C., Rasmussen, J., Sørensen, P., and Olesen, J. E. (2018). Nitrogen leaching: a crop rotation perspective on the effect of N surplus, field management and use of catch crops. *Agric. Ecosyst. Environ.* 255, 1–11. doi:10.1016/j.agee.2017.12.009

Dunn, A., Julien, G., Ernst, W., Cook, A., Doe, K., and Jackman, P. (2011). Evaluation of buffer zone effectiveness in mitigating the risks associated with agricultural runoff in Prince Edward Island. *Sci. Total Environ.* 409, 868–882. doi:10.1016/j.scitotenv.2010.11.011

El-Khoury, A., Seidou, O., Lapen, D., Que, Z., Mohammadian, M., Sunohara, M., et al. (2015). Combined impacts of future climate and land use changes on discharge, nitrogen and phosphorus loads for a Canadian river basin. *Environ. Manag.* 151, 76–86. doi:10.1016/j.jenvman.2014.12.012

Gassman, P. W., Reyes, M. R., Green, C. H., and Arnold, J. G. (2007). The soil and water assessment tool: historical development, applications, and future research directions. *J. ASABE, Trans. ASABE* 50, 1211–1250. doi:10.13031/2013.23637

Grizard, P., MacQuarrie, K. T., and Jiang, Y. (2020). Land-use based modeling approach for determining freshwater nitrate loadings from small agricultural watersheds. *Water Qual. Res. J.* 55, 278–294. doi:10.13031/2013.23637

Gupta, H. V., Sorooshian, S., and Yapo, P. O. (1998). Toward improved calibration of hydrologic models: multiple and noncommensurable measures of information. *Water Resour. Res.* 34, 751–763. doi:10.1029/97wr03495

Gupta, H. V., Sorooshian, S., and Yapo, P. O. (1999). Status of automatic calibration for hydrologic models: Comparison with multilevel expert calibration. *J. Hydrol. Eng.* 4, 135–143. doi:10.1061/(asce)1084-0699(1999)4:2(135)

Haas, M. B., Guse, B., and Fohrer, N. (2017). Assessing the impacts of Best Management Practices on nitrate pollution in an agricultural dominated lowland catchment considering environmental protection versus economic development, *J. Environ. Manag.*, 196, 347–64.

Haidary, A., Amiri, B. J., Adamowski, J., et al. (2013). Assessing the Impacts of Four Land Use Types on the Water Quality of Wetlands in Japan. *Manage.* 27, 2217–2229. doi:10.1007/s11269-013-0284-5

Hua, B., Yang, J., Liu, F., Zhu, G., Deng, B., and Mao, J. (2018). Characterization of dissolved organic matter/nitrogen by fluorescence excitation-emission matrix spectroscopy and X-ray photoelectron spectroscopy for watershed management. *Chemosphere* 201, 708–715. doi:10.1016/j.chemosphere.2018.03.043

Jahanzad, E., Barker, A. V., Hashemi, M., Sadeghpour, A., and Eaton, T. (2017). Forage radish and winter pea cover crops outperformed rye in a potato cropping system. *Agron. J.* 109, 646–653. doi:10.2134/agronj2016.06.0342

Jiang, Y., Zebarth, B. J., Somers, G. H., MacLeod, J. A., and Savard, M. M. (2012). Nitrate leaching from potato production in Eastern Canada. In: He, Z., Larkin, R. P., Honeycutt, C. W. (Editors). *Springer, NY: Sustainable Potato Production: Global Case Studies,*. pp. 233–250.

Jiang, Y., Nishimura, P., van den Heuvel, M. R., MacQuarrie, K. T., Crane, C. S., Xing, Z., et al. (2015). Modeling land-based nitrogen loads from groundwater-dominated agricultural watersheds to estuaries to inform nutrient reduction planning. *J. Hydrol.* 529, 213–230. doi:10.1016/j.jhydrol.2015.07.033

Jiang, Y., Nyiraneza, J., Khakbazan, M., Geng, X., and Murray, B. J. (2019). Nitrate leaching and potato yield under varying plow timing and nitrogen rate. *Agrosystems Geosci. Environ.* 2, 1–14. doi:10.2134/age2019.05.0032

Jiang, Y., Nyiraneza, J., Noronha, C., Mills, A., Murnaghan, D., Kostic, A., et al. (2022). Nitrate leaching and potato tuber yield response to different crop rotations. *Field Crops Res.* 288, 108700. doi:10.1016/j.fcr.2022.108700

Jiang, Y., and Somers, G. (2009). Modeling effects of nitrate from non-point sources on groundwater quality in an agricultural watershed in Prince Edward Island, Canada. *Hydrogeol. J.* 17, 707–724. doi:10.1007/s10040-008-0390-2

Jiang, Y., Stetson, T., Philips, J., and Kostic, A. (2024). Reducing yearly variation in potato tuber yield using supplemental irrigation. *Potato Res.* 67, 1625–1651. doi:10.1007/s11540-024-09711-6

Jorgensen, E. E. (2002). *Advances in restoration science, number 2: opportunities in nitrogen management research: improving applications for proven technologies and identifying new tools for managing nitrogen flux and input in ecosystems*. Washington, DC: United States Environmental Protection Agency. (EPA) Issue Paper, EPA/600/S-02/003. 4p.

Kelling, K. A., Andraski, T. W., and Speth, P. E. (2019). Field evaluation of potato N needs following forage legumes. *Am. J. Potato Res.* 96, 62–68. doi:10.1007/s12230-018-9689-2

Kersebaum, K. C., Steidl, J., Bauer, O., and Piorr, H.-P. (2003). Modelling scenarios to assess the effects of different agricultural management and land use options to reduce diffuse nitrogen pollution into the river Elbe, Physics and Chemistry of the Earth, Parts A/B/C. 28, 12–13.

Koropeckyj-Cox, L., Christianson, R. D., and Yuan, Y. (2021). Effectiveness of conservation crop rotation for water pollutant reduction from agricultural areas. *Trans. ASABE* 64, 691–704. doi:10.13031/trans.14017

Krause, P., Boyle, D. P., and Bäse, F. (2005). Comparison of different efficiency criteria for hydrological model assessment. *Adv. Geosci.* 5, 89–97. doi:10.5194/adgeo-5-89-2005

Lee, S., Sadeghi, A. M., Yeo, I.-Y., McCarty, G. W., and Hively, W. D. (2017). Assessing the impacts of future climate conditions on the effectiveness of winter cover crops in reducing nitrate loads into the Chesapeake Bay watersheds using the SWAT model. *Trans. ASAE.* 60, 1939–1955. doi:10.13031/trans.12390

Liang, K., Jiang, Y., Nyiraneza, J., Fuller, K., Murnaghan, D., and Meng, F.-R. (2019). Nitrogen dynamics and leaching potential under conventional and alternative potato rotations in Atlantic Canada. *Field Crops Res.* 242, 107603. doi:10.1016/j.fcr.2019.107603

Liang, K., Jiang, Y., Qi, J., Fuller, K., Nyiraneza, J., and Meng, F.-R. (2020). Characterizing the impacts of land use on nitrate load and water yield in an agricultural watershed in Atlantic Canada. *Sci. Total Environ.* 729, 138793. doi:10.1016/j.scitotenv.2020.138793

Liao, S. L., Savard, M., Somers, G., Paradis, D., and Jiang, Y. (2005). Preliminary results from water-isotope characterization of groundwater, surface water, and precipitation in the Wilmot River watershed, Prince Edward Island. (Natural Resources Canada, Geological Survey of Canada).

Masunga, R. H., Uzokwe, U. N., Mlay, P. D., Odeh, I., Singh, A., Buchan, D., and De Neve, S. (2016). Nitrogen mineralization dynamics of different valuable organic amendments commonly used in agriculture, *Appl. Soil Ecol.*, 101, 185–193.

Meisinger, J. J., and Delgado, J. A. (2002). Principles for managing nitrogen leaching. *J. Soil Water Conserv*, 57, 485–498.

Moriasi, D. N., Arnold, J. G., Van Liew, M. W., Bingner, R. L., Harmel, R. D., and Veith, T. L. (2007). Model evaluation guidelines for systematic quantification of accuracy in watershed simulations. *Trans. ASAE* 50, 885–900. doi:10.13031/2013.23637

Myrbeck, Å. (2014). *Soil tillage influences on soil mineral nitrogen and nitrate leaching in Swedish arable soils*. Ultuna, Uppsala, Sweden: Doctoral Thesis Swedish University of Agricultural Sciences. Available online at: https://pub.epsilon.slu.se/11461/1/myrbeck_a_140828.pdf.

Neeteson, J. J. (1989). "Effects of legumes on soil mineral nitrogen and response of potatoes to nitrogen fertilizer," in *Effects of crop rotation on potato production in the temperate zones*. Editors J. Vos, C. D. Van Loon, and G. J. Bollen (Dordrecht, Netherlands: Kluwer Academic Publishers). doi:10.1007/978-94-009-2474-1_8

Neter, J., Kutner, M. H., Nachtsheim, C. J., and Wasserman, W. (1996). Applied linear statistical models.

Pai, N., and Saraswat, D. (2011). SWAT2009_LUC: a tool to activate the land use change module in SWAT 2009. *Trans. ASAE* 54, 1649–1658. doi:10.13031/2013.39854

Paradis, D., Ballard, J., Savard, M., Lefebvre, R., Jiang, Y., Somers, G., et al. (2006). "Impact of agricultural activities on nitrates in ground and surface water in the Wilmot Watershed, PEI, Canada," in *59th Canadian geotechnical conference and the 7th joint CGS/IAH-CNC conference* (Vancouver), 1–4.

Pavlovskii, I., Jiang, Y., Danielescu, S., and L. Kurylyk, B. L. (2023). Influence of precipitation event magnitude on baseflow and coastal nitrate export for Prince Edward Island, Canada. *Hydrol. Process.* 37. doi:10.1002/hyp.14892

Peralta, J. M. A., and Stockle, C. O. (2002). Dynamics of nitrate leaching under irrigated potato rotation in Washington State: a long-term simulation study. *Agric. Ecosyst. Environ.* 88, 23–34. doi:10.1016/s0167-8809(01)00157-8

Prince Edward Island Agricultural Insurance corporation (PEIAIC) (2022). 2022 spring AgriInsurance agreement at. Available online at: https://www.

princeedwardisland.ca/sites/default/files/publications/af_agriinsurance_cropsagreement.pdf (Accessed June 13, 2022).

Prince Edward Island Government. (2014). Potato fertilization. *PEI analytical Laboratories*. Available online at: https://www.gov.pe.ca/photos/original/af_fact_potfer.pdf. Accessed 12 July 2018.

Prunty, L., and Greenland, R. (1997). Nitrate leaching using two potato-corn N-fertilizer plans on sandy soil. *Agric. Ecosyst. Environ.* 65, 1–13. doi:10.1016/s0167-8809(97)00043-1

Pushpalatha, R., Perrin, C., Le Moine, N., and Andréassian, V. (2012). A review of efficiency criteria suitable for evaluating low-flow simulations. *J. Hydrol.* 420, 171–182. doi:10.1016/j.jhydrol.2011.11.055

Qi, J., Li, S., Li, Q., Xing, Z., Bourque, P., and Meng, F.-R. (2015). Modifying the soil temperature module in SWAT for application in atlantic Canada ---Module development, validation and impacts on watershed modelling. doi:10.13140/RG.2.2.31949.49124

Salam, A. A., Bailey, R. T., White, J. T., Arnold, J. G., White, M. J., Čerkasova, N., et al. (2024). A framework for parameter estimation, sensitivity analysis, and uncertainty analysis for holistic hydrologic modeling using SWAT+. *Hydrol. Earth Syst. Sci.*, 28, 21–48. doi:10.5194/hess-28-21-2024

Savard, M. M., Paradis, D., Somers, G., Liao, S., and van Bochove, E. (2007). Winter nitrification contributes to excess NO3− in groundwater of an agricultural region: a dual-isotope study. *Water Resour. Res.* 43, W06422. doi:10.1029/2006wr005469

Schilling, K., and Zhang, Y.-K. (2004). Baseflow contribution to nitrate-nitrogen export from a large, agricultural watershed, USA. *J. Hydrol.* 295, 305–316. doi:10.1016/j.jhydrol.2004.03.010

Sith, R., Watanabe, A., Nakamura, T., Yamamoto, T., and Nadaoka, K. (2019). Assessment of water quality and evaluation of best management practices in a small agricultural watershed adjacent to Coral Reef area in Japan. *Agric. Water Manag.* 213, 659–673. doi:10.1016/j.agwat.2018.11.014

Steiness, M., Jessen, S., van't Veen, S. G. M., Kofod, T., Hojberg, A. L., and Engesgaard, P. (2021). Nitrogen-loads to streams: importance of bypass flow and nitrate removal processes. *J. Geophys. Res. Biogeosci.* 126, e2020JG006111. doi:10.1029/2020JG006111

Tang, X., Zhang, J., Wang, G., Jin, J., Liu, C., Liu, Y., et al. (2021). Uncertainty analysis of SWAT modeling in the Lancang River Basin using four different algorithms. *Water* 13, 341. doi:10.3390/w13030341

Torstensson, G., Aronsson, H., and Bergström, L. (2006). Nutrient use efficiencies and leaching of organic and conventional cropping systems in Sweden. *J. Agron.* 98, 603–615. doi:10.2134/agronj2005.0224

Ullrich, A., and Volk, M. (2009). Application of the Soil and Water Assessment Tool (SWAT) to predict the impact of alternative management practices on water quality and quantity. *Agric. Water Manag.* 96, 1207–1217. doi:10.1016/j.agwat.2009.03.010

van de Poll, H. W. (1989). Lithostratigraphy of the Prince edward island redbeds. *Atl. Geol.* 25, 23–35. doi:10.4138/1668

Vörösmarty, C. J., McIntyre, P. B., Gessner, M. O., Dudgeon, D., Prusevich, A., Green, P., et al. (2010). Global threats to human water security and river biodiversity. *Nature* 467, 555–561. doi:10.1038/nature09440

Vos, J., Van Loon, C., and Bollen, G. (2012). "Effects of crop rotation on potato production in the temperate zones," in *Proceedings of the international conference on effects of crop rotation on potato production in the temperate zones, held august 14–19, 1988*. Wageningen, Netherlands: Springer Science and Business Media.

Wang, C., Jiang, R., Boithias, L., Sauvage, S., Sánchez-Pérez, J.-M., Mao, X., et al. (2016). Assessing potassium environmental losses from a dairy farming watershed with the modified SWAT model. *Agric. Water Manag.* 175, 91–104. doi:10.1016/j.agwat.2016.02.007

Wang, Q., Liu, R., Men, C., Guo, L., and Miao, Y. (2018). Effects of dynamic land use inputs on improvement of SWAT model performance and uncertainty analysis of outputs. *J. Hydrol.* 563, 874–886. doi:10.1016/j.jhydrol.2018.06.063

Wherry, S. A., Tesoriero, A. J., and Terziotti, S. (2021). Factors affecting nitrate concentrations in stream base flow. *Environ. Sci. Technol.* 55, 902–911. doi:10.1021/acs.est.0c02495

White, K. L., and Chaubey, I. (2005). Sensitivity analysis, calibration, and validations for a multisite and multivariable SWAT model 1. *JAWRA J. Am. Water Resour. Assoc.* 41, 1077–1089. doi:10.1111/j.1752-1688.2005.tb03786.x

Whittaker, J., Nyiraneza, J., Zebarth, B. J., Jiang, Y., and Burton, D. L. (2023). The effects of forage grasses and legumes on subsequent potato yield, nitrogen cycling, and soil properties. *Field Crops Res.* 290, 108747. doi:10.1016/j.fcr.2022.108747

Wyngaarden, S. L., Gaudin, A. C. M., Deen, W., and Martin, R. C. (2015). Expanding red clover (*Trifolium pratense*) usage in the corn–soy–wheat rotation. *Sustainability* 7, 15487–15509. doi:10.3390/su71115487

Yang, X., Liu, Q., Fu, G., He, Y., Luo, X., and Zheng, Z. (2016). Spatiotemporal patterns and source attribution of nitrogen load in a river basin with complex pollution sources. *Water Res.* 94, 187–199. doi:10.1016/j.watres.2016.02.040

Yang, X. M., Drury, C. F., Dan Reynolds, W. D., and Reeb, M. D. (2024). Legume cover crop as a primary nitrogen source in an organic crop rotation in Ontario, Canada: impacts on corn, soybean and winter wheat yields. *Agric.* 14, 19–31. doi:10.1007/s13165-023-00452-3

Zebarth, B., Drury, C., Tremblay, N., and Cambouris, A. (2009). Opportunities for improved fertilizer nitrogen management in production of arable crops in eastern Canada: a review. *Can. J. Soil Sci.* 89, 113–132. doi:10.4141/cjss07102

Zebarth, B. J., Danielescu, S., Nyiraneza, J., Ryan, M. C., Jiang, Y., Grimmett, M., et al. (2015). Controls on nitrate loading and implications for BMPs under intensive potato production systems in Prince Edward Island, Canada. *GROUND WATER Monit. R.* 35, 30–42. doi:10.1111/gwmr.12088

frontiers | Frontiers in Environmental Science

TYPE Original Research
PUBLISHED 27 October 2025
DOI 10.3389/fenvs.2025.1651136

Check for updates

OPEN ACCESS

EDITED BY
Jana Levison,
University of Guelph, Canada

REVIEWED BY
Andreas Bauwe,
University of Rostock, Germany
Ali Moridi,
Shahid Beheshti University, Iran

*CORRESPONDENCE
Junyu Qi,
junyuqi@umd.edu

RECEIVED 20 June 2025
ACCEPTED 08 October 2025
PUBLISHED 27 October 2025

CITATION
Qi J, Malone R, Liang K, Cole K, Emmett B, Moriasi D, Shahid MR and Castellano M (2025) Comparative modeling of nitrogen losses in a tile-drained watershed using SWAT model: uncertainty and calibration considerations. *Front. Environ. Sci.* 13:1651136. doi: 10.3389/fenvs.2025.1651136

COPYRIGHT
© 2025 Qi, Malone, Liang, Cole, Emmett, Moriasi, Shahid and Castellano. This is an open-access article distributed under the terms of the Creative Commons Attribution License (CC BY). The use, distribution or reproduction in other forums is permitted, provided the original author(s) and the copyright owner(s) are credited and that the original publication in this journal is cited, in accordance with accepted academic practice. No use, distribution or reproduction is permitted which does not comply with these terms.

Comparative modeling of nitrogen losses in a tile-drained watershed using SWAT model: uncertainty and calibration considerations

Junyu Qi[1]*, Robert Malone[2], Kang Liang[3], Kevin Cole[2], Bryan Emmett[2], Daniel Moriasi[2], Muhammad Rizwan Shahid[4] and Michael Castellano[4]

[1]Earth System Science Interdisciplinary Center, University of Maryland, College Park, MD, United States, [2]USDA-ARS National Laboratory for Agriculture and the Environment, Ames, IA, United States, [3]School of Natural Resource Sciences, North Dakota State University, Fargo, ND, United States, [4]Department of Agronomy, Iowa State University, Ames, IA, United States

Ecohydrological models are critical for understanding coupled hydrologic–biogeochemical processes in tile-drained watersheds and for assessing management options. Despite recent advances in SWAT's hydrological and biogeochemical processes, there has been limited evaluation of both the original and new tile drainage and nitrogen (N) modules. We therefore applied a comparative modeling approach in a typical Midwestern tile-drained watershed, evaluating eight configurations that vary tile-drainage module (original/new), tile parameter treatment (calibrated/default), and N module (original/new) to assess performance for N-loss simulation. Using daily streamflow and nitrate (NO_3^-) load records from three monitoring sites, we conducted calibration, validation, sensitivity analysis, and uncertainty assessment. Each configuration effectively reproduced daily and monthly dynamics, although high-flow and associated NO_3^- load peaks were underestimated. We found that the new tile module generally improved streamflow simulations, particularly under tile parameter calibration conditions, while the new N module consistently enhanced NO_3^- load simulations compared to the original module. Despite improvements in streamflow and NO_3^- loads with the new tile and N modules, the additional processes in the new N module can magnify uncertainty in N-gas-flux estimates when calibration observations are scarce. We recommend applying the new N module in conjunction with additional measurements—such as soil moisture and nitrous oxide (N_2O) fluxes—to constrain better N gas flux estimates beyond outlet NO_3^- load data. If such observations are unavailable, careful calibration with reasonable estimates may still help constrain soil N cycling and improve overall N budget accuracy.

KEYWORDS

tile drainage, nitrate leaching, nitrogen gas flux, SWAT, century

1 Introduction

Tile drainage is a prevalent agricultural practice in the Midwest USA, particularly in regions characterized by flat topography and clayey soils that impede natural drainage (Skaggs et al., 1994; Moriasi et al., 2012). This system, which involves the installation of subsurface drainage pipes, aims to enhance soil aeration and crop productivity by managing excess water levels (Skaggs et al., 1994; Schilling and Helmers, 2008). However, while tile drainage effectively alleviates waterlogging and improves agricultural yields, it also poses significant environmental challenges (Baker and Johnson, 1977; Logan et al., 1994). Tile drainage significantly influences streamflow and nutrient transport by modifying hydrological pathways and nutrient cycling processes (Li et al., 2010; Crossman et al., 2014). Compared to non-tiled systems, tile-drained watersheds exhibit distinct distributions of water balance components, including surface runoff, lateral flow, shallow groundwater flow, and aquifer recharge (Schilling and Helmers, 2008; May et al., 2023). Additionally, tile drainage affects water quality by reducing surface runoff and erosion, increasing soil aeration—which promotes mineralization but limits denitrification—and enhancing nitrate (NO_3^-) leaching into surface waters (Ikenberry et al., 2017; Ford et al., 2018).

In the Midwest, where intensive agriculture and heavy fertilizer use are common, the risk of NO_3^- leaching is significantly elevated (Dinnes et al., 2002). Research indicates that tile drainage systems accelerate NO_3^- transport from agricultural fields to surface waters, raising water quality and public health concerns (Zucker and Brown, 1998). Beyond nitrogen (N) loss to freshwater systems, tile drainage also influences N gas fluxes, including ammonia volatilization (NH_3) and fluxes of nitrous oxide (N_2O), nitric oxide (NO), and dinitrogen (N_2), contributing to environmental concerns (Gu et al., 2013; Nash et al., 2015). The interactions between tile drainage, N cycling, and hydrological processes are complex and influenced by factors such as soil moisture, temperature, and fertilizer application timing and rates (Burton et al., 2024). A comprehensive understanding of N loss dynamics in tile-drained systems is essential for developing effective management strategies that minimize environmental impacts while maintaining agricultural productivity (Awale et al., 2015). Key priorities include investigating the mechanisms driving NO_3^- leaching and N gas fluxes, their environmental consequences, and potential mitigation strategies (Hama-Aziz et al., 2017; Fabrizzi et al., 2024).

Ecohydrological models play a key role in simulating watershed hydrology, identifying and quantifying N-loss pathways, and guiding the development of effective BMPs for tile-drained systems (Moridi, 2019; Ghimire et al., 2020; Wang et al., 2021b; Yousefi and Moridi, 2022). By integrating hydrologic, soil, and nutrient-cycling processes, they capture the coupled hydrologic–biogeochemical interactions that govern N transport (Groffman et al., 2009; Wang et al., 2021a; Chen et al., 2024). The Soil and Water Assessment Tool (SWAT), a leading watershed-scale ecohydrological model, is widely used to test management scenarios under varying conditions and to pinpoint strategies that reduce N losses. (Arnold et al., 1998). By accurately simulating N transport and transformation in agricultural systems, SWAT provides valuable insights into the effects of land management decisions on water quality and soil health (Nazari Mejdar et al., 2023). The SWAT model's representation of tile drainage systems and nutrient cycling processes has undergone progressive development over time. Initially, a simple tile drainage module was introduced (Du et al., 2005; Du et al., 2006), followed by the development of a more physically-based tile drainage module (Moriasi et al., 2012; Moriasi et al., 2013b). Both modules have been successfully applied in field- and watershed-scale studies, enhancing SWAT's capability to simulate subsurface drainage dynamics. For N cycling, SWAT's original soil N mineralization algorithm integrates immobilization, making it a net mineralization model (Seligman and Keulen, 1980). The model also incorporates ammonia volatilization and nitrification (Reddy et al., 1979) and accounts for NO_3^- loss through denitrification (Neitsch et al., 2011). Acknowledging the close interconnection between soil carbon (C) and N cycling, recent advancements in the SWAT model have enhanced its capability to simulate soil organic C dynamics and N gas fluxes using the Century/DayCent model algorithms (Zhang et al., 2013; Yang et al., 2017; Liang et al., 2022; Liang et al., 2023; Tijjani et al., 2023; Tijjani et al., 2024). These enhancements could potentially increase SWAT's effectiveness in evaluating the impacts of tile drainage on N losses through various pathways, thereby improving its applicability in managing agricultural watersheds and conducting water quality studies.

Since model prediction uncertainty largely stems from input data, model structure, and model parameters (Refsgaard et al., 2006; Abbaspour K. et al., 2007; Abbaspour K. C. et al., 2007; Abbaspour, 2013), adding more biogeochemical processes can increase uncertainty. While incorporating extensive field observations is required to constrain parameters and reduce uncertainty (Herrera et al., 2022), large-scale data collection is often lacking. In such cases, soft/estimated data provide a practical alternative for improving model calibration (Arnold et al., 2015; Nelson et al., 2018). Despite advances in simulating tile drainage and N cycling, comparative evaluations of different SWAT versions remain scarce—particularly regarding their representation of N cycling within tile-drained systems. Comparative assessments of model versions and/or configurations offer several key benefits: 1) Identifying model strengths and weaknesses across different configurations, improving model selection for specific research and management objectives and/or applications (Kujawa et al., 2020). 2) Improving our understanding of model uncertainty, especially regarding how different representations of processes affect the predictions of flow pathways and N losses (Narsimlu et al., 2015). And 3) Refining model calibration approaches by determining the types and resolutions of data needed for accurate parameterization (Perrin et al., 2001). To date, no studies have simultaneously evaluated the new and original SWAT tile drainage and N modules, and comprehensive comparisons between the updated and original versions remain largely absent. Therefore, the main objective of this study, and a novel contribution, is a comparative modeling evaluation of SWAT's ability to simulate N losses in a typical Midwestern tile-drained watershed using eight configurations spanning tile drainage module (original/new), tile-parameter treatment (calibrated/default), and N module (original/new). Overall, we aimed to identify the key module structures and processes that most significantly contribute to prediction uncertainty, and to determine the additional observational and/or soft data needed to improve model calibration and accuracy.

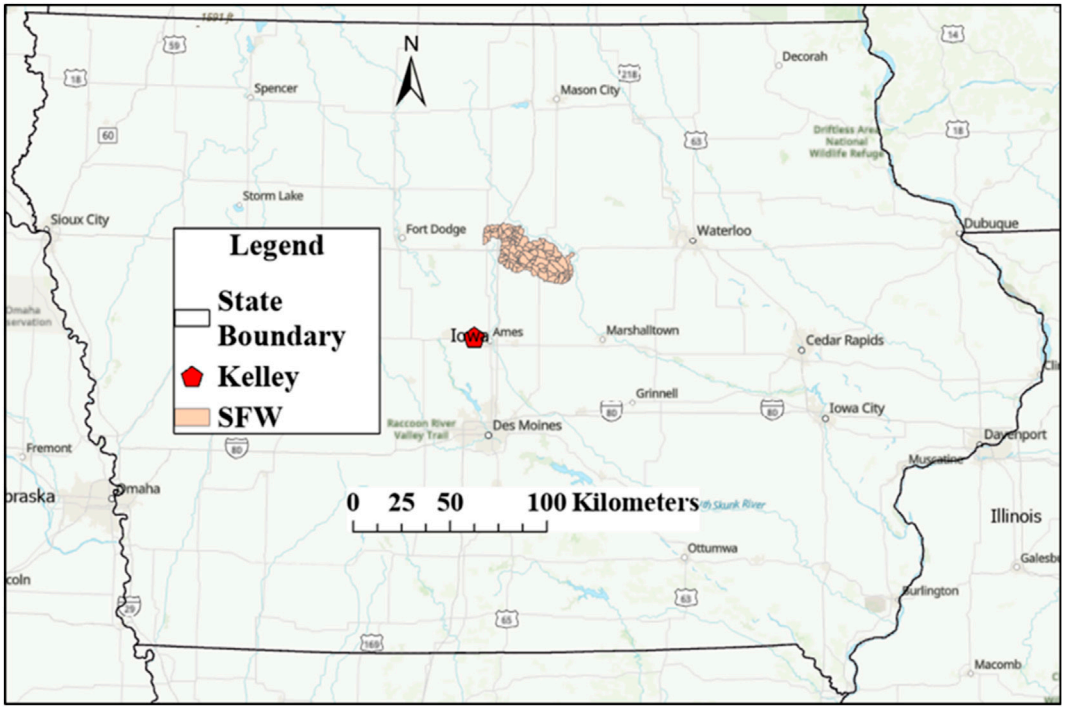


FIGURE 1
Location of the South Fork of the Iowa River Watershed (SFW) and the Kelley experimental site in Iowa.

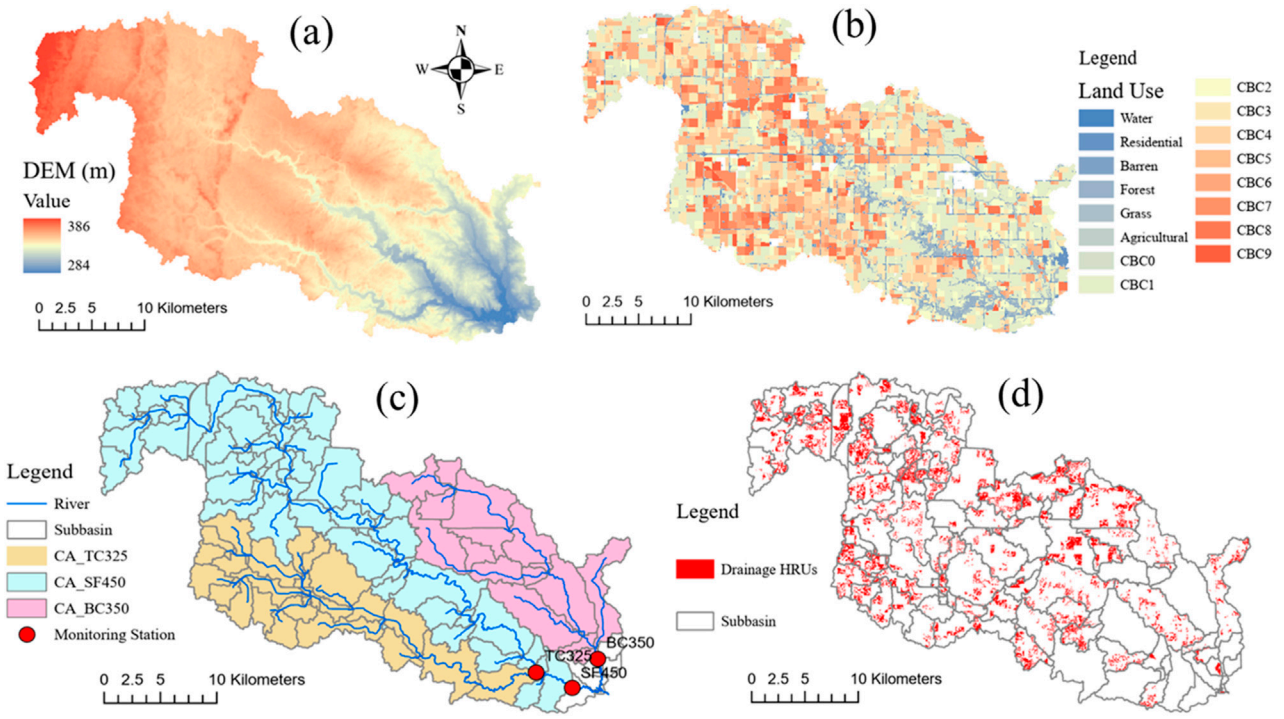


FIGURE 2
The South Fork of the Iowa River Watershed (SFW) maps of **(a)** DEM, **(b)** Land use (see Supplementary Table S1 for explanation), **(c)** Control areas of monitoring stations (see Supplementary Table S3), and **(d)** HRUs setup with tile drainage distributed in subbasins.

2 Materials and methods

2.1 Study area and data collection

The Iowa's South Fork of the Iowa River Watershed (SFW; Figure 1) encompasses an area of 775 km^2, including the tributaries of South Fork (containing Tipton Creek) and Beaver Creek (Figure 2c; Supplementary Table S3). It serves as a representative example of the Des Moines Lobe, the primary landform region in north-central Iowa. The terrain is relatively young, having developed approximately 10,000 years after the last glacial retreat, resulting in natural stream incision and alluvial valley formation primarily in the lower sections of the watershed (Figure 2a). The region's soils are highly productive, dominated by the Clarion-Nicollet-Webster soil association, which consists of a sequence of well-drained Typic Hapludolls, somewhat poorly drained Aquic Hapludolls, and poorly drained Typic Haplaquolls (Tomer et al., 2008b). The average annual precipitation in the SFW during the study period (2001–2018) was 894 mm, with approximately 62% falling during the growing season. The daily temperature can drop to as low as −13 °C in January and rise to as high as 29 °C in July (Bailey et al., 2022). Currently, corn and soybean rotations cover approximately 85% of the land area (Figure 2b), and animal feeding operations, primarily for swine, are prevalent, particularly in the Tipton Creek catchment (Tomer et al., 2008a).

Cropping rotations were determined using annual classified satellite data made available by the USDA National Agricultural Statistics Service (NASS). Ten years of NASS crop-cover data (2000–2009) were overlaid to identify dominant crop rotations occurring on crop lands in the watershed (Supplementary Table S1). Crop lands were identified using digitized agricultural field boundaries within the watershed obtained from local Farm Service Agency (USDA-FSA) offices. Non-crop land was dominantly hay and wetland forest, which were typically located in riparian valleys. Roadways, farmsteads, and towns were classified as residential land. The management schedules for corn and soybean are presented in Supplementary Table S2, based on the information provided by Tomer et al. (2008a).

Artificial drainage was installed to allow agricultural production, beginning more than 100 years ago. Although the location of individual drains in fields has not been mapped, previous studies have estimated that up to 80% of the watershed may be artificially drained (Green et al., 2006). Approximately 35% of the watershed's soils are classified as well-drained, but most are present on steeper slopes that are not farmed or are surrounded by poorly drained soils. The drainage districts tend to coincide with the watershed subbasins where poorly drained soils are common. This estimated value includes all of the soils that are not well drained and a few that are well drained but are surrounded by poorly drained soil.

Three stream gauging stations were utilized to provide long-term observations of daily streamflow and NO_3^- load (Supplementary Table S3). These stations monitor the three major tributaries: South Fork (USGS#05451210, near New Providence), Tipton Creek, and Beaver Creek (Figure 2c). Detailed methodologies for streamflow monitoring and water sampling can be found in Tomer et al. (2008b). Nitrate concentrations in our dataset were estimated using linear interpolation between samples collected at least weekly. Sampling included weekly point samples taken in the thalweg and automated composite samples collected during runoff events using a peristaltic pump. A computerized data logger controlled the composite sampler, triggering flow-paced sampling based on the site's rating curve, with one composite sample analyzed per event. The weekly and event-based sample results were integrated into a time-series management system, which applied linear interpolation to generate a 10-min resolution concentration record. This high-resolution time series was then used to calculate daily mean concentrations, which served as the basis for daily NO_3^- load estimates (i.e., concentration × daily total stream flow).

2.2 The development of tile drainage and N cycling processes for SWAT

The SWAT model is the most widely used watershed-scale ecohydrological model globally for evaluating water quantity and quality affected by land use and management practices. It can simulate tile drainage systems using both a simplified tile module and a more physically based module. While the SWAT model has been employed for tile drainage simulations, its application to NO_3^- loss through tile systems has rarely been reported. The model's original soil N mineralization processes were based on the PAPRAN model (Seligman and Keulen, 1980), which incorporates immobilization, making it a net mineralization algorithm. It considers fresh organic N and two humic N pools (active and stable). Mineralized N is directly added to the NO_3^- pool, while ammonium (NH_4^+) is introduced into the soil system through fertilization, which can then be lost *via* ammonia volatilization and nitrification, using methods developed by Reddy et al. (1979). The original SWAT model also calculates NO_3^- loss through denitrification, incorporating a threshold for nutrient cycling water factors necessary for denitrification to occur (Neitsch et al., 2011). To ascertain the amount of NO_3^- transported with water, the concentration of NO_3^- in the mobile water is first calculated, which is then multiplied by the volume of water moving through the tile drainage pathway to determine the mass of NO_3^- lost from the soil layer containing the tile.

Recognizing the close interconnection between soil C and N cycling processes, recent advancements in the SWAT model enhance its ability to simulate soil organic C dynamics and N gas fluxes (Zhang et al., 2013; Yang et al., 2017; Liang et al., 2022; Liang et al., 2023; Tijjani et al., 2023; Tijjani et al., 2024). These improvements make it more applicable for studies on water quality, soil health, and BMPs assessment. Below, we briefly outline these advancements and highlight how the updated model differs from the original version.

2.2.1 The new soil N module

The core algorithms for C and N cycling processes from the Century model (Parton et al., 1994; Izaurralde et al., 2006) have been modified and integrated into the SWAT model to enable a more comprehensive simulation of soil C and N dynamics within the soil profile (Figure 3) (Zhang et al., 2013). Furthermore, DayCent-based N_2O production and fluxes (Del Grosso et al., 2000; Parton et al., 2001) have also been incorporated into the SWAT model (Figure 3) (Yang et al., 2017). Thus, this enhanced SWAT model simulates N

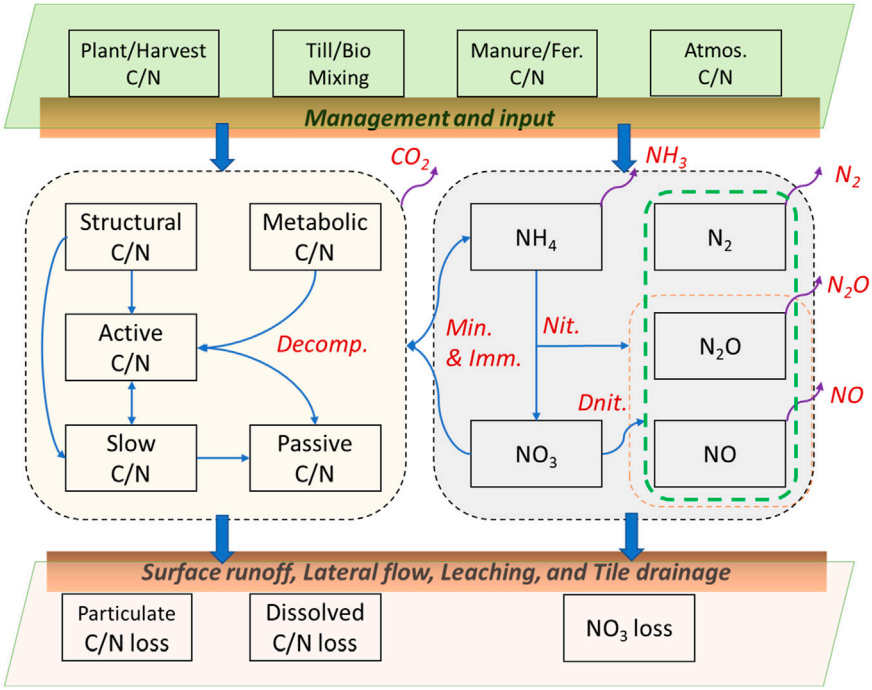


FIGURE 3
Schematic diagram for Century/DayCent-based soil organic C/N decomposition/mineralization/immobilization and N gas flux algorithms integrated in SWAT.

cycling processes within an agroecosystem by incorporating key steps like N fixation, mineralization, nitrification, denitrification, plant uptake, and leaching, allowing it to track the movement of N through different soil pools and between the atmosphere, vegetation, and soil, with a particular focus on the daily dynamics of these processes. Comprehensive details on soil C and N cycling processes and validation of the enhanced SWAT model are available in related studies (Parton et al., 1994; Izaurralde et al., 2006; Zhang et al., 2013; Liang et al., 2022; Liang et al., 2023; Tijjani et al., 2023; Luo et al., 2024; Tijjani et al., 2024).

In comparison to the original N module in SWAT (Neitsch et al., 2011), the new N module is significantly more complex, featuring additional parameters that simulate N_2O fluxes resulting from both nitrification and denitrification processes (Figure 3; Table 1). The new N module also simulates the production of NO and N_2 as byproducts of the nitrification and denitrification reaction sequence (Figure 3). Detailed information on N gas fluxes simulation refers to Yang et al. (2017).

2.2.2 Tile drainage modules

In SWAT, tile drainage can be calculated using two modules (Guo et al., 2018). The original tile drainage algorithm calculates tile flow as a function of water table depth, tile depth, and the time required to drain the soil to field capacity, assuming that the tile systems have equidistant tile spacing and size (Table 1) (Arnold et al., 1999; Du et al., 2005; Green et al., 2006). The new tile drainage algorithm computes tile flow using Hooghoudt's steady state and Kirkham (van Schilfgaarde et al., 1957) tile drain equations that are a function of water table depth, tile drain depth, size, and spacing (Table 1), which are also used in the widely used DRAINMOD model (Skaggs et al., 2012). Previous studies incorporated and tested these equations within SWAT (Moriasi D. et al., 2007; Moriasi et al., 2012). These two methods were integrated with the "tip-bucket" soil water movement algorithm to simulate soil water balance for the drainage-based soil systems. Both methods for calculating tile drainage have been thoroughly tested against field and watershed scale drainage observations (Green et al., 2006; Moriasi et al., 2013b). Few studies have successfully simulated NO_3^- losses through tile drainage using the SWAT model (Schilling and Wolter, 2009; Moriasi et al., 2013a; Moriasi et al., 2013b; Gassman et al., 2014; Ikenberry et al., 2017).

2.3 Model setup, calibration, sensitivity and uncertainty analysis

Using a 10 m grid Digital Elevation Model (DEM), the SFW was divided into 115 subbasins, which were further segmented into 385 hydrologic response units (HRUs) based on the SSURGO database, a field-level land use map, and two slope categories (0%–2% and >2%). Typical management schedules for corn–soybean rotations were derived from the referenced cropland management dataset (Tomer et al., 2008a) and supplemented with estimates from Iowa State University Extension and Outreach. For instance, before the corn year, 75% of the total annual manure application was applied in the fall, while the remaining 25% was applied in the spring of the corn year (Supplementary Table S2). The model utilized NLDAS2 weather data for its inputs (Xia et al., 2012; Qi et al., 2019c). The presence of subsurface drains was assumed for all areas with hydric soils, with

TABLE 1 Model parameters considered in model calibration.

Model	Parameter	Default/Used	Explanation
Hydrologic processes	ICN.bsn	1[a]	Daily curve number calculation method
	CNCOEF.bsn	1	Plant ET curve number coefficient
	CN2.mgt	varied/varied	Initial SCS CN II value
	SURLAG.hru	2	Surface runoff lag time in the HRU [days]
	ESCO.hru	0.95	Soil evaporation compensation factor
	EPCO.hru	1	Plant uptake compensation factor
	GWQMN.gw	1,000	Threshold depth of water for return flow to occur [mm]
	GW_REVAP.gw	0.02	Groundwater "revap" coefficient
	REVAPMN.gw	750	Threshold depth of water for "revap" to occur [mm]
	ALPHA_BF.gw	0.048	Baseflow alpha factor [days]
	GW_DELAY.gw	31	Groundwater delay [days]
Original tile module	GDRAIN.mgt	96	Drain tile lag time [hours]
	TDRAIN.mgt	24	Time to drain soil to field capacity [hours]
	DDRAIN.mgt	1,000	Depth to the sub-surface drain [mm]
	DEP_IMP.hru	2,500	Depth to impervious layer [mm]
	ITDRN.bsn	0[a]	Tile drainage equations flag
	IWTDN.bsn	0[a]	Water table depth algorithms flag
New tile module	LATKSATF.bsn	1.4	Multiplication factor to determine lateral ksat
	PC_BSN.bsn	0	Pump capacity [mm h]
	DRAIN_CO.bsn	35	Drainage coefficient [mm d]
	SDRAIN.bsn	12,000	Distance between two drain or tile tubes [mm]
	RE_BSN.bsn	20	Effective radius of drains [mm]
	DDRAIN.mgt	1,000	Depth to the sub-surface drain [mm]
	DEP_IMP.hru	2,500	Depth to impervious layer [mm]
	ITDRN.bsn	1[a]	Tile drainage equations flag
	IWTDN.bsn	1[a]	Water table depth algorithms flag
	ISMAX.bsn	1[a]	Max depressional storage code
Original N module	RSDCO_PL.plant	0.05	Residue decomposition coefficient
	SDNCO.bsn	1.1	Denitrification threshold water content
	CDN.bsn	1.4	Denitrification exponential rate coefficient
	CMN.bsn	0.0003	Rate factor for humus mineralization of active organic N
	N_UPDIS.bsn	0.2	Nitrogen percolation coefficient
	NPERCO.bsn	20	Nitrogen uptake distribution parameter
New N module	CMFf1[b]	1	Multiplication factor for CMF for the first soil layer
	CMFf2[b]	1	Multiplication factor for CMF for other soil layers
	FHSf[b]	1	Multiplication factor for FHS
	MaxRate[c]	0.15	Max fraction of ammonia nitrified during nitrification
	wfps_adj[c]	1.0	Adjustment on inflection point for water-filled pore space effect on denitrification curve

(Continued on following page)

TABLE 1 (*Continued*) Model parameters considered in model calibration.

Model	Parameter	Default/Used	Explanation
	NPERCO.bsn	0.2	Nitrogen percolation coefficient
	N_UPDIS.bsn	20	Nitrogen uptake distribution parameter

[a]Parameters for setup different modules and not changed during calibration.
[b]Newly introduced parameters (see Supplementary Material).
[c]Parameters described in Yang et al. (2017).

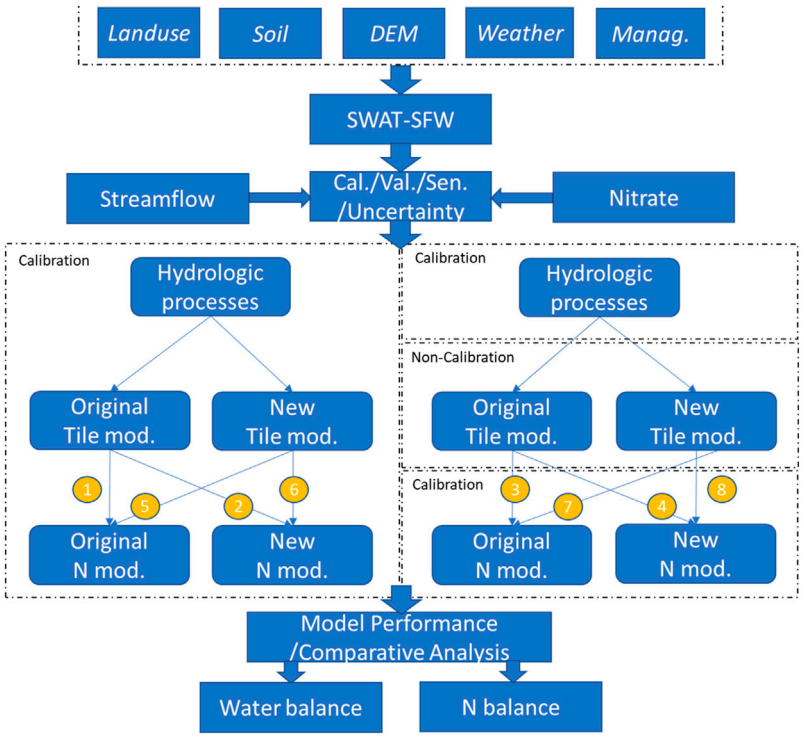


FIGURE 4
Flowchart of the study design, including SWAT setup; calibration and validation; sensitivity and uncertainty analyses; and the eight modeling configurations. The yellow circles represent the scenario numbers (Tables 2–5).

adjacent land also included due to the practice of draining a field if any of its interior area has poorly drained soils (Bailey et al., 2022). Therefore, an HRU was designated as a drain if it is covered by hydric soil (Figure 2d). The Penman-Monteith method was employed to estimate potential evapotranspiration, while the variable storage routing method was used for in-stream routing. Annual average wet and dry N deposition input was derived from the Clean Air Status and Trends Network (CASTNET).

The observed daily streamflow and NO_3^- load were evenly divided into calibration and validation periods (Supplementary Table S3). Before the calibration period, we used a 1-year (2000) warm-up period to initialize the model. Selected parameters for model calibration are shown in Table 1. We considered previous studies in the same watershed when selecting hydrologic, tile drainage, and soil N cycling parameters (Green et al., 2006; Moriasi et al., 2012; Moriasi et al., 2013b; Yang et al., 2017; Bailey et al., 2022). We employed a multi-station procedure to calibrate the streamflow and NO_3^- loads. The first step was to calibrate the streamflow of three stations, which is the key for the following water quality calibration. Following discharge calibration, the NO_3^- load of three stations was calibrated (Figure 4).

The Sequential Uncertainty Fitting algorithm version 2 (SUFI-2) method in SWAT-CUP (Abbaspour K. et al., 2007) was used to conduct calibration for daily flow rate and NO_3^- loads. It was also used to conduct parameter sensitivity and uncertainty analysis. Model performance was assessed according to percent bias (Pbias; Equation 1), coefficient of determination (R^2; Equation 2), and Kling-Gupta efficiencies (KGE; Equation 3) (Knoben et al., 2019), given as:

$$Pbias = 100 \times \frac{\sum_{i=1}^{N}(P_i - O_i)}{\sum_{i=1}^{N} O_i} \quad (1)$$

$$R^2 = \left(\frac{\sum_{i=1}^{n}\left(O_i - O_{avg}\right) \cdot \left(P_i - P_{avg}\right)}{\left[\sum_{i=1}^{n}\left(O_i - O_{avg}\right)^2 \cdot \sum_{i=1}^{n}\left(P_i - P_{avg}\right)^2\right]^{0.5}} \right)^2 \quad (2)$$

$$KGE = 1 - \sqrt{(r-1)^2 + (\alpha - 1)^2 + (\beta - 1)^2} \quad (3)$$

where O_i and P_i are the observed and modeled data, O_{avg} and P_{avg} their averages, r the linear correlation between observed and modeled data, α the flow variability error, and β bias term. Model performance criteria were established based on the guidelines provided by Moriasi DN. et al. (2007), operating under the assumption that the evaluation criteria for Nash-Sutcliffe Efficiency (*NSE*) are also applicable to R^2 and *KGE*. *KGE* provides a more comprehensive assessment of model performance by evaluating not only the correlation between observed and simulated values but also accounting for the variability and bias in the simulations. Unlike *NSE*, which can be overly sensitive to outliers and can yield misleading results if the mean observed value is low, *KGE* incorporates multiple aspects of model performance. This makes *KGE* a more robust metric, particularly in complex hydrological systems where various factors can influence model outputs. The *KGE* was used as the objective function for calibrating daily streamflow and NO_3^- load, incorporating data from three monitoring stations with equal weighting in the function.

Parameter sensitivities were determined using the following multiple regression equation, based on results running the SUFI-2 procedure of SWAT-CUP multiple times, given as (Equation 4):

$$g = \alpha + \sum_{i=1}^{m} \beta_i \cdot b_i \quad (4)$$

where g is the objective function value, α and β_i are regression coefficients, b_i is the calibration parameter, and m is the number of parameters considered. *KGE* was used as the objective function value. The Student's t-test was used to quantify the statistical significance of each parameter, with a p-value <0.05 indicating a parameter as sensitive in the present study. The global sensitivity analysis approach estimates the change in the objective function resulting from changes in each parameter while all other parameters are changing (Abbaspour K. et al., 2007), and as a result, it does not provide an absolute measure of the sensitivity but rather the relative sensitivity.

Prediction uncertainty was estimated through the SUFI-2 procedure (Abbaspour K. et al., 2007). In SUFI-2, the uncertainties in model structure, parameters, and input data are not separately estimated but are attributed as total model uncertainty to the parameters (Abbaspour K. et al., 2007). The Latin hypercube sampling method is used in SUFI-2 for vast parameter value combinations, and resultant model simulations are used to calculate the percentage of measured data bracketed by the 95 Percent Prediction Uncertainty (often referred to as 95PPU), which is measured by the p-factor. The range of the p-factor varies from 0.0 to 1.0, with values close to 1.0 (all observations bracketed by the prediction uncertainty) indicating very strong model performance and small prediction uncertainty. The r-factor is the average thickness of the 95PPU bands divided by the standard deviation of the observed data. The r-factor varying between 0 and 1.0 indicates acceptable prediction uncertainty estimation (Abbaspour K. et al., 2007; Abbaspour, 2013). In general, a trade-off between p-factor and r-factor exists for model uncertainty evaluation. A larger p-factor can be achieved at the expense of a larger r-factor, and *vice versa*. A model with a balance between the two factors can provide acceptable prediction uncertainty (Qi et al., 2019b).

2.4 Comparison of model configurations

We considered eight model configurations, which included: original and new tile drainage modules × calibration and non-calibration of tile drainage modules × original N module and new N module. Figure 4 illustrates the design of the eight model configurations and the step-wise calibration procedure. Here, we aimed to evaluate model performance under scenarios with calibrated and non-calibrated tile drainage parameters (Table 1), reflecting practical conditions where tile parameters may or may not be accurately known (Green et al., 2006; Moriasi et al., 2012; Schilling et al., 2019). For each of the eight model configurations, we independently calibrated the same set of parameters (Table 1). We then analyzed the eight simulations for water and soil N balance at the watershed scale and discussed the results as compared with previous studies. We calculated the average, standard deviation (SD), and coefficient of variation (CV) for water and N balance components across eight modeling simulations. The CV is a useful statistic that measures the relative variability of model outputs by comparing the standard deviation to the mean. The CV can help identify which processes exhibit greater variability across different model configurations (Butts et al., 2004). By assessing the CV of different outputs, we can prioritize areas that may need further investigation or refinement in model structure and parameterization.

3 Results and discussions

3.1 Model performance evaluation

The performance evaluation metrics for daily streamflow and NO_3^- load across the eight model configurations at the three outlets are summarized in Tables 2 and 3. The best-fit parameters for the eight model configurations are presented in Supplementary Tables S4 and S5. For daily streamflow simulations, R^2 values ranged from 0.40 to 0.68, and *KGE* values from 0.46 to 0.80 during the calibration period, with *Pbias* between −7.7% and 19.6% across all eight model configurations and three stations. During the validation period, R^2 values ranged from 0.49 to 0.68, *KGE* values from 0.51 to 0.77, and *Pbias* ranged between −27.2% and −11.4%. Overall, the model satisfactorily predicted daily streamflow across all configurations, though it generally underestimated streamflow during the validation period. For daily NO_3^- load simulations, during the calibration period, R^2 and *KGE* values ranged from 0.33 to 0.57 and 0.39 to 0.60, respectively, with *Pbias* between −52.7% and −14.3%. During validation, the performance decreased, with R^2 values from 0.21 to 0.48, *KGE* values from 0.05 to 0.58, and *Pbias* values ranging between −45.4% and −7.6% across all configurations and stations (Table 3). All models consistently tended to underestimate daily NO_3^- loads. Nevertheless, the new N module typically delivered superior performance over the original N module in predicting daily NO_3^- loads, regardless of tile module configuration (Table 3).

We also evaluated daily and monthly simulations of streamflow and NO_3^- load for the combined calibration and validation periods (Supplementary Tables S6 and S7). Overall, daily streamflow showed R^2 of 0.52–0.68, *KGE* of 0.63–0.79, and *Pbias* of −15% to −2%, while

TABLE 2 Model performance evaluation for daily streamflow at three monitoring stations.

	Model configuration			Calibration									Validation								
				BC350			SF450			TC325			BC350			SF450			TC325		
#	Tile	Cali. Tile	N Mod	Pbias	R^2	KGE	Pbias	R^2	KGE	Pbias	R^2	KGE	Pbias	R^2	KGE	Pbias	R^2	KGE	Pbias	R^2	KGE
1	Ori	Yes	Ori	13.2	0.58	0.69	−3.6	0.57	0.76	15.8	0.41	0.48	−23.5	0.51	0.57	−17.3	0.58	0.70	−15.6	0.58	0.68
2			New	14.5	0.58	0.69	−1.8	0.57	0.75	18.2	0.40	0.46	−21.5	0.50	0.57	−14.7	0.57	0.71	−14.1	0.57	0.68
3		No	Ori	9.0	0.58	0.67	−7.7	0.68	0.79	7.8	0.51	0.66	−27.2	0.50	0.51	−20.9	0.68	0.70	−17.6	0.67	0.75
4			New	10.4	0.57	0.67	−6.0	0.67	0.79	9.4	0.50	0.65	−25.5	0.49	0.52	−18.9	0.68	0.72	−16.4	0.66	0.75
5	New	Yes	Ori	14.9	0.62	0.74	−1.8	0.65	0.79	16.8	0.52	0.48	−20.5	0.52	0.62	−13.8	0.65	0.76	−13.8	0.67	0.69
6			New	16.0	0.61	0.72	−0.1	0.64	0.79	19.1	0.51	0.46	−18.9	0.52	0.63	−11.7	0.65	0.77	−12.5	0.66	0.69
7		No	Ori	15.0	0.60	0.72	−1.5	0.64	0.80	17.7	0.49	0.50	−20.2	0.50	0.60	−13.6	0.65	0.76	−13.6	0.66	0.72
8			New	16.4	0.60	0.71	0.2	0.63	0.79	19.6	0.49	0.49	−18.7	0.50	0.60	−11.4	0.64	0.77	−12.4	0.64	0.72

Pbias values (%) indicate the model bias, with negative values representing underestimation and positive values representing overestimation.

10.3389/fenvs.2025.1651136

TABLE 3 Model performance evaluation for daily NO_3^- load at three monitoring stations.

	Model configuration			Calibration									Validation								
				BC350			SF450			TC325			BC350			SF450			TC325		
#	Tile	Cali. Tile	N Mod	Pbias	R^2	KGE	Pbias	R^2	KGE	Pbias	R^2	KGE	Pbias	R^2	KGE	Pbias	R^2	KGE	Pbias	R^2	KGE
1	Ori	Yes	Ori	−25.8	0.33	0.45	−19.6	0.52	0.47	−43.9	0.52	0.47	−34.1	0.35	0.42	−34.8	0.41	0.48	−16.5	0.41	0.05
2			New	−19.4	0.38	0.54	−20.5	0.54	0.59	−44.9	0.57	0.47	−30.2	0.42	0.51	−35.7	0.43	0.50	−14.5	0.44	0.23
3		No	Ori	−17.6	0.35	0.50	−14.7	0.51	0.51	−45.9	0.48	0.45	−37.1	0.28	0.40	−40.2	0.21	0.32	−10.3	0.45	0.13
4			New	−14.3	0.38	0.55	−15.2	0.56	0.60	−45.5	0.55	0.46	−31.2	0.34	0.48	−33.7	0.29	0.42	−7.6	0.48	0.19
5	New	Yes	Ori	−28.3	0.34	0.45	−27.8	0.48	0.49	−52.7	0.47	0.39	−38.8	0.39	0.45	−45.4	0.33	0.36	−24.5	0.42	0.16
6			New	−16.6	0.40	0.54	−22.2	0.53	0.59	−46.8	0.53	0.44	−25.1	0.47	0.58	−34.3	0.41	0.48	−15.2	0.47	0.21
7		No	Ori	−26.3	0.34	0.44	−23.8	0.48	0.47	−49.4	0.47	0.41	−35.5	0.39	0.46	−39.9	0.38	0.45	−21.5	0.42	0.11
8			New	−19.6	0.40	0.55	−21.9	0.52	0.58	−47.6	0.54	0.43	−28.0	0.45	0.56	−32.1	0.42	0.52	−15.6	0.46	0.22

Pbias values (%) indicate the model bias, with negative values representing underestimation and positive values representing overestimation.

10.3389/fenvs.2025.1651136

TABLE 4 Annual average water budgets (in mm H_2O) in the south fork of the iowa river watershed (SFW) for the eight model configurations over 2001–2018.

#	Tile	Cali. Tile	N Mod	PCP	PET	ET	SurQ	LatQ	GwQ	DrainQ	Recharge	Yield
1	Ori	Yes	Ori. N	894	1,137	602	46	4	61	186	66	301
2			New N	894	1,137	595	44	4	63	194	67	308
3		No	Ori. N	894	1,137	613	106	14	48	119	51	288
4			New N	894	1,137	607	103	14	49	125	53	294
5	New	Yes	Ori. N	894	1,137	591	110	3	52	142	55	311
6			New N	894	1,137	587	108	3	53	147	57	315
7		No	Ori. N	894	1,137	591	96	3	55	156	58	312
8			New N	894	1,137	586	94	3	56	160	59	316
			AVE	894	1,137	597	88	6	55	154	58	306
			SD	0	0	9	26	5	5	25	5	9
			CV	0	0	0.02	0.29	0.73	0.09	0.16	0.09	0.03
Green 2006 (1995–2004)				768	1,191	569	38	7	11	136		192
Bailey 2022 (2002–2012)				889		601	145	22	7	142	123	316

Abbreviations: PCP, precipitation; SurQ, surface runoff; LatQ, lateral flow; GwQ, groundwater flow; DrainQ; tile drainage; Recharge indicates soil water percolation to aquifer.

daily NO_3^- load had R^2 of 0.32–0.47, *KGE* of 0.18–0.57, and *Pbias* of −30% to −12% across all configurations and stations. Monthly simulations generally yielded better model performance compared to daily simulations across all configurations and stations. For monthly streamflow, R^2 and *KGE* values exceeded 0.69 and 0.79, respectively, with *Pbias* values ranging between −15% and −2%. Monthly NO_3^- load had R^2 values ranging from 0.37 to 0.59, *KGE* values from 0.32 to 0.63, and *Pbias* from −30% to −14%. According to the performance criteria recommended by Moriasi DN. et al. (2007) for monthly simulations (assumed applicable for R^2 and *KGE*), the majority of simulations achieved satisfactory results.

Overall, the new tile module improved daily and monthly streamflow simulations over the original, especially under the tile parameter calibration condition (Supplementary Tables S6 and S7). In addition, we did not observe a clear improvement in model performance when calibrating additional tile parameters for either the original or the new tile modules. In fact, in many cases, the original tile model without calibrated parameters provided better simulations of daily streamflow. This may be caused by the fact that adding more tile parameters to the hydrological parameter set increases model complexity, making it more difficult for auto-calibration to consistently capture the global optimum of the objective function (*KGE* in our case). It is recommended to maintain a balance between the number of parameters included and computational cost when using semi-distributed hydrological models such as SWAT (including more parameters does not necessarily lead to better results), and observed parameters should be utilized whenever possible.

Previous studies using SWAT to simulate daily streamflow highlighted persistent challenges in accurately capturing peak-flow events (Qi et al., 2019b; Kumar et al., 2024). Underestimation of streamflow during high-flow conditions directly contributes to the underestimation of NO_3^- loads (Qi et al., 2019a). Another critical reason for underestimating NO_3^- loads could be SWAT's simplified representation of NO_3^- transport through tile drainage systems. Unlike the explicit numerical approach used by models such as DRAINMOD, which solves the advective-dispersive-reactive equation (Helwig et al., 2002), SWAT's simplified coupling of soil water flow with NO_3^- leaching may require further refinement. Additionally, the model performance at the TC325 station for NO_3^- loads was consistently lower compared to the other two stations. This discrepancy is likely related to the significant presence of animal feeding operations, particularly swine production, within the Tipton Creek area (Tomer et al., 2008a; Tomer et al., 2008b). Due to insufficient information, the temporal and spatial patterns of manure application were not adequately represented in the model's fertilization operations (Figure 2).

3.2 Model sensitivity and uncertainty analysis

We selected the most sensitive parameters affecting daily streamflow and NO_3^- load at the watershed outlets based on findings from previous studies for model calibration (Green et al., 2006; Moriasi et al., 2012; Moriasi et al., 2013a; Moriasi et al., 2013b). These parameters were then used for further sensitivity analysis, as summarized in Table 1. Sensitivity was assessed using p-values from Student's t-tests, with the results presented in Supplementary Tables S8 and S9.

For daily streamflow, the most sensitive parameters in the original tile module without tile parameter calibration were primarily related to surface runoff and soil moisture (such as *SURLAG*, *ESCO*, *EPCO*, and *CN2*; see Table 1 for explanation; Supplementary Table S8). Although groundwater parameters were included in the calibration process, they did not show significant sensitivity to daily streamflow under this configuration. However, when tile parameters were calibrated, the

TABLE 5 Annual nitrogen budgets (kg N ha^{-1}) for the entire south fork of the iowa river watershed (SFW) under eight model configurations (2001–2018); values in brackets represent nitrification gas fluxes.

#	Tile	Cali. Tile	N Mod	FerMN	FerON	Atm	Rsd	Fix	NetMin	Uptake	Dnit	Vol	N_2O	NO	N_2	Drain	SurQ	LatQ	Leach	GwQ	ONloss	YldN	ΔMN	ΔTN
1	Ori	Yes	Ori. N	90	55	21	79	79	106	210	29	1	—	—	—	25	1	1	9	0.3	10	131	−60	37
2			New N	90	55	21	102	52	146	191	24	3	10 (0.8)	6 (2)	10	25	1	1	8	0.2	1	142	1	12
3		No	Ori. N	90	55	21	92	70	141	164	29	1	—	—	—	22	3	2	8	0.2	18	142	21	9
4			New N	90	55	21	128	43	181	278	13	1	6 (1)	5 (2.7)	6	23	3	2	8	0.2	1	150	−41	3
5	New	Yes	Ori. N	90	55	21	99	61	161	237	33	1	—	—	—	27	2	1	10	0.4	20	138	−39	−6
6			New N	90	55	21	119	42	178	220	27	2	12 (0.9)	7 (2.5)	11	23	3	1	8	0.3	1	142	2	−4
7		No	Ori. N	90	55	21	96	61	159	233	33	1	—	—	—	30	2	1	10	0.4	16	137	−40	−3
8			New N	90	55	21	113	44	160	210	19	2	9 (0.9)	6 (2.4)	8	24	3	1	8	0.3	1	140	2	9
			Ave	90	55	21	103	56	154	218	26	2	9	6	9	25	2	1	9	0.3	9	140	−19	7
			SD	—	—	—	15	13	22	31	7	0	2	1	2	2	1	1	1	0.1	8	5	27	13
			CV	—	—	—	0.1	0.2	0.1	0.1	0.3	0.3	0.2	0.1	0.2	0.1	0.3	0.6	0.1	0.3	0.9	0.0	−1.4	1.8
Li 2008 (2002–2005)				132	—	—	—	127	120	329	9	—	—	—	—	45	—	—	—	—	—	—	−3	—
Gillette 2018 (2002–2009)				117	—	—	—	98	117	267	17	—	7	—	—	48	—	—	—	—	—	—	−2	—

Abbreviations: FerMN, mineral N fertilization; FerON, organic N fertilization; Atm, atmospheric deposition; Rsd, residue organic N; Fix, organic N fixation by legume; NetMin, net mineralization; Uptake, plant uptake; Dnit, denitrification; Vol, volatilization; N_2O and NO, N_2O and NO, fluxes from both nitrification and denitrification; N_2, N_2 flux from denitrification; Drain, NO_3^- loss *via* drainage; SurQ, NO_3^- loss *via* surface runoff; LatQ; NO_3^- loss *via* lateral flow; Leach; NO_3^- leaching to aquifer; GwQ, NO_3^- contribution to stream by groundwater flow; ONloss, organic N loss *via* surface runoff; YldN, N removed in yield; ΔMN (soil mineral N change) = fertilized mineral N + atmospheric deposition N + net mineralization N–uptake N–denitrification (when using the ori. N module) – (N_2O + N_2+NO; when using the new N module) – volatilization N–drainage N–surface runoff N–lateral flow N–leaching N; ΔON (total soil N change) = fertilized mineral N + fertilized organic N + atmospheric deposition N + organic fixation N–denitrification (when using the ori. N module) – (N_2O + N_2+NO; when using the new N module) – volatilization N–drainage N–surface runoff N–lateral flow N–leaching N–organic N loss–crop yield N.

10.3389/fenvs.2025.1651136

most sensitive parameters shifted to include both groundwater (such as *GWQMN*, *GW_REVAP*, and *REVAPMN*) and tile drainage (such as *DEP_IMP* and *GDRAIN*) parameters (Tables 1; Supplementary Table S8). A similar pattern was observed in the new tile drainage module, suggesting that calibrating tile parameters increases the sensitivity of groundwater parameters to streamflow simulation. Despite these shifts in sensitivity, the overall model performance did not improve when tile parameters were calibrated compared to configurations without tile calibration (Table 2). This could be due to the relatively low contribution of groundwater discharge to streamflow compared to surface runoff and drainage flow in the SFW (Supplementary Table S12).

Regarding the daily NO_3^- load, the parameters found to be most sensitive for the original N module were primarily associated with denitrification processes (*CDN*) and mineralization processes (*CMN*) (Tables 1; Supplementary Table S9). In contrast, parameters controlling organic matter decomposition rates and the initial fraction of fresh humus (*FHS*)—notably *CMFm2* and *fFHS* (Table 1; Supplementary Table S9)—showed high sensitivity for the new N module. Additionally, the parameter governing denitrification processes (i.e., *wfps_adj)* was also very sensitive (Table 3). Upon examination of the denitrification-related parameters (Supplementary Tables S4 and S5), we found that low values of *wfps_adj* were associated with increased denitrification rates for the new N module (A detailed discussion of this parameter is provided in the Supplementary Material).

Supplementary Tables S10 and S11 present the p-factor and r-factor values for the estimated 95PPU bands of daily streamflow and NO_3^- fluxes across the eight model configurations. The p-factor values showed that the 95PPU bands captured 27%–52% of observed daily streamflow and only 14%–34% of observed NO_3^- loads. The r-factor ranged from 0.32 to 0.59 for observed daily streamflow and from 0.26 to 0.60 for observed NO_3^- loads. Overall, the low p-factor values indicated a high level of uncertainty in the predictions of both daily streamflow and NO_3^- load across three monitoring stations. This overall decrease in p-factor from streamflow to NO_3^- load suggested that modeling uncertainty was greater for NO_3^- load than for streamflow simulation. This result was expected, as streamflow simulation was primarily influenced by hydrological processes, whereas NO_3^- simulation depended on both hydrological and biogeochemical processes. The added complexity of N cycling introduced greater challenges, contributing to the lower p-factor values observed for NO_3^- predictions compared to streamflow.

3.3 Water balance assessment across model configurations

Table 4 shows the annual water budget for the eight model configurations in the SFW. Average, SD, and CV were also calculated for the water budget across eight model configurations. The average annual precipitation in the watershed from 2001 to 2018 was 894 mm, while the average annual potential evapotranspiration (PET) was 1,137 mm. Actual evapotranspiration (ET) ranged from 586 to 613 mm, with an average of 597 mm, which represents about 67% of the average annual precipitation (Supplementary Table S12). The total water yield (= surface runoff + lateral flow + groundwater flow + drainage flow) accounted for approximately 34% of the average annual precipitation (Supplementary Table S12). Surface runoff varied between 44 and 110 mm, averaging 88 mm, which constitutes about 31% of the total water yield. Baseflow ranged from 48 to 63 mm, with an average of 55 mm, making up about 18% of the total water yield (Supplementary Table S12). Drainage flow ranged from 119 to 194 mm, averaging 154 mm, which accounts for approximately 50% of the total water yield (Supplementary Table S12). Lateral flow ranged from 3 to 14 mm, averaging 6 mm, making up about only 2% of the total water yield (Supplementary Table S12).

Lateral flow showed the highest coefficient of variation (CV = 0.7), although its magnitude was an order of magnitude lower than that of surface runoff and drainage flow. We also observed significantly greater variation between calibration and non-calibration model configurations for the original tile module compared to the new tile module for both surface runoff and drainage flow. When calibrated, the original tile module generated considerably less surface runoff and more drainage flow than in the non-calibrated condition, whereas the new tile drainage module showed similar results regardless of calibration. Interestingly, the non-calibrated original tile module produced results more comparable to the new tile module under both calibration and non-calibration conditions. These results suggest that obtaining consistent and reliable results necessitates more detailed information about actual field conditions, as relying solely on parameter calibration without accurate tile data may lead to a skewed water budget for tile drainage systems.

Table 4 also shows the comparison between previous studies and this study on water budget, and Supplementary Table S12 shows important hydrological component ratios at the SFW. It should be noted that the study area of Bailey et al. (2022), which used SF450 as the outlet, was smaller than the area considered in this study (Figure 2). This study had close annual precipitation of 894 mm to Bailey et al. (2022)(889 mm) both of which were higher than that of Green et al. (2006) (768 mm) due to different study periods. Accordingly, the ET values were also close between this study and that of Bailey et al. (2022) (601 mm) and greater than that of Green et al. (2006) (569 mm). Total water yield—comprising surface runoff, lateral flow, groundwater flow, and tile drainage flow—accounted for 32%–35% of annual precipitation. This figure surpassed the 25% reported by Green et al. (2006) but fell short of the 36% noted by Bailey et al. (2022). Surface runoff represented 5%–12% of annual precipitation, higher than the 5% documented by Green et al. (2006) but lower than the 16% observed by Bailey et al. (2022). A similar trend was seen in the contribution of surface runoff to total water yield, with our study accounting for 14%–37%, most of which were greater than the 20% cited by Green et al. (2006) and less than the 46% reported by Bailey et al. (2022).

Total subsurface flow, which includes lateral flow, groundwater flow, and tile drainage flow, accounted for 20%–29% of annual precipitation in this study, most of which were higher than the 20% reported by Green et al. (2006) and the 19% noted by Bailey et al. (2022). The increase was primarily due to the groundwater discharge simulated in this study, which constituted 17%–20% of total water yield, significantly higher than the 6% from Green et al. (2006) and 2% from Bailey et al. (2022). In contrast, the lateral flow represented only 1%–5% of total water yield, most of which was less than the 4% from Green et al. (2006) and 7% from Bailey et al. (2022). This made

lateral flow the smallest contributor to total water yields in both this study and Green et al. (2006), whereas Bailey et al. (2022) identified groundwater flow as the least contributor. Our drainage flow accounted for 13%–22% of annual precipitation, which was close to the 16% reported by Bailey et al. (2022) and 18% estimated by Green et al. (2006). Moreover, drainage flow made up 41%–63% of total water yield, most of which exceeded the 45% from Bailey et al. (2022) but fell short of the 71% reported by Green et al. (2006). The fraction of drainage flow in total water yield aligns with the range of 46%–54% reported by Schilling et al. (2019) in their analytical and SWAT modeling of a similar drained watershed (Boon River watershed) in the Des Moines Lobe of north-central Iowa.

Overall, our results using both tile modules to analyze the water budget in the SFW were mostly consistent with the findings of the SWAT modeling study by Green et al. (2006) and the SWAT + MODFLOW modeling study by Bailey et al. (2022). Additionally, our findings aligned with the fieldwork conducted by Tomer et al. (2008b), demonstrating the robustness of the two tile modules in simulating hydrological processes within tile-drained agricultural ecosystems.

3.4 Nitrogen balance assessment across model configurations

Table 5 presents the average annual N budget for the entire SFW across eight model configurations for the period 2001–2018. Average, SD, and CV were also calculated for the N budget. The average annual N fertilization amounted to 90 kg N ha^{-1} in mineral form and 55 kg N ha^{-1} in organic form (Supplementary Table S2). Average annual atmospheric deposition of N was about 21 kg N ha^{-1}. Biological N fixation ranged from 42 to 79 kg N ha^{-1}, averaging 56 kg N ha^{-1}. Residue-derived organic N inputs to the soil ranged from 79 to 128 kg N ha^{-1}, averaging 103 kg N ha^{-1}. Net mineralization of organic matter produced 106–181 kg N ha^{-1}, averaging 154 kg N ha^{-1}. Plant uptake ranged from 164 to 278 kg N ha^{-1}, averaging 218 kg N ha^{-1}. Denitrification loss ranged from 13 to 33 kg N ha^{-1}, averaging 26 kg N ha^{-1}, while volatilization (NH_3) ranged from 1 to 3 kg N ha^{-1}, averaging 2 kg N ha^{-1}. The NO_3^- loss *via* drainage flow ranged from 22 to 30 kg N ha^{-1}, averaging 25 kg N ha^{-1}, and leaching NO_3^- ranged from 8 to 10 kg N ha^{-1}, averaging 9 kg N ha^{-1}. The NO_3^- loss *via* surface runoff, lateral flow, and groundwater averaged 2, 1, and 0.3 kg N ha^{-1} across eight model configurations (Table 5). Organic N losses *via* surface runoff ranged from 1 to 20 kg N ha^{-1} with a high CV of 0.9. Organic N removed through crop harvest ranged from 131 to 150 kg N ha^{-1}. N_2O fluxes ranged from 6 to 12 kg N ha^{-1}, NO fluxes from 5 to 7 kg N ha^{-1}, and N_2 fluxes from 6 to 11 kg N ha^{-1}. In addition, we calculated changes in mineral N and total N in the soil profile, which ranged from −60 to 21 kg N ha^{-1} (with a high |CV| = 1.4) and from −6–37 kg N ha^{-1} (with a high CV of 1.8), respectively.

Since no prior studies on N balance have been conducted in the SFW, we compared our results with those from research performed at the nearby Kelley experimental site (Figure 1) (Li et al., 2008; Gillette et al., 2018). Two ecosystem modeling efforts have been undertaken at the Kelley site over different periods to assess the effects of cover crops on NO_3^- loss through tile drainage and N_2O fluxes. For our analysis, we chose results from the control scenario that did not include cover crops, as the majority of agricultural land in the SFW does not utilize cover crops. Table 5 presents a comparison between the previous studies at the Kelley site and our findings regarding N budgets, and Supplementary Table S13 also lists key component ratios. It is noted that we assumed identical atmospheric deposition for both sites, and the two previous studies did not report all balance components.

At the SFW, the annual N uptake comprised 65%–97% of the total mineral N input, which includes mineral fertilization, atmospheric deposition, and net mineralization. Denitrification accounted for approximately 7%–13% of the total input, while N_2O contributed about 2%–4%. Drainage losses were 8%–12% of total input. Compared to the Kelley site, the SFW had higher N fertilization, resulting in higher net mineralization than at the Kelley site. Nitrogen fixation at the SFW site was lower, likely due to higher overall nitrogen application rates compared to the Kelley site. Another possible reason for the underestimation of N fixation could be inadequate calibration of crop growth processes. Additional observations of crop yield and/or biomass would help improve the simulation of crop growth–induced N dynamics. The N uptake to total mineral N input ratio in the SFW was less than the 1.1 reported by Gillette et al. (2018) and the 1.21 from Li et al. (2008) at the Kelley site, indicating less N use efficiency in the SFW. Additionally, denitrification was higher in the SFW—particularly when using the original N module—compared with the Kelley site, with denitrification ratios over total input at 0.07–0.13 for this study compared to 0.07 for Gillette et al. (2018) and 0.03 for Li et al. (2008). Simulated total N_2O fluxes were also greater in the SFW than in the Kelley site, although the N_2O to input ratio was similar (0.02–0.04). In contrast, NO_3^- loss *via* drainage flow was lower in the SFW than at the Kelley site, with a drainage N loss to input ratio of 0.08–0.12, which is less than the ratios of 0.17 from Li et al. (2008) and 0.19 from Gillette et al. (2018).

Simulated denitrification in the new N module was consistently lower than in the original module across all tile configurations (13–27 vs 29–33, respectively). As a result, the original module estimated denitrification rates that exceeded simulated drainage NO_3^- losses, while the new module produced estimates below those losses (Table 5). Although denitrification rates could not be validated in SFW due to a lack of observations, the results from the new N module aligned more closely with those from the Kelley site, suggesting improved denitrification simulation. In addition, denitrification simulated by the new N module was more sensitive to soil moisture than in the original module, as reflected in the differences among tile drainage modules and their calibration approaches. For example, the new N module showed substantial discrepancies in denitrification between calibrated and non-calibrated configurations (24 vs 13 kg N ha^{-1} with the original tile module; 27 vs 19 kg N ha^{-1} with the new tile module), whereas the original N module produced more consistent results (29 and 33 kg N ha^{-1} with the new and original tile modules, respectively).

Most N gas fluxes originated from denitrification and were near the upper range of literature-reported values, particularly for NO and N_2O (Bouwman et al., 2002; Hoben et al., 2011; Castellano et al., 2012; Butterbach-Bahl et al., 2013; Castellano et al., 2019; Ma et al., 2022). And most of the N_2O results were also greater than that reported in Gillette et al. (2018). Although the new N module

improved denitrification simulation, an accurate representation of N gas fluxes still requires additional field measurements. In particular, the NO: N_2O: N_2 ratios are strongly influenced by soil moisture dynamics (Potter et al., 1996; Parton et al., 2001), emphasizing the importance of complementary observations (e.g., soil moisture and routinely measured N_2O fluxes) to better constrain model parameters and improve watershed-scale N budget assessments. For instance, the DayCent model represents the topsoil with finer vertical resolution (typically 2 cm for the first layer and 3 cm for the second) compared to SWAT, which uses a fixed 1 cm first layer and approximately 20 cm for the second. This coarser layering in SWAT necessitates careful calibration against observed soil moisture, which strongly influences N gas fluxes.

Furthermore, we found that the new N module simulated substantially lower organic N losses *via* surface runoff compared to the original N module (1 vs 10–20 kg N ha^{-1}), regardless of the tile module configuration (Table 5). This result indicates that, according to the new N module, residue and soil organic matter in the surface layer decomposed more rapidly than simulated by the original N module. One potential solution to the underestimation of organic N loss *via* surface runoff is to incorporate a passive humus pool, which is currently not represented for the surface soil layer (Zhang et al., 2013). Additionally, the large variability in soil mineral N and total soil N changes across the eight model configurations underscores the substantial uncertainty in soil N cycling processes. The general positive changes in soil N (Table 5) suggest that the system may have been accumulating N, potentially contributing to legacy N. Since the current SWAT model cannot simulate legacy N storage and release, this limitation may partly explain the underestimation of NO_3^- loads at the outlets. It is worth noting that the SFW produced an excessive NO_3^- load, with an average NO_3^- yield of ~38 kg N ha^{-1} yr^{-1} at station SF450 for 2001–2018 (See the comparison with USGS estimations in Supplementary Figure S2), whereas multiyear average NO_3^- yields in Iowa typically range from 15 to 30 kg N ha^{-1} yr^{-1} (Jones et al., 2018a; Jones et al., 2018b).

In contrast to the large variations in simulated denitrification and associated N gas fluxes, we found that drainage NO_3^- losses were much more consistent across different model configurations. In addition, all models tended to simulate relatively low volatilization. Although few studies have reported volatilization results using SWAT, our findings highlight the need to improve its representation in the model (Lian et al., 2021). Compared to the original N module, the new N module was more sensitive to environmental changes. This requires careful monitoring of changes in organic C and N, as well as decomposition and mineralization rates. The original N module has the advantage of providing relatively stable and reasonable N cycling simulations without needing to account for C processes in detail. In contrast, the new N module necessitates careful calibration of initial humus pool partitioning, as it relies on these pools for accurate simulations (see sensitivity analysis).

3.5 Limitation and future research

While the simulation results for streamflow were robust, the accuracy of NO_3^- load simulations was comparatively lower. It is widely recognized that SWAT and other hydrological models generally perform better in simulating hydrological processes than in nutrient cycling. In this study, one contributing factor to the reduced performance in simulating NO_3^- was the insufficient representation of NO_3^- leaching processes, especially as affected by tile drainage. Improving this aspect may necessitate further development of a more physically-based model to enhance future outcomes. In addition, the interaction of tile drainage with streamflow is more intricate than what the current model configuration can capture. Features such as potholes or depressions that receive inflow can be considered in the modeling, but the added complexity of these landscape hydrological pathways may reduce overall model performance and complicate the calibration process (Du et al., 2005; Beeson et al., 2011; Beeson et al., 2014). Another reason for the underestimation of NO_3^- load is the lack of accurate input data, such as the quantity and timing of mineral fertilizer and manure applications, as well as detailed crop management practices, all of which strongly influence soil N dynamics (Ren et al., 2022; Niroula et al., 2023).

This study illustrates a common challenge encountered in the application of the SWAT model, where only discharge and water quality data are available from limited subbasin outlets. The calibration of soil water and nutrient parameters using water quantity and quality data with the original soil N module is widely used within the SWAT community. However, when more complex hydrological and biogeochemical processes, such as tile drainage and N gas fluxes, are incorporated into the model, relying solely on outlet water data to calibrate soil process parameters can lead to significant uncertainty in predictions (Arnold et al., 2015). The new N module adopts the Century/DayCent model approach to simulate N gas fluxes, including N_2O, NO, and N_2, originating from nitrification and denitrification (Figure 3). To effectively use the more complex model and reduce prediction uncertainty, additional observations—such as soil moisture and the commonly measured N_2O flux—is needed (Del Grosso et al., 2020). Although SWAT employs a simplified "tipping-bucket" soil water module, it can provide reasonable estimates of soil water dynamics when calibrated with soil moisture data (Qi et al., 2018). In addition, except for requiring additional field observations, it is important to simulate nutrient dynamics within a watershed—not just loads at the outlet—using soft data (Arnold et al., 2015). Proper process representation supported by soft data can significantly improve model calibration and validation. Soft data sources may include peer-reviewed literature, technical reports, theses, and field surveys.

4 Conclusion

This study used a comparative modeling framework to evaluate SWAT's ability to simulate watershed-scale tile drainage and N losses (NO_3^- leaching and N-gas fluxes) in a representative Midwestern tile-drained watershed. Eight configurations were tested by pairing original vs. new tile-drainage modules, calibrated vs. default tile parameters, and original vs. new N modules. Daily streamflow and NO_3^- loads from three monitoring stations (two: 2001–2018; one: 2001–2010) supported calibration, validation, sensitivity, and uncertainty analyses, and watershed-scale water and N balances were

compared with prior work, including the nearby Kelley experimental site.

Model evaluation indicated that all eight model configurations effectively simulated daily and monthly streamflow and NO_3^- loads, though they tended to underestimate peak streamflow and NO_3^- loads. The watershed-scale water balance terms mostly fell within the range reported in previous studies. We found that the new tile module generally enhanced daily streamflow predictions compared to the original module, particularly under the conditions of calibrated tile parameters. For both the new and original tile modules, further calibration of additional tile parameters did not lead to noticeable improvements in daily streamflow. Meanwhile, the new N module consistently outperformed the original N module in simulating daily and monthly NO_3^- loads, regardless of the tile module configuration used. Parameter sensitivity and uncertainty analyses revealed high uncertainty, particularly for NO_3^- load predictions at all three monitoring stations due to the complexity of N cycling processes. Specifically, we found that denitrification and associated N gas fluxes (inducing N_2O, NO, and N_2) varied across configurations, reflecting fundamental differences between the original and new N modules. The N budget also deviated from values reported at the Kelley site, indicating that relying solely on outlet NO_3^- load data is insufficient to capture key soil N cycling processes.

The new tile module is preferable for streamflow simulation, and the new N module strengthens NO_3^- load predictions; however, the expanded process representation for N gases amplifies uncertainty when calibration data are sparse. To reduce uncertainty in denitrification and N-gas estimates, multi-constraint calibration is recommended—pair outlet NO_3^- loads with supplemental observations (e.g., soil moisture and N_2O fluxes) and/or soft data. The comparative approach proved effective for identifying process controls and data gaps, guiding targeted monitoring to improve SWAT performance in tile-drained watersheds. In sum, the comparative evaluation clarifies where SWAT performs robustly (streamflow, NO_3^- loads) and where additional observations are essential (N-gas fluxes), providing actionable direction for future model development, calibration strategies, and data collection in tile-drained systems.

Data availability statement

The raw data supporting the conclusions of this article will be made available by the authors, without undue reservation.

Author contributions

JQ: Project administration, Funding acquisition, Formal Analysis, Software, Writing – review and editing, Conceptualization, Methodology, Writing – original draft. RM: Writing – review and editing, Resources, Data curation, Investigation, Validation. KL: Data curation, Methodology, Investigation, Resources, Writing – review and editing. KC: Writing – review and editing, Resources, Data curation. BE: Resources, Validation, Writing – review and editing, Data curation, Investigation. DM: Data curation, Investigation, Writing – review and editing, Supervision. MS: Writing – review and editing, Data curation, Resources. MC: Writing – review and editing, Resources, Data curation.

Funding

The author(s) declare that financial support was received for the research and/or publication of this article. The funding support for this study was provided by the U.S. Department of Agriculture, the National Institute of Food and Agriculture (2021-67019-33684 and 2023-67019-39221). This research was a contribution from the Long-Term Agroecosystem Research (LTAR) network. LTAR is supported by the United States Department of Agriculture. The USDA is an equal opportunity provider and employer.

Conflict of interest

The authors declare that the research was conducted in the absence of any commercial or financial relationships that could be construed as a potential conflict of interest.

Generative AI statement

The author(s) declare that no Generative AI was used in the creation of this manuscript.

Any alternative text (alt text) provided alongside figures in this article has been generated by Frontiers with the support of artificial intelligence and reasonable efforts have been made to ensure accuracy, including review by the authors wherever possible. If you identify any issues, please contact us.

Publisher's note

All claims expressed in this article are solely those of the authors and do not necessarily represent those of their affiliated organizations, or those of the publisher, the editors and the reviewers. Any product that may be evaluated in this article, or claim that may be made by its manufacturer, is not guaranteed or endorsed by the publisher.

Supplementary material

The Supplementary Material for this article can be found online at: https://www.frontiersin.org/articles/10.3389/fenvs.2025.1651136/full#supplementary-material

References

Abbaspour, K. C. (2013). *SWAT-CUP 2012: SWAT calibration and uncertainty programs–a user manual*. Dübendorf, Switzerland: Eawag, 103.

Abbaspour, K. C., Vejdani, M., Haghighat, S., and Yang, J. (2007a). "SWAT-CUP calibration and uncertainty programs for SWAT," in MODSIM 2007 international congress on modelling and simulation, modelling and simulation society of Australia and New Zealand. Dübendorf, Switzerland: Swiss Federal Institute of Aquatic Science and Technology, 1596–1602.

Abbaspour, K. C., Yang, J., Maximov, I., Siber, R., Bogner, K., Mieleitner, J., et al. (2007b). Modelling hydrology and water quality in the pre-alpine/alpine Thur watershed using SWAT. *J. Hydrol.* 333 (2-4), 413–430. doi:10.1016/j.jhydrol.2006.09.014

Arnold, J. G., Srinivasan, R., Muttiah, R. S., and Williams, J. R. (1998). Large area hydrologic modeling and assessment part I: model development. *JAWRA J. Am. Water Resour. Assoc.* 34 (1), 73–89. doi:10.1111/j.1752-1688.1998.tb05961.x

Arnold, J., Gassman, P., King, K., Saleh, A., and Sunday, U. (1999). Validation of the subsurface tile flow component in the SWAT model. *Trans. ASAE*, 99–2138.

Arnold, J. G., Youssef, M. A., Yen, H., White, M. J., Sheshukov, A. Y., Sadeghi, A. M., et al. (2015). Hydrological processes and model representation: impact of soft data on calibration. *Trans. ASABE* 58 (6), 1637–1660. doi:10.13031/trans.58.10726

Awale, R., Chatterjee, A., Kandel, H., and Ransom, J. K. (2015). Tile drainage and nitrogen fertilizer management influences on nitrogen availability, losses, and crop yields. *Open J. Soil Sci.* 5 (10), 211–226. doi:10.4236/ojss.2015.510021

Bailey, R. T., Bieger, K., Flores, L., and Tomer, M. (2022). Evaluating the contribution of subsurface drainage to watershed water yield using SWAT+ with groundwater modeling. *Sci. Total Environ.* 802, 149962. doi:10.1016/j.scitotenv.2021.149962

Baker, J., and Johnson, H. (1977). Impact of subsurface drainage on water quality. Proceedings, third national drainage symposium, Chicago, United States, December 1976, 91–298.

Beeson, P., Doraiswamy, P., Sadeghi, A., Di Luzio, M., Tomer, M., Arnold, J., et al. (2011). Treatments of precipitation inputs to hydrologic models. *Trans. ASABE* 54 (6), 2011–2020. doi:10.13031/2013.40652

Beeson, P. C., Sadeghi, A. M., Lang, M. W., Tomer, M. D., and Daughtry, C. S. (2014). Sediment delivery estimates in water quality models altered by resolution and source of topographic data. *J. Environ. Qual.* 43 (1), 26–36. doi:10.2134/jeq2012.0148

Bouwman, A., Boumans, L., and Batjes, N. (2002). Emissions of N_2O and NO from fertilized fields: summary of available measurement data. *Glob. Biogeochem. Cycles* 16 (4), 6-1-6–13. doi:10.1029/2001gb001811

Burton, D. L., Wilts, H., and Macleod, J. (2024). Dissolved nitrous oxide emissions associated with agricultural drainage water as influenced by manure application. *Front. Environ. Sci.* 12, 1479754. doi:10.3389/fenvs.2024.1479754

Butterbach-Bahl, K., Baggs, E. M., Dannenmann, M., Kiese, R., and Zechmeister-Boltenstern, S. (2013). Nitrous oxide emissions from soils: how well do we understand the processes and their controls? *Philosophical Trans. R. Soc. B Biol. Sci.* 368 (1621), 20130122. doi:10.1098/rstb.2013.0122

Butts, M. B., Payne, J. T., Kristensen, M., and Madsen, H. (2004). An evaluation of the impact of model structure on hydrological modelling uncertainty for streamflow simulation. *J. Hydrol.* 298 (1-4), 242–266. doi:10.1016/j.jhydrol.2004.03.042

Castellano, M., Helmers, M., Sawyer, J., Christianson, L., and Barker, D. (2012). Nitrogen, carbon, and phosphorus balances in Iowa cropping systems: sustaining the soil resource. 2012 Integrated crop management conference - Iowa State University.

Castellano, M. J., Archontoulis, S. V., Helmers, M. J., Poffenbarger, H. J., and Six, J. (2019). Sustainable intensification of agricultural drainage. *Nat. Sustain.* 2 (10), 914–921. doi:10.1038/s41893-019-0393-0

Chen, R., Shen, W., Chen, Z., Guo, J., Yang, L., Fei, G., et al. (2024). Modulation of soil nitrous oxide emissions and nitrogen leaching by hillslope hydrological processes. *Sci. Total Environ.* 951, 175637. doi:10.1016/j.scitotenv.2024.175637

Crossman, J., Futter, M., Whitehead, P. G., Stainsby, E., Baulch, H., Jin, L., et al. (2014). Flow pathways and nutrient transport mechanisms drive hydrochemical sensitivity to climate change across catchments with different geology and topography. *Hydrology Earth Syst. Sci.* 18 (12), 5125–5148. doi:10.5194/hess-18-5125-2014

Del Grosso, S., Parton, W., Mosier, A., Ojima, D., Kulmala, A., and Phongpan, S. (2000). General model for N_2O and N_2 gas emissions from soils due to dentrification. *Glob. Biogeochem. Cycles* 14 (4), 1045–1060. doi:10.1029/1999gb001225

Del Grosso, S. J., Smith, W., Kraus, D., Massad, R. S., Vogeler, I., and Fuchs, K. (2020). Approaches and concepts of modelling denitrification: increased process understanding using observational data can reduce uncertainties. *Curr. Opin. Environ. Sustain.* 47, 37–45. doi:10.1016/j.cosust.2020.07.003

Dinnes, D. L., Karlen, D. L., Jaynes, D. B., Kaspar, T. C., Hatfield, J. L., Colvin, T. S., et al. (2002). Nitrogen management strategies to reduce nitrate leaching in tile-drained midwestern soils. *Agron. J.* 94 (1), 153–171. doi:10.2134/agronj2002.1530

Du, B., Arnold, J., Saleh, A., and Jaynes, D. (2005). Development and application of SWAT to landscapes with tiles and potholes. *Trans. ASAE* 48 (3), 1121–1133. doi:10.13031/2013.18522

Du, B., Saleh, A., Jaynes, D., and Arnold, J. (2006). Evaluation of SWAT in simulating nitrate nitrogen and atrazine fates in a watershed with tiles and potholes. *Trans. ASABE* 49 (4), 949–959. doi:10.13031/2013.21746

Fabrizzi, K. P., Fernández, F., G., Venterea, R. T., and Naeve, S. L. (2024). *Nitrous oxide emissions from soybean in response to drained and undrained soils and previous corn nitrogen management*. 53 (4), 407–417.

Ford, W. I., King, K., and Williams, M. R. (2018). Upland and in-stream controls on baseflow nutrient dynamics in tile-drained agroecosystem watersheds. *J. Hydrol.* 556, 800–812. doi:10.1016/j.jhydrol.2017.12.009

Gassman, P. W., Sadeghi, A. M., and Srinivasan, R. (2014). Applications of the SWAT model special section: overview and insights. *J. Environ. Qual.* 43 (1), 1–8. doi:10.2134/jeq2013.11.0466

Ghimire, U., Shrestha, N. K., Biswas, A., Wagner-Riddle, C., Yang, W., Prasher, S., et al. (2020). A review of ongoing advancements in soil and water assessment tool (SWAT) for nitrous oxide (N_2O) modeling. *Atmosphere* 11 (5), 450. doi:10.3390/atmos11050450

Gillette, K., Malone, R., Kaspar, T., Ma, L., Parkin, T., Jaynes, D., et al. (2018). N loss to drain flow and N_2O emissions from a corn-soybean rotation with winter rye. *Sci. Total Environ.* 618, 982–997. doi:10.1016/j.scitotenv.2017.09.054

Green, C., Tomer, M., Di Luzio, M., and Arnold, J. (2006). Hydrologic evaluation of the soil and water assessment tool for a large tile-drained watershed in Iowa. *Trans. ASABE* 49 (2), 413–422. doi:10.13031/2013.20415

Groffman, P. M., Butterbach-Bahl, K., Fulweiler, R. W., Gold, A. J., Morse, J. L., Stander, E. K., et al. (2009). Challenges to incorporating spatially and temporally explicit phenomena (hotspots and hot moments) in denitrification models. *Biogeochemistry* 93, 49–77. doi:10.1007/s10533-008-9277-5

Gu, J., Nicoullaud, B., Rochette, P., Grossel, A., Hénault, C., Cellier, P., et al. (2013). A regional experiment suggests that soil texture is a major control of N_2O emissions from tile-drained winter wheat fields during the fertilization period. *Soil Biol. Biochem.* 60, 134–141. doi:10.1016/j.soilbio.2013.01.029

Guo, T., Gitau, M., Merwade, V., Arnold, J., Srinivasan, R., Hirschi, M., et al. (2018). Comparison of performance of tile drainage routines in SWAT 2009 and 2012 in an extensively tile-drained watershed in the Midwest. *Hydrology Earth Syst. Sci.* 22 (1), 89–110. doi:10.5194/hess-22-89-2018

Hama-Aziz, Z. Q., Hiscock, K. M., and Cooper, R. J. (2017). Dissolved nitrous oxide (N_2O) dynamics in agricultural field drains and headwater streams in an intensive arable catchment. *Hydrol. Process.* 31 (6), 1371–1381. doi:10.1002/hyp.11111

Helwig, T. G., Madramootoo, C. A., and Dodds, G. T. (2002). Modelling nitrate losses in drainage water using DRAINMOD 5.0. *Agric. Water Manag.* 56 (2), 153–168. doi:10.1016/s0378-3774(02)00005-7

Herrera, P. A., Marazuela, M. A., and Hofmann, T. (2022). Parameter estimation and uncertainty analysis in hydrological modeling. *Wiley Interdiscip. Rev. Water* 9 (1), e1569. doi:10.1002/wat2.1569

Hoben, J., Gehl, R., Millar, N., Grace, P., and Robertson, G. (2011). Nonlinear nitrous oxide (N_2O) response to nitrogen fertilizer in on-farm corn crops of the US Midwest. *Glob. Change Biol.* 17 (2), 1140–1152. doi:10.1111/j.1365-2486.2010.02349.x

Ikenberry, C. D., Soupir, M. L., Helmers, M. J., Crumpton, W. G., Arnold, J. G., and Gassman, P. W. (2017). Simulation of daily flow pathways, tile-drain nitrate concentrations, and soil-nitrogen dynamics using SWAT. *JAWRA J. Am. Water Resour. Assoc.* 53 (6), 1251–1266. doi:10.1111/1752-1688.12569

Izaurralde, R., Williams, J. R., Mcgill, W. B., Rosenberg, N. J., and Jakas, M. Q. (2006). Simulating soil C dynamics with EPIC: model description and testing against long-term data. *Ecol. Model.* 192 (3-4), 362–384. doi:10.1016/j.ecolmodel.2005.07.010

Jones, C. S., Nielsen, J. K., Schilling, K. E., and Weber, L. J. (2018a). Iowa stream nitrate and the Gulf of Mexico. *PLoS One* 13 (4), e0195930. doi:10.1371/journal.pone.0195930

Jones, C. S., Schilling, K. E., Simpson, I. M., and Wolter, C. F. (2018b). Iowa stream nitrate, discharge and precipitation: 30-year perspective. *Environ. Manag.* 62 (4), 709–720. doi:10.1007/s00267-018-1074-x

Knoben, W. J., Freer, J. E., and Woods, R. A. (2019). Inherent benchmark or not? Comparing Nash–Sutcliffe and Kling–Gupta efficiency scores. *Hydrology Earth Syst. Sci.* 23 (10), 4323–4331. doi:10.5194/hess-23-4323-2019

Kujawa, H., Kalcic, M., Martin, J., Aloysius, N., Apostel, A., Kast, J., et al. (2020). The hydrologic model as a source of nutrient loading uncertainty in a future climate. *Sci. Total Environ.* 724, 138004. doi:10.1016/j.scitotenv.2020.138004

Kumar, M., Tiwari, R. K., Rautela, K. S., Kumar, K., Khajuria, V., Verma, I., et al. (2024). Comparative assessment of process based models for simulating the hydrological response of the Himalayan River Basin. *Earth Syst. Environ.* 9, 299–313. doi:10.1007/s41748-024-00441-w

Li, L., Malone, R., Ma, L., Kaspar, T., Jaynes, D., Saseendran, S., et al. (2008). Winter cover crop effects on nitrate leaching in subsurface drainage as simulated by RZWQM-DSSAT. *Trans. ASABE* 51 (5), 1575–1583. doi:10.13031/2013.25314

Li, H., Sivapalan, M., Tian, F., and Liu, D. (2010). Water and nutrient balances in a large tile-drained agricultural catchment: a distributed modeling study. *Hydrol. Earth Syst. Sci.* 14 (11), 2259–2275. doi:10.5194/hess-14-2259-2010

Lian, Z., Ouyang, W., Liu, H., Zhang, D., and Liu, L. (2021). Ammonia volatilization modeling optimization for rice watersheds under climatic differences. *Sci. Total Environ.* 767, 144710. doi:10.1016/j.scitotenv.2020.144710

Liang, K., Qi, J., Zhang, X., and Deng, J. (2022). Replicating measured site-scale soil organic carbon dynamics in the US Corn Belt using the SWAT-C model. *Environ. Model. Softw.* 158, 105553. doi:10.1016/j.envsoft.2022.105553

Liang, K., Qi, J., Zhang, X., Emmett, B., Johnson, J. M., Malone, R. W., et al. (2023). Simulated nitrous oxide emissions from multiple agroecosystems in the US Corn Belt using the modified SWAT-C model. *Environ. Pollut.* 337, 122537. doi:10.1016/j.envpol.2023.122537

Logan, T., Eckert, D., and Beak, D. (1994). Tillage, crop and climatic effects of runoff and tile drainage losses of nitrate and four herbicides. *Soil Tillage Res.* 30 (1), 75–103. doi:10.1016/0167-1987(94)90151-1

Luo, X., Risal, A., Qi, J., Lee, S., Zhang, X., Alfieri, J. G., et al. (2024). Modeling lateral carbon fluxes for agroecosystems in the Mid-Atlantic region: control factors and importance for carbon budget. *Sci. Total Environ.* 912, 169128. doi:10.1016/j.scitotenv.2023.169128

Ma, R., Yu, K., Xiao, S., Liu, S., Ciais, P., and Zou, J. (2022). Data-driven estimates of fertilizer-induced soil NH_3, NO and N_2O emissions from croplands in China and their climate change impacts. *Glob. Change Biol.* 28 (3), 1008–1022. doi:10.1111/gcb.15975

May, H., Rixon, S., Gardner, S., Goel, P., Levison, J., and Binns, A. (2023). Investigating relationships between climate controls and nutrient flux in surface waters, sediments, and subsurface pathways in an agricultural clay catchment of the Great Lakes Basin. *Sci. Total Environ.* 864, 160979. doi:10.1016/j.scitotenv.2022.160979

Moriasi, D., Arnold, J., and Green, C. (2007a). *Incorporation of Hooghoudt and Kirkham tile drain equations into SWAT2005*. Netherlands: UNESCO-IHE Delft, 139–147.

Moriasi, D. N., Arnold, J. G., Van Liew, M. W., Bingner, R. L., Harmel, R. D., and Veith, T. L. (2007b). Model evaluation guidelines for systematic quantification of accuracy in watershed simulations. *Trans. ASABE* 50 (3), 885–900. doi:10.13031/2013.23153

Moriasi, D., Rossi, C., Arnold, J., and Tomer, M. (2012). Evaluating hydrology of the Soil and Water Assessment Tool (SWAT) with new tile drain equations. *J. Soil Water Conservat.* 67 (6), 513–524. doi:10.2489/jswc.67.6.513

Moriasi, D. N., Gowda, P. H., Arnold, J. G., Mulla, D. J., Ale, S., and Steiner, J. L. (2013a). Modeling the impact of nitrogen fertilizer application and tile drain configuration on nitrate leaching using SWAT. *Agric. Water Manag.* 130, 36–43. doi:10.1016/j.agwat.2013.08.003

Moriasi, D. N., Gowda, P. H., Arnold, J. G., Mulla, D. J., Ale, S., Steiner, J. L., et al. (2013b). Evaluation of the Hooghoudt and Kirkham tile drain equations in the Soil and Water Assessment Tool to simulate tile flow and nitrate-nitrogen. *J. Environ. Qual.* 42 (6), 1699–1710. doi:10.2134/jeq2013.01.0018

Moridi, A. (2019). A bankruptcy method for pollution load reallocation in river systems. *J. Hydroinformat.* 21 (1), 45–55. doi:10.2166/hydro.2018.156

Narsimlu, B., Gosain, A. K., Chahar, B. R., Singh, S. K., and Srivastava, P. K. (2015). SWAT model calibration and uncertainty analysis for streamflow prediction in the Kunwari River Basin, India, using sequential uncertainty fitting. *Environ. Process.* 2, 79–95. doi:10.1007/s40710-015-0064-8

Nash, P., Motavalli, P., Nelson, K., and Kremer, R. (2015). Ammonia and nitrous oxide gas loss with subsurface drainage and polymer-coated urea fertilizer in a poorly drained soil. *J. Soil Water Conservat.* 70 (4), 267–275. doi:10.2489/jswc.70.4.267

Nazari Mejdar, H., Moridi, A., and Najjar-Ghabel, S. (2023). Water quantity–quality assessment in the transboundary river basin under climate change: a case study. *J. Water Clim. Change* 14 (12), 4747–4762. doi:10.2166/wcc.2023.421

Neitsch, S. L., Williams, J. R., Arnold, J. G., and Kiniry, J. R. (2011). Soil and water assessment tool theoretical documentation version 2009. Temple, Texas, USA: Grassland. *Soil Water Res. Serv.*

Nelson, A., Moriasi, D., Talebizadeh, M., Steiner, J., Gowda, P., Starks, P., et al. (2018). Use of soft data for multicriteria calibration and validation of Agricultural Policy Environmental eXtender: impact on model simulations. *J. Soil Water Conservat.* 73 (6), 623–636. doi:10.2489/jswc.73.6.623

Niroula, S., Cai, X., and Mcisaac, G. (2023). Sustaining crop yield and water quality under climate change in intensively managed agricultural watersheds—the need for both adaptive and conservation measures. *Environ. Res. Lett.* 18 (12), 124029. doi:10.1088/1748-9326/ad085f

Parton, W. J., Ojima, D. S., Cole, C. V., and Schimel, D. S. (1994). A general model for soil organic matter dynamics: sensitivity to litter chemistry, texture and management. *Quantitative Model. Soil Form. Process.* 147–167. doi:10.2136/sssaspecpub39.c9

Parton, W., Holland, E., Del Grosso, S., Hartman, M., Martin, R., Mosier, A., et al. (2001). Generalized model for NO_x and N_2O emissions from soils. *J. Geophys. Res. Atmos.* 106 (D15), 17403–17419. doi:10.1029/2001jd900101

Perrin, C., Michel, C., and Andréassian, V. (2001). Does a large number of parameters enhance model performance? Comparative assessment of common catchment model structures on 429 catchments. *J. Hydrol.* 242 (3-4), 275–301. doi:10.1016/s0022-1694(00)00393-0

Potter, C. S., Matson, P. A., Vitousek, P. M., and Davidson, E. A. (1996). Process modeling of controls on nitrogen trace gas emissions from soils worldwide. *J. Geophys. Res. Atmos.* 101 (D1), 1361–1377. doi:10.1029/95jd02028

Qi, J., Zhang, X., Mccarty, G. W., Sadeghi, A. M., Cosh, M. H., Zeng, X., et al. (2018). Assessing the performance of a physically-based soil moisture module integrated within the Soil and Water Assessment Tool. *Environ. Model. Softw.* 109, 329–341. doi:10.1016/j.envsoft.2018.08.024

Qi, J., Du, X., Zhang, X., Lee, S., Wu, Y., Deng, J., et al. (2019a). Modeling riverine dissolved and particulate organic carbon fluxes from two small watersheds in the northeastern United States. *Environ. Model. Softw.* 124, 104601. doi:10.1016/j.envsoft.2019.104601

Qi, J., Lee, S., Zhang, X., Yang, Q., Mccarty, G. W., and Moglen, G. E. (2019b). Effects of surface runoff and infiltration partition methods on hydrological modeling: a comparison of four schemes in two watersheds in the Northeastern US. *J. Hydrol.* 581, 124415. doi:10.1016/j.jhydrol.2019.124415

Qi, J., Wang, Q., and Zhang, X. (2019c). On the use of NLDAS2 weather data for hydrologic modeling in the upper Mississippi River Basin. *Water* 11 (5), 960. doi:10.3390/w11050960

Reddy, K., Khaleel, R., Overcash, M., and Westerman, P. (1979). A nonpoint source model for land areas receiving animal wastes: II. Ammonia volatilization. *Trans. ASAE* 22 (6), 1398–1405. doi:10.13031/2013.35219

Refsgaard, J. C., Van Der Sluijs, J. P., Brown, J., and Van Der Keur, P. (2006). A framework for dealing with uncertainty due to model structure error. *Adv. Water Resour.* 29 (11), 1586–1597. doi:10.1016/j.advwatres.2005.11.013

Ren, D., Engel, B., and Tuinstra, M. R. (2022). Crop improvement influences on water quantity and quality processes in an agricultural watershed. *Water Res.* 217, 118353. doi:10.1016/j.watres.2022.118353

Schilling, K. E., and Helmers, M. (2008). Effects of subsurface drainage tiles on streamflow in Iowa agricultural watersheds: exploratory hydrograph analysis. *Hydrological Process. Int. J.* 22 (23), 4497–4506. doi:10.1002/hyp.7052

Schilling, K. E., and Wolter, C. F. (2009). Modeling nitrate-nitrogen load reduction strategies for the Des Moines River, Iowa using SWAT. *Environ. Manag.* 44 (4), 671–682. doi:10.1007/s00267-009-9364-y

Schilling, K. E., Gassman, P. W., Arenas-Amado, A., Jones, C. S., and Arnold, J. (2019). Quantifying the contribution of tile drainage to basin-scale water yield using analytical and numerical models. *Sci. Total Environ.* 657, 297–309. doi:10.1016/j.scitotenv.2018.11.340

Seligman, N., and Keulen, H. (1980). 4.10 PAPRAN: a simulation model of annual pasture production limited by rainfall and nitrogen. *Simul. nitrogen Behav. Soil-Plant Syst.* 192.

Skaggs, R. W., Breve, M., and Gilliam, J. (1994). Hydrologic and water quality impacts of agricultural drainage*. *Crit. Rev. Environ. Sci. Technol.* 24 (1), 1–32. doi:10.1080/10643389409388459

Skaggs, R. W., Youssef, M., and Chescheir, G. (2012). DRAINMOD: model use, calibration, and validation. *Trans. ASABE* 55 (4), 1509–1522. doi:10.13031/2013.42259

Tijjani, S. B., Qi, J., Giri, S., and Lathrop, R. (2023). Modeling land use and management practices impacts on soil organic carbon loss in an agricultural watershed in the Mid-Atlantic Region. *Water* 15 (20), 3534. doi:10.3390/w15203534

Tijjani, S. B., Giri, S., Lathrop, R., Qi, J., Karki, R., Schäfer, K. V., et al. (2024). Modeling carbon dynamics from a heterogeneous watershed in the mid-Atlantic USA: a distributed-calibration and independent verification (DCIV) approach. *Sci. Total Environ.* 956, 177271. doi:10.1016/j.scitotenv.2024.177271

Tomer, M., Moorman, T., James, D., Hadish, G., and Rossi, C. (2008a). Assessment of the Iowa River's south fork watershed: part 2. Conservation practices. *J. Soil Water Conservat.* 63 (6), 371–379. doi:10.2489/jswc.63.6.371

Tomer, M., Moorman, T., and Rossi, C. (2008b). Assessment of the Iowa River's South Fork watershed: part 1. water quality. *J. Soil Water Conservat.* 63 (6), 360–370. doi:10.2489/jswc.63.6.360

van Schilfgaarde, J., Engelund, F., Kirkham, D., Peterson, Jr, D. F., and Maasland, M. (1957). Theory of land drainage. Drainage of agricultural lands, 7, 79–285.

Wang, C., Amon, B., Schulz, K., and Mehdi, B. (2021a). Factors that influence nitrous oxide emissions from agricultural soils as well as their representation in simulation models: a review. *Agronomy* 11 (4), 770. doi:10.3390/agronomy11040770

Wang, C., Schürz, C., Zoboli, O., Zessner, M., Schulz, K., Watzinger, A., et al. (2021b). N_2O emissions from two Austrian agricultural catchments simulated with an N_2O

submodule developed for the SWAT model. *Atmosphere* 13 (1), 50. doi:10.3390/atmos13010050

Xia, Y., Mitchell, K., Ek, M., Sheffield, J., Cosgrove, B., Wood, E., et al. (2012). Continental-scale water and energy flux analysis and validation for the North American Land Data Assimilation System project phase 2 (NLDAS-2): 1. Intercomparison and application of model products. *J. Geophys. Res. Atmos.* 117 (D3). doi:10.1029/2011jd016048

Yang, Q., Zhang, X., Abraha, M., Del Grosso, S., Robertson, G., and Chen, J. (2017). Enhancing the soil and water assessment tool model for simulating N_2O emissions of three agricultural systems. *Ecosyst. Health Sustain.* 3 (2), e01259. doi:10.1002/ehs2.1259

Yousefi, H., and Moridi, A. (2022). Multiobjective optimization of agricultural planning considering climate change impacts: minab reservoir upstream watershed in Iran. *J. Irrigation Drainage Eng.* 148 (4), 04022007. doi:10.1061/(asce)ir.1943-4774.0001675

Zhang, X., Izaurralde, R. C., Arnold, J. G., Williams, J. R., and Srinivasan, R. (2013). Modifying the soil and water assessment tool to simulate cropland carbon flux: model development and initial evaluation. *Sci. Total Environ.* 463, 810–822. doi:10.1016/j.scitotenv.2013.06.056

Zucker, L. A., and Brown, L. C. (1998). *Agricultural drainage: water quality impacts and subsurface drainage studies in the Midwest*. Ohio: Ohio State University Extension.

frontiers | Frontiers in Environmental Science

TYPE Original Research
PUBLISHED 20 November 2024
DOI 10.3389/fenvs.2024.1415215

Check for updates

OPEN ACCESS

EDITED BY
Keith Schilling,
The University of Iowa, United States

REVIEWED BY
Wei Shui,
Fuzhou University, China
Ning Niu,
Henan University of Economic and Law, China

*CORRESPONDENCE
Weiqiang Chen,
chwqgis@henau.edu.cn

RECEIVED 12 April 2024
ACCEPTED 07 November 2024
PUBLISHED 20 November 2024

CITATION
Yu Y, Chen W, Ji G, Guo Y, Chen Y, Sheng S, Deng Y and Weng Q (2024) Simulation and attribution analysis of agricultural nitrogen non-point source pollution in Huang-Huai-Hai Plain based on the InVEST model.
Front. Environ. Sci. 12:1415215.
doi: 10.3389/fenvs.2024.1415215

COPYRIGHT
© 2024 Yu, Chen, Ji, Guo, Chen, Sheng, Deng and Weng. This is an open-access article distributed under the terms of the Creative Commons Attribution License (CC BY). The use, distribution or reproduction in other forums is permitted, provided the original author(s) and the copyright owner(s) are credited and that the original publication in this journal is cited, in accordance with accepted academic practice. No use, distribution or reproduction is permitted which does not comply with these terms.

Simulation and attribution analysis of agricultural nitrogen non-point source pollution in Huang-Huai-Hai Plain based on the InVEST model

Ying Yu[1], Weiqiang Chen[1]*, Guangxing Ji[1], Yulong Guo[1], Yinan Chen[1], Siyu Sheng[2], Yaru Deng[1] and Qianwen Weng[1]

[1]College of Resources and Environmental Sciences, Henan Agricultural University, Zhengzhou, China, [2]College of Public Administration, Central China Normal University, Wuhan, Hubei, China

The study of agricultural non-point source pollution (ANNSP) patterns and driving mechanisms is crucial for regional ecological management. This paper evaluates the sources of ANNSP in the Huang-Huai-Hai Plain for the years 2000, 2010, and 2020 using the source list method. Additionally, nitrogen source data for the InVEST model were supplemented and adjusted, and the nitrogen output load and proportions derived in farmland from both methods were compared. The temporal and spatial distribution of nitrogen emission intensity was analyzed based on InVEST model outputs. Key source areas were identified through hotspot analysis, and spatial driving factors were examined using geodetector. Key findings reveal: 1) While the source list method estimated a higher nitrogen output load, both methods concurred on the proportion of agricultural nitrogen. The main sources of nitrogen input were overuse of fertilizer and livestock breeding. 2) Over this period, nitrogen emission intensity declined, exhibiting a distinct spatial pattern of "northwest low, southeast high." 3) The extent of critical source areas underwent a dynamic shift, initially contracting before expanding. 4) Rainfall emerged as the primary driver of spatial variability in agricultural TN emission intensity. These insights offer critical reference points for achieving efficient ANNSP management in the Huang-Huai-Hai Plain.

KEYWORDS

agricultural nitrogen non-point source pollution, InVEST model, hotspot analysis, geodetector, Huang-Huai-Hai Plain

1 Introduction

In the crucible of China's economic metamorphosis, agriculture stands resolute as an enduring pillar, achieving commendable milestones and profoundly influencing global food security (Zhang et al., 2023). Despite these strides, the relentless march of urbanization has constricted arable lands, amplifying the demand for agricultural and livestock products. The pursuit of enhanced yields has strained the natural environment's capacity, resulting in soil and water pollution and the emergence of agricultural non-point source pollution challenges (Lu et al., 2023). This pollution not only imperils water quality (Wang et al., 2023c), but also stands as a chief instigator of eutrophication. The "Second National Census of Pollution Sources Bulletin" in 2020 unveiled that agricultural sources alone contribute 46.52% of total

nitrogen (TN) emissions, surpassing industrial and domestic counterparts. The genesis of agricultural non-point source pollution is intricately woven with climatic nuances, topographical peculiarities, land-use dynamics, and vegetative cover, rendering the monitoring, simulation, and mitigation of its impact a daunting task (Luo et al., 2023; Jolly et al., 2023; Wang et al., 2023a). The Huang-Huai-Hai Plain, as one of China's nine major agricultural regions (Shirazi et al., 2022), shoulders the crucial task of supplying grains. However, over the past two decades, this region has faced severe threats from agricultural non-point source pollution, elevating the risk of water eutrophication (Chang and Zhang, 2023; Yue et al., 2022). Consequently, effectively and economically addressing agricultural non-point source pollution in the Huang-Huai-Hai Plain has emerged as a focal and formidable challenge in current research.

In the realm of addressing agricultural non-point source pollution, the accurate estimation of pollutant loads stands as a pivotal undertaking. Within this context, non-point source pollution models emerge as indispensable tools, categorically classified into two primary domains: empirical models and mechanistic models. Empirical models, exemplified by the output coefficient approach, leverage a broad spectrum of empirical data, but can fall short in portraying the intricate migration pathways of pollutants. Limitations stem from the inherent constraints imposed by regional boundaries, hindering a holistic understanding of the environmental phenomena (Li et al., 2021b). In contrast, mechanistic models engage in a more comprehensive examination, integrating diverse factors such as hydrology, meteorology, and geography to delve into the intricate spatial and temporal variations of non-point source pollution (Ji et al., 2023). These models not only facilitate the identification of pollutant sources and the analysis of their concentrations but also compute pollutant output loads. Consequently, they furnish robust support for the formulation of agricultural non-point source pollution mitigation strategies and the assessment of preventative measures (Zuo et al., 2023). Amid the plethora of non-point source pollution models, distributed models have gained widespread popularity due to their proficiency in simulating and predicting the migration and transformation of pollutants within river basins. This category encompasses models such as the Soil and Water Assessment Tool (SWAT) (Zhu et al., 2023; Ding et al., 2023b), the Annualized Agricultural Non-point Source (AnnAGNPS) (Chao et al., 2023; Liu et al., 2023), the Hydrological Simulation Program-Fortran (HSPF) (Lee et al., 2023), and the Integrative Valuation of Ecosystem Services and Tradeoffs Tool (InVEST) model (Ding et al., 2023a). In the practical application of these models, the judicious selection of a model must account for various factors, including the unique characteristics of the study area, simulation scale, and data availability.

The InVEST model distinguishes itself from other models through its straightforward parameterization and transparent mechanisms for nutrient flow and transformation within water systems. This simplicity and clarity make it particularly well-suited for large-scale simulations of non-point source pollution (Li et al., 2021a; Scordo et al., 2018). The Nutrient Delivery Ratio (NDR) module, integral to the InVEST model, provides a scientific basis for decision makers by modelling and estimating the contribution of vegetation and soil to water purification, particularly in controlling nutrient pollutants in runoff. Globally, researchers utilize NDR modules to explore non-point source pollution within watersheds. For instance, in the White River Basin of the Midwest United States, NDR modules have effectively delineated areas with elevated nitrogen and phosphorus loads across varying land use scenarios (Han et al., 2021). Similarly, studies in the United Kingdom have underscored the utility of NDR modules in evaluating the relative contributions of nitrogen and phosphorus outputs (Redhead et al., 2018). In China, Yan et al. (2018) evaluated the impact of constructed wetlands on total nitrogen removal in the Jiulong River basin, while NDR modules were used to estimate nitrogen and phosphorus pollutants in the mountainous terrain of Baoxing County, Sichuan Province (Liu et al., 2019). Zhang et al. (2021a) investigated non-point source distributions in the farmland of the Haihe River Basin, identifying critical pollution sources. These examples provided exemplify the robustness and dependability of the NDR module in studying non-point source pollution.

Variations in nutrient levels within a river basin can be evident across diverse regions. Within these areas, the preponderance of pollutant outputs from a single area may constitute the principal fraction of the overall pollution load within the entire basin, exerting a decisive influence on water quality. These localized domains, denominated as critical source areas (CSAs) (Ghebremichael et al., 2013; Hoang et al., 2019), assume paramount importance in the context of water quality management. Effectively identifying and managing these CSAs is imperative for the control of non-point source pollution. Although the task of non-point source pollution control is acknowledged to be formidable and resource-intensive (Chen et al., 2023a; Hou et al., 2022), achieving the objectives of water quality management can be done with greater efficacy and precision. Consequently, research endeavors revolving around CSAs have increasingly gained prominence. The strategic identification of CSAs through distributed models enables the prioritization of limited resources towards targeted remediation efforts, thereby markedly enhancing intervention efficiency (Giri et al., 2012). Such an approach not only holds promise for bolstering the efficacy of pollution control measures but also underscores a paradigm shift towards more discerning and resource-efficient environmental management strategies.

Currently, significant progress has been achieved in estimating non-point source pollution loads and identifying CSAs (Zuo et al., 2022). However, there remains a gap in understanding the mechanisms driving pollution emissions (Duan and Li, 2023). Using the InVEST model, this study conducted simulations of Agricultural nitrogen non-point source pollution (ANNSP) across the Huang-Huai-Hai Plain for the years 2000, 2010, and 2020. The aim of this study was to analyze the spatio-temporal patterns of total nitrogen (TN) emission intensity, pinpoint critical source areas, and quantify the influence of various factors. The primary objective of this research is to offer scientific support for decision-making regarding the control of Agricultural nitrogen non-point source pollution in the Huang-Huai-Hai Plain and advance the sustainable development of agriculture and contribute to rural ecological revitalization.

2 Materials and methods

2.1 Study area

The Huang-Huai-Hai Plain, located in the north of China, resides within a continental monsoon climate characterized by

TABLE 1 Research data and sources.

Name	Detailed data	Source
DEM	30 m resolution	Geospatial Data Cloud https://www.gscloud.cn/
LULC	30 m resolution, LULC details for 2000, 2010 and 2020	Resources and Environmental Science and Data Center https://www.resdc.cn/
Meteorological data	Average annual rainfall data	Resources and Environmental Science and Data Center https://www.resdc.cn/
Agricultural area data	Data of China's nine major agricultural regionalization, China's agricultural maturing regionalization and China's nine major river basins	Resources and Environmental Science and Data Center https://www.resdc.cn/
Administrative boundary	Beijing, Tianjin, Hebei, Henan, Shandong within the scope of 47 municipalities	Resources and Environmental Science and Data Center https://www.resdc.cn/
Statistical data	Arable land area, nitrogen and compound fertilizer yield, crop yield, livestock breeding and rural population	Statistical Yearbook of China and provinces

warm temperate sub-humid conditions, fostering unique opportunities for agricultural advancement. With ample rainfall and abundant light and heat resources, this region offers an optimal natural milieu for crop cultivation (Zhao et al., 2022). Boasting a deep and fertile soil layer, the Huang-Huai-Hai Plain primarily engages in dry farming practices. Notably, it serves as a pivotal hub for the cultivation of staple grain crops like wheat and corn, cementing its status as a significant contributor to China's grain, cotton, and oil production (Liu et al., 2022).

This study specifically targets the Huang-Huai-Hai Plain, recognized among the nine principal agricultural regions designated by the Chinese Academy of Sciences. Encompassing Beijing, Tianjin, Shandong, Hebei, and Henan provinces, the area under investigation comprises 47 prefectures and cities. The study area encompasses a total expanse of 542, 30, 000 ha, experiencing an average rainfall of 715 mm over the span of 2000–2020 years. Within this domain, considerable regional disparities exist in both agricultural production and non-point source pollution.

2.2 Data sources

This study utilized the InVEST model to simulate the spatial and temporal dynamics of ANNSP across the Huang-Huai-Hai Plain. The model execution necessitated a range of data inputs, including Digital Elevation Model (DEM), land use and land cover (LULC), meteorological data, agricultural area data, administrative boundaries, and statistical data. The detailed specifics of the data employed in this investigation, alongside their respective sources, are comprehensively documented in Table 1.

2.3 Methods

2.3.1 InVEST model

The InVEST model leverages the robust capabilities of ArcGIS software and establishes a sophisticated framework for assessing ecosystem functions (Redhead et al., 2018). By integrating diverse natural data inputs, the model dynamically analyzes ecosystem service volumes, offering regional decision makers an intuitive, quantitative perspective on how ecosystem changes impact human wellbeing consequences. The InVEST model seeks to reconcile economic development with socio-ecological expectations, aiming to optimize sustainable resource allocation by promoting economic growth while safeguarding ecosystem health and resilience. Applied and validated in fields such as water conservation (Li et al., 2021a), habitat service quality assessment (Wu et al., 2021), and carbon storage estimation (Zhao et al., 2019), the model has garnered recognition for its accuracy and practical utility. Compared to similar models, InVEST stands out due to its straightforward parameters, clear mechanisms, and significant advantages in spatial information processing, database technology, mathematical calculations, and visual representation (Wei et al., 2022).

2.3.1.1 NDR module

The NDR module, integral to the InVEST model, is designed to simulate and assess nutrient transport within ecosystems. Built upon a hydrological framework, it replicates water volume, fluid dynamics, and flow paths, integrating crucial hydrological factors such as rainfall, evaporation, and runoff to precisely evaluate nutrient transport via runoff (Small et al., 2023). In this study, the NDR module adjusts total nitrogen (TN) input loads based on the watershed's Runoff Potential Index (RPI) grid to compute the nitrogen transport rate at each pixel, as outlined in Equations 1–5. This analysis focuses on surface nutrient transport dynamics.

$$load_{mod}(x,i) = load(x,i) \cdot RPI_i \tag{1}$$

$$RPI_i = RP_i / RP_a v \tag{2}$$

$$NDR_{surf,i} = NDR_{o,i}^{\left(1+\exp\left(\frac{IC_j - ICo}{k}\right)\right)^{-1}} \tag{3}$$

$$X_{\exp,i} = load_{surf,i} \cdot NDR_{surf,i} \tag{4}$$

$$X_{\exp,tot} = \sum_i X_{\exp,i} \tag{5}$$

Where $load_{mod}$ (x,i) is the nutrient load for each raster pixel i corrected. RPI_i is the runoff potential index. RP_i is the runoff agent on raster pixel i. $RP_a v$ is the average proxy parameter on the grid. $NDR_{surf,i}$ is the surface nitrogen transmission rate, $NDR_{o,i}$ is the nitrogen transmission rate retained by downstream pixels, IC_j is the

TABLE 2 Values of key parameters in the biophysical table.

LULC	*load_n*(kg/pixel)	*eff_n*	*crit_len_n*
Farmland	TN load	0.5	25
Forest land	2.9	0.8	280
Meadow	11	0.78	160
Water area	13	0.06	17
Unused land	15	0.02	25
Construction land	14	0.04	17
Wet land	9	0.02	11

TABLE 3 Correlation coefficient of straw return to fields.

Crop	R_i (kg/t)	C_i (kg/t)	F_i (%)	F_i (kg/t)
Paddy	0.97	0.82	71	7.95
Wheat	1.34	0.54	81	7.24
Corn	1.23	0.89	75	10.95
Potato	0.72	1.97	22	14.18
Soybean	1.53	0.89	18	13.62
Cotton	2.82	0.85	9	23.97
Oilseed	2.14	1.03	24	22.04

topographic index, IC_o and k are calibration parameters, $load_{surf,i}$ is the nitrogen load of surface pixel i corrected, $X_{exp,i}$ is the corrected nitrogen export load for each raster pixel i, $X_{exp,tot}$ is the corrected total nitrogen export load of all grids.

This study focused on surface nitrogen nutrients in farmland and simplified the parameters in the biophysical table (Table 2). Set the cumulative flow threshold to 2000 m^3/s, set the calibration parameter K to 2, and determine the *RPI* based on the annual rainfall.

2.3.2 Source list method

The source inventory method, widely recognized for its efficacy in identifying and quantifying pollution sources, particularly in estimating nitrogen contributions (Han et al., 2023a; Zhang et al., 2021a). In the context of China's agricultural and rural activities, significant non-point sources include fertilizer application, straw return to fields, livestock breeding, and rural life. The InVEST model leverages detailed pollution load data from the source inventory method to conduct comprehensive analyses of various pollution sources' impacts on ecosystem health. This process involves complex model operations addressing spatial dispersal, environmental transformation, and pollutant bioaccumulation. Moreover, Ding et al. (2023a) research underscores that statistical analysis of nitrogen output loads across farmland type further validates the InVEST model's predictions, enhancing its scientific accuracy and reliability. Crucially, the source inventory method not only quantifies the specific contributions of each pollution source to nitrogen pollution (Fu et al., 2023; Wang et al., 2023a) but also accurately identifies principal sources, providing a data foundation for targeted pollution management strategies.

2.3.2.1 Fertilizer application

The quantification of nitrogen within applied fertilizers was determined by transforming the pure nitrogen content of both nitrogen fertilizers and nitrogen-containing compound fertilizers into statistical data. For nitrogen-containing compound fertilizers, a standardized assumption was made regarding the ratios of nitrogen to phosphorus to potassium, establishing a uniform ratio of 1:1:1, as detailed by Li et al. (2023a). The calculation formula is expressed as Equation 6:

$$N_{fer} = N_f + \frac{N_{cf}}{3} \tag{6}$$

Where N_{fer} is the input quantity of nitrogen-containing fertilizers, N_f is the amount of nitrogen fertilizer applied, N_{cf} is the amount of nitrogen-containing compound fertilizer applied.

2.3.2.2 Straw return to fields

Within this investigation, the TN content arising from the practice of returning to cropped fields was assessed across seven distinct crop types. The computation of the nitrogen surface source pollution load induced by straw returning to fields necessitates a comprehensive consideration of factors, including straw type, yield, crop-to-straw ratio, nitrogen content, the proportion of straw returned to fields, and product coefficient, as elucidated by Liu et al. (2021). The numerical values for each parameter (Table3) are extracted from pertinent literature sources (Yin et al., 2018; Zhang et al., 2021b; Wang et al., 2023b). The calculation formula is expressed as Equation 7:

$$N_{str} = \sum_i Y_i \cdot R_i \cdot C_i \cdot F_i \cdot P_i \tag{7}$$

Where N_{str} is the TN input into farmland resulting from the practice of returning crop straw to fields, Y_i is the yield of crop i, R_i is the ratio of crop i to straw, C_i is the nitrogen content in crop i, F_i is the proportion of crop i's straw returned to fields, P_i is the pollution production coefficient of crop i.

2.3.2.3 Livestock breeding

The ANNSP loss load stemming from livestock breeding is computed by utilizing metrics such as breeding volume alongside coefficients for manure and urine pollution generation. As reported in statistical yearbooks, the spectrum of livestock and poultry farming primarily encompasses large animals (cows, horses, donkeys, mules), pigs, sheep, and poultry. The coefficients for manure and urine excretion stand at 61.1, 4.51, 2.28, and 0.275 kg· head/piece^{-1}· a^{-1}, respectively, as documented by Chen et al. (2023b) and Qiu et al. (2021). The calculation formula is expressed as Equation 8:

$$N_{lp} = \sum_i Q_i \cdot E_i \tag{8}$$

Where N_{lp} is the TN input into agriculture stemming from animal husbandry, Q_i is the quantity of livestock i at the end of the year, E_i is the coefficient of fecal excretion for livestock i.

2.3.2.4 Rural life

Within the purview of this inquiry, the TN load ascribed to rural settings emanates solely from domestic sewage, solid waste, and fecal

TABLE 4 Non-point source pollution pattern of study area.

Mode number	Pattern	TN loss coefficient (%)	TN base loss (kg/ha)
5	Northern Plateau Mountain Region - Gentle Slope - Terraced Fields - Arid Land - Single Cropping of Large Fields	0.120	0.210
11	Northern Plateau Mountain Region - Steep Slope - Terraced Fields - Arid Land - Garden Plot	0.220	0.990
12	Northern Plateau Mountain Region - Steep Slope - Terraced Fields - Arid Land - Single Cropping of Large Fields	0.105	0.120
18	Northeast Semi-humid Plain Region - Flat Land - Arid Land - Single Cropping of Large Fields	0.180	0.315
23	Huang-Huai-Hai Semi-humid Plain Region - Flat Land - Arid Land - Single Cropping of Large Fields	0.563	3.315
25	Huang-Huai-Hai Semi-humid Plain Region - Flat Land - Arid Land - Double or More Croppings of Large Fields	0.950	6.315
40	Southern Mountainous and Hilly Region - Gentle Slope - Terraced Fields - Arid Land - Double or More Croppings of Large Fields	1.270	14.865
46	Southern Mountainous and Hilly Region - Steep Slope - Terraced Fields - Arid Land - Double or More Croppings of Large Fields	0.333	1.605
52	Southern Mountainous and Hilly Region - Steep Slope - Terraced Fields - Paddy Fields - Rice-Wheat Rotation	0.519	15.690
57	Southern Mountainous and Hilly Region - Gentle Slope - Terraced Fields - Paddy Fields - Rice-Wheat Rotation	0.577	15.000

waste generated by the rural populace (Zou et al., 2020). The calculation formula is expressed as Equation 9:

$$N_{rl} = P_i \cdot W_i \tag{9}$$

Where N_{rl} is the TN input into agriculture originating from rural life, P_i is the number of individuals in the rural community, W_i is the pollution coefficient attributed to each rural resident, calculated based on the standard of 1.58 kg per person per year.

2.3.2.5 Loss pattern

According to the manual *Agricultural Pollution Source Fertilizer Loss Coefficient* determine the pollution emission coefficient of different land loss patterns. The formula for calculating nitrogen is based on the pollution loss load of the source list method as shown in Equation 10:

$$N = N_{fer,ij} \cdot E_j + Q_j + \left(N_{str} + N_{lp} + N_{rl}\right) \cdot U_i \tag{10}$$

Where N is the pollution TN discharge, E_j is the TN loss coefficient of non-point source pollution pattern j (Table 4), Q_j is the basic loss, U_i is the pollution emission factor for different sources.

2.3.3 Hotspot analysis

Utilizing the Getis-Ord G_i^* index, a statistical technique renowned for pinpointing clusters of elevated and diminished values, we conducted cold and hot spot zoning. This methodology, widely utilized in geographical research, enables the identification and interpretation of spatial distribution patterns (Tran et al., 2022). Subsequently, based on Getis-Ord G_i^* index, we categorized the hotspot analysis results into five distinct grades. This grading system facilitates a nuanced comprehension of nitrogen emission distribution, thereby aiding in the pinpointing of CSAs. The specific grading principles and calculation formulas are elaborated in Equations 11–13.

$$\bar{X} = \frac{\sum_{i=1}^{n} X_j}{n} \tag{11}$$

$$S = \sqrt{\frac{\sum_{i=1}^{n} X^2}{n-1} - \bar{X}} \tag{12}$$

$$G_i^* = \frac{\sum_{j=1}^{n} W_{ij} - \bar{X}\sum_{j=1}^{n} W_{ij}}{\sqrt{\frac{\sum_{j=1}^{n} {W_{ij}}^2 - \left(\sum_{j=1}^{n} W_{ij}\right)^2}{n-1}}} \tag{13}$$

Where G_i^* is the Getis-Ord index, X_j is the nitrogen emission intensity of unit j, $\bar{X}$ is the mean nitrogen emission intensity of all units, W_{ij} is the spatial weight coefficient between regions i or j, n is the total number of study units.

2.3.4 Geodetector

The Geodetector emerges as a potent instrument, endowed with the capacity for both factor detection and interactive detection, predicated on the resemblance between the contribution of driving factors and their spatial dispersion (Duan and Li, 2023). A meticulous examination involved statistical partitioning of TN emission intensity (Y). The subsequent phase involved the discretization of multiple independent variables, encompassing DEM (X_1), slope (X_2), annual rainfall (X_3), proportion of farmland in each city (X_4), TN input intensity (X_5), N_{fer} (X_6), N_{str} (X_7), N_{lp} (X_8), and N_{rl} (X_9). This study elucidates the impact of driving factors on spatial variations in nitrogen emission intensity, facilitating the identification of key individual factors

through the q value measure developed by Li et al. (2022) and Shi et al. (2023). The calculation formula is expressed as Equation 14:

$$q = 1 - \frac{\sum_{h=1}^{L} N_h \sigma_h^2}{N\sigma^2} \quad (14)$$

Where q represents the explanatory degree of X on Y, h is to the stratification of variable Y or factor X, N_h is the number of units in layer h, N represents the entire region, σ_h^2 and σ^2 denote the variances in layer h and the entire region, respectively. The q-value ranges from 0 to 1, with a larger value signifying a more pronounced explanatory power of X on Y. A heightened q value corresponds to a more robust driving effect of that factor on the spatial-temporal evolution of agricultural nitrogen non-point source pollution, while a diminished q value suggests a weaker effect.

3 Results and analysis

3.1 Comparison of InVEST model and source list method

The source list method offers a more comprehensive assessment of nitrogen pollution loads by recording and analyzing various nitrogen input sources. In contrast, the InVEST model may be constrained by its structure and parameter settings, limiting its ability to fully capture all significant nitrogen sources. Therefore, the source list method serves as a crucial supplement to the InVEST model, enhancing the accuracy of nitrogen input information. This study integrates the source list method with the InVEST model to provide a quantitative evaluation of nitrogen point source pollution. Focusing on farmland, a pivotal land use category, we calculated the agricultural surface nitrogen non-point source pollution load for each city and assessed its contribution to the overall load (Table 5), thereby illuminating the potential environmental consequences of agricultural activities. Notably, the source list method consistently yielded higher nitrogen output estimates than the InVEST model across the three temporal snapshots of 2000, 2010, and 2020. Nitrogen pollution is a dynamic process influenced by various factors, including climate change, land use changes, and agricultural management practices. The source list method is limited in its ability to detect small-scale variations in nitrogen pollution and cannot accurately simulate the loss and transformation of nitrogen fertilizers in agricultural settings. In contrast, the InVEST model incorporates a wider range of influential factors, offering a more comprehensive analysis of nitrogen dynamics.

Further scrutiny of farmland's nitrogen output contribution to the total nitrogen non-point source pollution load reveals that the source tabulation method consistently yielded percentages of 67.24%, 64.93%, and 65.37% across the analyzed periods, underscoring the persistence of farmland as the primary source of nitrogen pollution load. The InVEST model estimates, albeit slightly varying at 64.32%, 62.7%, and 62.43%, agree on the pivotal role of farmland nitrogen management in regional pollution control. This congruence resonates with the recent findings of Ding et al. (2023a), reinforcing the InVEST model's applicability and credibility in assessing agricultural nitrogen non-point source pollution. The similar nitrogen output ratios across farmland primarily stem from the consistent role of farmland as a major source of nitrogen pollution and the uniformity of agricultural management practices.

On the basis of detailed analysis of the input ratio of each nitrogen source (Table 6), this study clearly pointed out that fertilizer application and livestock breeding were the main pollution sources of agricultural TN load. Specifically, from 2000 to 2020, nitrogen fertilizer application and livestock farming accounted for a significant share of total TN output load, with the former contributing 54.66%–66.09%, and the latter contributing 24.56%–30.71%. This data distribution not only revealed the main drivers of agricultural nitrogen pollution, but also mapped the profound changes in the structure and mode of agricultural production. Looking at the dynamics over this time period, we notice a striking trend: with the acceleration of urbanization, the expansion of urban areas inevitably leads to the reduction of arable land, and while the absolute demand for agricultural output may fluctuate due to a variety of factors, agricultural activity itself shows a relatively concentrated growth trend. In this context, agricultural producers tend to increase the application amount of nitrogen fertilizer in order to maintain or increase production. Meanwhile, the large-scale development of animal husbandry has further aggravated the burden of nitrogen emissions.

3.2 Analysis of TN emission intensity

In this survey, the TN output load per hectare of farmland served as a quantitative indicator for assessing agricultural non-point source pollution (ANNSP) emission intensity across various cities, with classifications derived using the natural breaks method (Figure 2). Analysis of data from 2000, 2010, and 2020 reveals average TN output loads of 8.43 kg/ha, 4.08 kg/ha, and 3.66 kg/ha, respectively.

Temporally, a noteworthy decreasing trend in TN emission intensity was evident across all cities. Spatially, there existed significant heterogeneity in TN emission intensity, with an overarching pattern of "northwest low, southeast high," aligning with the distribution of TN output load. This implies that farmland exerts minimal influence on the spatial distribution of TN emission intensity. It is pertinent to highlight that throughout all study years, Xinyang exhibited the highest TN emission intensity, registering values of 27.28 kg/ha, 9.49 kg/ha, and 10.87 kg/ha, respectively. In contrast, Zhangjiakou consistently demonstrated the lowest TN emission intensity, with values of 0.67 kg/ha, 0.41 kg/ha, and 0.26 kg/ha, respectively.

The decline in agricultural TN emission intensity can be primarily attributed to the formulation and execution of pertinent policies. Since 2015, China's Ministry of Agriculture has spearheaded the implementation of the *Action Plan to Achieve Zero Growth in Fertilizer Use* by 2020. This strategic initiative aims at progressively curtailing fertilizer application through the adoption of scientific fertilization practices and enhanced fertilization techniques. Concurrently, heightened emphasis from local administrations on agricultural environmental preservation has propelled the widespread promotion of eco-friendly agricultural methodologies and

TABLE 5 Comparison of farmland TN output between InVEST model and source list method.

Time	Source list		InVEST	
	Value (t/a)	Percentage	Value (t/a)	Percentage
2000 Year	574,550	67.24%	274,445	64.32%
2010 Year	483,227	64.93%	149,293	62.70%
2020 Year	396,274	65.37%	120,251	62.43%

TABLE 6 Sources and proportion of TN input load in agriculture.

Type of contamination source	2000 Year		2010 Year		2020 Year	
	Value (t/a)	Percentage	Value (t/a)	Percentage	Value (t/a)	Percentage
Fertilizer application	694,647	54.66%	693,685	60.52%	612,922	66.09%
Straw return to fields	5,351	0.42%	7,886	0.69%	7,557	0.81%
Livestock breeding	390,267	30.71%	332,272	28.99%	227,784	24.56%
Rural life	180,578	14.21%	112,305	9.80%	79,105	8.53%

approaches. This concerted effort has incentivized farmers to embrace alternatives such as organic fertilizers, biofertilizers, and other substitutes for chemical fertilizers, thereby curbing fertilizer usage and subsequently mitigating TN emissions. Moreover, governmental oversight of ANNSP has intensified, ushering in measures such as farmland drainage regulation and livestock breeding pollution management. These interventions further contribute to the reduction of TN emission intensity, thus fostering positive strides towards agricultural sustainability and ecological preservation.

3.3 Identification of critical source areas

To delineate the CSAs of ANNSP in the Huang-Huai-Hai Plain, this study employed the ArcGIS hotspot analysis tool. We conducted an extensive examination of data from 2000, 2010, and 2020, focusing on the agricultural TN emission intensity of individual cities. By configuring various levels of confidence, we derived the classification outcomes of CSAs (Figure 3).

In 2000, 2010, and 2020, the cumulative TN loads from CSAs represented 26%, 7%, and 28% of the entire study area, respectively. Temporally, the CSAs displayed a trend of initial contraction followed by expansion. Specifically, the number of cities situated within CSAs decreased from 5 to 2, before rising to 6. Regarding spatial distribution, CSAs progressively extended from the southern to the southeastern areas of the study domain. Initially, in 2000, the CSAs were dispersed across the southeastern region of Henan Province, encompassing Xuchang, Luohe, Zhoukou, Zhumadian, and Xinyang. By 2010, the CSAs were predominantly concentrated in the southern expanse of Henan Province, specifically in Luohe and Zhumadian. By 2020, these regions were primarily situated in the southeastern territories of Henan and Shandong provinces, including Xinyang, Linyi, Qingdao, Rizhao, Weifang, and Zibo.

The CSAs are significantly influenced by factors such as terrain and agricultural practices. These factors contribute to notable variations in soil moisture conditions and erosion resistance compared to other regions. Consequently, nitrogen nutrients are more susceptible to loss through runoff and leaching in these areas. Addressing this challenge necessitates a focus on improving ANNSP management practices and optimizing cropping structures within these CSAs. The integration of 3S (Geographic Information System (GIS), Global Positioning (GPS) and Remote Sensing (RS)) technologies and mechanistic models facilitates a more precise identification of CSAs for ANNSP. By simulating pollutant migration paths, transformation processes, and output continuity, these technologies aid in pinpointing the most polluted areas and locations within the study region. In CSAs such as Henan and southeastern Shandong, GIS and RS technologies were leveraged to monitor soil moisture and rainfall, thereby informing agricultural production practices. Initiatives included the advancement of water-saving irrigation technologies to mitigate water and nitrogen loss, as well as the promotion of crop varieties tailored to local climatic and soil conditions to bolster resilience against erosion.

3.4 Spatial evolutionary drivers analysis

In this investigation, by employing Geodetector, we scrutinized the discrimination and identification of factors influencing agricultural TN emission intensity across various cities within the Huang-Huai-Hai Plain, aiming to elucidate the primary drivers impacting nitrogen emissions in the region (Figure 4). Our findings revealed temporal variations in the main influencing factors. Specifically, in 2000, key drivers included annual rainfall (X_3), TN input intensity (X_5), and DEM (X_1) (a). Conversely, by 2010, the primary factors shifted to encompass annual rainfall (X_3), N_{rl} (X_9), and the proportion of farmland in each city (X_4) (b). This transition can be attributed to extensive rural-to-urban migration

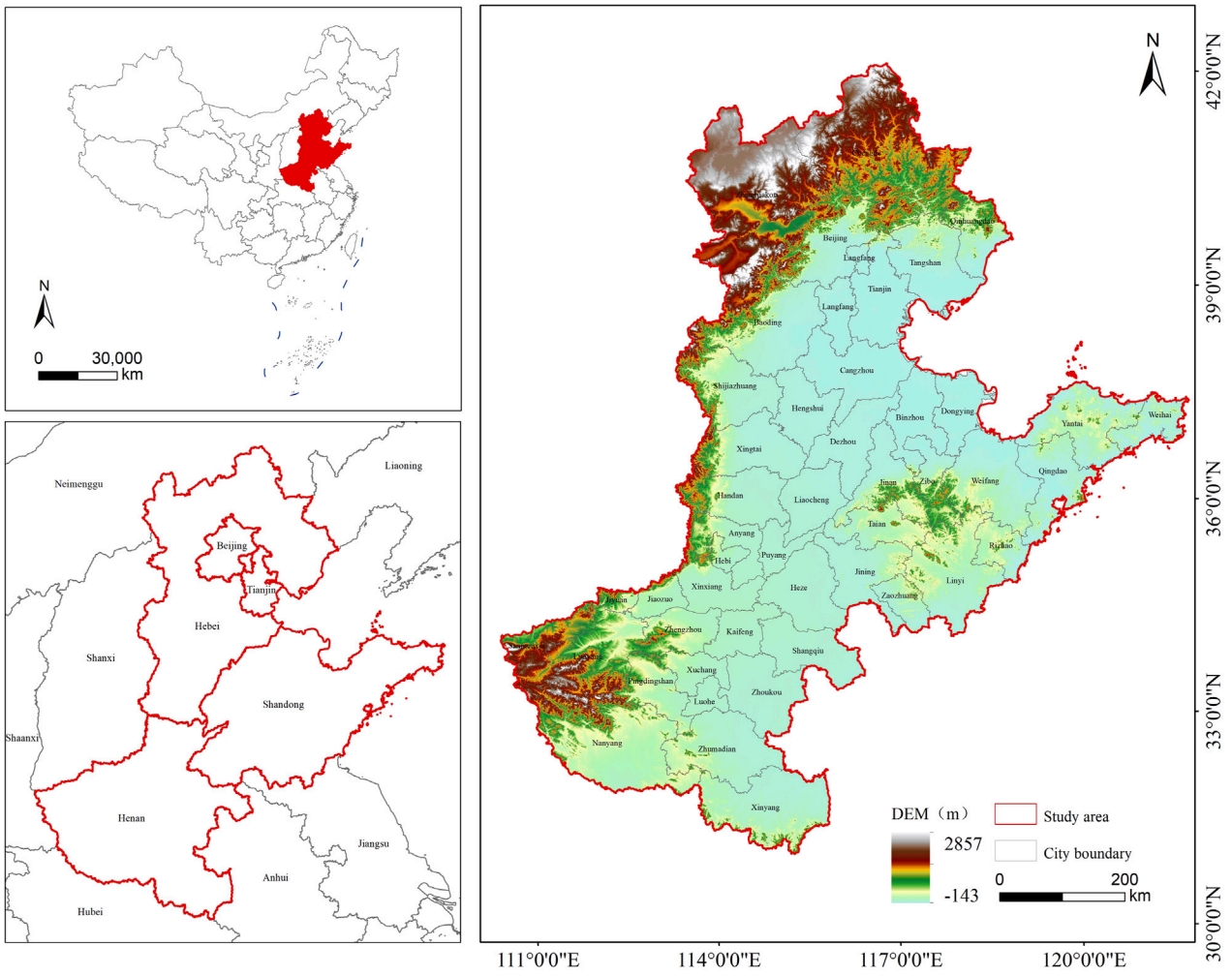


FIGURE 1
The location of the Huang-Huai-Hai Plain.

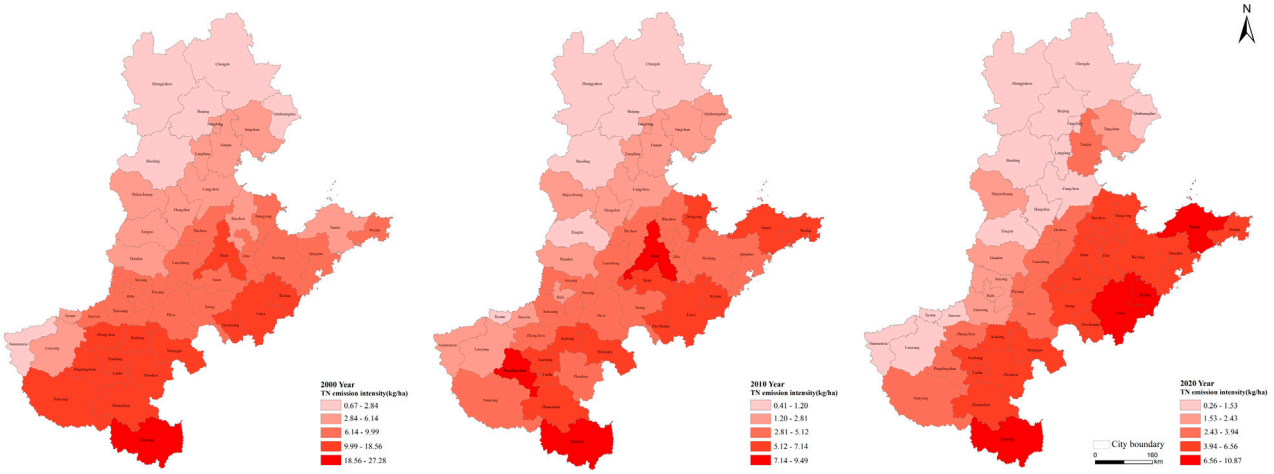


FIGURE 2
Agricultural TN emission intensity.

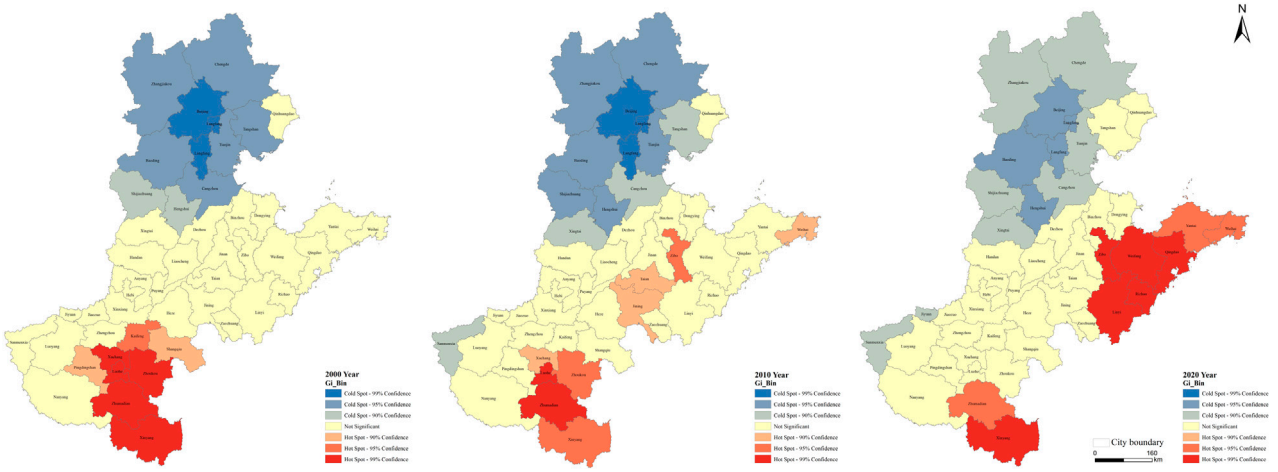


FIGURE 3
The classification outcomes of hotspot analysis.

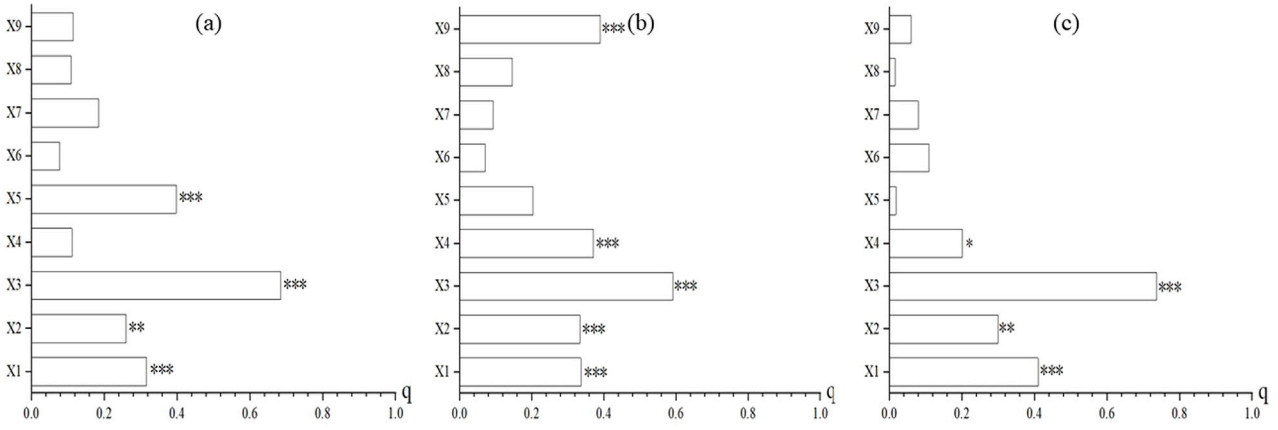


FIGURE 4
The contribution of driving factors. Note: **(A–C)** for the years 2000, 2010 and 2020, respectively. ***, ** and * are significant at 1%, 5% and 10% levels respectively.

between 2000 and 2010, alongside rapid declines in farmland concurrent with ongoing urbanization. Come 2020, the principal drivers comprised annual rainfall (X_3), DEM (X_1), and slope (X_2) (c). Notably, the enduring stability of annual rainfall (X_3) as a driving factor across time scales warrants attention. Furthermore, significance level analyses underscored the pivotal roles of rainfall and terrain in shaping agricultural TN emission intensity. Nitrogen pollutants are predominantly influenced by rainfall-runoff and erosion processes, leading to their ingress into water bodies, concomitant with changes in terrain elevation, ultimately polluting receiving waters.

Rainfall exerts a profound impact on pollution discharge, primarily influencing surface runoff and soil erosion, which can enhance soil nitrogen dissolution and facilitate nitrogen emissions. Additionally, rainfall interacts with topographic features, such as elevation and slope, exacerbating runoff and erosion in sloped areas, thereby intensifying nitrogen loss and acting as a crucial regulatory factor in agricultural nitrogen emissions. However, the spatio-temporal variability of rainfall impacts, constrained by regional and seasonal differences, complicates nitrogen pollution prevention and control. Consequently, effective ANNSP management strategies must account for the interplay between rainfall and terrain, implementing targeted measures to mitigate their adverse environmental effects.

4 Discussion

4.1 Comparison between source list method and InVEST model

This study employed the source list method to quantify primary nitrogen input sources in the Huang-Huai-Hai Plain and simulated the dynamic effects of agricultural nitrogen pollution on river

nitrogen flux for the years 2000, 2010, and 2020 using an optimized NDR module. By comparing the total agricultural nitrogen inflow estimated through the source list method with outputs from the InVEST model, we rigorously assessed the consistency and complementary strengths of these approaches in evaluating the contribution of farmland nitrogen pollution. The theoretical framework provided by Ding et al. (2023a) underpins this analysis. The findings indicate that fertilizer overapplication and inadequate livestock management are major drivers of agricultural nitrogen pollution in the region, aligning with the prevailing consensus (Zhou et al., 2023) and underscoring the pivotal role of agricultural practices in the regional nitrogen cycle. Notably, the source listing method offers comprehensive nitrogen input data and helps identify key sources potentially overlooked by the InVEST model, thereby enhancing the accuracy of nitrogen pollution assessments. Meanwhile, the InVEST model excels in simulating nitrogen dynamics under complex environmental conditions, particularly when considering multiple factors such as climate change, land use change, and agricultural practices. Although the two methods differ in total agricultural nitrogen emissions, this discrepancy is attributed to their varying sensitivities to complex environmental factors, rather than any fundamental shortcomings in model suitability.

4.2 Effects of simulation and attribution analysis of ANNSP

The ANNSP emissions within the Huang-Huai-Hai Plain manifest distinct spatial disparities, presenting formidable challenges for pollution management. To more efficiently address these concerns, each region must comprehensively assess its agricultural production status and objectives. Tailored agricultural non-point source pollution control measures should be devised, taking into account the unique characteristics of pollution sources, economic development levels, and environmental conservation imperatives. For instance, implementing and enhancing a contemporary fertilization technology infrastructure, advocating for environmentally friendly, scientifically guided, and precise fertilization practices (Tian et al., 2023), pioneering innovative approaches for crop residue utilization, and augmenting utilization efficiencies. Furthermore, there is a pressing need to delve deeper into the origins, systems, and holistic treatment of ANNSP (Wang et al., 2023a).

In the face of increasingly severe ANNSP issues, strengthening research and control efforts is particularly urgent. Considering economic costs and implementation difficulties, focusing governance on CSAs is a wise choice (Tao et al., 2023). By prioritizing strengthening management measures and reasonably arranging the layout of governance projects, investment efficiency can be significantly improved, land resources can be saved, pollution control difficulties can be reduced, and better achievement of expected governance goals can be achieved, coordinating the relationship between agricultural production and environmental protection (Han et al., 2023b). In CSAs like Henan and southeastern Shandong, 3S technology was employed to steer agricultural production. Advocate improving the comprehensive utilization efficiency of straw and water-saving irrigation technology to reduce the loss of water and nitrogen (Yin et al., 2018).

4.3 The improvement direction of research

In forthcoming applications, the integration of the InVEST model with the PLUS model (Zhu et al., 2024) and prospective climate scenario (Li et al., 2023b) data holds promise for advancing non-point source pollution prediction and analysis. Additionally, to achieve more effective ANNSP control, factors other than CSAs identification and management need to be considered. For example, the promotion and application of agricultural technology, the formulation and implementation of policies and regulations, farmers' environmental awareness and participation. These factors have important impacts on ANNSP control and management and need to be considered in future studies.

5 Conclusion

Based on the results of InVEST model, this study delved into the pivotal agricultural nitrogen non-point source pollution hotspots in the Huang-Huai-hai Plain and their tailored mitigation strategies. Key findings reveal:

(1) Although the source listi method yielded a higher load estimate than the InVEST model simulation, both concurred on the consistent proportion of output nitrogen from farmland. Over-fertilization and livestock breeding emerged as the primary contributors to TN loads within the agricultural landscape of the Huang-Huai-Hai Plain.
(2) Time-series analysis unveiled a pronounced decrease in nitrogen emission intensity, accompanied by a spatial pattern characterized by a gradual increase from northwest to southeast.
(3) Throughout the study period, the CSAs experienced a dynamic shift, initially narrowing and subsequently expanding. Notably, Xinyang City remained consistently situated within the CSAs.
(4) Factor detection analysis highlighted annual rainfall (X_3) as possessing the highest q-value in 2000, 2010, and 2020, underscoring rainfall as the primary driving factor shaping spatial variations in agricultural TN emission intensities across cities in the Huang-Huai-Hai Plain.

Data availability statement

The original contributions presented in the study are included in the article/supplementary material, further inquiries can be directed to the corresponding author.

Author contributions

YY: Conceptualization, Methodology, Writing–original draft. WC: Conceptualization, Funding acquisition, Writing–review and

editing. GJ: Data curation, Writing–review and editing. YG: Resources, Writing–review and editing. YC: Methodology, Writing–review and editing. SS: Writing–review and editing. YD: Formal Analysis, Writing–review and editing. QW: Supervision, Writing–review and editing.

Funding

The author(s) declare that financial support was received for the research, authorship, and/or publication of this article. This research was funded by the National Key Research and Development Project (2021YFD1700900).

Conflict of interest

The authors declare that the research was conducted in the absence of any commercial or financial relationships that could be construed as a potential conflict of interest.

Publisher's note

All claims expressed in this article are solely those of the authors and do not necessarily represent those of their affiliated organizations, or those of the publisher, the editors and the reviewers. Any product that may be evaluated in this article, or claim that may be made by its manufacturer, is not guaranteed or endorsed by the publisher.

References

Chang, D., and Zhang, Y. X. (2023). Farmland nutrient pollution and its evolutionary relationship with plantation economic development in China. *J. Environ. Manag.* 325, 116589. doi:10.1016/j.jenvman.2022.116589

Chao, X. B., Witthaus, L., Bingner, R., Jia, Y., Locke, M., and Lizotte, R. (2023). An integrated watershed and water quality modeling system to study lake water quality responses to agricultural management practices. *Environ. Model. Softw.* 164, 105691. doi:10.1016/j.envsoft.2023.105691

Chen, M. J., Janssen, A. B. G., de Klein, J. J. M., Du, X., Lei, Q., Li, Y., et al. (2023a). Comparing critical source areas for the sediment and nutrients of calibrated and uncalibrated models in a plateau watershed in southwest China. *J. Environ. Manag.* 326, 116712. doi:10.1016/j.jenvman.2022.116712

Chen, T., Lu, J. Y., Lu, T., Yang, X., Zhong, Z., Feng, H., et al. (2023b). Agricultural non-point source pollution and rural transformation in a plain river network: insights from Jiaxing city, China. *Environ. Pollut.* 333, 121953. doi:10.1016/j.envpol.2023.121953

Ding, L., Qi, C. C., and Zhang, W. Q. (2023a). Distribution characteristics of non-point source pollution of TP and identification of key source areas in Nanyi Lake (China) Basin: based on InVEST model and source list method. *Environ. Sci. Pollut. Res. Int* 30, 117464–117484. doi:10.1007/s11356-023-30405-y

Ding, W. L., Xia, J., She, D. X., Zhang, X., Chen, T., Huang, S., et al. (2023b). Assessing multivariate effect of best management practices on non-point source pollution management using the coupled Copula-SWAT model. *Ecol. Indic.* 153, 110393. doi:10.1016/j.ecolind.2023.110393

Duan, T. T., and Li, Y. X. (2023). A multiscale analysis of the spatially heterogeneous relationships between non-point source pollution -related processes and their main drivers in Chaohu Lake watershed, China. *Environ. Sci. Pollut. Res. Int* 30, 86940–86956. doi:10.1007/s11356-023-28233-1

Fu, D., Gong, Y., Chen, C. T., Gui, X., Liu, H., Chen, S., et al. (2023). Nitrogen and phosphorus loading characteristics of agricultural non-point sources in the tuojiang River Basin. *Water* 15, 3503. doi:10.3390/w15193503

Ghebremichael, L. T., Veith, T. L., and Hamlett, J. M. (2013). Integrated watershed- and farm-scale modeling framework for targeting critical source areas while maintaining farm economic viability. *J. Environ. Manag.* 114, 381–394. doi:10.1016/j.jenvman.2012.10.034

Giri, S., Nejadhashemi, A. P., and Woznicki, S. A. (2012). Evaluation of targeting methods for implementation of best management practices in the Saginaw River Watershed. *J. Environ. Manag.* 103, 24–40. doi:10.1016/j.jenvman.2012.02.033

Han, A. X., Liu, P. Y., Wang, B. F., and Zhu, A. (2023a). E-commerce development and its contribution to agricultural non-point source pollution control: evidence from 283 cities in China. *J. Environ. Manag.* 344, 118613. doi:10.1016/j.jenvman.2023.118613

Han, B. S., Reidy, A., and Li, A. H. (2021). Modeling nutrient release with compiled data in a typical Midwest watershed. *Ecol. Indic.* 121, 107213. doi:10.1016/j.ecolind.2020.107213

Han, Y., Liu, Z., Chen, Y. F., Liu, H., Song, L., et al. (2023b). Assessing non-point source pollution in an apple-dominant basin and associated best fertilizer management based on SWAT modeling. *Int. Soil Water Conservation Res.* 11, 353–364. doi:10.1016/j.iswcr.2022.10.002

Hoang, L., Mukundan, R., Moore, K. E. B., Owens, E. M., and Steenhuis, T. S. (2019). Phosphorus reduction in the New York City water supply system: a water-quality success story confirmed with data and modeling. *Ecol. Eng.* 135, 75–88. doi:10.1016/j.ecoleng.2019.04.029

Hou, L., Zhou, Z. Y., Wang, R. Y., Li, J., Dong, F., and Liu, J. (2022). Research on the non-point source pollution characteristics of important drinking water sources. *Water* 14, 211. doi:10.3390/w14020211

Ji, Y., Gao, D. M., Liu, Q. L., Su, J., Liu, Y., Zhao, J., et al. (2023). An integrated framework for agricultural non-point source pollution control technology evaluation: application of an improved multiple attribute decision making method. *Expert Syst. Appl.* 229, 120319. doi:10.1016/j.eswa.2023.120319

Jolly, Y. N., Rakib, M. R. J., Kumar, R., Sultana, S., Rahman, S. M. M., Kabir, J., et al. (2023). Evaluation of surface water quality near pollution sources in Buriganga River and deciphering their probable emergence, ecological, and health risk aspects. *Regional Stud. Mar. Sci.* 63, 102988. doi:10.1016/j.rsma.2023.102988

Lee, H., Kim, H., Kim, J., Jun, S. M., Hwang, S., Song, J. H., et al. (2023). Analysis of the effects of low impact development practices on hydrological components using HSPF. *J. Hydro-Environment Res.* 46, 72–85. doi:10.1016/j.jher.2023.01.001

Li, B. Z., Guo, B., Zhu, Q. B., and Zhuo, N. (2023a). Impact of technical training and personalized information support on farmers' fertilization behavior: evidence from China. *Sustainability* 15, 8925. doi:10.3390/su15118925

Li, M. Y., Liang, D., Xia, J., Song, J., Cheng, D., Wu, J., et al. (2021a). Evaluation of water conservation function of danjiang River Basin in qinling mountains, China based on InVEST model. *J. Environ. Manag.* 286, 112212. doi:10.1016/j.jenvman.2021.112212

Li, Q., Yang, Z. H., Yue, Y., and Zhong, H. (2021b). Variation of total phosphorus concentration and loads in the upper Yangtze River and contribution of non-point sources. *Water Supply* 21, 1687–1700. doi:10.2166/ws.2021.015

Li, Q. S., Zhang, J. C., Zhang, J. W., Gao, H., Chen, W., Huang, J., et al. (2023b). Spatial and temporal distribution characteristics and prediction analysis of nitrogen and phosphorus surface source pollution in Shandong Province under the climate and land use changes. *Front. Ecol. Evol.* 11. doi:10.3389/fevo.2023.1231394

Li, X. C., Niu, Y., He, Q. N., and Wang, H. (2022). Identifying driving factors of the runoff coefficient based on the geographic detector model in the upper reaches of Huaihe River Basin. *Open Geosci.* 14, 1421–1433. doi:10.1515/geo-2022-0438

Liu, B. Y., Lin, B. J., Li, X. X., Virk, A. L., N'dri Yves, B., Zhao, X., et al. (2021). Appropriate farming practices of summer maize in the North China Plain: reducing nitrogen use to promote sustainable agricultural development. *Resour. Conservation Recycl.* 175, 105889. doi:10.1016/j.resconrec.2021.105889

Liu, C., Qu, L. Q., Clausen, J., Lei, T., and Yang, X. (2023). Impact of riparian buffer zone design on surface water quality at the watershed scale, a case study in the jinghe watershed in China. *Water* 15, 2696. doi:10.3390/w15152696

Liu, J., Fu, B., Zhang, C. H., and Wang, Y. k. (2019). Modelling spatial variation in the treatment costs of non-point source pollution in mountainous regions of southwest China. *J. Mt. Sci.* 16 (8), 1901–1912. doi:10.1007/s11629-018-5051-x

Liu, J., Sun, B., Shen, H. L., Ding, P., Ning, D., Zhang, J., et al. (2022). Crop water requirement and utilization efficiency-based planting structure optimization in the southern Huang-Huai-Hai Plain. *Agronomy-Basel* 12, 2219. doi:10.3390/agronomy12092219

Lu, Y. R., Wang, C., Yang, R. J., Sun, M., Zhang, L., Zhang, Y., et al. (2023). Research on the progress of agricultural non-point source pollution management in China: a review. *Sustainability* 15, 13308. doi:10.3390/su151813308

Luo, M., Liu, X. X., Legesse, N., Liu, Y., Wu, S., Han, F. X., et al. (2023). Evaluation of agricultural non-point source pollution: a review. *Water Air Soil Pollut.* 234, 657. doi:10.1007/s11270-023-06686-x

Qiu, W. W., Zhong, Z. B., and Li, Z. L. (2021). Agricultural non-point source pollution in China: evaluation, convergence characteristics and spatial effects. *Chin. Geogr. Sci.* 31, 571–584. doi:10.1007/s11769-021-1200-1

Redhead, J. W., May, L., Oliver, T. H., Hamel, P., Sharp, R., and Bullock, J. M. (2018). National scale evaluation of the InVEST nutrient retention model in the United Kingdom. *Sci. Total Environ.* 610, 666–677. doi:10.1016/j.scitotenv.2017.08.092

Scordo, F., Lavender, T. M., Seitz, C., Perillo, V. L., Rusak, J. A., Piccolo, M. C., et al. (2018). Modeling water yield: assessing the role of site and region-specific attributes in determining model performance of the InVEST seasonal water yield model. *Water* 10, 1496. doi:10.3390/w10111496

Shi, S. H., Wang, X. L., Hu, Z. R., Zhao, X., Zhang, S., Hou, M., et al. (2023). Geographic detector -based quantitative assessment enhances attribution analysis of climate and topography factors to vegetation variation for spatial heterogeneity and coupling. *Glob. Ecol. Conservation* 42, e02398. doi:10.1016/j.gecco.2023.e02398

Shirazi, S. Z., Mei, X. R., Liu, B. C., and Liu, Y. (2022). Estimating potential yield and change in water budget for wheat and maize across Huang-Huai-Hai Plain in the future. *Agric. Water Manag.* 260, 107282. doi:10.1016/j.agwat.2021.107282

Small, G. E., Martensson, N., Janke, B. D., and Metson, G. S. (2023). Potential for high contribution of urban gardens to nutrient export in urban watersheds. *Landsc. Urban Plan.* 229, 104602. doi:10.1016/j.landurbplan.2022.104602

Tao, W., Wei, J., and Wang, N. L. (2023). The characteristics of non-point source nitrogen pollution in the lower reaches of huangshui basin in western China based on SWAT model. *Water Air Soil Pollut.* 234, 491. doi:10.1007/s11270-023-06480-9

Tian, M. L., Liu, R. F., Wang, J., Liang, J., Nian, Y., and Ma, H. (2023). Impact of environmental values and information awareness on the adoption of soil testing and formula fertilization technology by farmers-A case study considering social networks. *Agricilture-Basel* 13, 2008. doi:10.3390/agriculture13102008

Tran, D. X., Pearson, D., Palmer, A., Gray, D., Lowry, J., and Dominati, E. J. (2022). A comprehensive spatially-explicit analysis of agricultural landscape multifunctionality using a New Zealand hill country farm case study. *Agric. Syst.* 203, 103494. doi:10.1016/j.agsy.2022.103494

Wang, J. L., Fu, Z. S., Qiao, H. X., Bi, Y., and Liu, F. (2023a). Identifying the spatial risk patterns of agricultural non-point source pollution in a Basin of the upper yangtze river. *Agronomy-Basel* 13, 2776. doi:10.3390/agronomy13112776

Wang, L., Wang, E. L., Qian, X., Gao, Y., Zhang, H., Li, Z., et al. (2023b). Optimal straw management co-benefits crop yield and soil carbon sequestration of intensive farming systems. *Land Degrad. and Dev.* 34, 2322–2333. doi:10.1002/ldr.4610

Wang, M. M., Jiang, T. H., Mao, Y. B., Wang, F., Yu, J., and Zhu, C. (2023c). Current situation of agricultural non-point source pollution and its control. *Water Air Soil Pollut.* 234, 471. doi:10.1007/s11270-023-06462-x

Wei, Q. Q., Abudureheman, M., Halike, A., Yao, K., Yao, L., Tang, H., et al. (2022). Temporal and spatial variation analysis of habitat quality on the PLUS-InVEST model for Ebinur Lake Basin, China. *Ecol. Indic.* 145, 109632. doi:10.1016/j.ecolind.2022.109632

Wu, L. L., Sun, C. G., Fan, F., et al. (2021). Estimating the characteristic spatiotemporal variation in habitat quality using the InVEST model-a case study from Guangdong-Hong Kong-Macao Greater Bay area. *Remote Sens.* 13, 1008. doi:10.3390/rs13051008

Yan, Y. Y., Guan, Q. S., Wang, M., Su, X., Wu, G., Chiang, P., et al. (2018). Assessment of nitrogen reduction by constructed wetland based on InVEST: a case study of the Jiulong River Watershed, China. *Mar. Pollut. Bull.* 133, 349–356. doi:10.1016/j.marpolbul.2018.05.050

Yin, H. J., Zhao, W. Q., Li, T., Cheng, X., and Liu, Q. (2018). Balancing straw returning and chemical fertilizers in China: role of straw nutrient resources. *Renewable& Sustain. Energy Rev.* 81, 2695–2702. doi:10.1016/j.rser.2017.06.076

Yue, Y. J., Yang, W. Q., and Wang, L. (2022). Assessment of drought risk for winter wheat on the Huanghuaihai Plain under climate change using an EPIC model-based approach. *Int. J. Digital Earth* 15, 690–711. doi:10.1080/17538947.2022.2055174

Zhang, Q. L., Hu, H. T., Wang, D. Y., et al. (2021a). Spatial distribution of nitrogen and phosphorus in Haihe Basin and their determinants. *J. Irrigation Drainage* 40 (4), 97–106. doi:10.13522/j.cnki.ggps.2020411

Zhang, S. J., Zhang, G., Wang, D. J., and Liu, Q. (2021b). Long-term straw return with N addition alters reactive nitrogen runoff loss and the bacterial community during rice growth stages. *J. Environ. Manag.* 292, 112772. doi:10.1016/j.jenvman.2021.112772

Zhang, X., Sun, S. H., and Yao, S. B. (2023). Spatiotemporal distribution and dynamic evolution of grain productivity efficiency in the Yellow River Basin of China. *Environ. Dev. Sustain.* 26, 12005–12030. doi:10.1007/s10668-023-03619-w

Zhao, M. M., He, Z. B., Du, J., Chen, L., Lin, P., and Fang, S. (2019). Assessing the effects of ecological engineering on carbon storage by linking the CA-Markov and InVEST models. *Ecol. Indic.* 98, 29–38. doi:10.1016/j.ecolind.2018.10.052

Zhao, Y. X., Xiao, D. P., Bai, H. Z., Liu, D. L., Tang, J., Qi, Y., et al. (2022). Climate change impact on yield and water use of rice-wheat rotation system in the Huang-Huai-Hai Plain, China. *Biology-Basel* 11, 1265. doi:10.3390/biology11091265

Zhou, J. H., Liu, X. H., Liu, X. J., Wang, W., and Wang, L. (2023). Assessing agricultural non-point source pollution loads in typical basins of upper Yellow River by incorporating critical impacting factors. *Process Saf. Environ. Prot.* 177, 17–28. doi:10.1016/j.psep.2023.07.003

Zhu, K. W., Zhang, Y., Tian, X. S., Guan, D., Zhang, S., He, Y., et al. (2024). Evolutionary trend analysis of agricultural non-point source pollution load in chongqing based on land use simulation. *Agronomy* 14, 737. doi:10.3390/agronomy14040737

Zhu, Z. C., Fu, C. S., Wu, H. W., Zhang, H., Cao, Y., et al. (2023). What influences does grazing bring about to stream nutrient fluxes in alpine meadows? *Agric. Water Manag.* 289, 108502. doi:10.1016/j.agwat.2023.108502

Zou, L. L., Liu, Y. S., Wang, Y. S., and Hu, X. (2020). Assessment and analysis of agricultural non-point source pollution loads in China: 1978-2017. *J. Environ. Manag.* 263, 110400. doi:10.1016/j.jenvman.2020.110400

Zuo, D. P., Bi, Y. Q., Song, Y. H., Xu, Z., Wang, G., Ma, G., et al. (2023). The response of non-point source pollution to land use change and risk assessment based on model simulation and grey water footprint theory in an agricultural river basin of Yangtze River, China. *Ecol. Indic.* 154, 110581. doi:10.1016/j.ecolind.2023.110581

Zuo, D. P., Han, Y. A., Gao, X. X., Ma, G., Xu, Z., Bi, Y., et al. (2022). Identification of priority management areas for non-point source pollution based on critical source areas in an agricultural watershed of Northeast China. *Environ. Res.* 214, 113892. doi:10.1016/j.envres.2022.113892

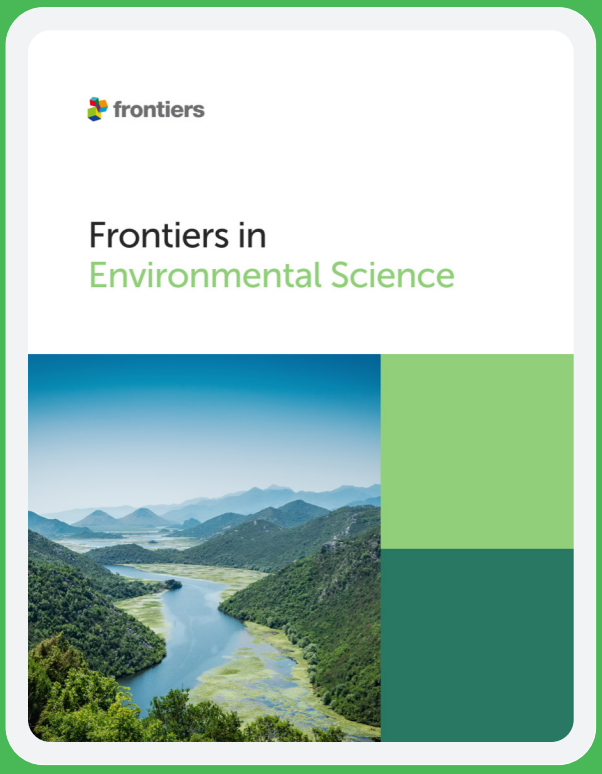
Frontiers in Environmental Science

Explores the anthropogenic impact on our natural world

An innovative journal that advances knowledge of the natural world and its intersections with human society. It supports the formulation of policies that lead to a more inhabitable and sustainable world.

Discover the latest Research Topics

See more →



Frontiers

Avenue du Tribunal-Fédéral 34
1005 Lausanne, Switzerland
frontiersin.org

Contact us

+41 (0)21 510 17 00
frontiersin.org/about/contact